GENERAL REPORT

Proceedings of the

ATHENS WORKSHOP
Jan. 20 & 21, 2006

ETC-12

Geotechnical EVALUATION *and* APPLICATION of the Seismic Eurocode EC 8
2003-2006

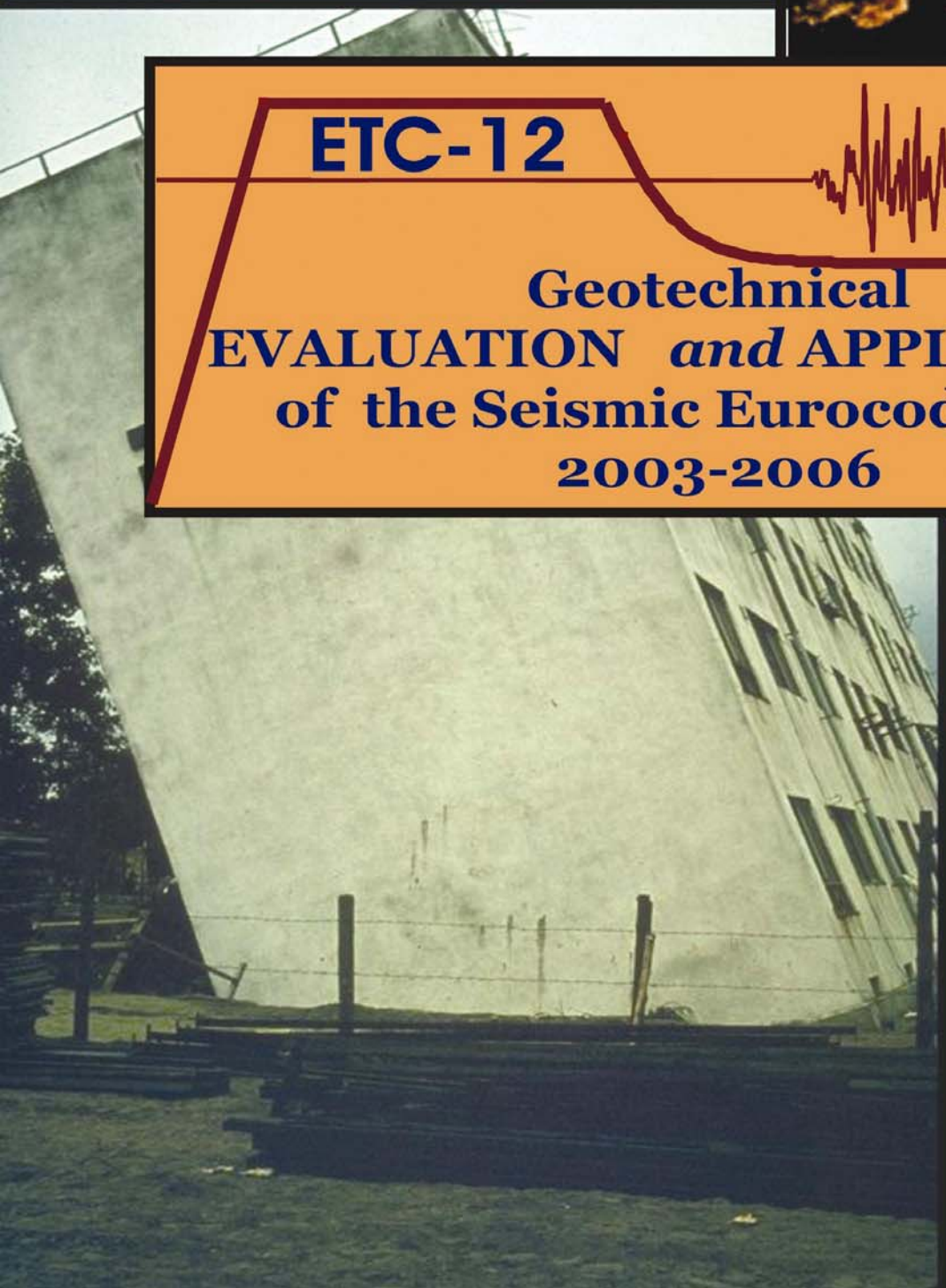

Edited by:
G. Bouckovalas

National
Technical
University of
Athens

Greece

This document is ready to print in duplex

P R E F A C E

The European Technical Committee ETC-12 became active in January 2003, following the invitation of Prof. Seco e Pinto, Vice President for Europe of the ISSMFE at the time, to Profs. George Gazetas and George Bouckovalas to act as Chairman and Co-chairman respectively.

Based on research and practical experience related to the geotechnical issues of Seismic Eurocode EC-8, but also on availability, eight more European experts were consequently selected, and kindly accepted to become members. Thus, the **Active Members** of ETC-12 are:

CORE MEMBERS		**MEMBERS**
G. Gazetas (Greece)	*Chairman*	M. Maugeri (Italy)
G. Bouckovalas (Greece)	*Co-chairman*	R. Paolucci (Italy)
A. Ansal (Turkey)		K. Pitilakis (Greece)
A. Pecker (France)		A. Simonelli (Italy)
D. LoPresti (Italy)		Ch. Vrettos (Germany)

The **Terms of Reference** agreed upon by the Committee Members are as follows:

TERMS OF REFERENCE

The Committee will concentrate on ***Part 5*** and the section of ***Part 1 dealing with soil categories and response spectra.***

The scope of the Committee will be :

(1) To provide ***general and specific comments*** on the code from the point of view of geotechnical earthquake engineering practice, and in light of the latest research. Such comments may be utilized during the 5–year period of tentative application of EC-8, to effect changes.

(2) To address issues of ***compatibility with EC7*** and recommend solutions.

(3) To ***apply EC8*** to a number of simple but realistic comparative case studies, referring to:

- Response spectra
- Shallow foundations
- Piled foundations
- Retaining structures
- Embankments
- Liquefaction

The application will utilize the EC7/EC8 partial safety factors, and the comparison can be made against other national or international codes, “exact” solutions, and so on.

(4) To ***report*** some the preliminary findings at the European Conference ECSMGE in Prague (on Friday 29 August 2003) and the final findings at the International Conference (ICSMGE) in Osaka (2005).

The activities of the Committee were essentially concluded about three years later, with the "**Athens ETC-12 Workshop**" (21 & 22/01/2006), where all Members, as well as invited colleagues, presented their contributions in accordance with the above Terms of Reference.

The following report presents the Proceedings of this Workshop, including:

- all **individual contributions**,
- a **General Report** with the main comments, concerns and proposals of the ETC-12 members regarding the present form of EC-8, as well as
- a **Summary** of proposed recommendations.

It is our hope that this joint 3-year effort will prove useful to the Permanent EC-8 Committee in considering possible future updates of the code.

During the entire term of ETC-12, there was continuous support and inspiration from the current ISSMGE President, Professor P.S. Pinto. Furthermore, Professor R. Frank, the ISSMGE Vice President for Europe, had an active participation during the Athens ETC-12 Workshop. These contributions are gratefully acknowledged by all Committee Members.

G. GAZETAS & **G. BOUCKOVALAS**

TABLE OF CONTENTS

SUMMARY & RECOMMENDATIONS

The Athens ETC-12 workshop was held on January 20 & 21, 2006 at the campus of the National Technical University (NTUA). Its scope was to report on the final findings of the ETC-12 members and their colleagues, along the lines defined by the adopted Terms of Reference for the 2003-2006 period. In other words, it replaced the ETC-12 meeting of September 2005, which was scheduled to take place during the International Conference (ICSMGE) in Osaka. Attendance reached about 40 European experts, from France, Germany, Greece, Italy and Turkey.

A total of eighteen (18) contributions were submitted for oral and written presentation, covering the majority of geotechnical aspects addressed by the EC-8. These contributions were presented during the first day of the workshop (Table I), with a brief discussion period allowed between the presentations. The main findings of the first day were summarized during the second day of the workshop, by means of eight (8) Summary Reports prepared by the ETC-12 members (Table II). Following each summary report, time was given for extensive floor discussion. Second day sessions were preceded by introductory remarks, regarding the general philosophy and objectives, as well as the present status of EC-8, kindly provided by Prof. *Roger Frank* (Vice President for Europe of the ISSMGE) and Prof. *Alain Pecker* (member of the EC-8 preparation committee).

The Summary Reports, and the discussion which followed them, are presented herein in the form of a General Report, which provides the main comments, concerns and proposals of all workshop participants regarding the present form of EC-8. It is the opinion of the active ETC-12 members that this report could provide the base for a future update of the code, with priority given to the proposed revisions which are summarized below:

GROUND CONDITIONS AND SEISMIC ACTIONS

(EC-8 Part 1: chapter 3, Part 5: chapter 2)

1. Replace the *average shear wave velocity* $V_{S,30}$ with the *average shear wave velocity* $V_{S,av.}$ *of the soil-like formations* which lay above the bedrock (rock or other rock-like material with V_S*>800m/s*), defined as:

$$V_{S,av.} = \frac{H}{\sum_{i=1,N} \frac{h_i}{V_i}} \qquad where \quad H = \sum_{i=1,N} h_i \le 30m$$

[*G. Gazetas and G. Bouckovalas propose to increase the 30m limiting soil depth to 50m. In any case, this value may be defined in the National Annex of each Country*]

2. Fill the gaps in the existing definition of Ground Types in terms of $V_{S,30}$ *(*$V_{S,av.}$*)* and *H*. Either of Figures 1.1b and 1.1c in the General Report may be used for that purpose.

3. Categorize deep and soft soil sites (e.g. with $T_{S,el}$*=4H/*$V_{S,av.}$ *> 0.80s*) to Ground Type S1, acknowledging the objective difficulties encountered in assessing the associated seismic response.

4. Define the Soil Factors for strong/weak motions based on a_g rather on *M*. In this case, the limiting value of *M=5.5* could be replaced with the limiting value of a_g*=0.15g*. The definition of Elastic Response Spectra in terms of *M* needs not be changed.

5. State clearly that N_{SPT} is not a reliable index, and should not be used for the categorization of clayey and gravely soil formations.

TABLE I: Workshop programme of Friday January 20, 2006

3:00 p.m.	**OPPENING ADDRESS** - *G. Bouckovalas*
3:30 p.m.	**SESSION 1** - *M. Maugeri, G. Lanzo*
	- Design response spectra and soil classification for seismic code provisions. *K. Pitilakis, Ch. Gazepis, A. Anastasiadis* - Compatibility of EC-8 ground types and site effects with 1-D wave propagation theory. *G. Bouckovalas, A. Papadimitriou, D. Karamitros* - Dynamic soil characterization according to EC-8 and its effects on the assessment of seismic actions. *D. Lo Presti,E.Mensi, N. Squeglia* - Selection and scaling of real acceleration time histories for site response analyses. *A. Ansal, E. Durukal, G. Tonuk* - Site Characterization at the Catania city, Italy. *A. Cavallaro, S. Grasso, M. Maugeri*
4:45 p.m.	**SESSION 2** - *K. Pitilakis, E. Cascone*
	- Some comments on the EC-8 prescriptions for the evaluation of soil liquefaction. *D. Lo Presti, E. Mensi, N. Squeglia* - Liquefaction: a contribution to the Eurocodes from the Italian guidelines "Geotechnical Aspects of the Design in Seismic Areas". *F. Santucci de Magistris* - Application of EC-8 for the assessment of liquefaction potential and for the seismic response of a river embankment. *Ch. Vrettos* - A modified Newmark-type analysis according to EC-8 requirements for seismic stability of natural slopes. *G. Biondi, M. Maugeri* - Slope stability analysis according to EC-8 and Italian seismic regulations. *A. L. Simonelli, S. Sica, F. Moccia*
6:00 p.m.	**B R E A K**
6:30 p.m.	**SESSION 3** - *G. Gazetas, F. Santucci de Magistris*
	- Numerical investigation of 3D seismic amplification by real steep topographic profiles and check of the EC-8 topographic amplification coefficients. *R. Paolucci* - Aggravation of seismic ground motion due to slope topography. *A.Papadimitriou, G. Bouckovalas* - Numerical study of topography effects at the Nicastro (southen Italy) cliff and comparison with EC-8 recommendations. *A. Pagliaroli,G. Lanzo, B. D'Elia* - Pseudo-static and pseudo-dynamic gravity wall design according to EC-8. *A. L. Simonelli* - Pseudo-static seismic design of embedded retaining structures. *L. Callisto*
7:45 p.m.	**SESSION 4** - *A. Simonelli, A. Kaynia, G. Tonuk*
	- Soil plasticity and uplifting effects on soil-structure interaction. *G. Abate, M.R. Massimino, M. Maugeri* - Suplementary criteria for shallow foundation design close to seismically active faults. *R. Paolucci, M.T. Yilmaz* - On the design of structures to resist fault displacements, with application in Greece. *I. Anastasopoulos, G. Gazetas* - Suggestions and comments on EC-8 geotechnical provisions: *K. Pitilakis*

TABLE II: Workshop programme of Saturday January 21, 2006

DISCUSSION SESSION ***R. Frank, A. Pecker, A. Ansal, G. Gazetas.***	
9:30 a.m.	**Ground conditions and seismic actions** (EC-8 Part 1: chapter 3, Part 5: chapter 2). *G. Bouckovalas, A. Anastasiadis*
10:00 a.m.	**Topography effects** (EC-8 Part 5: annex A). *K. Pitilakis, Ach. Papadimitriou*
10:30 a.m.	**Ground properties** (EC-8 Part 1: chapter 3, Part 5: chapter 3 & section 4.2). *D. Lo Presti, N.Squeglia*
11:00 a.m.	**Proximity to seismically active faults** (EC-8 Part 5: paragraph 4.1.1). *R. Paolucci, ...*
11:30 a.m.	**B R E A K**
12:00 a.m.	**Slope stability** (EC-8 Part 5: paragraph 4.1.2). *M. Maugeri, M.R. Massimino*
12:30 a.m.	**Potentially liquefiable soils** (EC-8 Part 5: paragraph 4.1.3 & annex B). *D. Lo Presti, Ch. Vrettos*
1:00 p.m.	**a. Shallow foundations** (EC-8 Part 5: chapters 5 and annex F) **b. Deep foundations** (EC-8 Part 5: paragraph 5.4.2, chapter 6 and annex C) **c. Soil-structure interaction** (EC-8 Part 5: chapter 6 and annex D) *G. Gazetas*
1:45 p.m.	**Earth retaining structures** (EC-8 Part 5: chapter 7 and annex E). *A. Simonelli*
2:15 p.m.	**CLOSURE**

TOPOGRAPHY EFFECTS
(*EC-8 Part 5: annex A*)

6. Characterize cases of irregular (ground surface or bedrock) topography as Ground Type S3, where the definition of seismic actions requires a special site exploration and study. The simple cases considered in Annex A, as well as cases where topography effects are not important (e.g. average inclination $i<15^o$ or height $H<30m$ and average shear wave velocity V_S>300m/s) should be excluded from this category.

7. For cliffs and step-like slopes, the distance behind the crest where topography aggravation persists should be defined. Until more refined studies become available on this topic, it is recommended to use the topography aggravation factors of Annex A within a distance *H* behind the crest, and reduce them (linearly) to the free field values (S_T=1.00) at distances greater than 5H.

8. Add criteria for simple cases of alluvial valleys subjected to weak ground motions.

GROUND PROPERTIES
(EC-8 Part 1: chapter 3, Part 5: chapter 3 & section 4.2)

9. Omit article 4.2.2 (7) and section 4.2.3 from Part 5, as they may over-simplify the assessment of internal soil damping and the dependency of dynamic soil properties upon strain level. Add the following articles in their place:

4.2.2 (7) *In all calculations involving the dynamic soil properties under stable conditions, the soil stiffness and internal damping parameters should be compatible with the strain levels induced by the design earthquake.*

4.2.2 (8) *For the design cases specified in (5) above, it is strongly recommended to measure internal soil damping and dynamic soil stiffness, at various strain levels, by appropriate laboratory or field techniques. For all other cases, or in lack of direct measurements, well documented empirical correlations may be used instead, allowing for the associated scatter.*

PROXIMITY TO SEISMICALLY ACTIVE FAULTS

(EC-8 Part 5: paragraph 4.1.1)

10. Modify article 4.1.1 (1)P as follows:

(1)P *…shall generally not be erected in the immediate vicinity of tectonic faults, recognized … national authorities, without proper seismotectonic and structural studies.*

11. Define the *"immediate vicinity"* in quantitative terms, e.g:

Fault Type	**Distance from Fault Trace** [(1)] **(m)**	
	on Standing (Foot) wall	**on Moving (Hanging) wall**
Strike-Slip	30	30
Normal	30+1.5H [(2)]	30
Reverse	30+2.0H [(2)]	30

(1) *The fault trace is defined at the bedrock (Ground Type A of Table 3.1, Part 1).* ***(2)*** *H is the soil thickness above bedrock.*

Note that, in the above distances, 30m is a gross estimate of the potential error in locating a fault trace in rock or rock-like formations, while the remaining part (*1.5H* or *2.0H*) accounts for the deviation of the fault trace due to propagation through soil-like materials, as well as, for the width of the intensely distorted zone on the surface of such materials. For normal and reverse faults, *R. Paolucci* proposes to increase the 30m distance to 50m.

12. Revise article 4.1.1 (3) P as follows:

(3)P *Special ~~geological investigations~~ geological, seismological and seismotectonic studies shall be carried out……near potentially active faults, in order to determine the ensuing hazard in terms of base rock dislocation ~~and severity of ground shaking~~.*

13. Include article 4.1.1 (4):

(4) *For buildings specified in (1)P above, a structural analysis is required to show that the structure-foundation system can withstand without damage a permanent ground movement, consistent with the probable fault displacement, applied at various locations within the foundation area. In case that the soil-foundation interaction is taken into account, proper attention should be given to the numerical simulation of the structure-soil interface, as well as the soil response under very large shear strains (e.g.>5%.)*

SLOPE STABILITY

(EC-8 Part 5: paragraph 4.1.2)

14. Modify article 4.1.2 (8)P as follows:

(8)P *Simplified methods, such as the pseudo-static ones, shall not be used for soils capable of developing high pore water pressures or significant degradation of stiffness under cyclic*

loading. Furthermore, the horizontal seismic force F_H specified in 4.1.2(5)P should be appropriately increased for "shallow" failure surfaces (e.g. with z/h<0.40, where z=height of failure surface and h= total height of slope).

15. Add the following article 4.1.2 (9)P:

4.1.2(9)P *For the special cases prescribed in (8)P above, it will be necessary to perform numerical analyses or apply improved analytical methods which can take effectively into account the possible effects of excess pore pressure build up, shear strength degradation and spatial (within the embankment) PGA variability.*

POTENTIALLY LIQUEFIABLE SOILS
(EC-8 Part 5: paragraph 4.1.3, annex B)

16. Revise the last sentence of article (3)P as follows:

"…(CPT), as well as the determination of grain size distribution curves, fines content and plasticity (Atterberg) limits in the laboratory. For structures of high importance, more advanced laboratory tests may also be performed (e.g. cyclic triaxial, torsional or simple shear tests) for a more complete evaluation of the liquefaction resistance."

17. Move articles (4)P, (5) and (6) to Annex B, as they are method-specific.

18. Article (7) may be omitted.

19. In the conditions stated in article (8) include:

- *the sands do not meet the gradation criteria of Fig. ….* (include Fig. 6.1 of the General Report)

20. Replace article (9) as follows:

(9) *Any established method, which is based on sound geotechnical and soil dynamics procedures, and supported by experience and field observations, is in principle acceptable for assessing the liquefaction potential.*

21. Revise Eq. 4.1 as follows:

$$\tau_e = m\alpha_{gR}\gamma_I\sigma_{vo}r_d \qquad (4.1)$$

where m=0.80-0.90, and

$$r_d = \begin{cases} 1.00 - 0.007z & (\text{if } z \le 10 \text{ m}) \\ 1.18 - 0.025z & (\text{if } 10 \le z \le 25\text{m}) \\ 0.55 & (\text{if } z > 25\text{m}) \end{cases}$$

[*The definition of r_d could also be moved to Annex B, as it is method specific*]

22. Add the following article, after present article 12(P) :

(…) In the case of sloping ground, or level ground with a step-like topographic irregularity (e.g. at river banks) liquefaction may lead to large, nearly horizontal displacements due to lateral spreading. These displacements, as well as their effect on the stability of shallow and deep foundations must be assessed using well established (empirical or other) methodologies supported by experience and field observations. In these cases also, adequate foundation safety shall be obtained by appropriate ground improvement methods and/or by pile foundations transferring loads to firm soil layers.

23. Revise present article (14) as follows:

"…… due to the large forces induced in the piles by the loss of soil support in the liquefiable soil layers, the possible lateral ground displacement, and the inevitable ….."

SHALLOW and DEEP FOUNDATIONS, SOIL-STRUCTURE INTERACTION
(EC-8 Part 5: chapters 5 & 6, annexes C, D & F)

24. State that uplifting and simultaneous mobilization of bearing capacity mechanisms do not imply failure, but may lead to unacceptable permanent displacements and rotations.

25. Second order (P-δ) effects play an important (detrimental) role on the dynamic response of slender structures. Therefore, they should be considered in the analysis procedures when a slenderness ratio of 2.0 or more is encountered.

26. It is well understood that dynamic overturning is highly sensitive to the excitation frequency and the size of the structure. In any case the minimum acceleration for overturning under dynamic conditions is higher than the static limiting value (b/h in g) especially when a short-period shaking or a large structure is considered. A lower bound (conservative estimate) of this trend can be obtained from the following expression:

$$A_{over,dyn} = \frac{b}{h}\sqrt{1+\left(\frac{\omega_{\mathrm{E}}}{p}\right)^2}$$

Where $\omega_E=2\pi/T_E$ is the predominant excitation frequency and $p = \sqrt{mgR/J_o}$ is a size parameter (J_o is the structure mass moment of inertia with respect to the corner of the foundation and $R = \sqrt{b^2 + h^2}$ is the "effective" diameter - see Fig. 7.1 of General Report). A period of 2.0sec ($\omega_E=\pi$) is considered as representative of static loading conditions whereas for civil engineering structures a value of $p = 1.5 \cong \pi/2$ can be estimated as an upper limit. In this way, the overturning acceleration for design against earthquake loading is suggested to be calculated as:

$$A_{over,dyn} = 2\left(\frac{b}{h}\right)g$$

If the vertical load of the foundation will be $N < 0.3N_{ult}$ where N_{ult} is the ultimate load capacity. This inequality ensures that inelastic soil deformations will be small and concentrated in the vicinity of the pivot points. For larger values of the vertical load N, a DSSI analysis in the time-domain is required to investigate the overturning potential.

27. In the realm of a capacity-based design, the computed angle of rotation can exceed the elastic threshold or even the "yield" angle θ_{ult} that corresponds the maximum moment M_{ult}. However, the maximum angle shall be bounded by the inequality $\theta_{\max} < \theta_c = 0.40 \cdot b/h$ if large permanent rotations must be avoided.

28. Equivalent-linear SSI procedures in time or frequency domain should be adopted only if the following conditions are concurrently satisfied: (1) $N < 0.3N_{ult}$ and (2) $M_{over} < 0.5Nb$ where M_{over} is the overturning moment onto the foundation.

EARTH RETAINING STRUCTURES
(EC-8 Part 5: chapter 7, annex E)

29. Revise Table 7.1 of section 7.3.2.2 as follows:

Table 7.1: Factor affecting the horizontal seismic coefficient

Type of retaining structure	***r***
Free gravity walls that can accept a displacement $d_r > 200\alpha S$ (mm)	*2.00*
As above with $d_r = 100aS \div 200aS$ (mm)	*1.50*
Flexural reinforced walls, anchored or braced walls, reinforced concrete walls founded on vertical piles that can accept a displacement $d_r < 100aS$ (mm)	*1.25*
As above, or restrained basement walls and bridge abutments, with $d_r = 0$	*1.00*

30. Allow for some shearing resistance between soil and wall (e.g. $\delta_d=1/3\ \varphi_d$) in passive earth pressure calculations, in order to avoid unrealistic (over-) design of embedded retaining structures with limited allowable displacements.

General Report of the Athens ETC-12 Workshop on the Evaluation and Application of Seismic Eurocode EC-8

The following General Report is based on the Summary Reports presented during the second day of the Athens Workshop, and the discussion which followed them.

1. GROUND CONDITIONS AND SEISMIC ACTIONS

(EC-8 Part 1: chapter 3, Part 5: chapter 2)

G. Bouckovalas[1], A. Anastasiadis[2]
[1]National Ttechnical University of Athens, Greece,
[2]Aristotle University of Thessaloniki, Greece

Ground conditions and seismic actions are considered in five (5) workshop contributions: by *Bouckovalas et al*., *Pitilakis et al*., *Cavallaro et al*., *Lo Presti et al*. and *Ansal et al*. The first two, rely on thorough parametric analyses to check the general accuracy of EC-8 provisions and propose possible improvements, while the next two rely on extensive site-specific ground response analyses, performed as part of major Seismic Microzonation studies, to check the applicability of EC-8 in practice. Finally, *Ansal* et al. examines the effect of various ground motion scaling parameters on the results of site- and earthquake hazard-specific ground response analyses.

In the following, we focus upon four (4) basic issues addressed directly or indirectly in the above contributions: the number and the definition at *Ground Types*, the associated *Soil Factors* and *Elastic Response Spectra*, as well as the *Scaling Parameters* for time-history representation of the input seismic motion. Note that a number of other practical issues is also addressed in the articles, which are worth of careful study and consideration, but could not be included in the following summary presentation without sacrificing the coherence at the general report.

Ground Types.- Figure 1.1 summarizes the Ground Types proposed by EC-8, modified by Cavallaro et al. for the Seismic Microzonation of Catania, as well as the ground types alternatively proposed by *Bouckovalas et al*. and *Pitilakis et al*.. The presentation uses ($V_{s,30}$ vs. H) or (V_s vs. H) diagrams, where H is the depth to the bedrock, $V_{s,30}$ is the average shear wave velocity over the first 30m of depth, while V_s is the average shear wave velocity over the soil depth H. Note that in the presentation of Fig. 1.1a, the sentence " ... *of several tens of meters*" used in the EC-8 description of ground types was interpreted as H≥30m.

The first thing to observe in this figure is that there is a gap in the EC-8 definition of ground types (Fig 1.1a). For instance, it is not clear how to categorize soil profiles with:

- $V_{s,30}$=100÷360 m/s and H= 20÷30m, or
- $V_{s,30}$ > 360 m/s and H=5÷30m

Secondly, it is noted that in the proposals of *Bouckovalas et al*. and *Pitilakis et al*., $V_{s,30}$ has been replaced by V_s. The logic behind this change is explained in detail in the two relevant articles. In brief, $V_{s,30}$ may be an overrated indicator of soil stiffness in the case of soft but shallow soil profiles (H<30m) and an underrated indicator for deep profiles (H>>30m), or for profiles with an abrupt stiffness change between 30m of depth and the deeper laying bedrock. However, during discussion of this topic, in the second day of the workshop, it was pointed out that the geotechnical investigation of depths greater than 30m may face objective difficulties and will be often abandoned in practice. Hence, in a short of compromise, it was suggested to use V_s when the depth to bedrock is 30m or less, and $V_{s,30}$ for deeper soil profiles.

Finally, there seems to be a more general trend towards an increased number of ground types. Namely:

- *Cavallaro et al*. split EC-8 ground types B, C and D into B_1 & B_2, C_1 & C_2 and D_1 & D_2, thus increasing the total number of ground types to nine (9).

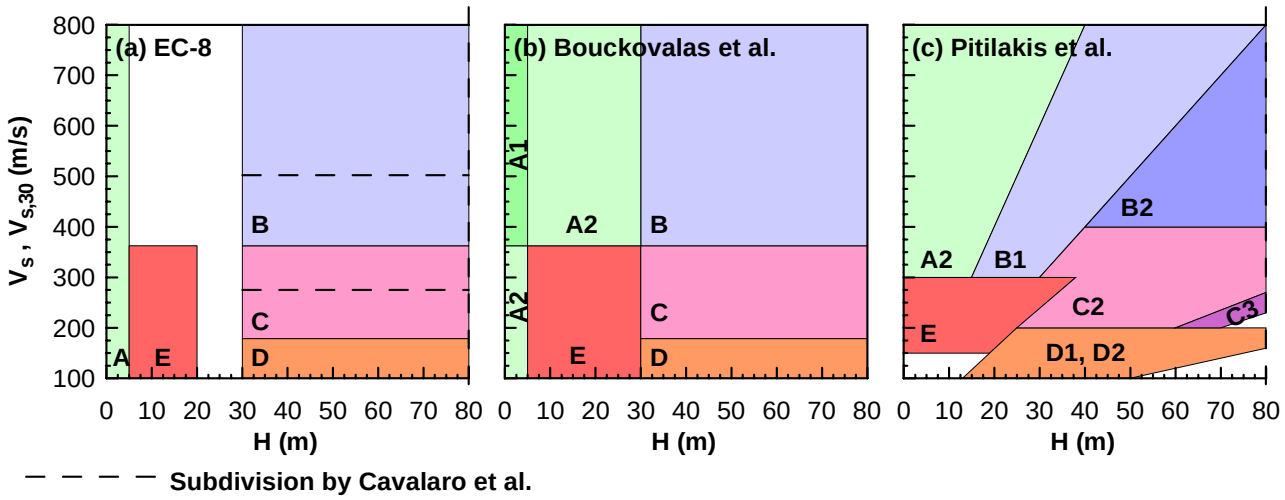

Fig 1.1: Definition of ground types according to (a) EC-8, (b) Bouckovalas et al. (2006), (c) Pitilakis et al. (2006)

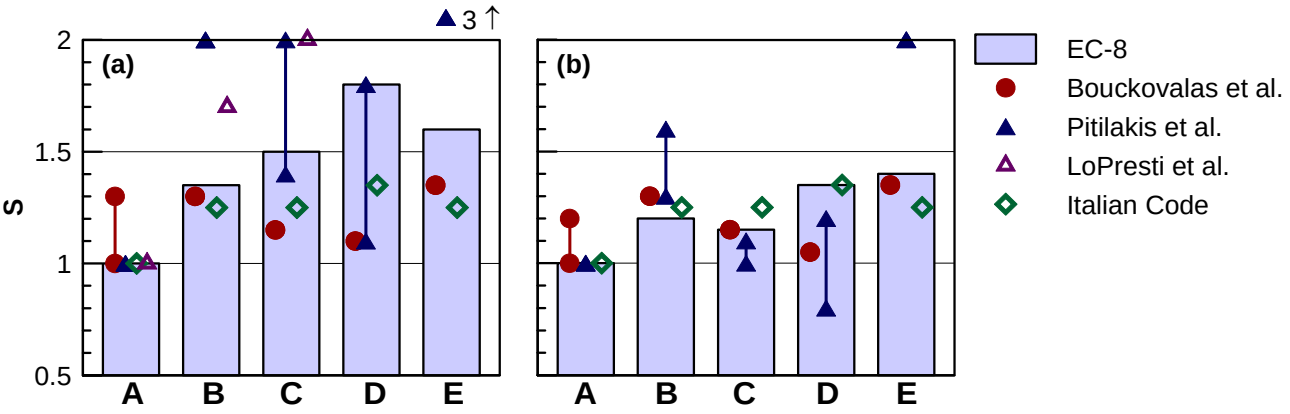

Fig 1.2: Comparison of Soil Factors for (a) weak ground motions with M<5.5 or PGA<0.20g and (b) strong ground motions with M>5.5 or PGA>0.20g

- *Bouckovalas* et al. increase the EC-8 ground types to seven (7), by introducing an intermediate ground type (A_2) which includes very shallow but soft soil deposits (H<5m and V_S=100÷360 m/s) but also closes the existing gap between ground types A and B (for V_s>360 and H=5÷30m).
- *Pitilakis et al*. increase ground types to twelve (12) by splitting and redefining EC-8 ground types, A, B, C and D according to the (elastic) fundamental soil period of the soil column T_o.

Although none of the above proposals found unanimous approval by the workshop participants, it was generally agreed that more ground types are needed, while their definition should directly or indirectly refer to the fundamental vibration period of the soil column.

Soil Factors.- Figures 1.2a and 1.2b summarize the soil factors proposed by EC-8, for "strong" and "weak" ground motions respectively, in comparison with the soil factors adopted in the Italian Code, as well as those analytically computed by *Bouckovalas et al.*, *Pitilakis et al.* and *Lo Presti et al.*. Observe that all soil factors for "strong" motions (M>5.5 or PGA>0,20g), in Fig. 1.2a, are in a good overall agreement. As a possible fine-tuning correction, soil factors for ground types B and E should be somewhat

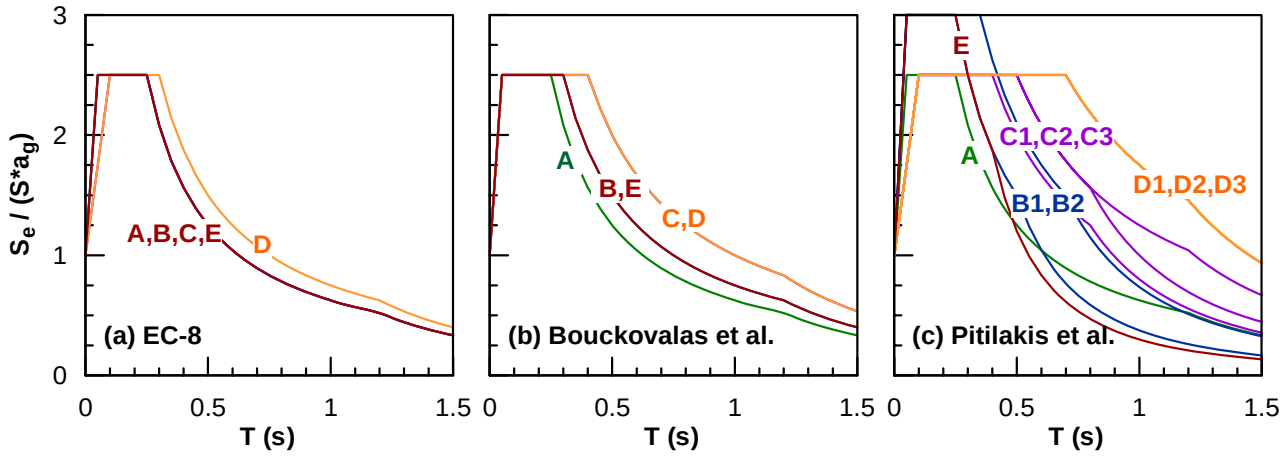

Fig 1.3: Comparison of Normalized Elastic Response Spectra for weak ground motions with M<5.5 or PGA<0.20g

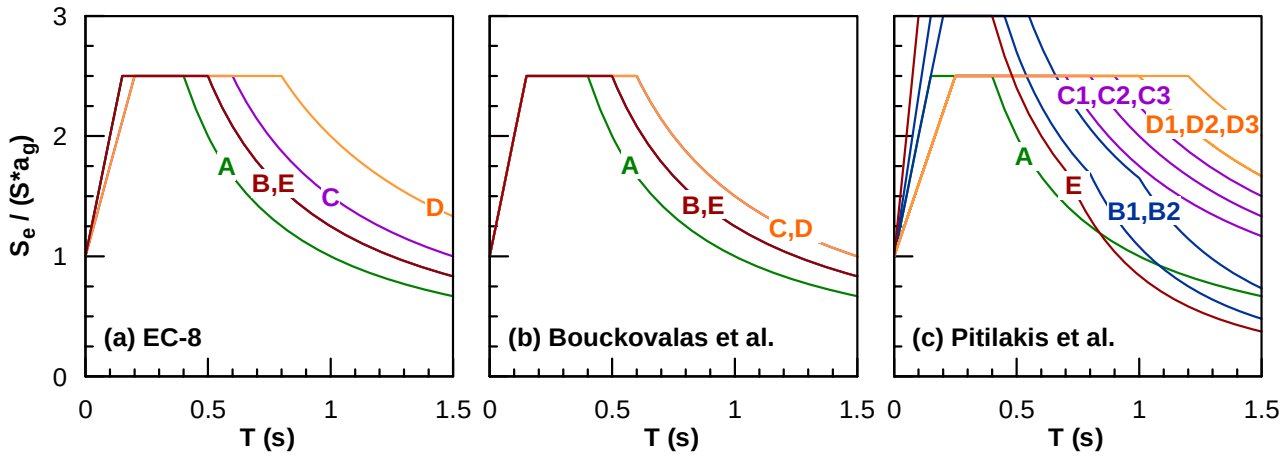

Fig 1.4: Comparison of Normalized Elastic Response Spectra for strong ground motions with M>5.5 or PGA>0.20g

increased, while the soil factor for ground type D should be equally decreased.

However, the picture becomes quite different for "weak" motions (M≤5.5 or PGA≤0,20g), in Fig 1.2b. First of all, the scatter of the analytical predictions is now significant, betraying a higher sensitivity of the seismic ground response analyses to the input data parameters, e.g. the input motion characteristics or the detailed variation of soil stiffness with depth. In addition, the EC-8 values pose as a lower (non-conservative) bound to analytical predictions for ground types B, C and E, and as an upper (conservative) bound for ground type D.

Normalized Elastic Response Spectra (NERS).- Figure 1.3 compares the NERS proposed by EC-8, with those proposed by *Bouckovalas et al*. and *Pitilakis et al*. for strong Ground Motions (M>5.5 or PGA>0.20g). A similar comparison is shown in Fig 1.4 for "weak" ground motions (M≤5.5 or PGA≤0,20g).

In gross terms, *Bouckovalas et al*. maintain the EC-8 provisions, altering slightly the period limits T_B and T_C for certain ground types (D for "strong" ground motion and E for "weak" ground motion). On the other hand, *Pitilakis et al*. propose drastic changes, increasing the significant period range of the spectra ($T_B \div T_C$), as well as, the peak normalized spectral acceleration which is set

equal to 2.5 by EC-8. As a result, spectral accelerations are increased for practically all ground types and seismic motion magnitudes.

Before concluding on the NERS, it is worth noting here the view expressed by Gazetas and Mylonakis (see Fig. 7.2, later herein), namely that the current procedure for obtaining design spectra may not be adequate for the study of soil-structure systems.

Scaling of Input Seismic Motion.- The EC-8 explicitly states (Part 1, Paragraph 3.2) that recorded or simulated accelerograms should be scaled to the PGA for the zone (site) under consideration. *Ansal et al*. showed that this requirement leads to optimum consistency of analytical predictions only for problems where PGA is the basic damage parameter (e.g. liquefaction susceptibility or slope stability). On the contrary, they proposed to scale input motions according to the Arias intensity in cases where seismic design depends on spectral acceleration (e.g. seismic design of above ground structures).

The workshop participants agreed to that view, and proposed that input motions should be generally scaled according to the basic damage parameters that will be used in subsequent design stages. For instance, scaling according to PGV was recommended for problems involving the computation of permanent ground or foundation displacements.

Other issues.– Apart from the above, the workshop participant discussed whether "strong" and "weak" ground motions should be defined in terms of earthquake magnitude M or in terms of PGA and the predominant excitation period. In addition, a lot of skepticism was expressed with regard to the current trend to proceed towards a much more detailed set of code provisions for soil effects, with the hope that the need for site-specific ground response analyses is finally limited to important structures and special soil conditions. The prevailing view on this matter was that such an approach may prove neither possible nor practical for one reason at least: the number of ground and earthquake motion parameters which have to be considered in order to ensure accuracy in a wide spectrum at applications, is rather too large for any code standards.

2. TOPOGRAPHY EFFECTS

(*EC-8 Part 5: annex A*)

K. Pitilakis, Ach. Papadimitriou

[1]Aristotle University of Thessaloniki, Greece

[2]National technical University of Athens, Greece

The contributions presented in the ETC-12 Workshop that deal directly or indirectly with the issue of topographic amplification of seismic ground motion are summarized in Table 2.1. A distinction is made in this Table as to the specific topographic geometry studied, i.e. cliff, slope or ridge. In addition, a paper that deals with the effects of the "topography" of the bedrock basin is also included in this discussion.

Studying and compiling the comments and proposed modifications for the various types of topographic geometries, the following can be reported:

"Cliff" topography.-

- *Pitilakis* and *Pagliaroli et al* propose that the topographic amplification factor S_T should be made frequency-dependent, although *Paolucci* finds the use of an average value for all frequencies as a satisfactory approach. In particular, *Pagliaroli et al* propose that the spectral amplification variation of S_T should take into account the 2D resonance frequency, whereas *Pitilakis* proclaims that the S_T should have higher values at high frequencies.
- Overall, the S_T=1.2÷1.4 values for the PGA that are prescribed by the EC-8 are found reasonable by *Pitilakis* as well as *Paolucci*, whereas *Pagliaroli et al* proclaim higher values to be more representative, a fact that is possibly an outcome of the elastic analyses they compiled and performed.
- For special cases of high (H>60m) and steep isolated cliffs, with an average $i>30^o$ and a maximum $i>60^o$, that have comparable length L and width W at the crest ($1/3 < L/W < 3$), *Paolucci* proclaims the use of $S_T \geq 1.6$ for PGA (at the crest). The foregoing values in parentheses are considered indicative and require further investigation, as agreed by *Paolucci* that proposed them.
- According to *Pitilakis*, the peak vertical accelerations increase close to the crest, while the distance to the free-field away from the cliff is less than one wavelength or 2÷3H.

TABLE 2.1 List of contributions dealing with topographic amplification factors

Contribution	Paper / Summary	Studied Geometry
Suggestion & comments on… topography effects *K. Pitilakis*	Summary	Cliff
Numerical investigation of 3D seismic amplification by real steep topographic profiles and check of the EC-8 topographic amplification coefficients *R. Paolucci*	Paper	Cliff, Ridge
Aggravation of seismic ground motion due to slope topography *A. Papadimitriou, G. Bouckovalas*	Paper	Slope
Numerical study of the topography effects at the Nicastro (southern Italy) cliff and comparison with EC-8 recommendations *A. Pagliaroli, G. Lanzo, B. D'Elia*	Paper	Cliff
Topographic amplification factors *G. Gazetas, D. Assimaki*	Summary	Slope
2D valley (basin) effects on seismic ground motions *P. Psarropoulos, G. Gazetas*	Summary	Basin

In general, *Pitilakis* believes that the most critical parameters of this problem are the geometry and the soil stratification, slope inclination, wave length, azimuth, amplitude and frequency content of the incident motion.

"Slope" topography.-

- Both related contributions, *Papadimitriou & Bouckovalas* and *Gazetas & Assimaki*, agree that there should be two (2) topographic amplification factors, S_{hT} and S_{vT}, one for the horizontal and another for the "parasitic" vertical seismic ground motion. Furthermore, both related contributions agree that these factors are spatially variable and, especially for the former, they both provide specific functions of spatial variation.
- For the S_{hT} *Gazetas & Assimaki* propose that it is frequency-dependent, with the peak value of 1.4 being assigned at T=0, a plateau of 1.2 being assigned for the peak spectral amplification period range ($T_B<T<T_C$) and a value of 1.0 to be assigned at periods $T\geq 1$s. Moreover, they argue that for the frequencies of greatest practical interest, topography effects are significant only with soft and moderately stiff soils.

On the contrary, *Papadimitriou & Bouckovalas* show that a frequency – independent value for S_{hT} suffices, and provide a specific relation for its estimation on the basis of the soil conditions, the slope geometry and the input motion characteristics.

- For the S_{vT}, *Papadimitriou & Bouckovalas* proclaim that it could be considered as a frequency-independent parameter and provide a specific relation for its estimation on the basis of the soil conditions, the slope geometry and the input motion characteristics.
- *Papadimitriou & Bouckovalas* show that topography effects should be considered only when $H/\lambda>0.16$ and $i>17^o$, where λ is the predominant wavelength of the shear waves. For comparison, the current criteria for considering topography effects are $H>30$m and $i>15^o$.

"Ridge" topography.- According to *Paolucci*, the frequency - independent aggravation factors proposed by EC-8 for horizontal motion, $S_T=1.2$ and 1.4 for average inclinations $i < 30^o$ and $i > 30^o$ respectively, are satisfactory.

"Basin" geomorphology.- According to *Psarropoulos & Gazetas*, 2D valley (basin) effects are significant only in weak and moderately weak motions. For strong motions, 1D analysis usually suffices, especially for locations far from the valley edges.

Furthermore, site response studies in a 2D valley, that of Euroseistest (*Makra et al. 2001; 2005*), showed that the additional to 1D resonance caused due to lateral propagation of locally generated (at the discontinuities) surface waves, quantified in terms of an

aggravation factor, attains a roughly constant value between 2 and 3 in the period range of 0.1 to 3.0s for weak and moderate ground motions respectively.

Despite the above evidence, there was general consensus that it is still premature to propose a geomorphic amplification factor for this type of topography.

Discussion.- In order to guide the discussion that took place on Saturday January 21st 2006, the following set of seven (7) questions was set to the audience:

[1] Although the constant values of S_T of EC-8 for horizontal motion are generally found reasonable, should S_T be refined by becoming a function of ground inclination i, the normalized height H/λ, or other parameters?

[2] Is the S_T for horizontal motion a frequency-dependent parameter, and if yes is the technical community ready to adopt in EC-8 a specific S_T spectrum (e.g. taking into account the resonance frequency)?

[3] Although the spatial variation of S_T for horizontal motion is generally acknowledged, is the technical community ready to adopt in EC-8 a specific S_T – distance from the topographic feature function?

[4] Although the generation of parasitic vertical motion near the topographic feature is generally acknowledged, is the technical community ready to adopt in EC-8 a 2nd topographic amplification factor S_{vT} for the vertical ground motion?

[5] Should there be a change to the criteria of EC-8 ($H > 30m$, $i > 15^o$) for neglecting topography effects?

[6] For special cases of high ($H>60$ m) and steep isolated cliffs (with an average $i > 30^o$ and a maximum $i > 60^o$) that have comparable length L and width W at the crest ($1/3 < L/W < 3$), should a really high value of $S_T \geq 1.7$ for PGA at the crest be adopted in EC-8 (with the foregoing values in parentheses being considered indicative)?

[7] What is the significance of the impedance contrast on topography effects?

During discussion, the following opinions were heard, in reference to the foregoing posed topics for possible discussion (numbers in brackets):

- *Paolucci* mentioned the difficulty of estimating the predominant wavelength λ of the shear waves and the difficulty that this issue imposes on using it as a parameter in an estimator equation of S_T [1]. He continued into underlining the importance of the angle of incidence in the values of S_T, a fact that makes the whole issue of an estimator equation of S_T even more complex [1].
- *Paolucci* agreed that S_T is frequency-dependent, but considers it premature to propose a related spectrum [2].
- *Bouckovalas* underlined the need for proposing a specific S_T – distance function [3]. This opinion was shared by all, based also on the closing remarks of *Pitilakis*, who expressed his doubts as to whether we are ready to propose a specific form for this function.
- *Bouckovalas* expressed the opinion that a 2nd topographic amplification factor S_{vT} should be addressed in a future modification of EC-8 [4].
- *Papadimitriou* mentioned the significance of taking into account the predominant wavelength λ of the shear waves in neglecting or not topography effects [5], but acknowledged the practical problem of its estimation, mentioned earlier by *Paolucci*.
- *Bouckovalas* and *Gazetas* both agreed that such tall and steep cliffs are very special cases and that if they become an objective of code provisions this should be performed in the National Annexes of countries that have such geological features [6]. This opinion was shared by all, based on the closing remarks of *Pitilakis*.
- *Vrettos* posed the rhetorical question as to whether dams could be considered as topographic features and if the engineer should use the topographic amplification factors in his dam design. *Gazetas* mentioned that this is not the same issue, since for dams the impedance contrast between the dam body and the natural soil is usually large, unlike natural topographic features, and since topographic features are usually of much milder geometry and of stiffer natural materials than dams. *Pecker* added that ICOLD has set forward specific regulations for large dams and that EC-8 should not deal with this issue.

- In closure, *Pecker* said that the Annex A for Topographic Amplification Factors is informative and needn't become more specific or detailed. On the other hand, he prompted all countries to implement detailed related provisions in their National Annexes.
- Finally, all agreed that there is no good validation from seismic arrays on the quantitative aspects of topographic effects and hence most related research and results (as well as the provisions of Informative Annex A) come from numerical studies, a fact that all agree to be a problem.

3. GROUND PROPERTIES

(EC-8 Part 1: chapter 3, Part 5: chapter 3 & section 4.2)

D. Lo Presti[1], N. Squeglia[1]

[1] University of Pisa, Italy

Some contributions have considered the problems related to the assessment of ground properties (*Lo Presti et al., Cavallaro et al., Pitilakis et al., Bouckovalas et al*), mainly addressing the following questions:

- Shall we continue to use V_{s30}?
- Are soil types enough (A, B, C, D, E, S1, S2)?
- Do we obtain the same soil type using V_{s30}, N_{spt} or S_u?

Discussion.- The first two questions have been discussed in a previous session devoted to the definition of seismic actions. The present discussion is therefore restricted to the assessment of necessary parameters (Table 3.1). Anyway, during discussion, it has been reminded that clause (4) of Chapter 3 (EC8 Part 1) states: "*Further sub-division of this classification (Table 3.1 Ground Types) is permitted to conform to special ground conditions*".

Discussion can be summarized as follows:

- Generally, the same soil type is obtained from V_{s30} or N_{SPT}. This indication has been given by *Lo Presti et al*. and mainly concerns soil types A, B and C. It appears necessary to extend this check to other soil types and also to consider classification based on the undrained shear strength. With this respect the database shown by *Pitilakis et al.* could be used.

Table 3.1: Relevant soil parameters

Purpose	Available investigation	Parameter
Soil type	Seismic, SPT, TX (UU-CU), FVT, CPT	V_{s30}, N_{spt}, S_u
Drained strength	DS, TX(CU-CD), CPT, SPT	c', ϕ'
Undrained strength	CPT, FVT, TX , SPT, Seismic, CLTX	CSR, $\tau_{cyc,u}$, S_u
Stiffness & Damping	RCT, CLTST, CLTX	G, D

Seismic = Down-hole, Cross-hole, SASW, SH - Seismic Refraction, etc.; SPT Standard Penetration Tests; TX = Triaxial Tests; FVT = Field Vane Test; CPT = Cone Penetration Test, CLTX = Cyclic Loading Triaxial Tests, RCT = Resonant Column Test; CLTST = Cyclic loading torsional shear test.

- *Simonelli* stressed that N_{SPT} may be appropriate for coarse grained soils (e.g. sands) but not for fine grained soils (e.g. clays) which have to be categorized according to S_u. Furthermore, he pointed out that the threshold values of the various geotechnical parameters adopted by EC-8 should be computed on the base of empirical correlations with more reliable, soil-specific parameters which are not presently considered by the code.
- Use of N_{SPT} to predict shear wave velocity is, on the other hand, strongly discouraged based on the evidence presented by *Lo Presti et al.*.
- *Cavallaro et al.* suggested using more advanced laboratory tests in order to determine the cyclic degradation of stiffness, damping and soil strength and the pore pressure build-up with number of cycles and strain level. More specifically the use of advanced cyclic triaxial tests, equipped for local strain measurements is suggested.
- It is observed that CSR, and $\tau_{cyc,u}$ represent the same parameter, that is the cyclic undrained shear strength of granular soils. Obviously CSR is a normalized parameter. More importantly it is recommended to assess the above parameters either from in situ tests or from

laboratory tests performed on specimens retrieved by means of in situ-freezing method.

- It is suggested to check how the stiffness and damping degradation reported in EC8 works in comparison to experimentally determined curves in well characterized soils.

Proposed Changes.-It was proposed to change the definition of Type E soil (Part 1 Chapter 3, Table 3.1 on Ground Type). The present definition states:

"*A soil profile consisting of a surface alluvium layer with V_{s30} values of type C or D and thickness varying between about 5 m and 20 m underlain by a stiffer material with V_{s30} > 800 m/s*".

This is suggested to change to:

"*A soil profile consisting of a surface alluvium layer with average shear wave velocity (V_S) values of type C or D and thickness varying between about 5 m and 20 m underlain by a stiffer material with V_S> 800 m/s*".

The above change draws upon the general remark that it does not make sense to determine V_{s30} for a layer with a maximum thickness of 20m (i.e.< 30m).

Finally, some participants expressed the view that the following statement (Part 5, chapter 4.2) could be omitted:

"(6) For all other cases, where the material vibration periods of the soil need to be determined, the Vs profile may be estimated by empirical correlations, using the in situ penetration resistance or other geotechnical properties, allowing for the scatter of such correlations".

4. PROXIMITY TO SEISMICALLY ACTIVE FAULTS

(EC-8 Part 5: paragraph 4.1.1)

***R. Paolucci*[1]**

[1] *Department of Structural Engineering, Politecnico di Milano, Italy*

Two relevant contributions have been presented and discussed in the ETC-12 Athens workshop of January 20 and 21, 2006, namely:

- *"Supplementary criteria for shallow foundation design close to seismically active faults", by R. Paolucci and T. Yilmaz, and*
- *"On the design of structures to resist fault displacement, with applications in Greece", by I. Anastasopoulsos and G. Gazetas*.

These contributions can be considered as complementary, in the sense that, while *Paolucci* and *Yilmaz* pointed out the need for introducing simplified design criteria for foundations to resist fault displacements, to cope with the numerous cases where active fault mapping is missing or not reliable, and proposed some criteria based on limit analysis concepts, *Anastasopoulos* and *Gazetas* used nonlinear finite element simulations to show how to deal with the design and verification of structures against fault displacements, by considering three real cases in Greece, namely: (a) the design of a three-span road bridge, (b) the fault-resistant design of a housing complex and (c) the design of a highway cut-and-cover tunnel.

Main Findings. - The main findings related to the ETC-12 activity on this topic can be summarized as follows.

(a) *Preventing construction in the proximity of seismically active faults does not completely avert the related risk, so that rational criteria to improve the structural performance against the fault-rupture hazard should be introduced.* This statement is justified by the following considerations:

(a.1) The accurate location of most seismic faults is still subject to debate and it is generally not detailed enough for engineering purposes.

(a.2) Even when the main fault trace location can be mapped reliably enough, secondary fault-ruptures may also occur, so that buildings constructed outside the mapped area can be still subject to fault breakage.

(a.3) Even not-engineered structures can sustain relatively large fault displacements, as shown by recent earthquakes. Indeed, the presence of a structure may lead to diversion of the rupture path, as well as to smoothing of the surface displacement profile caused by the emerging fault rupture.

(a.4) Large and spatially extended infrastructures cannot avoid in many cases crossing known (or unknown) seismically active faults. In this case, some criteria to help the designer to deal with the complicated interaction between fault rupture and the structural system are needed.

(b) *Seismic hazard studies in terms of fault-rupture induced surface breakage are strongly recommended.* This is because:

(b.1) The likelihood of a fault rupture event may be much smaller than the standard 10% exceedance probability in 50 years, for ultimate limit state design of structures, even in the proximity of well recognized and mapped seismically active faults. Excluding the East- and North-Anatolian faults, in the European context the seismic activity of the mapped faults is generally low, with slip rates less than 1 mm/year and recurrence periods of the critical event, i.e., the large earthquake that may induce a significant surface fault breakage, larger than 1000 years. Therefore there is a need to homogenize the hazard level for design against dynamic excitations and fault-rupture event.

(b.2) As a consequence, the quantitative evaluation, by probabilistic seismic hazard analysis tools, of the return period of the fault-rupture event is strongly recommended.

(c) *In case of important structures and infra-structures, the use of numerical methods for determination of the seismic action effects induced by fault-rupture cannot be avoided. However, they must rely upon an accurate treatment of the strongly nonlinear effects under investigation.* More specifically:

(c.1) A constitutive soil model well calibrated to capture the behavior at large shear strains must be used: investigations carried out within the QUAKER project showed that the use of the Mohr-Coulomb model coupled with the treatment of the numerical problem in large deformations is a good recipe for accurately propagating from the numerical point of view the fault rupture within the surface soil.

(c.2) Suitable interface elements must be considered to take into account foundation sliding or uplift induced by the emerging fault rupture.

(c.3) The uncertainty of fault outcropping location with respect to the structure should be taken into account.

(c.4) The uncertainty on the amount of fault displacement should also be considered, to be calibrated based on empirical formulas (see e.g. Wells and Coppersmith, 1994).

(d) *Some simple design criteria can be proposed for improving the structural performance in the presence of surface fault breakage*. For instance:

(d.1) Heavy structures, with continuous and rigid foundation systems, are one of the key rules. For simple shallow foundation systems, reference can be made to available solutions and charts defining the minimum vertical load required to divert the fault rupture (see Berrill, 1983; Yilmaz and Paolucci, 2006; Paolucci and Yilmaz, 2006).

(d.2) Deep foundation systems, such as pile or pier foundations, should be considered with special care since they may not rely on the diversion mechanism previously noted. First, the pile heads should be connected by a rigid cap, or tie beams, in order to avoid differential movements at the base of the structure. Second, even in the presence of rigid connections among pile heads, the stresses applied by the foundation to the soil surface are generally small, since most of the load is transferred by the piles: therefore, the conditions for foundation diversion will not be satisfied.

Note that, the ETC-12 activity on this topic has been mainly based on recent findings from the EU-funded research project QUAKER ("Fault-Rupture and Strong Shaking Effects on the Safety of Composite Foundations and Pipeline Systems" (see www.dundee.ac.uk/civileng/quaker). Thus, the conclusive technical reports that are about to be issued within the Quaker project may serve as an updated reference for this topic.

5. SLOPE STABILITY

(EC-8 Part 5: paragraph 4.1.2)

G. Biondi[1], E. Cascone[2], M. Maugeri[1]
[1]University of Catania, Italy
[2]University of Messina, Italy

The contribution of ETC-12 to the evaluation of seismic slope stability is expressed in two papers. In the paper by *Simonelli et al.* the results of the pseudo-static approach are compared with those of the sliding block analysis; the paper by *Biondi & Maugeri* summarizes the result of previous studies (Biondi et al., 2002; Biondi & Maugeri 2005) and propose a procedure to perform a sliding

block analysis taking into account the effect of the soil shear strength reduction due to cyclic loading.

EC8 provisions for slope stability.- The Eurocode prescribes the evaluation of the stability of natural slopes with respect to a design earthquake to ensure safety and serviceability of the structures erected on or near the slope. The limit state is defined as the state "*beyond which unacceptably large permanent displacements of the ground mass take place within a depth that is significant both for the structural and functional effects on the structures*".

The study of the seismic response of slopes is a complex problem that should be studied using dynamic methods of analysis. These range from highly simplified to rigorous methods and consequently require different levels of complexity in terms of characterization of material properties and modelling of stress-strain soil behaviour.

According to EC8 the seismic stability of slopes can be evaluated using finite element dynamic analysis, the sliding block approach or simplified pseudo-static methods. The use of simplified pseudo-static methods is subjected to restrictions related to: abrupt irregularities in soil topography, complex soil stratigraphy and soils capable of developing high pore water pressure or exhibiting stiffness degradation during cyclic loading.

For natural slopes the sliding block approach represents a good compromise between conventional pseudo-static methods and refined dynamic analysis in view of the uncertainties involved in the specification of seismic and geotechnical input data.

Pseudo-static versus traditional sliding block analysis. - *Simonelli et al.* presented a comparison between the results of a stability analysis performed in accordance to the Italian seismic code and to the provisions of EC-8. The comparison is firstly presented in terms of values of pseudo-static safety factor computed for several slope schemes using the values of the seismic coefficient prescribed by the previous Italian seismic code (D.M.16.01.96) and those obtained combining the provision of EC-8 with the more recent Italian code (OPCM 3274/2003) which provides the values of peak ground acceleration in Italy. The reference scheme for the analyses is the infinite slope.

The comparison shows considerable differences in the values of the pseudo-static safety factor that is significantly smaller when the seismic coefficients are evaluated applying the EC-8 and the ground acceleration values provided by the new Italian seismic code (OPCM 3274/2003), including the soil amplification factor S and the topography factor S_T. This dramatic reduction of the pseudo-static safety factor points out the need for a displacement-based analysis. Then, the results of the previous described pseudo-static analysis are compared in the paper with the result of a Newmark-type analysis. For this purpose the sliding block approach was applied parametrically referring to different slope schemes and using a set of records of some recent Italian earthquakes scaled to the peak ground acceleration values prescribed for each seismic zone by the new Italian seismic code (OPCM 3274/2003). *Simonelli et al.* evaluated upper bound curves of the computed permanent displacement D, to be used as design charts for artificial embankments. The design procedure is illustrated in Fig. 5.1 for the seismic Zone 1 of the OPCM 3274 (A_{max}=0.35g) assuming a value of the angle of shear strength of the embankment soil φ'=45°.

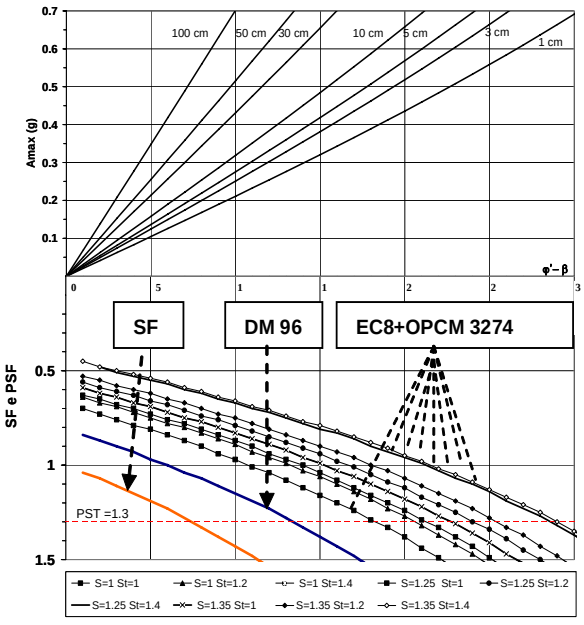

Fig. 5.1: Example of design chart proposed by Simonelli et al..

The upper part of the figure shows the iso-displacement curves as function of the maximum ground acceleration A_{max} and the difference between φ' and the slope angle β. Fixing an admissible value of D and knowing A_{max}, the slope of the embankment can be consequently defined.
In the lower part of the figure, the results of the pseudo-static application are shown as well, to allow for an immediate comparison between the two approaches. It is evident that the slope performance predicted by the displacement approach seems consistent with the previous Italian seismic code (DM96) that prescribes much lower values of the seismic coefficients (0.04g-0.1g) to be adopted in a pseudo-static analysis. Thus to maintain the use of the pseudo-static approach, which is well consolidated in the engineering practice, a better correlation between peak ground accelerations and pseudo-static coefficients is needed.

Pore pressure and cyclic degradation effects.- The paper by *Biondi & Maugeri* focuses on the influence of the soil cyclic behaviour on the displacement response of natural slopes and presents a procedure to perform a modified Newmark-type analysis that embodies the EC-8 requirements concerning the effect of excess pore pressure and soil cyclic degradation. The need for a new modified Newmark-type analysis is outlined in the paper through a critical literature review. Available procedures do not provide practical tools to detect the occurrence of weakening instabilities and their effect on the displacement response of a slope; moreover no suggestions are provided to detect the proper approach for a reliable displacement analysis. The procedure proposed in the paper summarizes experience gained during previous studies (e.g. *Biondi et al., 2002, Biondi & Maugeri, 2005*).

In detail, the procedure takes into account the effects of pore pressure build-up in cohesionless slopes and cyclic strength degradation in cohesive slopes on the following seismic design aspects: reduction of critical acceleration, permanent displacement accumulation and, finally, post-seismic slope stability. In the procedure some stability charts are introduced in terms of threshold values of earthquake-induced pore pressure ratio or in terms of threshold values of degradation index. The charts allow to detect the effect of shear strength degradation on the seismic and post-seismic stability condition of the slope and to detect the more reliable method for the displacement analysis. The procedure was applied to several infinite slope schemes performing a parametric analysis to detect the influence of each of the involved parameters.

An example of displacement response computed with the proposed procedure is presented in Figs. 5.2 and 5.3 for cohesionless and for cohesive slopes respectively. The influence of the parameters involved in the cyclic behaviour of soils (relative density D_r of sandy soils, degradation index t of cohesive soils) is clearly shown in the displacement time-histories. The displacement time histories evaluated using

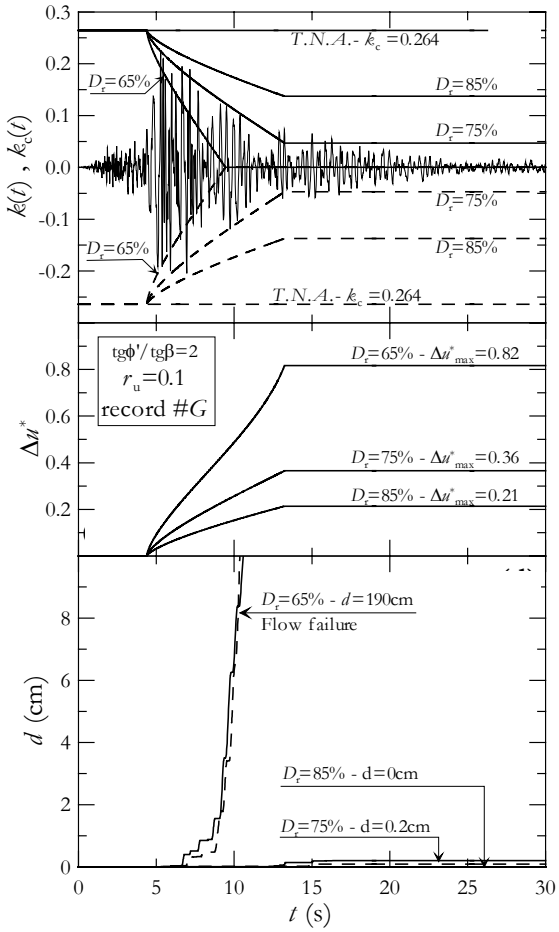

Fig. 5.2: Example of displacement analysis performed using the procedure by Biondi et al. (2002) for sandy slopes.

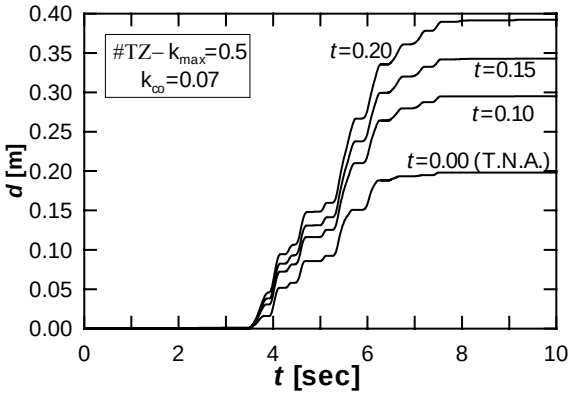

Fig. 5.3: Example of displacement analysis performed using the procedure by Biondi and Maugeri (2005) for clay slopes.

the traditional Newmark-type analysis (*T.N.A.*) are also shown in the figures for comparison. It is apparent that the traditional analysis is not capable to predict the slope response when considerable reduction of the soil shear strength takes place. The results presented in the paper show that the displacement response is significantly affected by the choice of the pore pressure generation model, the selection of the time interval in which it takes place, the selection of appropriate values of the cycles involved in the degradation effect and, finally, the computed degradation path of the critical acceleration.

Concluding remarks.- The main conclusions of the two papers on seismic slope stability offer issues for possible improvements in future revisions of EC8. Namely, the workshop participants agreed on the following topics:

- Since the pseudo-static approach is well consolidated in engineering practice, it would be very useful to maintain it in EC8. For this purpose, a better correlation between peak ground accelerations and pseudo-static coefficients is needed together with a procedure for reliable displacement analysis.
- Due to the influence of cyclic pore pressure build-up and shear strength degradation on the displacement response of a slope, the need for a modified Newmark-type analysis, capable of accounting for such effects, is apparent. It is realised that EC-8 cannot go in such detail. Still, the need for such (special) studies could be pointed out in connection with high seismicity areas and installations of high importance.

6. POTENTIALLY LIQUEFIABLE SOILS

(EC-8 Part 5: paragraph 4.1.3, annex B)

D. Lo Presti[1], N. Squeglia[1]

[1] *University of Pisa, Italy*

Some contributions have considered the problems related to the assessment of soil liquefaction and more specifically *Lo Presti, Mensi & Squeglia, Santucci de Magistris,* and *Vrettos.* Additional written comments have been provided by *Pitilakis* and *Ansal*. The written contributions mainly concern two different aspects:

- Criteria for neglecting liquefaction analyses.
- Suggested methods for analysis.

In the following, the discussion on these two topics, as well as the suggested EC8 (Part 5-section 4.1.3 and Annex B) changes, are summarized. In cases where there is not full agreement among contributors, the different views are briefly reported.

Liquefaction Criteria.- As for the first point the following observations have been done:

- The compositional criterion of EC8 mainly refers to the amount of fine (clay or silt) fraction. It has been observed in practice that such a criterion is rather too wide and would include many cohesive soils which is well known that are liquefaction resistant. It is suggested to replace the above criterion by the Chinese criteria or their recent evolution (Seed et al. 2003). As an alternative it is also suggested to include a criterion based on the grain size curve (see *Santucci de Magistris*). The need of knowing grain size distribution, fines content and plasticity index has been also pointed out by *Ansal*.
- The historical criterion assumes that analyses can be neglected if $a_{gR}\cdot\gamma_I\cdot S<0.15$. However, it has been observed that it is very hard to establish a value of the soil parameter S for liquefiable soils. There is evidence to indicate that it could be less than one, but, at the moment, its value is still under debate. It is therefore suggested to use the above criterion but assume that S=1.00. As for the importance factor (γ_I), it should not be less than one. Such low values apply when considering return periods smaller than those established for the ULS (i.e. temporary structures, DLS, etc.). However, as the liquefaction risk analysis is a mandatory part of the siting process (see chapter 4.1), the

reference return period of 475 yrs, or a greater value, should be considered.

- EC-8 indicates that if $(N_1)_{60}$ is greater than 20 or 30 (the later for clean sands), liquefaction analyses can be omitted. It has been observed that 20 or 30 blowcounts in fine sands indicate a very dense material, while in a coarse sand could correspond to a loose state. Thus, a number of participants suggested to omit such a criterion. On the contrary, *Santucci de Magistris* proposes to extend such a criterion to more coarse grained soils, based on CPT tip resistance and shear wave velocity measurements.
- The depth criterion prescribes that analyses can be omitted if the liquefiable layer is at a depth greater than 15 m. On the other hand, it has been observed that the effects of liquefaction are negligible if the thickness of the liquefiable layer (H_1) is equal or less to that of the overlying non-liquefiable layer (H_2). Thus, it has been suggested to replace the actual depth criterion by conservatively assuming that analyses can be neglected if $H_2>2H_1$.

Gazetas noted that such a criterion could prove unconservative in sloping areas, while *Ansal* suggested to omit liquefaction analyses for depths greater than 20m. Furthermore, *Bouckovalas* claimed that the depth criterion depends on the particular type of foundation or earth structure under consideration, and consequently it should be omitted from the code.

Analysis Methods.- As for the analyses of the liquefaction potential, the following (remarks) have been done:

- Analyses should be performed referring to the actual ground accelerations for the design earthquake and not to the "effective" values prescribed by codes. This includes both soil parameter (S or site amplification parameter) and design ground acceleration on type A soil (a_{gR}) (*Vrettos, Lo Presti et al., Pitilakis, Santucci de Magistris*);
- Analyses should not be exclusively performed for free-field conditions, but eventually considering the structure itself as well (embankment, building, pier bridge, tank etc), and the modification of loading and foundation conditions (*Pitilakis*). However, *Bouckovalas* points out that the methods required to do so are not yet well established and widely accepted, so that they can be readily included to seismic codes.
- Variation of acceleration with depth, even in the framework of the simplified approach (r_d parameter), should be considered (*Santucci de Magistris, Ansal, Vrettos*).
- As for the Magnitude Scaling Factor, it is suggested to refer to less conservative correlations based mostly on European earthquakes (*Pitilakis*).

Proposed Changes.- In extent of the above discussion, the following changes of section 4.1.3 on potentially liquefiable soils have been proposed:

- Clause (3)P: present formulation "Investigations required for this purpose shall as a minimum include the execution of in situ Standard Penetration Tests (SPT) or of Cone Penetration Tests (CPT), as well as the determination of grain size distribution curves in the laboratory." Proposed change: "Investigations required for this purpose shall as a minimum include the execution of in situ Standard Penetration Tests (SPT) or of Cone Penetration Tests (CPT), as well as the determination of grain size distribution curves, fines content and plasticity in the laboratory".
- Clause (4)P Present formulation: "For depth less than 3 m, the measured SPT values should be reduced by 25%". Proposed change: Omit this part.
- Clause (5) The present formulation should be replaced by the following sentences: "Normalization of the measured N_{SPT} with respect to the effects mentioned in clause (4)P, and in order to account for rod length, non-standardized sampler and borehole diameter may be done in the following way: $N_1(60) = N_{SPT} \cdot C_N \cdot C_E \cdot C_S \cdot C_R \cdot C_B$. Where N_{SPT} is the measured value, $N_{1(60)}$ the computed one and C_N, C_E, C_S, C_R, C_B are correction factors. Possible values and expressions of correction factors are given in Annex B".
- Clause (7). *Ansal* proposes to replace the present formulation in the following way: "For buildings on shallow foundations, evaluation of the liquefaction susceptibility may be omitted when the saturated sandy soils are found at depths greater than 20 m from the ground surface". On the contrary, *Lo Presti et al.* propose the following formulation "For buildings on shallow foundations (in non-

sloping areas), evaluation of the liquefaction susceptibility may be omitted when the saturated sandy soils are found at depths greater than 2H from the ground surface, where H is the thickness of a non-liquefiable top layer". Furthermore, *Bouckovalas* proposed to relate the minimum depth to liquefaction with the width B of he footing e.g. (e.g. 2.5B for strip footings). The seriously diverting opinions on this matter is an indication that it has not been yet resolved, and consequently the relevant clause may be omitted from the code.

- Clause (8). Lo Presti et al. propose the following formulation: "Neglecting the liquefaction hazard is not permitted when $\alpha_{gR} \cdot \gamma_I > 0.15$ (with $\gamma_I \geq 1.0$) and simultaneously, the following conditions are fulfilled: a) clay fraction (d<0.002 mm, CF) < 10 %; b) liquid limit (LL) < 32%; c) water content (W_n) > 0.9LL". *Ansal* proposes to maintain the present formulation by adding the following conditions "the depth of ground water level is greater than 15 m from the ground surface". *Santucci de Magistris* proposes to adding the following conditions to neglect the liquefaction hazard:
  - Moment magnitude M_w of the expected earthquake lower than 5.0;
  - Maximum expected horizontal acceleration at the ground level, in free-field conditions, lower than 0.1g; and,
  - The grading curve of the material external to the bounding curves reported in Figure 6.1 for the case of uniform (Uc < 3.5) or non-uniform soils (Uc > 3.5).

- Equation 4.1 should be replaced by the following expression: $\tau_l = m\alpha_{gR}\gamma_I\sigma_{vo}r_d$ with m=0.80-0.90 (as α_{gR} is already an effective and not the peak seismic ground acceleration). The stress reduction factor r_d may be computed by means of the following expressions r_d= 1.0 - 0.00765z (if z≤9.15 m); r_d=1.174 - 0.0267z (if 9.15≤z≤23m).
- Annex B – Section B2 should be modified as follows: "Analysis based on the SPT blowcount. The normalized index $N_{1(60)}$ is obtained as prescribed in 4.1.3. The following values and expressions are suggested for the correction factors: $C_N=(100/\sigma'_{vo})^{0.5}$; C_E=ER/60; C_B=1.0–1.05–1.15 (for borehole diameter of Φ = 65 –115; 150; 200 mm respectively);

Table B1: Correction factor for silty sands

FC (%)	α	β
≤ 5	0	1.0
5 -35	$\alpha = \exp(1.76-190/FC^2)$	$\beta=(0.99+FC^{1.5}/1000)$
>35	5.0	1.2

Table B2 Correction factor for Magnitude different than 7.5

Ms	CM
5.5	2.86
6.0	2.20
6.5	1.69
7.0	1.30
8.0	0.67

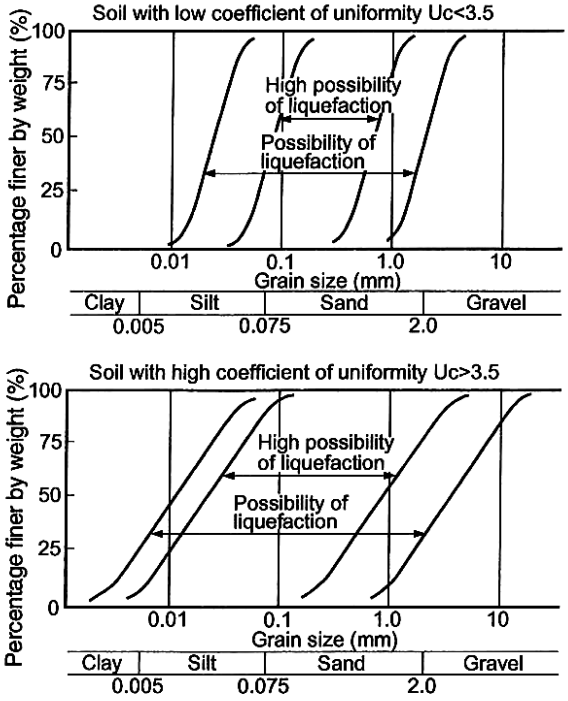

Fig 6.1: Grading curves for a preliminary evaluation of the liquefaction potential for soil with low and high coefficient of uniformity (after Tsuchida, 1970)

C_R=0.75–0.8–0.85–0.95–1.0 (if rod length is respectively L<3 m; 3<L< 4; 4<L<6; 6<L<10; 10<L<30); C_S=1.0 (standard sampler) or 1.3 (Standard sampler not using liners). ER=energy ratio of a given SPT equipment; σ'_{vo}=vertical effective geostatic stress. The cyclic resistance ratio for a Magnitude (M_s) of 7.5 in the case of clean sands may be

computed by means of the following equation:

$$CRR_{7.5} = 1/[34-(N_1)_{60}]+(N_1)_{60}/135+ 50/[10(N_1)_{60} +45]^2–1/200 \quad \text{(eq. B1)}$$

In the case of sand containing fines it is possible to correct the measured penetration resistance $(N_1)_{60}$ by means of the following expressions:

$$(N_1)_{60cs}=\alpha+\beta(N_1)_{60}$$

The α and β parameters are reported in table B1 according to the fines content FC. Table B2 gives the factor CM which should be multiplied by the $CRR_{7.5}$ for Surface-Wave Magnitude different than 7.5.

- Annex B – Section B3 should be modified as follows. “Analysis based on CPT. Based on numerous studies on the correlation between CPT cone resistance and soil resistance to liquefaction, relationships similar to eq. B1 have been established. Such direct correlations must be preferred to indirect correlations using a relationship between the SPT blow-count and the CPT cone resistance”
- Annex B: Figure B1 should be omitted.

7. SHALLOW and DEEP FOUNDATIONS, SOIL-STRUCTURE INTERACTION

(EC-8 Part 5: chapters 5 & 6, annexes C, D & F)

G. Gazetas
National Technical University of Athens, Greece

Shallow foundations: soil yielding and base uplift.- Capacity design requirements in seismic codes restrict foundation uplifting and do not allow mobilization of bearing capacity mechanisms. However, observations in recent earthquakes, design of large footings for bridge piers, and retrofitting analyses of existing structures to resist strong shaking, have all shown that such restrictions are often impossible or even unnecessary to satisfy. To investigate the consequences of “plastic hinging” in the foundation, the response of slender 1-dof structures with a foundation mat has been explored analytically and numerically (Apostolou and Gazetas, 2005).

As their predominant mode of response is rocking, such systems are vulnerable to plastic hinge development below ground level under strong seismic excitation. Thus, non-linear soil-foundation effects associated with large deformations due to base uplifting and soil failure have been examined and compared with the conventional linear approach. The interplay between foundation uplifting and soil failure of the bearing capacity type has been elucidated under static and dynamic conditions, and the consequences of considering nonlinear phenomena related to foundation has been explored.

Based on the aforementioned studies, as well as on relevant results from the numerical case study presented by *Abate et al.* in the Workshop, the following modifications and additions are proposed for Chapter 6 and Annex D of EC8:

(a) Uplifting and simultaneous mobilization of bearing capacity mechanisms do not imply failure, but may lead to unacceptable permanent displacements and rotations.

(b) Second order (P-δ) effects play an important (detrimental) role on the dynamic response of slender structures. Therefore, they should be considered in the analysis procedures when a slenderness ratio of 2 or more is encountered.

(c) It is well understood that dynamic overturning is highly sensitive to the excitation frequency and the size of the structure. In any case the minimum acceleration for overturning under dynamic conditions is higher than the static limiting value (b/h in g) especially when short-period shaking or a large structure is considered. A lower bound (conservative estimate) of this trend can be obtained from the following expression:

$$A_{over,dyn} = \frac{b}{h}\sqrt{1+\left(\frac{\omega_E}{p}\right)^2}$$

Where $\omega_E=2\pi/T_E$ is the predominant excitation frequency and $p=\sqrt{mgR/J_o}$ is a size parameter (J_o is the structure mass moment of inertia with respect to the corner of the foundation and $R=\sqrt{b^2+h^2}$ is the “effective” diameter - see Fig. 7.1). A period of 2.0sec ($\omega_E=\pi$) is considered as a representative of static loading conditions whereas for civil engineering structures a value of $p=1.5\cong\pi/2$ can be estimated as an upper limit. In this way, the overturning acceleration

for design against earthquake loading is suggested to be calculated as:

$$A_{over,dyn} = 2 \cdot \frac{b}{h} g$$

If the vertical load of the foundation will be $N < 0.3N_{ult}$ where N_{ult} is the ultimate load capacity. This inequality ensures that inelastic soil deformations will be small and concentrated in the vicinity of the pivot points. For larger values of the vertical load N, a DSSI analysis in the time-domain is required to investigate the overturning potential.

(d) In the realm of a capacity-based design, the computed angle of rotation can exceed the elastic threshold or even the "yield" angle θ_{ult} that corresponds the maximum moment M_{ult}. However, the maximum angle shall be bounded by the inequality $\theta_{max}<\theta_c=0.40 \cdot b/h$ if large permanent rotations must be avoided.

(e) Equivalent-linear SSI procedures in time or frequency domain should be adopted only if the following conditions are concurrently satisfied: (1) $N < 0.3N_{ult}$ and (2) $M_{over} < 0.5Nb$ where M_{over} is the overturning moment onto the foundation.

Capacity Design of Pile Foundations.- In all seismic codes, piles are designed to remain structurally elastic, although EC8 in its wisdom

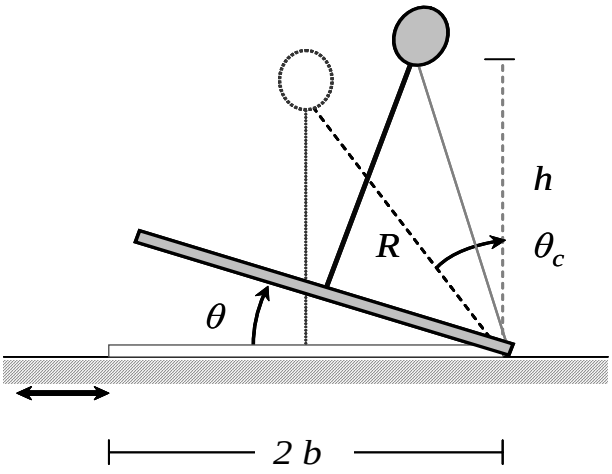

Fig. 7.1: Rocking of a rigid one-story structure on rigid base.

allows that *piles "under certain conditions be allowed to develop a plastic hinge at their head"*. The main reasons are: (i) the location of plastic hinges is not approachable for post-seismic inspection and repair, and (ii) failure due to yielding in the pile prior to exceeding soil capacity, is of undesirably *brittle* nature. By contrast, if soil capacity is mobilized first, the failure mode is ductile. Besides, the intensely hysteretic behaviour implied by the soil failure mode tends to be beneficial for structural performance.

However, numerous examples in Kobe during the 1995 Earthquake revealed that : (i) yielding of piles in strong seismic shaking is unavoidable, especially in soft / loose soils, and (ii) inspection of piles after the earthquake is often a feasible, although not a trivial operation. Moreover:

(a) The lateral confinement provided by the soil plays a very significant role in pile response. The soil confining pressure increases the effective confinement of the section and retards the development of high levels of localized plastic rotation, thus providing a sizable increase in ductility capacity. Sufficient displacement ductility may be obtained in a pile shaft with transverse reinforcement ratio, ρ_t, as low as 0.003 (Pristley et al., 1996; Budek et al., 2004).

(b) The presence of soil confinement leads to increased plastic hinge lengths, thus preventing high localized curvature (Tassios, 2004). Therefore, the piles retain much of their axial load carrying capacity after yielding.

(c) As the reconstruction of the Kobe Route 3 by Hanshin Expressway proved, a capped pile group in which the piles have cracked, retaining only ½ of their initial un-cracked *structural rigidity, EI*, still preserves 80% of its *overall lateral stiffness, K_H, thanks* to the participation of the surrounding soil (Gazetas et al., 2005).

The above evidence supports the idea of allowing plastic deformation of piles due to inertial and kinematic loading, in future updates of the code.

SSI and Seismic Code Spectra.- Smooth design acceleration spectra, the result of statistical processing of a large number of elastic response spectra of actual recordings, have been universally accepted as the way to specify the earthquake loading in seismic codes. Design acceleration spectra have an essentially constant acceleration branch and a declining acceleration branch (with the exception of a rather insignificant ascending-

acceleration region of very small periods). The period range of the constant-acceleration plateau is larger (up to 1 sec) for the softer soils.

The main effect of soil-structure interaction is the increase in the fundamental period of the structure. This increase in natural period arising from soil deformability, along with the aforementioned conventional description of acceleration spectra, leads almost invariably to smaller accelerations and stresses in the structure and its foundation. Thus, the importance of accounting for SSI effects has been often dismissed, to be "*on the safe side"*.

This beneficial role of SSI has been turned into a dogma. For example, according to EC8/5, Annex D : **"** *D2 For the majority of usual building structures, the effects of SSI tend to be beneficial, since they reduce the bending moments and shear forces acting in the various members of the superstructure...*.**"**

Since design spectra are derived conservatively, the above statement may indeed hold true for a large class of structures and seismic environments. But not always. There is evidence documented in numerous case histories that the perceived beneficial role of SSI is an oversimplification that may lead to unsafe design for both the superstructure and the foundation.

To elucidate this, we could compare for instance the conventional design spectrum for soft deep soil with four well known actual response spectra: Brancea (Bucharest) 1977, Michoacan [Mexico City (SCT)] 1985, Kobe (Fukiai, Takatori) 1995. We will observe that all the recorded spectra attain their maxima at periods exceeding 1.0 second. The large spectral values of some of these records are undoubtedly the result of resonance of the soil deposit with the incoming seismic waves. Another phenomenon, however, of seismological rather than geotechnical nature, the "forward fault-rupture directivity", may be an important contributing factor in the large spectral values at T>0.50s in near-fault seismic motions.

It is therefore apparent that, as a result of soil (or seismological) factors, an increase in the fundamental period due to SSI may lead to increased response (despite a possible increase in damping), which contradicts the expectation incited by the conventional design spectrum.

The reason for this unrealistic shape is because the spectra of motions recorded on soft soil attain their maxima at different, well separated periods and, thereby, averaging them eliminates their peaks causing this effect. In contrast, when plotted against the normalized periods T/T_g and T/T_a the average spectrum exhibits a characteristic peak at values of T/T_g close to 1, which reproduces the trends observed in actual spectra! Notwithstanding the fact that determining the characteristic soil period for a given site is not always easy, it is clear that current provisions treat seismic demand in soft soils in a non-rational way, and may provide designers with misleading (and unsafe) information on the significance of SSI effects.

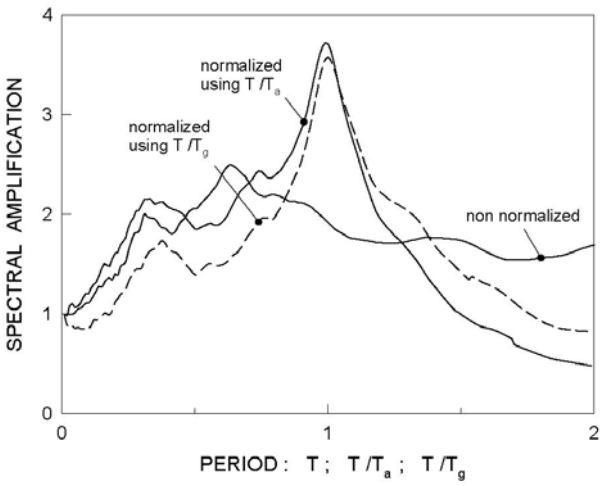

Fig. 7.2: Average acceleration spectra based on 24 actual motions recorded on soft soil. The periods are normalized before averaging with: (a) period of peak spectral acceleration (T_a) ; (b) period of peak spectral velocity (T_g) ; β = 5% (After Mylonakis & Gazetas 2000).

It is therefore proposed that in a future revision of EC8 design spectra for evaluating SSI effects be of the form plotted in Fig. 7.2 :

$$S_a = S_a\,(T/T_g)$$

Such spectra will have to be developed using techniques similar to those used for the development of current design spectra. There is nothing strange with having different design

spectra for assessing SSI --- this type of spectra will be the “critical” loading for this “mode” of response*.*

8. EARTH RETAINING STRUCTURES

(EC-8 Part 5: chapter 7, annex E)

A.L. Simonelli
University of Sannio, Benevento, Italy

Two contributions on earth retaining structures have been presented at the Workshop: one paper, by *A.L. Simonelli*, deals mainly with gravity walls, while the other, by *L. Callisto*, deals specifically with embedded retaining structures.

The focal theme of both papers is the evaluation of the effectiveness of the analysis methods proposed in the Eurocode. In Ch. 7.3 it is stated that “Any established method based on the procedures of structural and soil dynamics, and supported by experience and observations, is in principle acceptable for assessing the safety of an earth retaining structure”; and that aspects such as non linear behaviour of soils, inertial effects of the masses of soil, structure and gravity loads, hydrodynamic effects of water, compatibility between deformation of soil, structure and eventual tiebacks should be accounted for. Nevertheless, the Code then describes in detail the pseudo-static analysis, regarded as the main simplified method.

In the paper by *Simonelli*, the EC8 pseudo-static approach is utilized to verify four (4) reference gravity walls designed in the different seismic zones of Italy, according to the pre-existing national Code (D.M. LL.PP. 16.1.96): the result of the application is that the old walls would be strongly underdimensioned. Then the behaviour of the same walls is checked by more reliable simplified dynamic analyses, applied according to EC8 rules: the results seem to substantially validate the old D.M. 96 designs, and definitely confirm that the EC8 pseudo-static approach is over-conservative. In the same paper some critical remarks are pointed out, regarding the choice of the value of the factor *r*, the design approaches and the partial safety factors adopted for the ULS analysis and the evaluation of water pressure behind the wall in the case of low permeability soils.

In his paper, *Callisto* illustrates the main problems which arise in the application of the EC8 pseudo-static method to the embedded retaining structures, putting in evidence the differences with gravity walls’ analysis. The main uncertainties in embedded structures’ pseudo-static analysis are related to the evaluation of: passive resistance, seismic earth pressures in layered deposits, pore water pressure, especially under undrained conditions, and seismic coefficients.

Discussion.- In order to guide the discussion session on earth retaining structures, the writer suggested the following crucial points to be dealt with, beginning with general aspects (regarding both gravity and retaining walls):

[1] *pseudostatic approach: calibration of the method on the basis of dynamic analysis results;*
[2] *design approaches and partial safety factors: congruency between EN1990, EN1998 and EN1997;*
[3] *water pressure in the case of low permeability soil;*
[4] *dynamic analysis: proper definition of representative seismic input motion;*

and continuing with specific aspects related to gravity walls:

[5] *correlation between the reduction factor* ***r*** *and the wall acceptable displacement* $\boldsymbol{d_r}$*;*

and embedded retaining structures:

[6] *evaluation of the passive resistance;*
[7] *evaluation of the seismic coefficients (*k_h*,* k_v*) assuming a factor* ***r*** *value equal to 1;*

The discussion was very fruitful; the main findings for each of the above point listed above are as follows.

[1] The pseudo-static method provides much more conservative results than the dynamic analysis. Since it is recognized that the latter is more reliable, remedial actions are necessary in order to make EC8 pseudostatic design more effective (adoption of model coefficients, or the re-calibration of factors such as ***r***, on the basis of dynamic analysis results). It is recognized that the pseudo-static approach should be maintained, since this kind of analysis is well consolidated in the engineering practice.

[2] After an intense discussion, with the significant contribution of *Roger Frank*; it has

been confirmed that the procedures for the ULS seismic design stated in EC8 are compatible with the rules of EN1990, and are not in conflict with the design approaches and partial safety factors listed in EN1997. In the writer's opinion, it could be stated that the seismic design is performed according to the design approach DA1, combination 2 (DA1C2).

[3] The writer underlines that, although EC8 pseudo-static method takes into account the inertial forces of the water in a saturated soil, both in the case of dynamically pervious and dynamically impervious materials (EC8 Part 5, Annex E), it always assumes that the soil behaves in drained conditions, since the effective stresses are computed by means of the submerged unit weight of the soil γ', and no earthquake induced excess pore pressure (Δu) is taken into account. *Callisto* stresses this problem, with reference to the embedded structures that are frequently located in low permeability soils; in this case, the initial pore water pressures must also be carefully evaluated. It is recognized that indications should be given for the application of the pseudo-static method in the case of undrained response of the soil under seismic loading.

[4] This aspect has been widely discussed in a previous session on seismic actions (chaired by *Bouckovalas*); here it can be resumed that for simplified dynamic analysis of gravity retaining walls (such as for slopes) the adoption of a number of recorded accelerograms scaled to the PGV expected at the specific site is the best choice. In the case of embedded structures, the frequency content of the seismic signals must also be checked, since it can strongly affect the soil-structure interaction (SSI) phenomenon.

[5] As regards gravity walls, the writer observed that the correlation between the reduction factor ***r*** and the wall acceptable displacement $\boldsymbol{d_r}$ (Table 7.1 of EC8 Part 5, Ch.7) was not very clear (for details see Table 2 and Fig. 3 of the paper by *Simonelli)*. *Alain Pecker* confirmed that the threshold values $\boldsymbol{d_r}$ represent the upper limit values for the acceptable displacements, hence validating the interpretation of the correlation as illustrated in Fig. 8.1. However, in this case the ***r*** = 2 value should also be extended to walls that can accept displacements greater than 300 α S; as a consequence, the first line of the previously cited Table 7.1 (in EC8 Part 5) should be changed from its present version:

- *"Free gravity walls that can accept a displacement up to* $\boldsymbol{d_r}$ *= 300* α *S (mm)";*

to the new one:

- *"Free gravity walls that can accept a displacement* $\boldsymbol{d_r} \geq$ *200* α *S (mm)".*

[6] The problem of a correct evaluation of the passive resistance, which is of primary importance for embedded structures, was

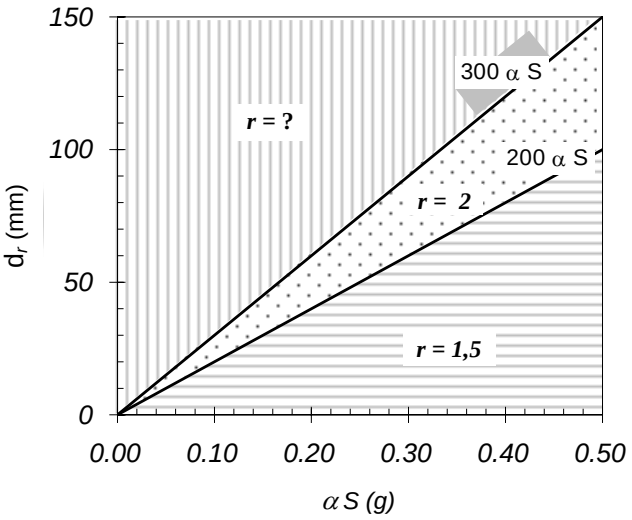

Fig. 8.1: Graphic interpretations of the present correlation among the ***r*** factor, the acceptable displacement $\boldsymbol{d_r}$ (free gravity wall) and the peak ground acceleration (see EC8 Part5, Table 7.1).

stressed by *Callisto*. It is well-known, Mononobe and Okabe theory overestimates the passive resistance in the case of high values of the soil-wall friction angle δ. In the EC8, this problem is overcome by assuming δ=0; on the contrary, this hypothesis is very severe since it strongly reduces the passive resistance of rough embedded walls. In conclusion, it seems reasonable to suggest different approaches (e.g. those based on limit analysis) for the evaluation of the passive resistance.

[7] Application of the pseudo-static method to embedded structures, with the adoption of a factor ***r*** value equal to 1, implies that the inertial forces are proportional to the

maximum acceleration value expected at the ground surface, which is also considered constant with depth. *Callisto* illustrates the over-conservativeness of the ***r*** =1 hypothesis, which in turn could be reasonable only in the case of a "fragile" behaviour of the soil-structure system (e.g. fragile failure either of a pre-stressed anchor, or of the soil, or the wall structure). As a matter of fact, it is recognized that the application of the pseudo-static method with the assumptions of ***r*** =1 (together with the evaluation of passive resistance with δ=0) would produce over-conservative and unacceptable results. In order to successfully apply the pseudo-static method, the soil-embedded structure system should be conceived to ensure a ductile behaviour of the entire system, hence allowing the adoption of a reduction factor ***r*** greater than 1; moreover specific studies could allow the evaluation of further reduction of the seismic acceleration with depth. In conclusion, it is a common opinion that dynamic analyses would be more suitable for studying the complex interaction between the soil and the embedded structures under seismic loading, and probably could provide reliable indications on the values of the equivalent accelerations to be adopted in the pseudo-static approach.

Apart from the above, other issues such as soil layering have been cited, but they have not been dealt with. Some of them will be probably discussed in the future, while others probably can not be properly developed inside a normative document.

ACKNOWLEDGEMENTS

The technical firms ATTIKO METRO, EDRASIS-Ch. PSALLIDAS and ISTRIA , as well as the School of Civil Engineering of N.T.U.A., kindly offered financial support for the Athens ETC-12 Workshop. In addition, N.T.U.A. provided the conference hall. These contributions are gratefully acknowledged by the ETC-12 members.

LIST OF WRITTEN CONTRIBUTIONS

Abate G., Massimino M. R., Maugeri M. (2006), "Soil plasticity and uplifting effects on soil-structure interaction", *Workshop of ETC12 Evaluation Committee for the Application of EC8*, Athens, January 20-21.

Anastasopoulsos I., Gazetas G. (2006), "On the design of structures to resist fault displacements, with application in Greece", *Workshop of ETC12 Evaluation Committee for the Application of EC8*, Athens, January 20-21.

Ansal A., Durukal E., Tonuk G. (2006), "Selection and scaling of real acceleration time histories for site response analyses", *Workshop of ETC12 Evaluation Committee for the Application of EC8*, Athens, January 20-21.

Biondi G., Maugeri M. (2006), "A modified Newmark-type analysis according to EC-8 requirements for seismic stability of natural slopes", *Workshop of ETC12 Evaluation Committee for the Application of EC8*, Athens, January 20-21.

Bouckovalas G., Papadimitriou A., Karamitros D. (2006), "Compatibility of EC-8 ground types and site effects with 1-D wave propagation theory", *Workshop of ETC12 Evaluation Committee for the Application of EC8*, Athens, January 20-21.

Callisto L. (2006), "Pseudo-static seismic design of embedded retaining structures", *Workshop of ETC12 Evaluation Committee for the Application of EC8*, Athens, January 20-21.

Cavallaro A., Grasso S., Maugeri M. (2006) "Site Characterization at the Catania city, Italy", *Workshop of ETC12 Evaluation Committee for the Application of EC8*, Athens, January 20-21.

Gazetas G & Assimaki D. (2006), " Topographic Amplification Factors", *Workshop of ETC12 Evaluation Committee for the Application of EC8*, Athens, January 20-21.

Lo Presti D., Mensi E., Squeglia N. (2006), "Some comments on the EC-8 prescriptions for the evaluation of soil liquefaction", *Workshop of ETC12 Evaluation Committee for the Application of EC8*, Athens, January 20-21.

Lo Presti D., Mensi E., Squeglia N. (2006), "Dynamic soil characterization according to EC-8 and its effects on the assessment of seismic actions", *Workshop of ETC12 Evaluation Committee for the Application of EC8*, Athens, January 20-21.

Pagliaroli A., Lanzo G., D'Elia B. (2006), "Numerical study of topography effects at the Nicastro (southen Italy) cliff and comparison with EC-8 recommendations", *Workshop of ETC12 Evaluation Committee for the Application of EC8*, Athens, January 20-21.

Paolucci R. (2006), “Numerical investigation of 3D seismic amplification by real steep topographic profiles and check of the EC-8 topographic amplification coefficients”, *Workshop of ETC12 Evaluation Committee for the Application of EC8*, Athens, January 20-21.

Paolucci R., Yilmaz M.T. (2006), “Supplementary criteria for shallow foundation design close to seismically active faults”, *Workshop of ETC12 Evaluation Committee for the Application of EC8*, Athens, January 20-21.

Papadimitriou Ach., Bouckovalas G. (2006), “Aggravation of seismic ground motion due to slope topography”, *Workshop of ETC12 Evaluation Committee for the Application of EC8*, Athens, January 20-21.

Pitilakis K., Gazepis Ch., Anastasiadis A. (2006) “Design response spectra and soil classification for seismic code provisions”, Workshop of ETC12 Evaluation Committee for the Application of EC8, Athens, January 20-21.

Psarropoulos P., Gazetas G., (2006), “ 2 D Valley (Basin) Effects on Seismic Ground Motions”, *Workshop of ETC12 Evaluation Committee for the Application of EC8*, Athens, January 20-21.

Santucci de Magistris F. (2006), “Liquefaction: a contribution to the Eurocodes from the Italian guidelines “Geotechnical Aspects of the Design in Seismic Areas”, *Workshop of ETC12 Evaluation Committee for the Application of EC8*, Athens, January 20-21.

Simonelli A. L., Sica S., Moccia F. (2006), “Slope stability analysis according to EC-8 and Italian seismic regulations”, *Workshop of ETC12 Evaluation Committee for the Application of EC8*, Athens, January 20-21.

Simonelli A. L. (2006), “Pseudo-static and pseudo-dynamic gravity wall design according to EC-8”, *Workshop of ETC12 Evaluation Committee for the Application of EC8*, Athens, January 20-21.

Vrettos Ch. (2006), “Application of EC-8 for the assessment of liquefaction potential and for the seismic response of a river embankment”, *Workshop of ETC12 Evaluation Committee for the Application of EC8*, Athens, January 20-21.

ADDITIONAL REFERENCES

Apostolou M., Gazetas G., (2005), “ Rocking of Foundations under Strong Shaking : Mobilisation of Bearing Capacity and Displacement Demands”, *Proceedings of the 1st Greece-Japan Workshop : Seismic Design, Observation, and Retrofit of Foundations, Athens,* editors : George Gazetas, Yozo Goto, Takashi Tazoh, pp.131-140.

Berrill, J.B. (1983). “Two-dimensional analysis of the effect of fault rupture on buildings with shallow foundations,” *Soil Dynamics and Earthquake Engineering*, Vol. 2, pp. 156-160.

Biondi, G., Cascone, E., and Maugeri, M. (2002): “Flow and Deformation Failure of Sandy Slopes”, Soil Dynamics and Earthquake Engineering, Elsevier, Vol.22, pp.1103-1114.

Biondi, G. & Maugeri, M. (2005): “Effect of cyclic behaviour of soils on seismic response of clay slopes” Proc. Satellite Conf. of the 16th Int. Conf. on Soil Mechanics and Geothecnical Engineering, September 12-16, Osaka, Japan.

DM LL.PP. 16/1/96, Norme tecniche per le costruzioni in zone sismiche, Gazzetta Ufficiale della Repubblica Italiana, n. 29 del 5/2/1996.

Gazetas G., (2006), “Seismic Analysis of Shallow Foundations : Beyond EC8***”,*** *XX National Italian Geotechnical Conference : “La Progettazione Geotechnica con gli Eurocodici”* (Geotechnical Design with Eurocodes), Torino, Italy, 22-23 November 2005.

Gazetas G., Anastasopoulos I., Gerolymos N., Mylonakis G., Syngros C., (2006), “The Collapse of the Hanshin Expressway (Fukae) Bridge, Kobe 1995 : Soil-Foundation-Structure Interaction, Reconstruction, Seismic Isolation”, *Entwicklungen in der Bodenmechanik, Bodendynamik und Geotechnik,* Festschrift zum 60. Geburtstag von Univ.-Professor Dr.-Ing.habil. Stavros Savidis, (Herausgegeben von Dr. –Ing.Frank Rackwitz), pp. 93-120.

Gazetas G., Apostolou M., (2004), “Nonlinear Soil-Foundation Interaction : Uplifting and Soil Yielding”, *Prodeedings of the 3rd Joint US-Japan Workshop on SSI,* Menlo Park CA.

Gazetas G., Apostolou M., and J. Anastasopoulos, (2003), “Seismic Uplifiting of Foundations on Soft Soil, with Examples from Adapazari (Izmit 1999 earthquake)”, *Proceedings of the International Conference organized by British Geotechnical Association : Foundations, Innovations, Observations, Design and Practice,* (ed. T. Newson), Dundee, 2- 5 September, pp.37-49.

Makra K., D. Raptakis, F.J. Ghavez-Garcia, K. Pitilakis (2001), “Site effects and design provisions: the case of EUROSEISTEST”, *Pure and Applied Geophysics*, Vol. 158 (2), 2349-2367.

Makra K., F.J. Ghavez-Garcia, D. Raptakis, K. Pitilakis (2005), “Parametric analysis of the

seismic response of 2D sedimentary valley: Implications for code implementations of complex site effetcts", *Soil Dynamics and earthquake Engineering*, 25, 303-315.

Mylonakis G., Gazetas G., (2000), "Seismic Soil-Structure Interaction: Beneficial or Detrimental?", *Journal of Earthquake Engineering,* Vol. 4, No. 3, pp. 277-301.

OPCM n. 3274 (20/3/03), Primi elementi in materia di criteri generali per la classificazione sismica del territorio nazionale e di normative tecniche per le costruzioni in zona sismica, Gazzetta Ufficiale della Repubblica Italiana, n. 105 dell' 8/5/03.

Priestely M.J. N., Seible F., Calvi G.M. (1996), "Seismic Design and Retrofit of Bridges", Jonh Wiley.

Yilmaz, M.T. and R. Paolucci (2006). "Earthquake fault rupture – shallow foundation interaction in undrained soils", submitted for publication to *Earthquake Engineering and Structural Dynamics*.

Wells, D. and K. Coppersmith (1994). "New empirical relationships among magnitude, rupture length, rupture width, rupture area, and surface displacement". *Bulletin of the Seismological Society of America*, Vol. 84, 974-1002.

SESSION 1: Seismic Ground Response

DESIGN RESPONSE SPECTRA AND SOIL CLASSIFICATION FOR SEISMIC CODE PROVISIONS

Kyriazis PITILAKIS [1], Christos GAZEPIS[2], Anastasios ANASTASIADIS[3]

SUMMARY

We are proposing improved spectral amplification factors for different site conditions based on an extensive theoretical and experimental study of the characteristics of seismic ground response. We have analyzed a large set of worldwide well-documented strong motion recordings and we have performed a large number of theoretical analyses (~600) of various representative models of realistic site conditions. Special emphasis is given to the non-linear soil behavior, the impedance contrast between bedrock and soil deposits, the thickness of soil deposits and the presence of a lower stiffness soil layer near the ground surface. The selected soil models and the applied numerical code were validated with real recordings at about 100 well-documented sites in Greece and worldwide. We determined statistically the basic parameters that influence the characteristics of seismic vibration in the defined soil categories and we are presenting herein an improved categorization of subsoil conditions (including parameters like the thickness of the soil deposits, the depth of the bedrock, the fundamental period of the site, the stratigraphy, the soil type, the mean Vs value of the whole deposit etc.) and corresponding response spectra, aiming to contribute to the ongoing discussion on the improvement of seismic regulations (i.e. EC8 Draft).

INTRODUCTION

Seismic ground response characteristics, defined generally as "site effects", are inevitably reflected in seismic code provisions. The selection of appropriate elastic response spectra according to soil categories and seismic intensity is the simplest way to account for site effects both for engineering projects and for a general-purpose microzonation study. Contemporary seismic codes (IBC 2000, UBC97, EC8) have largely accepted the significant role of site effects and attempt to incorporate their influence either by means of a constant amplification factor exclusively dependent on the soil class or including additional parameters like the shaking intensity, near field conditions, etc. Even though concerning site classification different approaches exist, the basic idea of the mean value of shear wave velocity over the last few decades of meters (30m or other) is considered to be a sound parameter for site classification. However soil classification exclusively based in terms of $V_{S,30}$ assumption, is a rather simplified hypothesis, misleading in many cases, which can potentially lead to erroneous results, especially in cases of deep soil formations or abrupt stiffness change between the soil layer at -30m and the bedrock laying deeper, (Seed [3], Borcherdt [4], Martin [5], Dickenson [6], Dobry [7], Marek [8], Pitilakis [9]) On the other hand,

[1] Professor, Department of Civil Engineering, Aristotle Univeristy of Thessaloniki, Lab of Soil Mechanics & Foundations, Research Unit of Soil Dynamics and Geotechnical Earthquake Engineering GREECE, Email: pitilakis@geo.civil.auth.gr
[2] Civil Engineer, Department of Civil Engineering, Aristotle University of Thessaloniki, Lab of Soil Mechanics & Foundations, GREECE, Email: gazepis@hotmail.com
[3] Researcher, Institute of Engineering Seismology & Earthquake Engineering, ITSAK, GREECE, Email: anastas@itsak.gr

recent studies based on different sites, where the soil dynamic profile from the surface to the bedrock was well known, have shown that for low to medium intensity shaking (i.e. less than 0.2g or 0.1g), a linear approach for the assessment of the amplification functions could be satisfactory for a considerable number of soils. Nevertheless, such an approach has the obvious draw back of ignoring soil non-linearity, which might become important in the case of strong ground shaking intensity according to the soil type, stiffness and depth. Table 1 compares soil classification schemes in modern seismic codes worldwide applying the $V_{S,30}$ criterion. Current, design practice, either uses an oversimplified approach to soil classification (e.g. soil type in EAK2000), or ignores the effect of depth by accounting only for the average shear wave velocity over the 30m of a site profile. (e.g. EC8, UBC97).

Table 1. Comparison of soil classification in modern seismic codes worldwide

$V_{s,30}$ (m/sec)	180	360	760	1500
UBC/97 IBC/2000	S_E	S_D	S_C	S_B S_A
GREEK SEISMIC CODE EAK2000	D – C	C B A		Á
EC8 (ENV1998)	C	C B A		A
EC8 (prEN1998) (Draft4, 2001)	D	C	B	A
New Zealand, 2000 (Draft)	D (T>0.6s =>$V_{s,30}$<200)	C (T<0.6s =>$V_{s,30}$>200)	B	A
Japan, 1998 (Highway Bridges)	III (T>0.6s->$V_{s,30}$<200)	II (I) (T=0.2-0.6 s -> $V_{s,30}$=200-600)		I (T<0.2s ->$V_{s,30}$>600)
Turkey/98	$Z_4 – Z_3$	$Z_3 – Z_2$	$Z_3–Z_2– Z_1$	Z_1
AFPS/90	$S_3 – S_2$	$S_3–S_2–S_1$	$S_1 – S_0$	S_0

Among the important seismic site response factors are the impedance ratio between surface and underlying deposits, the soil type and the stratigraphy, the material damping and its potential variation with the intensity of the ground. Following the above, a site classification system should include adequate parameters describing the dynamic stiffness of the site and the depth of the deposit. Although earlier codes made use of natural ground period (To) as a means to classify site conditions (e.g. UBC 1976), recent codes as UBC97 and EC8 adopt the $V_{S,30}$ as the primary parameter for site classification, requiring a relatively extensive field investigation and overlooking the potential importance of depth to bedrock as a dominant factor in the site response.

The objective of this work is to develop site amplification factors that are both intensity and frequency dependent, based on a more refined site classification system that includes soil type, stratigraphy, depth and stiffness as key parameters.

METHODOLOGY

The procedure applied herein to propose site –dependent amplification factors is shown below:

- Creation of an extended database of high quality geotechnical and geophysical data of representative soil profiles in Greece and worldwide
- Selection of well constrained strong ground motion recordings with different PGA values, Mw magnitudes and covering a wide range of seismo-tectonic background. The good knowledge of site conditions such as soil stratification, Vs profile, shear modulus degradation curves, damping (G/Go-γ-D curves) and depth of the bedrock, was the basic criterion for the selection of the aforementioned recordings.
- Detailed analyses of the spectral characteristics of the selected recordings, comparison with code site classification categories (EC8, NEHRP, EAK), and evaluation of potential important differences due to the site classes defined
- Elaboration of improved representative site classification matrix using (a) the database, (b) the previous analyses of the recordings, (c) the soil categories proposed in modern codes (EC8, NEHRP) and (d) an engineering judgment based on the most common soil profiles found in Greece and worldwide. The classification scheme was deemed to perform adequate theoretical 1D equivalent linear computations of ground response with different soil profiles in terms of impedance contrast, dynamic soil properties, relative thickness and depth of the rigid or non-rigid bedrock.
- Selection of various "bedrock" input motion excitations, describing the essential characteristics of recordings on rock or on very stiff sites (frequency content, PGA values, seismo-tectonic background).
- Validation of the selected herein dynamic soil properties and soil profiles soil models with in-situ and laboratory data at similar soil and site conditions.
- Validation of the results of many 1D equivalent linear analyses (Schnabel [10]), in different well-documented soil profiles where reliable recordings were also available.
- Performance of an extended program of 1D analyses (>600).
- Elaboration of the results of the parametric studies in order to define homogeneous site response spectral characteristics, including spectral amplification factors for different site-soil classes, considering the soil type, the thickness of soil deposit, and the soil stiffness.

The soil models that were used in the analyses of seismic response cover an important breadth of different realistic soil conditions. Figure 1 presents the selected limits of certain characteristic parameters which, grouped as follows:

- Thickness of soil deposit varying from 20 to 110m.
- Shear wave velocity of bedrock varying from 750m/s to 2000m/s
- Fundamental period of site varying from 0.1sec to 1.5sec
- Mean shear wave velocity of upper 30m varying from 120m/sec to 837m/s
- Mean shear wave velocity of whole soil deposits varying from 100m/s to 858m/s
- Impedance ratio varying from 1.4 to 15.0

Depending on the criteria applied for the selection of the representative 1D profiles, the set of parametric analyses is separated in three groups:

- Soil models according to the EC8 site classification having (a) three different thickness (20m, 40m and 60m), (b) different mean Vs values for the whole profile (figure 2a) and c) shear wave velocity of the bedrock equal to 1500m/s.

- Homogenous clayey and sandy as well as “mixed soil” models, with various physical and mechanical properties (e.g. plasticity, relative density, etc) and shear wave velocity of bedrock varying from 750m/s to 2000m/s (Figure 2b).
- Non-homogeneous soil profiles having at different depths a “lower stiffness” soil layer of various thickness (Figure 2(c)). This particular case of soil conditions may be defined as a special site category in seismic codes (e.g. category E in EC8); this category is of specific interest as it is often met in practice in regions with loose soil deposits.

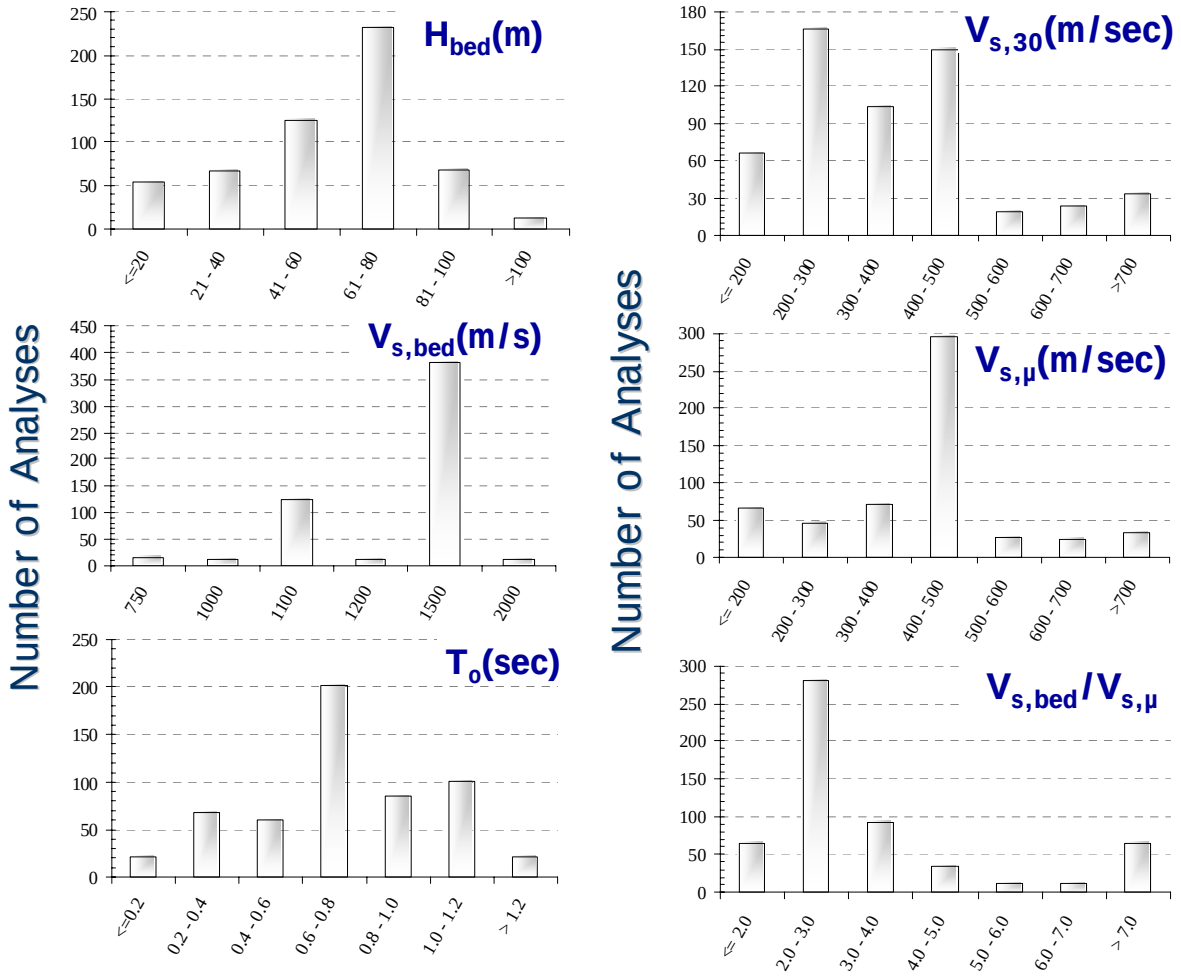

Figure 1. Soil models used in the theoretical analyses: Variation of (a) depth of bedrock, (b) Vs of bedrock ($Vs_{,bed}$) , (c) fundamental period of soil deposit, (d) fluctuation of mean value of $Vs_{,30}$, (e) mean shear wave velocity of soil deposit $Vs_{,m}$ and (f) impedance ratio $Vs_{,bed}$ / $Vs_{,m}$.

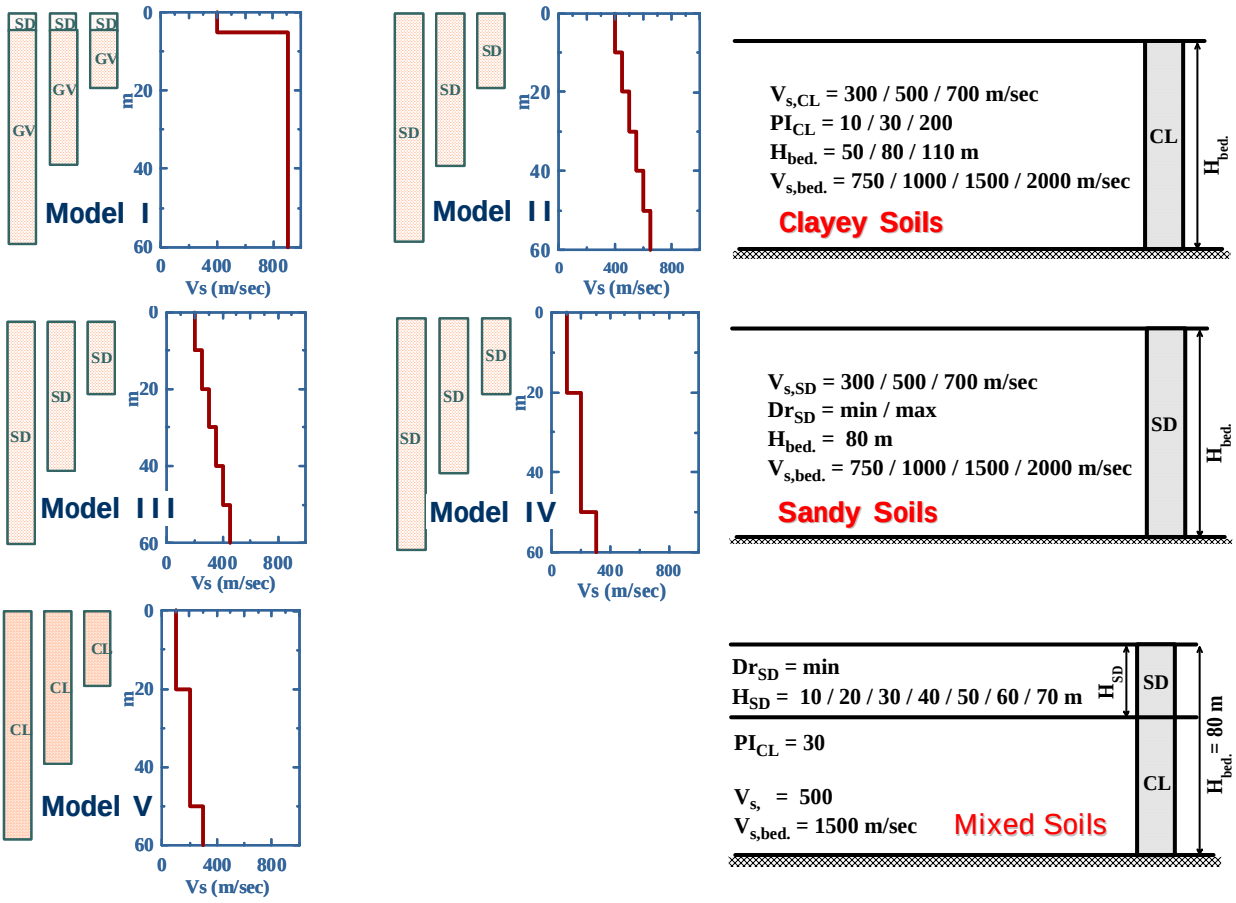

Figure 2. (a) Soil models according to EC8 classes, (b) Clayey, sandy and mixed soil models used in theoretical analyses.

For the seismic response study twelve real accelerograms were considered in the analyses. They were carefully selected to satisfy the following criteria: a) been recorded at rock sites, b) cover a wide range of peak acceleration values (0.01g to 0.7g) and frequency content and c) match the response spectra provided by Eurocode 8 and Greek seismic code for rock-site conditions.
The normalized acceleration response spectra for the proposed input motions are given in figure 3a, while figure 3b shows the comparison with EC8 and UBC97 response spectra, as well as with response spectra provided by empirical attenuation relationships (Ambraseys [11], Sabetta [12]).

Equivalent linear site response analyses were performed using CYBERQUAKE computer code [13]. Shear modulus reduction curves G/Go and damping ratio D_S, both depending on the shear strain specified from resonant column tests (Pitilakis [14,15,16]) and from the literature. Results of site response analysis in frequency domain using the equivalent linear approximation are considered accurate for the determination of PGA up to 3sec for generic purpose projects (Finn [17], Martin [5], Durward [18], Dobry [7], Dickenson [6]). For each earthquake-site model, a nonlinear site response analysis is performed in order to generate acceleration time history and the corresponding response spectrum with 5% damping ratio at ground surface. In total, more than 600 theoretical analyses of various well-documented soil models were performed.

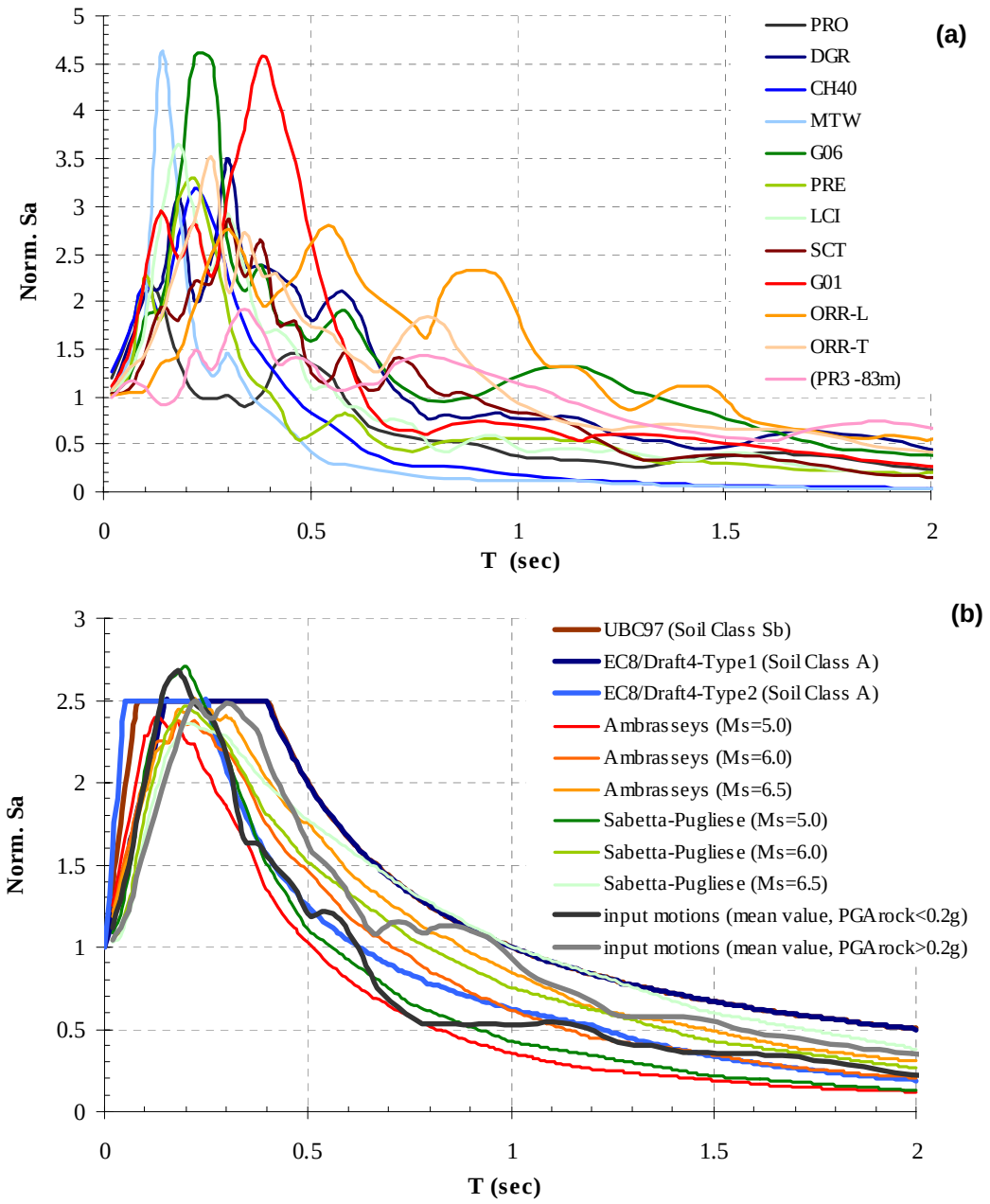

Figure 3. (a) Normalized acceleration response spectra of the 12 selected seismic excitations used in theoretical analyses, (b) acceleration response spectra at 'rock' sites: comparison of values proposed by seismic codes and empirical attenuation relationships.

PROPOSED SOIL AND SITE CLASSIFICATION

The classification of a site using simple qualitative criteria, as it is proposed by the Greek Seismic code (EAK), does not correspond to the present needs of an improved soil classification for site effect analyses or to the present state of knowledge. The absence of quantitative description parameters that constitute characteristic attributes of soil materials and site conditions, increase the uncertainty of choosing of suitable category. The majority of international seismic regulations (NEHRP/97, UBC/97, Ec8-

prEN1998/Draft4) recognizing the need for quantitative parameters adopts the $Vs_{,30}$ criterion in the definition of the site category. Even though the classification based on $Vs_{,30}$ overcomes the qualitative description's shortcomings ,it can potentially lead to erroneous results, according to the results of theoretical and experimental analyses that were done elsewhere (Pitilakis [16]) and have been conducted in the framework of this study. Many experimental and theoretical studies (Pitilakis [9], Raptakis [19], Makra [20]) confirm the important role of the basin and deep soil layers. The site classification proposed herein (Table 1) is an attempt to encompass the factors affecting seismic site response while minimizing the amount of data required for site characterization. Simple and widely used soil parameters are used for the description of different soil categories (N-SPT, mean shear wave velocity Vs, undrained strength Su).

The basic parameters that were adopted for the site classification scheme are summarized in below:

a) Qualitative description of common the soil-rock types like: healthy/slightly weathered/ segmented rock formations, very stiff to soft clays, very dense to loose sands etc. This qualitative description refers also to the proposed range of values of mean shear wave velocities.
b) Average estimated depth to the real bedrock or to a so-called "seismic bedrock" formation which is assigned to Vs>800 m/s.
c) Mean shear wave velocity Vs over the whole soil column until the bedrock.
d) The fundamental period of the site, which constitutes an indirect measure of stiffness and thickness of soil deposits.
e) Values from SPT tests, which constitute the most common in-situ geotechnical test and are commonly used to characterize soil deposits and to estimate the values of Vs.
f) The undrained shear strength and the plasticity index used for clayey soils.

According to the proposed site classification scheme the sites are classified into six basic categories (A, B, C, D, E and X) by their qualitative description and stiffness characteristics. This general form follows the general categories proposed by EC8, introducing at the same time some extra sub-classes that were pointed out at the theoretical study of seismic response, corresponding to common cases that are met in engineering practice. The subdivision of the basic categories A, B, C and D in sub-categories was based on the results of theoretical analyses highlighting the influence of depth to bedrock in the characteristics of seismic response.

SITE DEPENDED AMPLIFICATION FACTORS AND RESPONSE SPECTRA

For each soil category of Table 1 and for two levels of expected seismic intensity in rock site (Type 1 – PGArock>0.2g, Type 2 – PGArock<0.2g) spectral acceleration factors at the surface were determined. Figure 4 depicts a representative example of calculation procedure for site class C1.
The determination of smoothed acceleration spectra at the surface for each soil category was based on the estimated average spectral amplifications factors multiplying the EC8 rock site spectra. The applied procedure has as follows:

- Classification of soil models for seismic response analyses according to the defined soil categories.
- Statistical elaboration of the results of the theoretical 1D nonlinear ground response analyses in terms of spectral amplification factors (variation of mean values as a function of the period and the level of the expected intensity).

Table 1. Soil and Site Characterizatrion (Pitilakis [16]).

SOIL CATEG.		DESCRIPTION	To (sec)	REMARKS
A	A_1	Healthy rock formations		Vs ≥1500 m/s
	A_2	Slightly weathered/segmented rock formations,(thickness of weathered layer < 5.0m)	≤0.2	Weak layer: $V_s \geq 300$ m/s Rock form.: $V_s \geq 800$ m/s
		Geologic formations which resemble to rock formations in their mechanical properties and their composition (e.g. conglomerates)		$V_s \geq 800$ m/sec
B	B_1	Highly weathered rock formations whose weathered layer has a considerable thickness of 5.0 - 30.0m	≤ 0.4	Weathered layer: $V_{s\,(1)} \geq 300$ m/s
		Soft rock formations of great thickness or formations of similar stiffness and mechanical properties (e.g. stiff marls)		V_s = 400 - 800 m/s $N_{SPT(2)} > 50$ $S_{u(3)}$>200KPa
		Homogeneous soil formations of very dense sand – sand gravel and/or very stiff clay, and small thickness (less than 30.0m)		V_s = 400 - 800 m/s $N_{SPT} > 50$ S_u >200Kpa
	B_2	Homogeneous soil formations of very dense sand – sand gravel and/or very stiff clay, and medium thickness (30.0 - 60.0m), whose mechanical properties and stiffness increase with depth	≤0.8	V_s = 400 - 800 m/s $N_{SPT} > 50$ S_u >200Kpa
C	C_1	Soil formations of dense to very dense sand–sand gravel and/or stiff to very stiff clay, of great thickness (>60.0m), whose mechanical properties and strength are constant and/or increasing with depth	≤1.2	V_s = 400 - 800 m/s $N_{SPT} > 50$ S_u >200KPa
	C_2	Soil formations of medium dense sand – sand gravel and/or medium stiffness clay (PI > 15, fines percentage > 30%) of medium thickness (20.0m – 60.0m)	≤1.2	V_s = 200 - 400 m/s $N_{SPT} > 20$ S_u >70KPa
	C_3	Category C2 soil formations of great thickness (>60.0 m), homogenous or stratified that are not interrupted by any other soil formation with a thickness of more than 5.0m and of lower strength and Vs velocity	≤1.4	V_s = 200 - 400 m/s $N_{SPT} > 20$ Su >70KPa
D	D_1	Recent soil deposits of substantial thickness (up to 60m), with the prevailing formations being soft clays of a high plasticity index (PI>40), with a high water content and low values of strength parameters	≤ 2.0	V_s ≤200 m/s $N_{SPT} < 20$ Su <70KPa
	D_2	Recent soil deposits of substantial thickness (up to 60m), with prevailing fairly loose sandy to sandy-silty formations with a substantial fines percentage (so as not to be considered susceptible to liquefaction)	≤2.0	V_s ≤200 m/s $N_{SPT} < 20$
	D_3	Soil formations of category C with Vs >300m/s and great overall thickness (>60.0m), interrupted at the first 40 meters by soil layers of category D1 or D2 of a small thickness (5 – 15m),	≤ 1.2	
E		Surface soil formations of small thickness (5m - 20m), small strength and stiffness, likely to be classified in category C or D according to geotechnical properties, which overlie category A formations (Vs≥ 800 m/s).	≤ 0.5	Surface soil layers: V_s = 150 - 300 m/s
X		- Loose fine sandy-silty soils beneath the water table, susceptible to liquefaction (unless a special study proves no such danger, or if the soil's mechanical properties are improved). - Soils near well documented seismically active tectonic faults. - Steep slopes covered with loose lateral deposits. - Loose granular or soft silty-clayey soils, provided they have been proven to be hazardous in terms of dynamic compaction or loss of strength, Recent loose landfills. - Soils with a very high percentage in organic material.		

(1), (2), (3) : *mean values over the whole soil column until the bedrock.*

- Determination of normalized acceleration spectra for each site category, which result from the application of mean amplification factors to the equivalent normalized spectra for rock site conditions, described by the following equations:

$$0 \le T \le T_B : \ \frac{S_a(T)}{PGA_{rock}} = S \cdot \left[1 + \frac{T}{T_B} \cdot (\beta - 1) \right] \tag{1}$$

$$T_B \le T \le T_C : \ \frac{S_a(T)}{PGA_{rock}} = S \cdot \beta \tag{2}$$

$$T_C \le T \le T_D : \frac{S_a(T)}{PGA_{rock}} = S \cdot \beta \cdot \frac{T_C}{T} \tag{3}$$

$$T_D \le : \qquad \frac{S_a(T)}{PGA_{rock}} = S \cdot \beta \cdot T_C \left(\frac{T_D}{T^2} \right) \tag{4}$$

where, PGA_{rock} = design ground acceleration at rock-site conditions, T_B, T_C = limits of the constant spectral acceleration branch, T_D = value defining the beginning of the change of the slope branch and value defining the constant displacement response range of the spectrum, S = soil amplification parameter and β = spectral amplification parameter.

Table 2 and Figures 5 to 6 present the defined parameters and the acceleration response spectra for each site category of Table 1 and two levels of earthquake intensity (Type 1 – PGArock > 0.2g, Type 2 – PGArock < 0.2g).

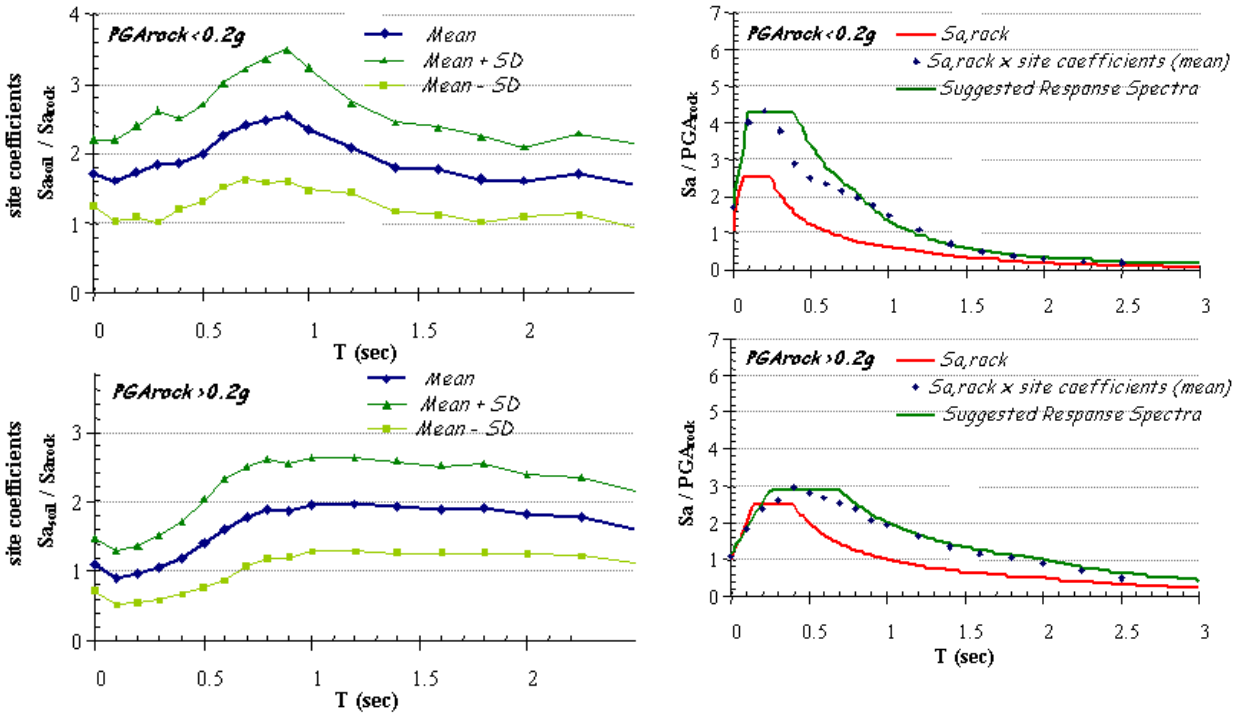

Figure 4. Site category C1: (a) Spectral amplification factors – Results of theoretical seismic response, (b) Proposed acceleration response spectra.

Table 2. Parameters of proposed acceleration response spectra.

Soil Category	*Proposed Acceleration Response Spectra*									
	$PGA_{rock}<0.2g$					$PGA_{rock}>0.2g$				
	T_B (sec)	T_C (sec)	T_D (sec)	S	β	T_B (sec)	T_C (sec)	T_D (sec)	S	β
A	0,05	0,25	1,2	**1,0**	2,5	0,15	0,4	2,0	**1,0**	2,5
B_1	0,05	0,25	0,5	**2,0**	3,0	0,15	0,45	0,8	**1,6**	3,0
B_2	0,05	0,35	0,7	**2,0**	3,0	0,20	0,55	1,0	**1,3**	3,0
C_1	0,1	0,4	0,8	**1,7**	2,5	0,25	0,7	2,0	**1,1**	2,5
C_2	0,1	0,5	0,8	**2,0**	2,5	0,25	0,8	2,0	**1,1**	2,5
C_3	0,1	0,5	1,2	**1,4**	2,5	0,25	0,9	2,2	**1,0**	2,5
D_1	0,1	0,7	1,2	**1,8**	2,5	0,25	1,0	2,0	**1,2**	2,5
D_2	0,1	0,7	1,2	**1,1**	2,5	0,25	1,0	2,0	**0,8**	2,5
D_3	0,1	0,7	1,2	**1,1**	2,5	0,25	1,2	2,0	**1,0**	2,5
E	0,05	0,25	0,4	**3,0**	3,0	0,1	0,4	0,7	**2,0**	3,0

Soil Category		PGA_{rock}<0.2g Type 2 - EC8				PGA_{rock}>0.2g Type 1 - EC8			
Proposed	EC8	S	S	β	β	S	S	β	β
A	A	1,0	1,0	2,5	2,5	1,0	1,0	2,5	2,5
B_1	B	2,0	1,35	3,0		1,6	1,2	3,0	
B_2		2,0		3,0		1,3		3,0	
C_1	C	1,7	1,5	2,5	2,5	1,1	1,5	2,5	2,5
C_2		2,0		2,5		1,1		2,5	
C_3		1,4		2,5		1,0		2,5	
D_1	D	1,8	1,8	2,5	2,5	1,2	1,35	2,5	2,5
D_2		1,1		2,5		0,8		2,5	
D_3		1,1		2,5		1,0		2,5	
E	E	3,0	1,6	3,0	2,5	2,0	1,4	3,0	2,5

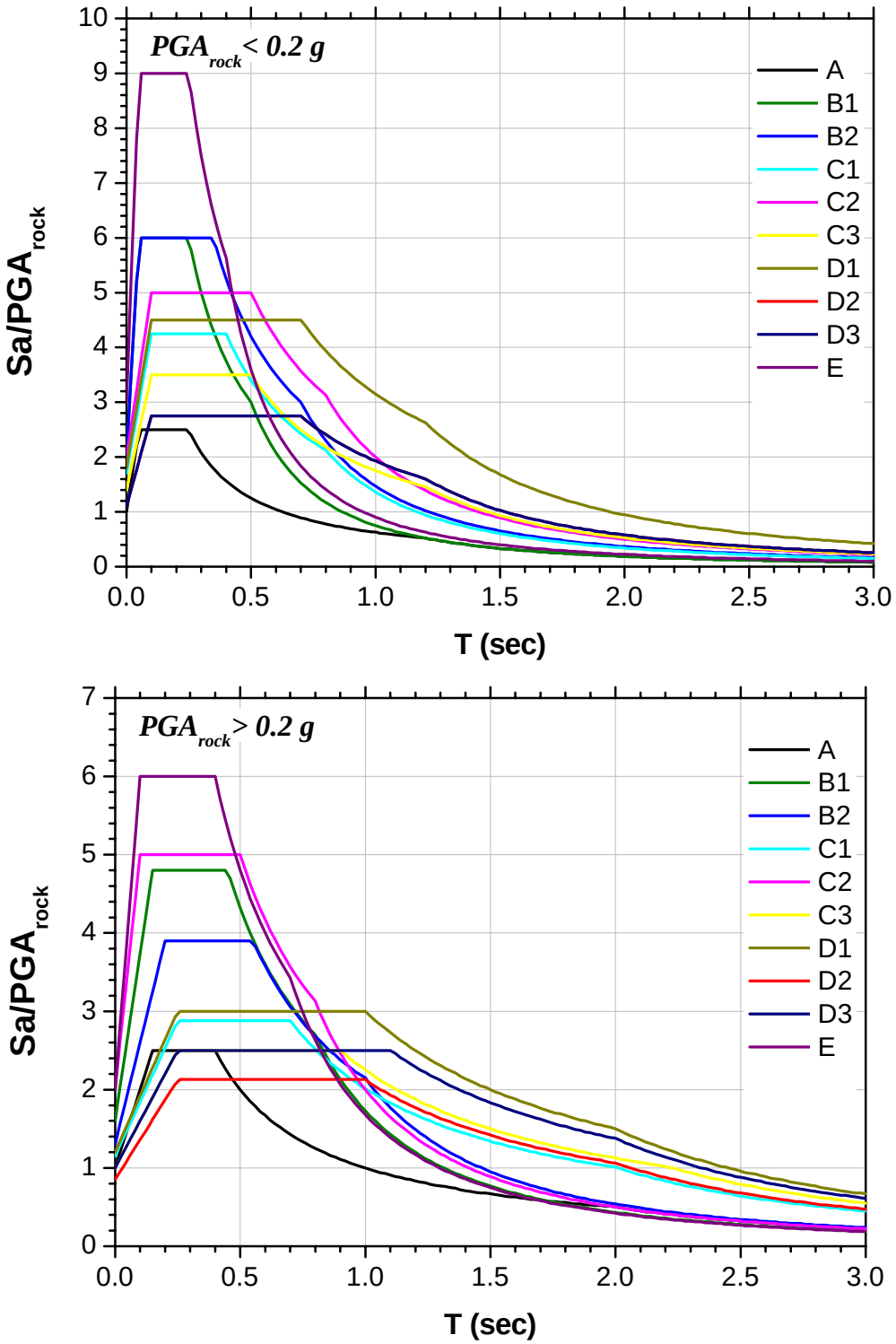

Figure 5. Proposed acceleration response spectra for each site category of table 1 and two levels of expected intensity (PGA_{rock} <0.2g and PGA_{rock}>0.2g) normalized with respect to the maximum acceleration at 'rock' site conditions (PGA_{rock}).

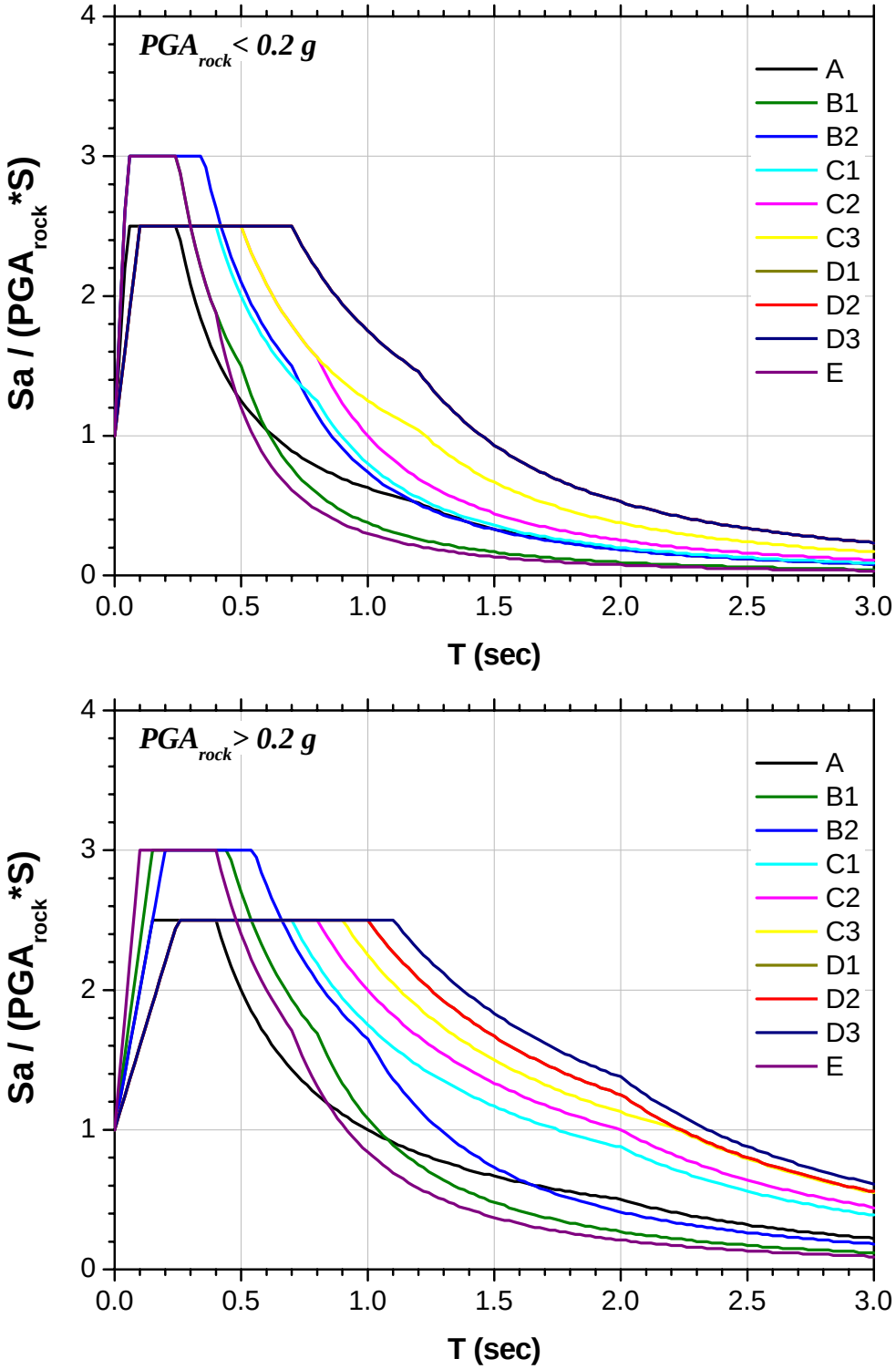

Figure 6. Normalized acceleration response spectra for each site category of Table 1 and two levels of earthquake intensity (PGA_{rock} <0.2g and PGA_{rock}>0.2g); normalized with respect to the maximum ground acceleration (PGA_{rock}*S).

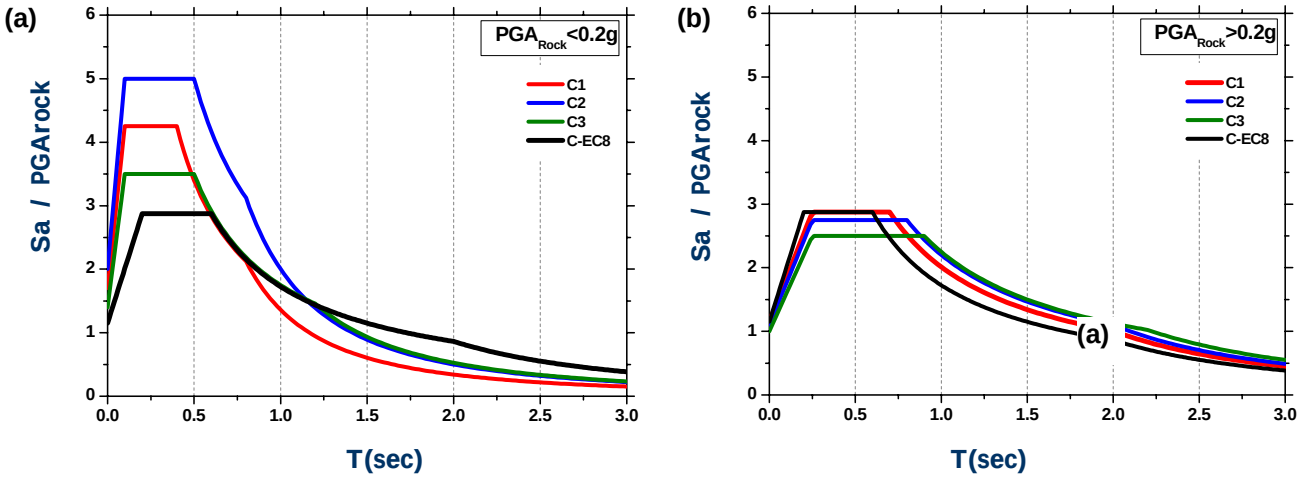

Figure 7. Acceleration response spectra for C soil sites: Comparison of proposed values with those provided by EC8 for (a) PGA_{rock}<0.2g and (b) PGA_{rock}>0.2g

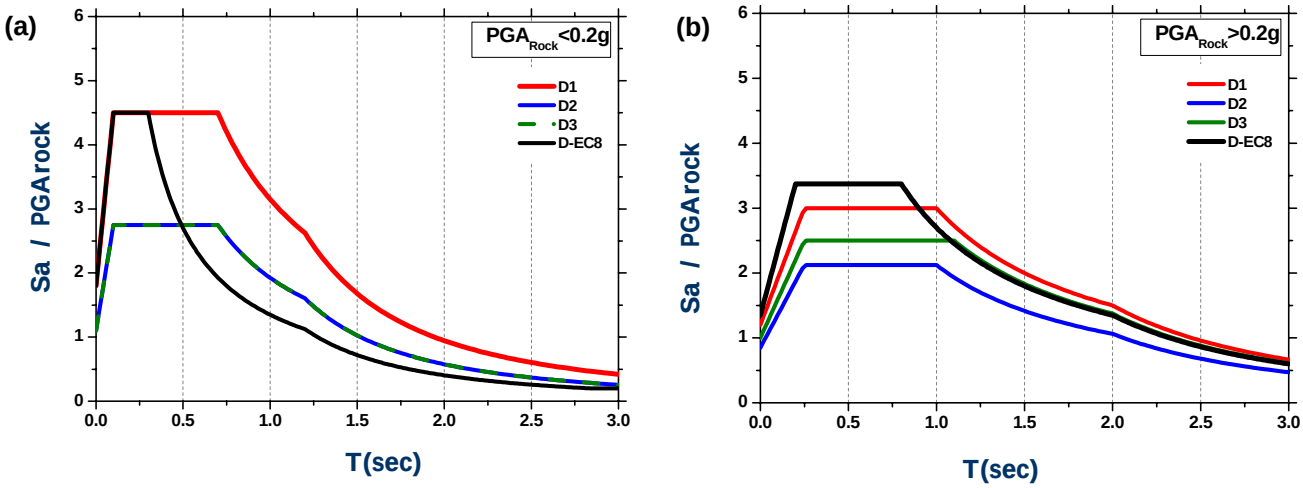

Figure 8. Acceleration response spectra for D soil sites: Comparison of proposed values with those provided by EC8 for (a) PGA_{rock}<0.2g and (b) PGA_{rock}>0.2g

In Figures 7 and 8 the proposed acceleration response spectra for C and D classes are compared with the EC8 spectra. The calculated values for C class (figure 7a), at low ground shaking intensity sites (PGA_{rock}<0.2g) show high amplification at low periods (0.1 to 0.5sec) presenting noticeable differences from those curves proposed by EC8. On the contrary, for high seismicity zones, where expected ground shaking acceleration at 'rock-like' conditions is higher than 0.2g (figure 7b), the proposed values fit reasonably well with EC8 spectra, except for C3 class. The calculated values for D1 class (figure 8a) at low ground shaking intensity sites (PGA_{rock}<0.2g) exhibit high spectral values at periods ranging from 0.1sec to 0.7sec, while D2, D3 classes exhibit lower spectral amplification, presenting noticeable differences compared to EC8. Moreover, in the case of strong ground shaking intensity (PGA_{rock}>0.2g) at D class sites the proposed values exhibit lower spectral amplification from those provided by EC8, due to

the influence of strong non-linear behavior. The differences reflect the effects of induced ground shaking intensity, soil depth, soil type, stiffness and stratification on the surface spectral amplification under 1D wave propagation.

CONCLUSIONS

Geotechnical and geophysical data stemming for various sites in Greece and Europe along with results from instrumental and theoretical methods were analyzed to evaluate an improved and refined geotechnical site classification scheme, to account for site effects in engineering design practice. The proposed classification scheme is based on a general characterization of the site conditions that includes soil thickness and bedrock depth, deposit stiffness and fundamental period. For each site category spectral amplification factors for two levels of expected intensity of "outcropping" ground shaking were determined. Finally, mean response acceleration spectra for each soil category with two level of ground shaking intensity are proposed, normalized to the response spectra provided by Eurocode 8 for rock-site conditions. We believe that the proposed site amplification coefficients, and normalized response spectra, reflect better the actual site conditions, while they take into consideration more accurately the effect of shaking intensity on soil non-linearity. However, further investigation has to be undertaken, enriching the number of the well-documented soil profiles and simultaneous strong motion recordings at different soil-site conditions.

ACKNOWLEDGMENTS

Financial support was provided by the Organization for Seismic Planning and Protection of Greece. This contribution is acknowledged.

REFERENCES

1. EAK(2000), Greek Seismic Code, Organization of Seismic Planning and Protection.
2. European Committee for Standardization (2001). "General rules, seismic actions and rules for buildings" EC8, Draft No4, Design of Structures for Earthquake Resistance, Part 1.
3. Seed, R.B., Dickenson, S.E., Mok, C.M. "Seismic response analysis of soft and deep cohesive sites: A brief summary at recent findings', 1991, Proceedings, CALTRANS First Annual Seismic Response Workshop, Sacramento, California.
4. Borcherdt, R.D. (1994) "Estimates of site dependent response spectra for design (methodology and justification)", Earthquake Spectra, 10: 617-653.
5. Martin GR, Dobry R. "Earthquake site response and seismic code provisions". NCEER Bull. 1994, 8(4): 1-6.
6. Dickenson, S. E., Seed, R. B. "Nonlinear dynamic response of soft and deep cohesive soil deposits", Proc. of Int. Workshop on Site Response, 1995, Yokosuka, Japan, 2: 67-81.
7. Dobry R, Borchert RD, Crouse CB, Idriss IM, Joyner WN, Martin GR, Power MS, Rinne EE, Seed RB. "New Site coefficients and site classification system used in recent building seismic code provisions". Earthquake Spectra, 2000, 16(1): 41-67.
8. Rodriguez-Marek, A., Bray, J.D., Abrahamson, N. "An empirical geotechnical seismic site response procedure". Earthquake Spectra, 2001, 17, No.1.
9. Pitilakis, K. D., Makra, K. A., Raptakis, D. G. "2D vs. 1D site effects with potential applications to seismic norms: The cases of EUROSEISTEST and Thessaloniki", 2001, Invited Lecture, Proc. XV ICSMGE Satellite Conference on Lessons Learned from Recent Strong Earthquakes, Istanbul, 123-133.
10. Schnabel P.B., Lysmer J., Seed H.B. "SHAKE - A computer program for earthquake response analysis of horizontally layered sites', 1972, Report No.EERC-72/12, University of California, Berkeley, 1972.

11. Ambraseys, N.N. (1995). “The prediction of earthquake peak acceleration in Europe”. Earthquake Engineering and Structural Dynamics, 24, pp.467-490.
12. Sabetta, F., Pugliese, A. (1996) “Estimation of Response Spectra and Simulation of Nonstationary Earthquake Ground Motions”. Bull. Seism. Soc. Am., 1996, 86(2):337-352.
13. Cyberquake. H.Modaressi, BRGM, 1998.
14. LSFE AUTH. “Database of Soil Mechanics and Geophysical data”. Laboratory of Soil Mechanics and Foundation Engineering Εργαστήριο Εδαφομηχανικής και Θεμελιώσεων, 2002.
15. Pitilakis K, Anastasiadis A. “Soil and site characterization for seismic response analysis”. XI ECEE, Paris, Inv.Lectures: 65-90, 1998.
16. Pitilakis, K. et al. “Experimental and theoretical analyses of site effects toward the improvement of soil classification and design spectra in EC8 and Greek Seismic Code”, 2003, Final Report Organization of Seismic Planning and Protection.
17. Finn WD, Iai S, Matsunaga Y. “The effects of site conditions on ground motions”. In Proc. Of 10th ECEE, 1995, 2607-2612.
18. Durward JA, Boore DM, Joyner WB. “The Amplitude Dependence of High-Frequency Spectral Decay: Constraint on Soil Non-Linearity”. Int.Workshop on Site Response, Yokosuka Japan, 1996, 82-103.
19. Raptakis, D. G., Chavez-Garcia F., Makra, K. A. and Pitilakis, K. D. “Site Effects at Euroseistest-I. 2D Determination of the Valley Structure and Confrontation of the Observations with 1D Analysis”. Soil Dynamics and Earthquake Engineering, 2000, 19(1): 1-22.
20. Makra, K., Raptakis, D., Chavez-Garcia, F. J., and Pitilakis, K. (2001) “Site effects and Design Provisions: The case of Euroseistest”, J. Pure and Applied Geophysics. 158(12): 2349-2367.

Compatibility of EC-8 Ground Types and Site Effects with 1-D Wave Propagation Theory

George D. Bouckovalas[1], Achilleas G. Papadimitriou[2], Dimitris Karamitros[3]

[1] *Professor, National Technical University of Athens, Greece*
[2] *Research Associate, National Technical University of Athens, Greece*
[3] *Civil Engineer, National Technical University of Athens, Greece*

Abstract

This paper comments on the EC-8 provisions for site effects on seismic actions, from the point of view of non-linear, 1-D seismic wave propagation theory. For this purpose, a large number of parametric analyses are performed using the recently proposed multi-variable relations of Bouckovalas and Papadimitriou (2003), which approximately reproduce the results of the equivalent linear method (*Shake 91*, Idriss and Sun 1992). In closure, a number of easy to implement and mostly quantitative modifications of EC-8 are proposed which do not alter its basic line of thought, but enhance the compatibility between its provisions and commonly performed theoretical analyses of seismic soil response

INTRODUCTION

The EC-8 divides soil sites into seven (7) "*Ground Types*", five (5) of which (i.e. A, B, C, D and E) have prescribed seismic actions and the remaining two (S1 and S2) require the execution of a special detailed study. The former five (5) ground types are identified in terms of their stratigraphic description, the approximate thickness H of recent soil deposits and the average values of the SPT blow count N_{SPT}, the undrained shear strength c_u and the shear wave velocity $V_{S,30}$ in the top 30m of the ground. In practice, the identification of the ground type is mainly based on H and $V_{S,30}$, the latter being computed irrespective of whether the top 30m include the bedrock or not. Furthermore, each ground type is assigned a different "*Soil Factor*" (S) that modifies the "*Design Ground Acceleration*" (a_g) relative to that of the basic (bedrock) ground type (A) and a different (normalized) horizontal elastic response spectrum $S_e(T)$, where T denotes the structural period. Soil factors S and (normalized) elastic response spectra (hereby denoted as *NERS*) are defined separately for areas of high and low seismicity, i.e. areas where the design earthquake has a (surface-wave) magnitude $M > 5.5$ and $M < 5.5$ respectively. The former set of S and *NERS* are denoted as Type 1 spectra in EC-8, while the latter as Type 2.

The above description of local soil effects is broadly approximate, but quite rational, as it accounts directly or indirectly for two basic factors which are known, from theory as well as from field evidence, to control the seismic soil response: the dynamic characteristics of the site (through H and $V_{S,30}$) and the seismic excitation characteristics (through the earthquake magnitude M). There is no doubt that, using the non-linear site period T_s, the predominant excitation period T_e and the peak seismic acceleration a_{max} and/or velocity v_{max} to define seismic actions would be a much more rigorous approach. Nevertheless, at the present state of geotechnical and seismological engineering practice, these parameters are not readily available to non-expert users of the code and consequently their use would have an overall negative effect.

For the foregoing reasons, our opinion is that the main line of thought of EC-8 should be preserved at the moment and any proposed modifications should aim to improve its agreement with well accepted theoretical and

field evidence. Hence, in the following, the EC-8 provisions for site effects are examined from a theoretical point of view. Namely, a large number of parametric analyses are performed in order to ascertain whether:

I. The EC-8 ground types cover adequately and uniquely all soil conditions which are often encountered in practice.
II. The EC-8 soil factors *S* and *NERS* are consistent with the corresponding ground types and seismicity levels.

OUTLINE OF METHODOLOGY

The foregoing parametric analyses are performed with a set of theory-based multi-variable relations, which approximately reproduce the results of the equivalent linear method (*Shake 91*, Idriss and Sun 1992). These relations were recently proposed by Bouckovalas and Papadimitriou (2003) and are outlined briefly in Appendix I.

To answer questions I and II of the introduction, the EC-8 code provisions had to be recast in terms of the parameters entering the foregoing multi-variable relations. As deduced by the equations in Appendix I, these relations are based on the definition of the elastic soil period $T_{s,o}$ which is used in Eq. (I-1) and in turn requires the definition of the (elastic) shear wave velocity V_S profile of the soil column down to a depth H where lies a uniform bedrock with shear wave velocity V_b. Hence, there was a need for interrelating this V_S profile to the $V_{S,30}$ value of EC-8 and this was performed via $V_{S,el}$, i.e. the average shear wave velocity of the soil column, which is related to $V_{S,30}$ as:

$$V_{S,el} = \begin{cases} \dfrac{H}{\dfrac{30}{V_{S,30}} - \dfrac{30-H}{V_b}} & ;\ H < 30\text{m} \\ V_{S,30}\left(\dfrac{H}{30}\right)^{a} & ;\quad H \geq 30\text{m} \end{cases} \qquad (1)$$

where a is the power of depth z (in m) in the assumed increasing $V_S = V_{S,30}(z/30)^a$ relation (e.g. a = 0 leads to a uniform profile). The value of V_b was varied from 800m/s up to 1200m/s in the analyses, keeping in mind that the underlying bedrock is rarely an extremely stiff rock with $V_b >> 1200$m/s.

Furthermore, the EC-8 provides different soil factors *S* and normalized elastic response spectra *NERS* on the basis of the (surface-wave) magnitude *M* of the design earthquake (Type 1: $M > 5.5$ and Type 2: $M < 5.5$). In accordance to the above, a distinction between strong and weak seismic motion is also made in the parametric analyses. In the multi-variable relations, this distinction is made in terms of the parameters quantifying the design acceleration time history at the outcropping bedrock, namely: a) its peak value a^b_{max}, b) its predominant period T_e and c) the number of equivalent uniform cycles n quantifying its duration. Thus, based on experience and being conservative in our estimates, the following ranges of values were adopted in the analyses:

Table 1: Quantification of strong and weak seismic motion

Parameter	$M < 5.5$	$M > 5.5$
a^b_{max} (g)	0.1 – 0.2	0.2 – 0.5
T_e (s)	0.1 – 0.25	0.2 – 0.4
n	3 – 6	4 – 8

In the sequel, parametric analyses were performed using the multi-variable relations of the Appendix in order to establish the variation of the soil factor *S* (denoted as A_a in Eq. I-2) as a function of H and $V_{S,30}$ or equivalently of H and $V_{S,el}$. The variation is studied separately for strong and weak seismic motion and in terms of its average value over the whole range of a^b_{max}, T_e and n outlined in Table 1. This procedure enables commentary on the rationality of the ground type definition process of the EC-8 and furthermore it allows for a separate estimation of design values for the soil factor *S* for all ground types and both earthquake magnitude ranges (Types 1 and 2).

Similarly, parametric analyses were performed using the multi-variable relations of the Appendix in order to establish the range of variation of the horizontal elastic response spectrum $S_e(T)$ for the various ground types and earthquake magnitudes ranges (Types 1 and 2). Having studied the variation of the soil factor *S* as described above, the emphasis was put on the amplification ratios A_{Sa}* of the normalized (horizontal) elastic response spectra (*NERS*), which are defined as

$$A_{Sa}{}^{*} = \frac{NERS \text{ for Ground Types A,B,C,D,E}}{NERS \text{ for Ground Type A}} \qquad (2)$$

The code provisioned values of A_{Sa}* are estimated on the basis of their definition in the EC-8 and are different for Types 1 and 2. These values are then compared to the values of A_{Sa}* resulting as average (± standard deviation) over the whole range of a^b_{max}, T_e and n outlined in Table 1 for Types 1 and 2 respectively.

SITE EFFECTS ON DESIGN GROUND ACCELERATION

Fig. 1 shows contours of computed soil factors, in terms of soil thickness (H) and average shear wave velocity ($V_{S,30}$), for soft bedrock (V_b = *800m/s*) and hard bedrock (V_b = *1200m/s*) conditions. In addition, Fig. 2 shows the range (average ± std. deviation) of computed S values for each ground type, and compares it to the EC-8 soil factors. In Fig. 1, we have included the H-$V_{S,30}$ range of EC-8 for the proposed ground types A to E. In doing so the expression "*several tens*" used in the definition of ground types was interpreted as "*depth larger than 30m*". Moreover, note that parametric analyses were not performed for cases with H > 80m, since such deep profiles should require a special study, in our opinion.

There are a number of noteworthy observations in these two figures pertaining to areas with M > 5.5 (Type 1), such as:

a) The definition of ground types is not complete, as sites with $V_{S,30}$ > 360 m/s and H = 5 – 30m , as well as sites with $V_{S,30}$ < 360 m/s and H = 20 – 30m do not seem to belong to any ground type.
b) Computed soil factors for ground type A are much higher than the proposed reference value of S = 1.00.
c) Except for ground type C, the EC-8 soil factors are not in agreement with theoretical predictions. The most remarkable difference is observed for ground type D where EC-8 proposes S = 1.35, as compared to computed values which range systematically between 0.95 and 1.10.

Similar observations are made in Figs. 3 and 4, which evaluate the EC-8 proposed soil factors for low seismicity areas (M < 5.5, Type 2), only that now differences are much larger and concern almost all ground types.

As a first step to improve the foregoing comparisons, the $V_{S,30}$ (= average shear wave velocity for the top 30m of soil and/or bedrock) was replaced with $V_{S,el}$ (= average shear wave velocity over the thickness H) that is given on the basis of Eq.(1). The new comparisons are shown in Figs. 5 & 6 for M > 5.5 and Figs. 7 & 8 for M < 5.5. Observe that soil factors S for ground type A range between 0.85 and 1.30, i.e. they have come closer to the reference value of S = 1.00.

As a second step, the ground types are re-defined as follows:

a) Ground type E was extended to sites with soil thickness up to 30m.
b) Ground type A was broken into two sub-groups (A1 and A2) with the following characteristics:
   - Ground Type A1: $V_{S,el}$ > 360 m/s & H < 5m
   - Ground Type A2:
     $V_{S,el}$ = 100 – 360m/s & H < 5m, or
     $V_{S,el}$ > 360 m/s & H = 5 – 30m

The new comparisons between theoretically predicted and EC-8 proposed soil factors are summarized in Figs. 9 & 10 for M > 5.5 and Figs. 11 & 12 for M < 5.5. Observe that ground type A1 has now become a truly reference soil condition with S = 1.00 ± 0.05. Furthermore, the range of S factors for the new ground type A2 is comparable to that of all pre-existing ground types, implying that it has not only filled an existing gap in the ground type definition process, but it also corresponds to a more or less uniform seismic ground acceleration.

However, there is still significant difference between the EC-8 proposed and the theoretical S factors for other than A1 sites. Thus, as a third step, the S factors may be re-defined as shown in the following Table 2:

Table 2: Theory-based soil factors S

Ground Type	Soil Factor S		
	M > 5.5	M < 5.5	average
A1	1.00	1.00	1.00
A2	1.20	1.30	1.25
B	1.30	1.30	1.30
C	1.15	1.15	1.15
D	1.05	1.10	1.10
E	1.35	1.35	1.35

As expected, S factors for Type 2 spectra (M < 5.5) are somewhat larger than those for Type 1. Yet, the difference between the two sets is small and thus an average set of seismicity independent S factors could be adopted.

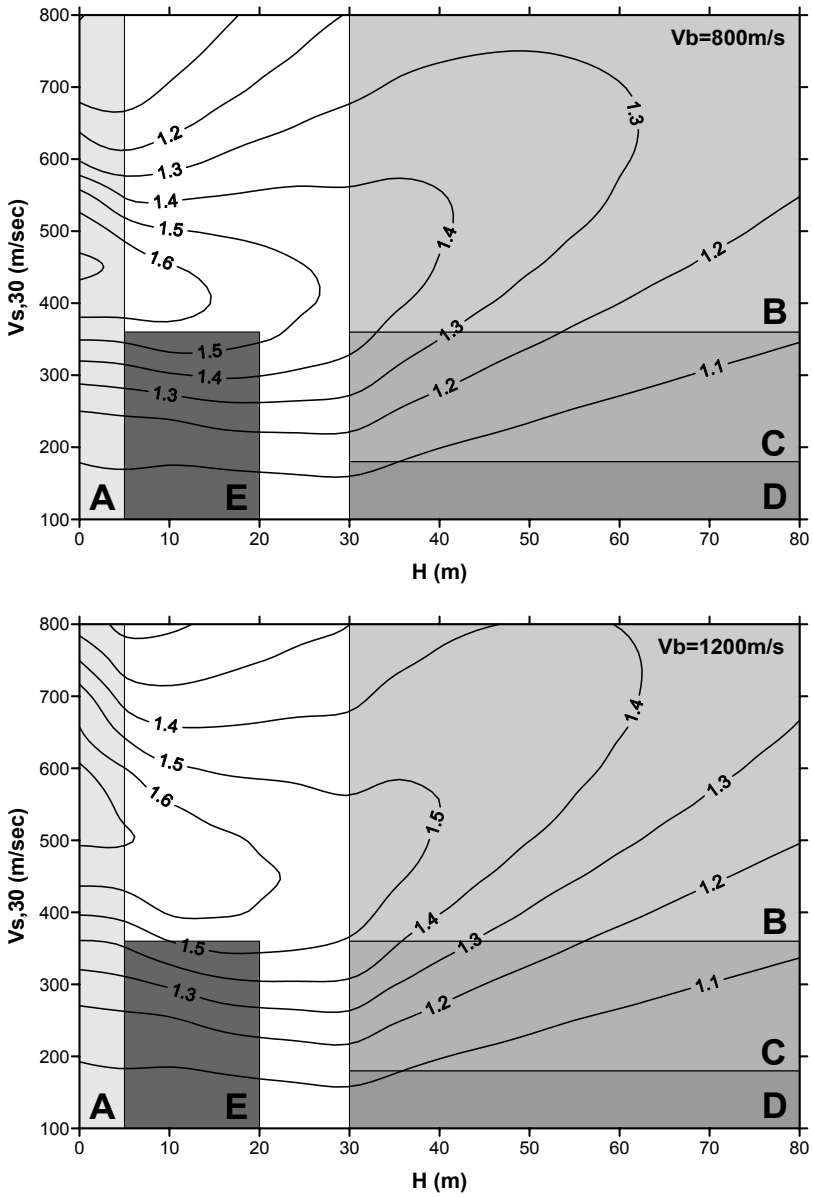

Fig 1 Ground type categorization on the basis of EC-8, as a function of H and $V_{s,30}$, and contours of average soil factor S variation from 1-D analyses: a) V_b = 800m/s, b) V_b = 1200m/s – Type 1 (M > 5.5)

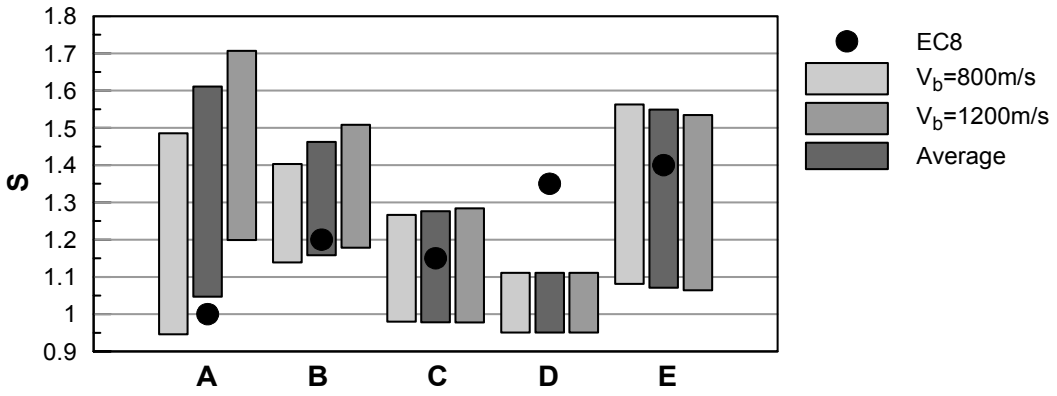

Fig 2 Soil factors S per ground type on the basis of EC-8, as a function of H and $V_{s,30}$, versus respective range of variation from 1-D analyses – Type 1 (M > 5.5)

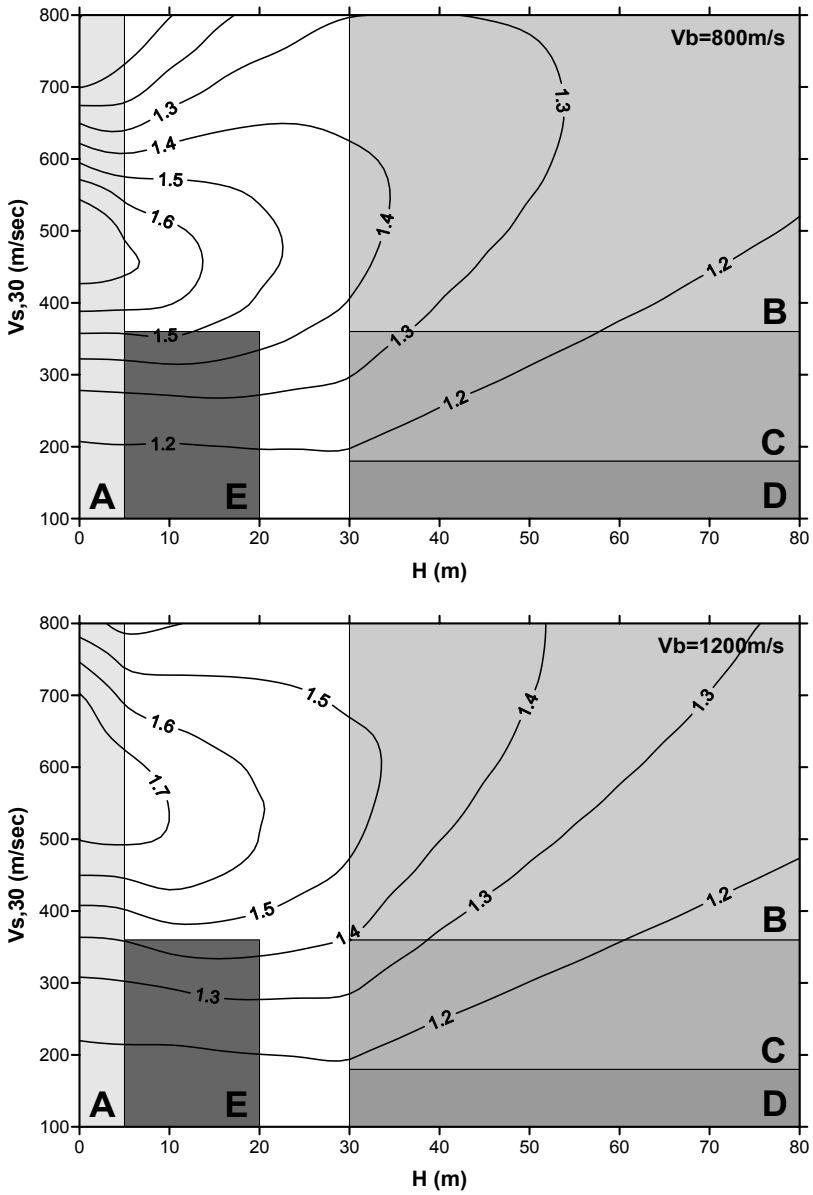

Fig 3 Ground type categorization on the basis of EC-8, as a function of H and $V_{s,30,}$ and contours of average soil factor S variation from 1-D analyses: a) V_b = 800m/s, b) V_b = 1200m/s – Type 2 ($M < 5.5$)

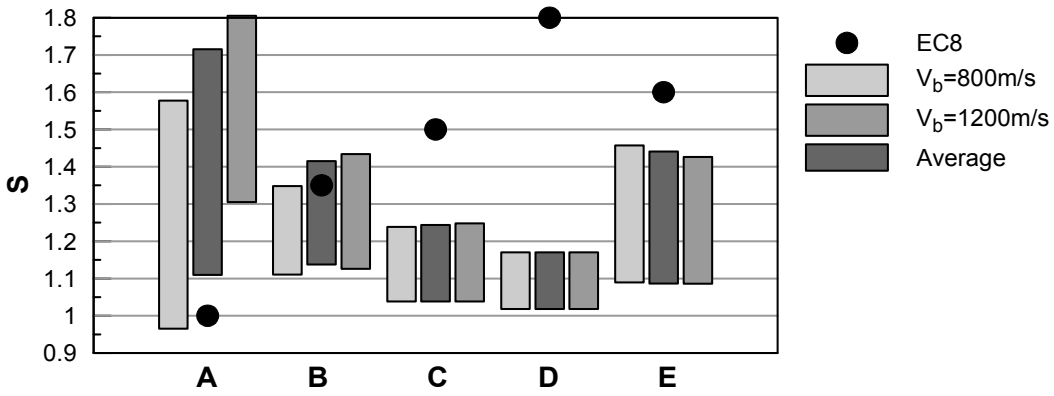

Fig 4 Soil factors S per ground type on the basis of EC-8, as a function of H and $V_{s,30}$, versus respective range of variation from 1-D analyses – Type 2 ($M < 5.5$)

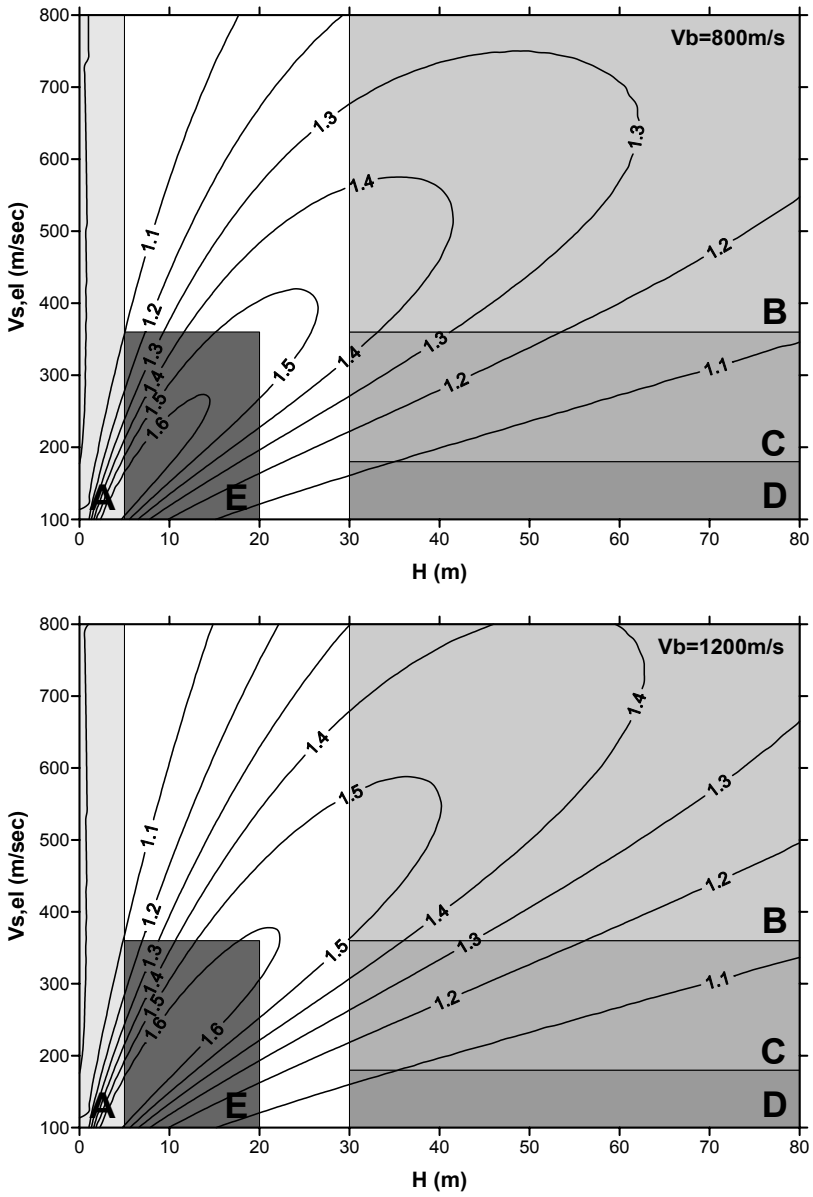

Fig 5 Ground type categorization on the basis of EC-8, as a function of H and equivalent $V_{s,el}$, and contours of average soil factor S variation from 1-D analyses: a) V_b = 800m/s, b) V_b = 1200m/s – Type 1 (M > 5.5)

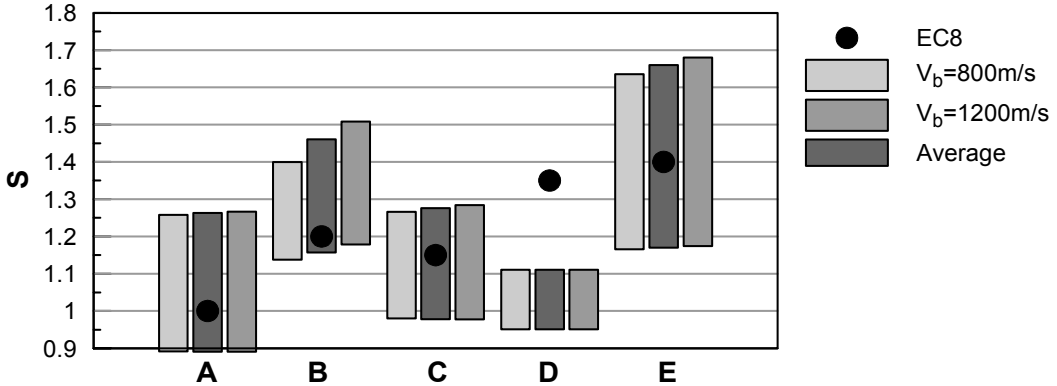

Fig 6 Soil factors S per ground type on the basis of EC-8, as a function of H and $V_{s,el}$, versus respective range of variation from 1-D analyses – Type 1 (M > 5.5)

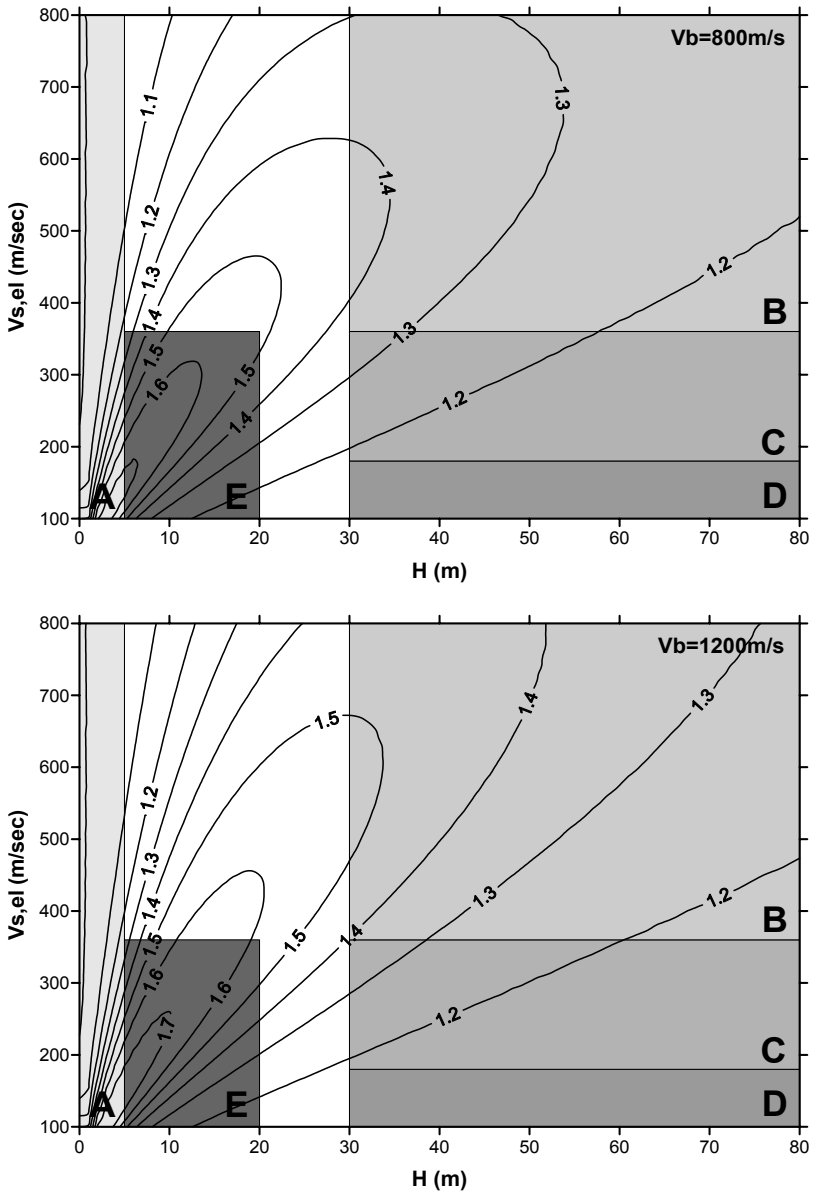

Fig 7 Ground type categorization on the basis of EC-8, as a function of H and equivalent $V_{s,el}$ and contours of average soil factor S variation from 1-D analyses: a) V_b = 800m/s, b) V_b = 1200m/s – Type 2 (M < 5.5)

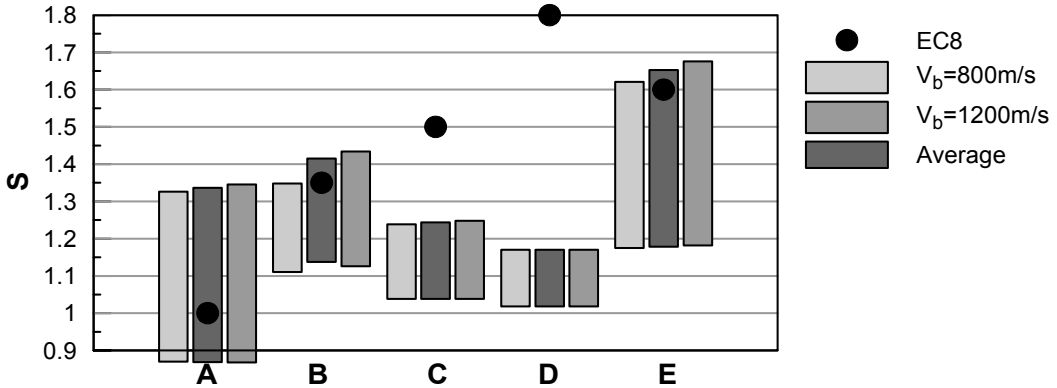

Fig 8 Soil factors S per ground type on the basis of EC-8, as a function of H and $V_{s,el}$, versus respective range of variation from 1-D analyses – Type 2 (M < 5.5)

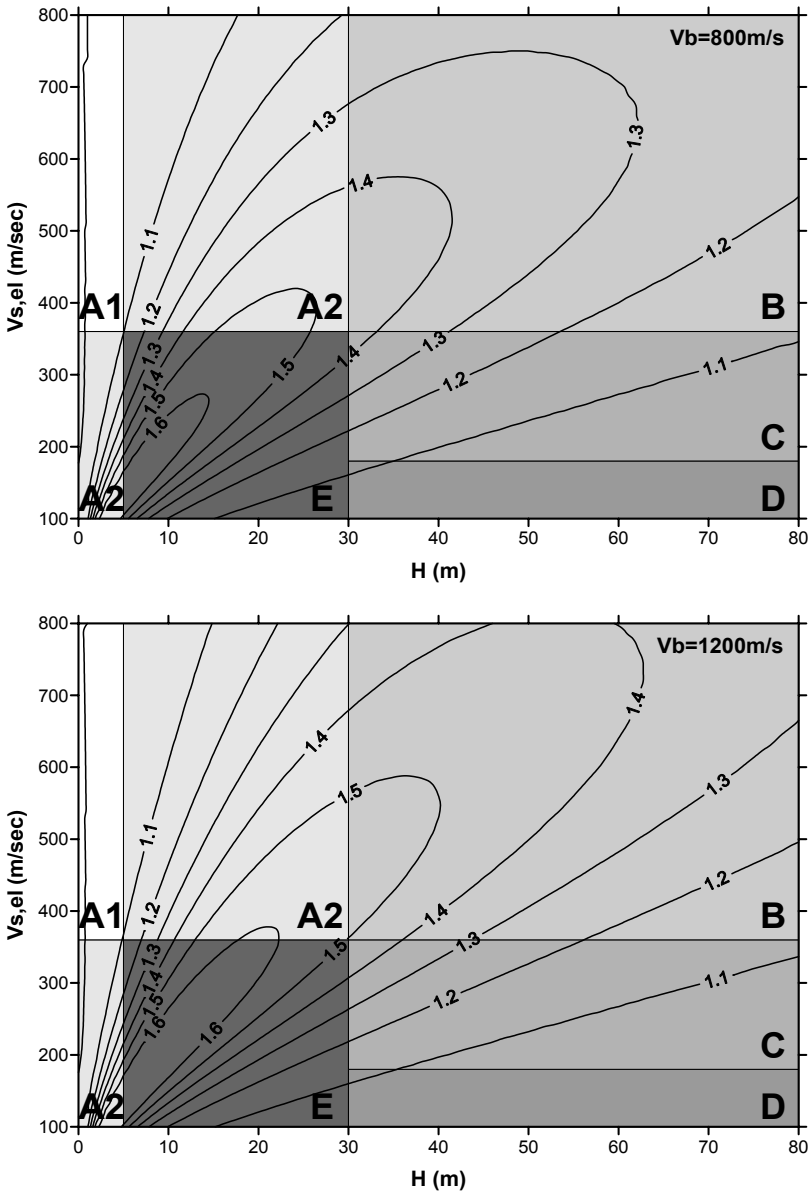

Fig 9 Proposed (modified EC-8) ground type categorization, as a function of H and $V_{s,el}$, and contours of average soil factor S variation from 1-D analyses: a) V_b = 800m/s, b) V_b = 1200m/s – Type 1 (M > 5.5)

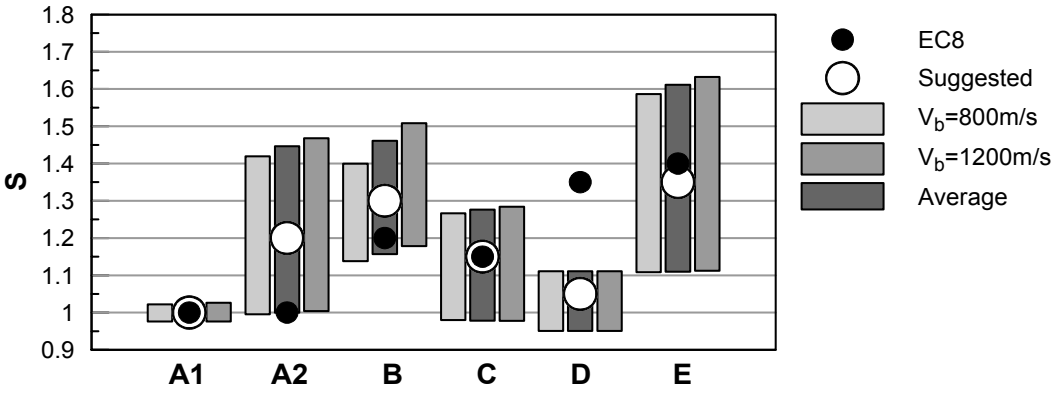

Fig 10 Adjusted soil factors S per ground type of the proposed modified EC-8 as computed from the 1-D analyses and comparison to the standing code provisions – Type 1 (M > 5.5)

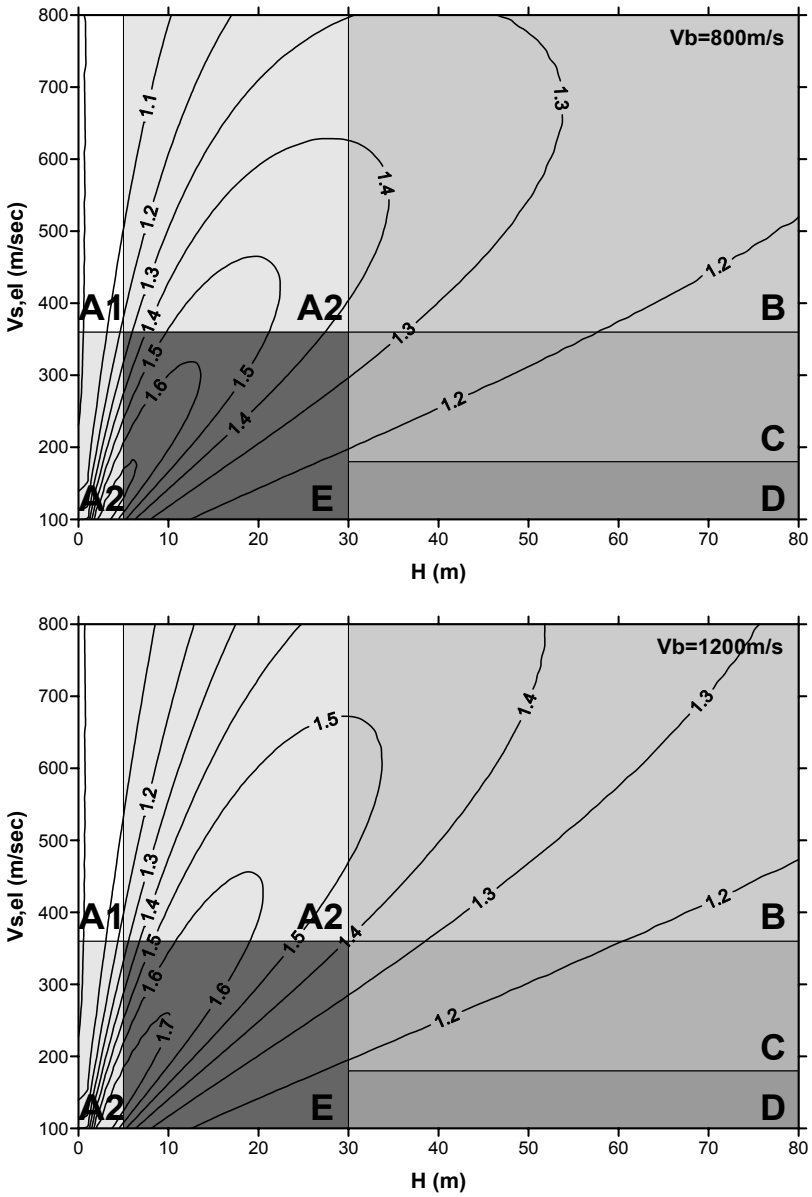

Fig 11 Proposed (modified EC-8) ground type categorization, as a function of H and $V_{s,el}$, and contours of average soil factor S variation from 1-D analyses: a) V_b = 800m/s, b) V_b = 1200m/s – Type 2 ($M < 5.5$)

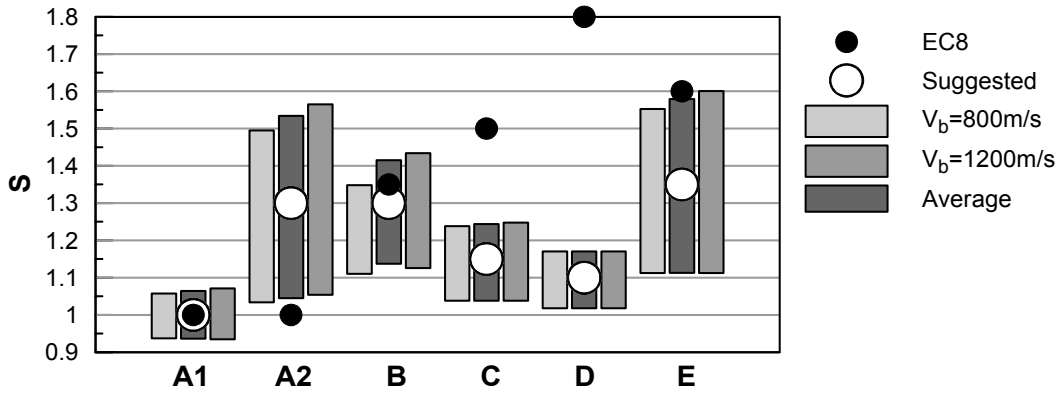

Fig 12 Adjusted soil factors S per ground type of the proposed modified EC-8 as computed from the 1-D analyses and comparison to the standing code provisions – Type 2 ($M < 5.5$)

SITE EFFECTS ON NORMALIZED ELASTIC RESPONSE SPECTRA (*NERS*)

Figs. 13 & 14 summarize theoretical predictions and EC-8 proposed *NERS* for high seismicity and low seismicity areas, respectively. The comparison is shown in terms of the normalized spectral amplification ratios A_{Sa}* for the different ground types. Theoretical predictions are shown as a gray band, defined by the mean curve and the ± one standard deviation curves. Observe the difference in the shapes of the theoretically predicted and the EC-8 proposed curves, which is most probably attributed to the smoothing that is commonly applied to code spectra. Eliminating this difference to a satisfactory degree would require drastic modification of the code spectra which, to our opinion, is not presently justified.

Hence, our attention was focused to improve fitting of the EC-8 *NERS* to the theoretical predictions, while maintaining their current general form. This was accomplished by keeping the reference *NERS* for ground type A unchanged and modifying appropriately the characteristic structural periods T_B and T_C for any of the remaining ground types. The new T_B and T_C values are summarized in Table 3, while the corresponding spectral amplification curves are drawn with bold line in Figs. 13 & 14.

Table 3: Modified structural periods T_B and T_C defining the design horizontal elastic response spectra

Ground Type	**M > 5.5** (Type 1)		**M < 5.5** (Type 2)	
	T_B **(s)**	T_C **(s)**	T_B **(s)**	T_C **(s)**
A1 & A2	0.15	0.40	0.05	0.25
B		0.50		0.30
C		0.60		0.40
D		0.60		0.40
E		0.50		0.30

CONCLUSION: PROPOSED MODIFIED EC-8

Based on the commentary and comparisons presented above, modifications are proposed to specific elements of Chapter 3 of EC-8. These elements are outlined below and the proposed modifications are denoted in bold face.

(a) Disregarding any reference to the N_{SPT} or undrained shear wave velocity c_u that were not addressed here, Table 3.1 that presents the ground types reads as follows:

Ground Type	***H*** **(m)**	$V_{S,el}$ **(m/s)**
A1	**0 – 5**	**> 360**
A2	**0 – 5**	**100 – 360**
	5 – 30	**360 – 800**
B	**30 – 80**	360 – 800
C	**30 – 80**	180 – 360
D	**30 – 80**	100 – 180
E	5 – **30**	100 – 360
S1	**any thickness**	< 100
S2	**> 80**	**any stiffness**
	liquefiable or sensitive soil	

(b) Table 3.2 that presents the parameters describing the recommended Type 1 elastic response spectrum (strong motion) reads as follows:

Ground Type	***S***	T_B **(s)**	T_C **(s)**	T_D **(s)**
A1	1.00	0.15	0.40	2.00
A2	**1.20**	0.15	0.40	2.00
B	**1.30**	0.15	0.50	2.00
C	1.15	**0.15**	0.60	2.00
D	**1.05**	**0.15**	**0.60**	2.00
E	**1.35**	0.15	0.50	2.00

(c) Table 3.3 that presents the parameters describing the recommended Type 2 elastic response spectrum (weak motion) reads as follows:

Ground Type	***S***	T_B **(s)**	T_C **(s)**	T_D **(s)**
A1	1.00	0.05	0.25	1.20
A2	**1.30**	0.05	0.25	1.20
B	**1.30**	0.05	**0.30**	1.20
C	**1.15**	**0.05**	**0.40**	1.20
D	**1.10**	**0.05**	**0.40**	1.20
E	**1.35**	0.05	**0.30**	1.20

(d) Given the small differences in the values of *S* in the elastic response spectra of Types 1 and 2, a unique set of *S* values could be alternatively used, namely:

	A1	**A2**	B	C	D	E
S	1.00	**1.25**	**1.30**	**1.15**	**1.10**	**1.35**

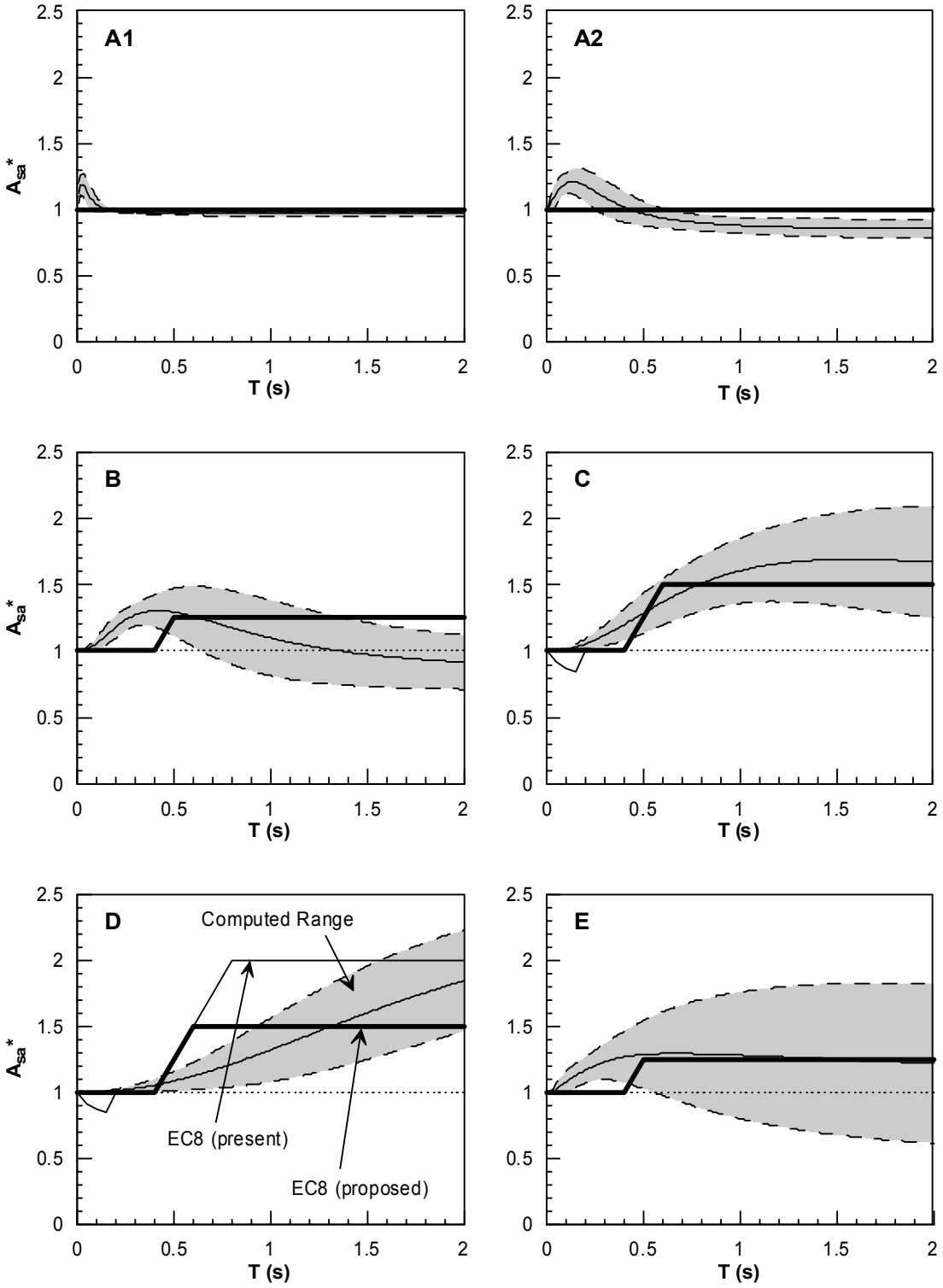

Fig 13 Normalized spectral amplification ratios A_{Sa}* per ground type from 1-D analyses and comparison to the standing and proposed modified EC-8 for High Seismicity (M > 5.5) areas – Type 1

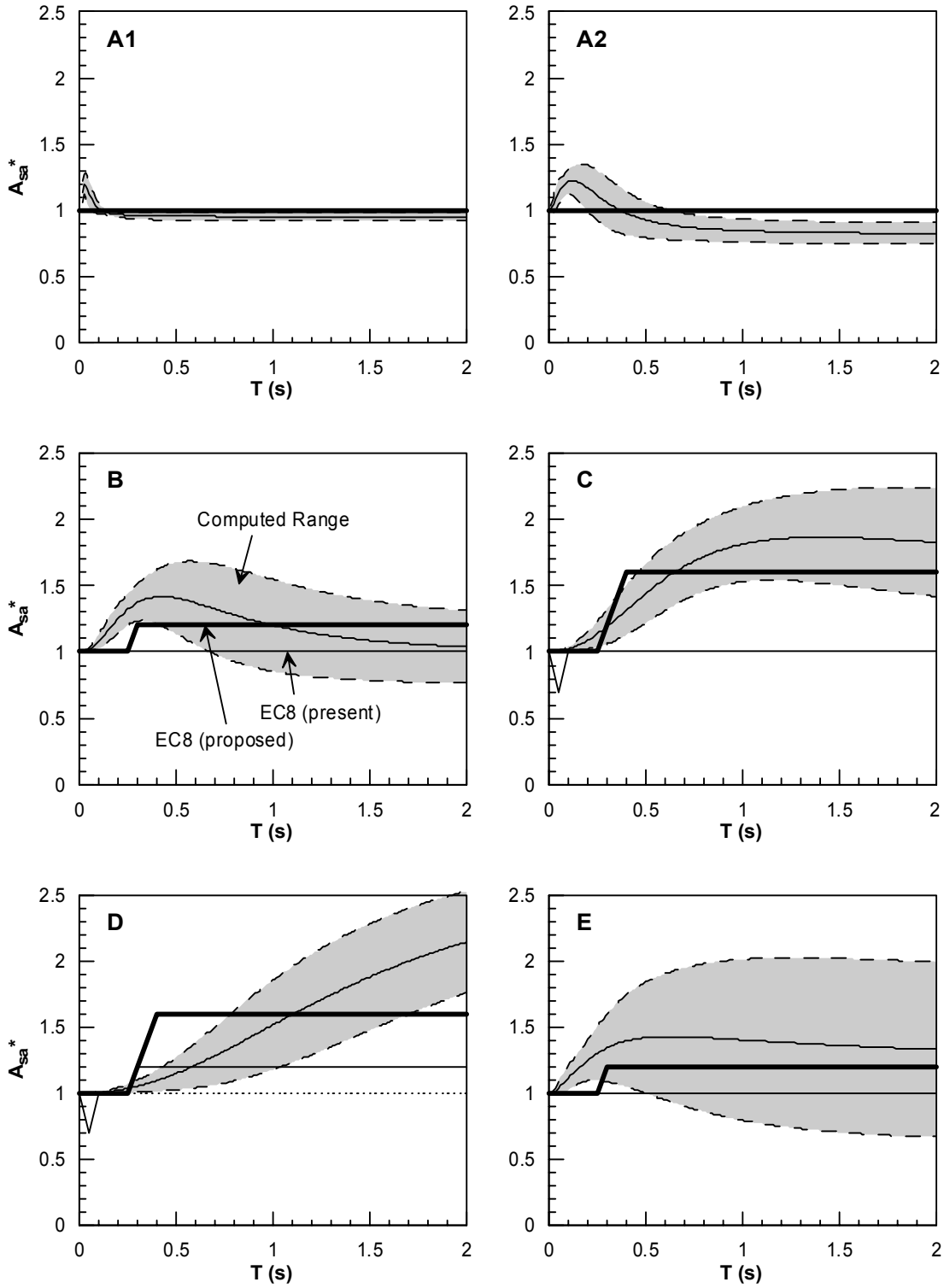

Fig 14 Normalized spectral amplification ratios A_{Sa}* per ground type from 1-D analyses and comparison to the standing and proposed modified EC-8 for Low Seismicity ($M < 5.5$) areas – Type 2

REFERENCES

Bouckovalas, G.D. and Papadimitriou A.G. (2003) "Multi-variable relations for soil effects on seismic ground motion", *Earthquake Engineering and Structural Dynamics*, 32(12), pp. 1867-1896

Idriss, I.M., and Sun, J.I. (1992) "Shake91: A computer program for conducting equivalent linear seismic response analysis of horizontally layered soil deposits", *User's Guide*, Center for Geotechnical Modeling, Civil Engineering Department, UC Davis

APPENDIX I

This appendix presents briefly the approximate relations used for the estimation of the effects of soil conditions on seismic ground motion. Further details can be found in Bouckovalas and Papadimitriou (2003).

In all of these relations, the basic parameter that dominates the response is the non-linear soil period T_s, which is given by:

$$\left(T_s/T_{s,o}\right)^2 = 1 + 5330\left(V_{s,o}\right)^{-1.3}\left(\frac{a^b{}_{max}}{g}\right)^{1.04} \qquad \text{(I-1)}$$

where $T_{s,o}$ is the linear (elastic) soil period, and $V_{s,o}$ is the average elastic shear wave in the soil column. Note that the evaluation of $T_{s,o}$ can be performed with various techniques from the literature, e.g. based on the average $V_{s,o}$, or the uniform V_s value that results to the same travel time of the S waves from the soil surface to the bedrock. Fig. I-1 shows examples of the effects of $a^b{}_{max}$ and $V_{s,o}$ on the value of the ratio $T_s/T_{s,o}$.

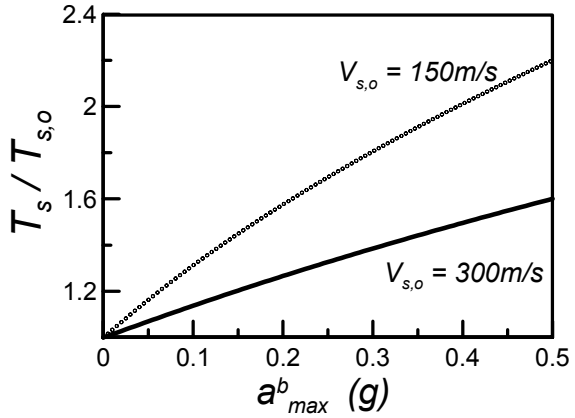

Fig. I-1: Effects of $a^b{}_{max}$ and $V_{s,o}$ on ratio $T_s/T_{s,o}$.

Peak Seismic Motion Parameters

This section presents the relations for the soil surface-to-bedrock outcrop peak acceleration and velocity ratios, A_a and A_V, respectively. The former is given by:

$$A_a = \frac{1 + C_{1,a}\left(T_s/T_e\right)^2}{\sqrt{\left[1-\left(T_s/T_e\right)^2\right]^2 + \left[C_{2,a}\left(T_s/T_e\right)\right]^2}} \qquad \text{(I-2)}$$

where,

$$C_{1,a} = 1.2\left(\frac{a^b{}_{max}}{g}\right)^{-0.17}\frac{n^{0.5}}{1+n^{0.5}} \qquad \text{(I-3)}$$

$$C_{2,a} = 1.05 + 0.57\left(T_b/T_s\right) \qquad \text{(I-4)}$$

Fig. I-2 shows examples of the effects of parameters $a^b{}_{max}$, n, T_b/T_s and T_s/T_e on the value of A_a, via Eq. (I-2). Observe that among the four parameters entering the relation for A_a, T_s/T_e is the most important and that A_a becomes maximum due to resonance for T_s/T_e = 1.

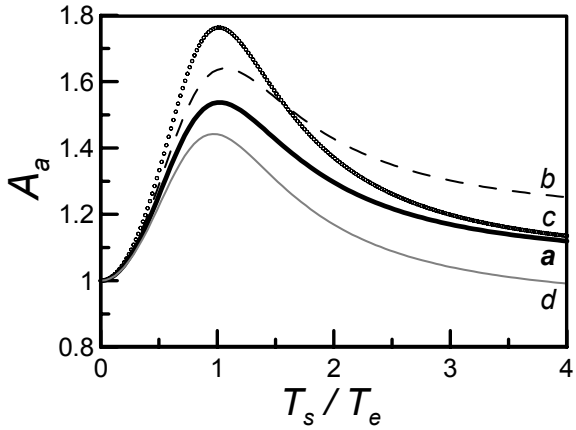

	$a^b{}_{max}$	T_b/T_s	n
a:	0.2g	0.5	4
b:	0.1g	0.5	4
c:	0.2g	0.2	4
d:	0.2g	0.5	2

Fig. I-2: Effects of $a^b{}_{max}$, T_b/T_s, n and T_s/T_e on A_a.

The relation for A_V is similar to Eq. (I-2), i.e.:

$$A_V = \frac{1 + C_{1,V}\left(T_s/1.5T_e\right)^2}{\sqrt{\left[1-\left(T_s/1.5T_e\right)^2\right]^2 + \left[C_{2,V}\left(T_s/1.5T_e\right)\right]^2}} \qquad \text{(I-5)}$$

where,

$$C_{1,V} = 0.88\left(\frac{a^b{}_{max}}{g}\right)^{-0.124} \quad \text{(I-6)}$$

$$C_{2,V} = 1.087 + 0.598\left(T_b/T_s\right) \quad \text{(I-7)}$$

Fig. I-3 shows examples of the effects of parameters a^b_{max}, T_b/T_s and T_s/T_e on the value of A_V. In this case also, T_s/T_e is the most important parameter. Note that A_V statistically becomes maximum at T_s/T_e = 1.5, since the predominant period of the velocity time history is usually higher than that of the respective acceleration history.

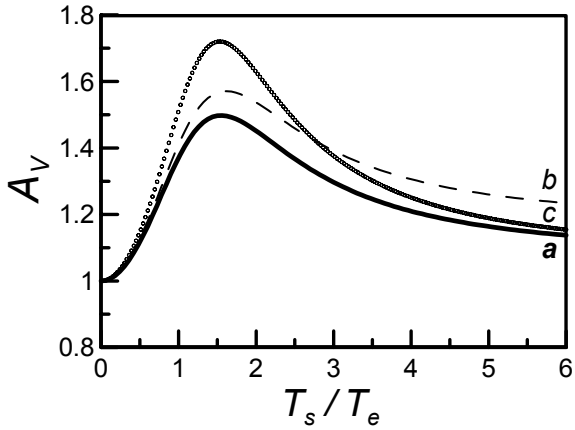

	a^b_{max}	T_b/T_s
***a**:*	0.2g	0.5
b:	0.1g	0.5
c:	0.2g	0.2

Fig. I-3: Effects of a^b_{max}, T_b/T_s and T_s/T_e on A_V.

Horizontal Elastic Response Spectra

To focus on the frequency content of the elastic response spectra, the emphasis was given on the normalized spectral acceleration for 5% critical damping, $S_a^* = S_a/a_{max}$. Thus, the corresponding soil surface-to-bedrock outcrop spectral ratio, A_{Sa}^*, is given by (I-8):

$$A_{Sa}^* = \frac{1 + A_{Sa,r}^* \left(T_s/T_e\right)^2}{\sqrt{\left[1 - \left(\frac{T_{str}}{T_s}\right)^2\right]^2 + \left[\left(\frac{1 + A_{Sa,r}^*}{A_{Sa,p}^*}\right)\left(\frac{T_{str}}{T_s}\right)\right]^2}}$$

where T_{str} is the fundamental structural period, and $A_{Sa,p}^*$ and $A_{Sa,r}^*$ are the peak and residual values of the normalized spectral amplification ratio A_{Sa}^*, as defined in Fig. I-4. Note that according to Eq. (I-8), the peak spectral amplification occurs for T_{str}/T_s = 1 due to resonance.

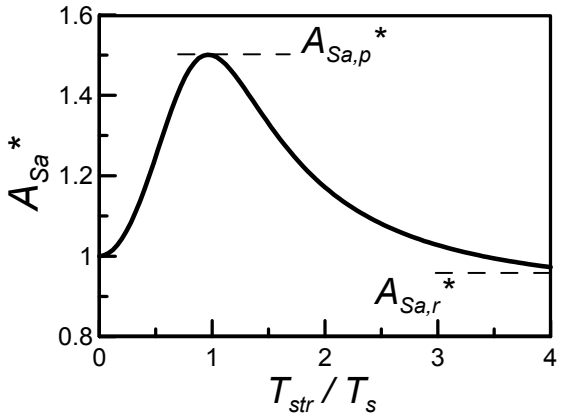

Fig. I-4: General form of normalized elastic spectral amplification ratio A_{Sa}^*.

Given the form of Eq. (I-8), the statistical analysis focused on $A_{Sa,p}^*$ and $A_{Sa,r}^*$, which gives, in turn (I-9):

$$A_{Sa,p}^* = \begin{cases} 1 + 0.318\left(\frac{T_s}{T_e}\right)^{0.058} \\ 1.318 + 0.279\left(\frac{T_b}{T_s}\right)^{-0.504} n^{-0.613}\left(\frac{T_s}{T_e} - 1\right) \\ 1.318 + 0.837\left(\frac{T_b}{T_s}\right)^{-0.504} n^{-0.613} \end{cases}$$

where Eqs. (I-9a) and (I-9c) hold for $T_s/T_e < 1$ and $T_s/T_e > 4$ respectively, while Eq. (I-9b) for $1 \le T_s/T_e \le 4$. The three-partite form of Eq. (I-9) is better understood in Fig. I-5.

Similarly, $A_{Sa,r}^*$ is given by a three-partite equation (I-10):

$$A_{Sa,r}^* = \begin{cases} 1 - 0.302\left(\frac{T_s}{T_e}\right) \\ 0.698 + 0.189\left(\frac{T_b}{T_s}\right)^{-0.474} n^{-0.406}\left(\frac{T_s}{T_e} - 1\right) \\ 0.698 + 0.945\left(\frac{T_b}{T_s}\right)^{-0.474} n^{-0.406} \end{cases}$$

where Eqs. (I-10a) and (I-10c) hold for $T_s/T_e < 1$ and $T_s/T_e > 6$ respectively, while Eq. (I-10b) for $1 \leq T_s/T_e \leq 6$. As above, Eq. (I-10) is better understood in Fig. I-6.

For both $A_{Sa,p}^*$ and $A_{Sa,r}^*$, T_s/T_e is the most important parameter, while a^b_{max} proved statistically insignificant.

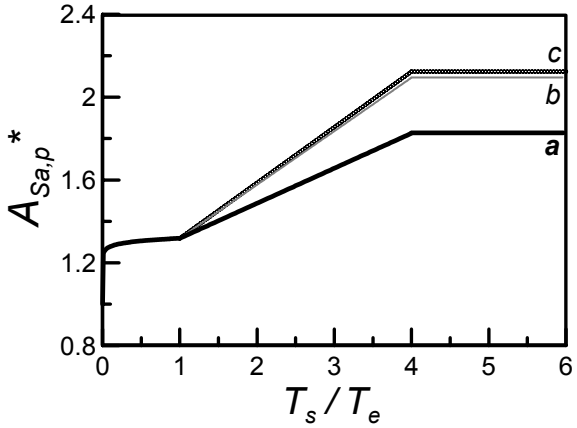

	T_b/T_s	n
***a**:*	0.5	4
b:	0.5	2
c:	0.2	4

Fig. I-5: Effects of T_b/T_s, n and T_s/T_e on $A_{Sa,p}^*$.

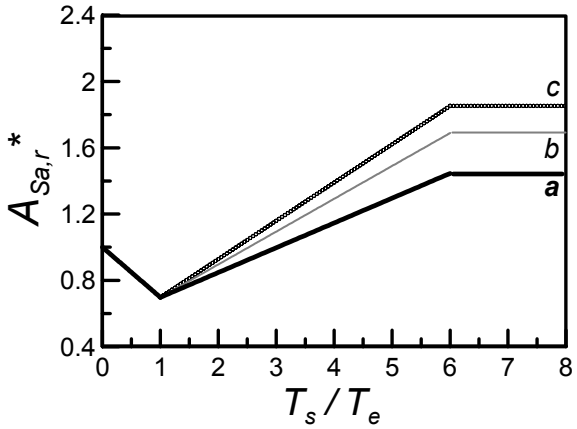

	T_b / T_s	n
***a**:*	0.5	4
b:	0.5	2
c:	0.2	4

Fig. I-6: Effects of T_b/T_s, n and T_s/T_e on $A_{Sa,r}^*$.

Dynamic soil characterization according to EC8 and its effects on the assessment of seismic actions

D. Lo Presti[1], E. Mensi[2], N. Squeglia[1], O. Pallara[2]

[1] *University of Pisa, Italy*
[2] *Politecnico di Torino, Italy*

Abstract

This paper compares the elastic response spectra, prescribed by EC8 (1998) part 1, to those inferred by means of 1D equivalent - linear analyses in a number of well characterized sites in Tuscany (Italy). Soil characterization has been done in the framework of a program supported by the Regional Government of Tuscany and devoted to the assessment of local site effects and to the reduction of seismic risk. Reference spectra have been selected according to the type of soil and expected Magnitude. Influence of the variability of soil properties and input motion on the response spectra is considered. Identification of the type of soil has been accomplished by means of both shear wave velocity profile ($V_{s,30}$) and penetration test results (N_{spt}). The limitations and capabilities of SPT is discussed. The relevant prescriptions of recently established Italian codes (OPCM - 3274 2003, Norme Tecniche per le Costruzioni 2005), which represent a partial implementation of EC8 in Italy, are also discussed.

INTRODUCTION

EC8 (1998) part 1, prescribes two sets (Type 1 & 2) of elastic response spectra, depending on the expected Magnitude of the design earthquake. Each set consists of five different spectra which depend on the type of soil. More precisely:

- the shape of the elastic response spectrum is taken the same for both the Ultimate Limit State (ULS) and the Damage Limitation State (DLS);
- the horizontal seismic action is described by two orthogonal independent components;
- the horizontal elastic response spectrum is defined by eqs. (1) to (4).

$$0 \le T \le T_B \qquad S_e(T) = a_g S[1 + \frac{T}{T_B}(\eta \cdot 2.5 - 1)] \qquad (1)$$

$$T_B \le T \le T_C \qquad S_e(T) = a_g S \cdot \eta \cdot 2.5 \qquad (2)$$

$$T_C \le T \le T_D \qquad S_e(T) = a_g S \cdot \eta \cdot 2.5 \frac{T_C}{T} \qquad (3)$$

$$T_D \le T \le 4s \quad S_e(T) = a_g S \cdot \eta \cdot 2.5 \frac{T_C T_D}{T^2} \qquad (4)$$

where: $S_e(T)$ = elastic spectrum ordinate; T = period of a SDOF system; $a_g = \gamma_I k \cdot a_{gR}$ is the design ground acceleration for type A soil, established by National Authorities, for a given reference return period T_{NCR} or reference probability of exceedance P_{NCR} in 50 years or a given life time of the construction T_L; γ_I = importance factor to account for different return period; k = modification factor to account for special regional situations; η = damping correction factor (η = 1 when the structural damping ξ = 5 %); T_B, T_C = limits for constant acceleration; T_D limit beyond which the elastic response displacement is constant; S = soil parameter.

National annexes should define appropriate values of k (it is suggested to assume k = 1) and, trough zonation maps, a_{gR}. Simple relationships are suggested between return period (T_R), probability of exceedance (P_R), life time of the construction (T_L) and importance

factor (γ_I):

$$T_R = -\frac{T_L}{\ln(1-P_R)} \quad (5)$$

$$\gamma_I = \left(\frac{P_{LR}}{P_L}\right)^{1/3} = \left(\frac{T_L}{T_{LR}}\right)^{1/3} \quad (6)$$

where: P_{LR} and T_{LR} are respectively reference probability of exceedance and life time of the construction.

Parameter S, and periods T_B, T_C, T_D depend on the type of soil. Table 1 and 2 summarize respectively for Type 1 & 2 elastic spectra the values prescribed for the above parameters. Type 2 elastic spectra should be used in the case that the earthquakes which mostly contribute to the seismic hazard (in the framework of a probabilistic approach) have Magnitude of surface wave $M_S \geq 5.5$.

Table 1 Parameters for type 1 Horizontal Elastic Spectrum

Soil	S	T_B (s)	T_C (s)	T_D (s)
A	1.0	0.15	0.40	2.0
B	1.2	0.15	0.50	2.0
C	1.15	0.20	0.60	2.0
D	1.35	0.20	0.80	2.0
E	1.4	0.15	0.50	2.0

Table 2 Parameters for type 2 Horizontal Elastic Spectrum

Soil	S	T_B (s)	T_C (s)	T_D (s)
A	1.0	0.05	0.25	1.2
B	1.35	0.05	0.25	1.2
C	1.5	0.10	0.25	1.2
D	1.8	0.10	0.30	1.2
E	1.6	0.05	0.25	1.2

Italian codes (OPCM – 3274 2003, Norme Tecniche per le Costruzioni 2005) define elastic spectra using equations (1) to (4), but different spectra are prescribed for ULS and DLS. The parameters that should be used for the ULS are reported in Table 3.

Table 3 Parameters for ULS Horizontal Elastic Spectrum (Italian Code)

Soil	S	T_B (s)	T_C (s)	T_D (s)
A	1.0	0.15	0.40	2.0
B, C, E	1.25	0.15	0.50	2.0
D	1.35	0.20	0.80	2.0

Spectra, prescribed by the Italian codes, do not depend on the expected Magnitude.

Soil types are defined in the same way by EC8, OPCM – 3274 and Norme Tecniche per le Costruzioni. Such a definition is based on stratigraphic profile, average shear wave velocity of the first 30 m (V_{s30}), number of blow/(30 cm) from SPT (N_{spt}), and undrained shear strength (C_u).

Table 4 summarizes the criteria, prescribed to identify the soil type, in terms of V_{s30} and N_{spt}. The above mentioned codes also consider very loose or soft soils (S1 and S2) which are not discussed in this paper.

Table 4 Ground conditions

Soil type	V_{s30} (m/s)	N_{spt} (blow/30cm)
A	> 800	-
B	360 - 800	> 50
C	180 - 360	15 -50
D	< 180	< 15
E	(*)	-

(*) Soil type E consists of 5 to 20 m of soil like C or D underlain by soil type A. This definition is expressed in EC8 not very clearly because refer to V_{s30}.

As for the seismic zonation, the Italian codes prescribe the design acceleration of Table 5.

Table 5 Design acceleration (Italy)

Zone	PGA	a_{gR}
1	< 0.05	0.05
2	0.05 – 0.15	0.15
3	0.15 – 0.25	0.25
4	> 0.25	0.35

PGA = Peak ground acceleration from probabilistic hazard studies.

Possible introduction of sub – zone with intermediate values of a_{gR} is under discussion.

VALIDATION OF DIFFERENT CRITERIA TO IDENTIFY SOIL TYPE

Available database

The available database consists of investigations performed in 62 sites located in 34 different towns of Tuscany. For each site, data consists of the following:

- stratigraphic profile from boreholes, with SPT measurements;
- shear wave velocity (V_S) profile from Down – Hole (DH) tests performed in

the boreholes;

- shear wave velocity (V_S) profile from seismic refraction tests performed generating both compression (P) and horizontally polarized shear waves (SH);
- resonant column tests (RCT), cyclic loading torsional shear tests (CLTST), cyclic loading triaxial tests (CLTX) performed on undisturbed samples (not available for all boreholes and any type of soil);
- dynamic penetration tests (DP), performed by using a cone 51 mm in diameter and with an apex angle of 60° (hammer weight and falling height are the same as for the SPT, blowcounts every 20 cm penetration). This type of tests has been performed in few sites.

The above mentioned investigations have been performed to verify the seismic requirements of existing public constructions (schools, etc.) in the light of the new Italian codes.

Local geology

Local geology mainly consists of the formations listed in Table 6.

Table 6 Geological formations

Geological formation	Thickness (m)	Range of V_s (m/s)
Holocene debris deposits (DT)	< 15	100 – 350
Holocene alluvial deposits (ALL – CT)	< 20	250 – 500
Pleistocene alluvial terrace (CT/MG – AT)	< 15	300 – 600
Plio – Pleistocene fluvial – lacustrine deposits (ARG – CG)	< 72	500 – 800
Oligocene sandstone (MG)	-	600 – 1500
Argille – Calcari (AC) (*)	-	700 – 1400

(*) Paleocene – Eocene Claystone-Limestone

Identification of soil type from SPT (DP), DH and SH tests

Ground conditions have been identified by means of Nspt and Vs30 at 18 sites. Only in three cases different indications have been obtained. In these 3 cases SPT results classify the soils in the category immediately above or below that selected on the basis of Vs30.

On the other hand, Figure 1 clearly shows the good correlation existing between V_{s30} obtained from DH tests and that inferred from SH tests. Use of surface test is therefore recommended to save costs. In any case, intrinsic limitations of each seismic method should be considered (see as an example Lo Presti et al. 2004).

Assessment of Vs from SPT (DP)

Shear wave velocity has been inferred from penetration test results. For this purpose the Otha and Goto (1978) equation and the Schnaid (1997) approach have been used.
More precisely, Ohta e Goto (1978) equation can be written in the following way:

$$V_s = 69 \cdot N_{60}^{0.17} \cdot Z^{0.2} \cdot F_A \cdot F_S \qquad (7)$$

where:
V_s = Shear wave velocity in m/s
N_{60} = blowcounts/30 cm normalized to an Energy Ratio ER = 60 %
Z = depth in m
F_A, F_S = Correction factors which accounts for deposit age and soil composition.

Penetration test results, terminated at 50 blowcounts, have been linearly extrapolated by considering the effective penetration after 50 blows.
DP test results have been converted into N_{60} by multiplying the data by 1.83 to account for different penetration and ER (usually 60 % in SPT and 74% in DP).

Comparison of shear wave velocities inferred from penetration tests, using Otha e Goto (1978) equation,and those directly measured in DH tests is shown in Figure 2. The Figure clearly shows that eq. (7), on average, underestimate of about 38 % the measured values with a SD of about 205 m/s. In any case, the correlation is quite poor.

More recently, Schnaid (1997) proposed empirical correlations between $\mathrm{Log}V_s/(N_1)_{60}$ & $\mathrm{Log}(N_1)_{60}$. This correlation has the advantage that, unlike Otha e Goto (1978) eq., the knowledge of soil composition is not necessary.

Figure 3 shows the experimental values of $\mathrm{Log}V_s/(N_1)_{60}$ & $\mathrm{Log}(N_1)_{60}$. The Figure also shows the empirical correlation obtained by regression analysis of the data.

$$\mathrm{Log}\left(\frac{V_s}{(N_1)_{60}}\right) = -0.927 \cdot (N_1)_{60} + 2.52 \qquad (8)$$

Figure 4 shows the shear wave velocities measured in DH tests and those inferred using eq. (8). Figure 4 clearly shows very poor correlation between measured and computed shear wave velocity.

Correlations between shear wave velocity and penetration resistance should be used very cautiously. It is recommended to use only correlations established for a specific site.

COMPUTED VS. PRESCRIBED RESPONSE SPECTRA

Elastic response spectra (ξ = 5%) have been computed at 19 different sites by means of 1D equivalent – linear analyses run by means of EERA (Bardet et al. 2000). Analyses have been repeated to accounts for local variability of shear wave velocity of strata.

The local variability refers to that observed at a given site by comparing stratigraphic profile, DH and SH data.

Laboratory tests (Resonant Column Test – RCT, Cyclic Loading Torsional Shear Test – CLTST, Cyclic Loading Triaxial Test – CLTX) were used to determine the variation of stiffness (G) and damping ratio (D) with shear strain (γ). For a given geologic formation the variability of stiffness and damping ratio has been considered by repeating the computations with the upper and lower envelopes of the G/Go-γ D-γ curves. Because of the limited number of laboratory tests, in comparison to the extension of the investigated area, the whole variability of a given geologic formation has been considered.

Input motion (accelerograms at the rock outcrop) has been obtained by means of the following procedure (Mensi et al. 2004, Lai et al. 2005):

- definition of PGA at each site by means of standard probabilistic hazard analysis;
- de-aggregation of the hazard analysis (T_R = 475 years) to obtain the Magnitude- distance couple which mostly contribute to determine the hazard. The following couples have been obtained: M=5.3 d=10.2 km (Mensi et al. 2004), M=5.4 d= 13 km (Lai et al. 2005);
- selection of free-field natural accelerograms seismically compatible with the M-d couples, given a certain tolerance. The largest tolerance was adopted by Lai et al. 2005 in order to guarantee the compatibility with the elastic response spectra prescribed by the Italian code. More specifically a tolerance of ΔM=0.2-0.5 and Δd=9-17 km and 5-20 km were adopted by Lai et al. (2005).

On the basis of the above described procedure, three accelerograms selected by Mensi et al. 2004 (A1, A2, A3) and another three selected by Lai et al. 2005 (A6.1, A6.2, A6.3) have been used.

As an alternative, an artificial accelerogram, obtained from the probabilistic elastic spectrum on rock, was used (Ferrini et al. 2000).

Figures 5a to 5f and 6a to 6f summarize respectively the G/Go-γ and D-γ curves used for the different geologic formations and the experimental data. Figures 7a to 7g show the input accelerograms.

It is worthwhile to remark that in the case of alluvial deposit (ALL) the plotted data refer to both undisturbed gravel samples, retrieved by means of in situ freezing method (Lo Presti et al. 2005) and undisturbed silty sand samples retrieved by means of conventional methods.

For each of the seven selected accelerograms the analyses summarized in Table 7 have been done.

Table 7 analyses performed

Case Number	Vs (bedrock)	Vs (surface layers)	G-γ D-γ envelopes
1	Max	Min	Max
2	Max	Min	Min
3	Min	Min	Max
4	Min	Min	Min
5	Max	Max	Max
6	Max	Max	Min

To evaluate analysis results, PGA, normalized elastic response spectra and a synthetic amplification parameter have been considered.

The amplification parameter is defined in the following way:

$$F_a = \frac{\int_{0.1}^{0.5} \text{PSA(deposit)}}{\int_{0.1}^{0.5} \text{PSA(outcrop)}} \qquad (9)$$

where: PSA = spectral acceleration computed at the top of the deposit or at outcrop, integrated between 0.1 and 0.5 s (corresponding to the most recurrent periods of the constructions existing in the study area).

The above definition of a synthetic amplification parameter is similar to that proposed by Pergalani et al. (1999).

Figures 8a to 8c show the PGA obtained at the top of soil deposits, by means of linear equivalent analyses at three sites, classified respectively as Type A, B and C soils.

Figure 8a refers to type A soil. Obviously, for this case no amplification exists and effects of different ground conditions and input accelerograms seems negligible. The level of a_{gR} (OPCM), prescribed by the Italian code for that area, according to the criteria shown in Table 5, and the PGA obtained from hazard study, are also reported in the Figure. The degree of conservativisme introduced by the criteria listed in Table 5 is evident.

Figures 8b and 8c refer to type B and C soil respectively. In these Figures the effect of both input accelerograms and ground conditions on PGA is seen. It appears that the variability of PGA because of differences in ground conditions is comparable to that due to differences in input motion.

Design accelerations have been plotted in Figures 8b and 8c. The design accelerations have been obtained multiplying a_{gR}, prescribed by the Italian Code, by the soil factor S prescribed for type B and C soils by OPCM 3274 (2003) and those prescribed by EC8 for the same type of soils in the case of type 1 (EC8-1) and 2 (EC8-2) spectra. It is evident that in some cases the prescribed design accelerations are lower than that obtained from linear – equivalent seismic response analyses, nonetheless the conservativisme introduced by Table 5 (OPCM).

Table 8 summarizes the average PGA, obtained from calculations for the three sites, and the design accelerations prescribed by OPCM and EC8.

Table 8 Computed PGA and prescribed design accelerations

Soil type	PGA(*)	OPCM	EC8-1	EC8-2
A	0.176	0.250	0.250 (-)	0.250 (-)
B	0.330	0.312	0.300	0.338
C	0.385	0.312	0.288	0.375

(*) Average; (-) value from Table 5

It is clear that for type B soil the case EC8-2 gives values of the design acceleration greater than that computed, while for type C soil the prescribed value is slightly lower than that computed. Not considering soil type A, where the above considerations are meaningless, the other cases (OPCM, EC8-1) prescribe design accelerations lower than those computed.

A general comparison between computed and prescribed design accelerations is reported in Table 9. More specifically, Table 9 indicate, for the 19 investigated sites the percentage of cases where the following condition is observed $F_a * PGA > Sa_{gR}$ (where: F_a is the synthetic amplification parameter, computed according to eq. 9; PGA = Peak Ground Acceleration on rock obtained from hazard analysis; S is the soil factor prescribed by OPCM and EC8; a_{gR} = design acceleration on rock as prescribed by OPCM, see Table 5).

Table 9

Condition	% of cases		
	OPCM	EC8-1	EC8-2
$F_a * PGA > Sa_{gR} + 0.025g$	39	43	7.0
$F_a * PGA > Sa_{gR} + 0.050g$	21	25	3.5
$F_a * PGA > Sa_{gR} + 0.150g$	3.5	3.5	3.5

It is therefore confirmed that only for the case EC8-2 the values of the soil parameter S, together with the prescriptions of the Italian code for the design acceleration on rock (Table 5) give design acceleration values greater than those prescribed, with very few exceptions.

A comparison between the computed

response spectra and the prescribed ones is shown in Figures 9a-b-c and 10a-b-c. The computed spectra have been normalized with respect to the PGA on rock, while the prescribed ones have been divided by a_{gR} of Table 5.

Figures clearly show that both input motion and ground conditions influence the response spectra. More specifically:

- natural accelerograms, (A1, A2, A3) selected to represent earthquakes with M=5.4 and d=13 km, lead to high spectral accelerations (PSA) in the high frequency range (T=0.1-0.2s) while PSA are much smaller than that prescribed by EC8 and OPCM 3274 at T>0.2 s;
- the second set of natural accelerograms (A6.1, A6.2, A6.3), selected considering a range of Magnitude and distances (ΔM=0.2-0.5; Δd=9-17 km; 5-20 km), give tha same picture, but the PSA spikes in the high frequency range are less pronounced and, at larger periods (T>0.2s) there is a better agreement between prescribed and computed spectra;
- the artificial accelerogram leads, on the whole, to a better agreement between computed and prescribed spectra;
- computed PSA may be greater than prescribed PSA for the most unfavorable ground conditions;
- Figures 9a-b-c and 10a-b-c are representative of sites where the average computed PGA at the top of soil deposit is greater than the prescribed one (about 40 % of the analyzed cases).

Figure 11 shows the average response spectrum obtained for a type B soil falling in the category where the computed PGA, at the top of soil deposit, is smaller than that prescribed. It is possible to see that the prescribed spectrum (EC8-2) is conservative for the full range of periods. In addition, it should be considered that the OPCM 3274 (2003) prescribe values of a_{gR} which are often much greater than those computed through hazard studies.

CONCLUSIONS

The following conclusions can be drawn:

- use of penetration test results to infer shear wave velocity profiles should be discouraged;
- it is recommended to use only correlations (N_{spt} – V_s) established for a specific site and only in the case of spatially uniform soil deposits;
- N_{spt} and V_s lead to consistent definition of soil type;
- use of seismic methods, even if not very accurate like seismic refraction with SH waves, is recommended as an economic way to determine the V_{s30} parameter;
- it is suggested to change the definition of soil type E in Table 3.1 (Ground Conditions) in the following way: “A surface alluvium like soil type C and D with thickness in between 5 to 20 m underlain by stiffer material like soil type A”;
- for the considered sites, mainly classified as type A, B and C soils, which are very popular, especially in the Mediterranean areas, the EC8 type 2 spectra and soil parameters (S) seem appropriate. The Magnitude which mainly contribute to the hazard of the considered sites is just below 5.5. The positive evaluation of EC8-2 spectra holds if prescribed PGA on type A soil of Table 5 are used.

ACKNOWLEDGEMENTS

The authors wouod like to thank dr. Ferrini (R.T.) for making available the database.

REFERENCES

Bardet, J.P., Ichii, K. and Lin C.H. (2000). “EERA – A Computer Program for Equivalent-Linear Earthquake Site Response Analyses of Layered Soil Deposits.”, Department of Civil Engineering, University of Southern California, http://geoinfo.usc.edu/gees.

Ferrini M. (coord.), Foti S., Lo Presti D., Luzi L., Pergalani F. Petrini V. Pochini A., Puccinelli A., Signanini P. & Socco V. 2000 *La riduzione del rischio sismico nella pianificazione del territorio: le indagini geologico tecniche e geofisiche per la*

valutazione degli effetti locali, CISM, Lucca 3-6 Maggio 2000.

Lai C., Strobbia C., Dall'ara (2005) Elaborazione di raccomandazioni e di linee guida per la definizione dell'input sismico e delle modellazioni da adottare nei territori della Regione Toscana nell'ambito dei progetti VEL – Parte 1. Eucentre Pavia Report

Lo Presti D., Lai C. & Foti S. 2004, Geophysical and Geotechnical Investigations for ground response analyses, in Recent Advances in Earthquake Geotechnical Engineering and Microzonation, Kluwer Academic Publisher, Editor A. Ansal, Capitolo di un libro. pp: 101-138.

Lo Presti D., Pallara O., Froio F., Rinolfi A., Jamiolkowski M. 2005 Stress-Strain-Strength Behaviour of Undisturbed and Reconstituted Gravely Soil Samples Submitted to RIG for possible publication, September 2005

Mensi E., Lai C., Spallarossa D. Pallara O. & Lo Presti D. (2004) Risposta sismica in alcune aree della Toscana : un confronto con le indicazioni dell'Ordinanza dell'OPCM 3274. Politecnico di Torino, Department of Structural and Geotechnical Engineering Report.

Norme Tecniche per le Costruzioni (2005) Ministero delle Infrastrutture e dei Trasporti. Decreto 14 Settembre 2005.

OPCM 3274 (2003) Primi elementi in materia di criteri generali per la classificazione sismica del territorio nazionale e di normative tecniche per le costruzioni in zona sismica. *Gazzetta Ufficiale della Repubblica Italiana 8 maggio 2003, n. 108.*

Ohta Y. & Goto N. (1978). Empirical Shear Wave Velocity Equations in Terms of Characteristic Soil Indexes. *Earthquake Engineering and Structural Dynamics*. 6.

Pergalani F., Romeo R., Luzi L., Petrini V., Pugliese A., Sano T. 1999. Seismic microzoning of the area struck by Umbria-Marche (Central Italy)Ms 5.9 earthquake of 26 september 1997. Soil Dyn. and Earth. Eng. 18, pp. 279-296.

Schnaid F. 1997 Panel Discussion. Evaluation of in situ tests in cohesive frictional materials. 14th Int. Conf. on SMGE. Hamburg. 4: 2189-2190

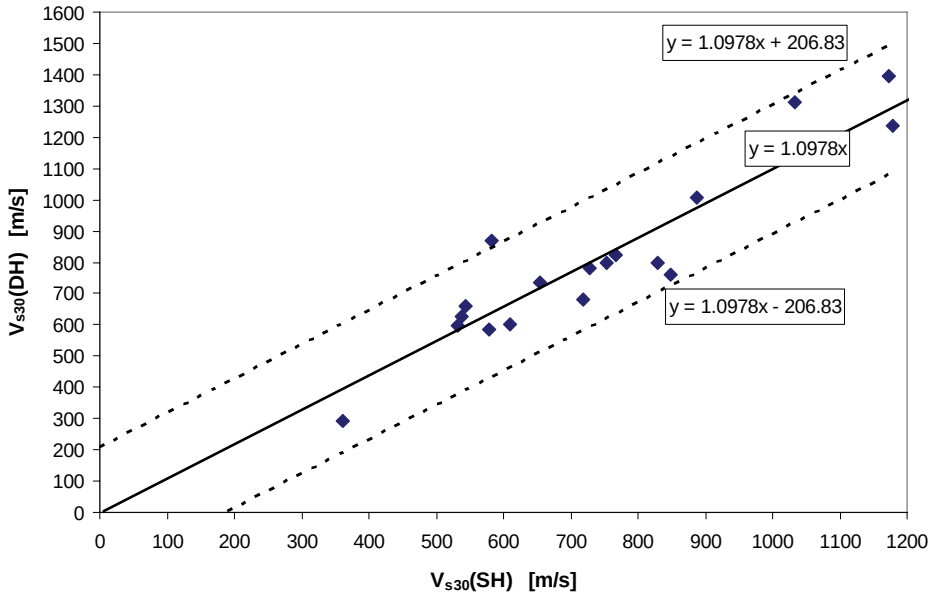

Fig 1: Average shear wave velocity from down-hole tests [V_{S30} (DH)] vs. that obtained from seismic refraction [V_{S30} (SH)]

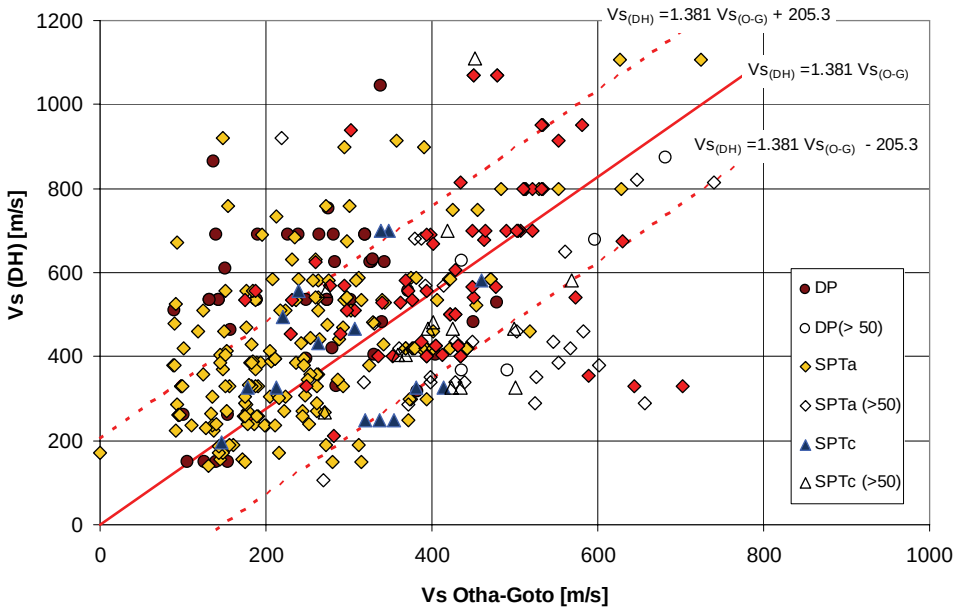

Fig 2: Measured shear wave velocity in down-hole tests vs. that inferred from N_{SPT} by means of Otha and Goto equation

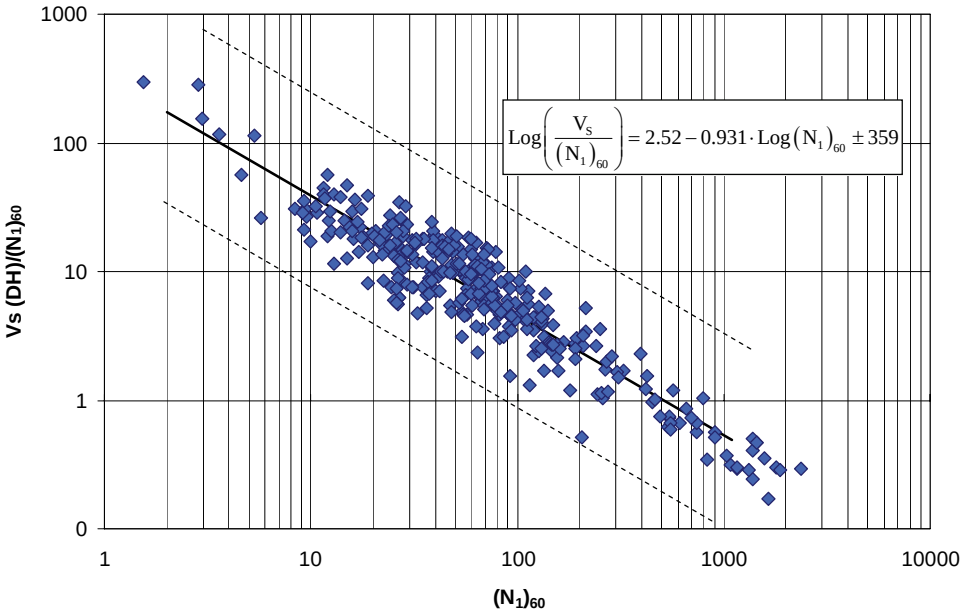

Fig 3: Normalized shear wave velocity vs. $(N_1)_{60}$ according to Schnaid (1997) approach

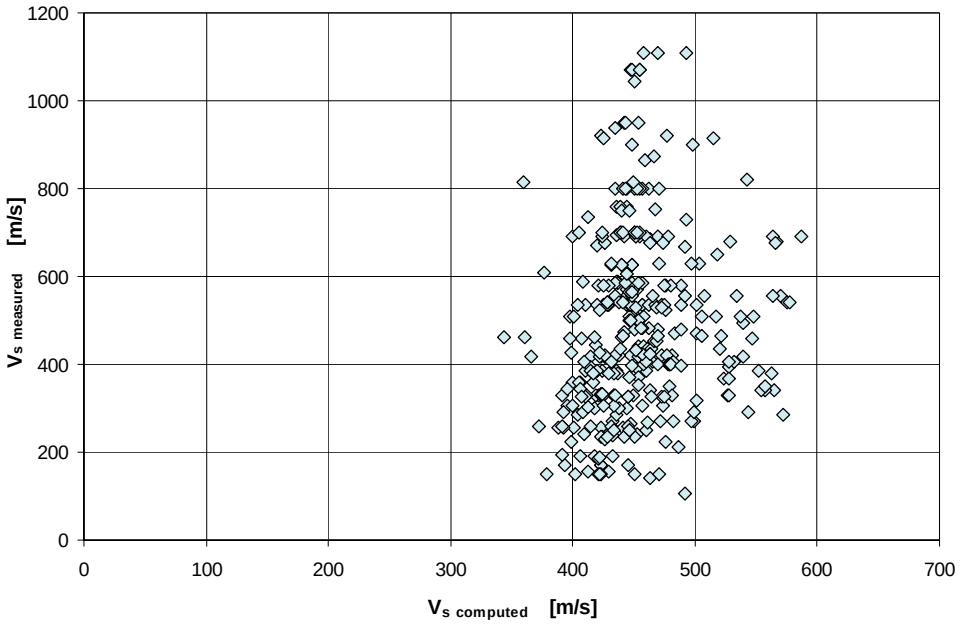

Fig 4: Measured (down-hole tests) vs. computed (according to Schnaid, 1997) shear wave velocity

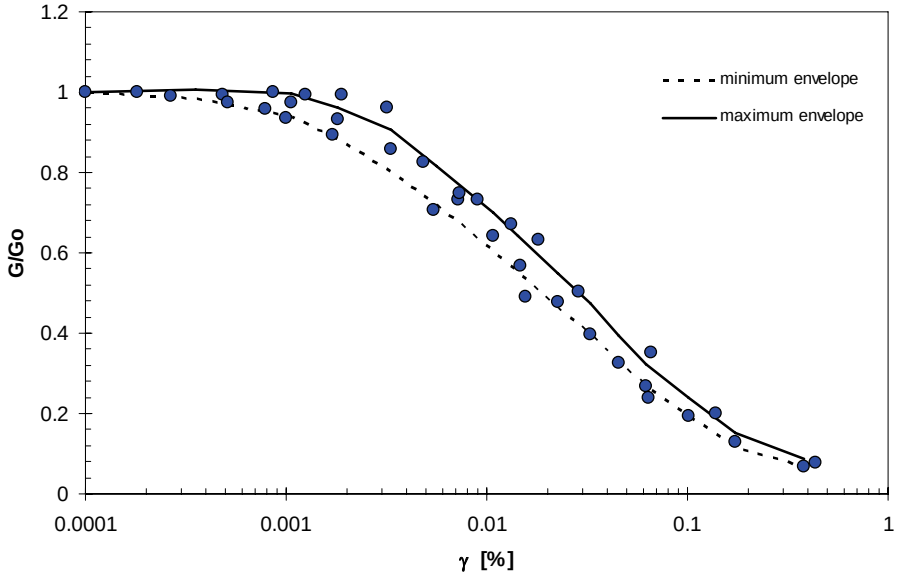

Fig 5a: Normalized stiffness vs. shear strain for Holocene Debris deposits (DT)

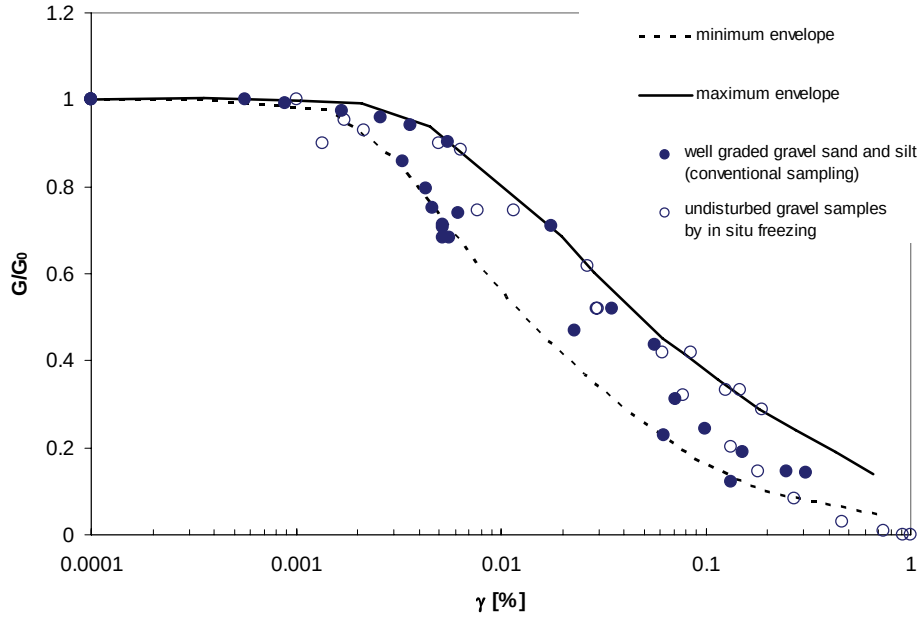

Fig 5b: Normalized stiffness vs. shear strain for Holocene Alluvial deposits (ALCT)

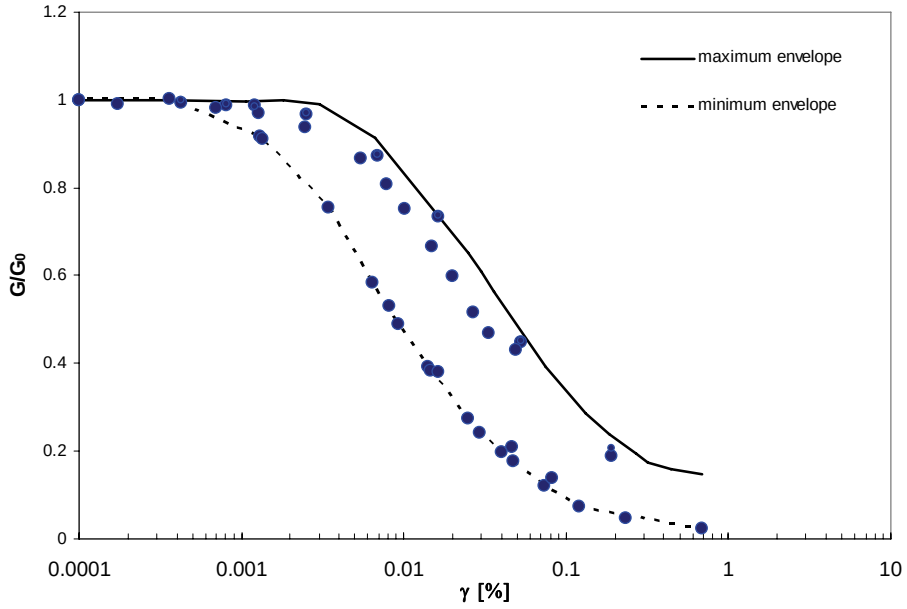

Fig 5c: Normalized stiffness vs. shear strain for Pleistocene Alluvial terrace (CT/MG-AT)

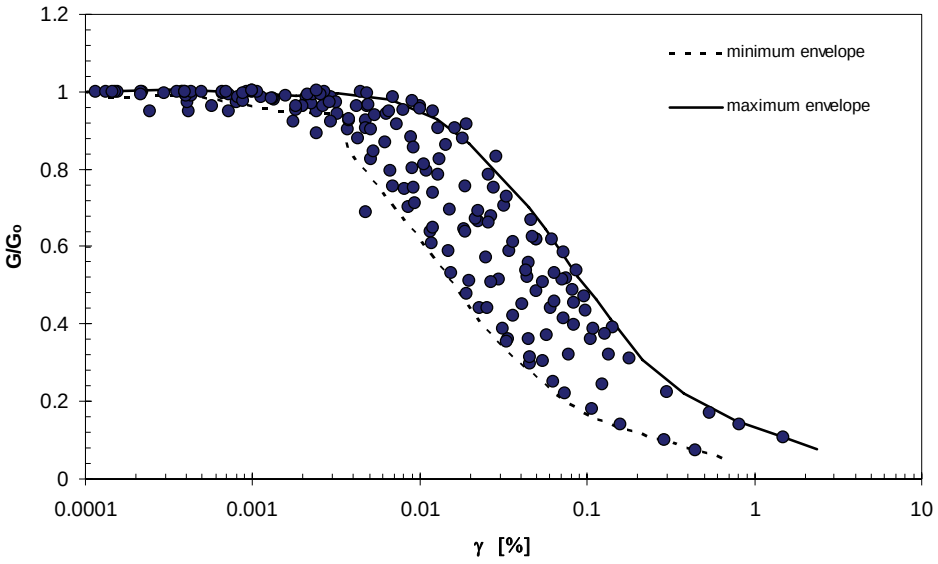

Fig 5d: Normalized stiffness vs. shear strain for Fluvial Lacustrine formations from Plio-Pleistocene (ARG-CG)

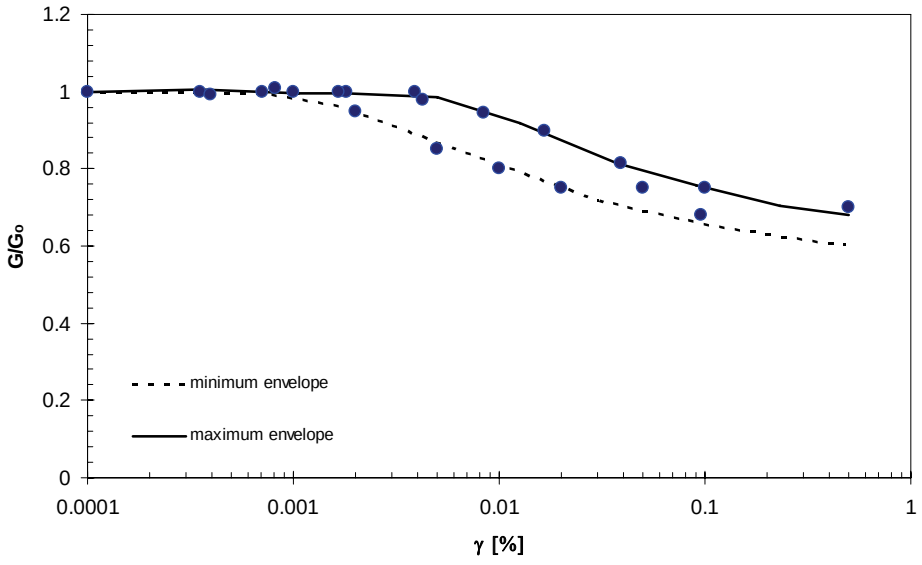

Fig 5e: Normalized stiffness vs. shear strain for Oligocene Sandstone (MG)

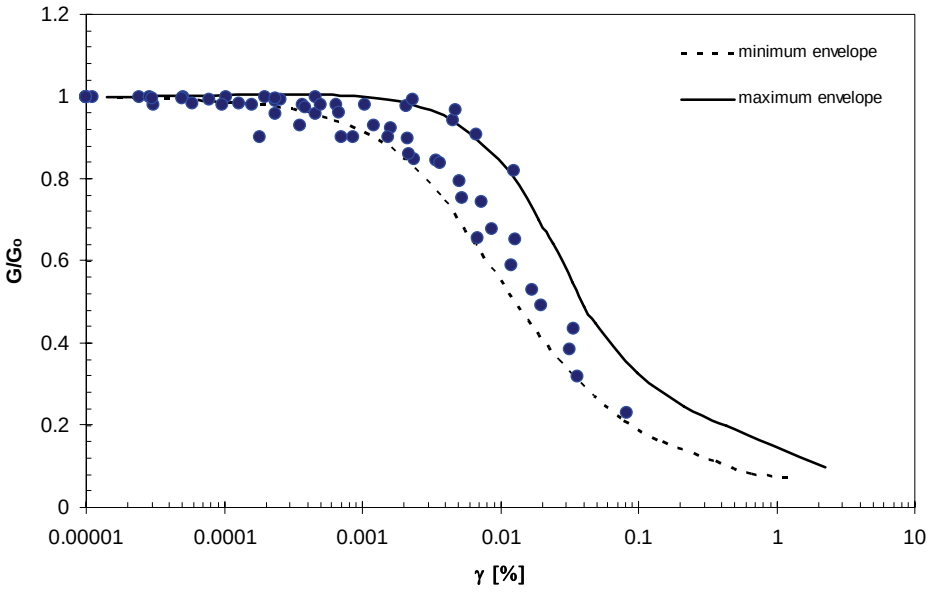

Fig 5f: Normalized stiffness vs. shear strain for Paleocene-Eocene claystone-limestone (AC)

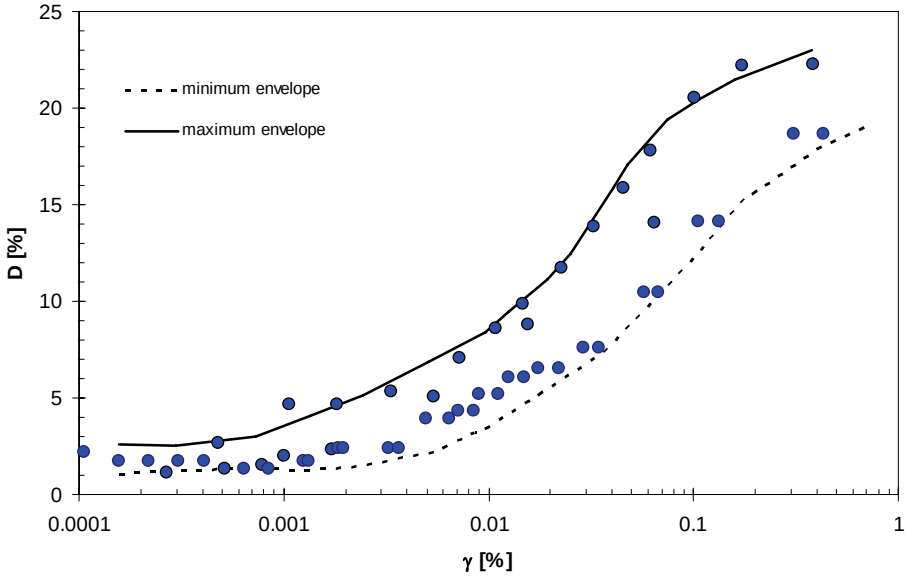

Fig 6a: Damping vs. shear strain for Holocene Debris deposits (DT)

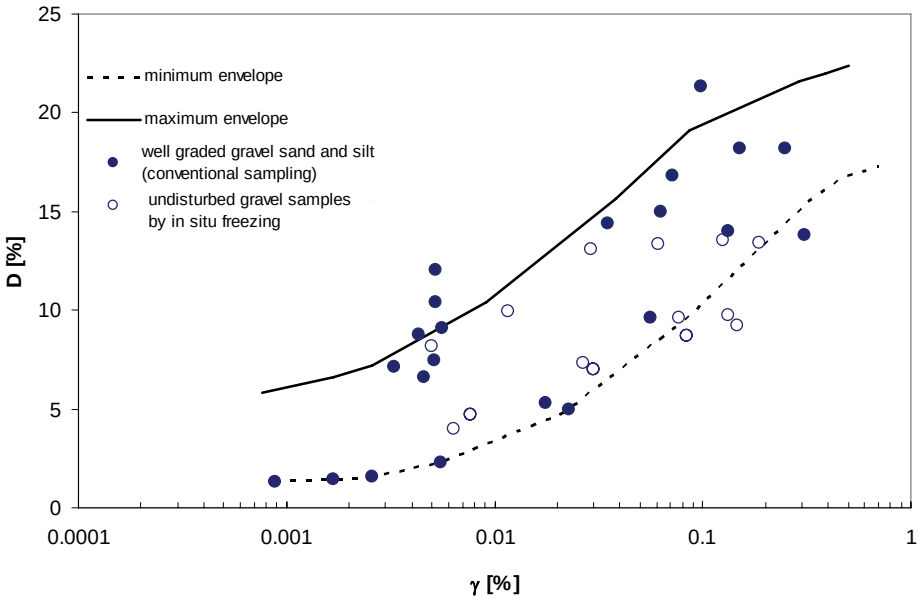

Fig 6b: Damping vs. shear strain for Holocene Alluvial deposits (ALCT)

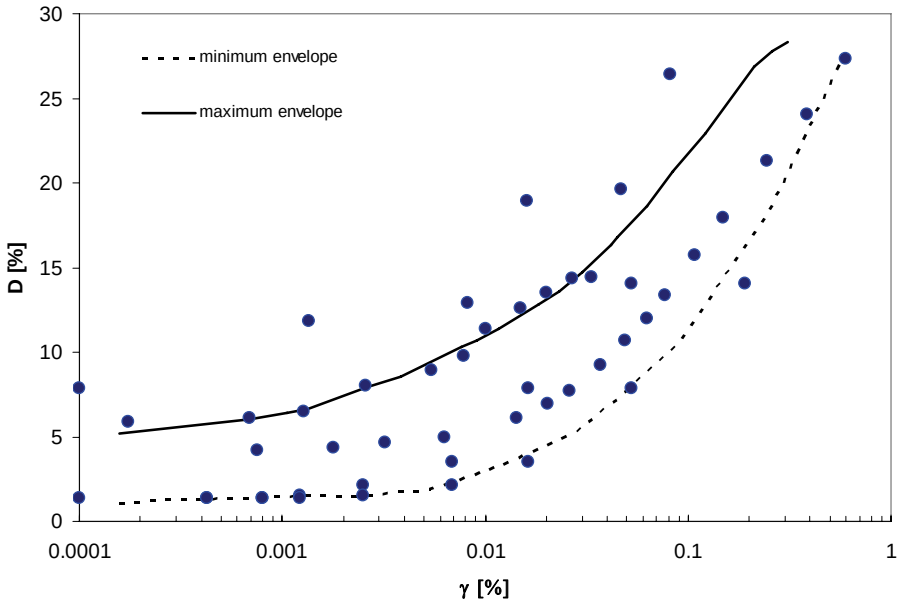

Fig 6c: Damping vs. shear strain for Pleistocene Alluvial terrace (CT/MG-AT)

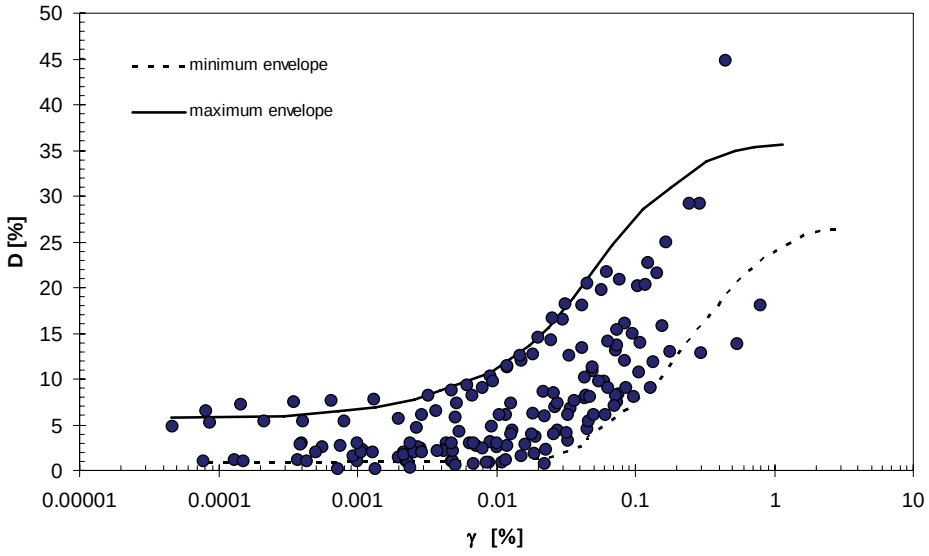

Fig 6d: Damping vs. shear strain for Fluvial Lacustrine formations from Plio-Pleistocene (ARG-CG)

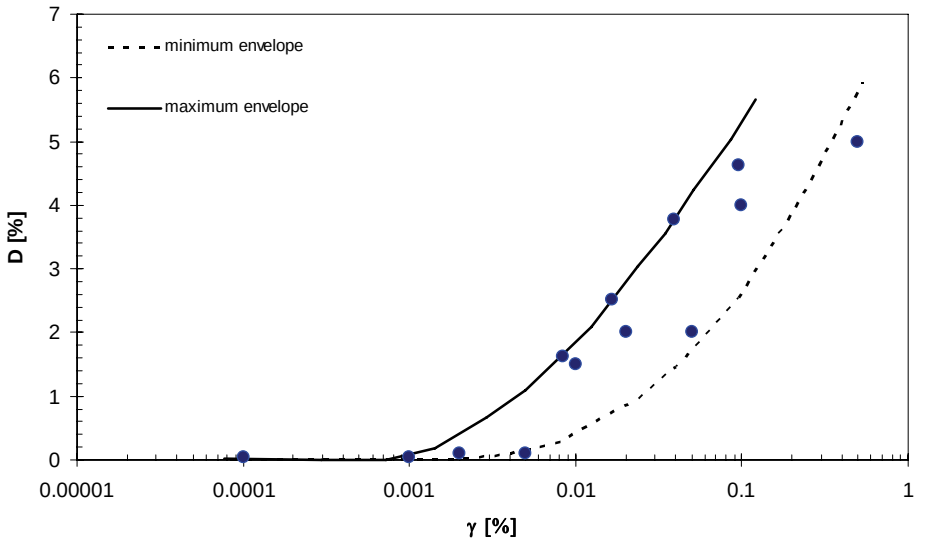

Fig 6e: Damping vs. shear strain for Oligocene Sandstone (MG)

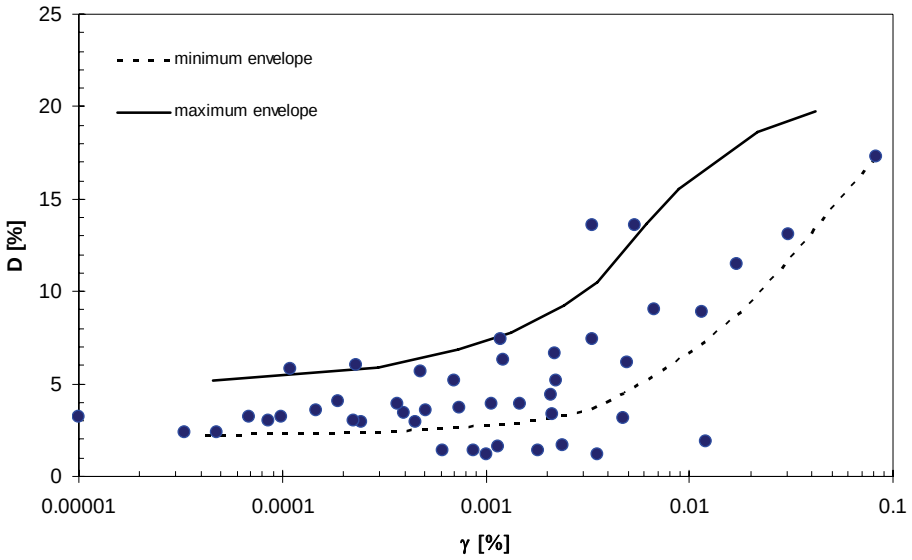

Fig 6f: Damping vs. shear strain for Paleocene-Eocene claystone-limestone (AC)

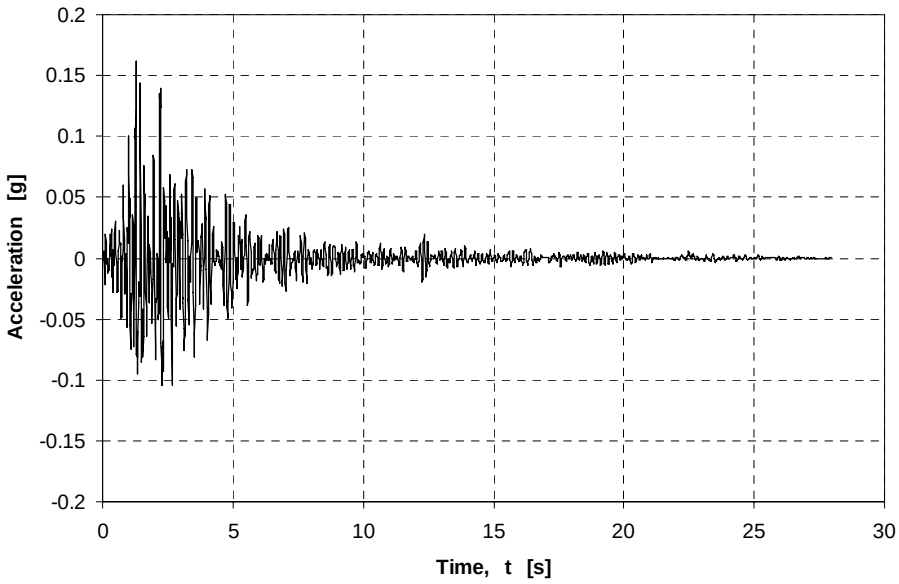

Fig 7a: Accelerogram A1 (Lazio - Italy, 1984 - Mensi et al. 2004)

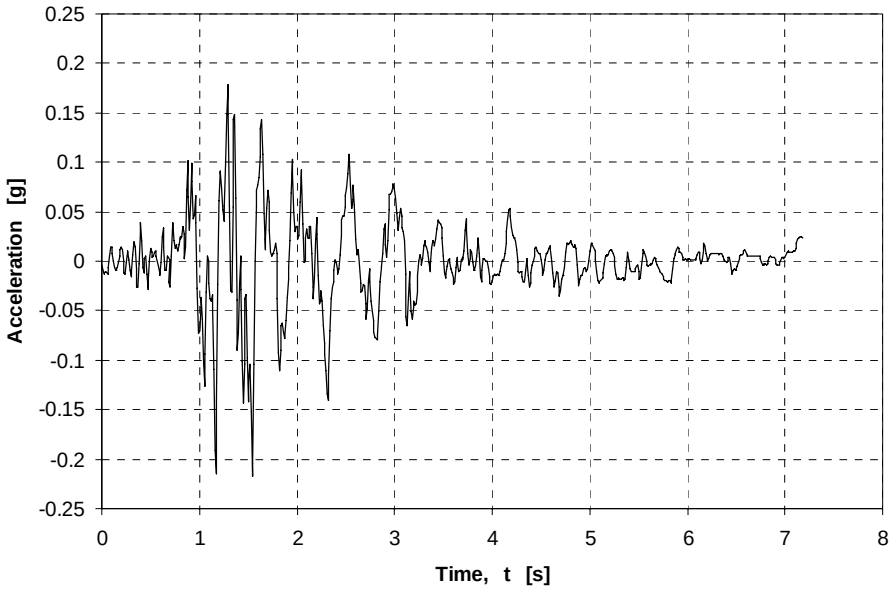

Fig 7b: Accelerogram A2 (Arnaia - Greece, 1985 - Mensi et al. 2004)

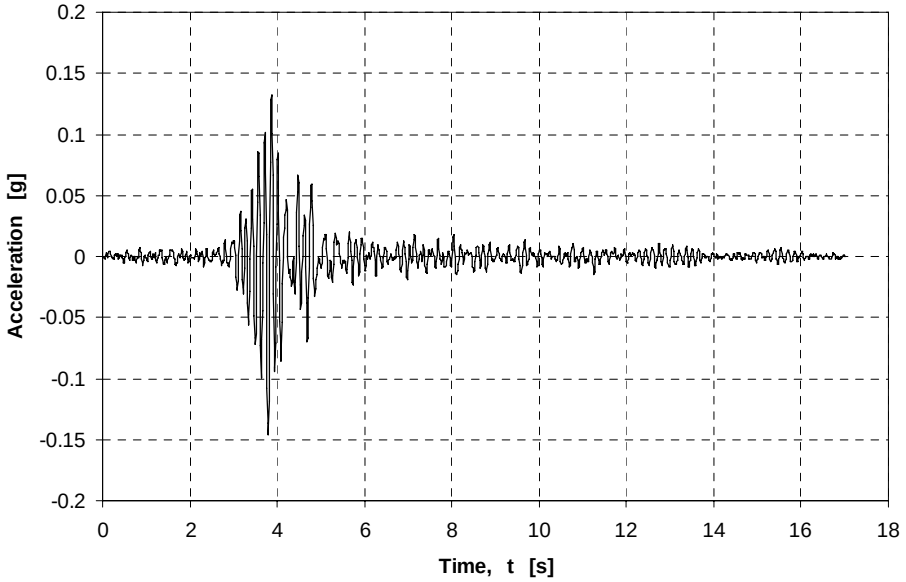

Fig 7c: Accelerogram A3 (Dursunbey - Turkey, 1979 - Mensi et al. 2004)

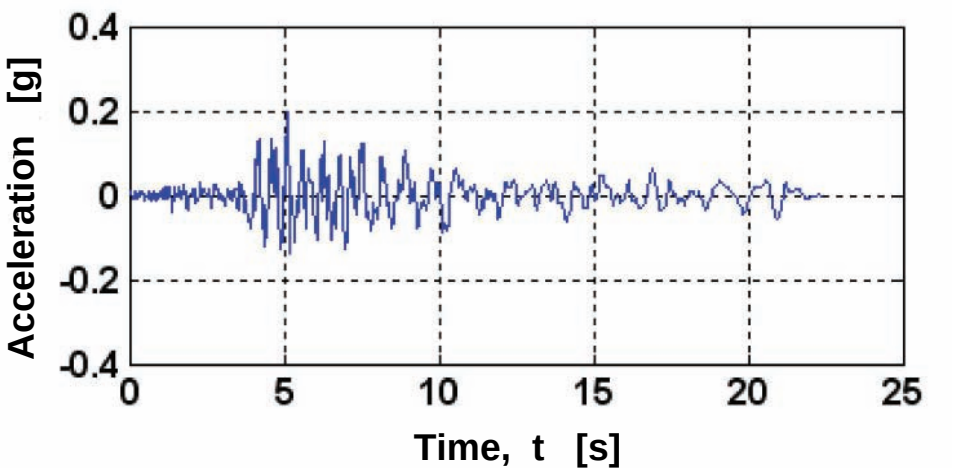

Fig 7d: Accelerogram A6.1 (Umbria/Marche - Italy, 1997 - Lai et al. 2005)

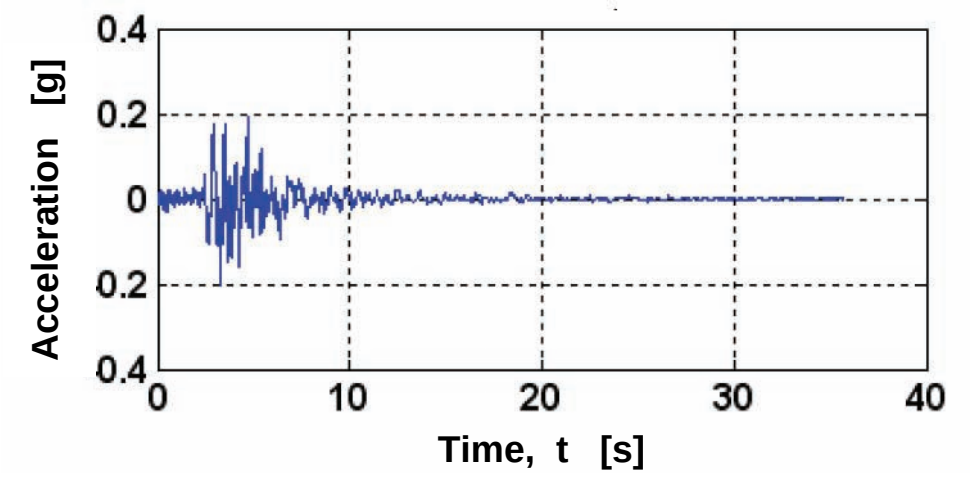

Fig 7e: Accelerogram A6.2 (Athene - Greece, 1999 - Lai et al. 2005)

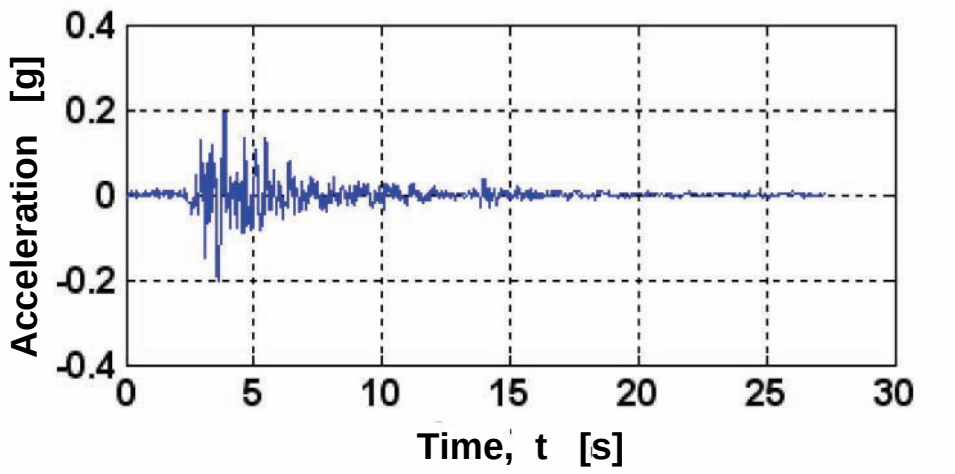

Fig 7f: Accelerogram A6.3 (North Algeria, 1980 - Lai et al. 2005)

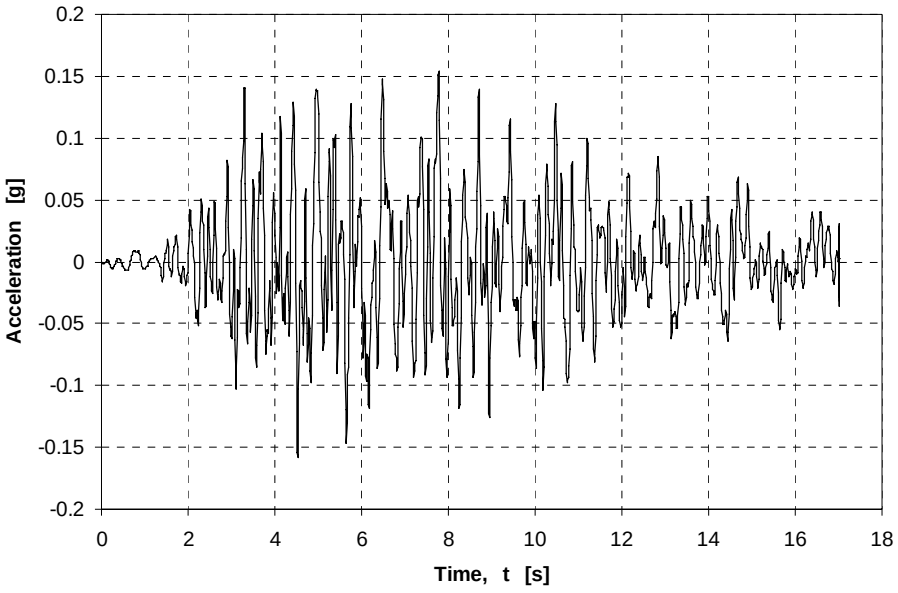

Fig 7g: Artificial accelerogram A7 (Ferrini etal. 2000)

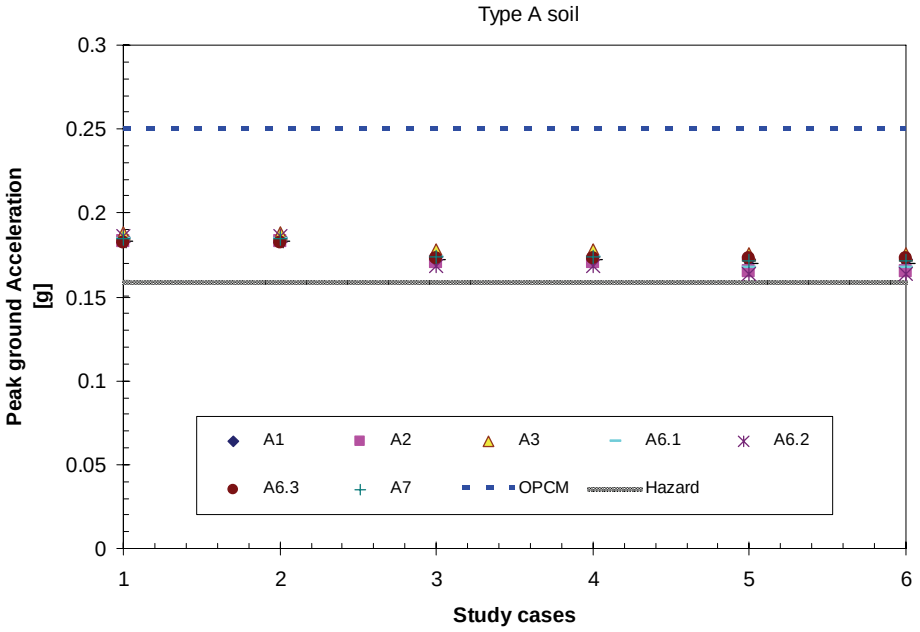

Fig 8a: Computed vs. prescribed PGA (type A soil)

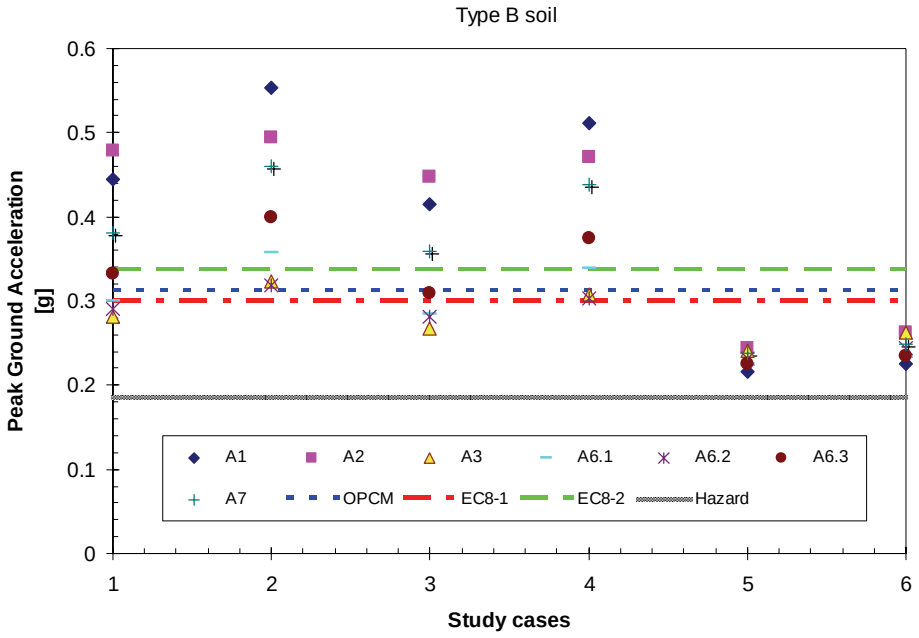

Fig 8b: Computed vs. prescribed PGA (type B soil)

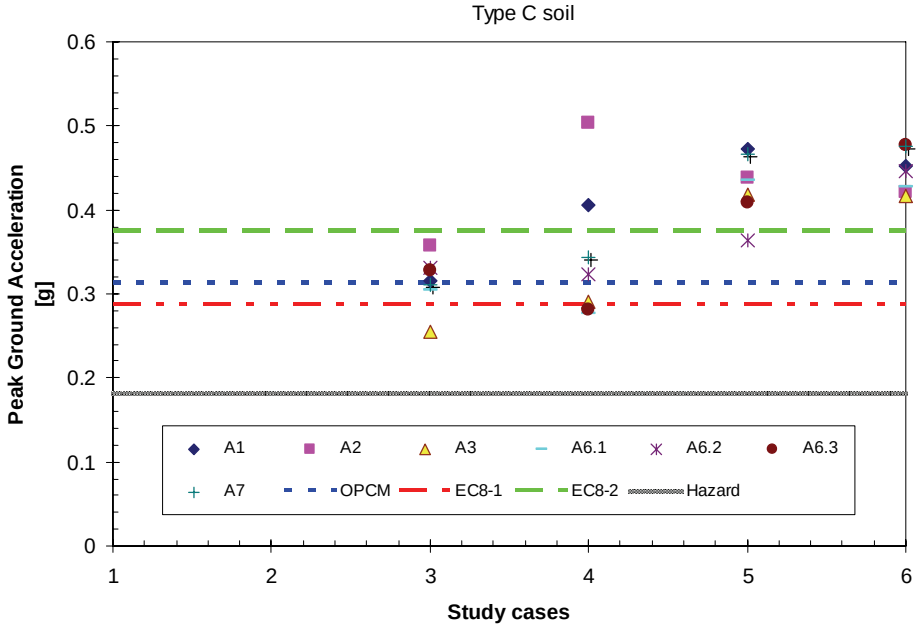

Fig 8c: Computed vs. prescribed PGA (type C soil)

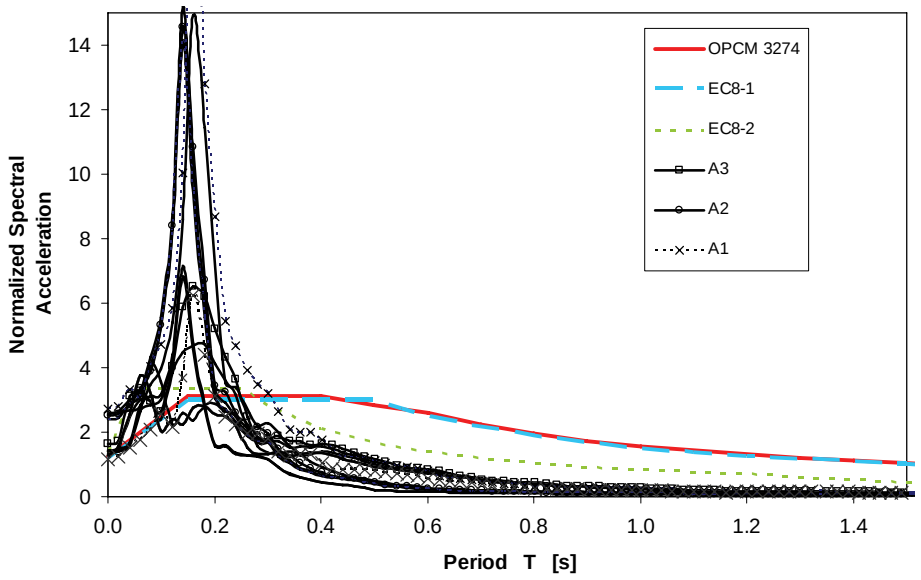

Fig 9a: Elastic Response spectrum – Type B soil – accelerograms A1-A2-A3: M = 5.3 d = 10.2 km

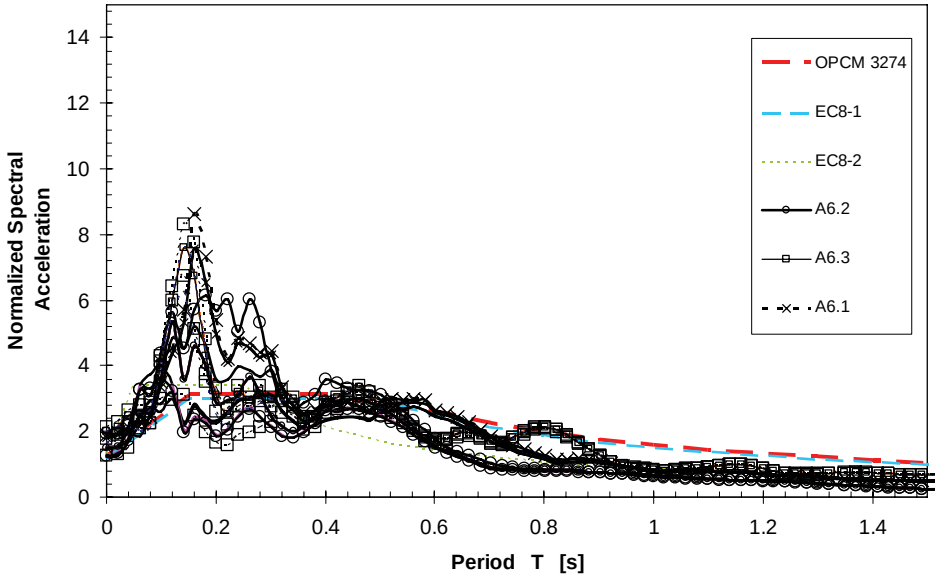

Fig 9b: Elastic Response Spectrum – Type B soil – Accelerograms A6.1-A6.2-A6.3: ΔM = 0.2-0.5 Δd = 9-17; 5-20 km

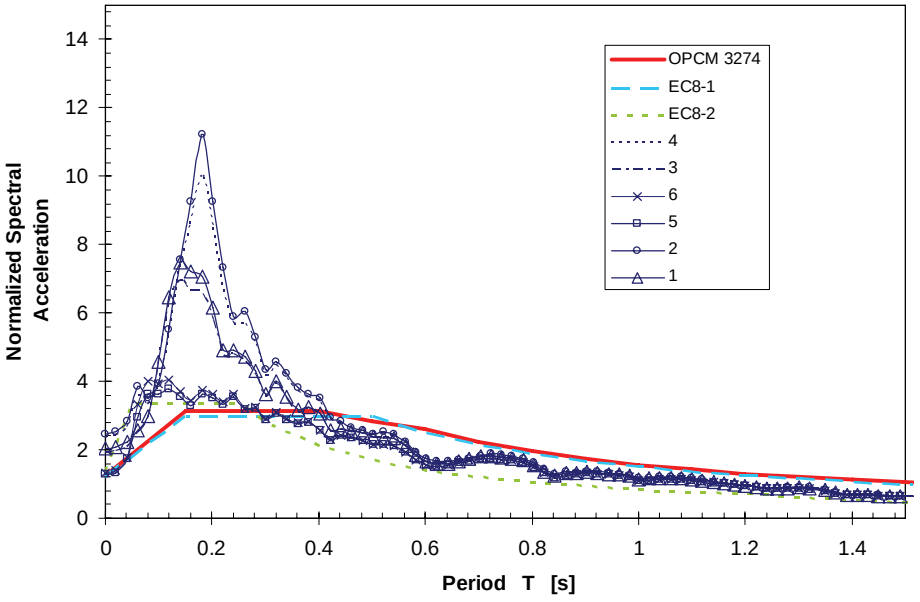

Fig 9c: Elastic Response spectrum – Type B soil (artificial accelerogram)

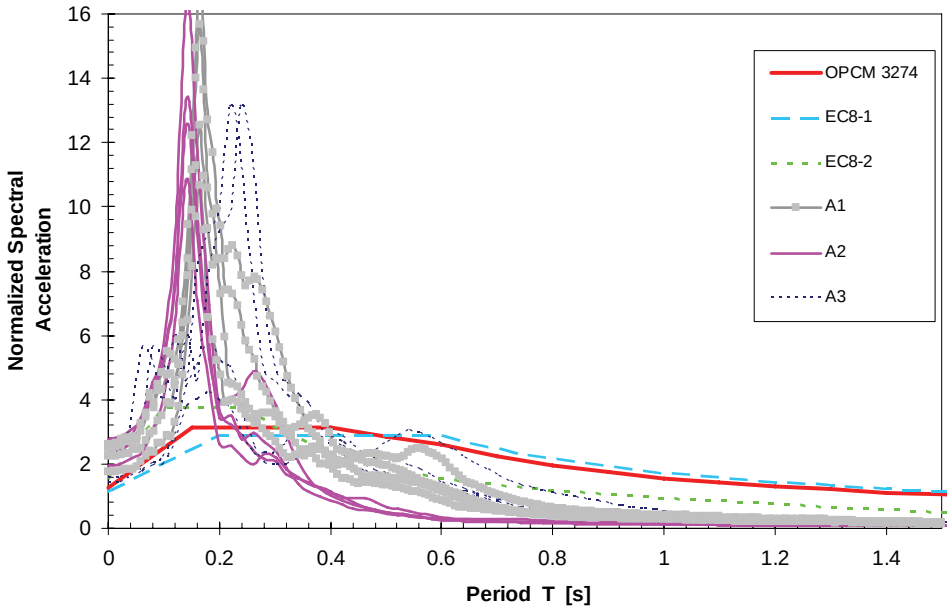

Fig 10a: Elastic Response Spectrum – Type C soil – Accelerograms A1-A2-A3: M = 5.3 d = 10.2 km

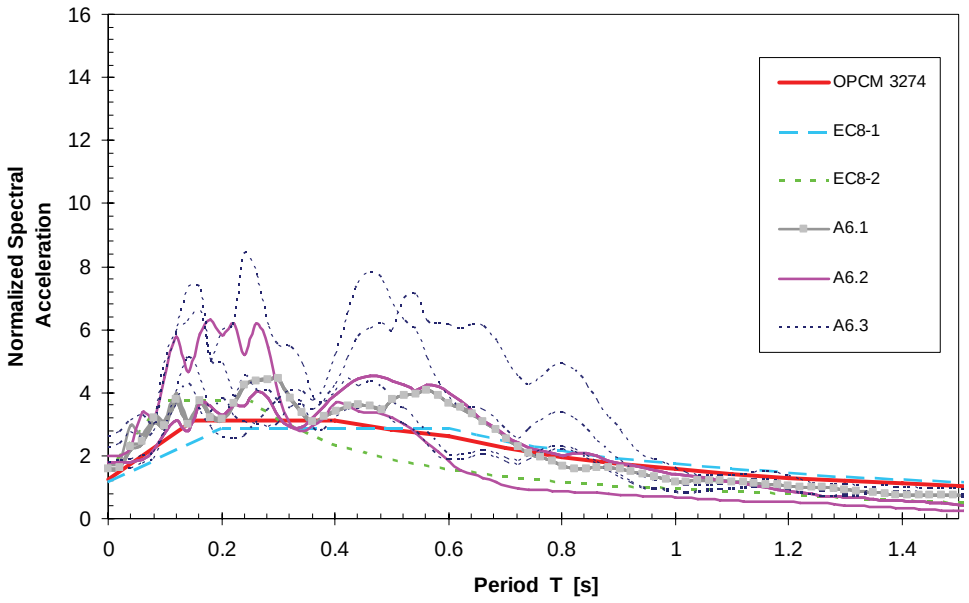

Fig 10b: Elastic Response Spectrum – Type C soil – Accelerograms A6.1-A6.2-A6.3: ΔM = 0.2-0.5 Δd = 9-17; 5-20 km

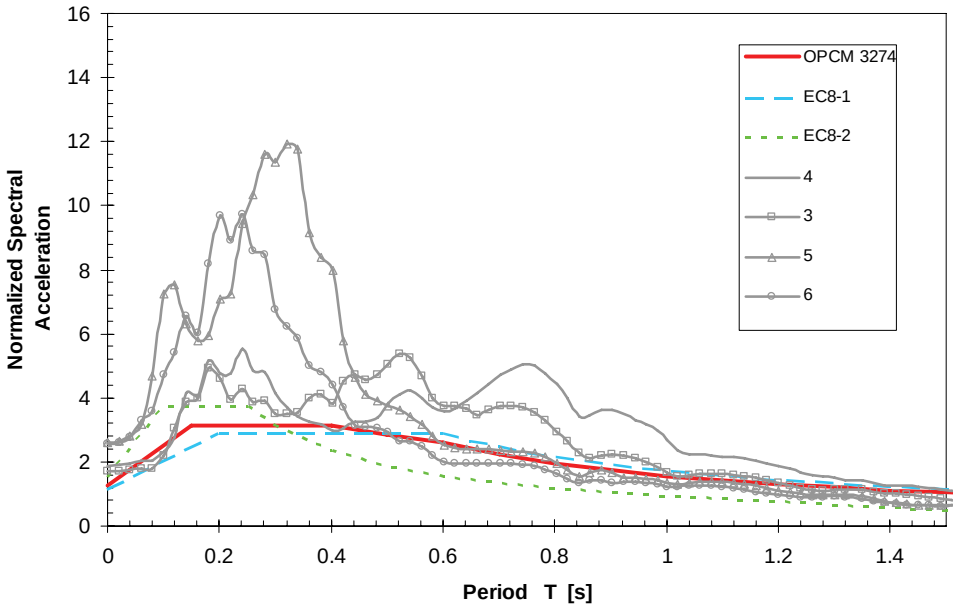

Fig 10c: Elastic Response Spectrum – Type C soil – Artificial Accelerogram

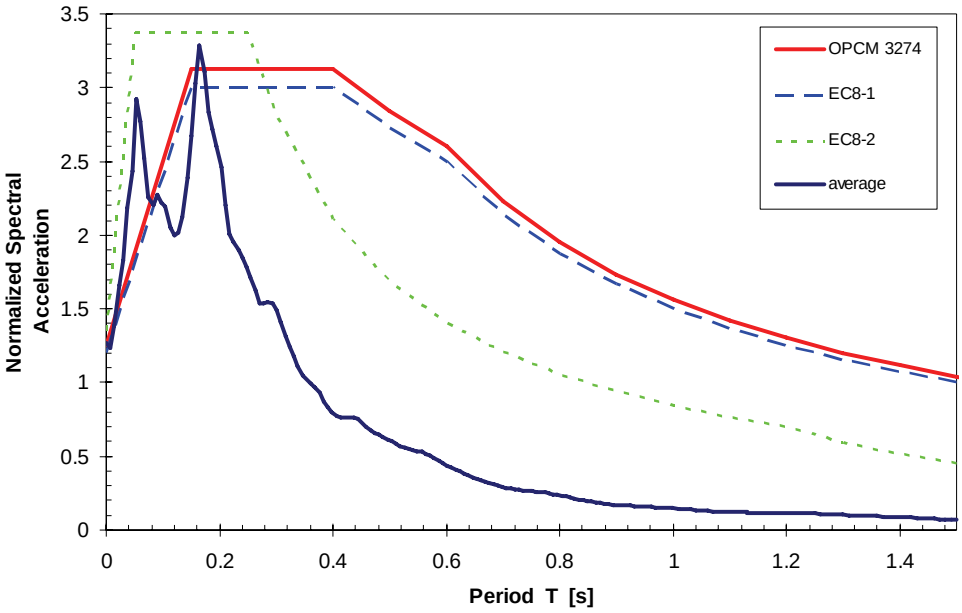

Fig 11: Computed average elastic response spectrum (Type B soil)

Selection and Scaling of Real Acceleration Time Histories for Site Response Analyses

Atilla Ansal, Eser Durukal, and Gökçe Tönük
Department of Earthquake Engineering, Kandilli Observatory and Earthquake Research Institute, Boğaziçi University, Istanbul, Turkey

Abstract

The response variability is investigated at two sites for a series of time histories selected as compatible or partly compatible with the site-specific earthquake hazard scaled to different intensity measures, as peak ground acceleration, peak ground velocity and Arias intensity. Using 1D equivalent linear site response model the uncertainty introduced by scaling and distance compatibility are evaluated with respect to the criteria set in EC8 for using real time histories for design purpose.

Keywords—*Ground motion scaling, site response*

INTRODUCTION

From the perspective of performance based earthquake engineering, there are three issues that need to be addressed by the geotechnical earthquake engineering community. The first concerns the selection of the damage parameter for different geotechnical structures. The second is related to the modeling of the uncertainty in the material properties of soils and of ground response. The third is about selection and scaling of ground motion to be used as input in the analyses [1].

The major uncertainty in ground response arises from the accuracy of selected site and material models and from the variability in the input earthquake motion [2, 3].

APPROACH

Using 1D equivalent linear model at two sites with pre-determined hazard levels, the resulting response variability is investigated under a series selected time histories compatible with the site-specific earthquake hazard in terms of expected fault mechanism, magnitude, and distance. Then using these selected set of records scaled to different intensity measures, namely to peak ground acceleration (PGA), peak ground velocity (PGV), and Arias intensity (AI), the analyses are repeated and the variability introduced by scaling is evaluated. Scaling of input time histories was carried out in time-domain that involves only the amplitude of the time series.

At the second stage the distance compatibility criteria is evaluated by conducting site response analysis using different sets of earthquake time histories recorded at different fault distances scaled in a similar manner.

IZMIR CASE STUDY

The first case study selected for evaluating the effects of scaling on site response is near the city of Izmir. The site response analyses were conducted using Shake91 [4] for the four soil profiles where in-hole shear wave measurements were performed previously. Even though these four borings are at the same site with spacing around 100m, the measured shear velocity profiles given in Fig. 1 indicates the variability in the site conditions at one large construction site where for all practical purposes only one site specific design spectra is needed.

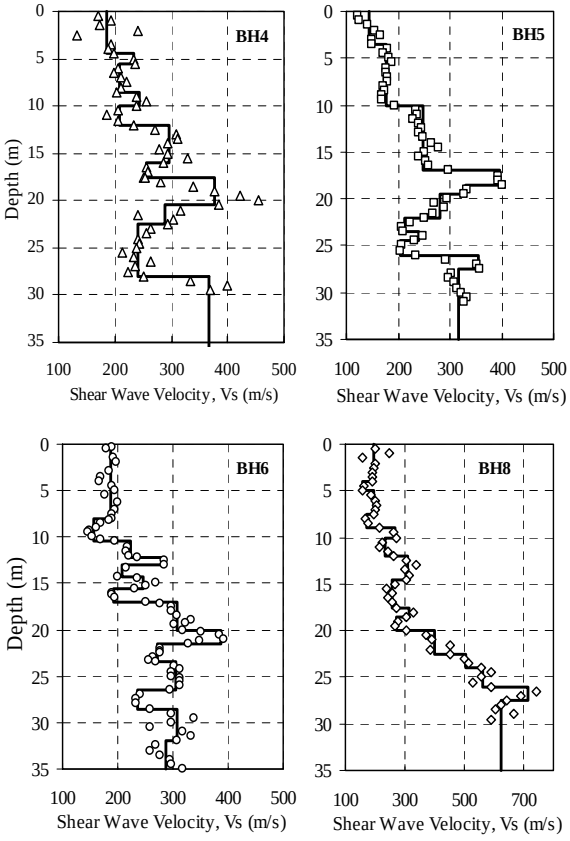

Fig. 1: Four soil profiles used in site response analyses for the first case study

The effects of scaling for each soil profile were evaluated separately and together to observe the effects of site variability in relation with the scaling of input ground motion. The scaled records were applied as outcrop motion where the engineering bedrock (Vs=750m/s) was taken at 45m depth.

The regional earthquake hazard analysis yielded an earthquake magnitude of 6.5-7 with an epicentre distance of 10-20km. The hazard compatible input earthquake data, composed of 20 acceleration time histories recorded between 10-20km epicentre distances, [5] are listed in Table 1. Site response analyses were conducted using scaling parameters determined from related empirical attenuation relationships [6, 7, 8, 9] as PGA=0.25g, PGV=30cm/s, and AI=55cm/s.

Table 1: Earthquake records used for Izmir case study

Station	Earthquake	Date	Mw	Re (km)	PGA (g)	
					EW	EW
1061	Düzce	11/12/99	7.1	15.6	0.134	0.107
1062	Düzce	11/12/99	7.1	13.3	0.257	0.114
531	Düzce	11/12/99	7.1	11.4	0.118	0.159
Arcelik	Kocaeli	08/17/99	7.4	17.0	0.218	0.149
Bolu	Düzce	11/12/99	7.1	17.6	0.728	0.822
Duzce	Kocaeli	08/17/99	7.4	12.7	0.312	0.358
Gebze	Kocaeli	08/17/99	7.4	17.0	0.244	0.137
117ELC	Imp.Valley	05/19/40	7.0	12.0	0.313	0.215
Joshua Tree	Landers	06/28/92	7.3	11.3	0.274	0.284
Morongo	Landers	06/28/92	7.3	17.7	0.188	0.140

The results are presented in terms of histograms of peak accelerations and spectral accelerations at 0.2s obtained by fitting an envelope NEHRP design spectra.

The peak ground acceleration histograms calculated for four soil profiles, shown separately in Fig. 2, indicates the importance of the variations in the soil profiles. Thus one option to account for these differences in the soil profile at the site is to consider the site response results obtained for four soil profiles together and determine the variation of peak ground acceleration with respect different scaling procedures adopted.

Based on the histograms for the calculated PGAs for all four borings for the three scaling option using the considered input motions, it seems that among three scaling procedures, taking into consideration all three parameters calculated to determine the variability in each set (kurtosis and normalized standard deviation being minimum, and range being the smallest), the PGA scaling appears to be the most suitable scaling parameter in terms of calculated peak ground accelerations on the ground surface if they happen to be the a suitable damage parameter (i.e. liquefaction susceptibility analysis).

The second comparison to observe the effects of the scaling schemes was performed with respect to spectral acceleration at 0.2s obtained from the best envelop NEHRP spectra fitted to each of the calculated acceleration response spectra. The results of these calculations are shown in Fig. 3.

In the case of spectral accelerations at 0.2s the characteristics of the statistical distributions have changed significantly. Arias intensity (AI) scaling yielded the smallest range and Kurtosis while PGA scaling yielded the largest range and Kurtosis. Thus with respect to spectral accelerations at 0.2s, AI scaling gave the most suitable solution with the smallest variability. In addition the lowest value of the spectral acceleration at 0.2s is also obtained from the AI scaling results.

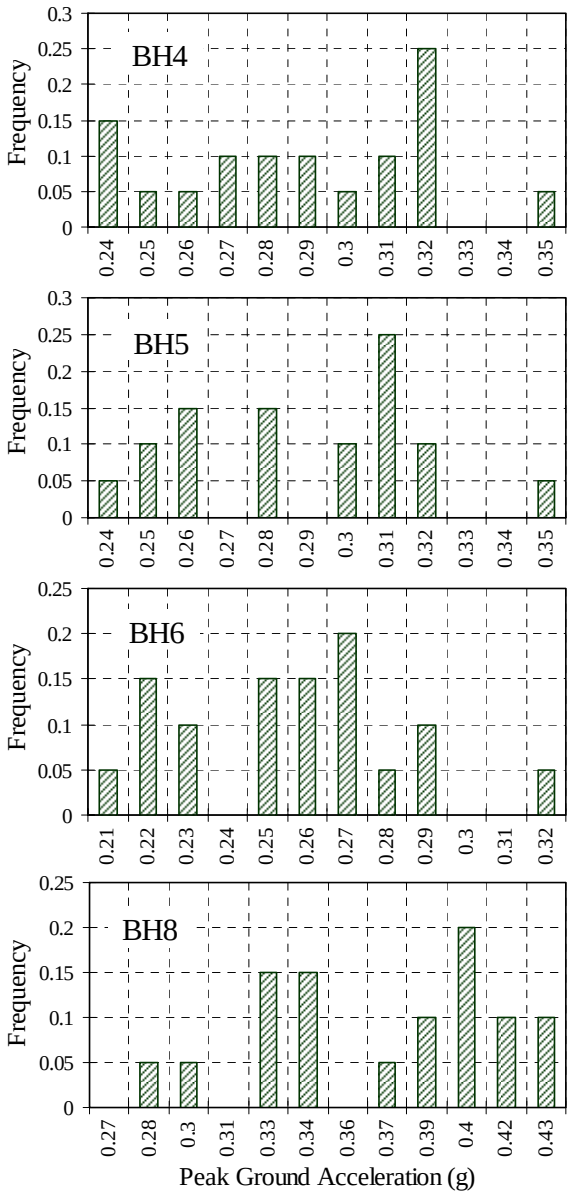

Fig. 2: Histograms of PGA on the ground surface for PGA scaled acceleration records for four soil profiles

If we consider spectral acceleration at 0.2s as the main damage parameter for the geotechnical engineering structures, than it is possible to suggest the use of AI scaling as the first option when conducting site response at a site to determine the design ground motions for geotechnical engineering structure.

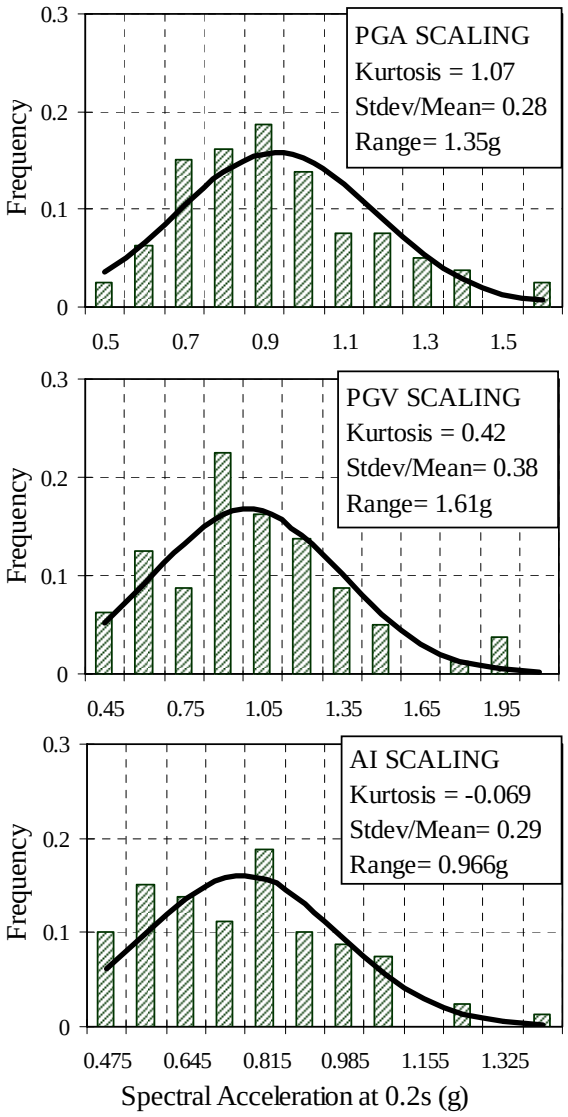

Fig. 3: Histograms of Sa(0.2s) on the ground surface for PGA, PGV, and AI scaled records

GÖLCÜK CASE STUDY

The second site is located in Gölcük; a town in the epicenter area of the 1999 Kocaeli, Turkey earthquake. Detailed site investigations were carried out in the town as a part of the post earthquake studies [10]. The soil profile selected for the parametric study is shown in Fig. 4.

The regional earthquake hazard is dominated by strike slip faulting, that generates earthquakes in the magnitude range of 7.0-7. 5.

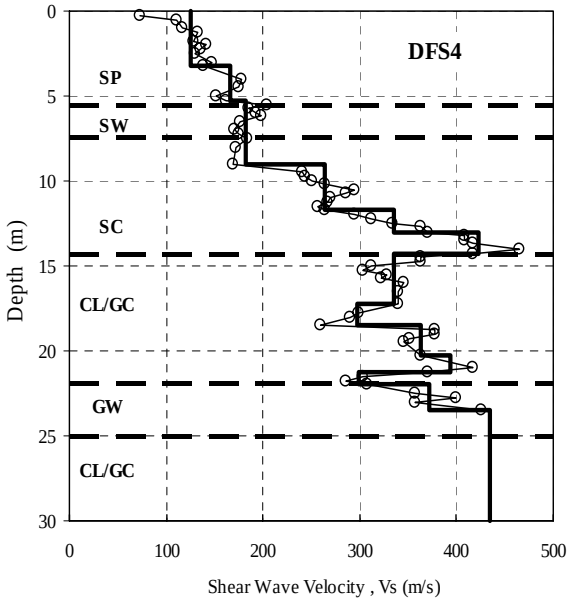

Fig. 4: Soil profile at Gölcük used in site response analyses

The ground motion data are obtained from PEER (http://peer.berkeley.edu/smcat). The selection criteria were earthquake mechanism as strike slip, magnitude range as 7.0-7.5; and distance range was taken as 10-40km that was grouped in 10km intervals. In the resulting data set there are records from three major events: Kocaeli, Turkey; Duzce, Turkey and Landers, USA earthquakes. The data, summarized in Table 2, are scaled to PGA=0.35g, PGV=30cm/s and AI=2m/s for site response analysis based on the empirical attenuation relationship proposed [7, 8, 9].

Table 2: Ground motion data set used in analyses Earthquake mechanism: strike-slip, Distance range: 10-20, 20-30 and 30-40km,

Station	Earthquake	Date	Mw	Re (km)	PGA (g)	
					EW	NS
10-20 km						
531	Düzce	11/12/99	7.1	11.4	0.118	0.159
1061	Düzce	11/12/99	7.1	15.6	0.134	0.107
1062	Düzce	11/12/99	7.1	13.3	0.257	0.114
Arcelik	Kocaeli	08/17/99	7.4	17.0	0.218	0.149
Gebze	Kocaeli	08/17/99	7.4	17.0	0.244	0.137
Joshua Tree	Landers	06/28/92	7.3	11.3	0.274	0.284
Morongo	Landers	06/28/92	7.3	17.7	0.188	0.140
20-30 km						
362	Düzce	11/12/99	7.1	27.4	0.026	0.042
12149 Desert	Landers	06/28/92	7.3	23.2	0.171	0.154
5070 NPS	Landers	06/28/92	7.3	24.2	0.136	0.134
23 Coolwater	Landers	06/28/92	7.3	21.2	0.283	0.417
100 MCF	Landers	06/28/92	7.3	21.2	0.126	0.125
30-40 km						
Lamont 1060	Düzce	11/12/99	7.1	30.2	0.053	0.028
Barstow	Landers	06/28/92	7.3	36.1	0.132	0.135
Göynük	Kocaeli	17/8/99	7.4	35.5	0.132	0.119
Iznik	Kocaeli	17/8/99	7.4	31.8	0.136	0.098
Palm Springs	Landers	06/28/92	7.3	37.5	0.076	0.089
Mudurnu	Düzce	11/12/99	7.1	33.6	0.12	0.056

The main purpose of the was to study the effects of releasing the distance requirement in selecting the previously recorded site specific hazard compatible earthquake time histories. The results are presented in terms of peak ground accelerations and response spectral accelerations at the ground surface. Ground motions scaled with respect to PGA, PGV and AI are used as input for the three sets of input motion for the site response analyses. The results obtained from the parametric study are shown in Fig. 5 with respect to the calculated elastic acceleration response spectra at the ground surface. The first left column of spectrum in Fig.5 shows the acceleration response spectrum calculated using the previously recorded time histories at a distance of 10-20km from the ruptured fault with no scaling, with PGA, PGV and Arias Intensity scaling. The last graph in the column shows the comparison among different scaling procedures in terms of average spectrum.

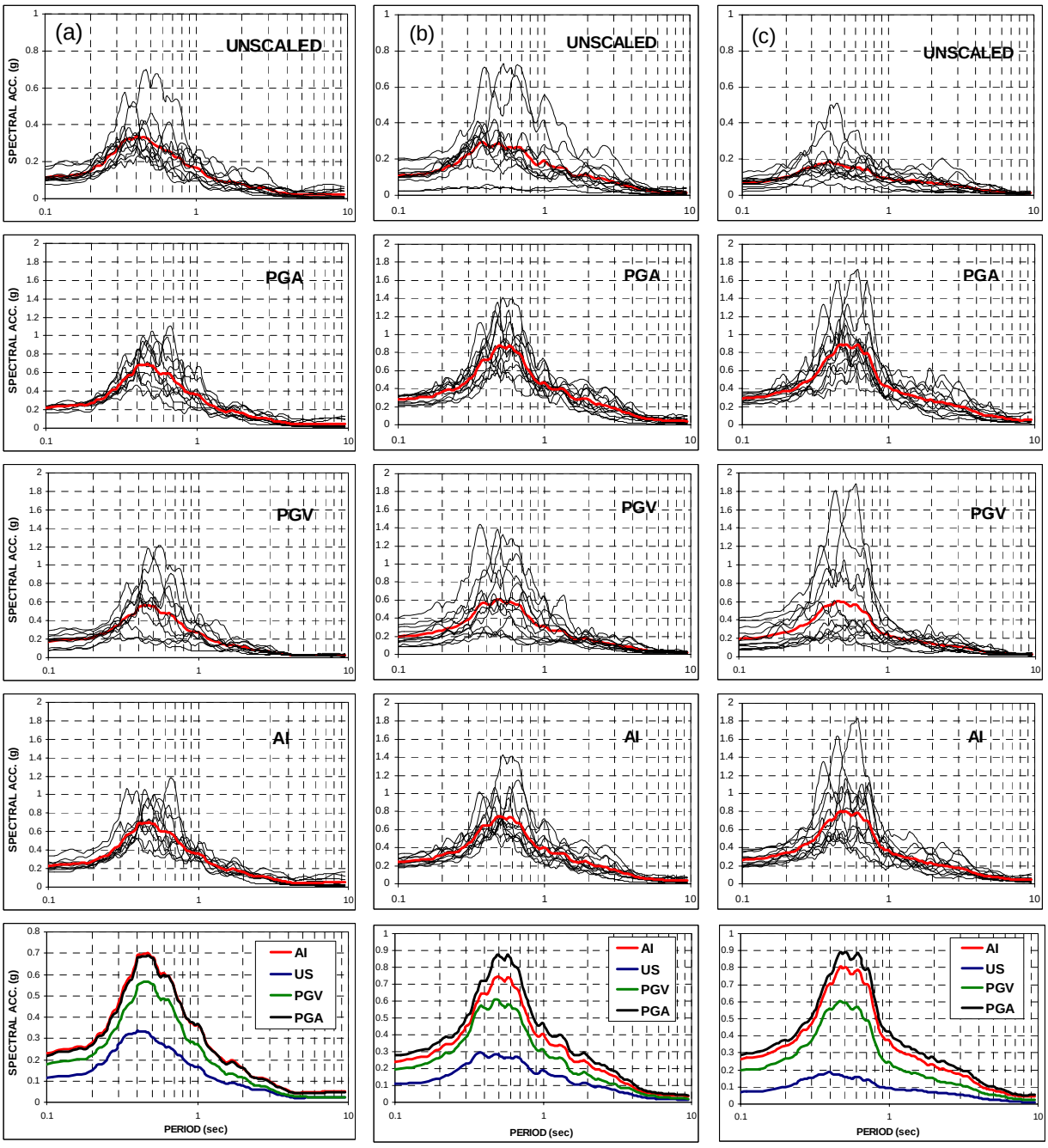

Fig.5: Calculated elastic acceleration response spectrum for three distance ranges (a)10-20km; (b)20-30km; (c) 30-40km using unscaled, PGA, PGV, and Arias Intensity scaled time histories

In the same fashion the middle column shows the results obtained by using time histories previously recorded at a distance of 20-30km and the third column on the very right shows the results obtained using time histories previously recorded at a distance of 30-40km from the ruptured fault.

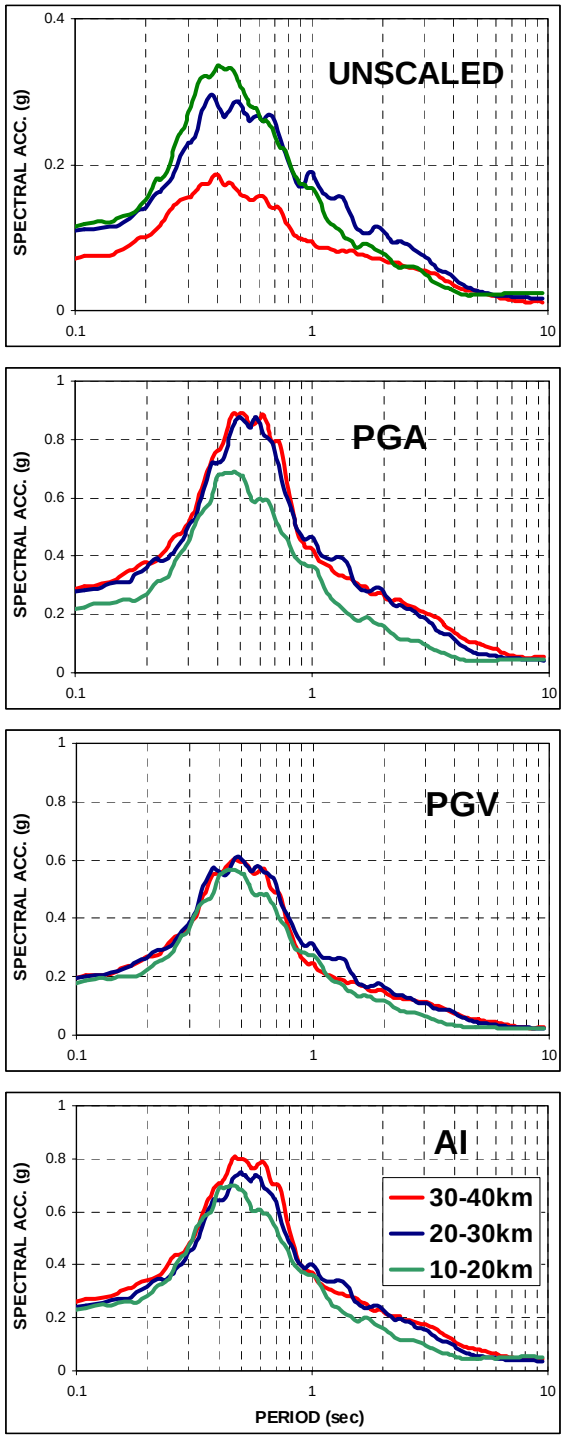

Fig. 6: Average spectral accelerations from site response analyses conducted using real time histories recorded at different distances with respect to scaling procedure

It is interesting to observe that PGA scaling always gave the highest spectral accelerations concerning other scaling procedures adopted in this study.

When you compare the results with respect to average spectral accelerations calculated using different time histories recorded at different distances as given in Fig. 6, there is a minor difference in PGA scaled input motions, in PGV or AI scaled records there is almost no difference. However, if one looks at the scatter and the change in the range of the calculated acceleration spectrum shown in Fig. 5, the distance to the faults appears to be an effective parameter. Even though the actual recorded time histories show the opposite trend, the scatter and range increases with the distance of the recorded time histories for the PGA, PGV and AI scaled input motions. This could lead to different spectral accelerations if the scatter is evaluated by statistical procedure in a probabilistic way. Therefore it would be recommendable to select the real time histories for site response analysis at compatible distance range as determined by the site specific hazard study.

The situation is similar in terms of the calculated peak ground accelerations as shown in Fig. 7. The scatter is much less for PGA scaled input motions as well as the scatter is less for all the scaled time histories recorded within 10-20km range.

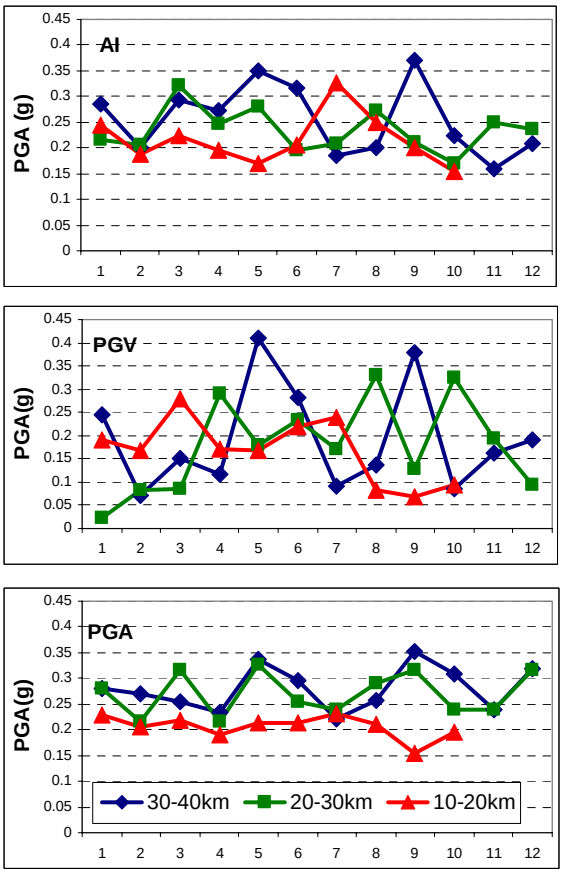

Fig. 6: Variation of peak ground accelerations from site response analyses using real time histories recorded at different distances with respect to scaling procedure

This again indicates that in the selection of real time history records for design purposes, it is necessary to use time histories that are compatible with the regional hazard assessment with respect to fault distance.

CONCLUSIONS

Although selected in accordance to the site-specific hazard parameters the ground motions may have different characteristics in time and frequency domain and thus play an important role by introducing a significant scatter in non-linear dynamic response. Scaling the records for time-domain analysis to values chosen consistent with site-specific hazard parameters is a way to handle this situation [11]. Scaling the input motion according to the most appropriate parameters so that the scatter of the model response is reduced is also important when design is required for different performance levels such as limit, serviceability etc. and also for displacement and acceleration sensitive structures and components [11].

In the first case study conducted it was observed that scaling with respect to Arias intensity especially in the case of spectral accelerations at 0.2s, yielded the most suitable scaling option among the three scaling procedures studied for conducting site response analyses if the damage parameter is selected as spectral accelerations. However, in the cases where damage parameter can be taken as peak ground accelerations (i.e liquefaction susceptibility or landslide hazard) than scaling with respect to peak acceleration should be preferred as suggested in EC8.

In the second case study, it appears that distance to the fault is one of the earthquake hazard parameters that may effect the outcome both with respect to peak ground or spectral accelerations, thus in selecting real time histories, the records need to be selected compatible with the regional hazard in terms of fault type, magnitude and fault distance.

Presented results are for the 10-40km distance and 6.5-7.5 magnitude range for two case studies. The analyses were carried out using SHAKE91 computer code thus the obtained results directly depend on the formulation adopted in this code.

REFERENCES

[1] Stewart, J. P., Chiou, S. J., Bray, J. D., Graves, R. W., Somerville, P. G., and Abrahamson, N. A., "Ground motion evaluation procedures for performance-based design," *Soil Dynamics and Earthquake Engineering*, Vol.22, No.9-12 , pp.765-772, 2002.

[2] Boore, D. M., "Can site response be predicted?" *Journal of Earthquake Engineering*, Vol.8, No.1, pp.1-42, 2004.

[3] Finn, W. D. L.., "State-of-the-art of geotechnical earthquake engineering practice," *Soil Dynamics and Earthquake Engineering*, Vol.20, pp.1-15, 2000.

[4] Idriss, I. M. and Sun J. I., "Shake91, A Computer Program for Conducting Equivalent Linear Seismic Response Analysis of Horizontally Layered Soil Deposits Modified based on the original SHAKE program Published in December 1972 by Schnabel, Lysmer and Seed", 1992.

[5] PEER Strong Motion Data Bank, http:// peer.berkeley.edu.

[6] Ambraseys, N. N., "The prediction of earthquake peak acceleration in Europe," *Earthquake Engineering and Structural Dynamics*, Vol.24, pp.467-490, 1995.

[7] Joyner, W. B. and Boore, D. M., "Measurement, characterization, and prediction of strong ground motion," *Earthquake Engineering and Soil Dynamics II – Recent Advances in Ground Motion Evaluation*, Geotechnical Special Publication 20, ASCE, New York, pp 43-102 , 1988.

[8] Travasarou, T., Bray, J. D., and Abrahamson, N. A., "Empirical attenuation relationship for arias intensity," *Earthquake Engineering and Structural Dynamics*, Vol.32, pp.1133-1155, 2003.

[9] Siyahi, B., Durukal, E., and Altaç, Z., "Evaluation of strong motion data from the Kocaeli and Düzce, Turkey Earthquakes in view of Arias intensity," *Proceedings 15ICSMGE Earthquake Geotechnical Engineering Satellite Conference on Lessons Learned from Recent Strong Earthquakes*, pp. 189-194, Istanbul, Turkey, 2001.

[10] Ansal, A., Togrol, E., Kurtulus, A., Iyisan, R., and Okur, V., "Near fault site effects during 1999 Kocaeli Earthquake", *Proc. 6th Int. Conf. on Seismic Zonation*, Cal., USA, 2000.

[11] Malhotra, P. K., "Strong-Motion Records for Site-Specific Analysis," *Earthquake Spectra*, Vol.19, No.3, pp.557-578, 2003.

Site Characterization at the Catania City, Italy

A. Cavallaro[1], S. Grasso[2] , M. Maugeri[2]

[1] *CNR-IBAM, Catania, Italy*
[2] *University of Catania, Italy*

Abstract

Site characterization is required for the identification of ground types and the associated response spectra as well as for requirements for siting and foundation soils. Requirements for siting regard slope stability and potentially liquefiable soils. Foundation soils regard mostly foundation system, soil-structure interaction and retaining structures. Ground investigation and studies must be designed according to the geotechnical problems to be solved.
In this paper the applicability of EC8 is discussed for the site characterization of the city of Catania (Italy), for identification of ground types and microzonation and for evaluation of slope stability, liquefaction potential and foundation stability, including soil-structure interaction.

INTRODUCTION

According to EC8, appropriate investigations should be carried out for identification of ground types and the associated response spectra (EC8 - part 1, 2003), as well as for that the construction site and the supporting ground, which should be free from risks of slope instability and permanent settlement caused by liquefaction in the event of an earthquake (EC8 - part 5, 2003).

Identification of ground types could be made on the basis of the stratigraphic profiles and the geotechnical parameters $v_{s,30}$, N_{SPT} and c_u. Due to the influence on the designed seismic action, the shear modulus G is required as well as the damping ξ. The evaluation of the dependence of the soil stiffness (G/G_{max}) and damping $\xi(\gamma)$ on the strain level is also required.

For slope stability analyses, soil strength parameters must be evaluated for undrained and drained conditions. For cohesive soils the appropriate strength parameter is the undrained shear strength c_u, taking into account the cyclic degradation effects under the earthquake loads. For cohesionless soils the appropriate strength parameter is the cyclic undrained shear strength $\tau_{cy,u}$ taking into account the possible pore pressure build-up. For quiescent slides where the chances of reactivation are higher, in addition to pore pressure build-up evaluation, large strain value of the ground strength parameters (i.e. residual strength) should be used. For liquefaction analyses a decrease in the shear strength and/or stiffness caused by the increase in pore water pressure in saturated cohesionless soil materials, during earthquake ground motions, should be evaluated. To this purpose a minimum site investigation required must include the execution of either in-situ Standard Penetration Test (SPT) or Cone Penetration Test (CPT) as well as the determination of grain size distribution curves in the laboratory.

The partial factor (γ_M) for material properties are recommended to be assumed as follow: for the undrained shear strength γ_{cu} = 1,4; for cyclic undrained shear strength $\gamma_{cy,u}$ = 1,25; for unconfined strength γ_{qu} = 1,4; for the angle of shearing resistance γ_{ϕ} = 1,25.

The applicability of EC8 is discussed for the site characterization of the city of Catania, in the framework of the Research Project: "Detailed Scenarios and Actions for Seismic Prevention of Damage in the Urban Area of Catania" (Maugeri, 2005). Ground investigation has been designed with the aim of solving two different problems: i) identification of ground

types and microzonation; ii) evaluation of slope stability, liquefaction potential and foundation stability, including soil-structure interaction, by several test sites.

IDENTIFICATION OF GROUND TYPES AND MICROZONATION

Identification of ground types for microzonation has been made by boreholes, SPT, CPT, and laboratory tests, including grain size distribution test, oedometer test, direct shear test and triaxial test (U-U, C-U, and C-D).

A database of about 1200 soil profiles detected by boreholes has been implemented in a Geographical Information System (GIS), as well as the geological map and the geotechnical data by SPT, CPT and laboratory tests (Grasso and Maugeri, 2005). The investigated urban area of Catania is about 45 Km^2, so the density of boreholes is about 25 for km^2. The EC8 recommend that the geological and geotechnical data shall be available in sufficient quantity, to allow the determination of an average ground type and/or the associated response spectra (see par. 4.2.2, part 5) without giving a minimum requirement. By the way the accuracy of the evaluation of the average ground type and associated response spectra depends very much on the quantity of boreholes for Km^2. It is very difficult to prescribe a minimum requirement because it depends on the spatial variability of geological and geotechnical units. Because of this extreme spatial variability, a minimum requirement has been fixed to 25 boreholes for km^2 for the Catania site.

Empirical correlations have been used for the evaluation of $v_{s,30}$ (Ohta and Goto, 1978; Yoshida and Motonori, 1988) for identifying ground types. Empirical correlations for the evaluation of G_o from q_c has suggested by Mayne and Rix (1993). Moreover empirical correlation between G_o and DMT results proposed by Hryciw (1990) has been also used. According to ground types given by Table 3.1 of EC8 a geotechnical map based on $v_{s,30}$ has been implemented in a GIS database (Fig. 1). In spite of extremely spatial variability, geotechnical map based on $v_{s,30}$ according to EC8 looks very uniform. Due to this extreme spatial variability of $v_{s,30}$, each soil type B, C and D have been subdivided into two different sub-types. In particular: soil type B has been subdivided into soil type B1 with $500<v_{s,30}<800$ and soil type B2 with $360<v_{s,30}<500$; soil type C has been subdivided into soil type C1 with $270<v_{s,30}<360$ and soil type C2 with $180<v_{s,30}<270$; soil type D has been subdivided into soil type D1 with $100<v_{s,30}<180$ and soil type D2 with $v_{s,30}<100$. A different and more detailed geotechnical map based on $v_{s,30}$ is reported in Fig. 2.

Considering soil profile given by boreholes there is also extreme variability with depth; so soil profiles seem very different from the profiles given by Table 3.1 of Eurocode EC8 and reported in Fig. 3. In particular very often soil profile is similar to that described in the Eurocode as soil E consisting of soil type C or D with thickness varying between about 5 m and 20 m, underlined by stiffer material, consisting of scoriaceous lava, with $v_{s,30}$ > 800 m/s. Nevertheless, as reported in Fig.4, it is possible to see that: i) the underlining stiffer material is

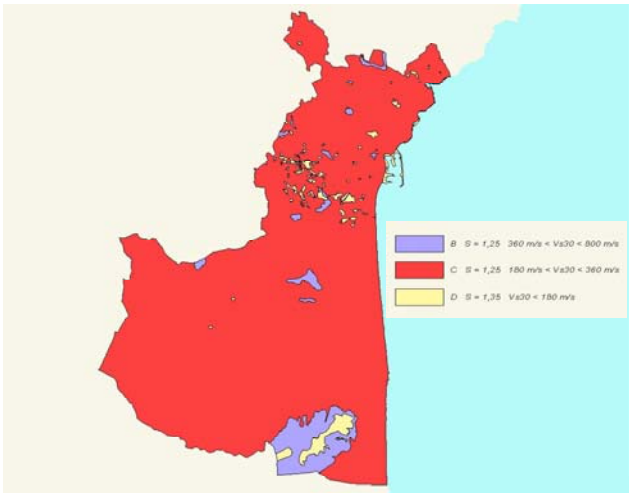

Fig 1: Geotechnical map based on $V_{s,30}$ according EC8

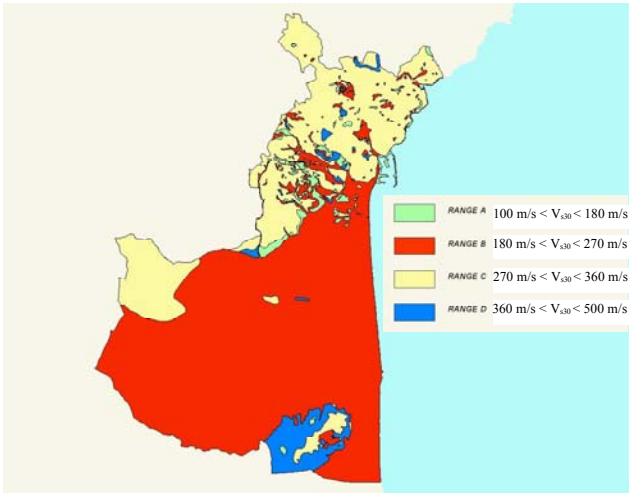

Fig 2: Detailed geotechnical map based on $V_{s,30}$

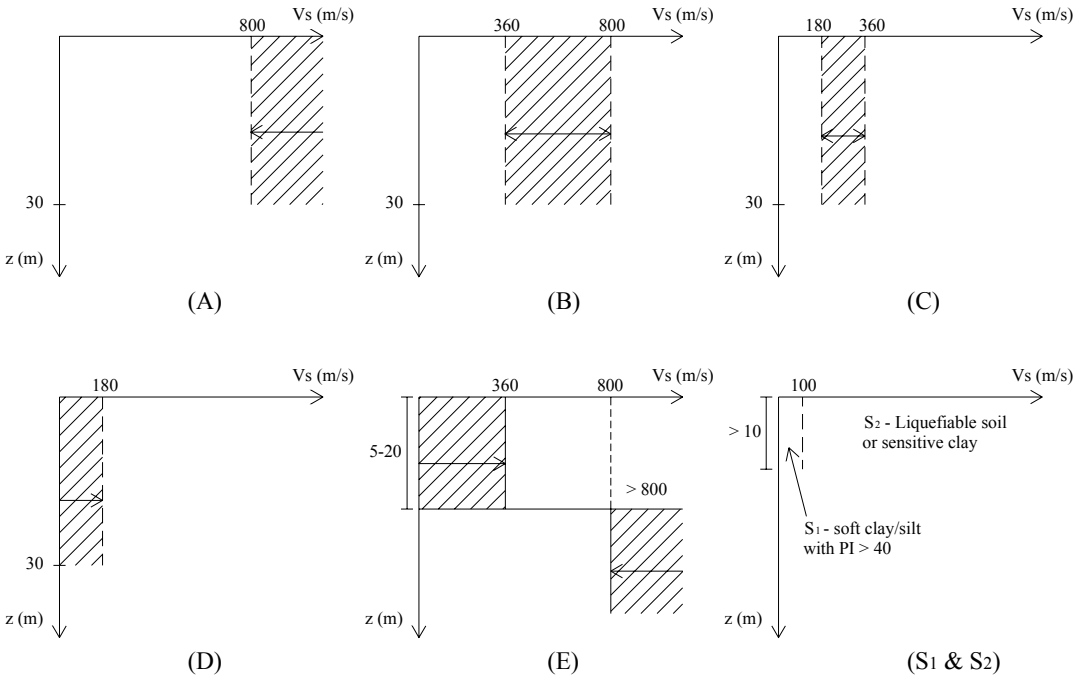

Fig 3: Ground types according to Table 3.1 of EC8.

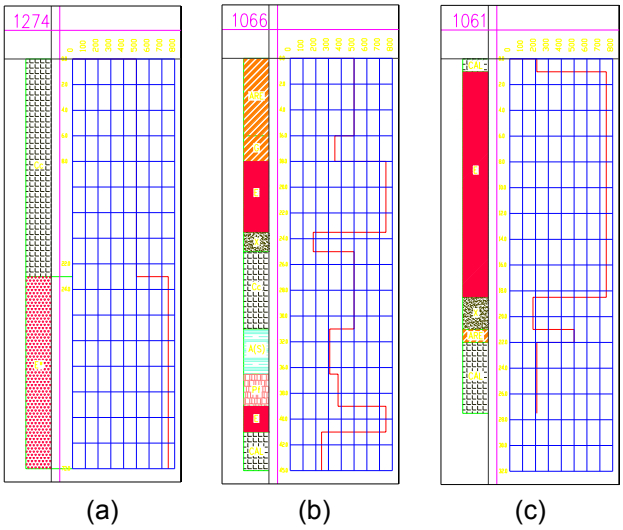

Fig 4: Soil profiles at Catania sites.

with 500 m/s<$v_{s,30}$<800m/s (Fig. 4a); ii) more than one underlining stiffer material with 500 m/s<$v_{s,30}$<800m/s are present (Fig. 4b); iii) the stiffer material is at the surface and it is underlined by softer material (Fig. 4c).

For the Sellano (Italy) soil Capilleri et al. (2003) suggested to subdivide soil type E in three different soil sub-type. Type E1 with 150<v_s<250 and depth = 20m; type E2 150<v_s<250 and depth = 15m or 250<v_s<360 and depth = 20m; type E3 250<v_s<360 and depth = 15m.

Also soft clay/silt soil of ground type S1 exists in the investigated area (Fig. 5a), as well as deposit of liquefiable soil of ground type S2 (Fig. 5b). In this situation of extreme soil variability in plan and in depth, the average shear wave velocity $v_{s,30}$ is not very significant because for ground type E if a soft soil is at the surface it is possible to have amplification of the ground motion, while if stiff and heavy thickness soil is at the surface resting over soft soil it is possible to have demagnification, with similar value for $v_{s,30}$.

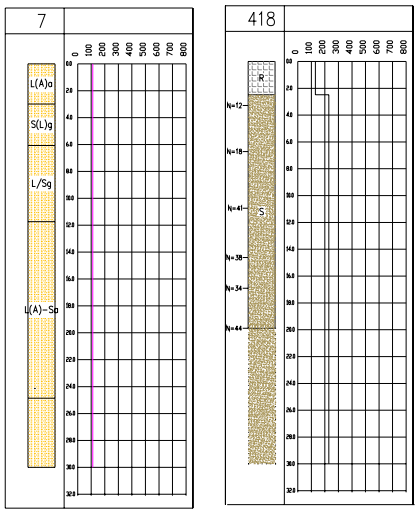

Fig 5: Ground types S1 (a) and S2 (b).

The inverse intercalation between soft

clay/silt soil and scoriaceous lava originated from Mount Etna Volcano is very common for the subsoil of Catania.

Moreover a stiff soil at a depth greater than 30 m could have significant influence on the associated response spectrum, so a depth greater than 30 m has to be taken into account for detailed soil profile.

Also soil stiffness and damping could have very significant influence on the associated response spectra. To this aim some test sites have been located to perform detailed site investigation and laboratory tests for the evaluation of the dependence of the soil stiffness (G/G_{max}) and damping $\xi(\gamma)$ on the shear strain level.

TEST SITES

Location

For detecting ground properties for the evaluation of slope stability, liquefaction potential and foundation stability, including soil-structure interaction, 12 test sites have been located (Fig. 6).

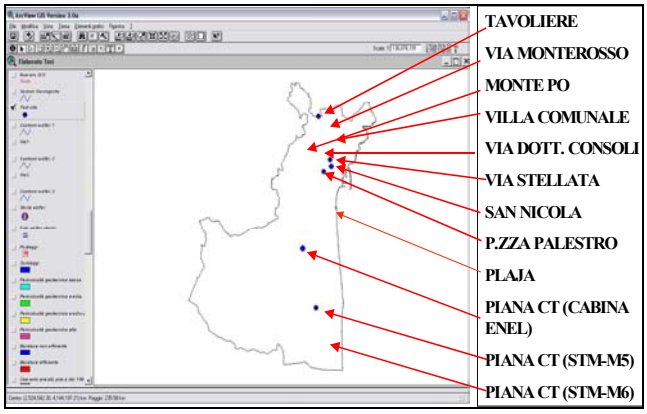

Fig 6: Test site location.

The three locations: No. 1 Piana di Catania (STM-M5); No. 2 Piana di Catania (ENEL box); No.12 Piana di Catania (STM-M6) are related to a clayey soil in the Catania plain.

The location No. 3 Playa beach is related to silica sandy liquefiable soil (Maugeri and Vannucchi, 1999).

The location No. 4 Tavoliere is related to stiff soil (scoriaceous lava) over soft soil. The locations No. 5 Via Stellata and No. 11 Villa Comunale are related to clayey soil in the central area. The location No. 6 Piazza Palestro is related to volcanic sand. The locations No. 7 San Nicola alla Rena Church and No. 9 Via Monterosso are related to scoriaceous lava. The location No. 8 Via Dottor Consoli is related to clayey soil in the central area.

The location No. 10 Monte Po is related to a layered soil made by a succession of Terreforti clays, sands and volcanic coarse. It is difficult to evaluate the $v_{s,30}$ and the average stiffness of this soil of the Monte Po hill, on which a landslide occurred in 1991 and can be reactivated by an earthquake (Biondi and Maugeri, 2005).

In the test sites boreholes, in-situ tests and laboratory tests performed on undisturbed samples retrieved from boreholes have been performed.

In-Situ Tests

In the 12 test sites have been performed: No. 25 boreholes, No. 12 SPT, No. 12 CPT, No. 1 C-H, No. 8 D-H, No. 4 Seismic Dilatometer Marchetti Test (SDMT). Shear wave velocity has been measured by different tests; for shear wave velocity and soil stiffness specific empirical correlations have been established with SPT and CPT.

The C-H test was performed at the location No. 1 Piana di Catania (STM–M5) (Maugeri et al., 1988). The D-H tests were performed at the following locations: No. 1 Piana di Catania (STM-M5) (Maugeri et al., 1988); No. 4 Tavoliere (Cavallaro and Maugeri, 1999); No. 5 Via Stellata (Cavallaro and Maugeri, 1999); No. 6 Piazza Palestro (Cavallaro and Maugeri, 2005); No. 7 San Nicola alla Rena Church (Cavallaro et al., 2001); No. 8 Via Dottor Consoli (Cavallaro et al., 2005); No. 9 Via Monterosso (Cavallaro et al., 2006a); No. 12 Piana di Catania (STM-M6) (Cavallaro et al., 2006b).

Using the theory of elasticity from v_s it has been evaluated the shear modulus at small strain (G_o).

The soil profile in terms of G_o has been evaluated and compared by different in situ and laboratory tests as well as empirical correlations (Figg. 7 and 8).

The new Seismic Dilatometer Marchetti Test (SDMT) is capable to measure shear wave velocity v_s, in addition to the material index (I_D), constrained modulus (M), undrained shear strength (c_u) and horizontal

stress index (K_d) (Marchetti, 1980).

SDMT were performed at the following locations: No. 3 Plaja beach; No. 10 Monte Po; No. 11 Villa Comunale; No.12 Piana di Catania (STM-M6) (Cavallaro et al., 2006b).

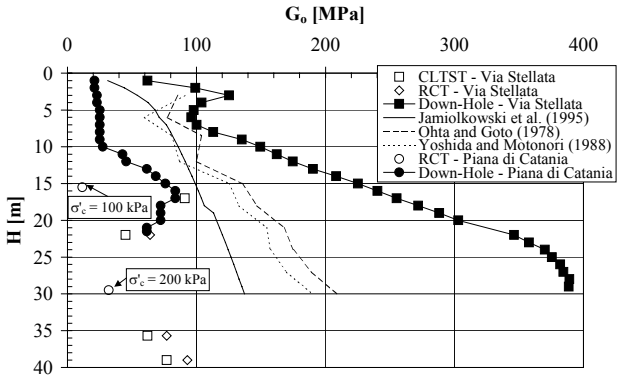

Fig 7: G_o by different measurements for Via Stellata site.

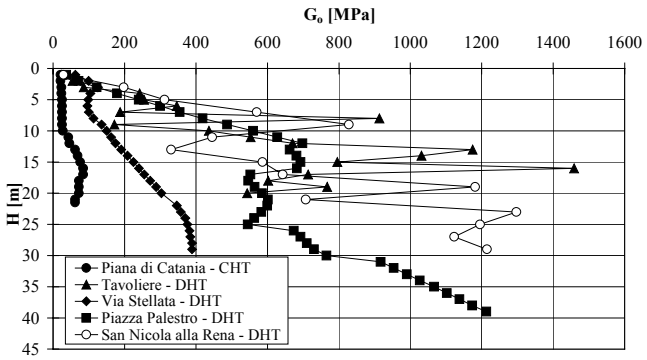

Fig 8: G_o for different test site.

In Fig. 9 is reported the v_s profile in addition to other DMT soil parameters. The v_s profile is very detailed because the measurement was taken every 0.5 m.

The recorded values are much more precise than the D-H results, because they are repeatable with an error lower than 1%. The SDMT has the advantage to take three independent measures (I_D, E_D, v_s).

The redundancy of measurements is very useful, for instance, for liquefaction analyses, which can be based either on v_s values or K_d values (Monaco et al., 2005). Comparisons between v_s measured by D-H and v_s measured by SDMT is reported in Fig. 10.

Moreover SDMT allows the evaluation of the dependence of the soil stiffness (G/G_{max}) on the shear strain level (Lehane and Fahey, 2004). The evaluation of $G(\gamma)$ at the shear strain of about 1 % has been compared with the results given by laboratory tests (Cavallaro et al., 2006b).

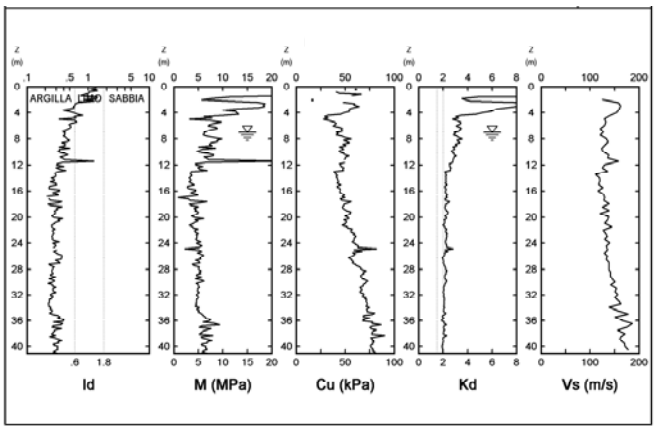

Fig 9: Summary of SDMTs in Catania STM-M6 area.

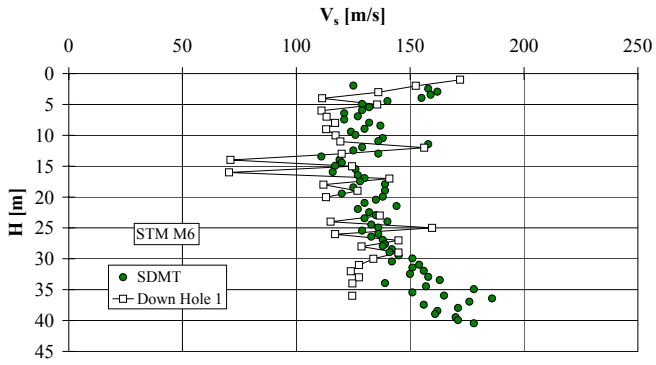

Fig 10: v_s by D-H and SDMT.

Laboratory Tests

Several laboratory tests have been performed in the static field, including grain size distribution test, oedometer test, direct shear test and triaxial test (U-U, C-U, and C-D). In the dynamic field the following tests have been performed: No. 20 Resonant Column Tests (RCT) and No. 15 Cyclic Loading Torsional Shear Tests (CLTST).

Resonant Column Tests have been performed in the following locations: No. 1 Piana di Catania (STM-M5) (Carrubba and Maugeri, 1988); No. 3 Plaja beach (Cascone, 1996; Cavallaro and Maugeri, 2004b, Cavallaro and Maugeri, 2005); No. 5 Via Stellata (Cavallaro et al., 1999; Maugeri and Cavallaro, 1999); No. 6 Piazza Palestro (Cavallaro and Maugeri, 2005); No. 7 San Nicola alla Rena Church (Cavallaro et al., 2001); No. 8 Via Dottor Consoli (Cavallaro et al., 2005). Cyclic Loading Torsional Shear Tests (CLTST) have been performed in the

following locations: No. 3 Plaja beach (Cascone, 1996); No. 5 Via Stellata (Cavallaro et al., 1999; Maugeri and Cavallaro, 1999); No. 6 Piazza Palestro (Cavallaro and Maugeri, 2005); No. 7 San Nicola alla Rena Church (Cavallaro et al., 2001); No. 8 Via Dottor Consoli (Cavallaro et al., 2005). In Fig. 11 is reported G(γ) obtained by RCT. The interpretation of the results are based on the Yokota et al. (1981) proposed equation:

$$\frac{G(\gamma)}{G_o} = \frac{1}{1+\alpha\gamma(\%)^{\beta}} \qquad (1)$$

in which:
G(γ) = strain dependent shear modulus;
γ = shear strain (in percent);
α, β = soil constants.

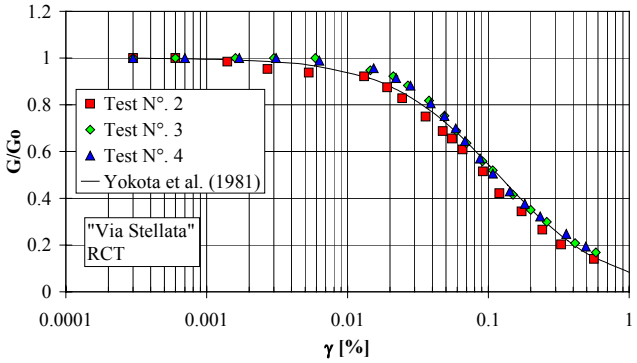

Fig 11: G/G_o-γ curves from RCT for "Via Stellata" site.

The expression (1) allows the computation of shear modulus degradation with strain level. The values of α and β, evaluated for each type of soil, are reported in Table 1.

In Fig. 12 are compared the values of G_o and G(γ) at about 1 % (Lehane and Fahey 2004) of shear strain obtained with RCT and SDMT for the Catania area.

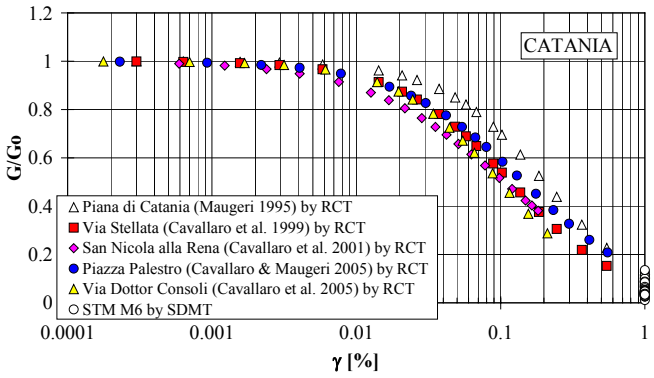

Fig 12: G/G_o vs shear strain for Catania area.

In Fig. 13 are reported $\xi(\gamma)$ values obtained by RCT.

As suggested by Yokota et al. (1981), the inverse variation of damping ratio with respect to the normalised shear modulus has an exponential form given by the following equation:

$$\xi(\gamma)(\%) = \eta \cdot \exp\left[-\lambda \cdot \frac{G(\gamma)}{G_o}\right] \qquad (2)$$

in which:
$\xi(\gamma)$ = strain dependent damping ratio;
γ = shear strain;
η, λ = soil constants.

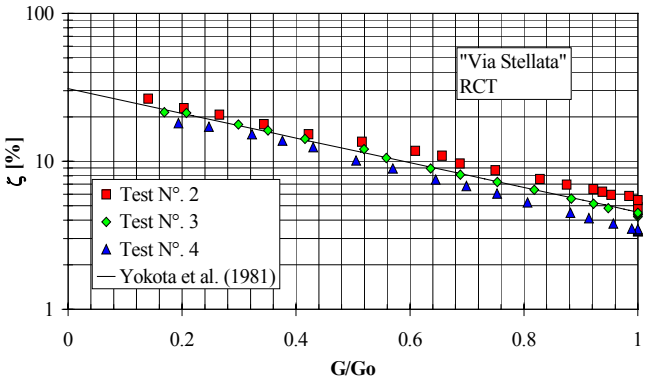

Fig 13: ξ-G/G_o curves from RCT for " Via Stellata " site.

The expression (2) allows the computation of damping increasing with strain level. The values of η and λ, evaluated for each type of soil, are reported in Table 1.

Sites No. 4 Tavoliere and No. 10 Monte Po are complex layered soils for which was difficult to evaluate the average stiffness and damping.

Moreover the degradation of the shear modulus and the increasing of damping with shear strain level have been compared (Fig. 14) with the behaviour based on plasticity index (I_P), proposed by Vucetic and Dobry (1991).

According to Eurocode requirements (see par. 3.1 part 5), cyclic degradation effects for clayey soil and pore pressure build-up, under the earthquake loads have been evaluated. Fig. 15 shows cyclic degradation for the test site No. 8 Via Dottor Consoli (Cavallaro et al., 2005). Cyclic degradation is very important for slope stability evaluation (Biondi and Maugeri, 2006).

Table 1: Soil constant values for evaluation of $G(\gamma)$ and $\xi(\gamma)$: sites No. 1, 2 and 12 clayey soil in the Catania plain; site No. 3 silica sandy soil; sites No. 5 and 11 clayey soil in the central area; site No. 6 volcanic sand; sites No. 7 and No. 9 scoriaceous lava; site No. 8 clayey soil in the central area.

Site	α	β	η	λ
1. Piana di Catania (STM–M5) 2. Piana di Catania (ENEL box) 12. Piana di Catania (STM-M6)	7.15	1.223	19.87	2.16
3. Plaja beach	9	0.815	80	4
4. Tavoliere	-	-	-	-
5. Via Stellata 11. Villa Comunale	11	1.119	31	1.92
6. Piazza Palestro	6.9	1	23	2.21
7. San Nicola alla Rena Church 9. Via Monterosso	7.5	0.897	90	4.5
8. Via Dottor Consoli	16	1.2	33	2.4
10. Monte Po	-	-	-	-

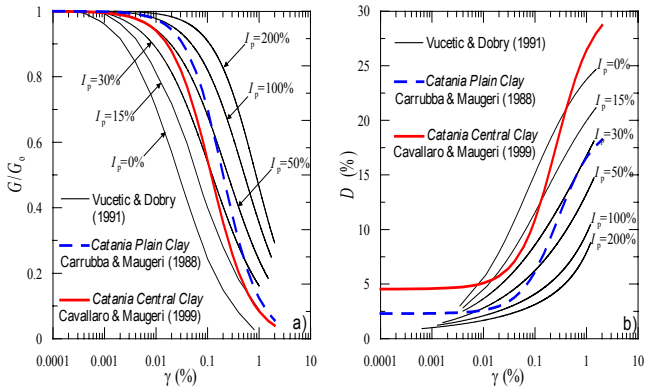

Fig 14: Comparison between the degradation of the shear modulus and the increasing of damping with shear strain level for Catania clay and plasticity index.

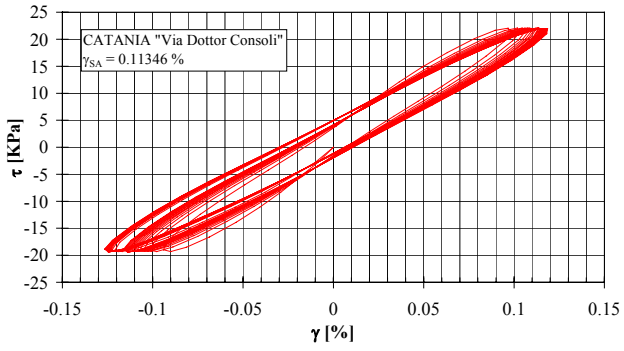

Fig 15: Cyclic soil degradation of "Via Dottor Consoli" site from CLTST.

The degradation index is related to the number of loading cycles N, by:

$$\delta = \frac{G_{eqN}}{G_{eq1}} = \frac{(\tau_{cN}/\gamma_c)}{(\tau_{c1}/\gamma_c)} = \frac{\tau_{cN}}{\tau_{c1}} = N^{-t} \qquad (3)$$

where t is the degradation parameter. For the Via Dottor Consoli clayey soil, for the 1st cycle is δ = 0.581 and t = 0.026; for the 29th cycle is δ = 0.225 and t = 0.441.

Fig. 16 show the pore-pressure build-up for sandy soil of test site No. 6, Piazza Palestro (Cavallaro and Maugeri, 2005). Pore pressure build-up is very important for liquefaction analyses and slope stability of cohesionless saturated soils (Biondi et al., 2000; 2002).

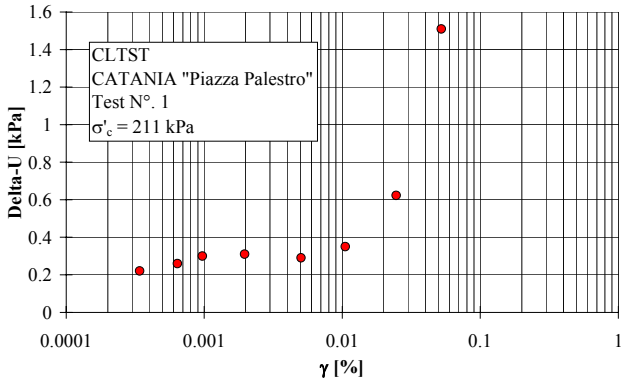

Fig 16: Pore pressure build-up of "Piazza Palestro" site from CLTST.

Although the evaluation of Young's modulus is not required by EC8 for soil, excepted for pile-head static stiffnesses (see annex C part 5) it has been evaluated by Cyclic Loading Triaxial Tests (CLT_xT) performed by the Double Ball Bearing Cyclic Triaxial Test designed by the University of Catania (Cavallaro, 1997). In the Fig. 17 are reported the results of CLT_xT tests performed for Noto soil (Cavallaro and Maugeri, 2003; Cavallaro and Maugeri, 2004a). Young's modulus (E) at small strain and Young's modulus degradation with strain level is important for soil-structure interaction (Abate et al., 2006).

Fig. 17 shows also a comparison between monotonic triaxial test with local and external measurements of E; of course the local measurements is more reliable.

Finally even if it is not required by EC8, the influence of shear strain rate on shear modulus (Tatsuoka and Kohata, 1995) has been evaluated for different cohesive soils

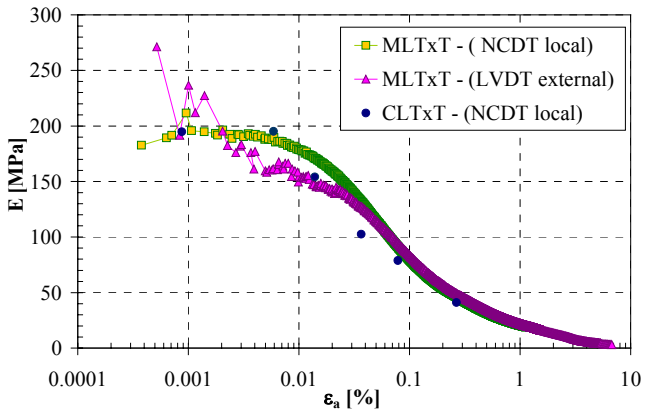

Fig 17: E-ε_a curves from MLTxT and CLTxT.

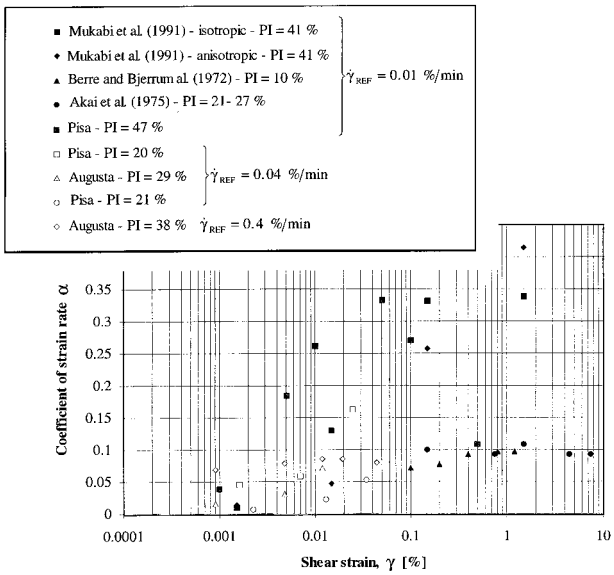

Fig 18: The coefficient of strain rate $\alpha(\gamma)$ for the evaluation of shear strain rate influence.

including test performed for Pisa and Augusta clay (Lo Presti et al., 1998), as reported in Fig. 18.

In particular, these data were obtained by means of T_x tests, CLTST and RCT performed on both remoulded and undisturbed clays. The data, on the whole, clearly show that $\alpha(\gamma)$ increases with the plasticity index and, for a given soil, with the shear strain level.

As is possible to see from Fig. 18 the influence of shear strain rate is relevant for Pisa and Augusta clay.

In spite the values of v_S, G_0, ξ_0 and E_0 are very relevant for solving many geotechnical problems, EC8 do not prescribe the assumptions of any partial factor γ_M for material properties. In general dynamic tests are much more accurate than static ones, thus the partial factor for material property can be lower than the static values. Also the proposed values for γ_{cu}, $\gamma_{cy,u}$, γ_{qu} and γ_ϕ can be reduced. By contrary model partial factor γ_{Rd} must be higher than the static values given by EC7; much more research work is needed for evaluating model partial factor in the dynamic field.

CONCLUSIONS

Site investigation requirements by EC8-Part 1 for identification of soil types are working with some difficulties in localities with extreme spatial variability of soil properties in plan and in depth, as in the case of the city of Catania.

A minimum requirement for quantity and quality of site investigation must be defined in relation to the spatial variability. In the case of spatial variability, sub-class of soil could be established, because of the influence of soil profile on the response spectra. For solving important geotechnical problems, the real soil profile must be considered. Also the depth of investigation must be increased from 30 m to 60-80 m in relation to the particular soil profile and particular geotechnical problem to be solved.

Site investigation requirements by EC8 - part 5 related to siting and foundation soil characterization include cyclic strength and stiffness evaluation, as well as damping evaluation at small and large shear strain. Moreover for cohesive soils the evaluation of cyclic degradation effects under earthquake loads is required as well as pore pressure build-up for cohesionless soils.

These evaluations, which are very important for slope stability analyses and potential liquefaction analyses, are not easy to perform and some more detailed on quality and quantity of in-situ and laboratory tests to be performed must be given. In this respect the new Seismic Dilatometer Marchetti Test (SDMT) seems to be very promising.

Finally much more attention by EC8 should be given to Young's modulus evaluation at small and large strain, which could be relevant for soil-structure interaction analyses. Lastly, the partial factors γ_M

proposed by EC8 for material properties can be reduced, while more research are needed for evaluating the model partial factors γ_{Rd}.

REFERENCES

Abate, G., Massimino, M.R. and Maugeri, M. (2006) "Soil Plasticity and Up-Lifting Effects on Soil-Structure Interaction", *Workshop of ETC12- Evaluation Committee for the Application of EC8*, Athens, January 20-21, 2006 (to appear).

Akai, K., Adachi T. and Ando N., (1975) "Existence of a Unique Stress-Strain-Time Relation of Clays", *Soils and Foundations*, Vol. 15, N°. 1, pp.1-16.

Berre, T. and Bjerrum, L., (1972) "Shear Strength of Normally Consolidated Clays", *Proc. Int. Conf. on SMFE*, Moscow, Paper N°. 1/6, pp. 39-49.

Biondi, G., Cascone, E., Maugeri, M. and Motta, E. (2000) "Seismic Response of Saturated Sohesionless Slopes", *Soil Dynamics and Earthquake Engineering*. Vol. 20, N° 1-4, pp. 209-215.

Biondi, G., Cascone, E. and Maugeri, M. (2002) "Flow and Deformation Failure of Sandy Slopes", *Soil Dynamics and Earthquake Engineering*, Vol.22, pp. 1103-1114.

Biondi, G. and Maugeri, M. (2005) "Seismic Response Analysis of Monte Po Hill (Catania)", In *Seismic Prevention of Damage: a Case Study in a Medietrranean City,* Editor M. Maugeri, WIT Press Southampton, pp. 177-195.

Biondi, G. and Maugeri, M. (2006) "Slope Stability by Modified Newmark Analysis", *Workshop of ETC12- Evaluation Committee for the Application of EC8*, Athens, January 20-21, 2006 (to appear).

Capilleri, P., Massimino, M.R. and Maugeri M. (2003b) "Site-Dependent Response Spectra at the Town of Sellano for the 1997-1998 Umbria –Marche Seismic Sequence", On: "*Geotechnical Analysis of Seismic Vulnerability of Monuments and Historical Sites*", Maugeri & Nova Eds., Pàtron , Bologna, pp. 139-168.

Carrubba, P. and Maugeri, M. (1988) "Determinazione delle Proprietà Dinamiche di un'Argilla Mediante Prove di Colonna Risonante", *Rivista Italiana di Geotecnica*, Vol. 22, N°. 2, pp. 101-113.

Cascone, E. (1996) "Analisi Sperimentale e Modellazione del Comportamento Dinamico dei Muri di Sostegno", *Ph. D. Thesis in Geotechnical Engineering*, University of Catania.

Cavallaro, A. (1997) "Influenza della Velocità di Deformazione sul Modulo di Taglio e sullo Smorzamento delle Argille", *Ph. D. Thesis in Geotechnical Engineering*, University of Catania.

Cavallaro, A., Maugeri, M., Lo Presti, D.C.F. and Pallara, O. (1999) "Characterizing Shear Modulus and Damping from in Situ and Laboratory Tests for the Seismic Area of Catania", *Second International Symposium on Pre-Failure Deformation Charac-teristics of Geomaterials*, Torino, 28-30 September 1999, pp. 51-58.

Cavallaro, A., Grasso, S. and Maugeri, M. (2001) "A Dynamic Geotechnical Characterisation of Soil at Saint Nicolò alla Rena Church Damaged by the South Eastern Sicily Earthquake of 13 December 1990", *Lesson Learned from Recent Strong Earthquake, Earthquake Geotechnical Engineering*, Satellite Conference to 15th ICSMGE, Istanbul 24 Agust, 2001, pp. 243-248.

Cavallaro, A., Lanzo, G., Pagliaroli, A. Lo Presti, D.C.F. and Maugeri, M., (2003) "A Comparative Study on Shear Modulus and Damping Ratio for a Cohesive Soil from Laboratory Tests", *Proceedings of the 3nd International Symposium on Deformation Characteristics of Geomaterials*, Lyon, 22 - 24 September 2003, pp. 257-265.

Cavallaro, A. and Maugeri, M. (2004a) "Modelling of Cyclic Behaviour of a Cohesive Soil by Shear Torsional and Triaxial Tests", *Proceedings of the International Conference on Cyclic Behaviour of Soils and Liquefaction Phenomena*, Bochum, 31 March - 02 April 2004.

Cavallaro, A. and Maugeri, M. (2004b) "Dynamic Geotechnical Characterization for the Microzonation of the Seismical Area of Catania", *Proceedings of the 5th International Conference on Case Histories in Geotechnical Engineering*, New York, 13 - 17 April 2004, paper n°. 3.23.

Cavallaro, A., Grasso, S. and Maugeri, M. (2005) "Site Characterisation and Site Response for a Cohesive Soil in the City of Catania", *Proc. of the Satellite Conference on Recent Developments in Earthquake Geotechnical Engineering*. Osaka University Nakanoshima

Center, Osaka City, Japan, September 10,2005, pp. 167-174.

Cavallaro, A. and Maugeri, M. (2005), "Non Linear Behaviour of Sandy Soil for the City of Catania", *Seismic Prevention of Damage: A Case Study in a Mediterranean City*, Wit Press Publishers, Editor by Maugeri M., pp. 115-132.

Cavallaro, A., Grasso, S. and Maugeri, M. (2006a) "Volcanic Soil Characterisation and Site Response Analysis in the City of Catania", *Proc. of the VIII National Conference on Earthquake Engineering (8thNCEE)*. San Francisco, USA, April 18-22, 2006 (to appear).

Cavallaro, A., Grasso, S. and Maugeri, M. (2006b) "Clay Soil Characterisation by the New Seismic Dilatometer Marchetti Test (SDMT)", *Proc. of the 2nd International Conference on the Flat Dilatometer*, Washington, April 2 - 5, 2006, (to appear).

Cavallaro, A. and Maugeri, M. (2005) "Non-Linear Behaviour of Sandy Soil for the City of Catania", In *Seismic Prevention of Damage: a Case Study in a Mediterranean City,* Editor M. Maugeri, WIT Press Southampton, pp. 115-132.

EC8 - Part 1 (2003) "Eurocode 8: Design of Structures for Earthquake Resistance - Part 1: General Rules, Seismic Actions and Rules for Buildings", December 2003 p. 215.

EC8 - Part 5 (2003) "Eurocode 8: Design of Structures for Earthquake Resistance - Part 5: Foundations, Retaining Structures and Geotechnical Aspects", December 2003 p. 44.

Grasso, S. and Maugeri, M. (2005) "Vulnerability of Physical Environment of the City of Catania Using GIS Technique", In *Seismic Prevention of Damage: a Case Study in a Medietrranean City,* Editor M. Maugeri, WIT Press Southampton, pp. 155-175.

Hryciw, R.D. (1990) "Small Strain Shear Modulus of Soil by Dilatometer", *JGED, ASCE*, VoL. 116, N°. 11, pp. 1700-1715.

Jamiolkowski, M., Lo Presti, D.C.F. and Pallara, O. (1995) "Role of In-Situ Testing in Geotechnical earthquake Engineering", *Proceedings of 3rd International Conference on Recent Advances in Geotechnical Earthquake Engineering and Soil Dynamic*, State of the Art 7, St. Louis, Missouri, April 2-7, 1995, Vol. II, pp. 1523-1546.

Lehane, B. and Fahey, M. (2004) "Using SCPT and DMT Data for Settlement Prediction in Sand", *Proceedings of the 2nd International Conference on Geotechnical Site Characterization, Porto, 20 - 22 September 2004,*, pp. 1673-1679.

Lo Presti, D.C.F., Maugeri, M., Cavallaro, A., and Pallara, O. (1998) "Shear Modulus and Damping of a Stiff Clay from in Situ and Laboratory Tests", *Proceedings of the 1st International Conference on Site Characterization*; Atlanta, 19 - 22 April 1998, pp. 1293-1300.

Marchetti, S. (1980) "In Situ Tests by Flat Dilatometer", *ASCE, Jnl GED,* Vol. 106, N°. 3, pp. 299-321.

Maugeri, M. (2005) "Seismic Prevention of Damage: a Case Study in a Medietrranean City", Editor M. Maugeri, WIT Press Southampton, 408 p.

Maugeri, M., Carrubba, A. and Carrubba, P. (1988) "Caratterizzazione Dinamica e Risposta del Terreno nella Zona Industriale di Catania", *Ingegneria Sismica*, n. 2, pp. 9-18.

Maugeri, M. and Cavallaro, A. (1999) "Non Linear Soil Behaviour of Catania Clays", *The Catania Project. Earthquake Damage Scenarios for High Risk Area in the Mediterranean*. Ed. E. Faccioli & V. Pessina. CNR-GNDT, Roma, pp. 38-41.

Maugeri, M. and Vannucchi, G. (1999) "Liquefaction Risk Analysis at S.G. La Rena, Catania, (Italy)", *Earthquake Resistant Engineering Structures (ERES 99)*, Catania, 15-17 June, 1999, pp. 301-310.

Mayne, P.W. and Rix, G.J. (1993) "G_{max}-q_c Relationships for Clays", *Geotechnical Testing Journal*, Vol. 16, N°. 1, pp. 54-60.

Monaco, P., Marchetti, S., Totani, G. and Calabrese, M. (2005) "Sand Liquefiability Assessment by Flat Dilatometer Test (DMT)", *Proc. XVI ICSMGE*, Osaka, 4, pp. 2693-2697.

Mukabi, J. N., Tatsuoka, F. and Hirose, K., (1991) "Effect of Strain Rate on Small Strain Stiffness of Kaolin in CU Triaxial Compression"; *Proc. 26th Japan National Conf. on SMFE*, Nagano, pp. 659-662.

Ohta, Y. and Goto, N. (1978) "Empirical Shear Wave Velocity Equations in Terms of Characteristic Soil Index", *Earthquake Engineering and Structural Dynamics,* Vol. 6.

Tatsuoka, F. and Kohata, Y. (1995) "Stiffness of Hard Soils and Soft Rocks in Engineering Applications", *Report of the Institute of Industrial Science*, The University of Tokyo, March 1995, Vol. 38, N°. 5.

Vucetic, M., Dobry, R. (1991) "Effect of soil plasticity on cyclic response". Journal of

Geotechnical Engineering, Vol. 117, No. 1, pp. 89-107

Yokota, K., Imai, T. and Konno, M. (1981) “Dynamic Deformation Characteristics of Soils Determined by Laboratory Tests”, *OYO Tec. Rep*. 3, pp. 13-37.

Yoshida, Y. and Motonori I. (1988) “Empirical Formulas for SPT Blow-Counts for Gravelly Soils“, *Proceedings of ISOPT-1,* Orlando, USA.

SESSION 2: Liquefaction - Slope Stability

Some Comments on the EC8 Prescriptions for the Evaluation of Soil Liquefaction.

D.C. F. Lo Presti[1], E. Mensi[2], N. Squeglia[1]

[1] *Università di Pisa, Italy*
[2] *Politecnico di Torino, Italy*

Abstract

Soil liquefaction is one of seismic induced phenomena frequently observed after an earthquake. In the present contribution prescription for the evaluation of soil liquefaction are analysed. After a critical description of criteria reported in the Eurocode 8, in comparison to Italian Code, some applications are presented and a proposal to modify the clauses (7) and (8) of paragraph 4.1.3 of the Eurocode 8 is put forward.

INTRODUCTION

EC8 [1998] and Italian Code [OPCM 3274, 2003] specify requirements for siting and foundation soils. More specifically, both the above-mentioned codes prescribe that the following hazards should be minimised:

- slope instability
- soil liquefaction
- excessive earthquake induced settlements
- fault rupture on ground surface

Such phenomena represent the most common seismic induced soil failures in a site. For example Table 1 [Keefer and Tannaci, 1981] shows data from 47 earthquakes (M=5.2÷8.6) occurred between 1811 and 1980. Almost in all cases fault activity has been observed on ground surface. Also slope instability induced by earthquake has been frequently observed, as well as soil liquefaction and densification.

The aim of present paper is a critical analysis of liquefaction risk assessment in the framework of EC8 and Italian Code.

In the present paper the following items have been analysed:

- definition of criteria for the evaluation of liquefaction susceptibility;
- application of simplified methods for the assessment of liquefaction risk to some real cases in Italy;
- definition of simplified criteria for the evaluation of liquefaction effects.

Table 1: Main geotechnical phenomena associated with earthquakes. [Keefer and Tannaci, 1981]

Observed Phenomena	Occurrence (% of historical earthquakes)
Surface expression of faulting	100
Landslide in soil	72
Landslide in rock	64
Surface fissuring not caused by faulting or soil liquefaction	57
Soil liquefaction	51
Soil compaction and settlements	51
Surface subsidence above underground openings	13
Snow avalanches	11
Cracks or falls in underground openings	9

LIQUEFACTION SUSCEPTIBILITY

There are three criteria by which liquefaction susceptibility can be assessed [Kramer, 1996; TC4 – ISSMGE, 1999]:

- historical;
- geologic;
- compositional.

Post-earthquake field investigations showed that liquefaction often recurs at the same location. Thus liquefaction case histories can be used to identify sites susceptible to liquefaction. On the contrary it is not possible to exclude the occurrence of soil liquefaction at location in which such phenomenon has never been observed before.

Figure 1 [TC4-ISSMGE, 1999] shows some statistical correlations between magnitudes and epicentre distance of the site in which soil liquefaction occurred. It can be noted that magnitude lower than 4.2 seems to be unable to induce soil liquefaction.

EC8 [1998] and the Italian Code prescribe the evaluation of liquefaction risk if the quantity $\gamma_i S \frac{a_g}{g}$ is greater than 0.15. In the expression γ_i is an importance factor, S is a coefficient related to soil profile, a_g/g is the ground acceleration defined in the code for each site (zonation maps from hazard analyses).

About this quantity the following considerations can be made:

- design ground acceleration defined by the Italian Code often do not corresponds to the values obtained from seismic hazard analyses (see Table 2). For example, if for a site seismic hazard analyses indicate a ground acceleration of 0.08g, related to a return period of 475y, the same site is classified for the Italian Code with a design ground acceleration of 0.15g. As a consequence the code introduces an additional safety factor that in the present example is about 2.
- in soils susceptible of liquefaction the elastic response spectrum is not defined as well as the coefficient S. The Italian Code suggests to use the highest value S = 1.35. Anyway, experimental evidences seem indicate that in such cases a reduction in amplification is possible [Kokusho, 1999]

The geologic criterion, not included in the Italian Code, indicates that soils susceptible of liquefaction are saturated (ground water table near the surface) Holocene deposits mainly of fluvial, colluvial and aeolian origin or in not well compacted human – made soil deposits.

Table 2: Design acceleration (Italy).

Zone	PGA	a_{gR}
1	< 0.05	0.05
2	0.05 – 0.15	0.15
3	0.15 – 0.25	0.25
4	> 0.25	0.35

About compositional and state criteria, EC8 and Italian Code can be superimposed. In both codes soils are not susceptible of liquefaction if one of the following three conditions occurs:

- clay fraction greater than 20% and $I_p > 10\%$;
- fine content greater than 35% and $(N_1)_{60} > 20$;
- $(N_1)_{60}$ greater than 25.

The quantity $(N_1)_{60}$ belongs to number of blows N_{SPT} measured by means of SPT referred to an efficiency of 60% and a stress state equal to atmospheric pressure. The procedures adopted to obtain $(N_1)_{60}$ from N_{SPT} are reported in Skempton [1986], Shmertmann and Palacios [1979], Kovacs and Salomone [1982] and Liao and Withmann [1986].

The compositional criterion reported in the Eurocode 8 and in the Italian Code lead to the following considerations:

- Ishihara [1993] and Seed et al. [2003] stated that cyclic strength of fine-grained soils with $I_p > 10\%$ is greater than that of non-plastic fine-grained soils. As a consequence it seems that the plasticity of fine content is more important of its quantity in defining cyclic strength. In fact the greater is the plastic index, the lower is liquefaction susceptibility;
- The limit of 20% for clay fraction seems too much conservative. Some examples reported in the following will show this item;
- The parameter $(N_1)_{60}$ is strongly affected by grain size distribution [Cubrinowski & Ishihara, 1999]. As a consequence the same value for $(N_1)_{60}$ (e.g. 20, the value indicated in the codes) refers to a high relative density for a fine sand, whereas refers to a very low relative density for a medium coarse sand. Also in this case the criterion reported above seems too much conservative.

In the Chinese Code [Wang, 1979; Seed & Idriss, 1982; Andrews & Martin, 2000], soils are

susceptible of liquefaction if all the condition listed in the following simultaneously occur:

- fine content (d < 0.005 mm) < 15%
- liquid limit (LL) < 35%
- water content (wn) > 0.9 LL.

An equivalent way to stress the condition about fine content and liquid limit are [Seed et Al., 2003]:

- clay fraction (d < 0.002 mm) < 10%
- liquid limit (LL) < 32 %.

In this criterion there is no reference to plastic index although liquid limit is strongly correlated to it. Seed et Al. [2003] suggest a criterion based on plastic properties of soils, as reported in figure 2. In writers opinion this criterion is more reasonable than that suggested in EC8 and Italian Code.

In any case a classification of soil based on laboratory tests is needed.

In conclusion, the writers suggest evaluating the liquefaction susceptibility by means of a correlation between the following information:

- site geology and litology;
- ground water level;
- intensity of expected seismic shaking

In the following some examples will be proposed to the reader in order to clarify the methods and the site investigation techniques.

SIMPLIFIED METHOD FOR THE ANALYSIS OF RISK OF LIQUEFACTION.

Risk of liquefaction.

A complete approach to the problem needs the following ingredients:

- definition of maximum acceleration at bedrock by means of a probabilistic seismic hazard analysis;
- definition of a couple Magnitude – distance with reference to a required return period by means of a process of deaggregation;
- selection of some accelerograms recorded in free-field condition compatible with the magnitude defined in the previous step;
- analysis of seismic response of a site in order to determine the maximum acceleration expected at ground surface and simulate the occurrence of soil liquefaction by means of algorithm that take into account the behaviour of liquefiable soils.

The complete analysis reported above need the knowledge of the following information:

- soil profile;
- shear wave velocity profile;
- ground water level position;
- G-γ and D-γ relationship for all soil layers;
- relationship between excess pore pressure and deformation and number of cycles of loading;
- strength parameters in terms of effective stress (c', φ') and/or cyclic undrained shear strength ($\tau_{cyc,u}$ or CRR)

Simplified analyses [Seed & Idriss, 1982; Seed et Al., 1985, Youd & Idriss, 2001] need the execution of the following steps:

- definition of the Cyclic Stress Ratio (CSR)
- definition of the Cyclic Resistance Ratio (CRR) by means of site tests;
- definition of expected number of cycles as function of Magnitude;
- safety factor calculation.

In order to evaluate CSR in a simple way, the following relations have been proposed:

$$\mathrm{CSR} = \frac{\tau_{av}}{\sigma'_{v0}} = 0.65 \frac{a_{max}}{g} \frac{\sigma_{v0}}{\sigma'_{v0}} r_d \qquad (2)$$

$r_d = 1.0 - 0.00765z$ if $z < 9.15$ m (3)

$r_d = 1.174 - 0.0267z$ if $9.15 < z < 23$ m (4)

where τ_{av} is the average shear stress in the soil, σ'_{v0} and σ_{v0} are respectively the geostatic effective and total vertical stress and r_d is a coefficient that takes into account soil deformability. Another relationship to evaluate CSR has been suggested by Seed et Al. [2003]. An evaluation of CRR is possible by means of the following expression:

$$\mathrm{CRR}_{7.5} = \frac{1}{34 - (N_1)_{60cs}} + \frac{(N_1)_{60cs}}{135} + \frac{50}{[10(N_1)_{60cs} + 45]^2} - \frac{1}{200} \qquad (5)$$

Where $(N_1)_{60cs}$ depends on $(N_1)_{60}$ by the expression

$$(N_1)_{60cs} = \alpha + \beta (N_1)_{60} \qquad (6)$$

in which α and β assume the following values

$\alpha = 0 \quad \beta = 1$ if FC < 5%

$\alpha = \exp(1.76-190/FC^2)$ $\beta = 0.99 + FC^{1.5}/1000$ if 5 < FC < 35%

$\alpha = 5 \quad \beta = 1.2$ if FC > 35%

The parameter $(N_1)_{60}$ depends on N_{spt} by means of the following expression

$$(N_1)_{60} = N_{SPT}\, C_N\, C_E\, C_B\, C_R\, C_S \qquad (7)$$

in which $C_N = (p_a/\sigma'_{v0})^{0.5}$ where p_a is the atmospheric pressure and σ'_{v0} is the geostatic effective vertical stress, C_E = ER/60 where ER is the efficiency (Energy Ratio) of test apparatus, C_B = 1.0 – 1.05 – 1.15 respectively for borehole diameter between 65 and 115 mm, between 115 and 150 mm and between 150 and 200 mm, C_R = 0.75 – 0.8 – 0.85 – 0.95 if the depth L of test respectively satisfy this conditions L < 3 m, 3 < L < 4, 4 < L < 6, 6 < L < 10, 10 < L < 30, C_S = 1 if European sampler has been employed or C_S = 1.3 for a Raymond sampler without liner.

Safety factor against liquefaction can be evaluated by means the following expression

$$F_L = \frac{(CRR)_{7.5}}{CSR} MSF \qquad (8)$$

in which MSF = $10^{2.24}$ / $M_w^{2.56}$ is a scale factor that takes into account seismic magnitude (i.e. the moment magnitude). In the Italian code the minimum value accepted of the safety factor is 1.25. The equation reported above applies to seismic magnitude greater than 5.25. Further expression can be found in Youd et Al. [2001] and Seed et Al. [2003].

If geostatic stress state or shear stress is particularly high the equation (8) must be written in the following way:

$$F_L = \frac{(CRR)_{7.5}}{CSR} MSF \cdot K_\sigma \cdot K_\alpha \qquad (9)$$

in which K_σ and K_α are factors taking into account respectively of geostatic stress state and shear stress. Further details about these coefficients can be found in Youd et Al. [2001] and Seed et Al. [2003].

Effects of liquefaction

The Italian code and the eurocode 8 let to neglect the risk of liquefaction if the elevation of the liquefiable stratum is more than 15 m below ground level. Such prescription is a consequence of the consideration that the effects of liquefaction of such stratum are not evident.

The recommendations of the Italian code and EC8 seem too much conservative if compared to that contained in TC4-ISSMGE [1999]. In fact the risk of liquefaction could be neglected if the thickness of non-liquefiable stratum is greater than the thickness of underlying liquefiable stratum.

SOME APPLICATION

A site in the north west of Tuscany has been analysed. The following information were available:

- seismic hazard analysis of the site [Mensi et Al., 2004; Lai et Al., 2005] with knowledge of PGA referred to various return period, Magnitude – distance couples which mostly contribute to the local hazard and some seismo compatible accelerograms on rock;
- seismic hazard analysis of the whole area [GNDT, 1999] which provides the PGA and the seismic intensity (MCS) at site for various return period;
- classification of the site with reference to Italian code (a_g/g = 0.25);
- soil profile deduced by a borehole up to 12 m from ground level;
- several LPT test performed accordingly to Crova et Al [1992];
- two SCPT carried out in the vicinity (2 m) of the borehole.

Seismic hazard analysis of the site [Mensi et Al., 2004; Lai et Al., 2005] gives the following parameters:

- a_{max}/g = 0.158 for a return period of 475y;
- M = 5.3 and d = 10.5 km;
- the accelerograms reported in figure 3.

Seismic hazard analysis of the whole area [GNDT, 1999] gives the following parameters:

- a_{max}/g = 0.159 for a return period of 475y
- I_0 = 7.8 (MCS) for the same return period.

Table 3: Grain size and LPT at Licciana Nardi site.

Sample	Depth	Pebbles	Gravel	Sand	Silt	d_{50}	N_{LPT}
-	[m]	%	%	%	%	mm	-
1	0.00-0.80	-	33	43	24	0.23	-
2	1.50-2.00	-	8	68	24	0.23	3
3	2.00-2.60	11	75	10	4	28.65	-
4	2.60-3.00	-	34	55	11	0.59	4
5	3.00-4.00	-	27	51	22	0.23	-
6	4.00-4.50	-	28	56	16	0.3	13
7	5.00-5.60	-	67	24	9	7	10
8	7.50-8.00	11	67	13	9	18.88	17
9	9.50-10.00	11	65	17	7	14.25	-
10	10.00-11.00	4	73	18	5	13.89	-
11	11.00-12.00	-	74	17	9	9.7	-

Table 4: Processing of N_{LPT} and CRR estimation.

z [m]	N_{LPT}	σ_v	σ'_v	C_N	C_R	d_{50}	C_{Lg}	$(N_1)_{60}$	FC	a	b	$(N_1)_{60cs}$	CRR
1.5	3	30	30	1.70	0.75	0.2	1.50	8.0	24	4.18	1.11	13.1	0.141
3	4	60	60	1.29	0.80	0.6	1.38	8.0	11	1.20	1.03	9.4	0.108
4.5	13	90	85	1.08	0.85	0.3	1.50	25.2	16	2.77	1.05	29.2	0.420
6	9	120	100	1.00	0.95	7	0.83	9.9	9	0.56	1.02	10.7	0.119
7.5	17	150	115	0.93	0.95	19	0.60	12.7	9	0.56	1.02	13.5	0.145
9	6	180	130	0.88	0.95	14	0.66	4.6	7	0.12	1.01	4.8	0.070

$C_E = 1.4$

Soil profile consists in an alternate sequence of sandy gravels and gravelly sands with different percentage of silt up to 12 m from ground surface, where the claystone have been located. Table 3 summarizes all the information deduced by the borehole. Figure 4 summarizes the results of LPT and SCPT tests. Water table has been located 4 m below ground level.

All the criteria described above (geological, historical and compositional) confirm the susceptibility of the site to liquefaction. As a consequence a (simplified) analysis of risk of liquefaction is needed.

Figure 5 shows the map of Tuscany where both condition of recent alluvial deposit (Geologic map of Tuscany) and seismic intensity greater than VIII [GNDT, 1999] are superimposed. As can be noted the extension of these areas are limited. The black dot indicates the location of site in discussion.

In order to apply the method described above, the definition of PGA is needed. If seismic hazard analysis of the site has not been carried out, the Italian code prescribes an acceleration of 0.338g for the site of this example. Alternatively it is possible to perform a ground response analysis using the accelerograms reported in figure 3 scaled with the peak acceleration of the site (0.158g). Such analysis, performed with the code EERA [Bardet, 2000] and soil data reported in Mensi et Al. [2004], gives a PGA of 0.21g.

Seismic magnitude of 5.3 has been estimated by means of deaggregation analysis [Mensi et Al., 2004]. Another way to estimate magnitude is the following equation [Karnik, 1969]

$$M_K = 0.531\ I_0 + 0.95 \qquad (12)$$

Since seismic intensity $I_0 = 7.8$, magnitude is 5.1, which is a value similar to that estimated with deaggregation analysis.

In Table 4 [Bozzola, 2003] calculations carried out to estimate $CRR_{7.5}$ have been summarized. Note that results from LPT have been corrected by a factor C_{Lg} depending on d_{50} [Tokimatsu, 1988].

In Table 5 calculations carried out to estimate CSR, MSF and F_L have been summarized. Subscripts (1) and (2) refer respectively to calculations based on PGA

prescribed by Italian code and seismic hazard analysis plus ground response analysis. It can be noticed that in the second case the values of F_L are greater than that of first case.

In the same site undisturbed samples were retrieved by means of in situ freezing method (Lo Presti et al., 2005) at a distance of about 20 m from the borehole where LPT has been performed. Three samples were retrieved from each depth between 2.0 m and 6.0 m below the ground level. It is important to remark that the retrieved samples exhibited a strong heterogeneity in term of grain size and relative density. Differences of grading and density were observed among samples retrieved from the same depth and in comparison to the results obtained from the not - far conventional borehole.

Table 5: Estimation of CSR and FL

r_d	CSR(1)	F_L(1)	CSR(2)	F_L(2)
0.99	0.217	1.586	0.135	2.549
0.98	0.214	1.226	0.133	1.969
0.97	0.224	4.553	0.140	7.317
0.95	0.251	1.155	0.156	1.856
0.94	0.270	1.307	0.168	2.100
0.93	0.283	0.606	0.177	0.974

M = 5.3; MSF = 2.43; a_{max} (OPCM2003) = 0.338;
a_{max} (Hazard analysis) = 0.219

Table 6: Test Conditions. Liquefaction tests - Frozen samples

z (m)	2.20-2.80	2.30-2.90	4.05-4.70
e (-)	0.290	0.333	0.332
σ'c (kPa)	47.6	45.8	54.1

Table 7: Liquefaction test results.

Dr (%)	σ_c (kPa)	σ_d (kPa)	N (-)	GC (%)	SC (%)	FC (%)
70	47.6	95 (0.98)	1	81	14	5
87	45.8	60 (0.66)	20	47	31	22
37	54.1	80 (0.74)	-	80	19	1

Liquefaction tests were run on isotropically consolidated specimens. More specifically, one – way cyclic compression loading triaxial tests were performed in undrained condition under stress control. Table 5 summarizes test condition at the end of consolidation. The deviator stress (σ_d), which was applied during undrained shearing, is also indicated in Table 7 and, in brackets, the cyclic stress ratio $(CSR = \frac{\sigma_d}{2 \cdot \sigma'_c})$.

Figure 6 compares the CSR, obtained in this research on undisturbed samples, to those obtained by Kokusho and Tanaka [1994] on gravely undisturbed samples. The CSR was defined as the normalized deviator stress, which causes 2% single amplitude axial strain in a given number of cycles. This condition coincides with a pore pressure ratio equal to 1.0 (zero –effective consolidation pressure). It is worthwhile to remark that the agreement with the data by Kokusho and Tanaka [1994] is a coincidence and the only possible conclusion is that the liquefaction strength of undisturbed samples is much larger than that usually obtained from reconstituted samples. It is also important to notice that only two of the three tested samples liquefied.

Table 7 summarizes the liquefaction-test results. More specifically, the table shows:

- relative density of the frozen samples;
- effective consolidation pressure;
- applied deviator stress and, in brackets, the CSR;
- number of loading cycles causing liquefaction;
- gravel (GC), sand (SC) and fine contents (FC).

It is worthwhile to remark that the liquefaction condition appears to be more controlled by compositional factors than global relative density. It should be stressed that the samples that liquefied exhibited a quite important percentage of medium to fine sand, whilst the sample that did not liquefy consists of gravel and coarse to medium sand.

Incidentally, the factory of safety against liquefaction obtained from the laboratory tests was quite greater than that inferred from in situ tests, performed at a distance of about 20 m.

In the end, some sites in Piedmont (Italy) that, on the Authors experience based on the considerations reported in the following, do not exhibit conditions for liquefaction susceptibility are discussed. On the contrary, according to EC8 and the Italian Code liquefaction analyses should be done with the conclusion that the mentioned sites are not suitable for construction. The available information is summarized in Table 8.

Table 8: Piedmont Sites.

Site	I_o (MCS)	M_k	a_{max}	Seismic Zone	N_{SPT}	z [m]
A	6.1	4.2	0.136	2	5	9
B	5.4	3.6	0.059	4	1 – 3	2.5
C	6.1	4.2	0.132	2	6	15

Peak ground acceleration has been computed for a return period of 475 years [GNDT, 1999]. Data shown indicate that zonation is not coherent with the hazard analysis especially for sites A e C that, more correctly, should be classified in zone 3.

It is worthwhile to remark that the sites and especially the considered layers consist of clayey silts with presence of organic matter, non – susceptible to liquefaction. Anyway, the compositional criteria of OPCM 3274 [2003] and EC8 [1998] lead to different conclusions. Limitations of the historical criterion of the above mentioned codes are also evident, especially for sites A and C where $a_{max} / g = 0.3375$ should be considered.

CLOSING REMARKS

The Authors propose to modify the clauses (7) and (8) of paragraph 4.1.3 in the following way:

(7) For buildings on shallow foundations, evaluation of the liquefaction susceptibility may be omitted when the saturated sandy soil layer of thickness H1 is found at depths H2>2H1 from the ground surface.

(8) Neglecting the liquefaction hazard is also permitted when a_{gR} < 0.15 g and the following conditions are fulfilled:

- clay fraction (d<0.002 mm) > 10%;
- limit liquid (LL) > 32 % ;
- water content (Wn) > 0.9 LL.

Criteria based on Nspt or (N1)60 should be omitted because of the great influence of grain size on the dynamic penetration resistance.

In spatially heterogeneous alluvial deposits the number of boreholes should be sufficient to verify the variability of ground conditions.

In well-graded coarse soils (from gravel to silt) the soil composition should be carefully checked in order to identify the presence of fine sands and silts. For this type of soils the global relative density does not appear as a relevant parameter.

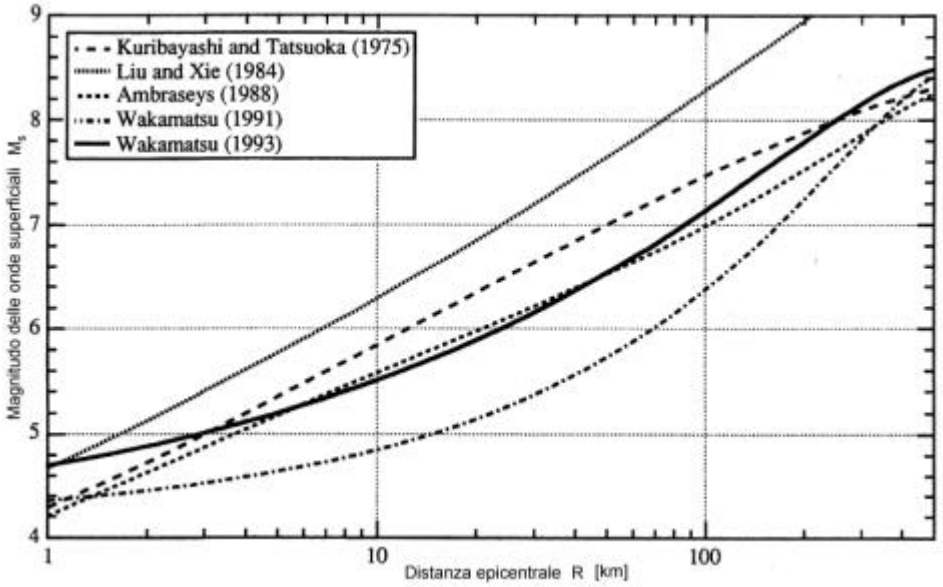

Fig 1: Historical criteria, Magnitude vs. epicentre distance.

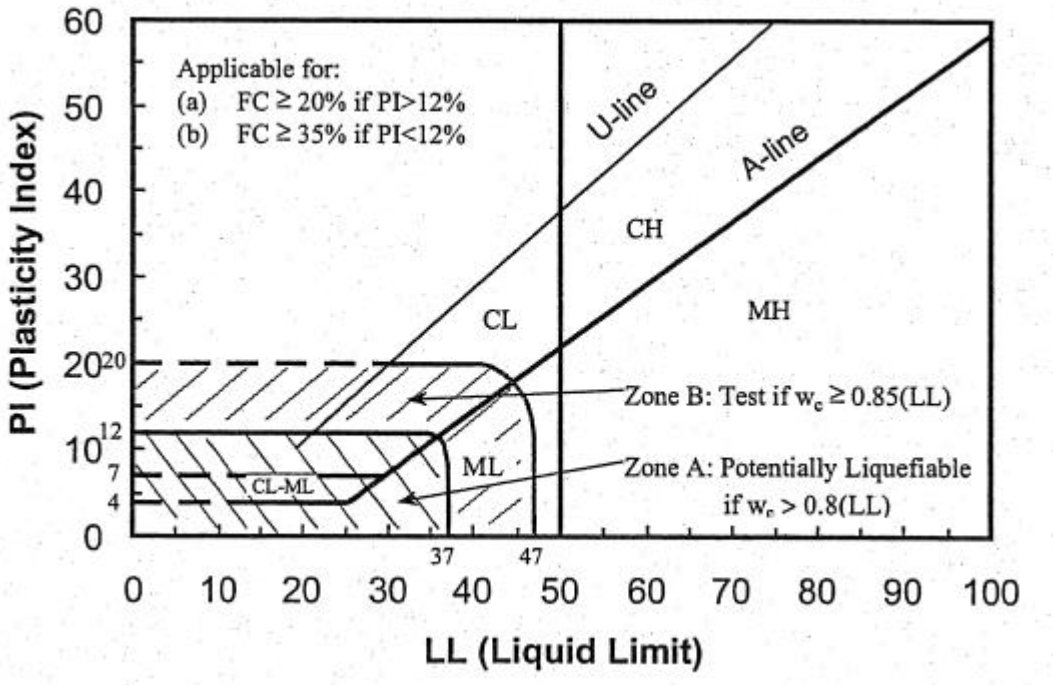

Fig. 2: Compositional Criterion by Seed et Al. [2003].

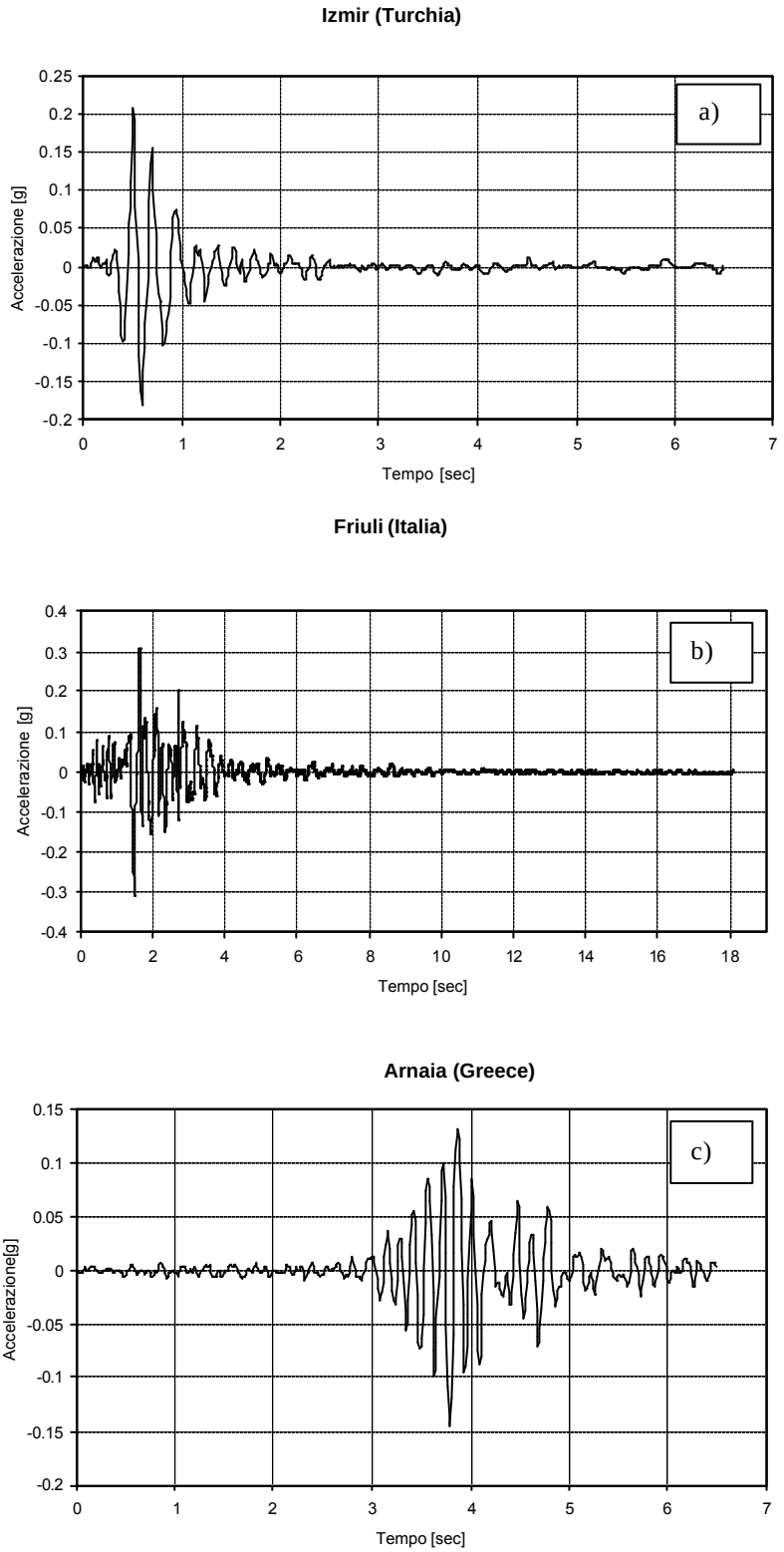

Fig. 3: Time histories of acceleration on bedrock: a) Izmir (Turkey), b) Friuli (Italy), c) Arnaia (Greece).

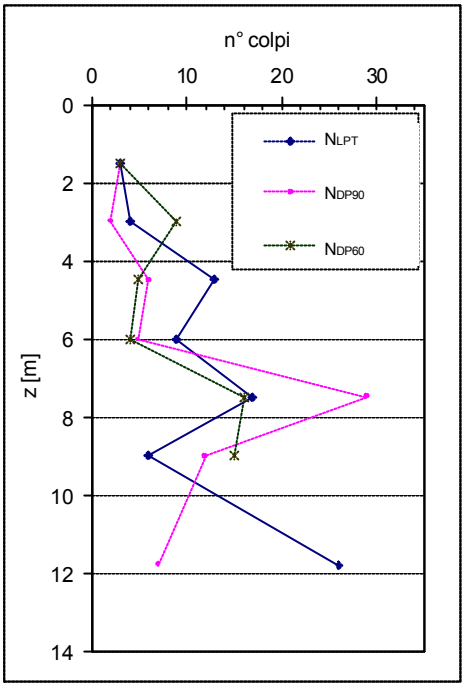

Fig. 4: Penetrometric resistance profile at Licciana Nardi site.

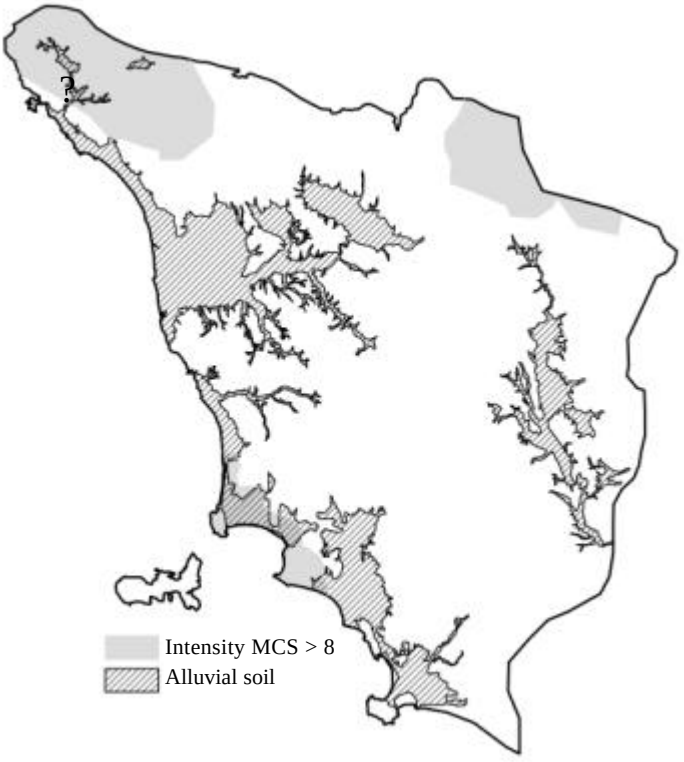

Fig. 5: Superposition of areas with MCS intensity greater than 8 and areas with alluvial soil [CGTONLINE, 2004]

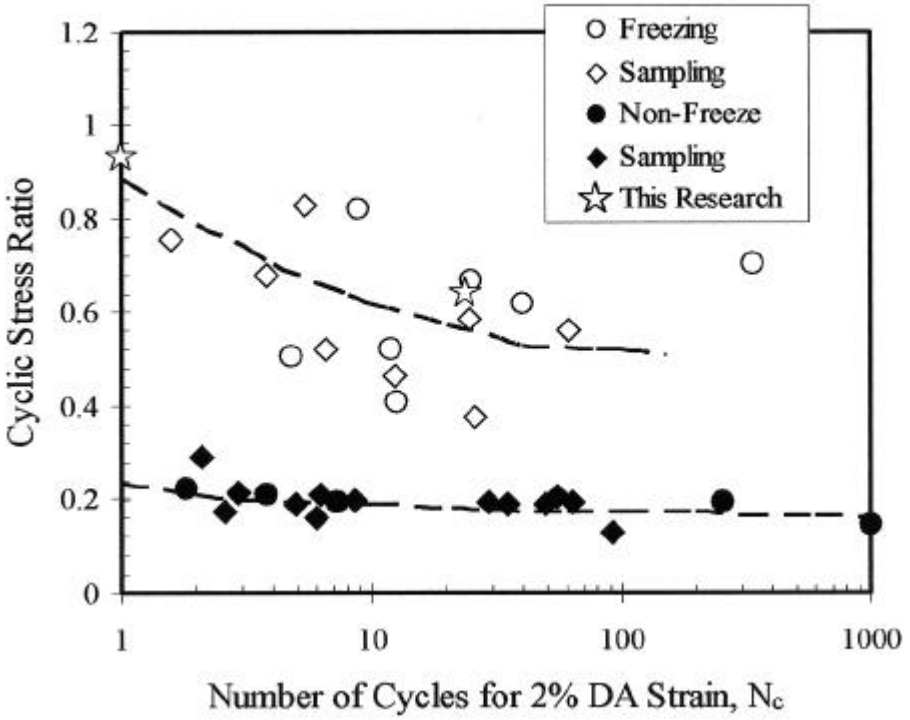

Fig. 6: Comparison between results obtained on undisturbed samples with that previously obtained by Kokusho and Tanaka [1994]

REFERENCES

Andrews D.C., Martin G.R. (2000), *Criteria for Liquefaction of Silty Soils,* 12th WCEE, Proceedings, Auckland, New Zealand.

Bardet, J.P., Ichii, K. and Lin C.H. (2000). *EERA – A Computer Program for Equivalent-Linear Earthquake Site Response Analyses of Layered Soil Deposits,* Department of Civil Engineering, University of Southern California, http://geoinfo.usc.edu/gees.

Bozzola F. 2003 *La tecnica del congelamento per il prelievo di campioni di terreno a grana grossa: vantaggi e benefici*. Tesi di Laurea, II Facoltà di Ingegneria Vercelli, Politecnico di Torino.

CGTONLINE (2004), *Carta Geologica della Toscana 1.250000,* Centro di Geotecnologie Università degli Studi di Siena, www.geotecnologie.unisi.it

Crova, R., Jamiolkowski, M., Lancellotta, R. and Lo Presti, D.C.F. (1992), *Geotechnical characterization of gravely soils at Messina Site, selected topics.* Proceedings of the Wroth Memorial Symposium, Thomas Telford, London, pp.199-218.

Cubrinovski M. & Ishihara K. (1999). *Empirical Correlation between SPT N-value and Relative Density of Sandy Soils.* Soils and Foundations. 5: 61-71.

Eurocode 8 (1998) *Design Provisions for Earthquake Resistance of Structures - Part 1-1:General Rules for the Representation of Seismic Actions." Part 5: Foundations, Retaining Structures and Geotechnical Aspects.*

GNDT (1999) *Servizio Sismico Nazionale Carta di pericolosità sismica 1999*

Ishihara K. (1993) *Liquefaction and flow failure during earthquakes.* The 33rd Rankine Lecture. Géotechnique 43(3): 351-415.

Karnik V. (1969) *Seismicity of the european area.* Reidel Publishing Company-Holland, vol. 1, parte II

Keefer D.K. & Tannaci N.E. (1981) *Bibliography on Landslides, Soil Liquefaction and Related Ground Failures in Selected Historic Earthquakes.* Open File Report 81-572, U.S. Department of Interior.

Kokusho T. (1999) *Effect of non-linear soil properties on seismic amplification in surface layers.* Proc. 2nd International Conference on Earthquake Geotechnical Engineering. Lisboa Portugal. Vol. 3: 913-918.

Kokusho T., Tanaka Y., (1994) *Dynamic properties of gravel layers investigated by in situ freezing sampling.* ASCE GSP no.44, Ground failures under seismic conditions, pp: 121 – 140.

Kovacs W.D., Salomone L.A. (1982). *SPT Hammer Energy Measurements.* Journal of Geotechnical Engineering, ASCE. GT4.

Kramer, S.L. (1996) *Geotechnical Earthquake Engineering*, Prentice-Hall, New Jersey, pp.653.

Kuribayashi,E. and Tatsuoka,F. (1975) *Brief Review of Soil Liquefaction During Eathquakes in Japan*, Soils and Foundations, Vol.15,no.4, pp.81-92

Lai C., Strobbia C., Dall'Ara (2005) *Convenzione tra Regione Toscana e Eucentre. Parte 1. Definizione dell'Input Sismico per i Territori della Lunigiana e della Garfagnana.*

Lo Presti D., Pallara O., Froio F., Rinolfi A., Jamiolkowski M. (2005) *Stress-Strain-Strength Behaviour of Undisturbed and Reconstituted Gravely Soil Samples* Submitted to Italian Geotechnical Journal for publication, September 2005

Liao S.C. & Withmann R.V. (1986). *Overburden Correction Factors for SPT in Sand*. Journal of GED, ASCE. 112(3): 373-377

Mensi E., Lai C., Spallarossa D. Pallara O. & Lo Presti D. (2004) *Risposta sismica in alcune aree della Toscana: un confronto con le indicazioni dell'Ordinanza dell'OPCM 3274*

OPCM 3274 (2003) *Primi elementi in materia di criteri generali per la classificazione sismica del territorio nazionale e di normative tecniche per le costruzioni in zona sismica*. Gazzetta Ufficiale della Repubblica Italiana 8maggio 2003, n. 108

Schmertmann J.H., Palacios, A. (1979). *Energy Dynamics of SPT.* Journal of GED, ASCE. 105(GT8): 909-926.

Seed H.B, Idriss I.M. (1982). *Ground motion and soil liquefaction during earthquakes. Monograph, EERI, Oakland, Ca. USA.*

Seed H.B. , Tokimatsu K. Harder L.F. , Chung (1985) *Influence of SPT procedures in soil liquefaction resistance evaluations*. Journal of GED, ASCE, 111(12), 1425-1445.

Seed R.B., Cetin O., Moss R.E.S., Kammarer A.M., Wu J., Pestana J.M., Riemer M.F., Sancio R.B., Bray J.D., Kayen R.E. & Faris A. (2003) *Recent Advances in Soil Liquefaction Engineering: a Unified and Consistent Framework.* 26th Annual ASCE Los Angeles Geotechnical Spring Seminar.

Skempton A.W. (1986). *Standard Penetration Tests Procedures & the Effects in Sands of Overburden Pressure, Relative Density, Particle Size, Ageing and Overconsolidation.* Géotechnique. 36(3): 425-447.

TC4-ISSMGE (1999). *Manual for Zonation on Seismic Geotechnical Hazards (Revised Version).* Technical Committee for Earthquake Geotechnical Engineering, TC4, ISSMGE,

Published by the Japanese Geotechnical Society.

Tokimatsu K. (1988) *Penetration Tests for Dynamic Problems.* Penetration Testing ISOPT-I. De Ruiter ed. Rotterdam

Wang W. (1979) *Some findings in soil liquefaction*. Research Report Water Conservancy and Hydroelectric Power Scientific Research Institute, Beijing, August.

Youd T.L., Idriss I.M. (2001). *Liquefaction Resistance of Soils: Summary Report from the 1996 NCEER and 1998 NCEER/NSF Workshops on Evaluation of Liquefaction resistance of Soils.* Journal of Geotechnical and Geoenvironmental Engineering. 127(4): 297-313.

Liquefaction: a contribution to the Eurocodes from the Italian Guideline "Geotechnical Aspects of the Design in Seismic Areas"

Filippo Santucci de Magistris[1]

[1] *University of Molise, Engineering Faculty, Teramo (CB), Italy*

Abstract

With reference to the phenomenon of the liquefaction, the paper summarizes a chapter of the Italian Guidelines "Geotechnical Aspects of the Design in Seismic Areas" to highlight some key points of this topic reported in Eurocode 8. A calculation example for the city of Naples is here developed, to show that the liquefaction could be of some concern also in Italy, where new design accelerations are recently adopted in the national seismic codes.

FOREWARD

In the morning of October 31, 2002 a moderate earthquake (moment magnitude M_w=5.78) hit the Molise region, approximately 200 km E of Rome. The earthquake had a great impact on the Italian public, since it caused the collapse of a primary school and the death of 27 students and a teacher.

As a consequence, some new seismic codes and laws were rapidly introduced in Italy, mainly inspired to the Eurocode 8, causing great interest and some concerns for the earthquake engineering in the national technical community.

At the same time, the Italian Geotechnical Society established a working group in order to write some guidelines for the "Geotechnical Aspect of the Design in Seismic Areas" (AGI, 2005).

Such guidelines follows the so called "performance based design approach", requiring the analysis of geotechnical systems under two different seismic event of different returning period. That is, for frequent earthquakes it is required that the geotechnical systems exhibit a good performance, satisfying typical requirements of a "Damage Limit State". Instead, for rare events it is required that the geotechnical systems exhibit different performances (from the "Damage Limit State" to the "Ultimate Limit State") according to the type and the destination of the construction. The "performance based design method" requires three different level of analysis varying from the traditional empirical and pseudo-static approaches up to the pseudo-dynamic or even fully dynamic study, according to the importance and the requirements necessary to the construction.

In the siting section of the guidelines, a chapter with an annex was devoted to the liquefaction (Santucci de Magistris, 2005 a, b). The chapter was summarized here, highlighting some key aspects of the paragraphs of the Eurocodes devoted to the same topic.

THE PROBLEM OF THE LIQUEFACTION IN ITALY

As it is well known, the liquefaction hazard depends on both the nature of the seismic motion (in terms of amplitude, frequency content and duration) and the nature of the soils.

Liquefaction is considered one of the major threats for geotechnical systems under seismic loading, being able to cause the failure of building foundation and infrastructures. However, it is a common opinion in the Italian technical community that this phenomenon is of minor concern in our country. This opinion is mainly supported from the apparent lack of well-documented case histories of liquefaction in

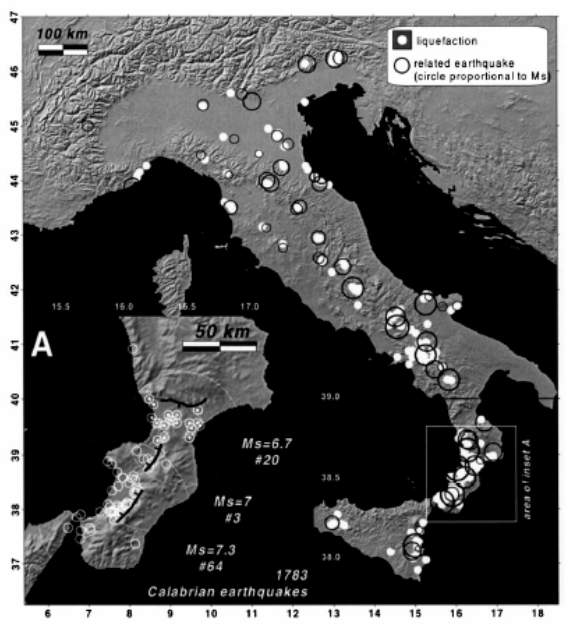

Fig 1: Distribution map of liquefaction case histories in Italy (after Galli, 2000).

Italy. Nevertheless, it is sometimes difficult to recognize the liquefaction in the field, and particularly difficult through the historical description of earthquake-induced effects (Galli and Meloni, 1993). In spite of the above, a catalogue of liquefaction phenomena in Italy is available and recently updated (Galli et al., 1999) and Fig 1 shows the related distribution map of liquefaction cases in Italy (Galli, 2000). From Fig 1 it appears that this phenomenon should be of some concern in our country, especially in the most seismic active regions.

The engineering methods to evaluate the liquefaction susceptivity mainly were published from American and Japanese researchers. As a consequence, indications in this paper, apart from the Eurocodes devoted to the design in seismic areas (EN 1998-1 e EN 1998-5) mainly derives from recommendations and guidelines (i.e., BSSC, 2003; CGS, 1997; CGS, 2004; ISSMGE-TC4, 1999; MCEER, 1995; NESC, 2000; NRC, 2003; PIANC, 2001; SCEC, 1999; SCEC, 2002), conference (i.e., the 11th ICSDEE & 3rd ICEGE, 2004) and journal paper (i.e., the very often quoted Youd et al., 2001 that summarised two workshops held in 1996 and 1998) written by Authors working outside Europe.

GENERALITY IN LIQUEFACTION ANALYSIS

Before describing the methods to evaluate the liquefaction potential, that is one of the main concerns about liquefaction in the Eurocodes, it is worth recalling here some statements from Santucci de Magistris (2005a) on the solution of a liquefaction problem.

Generally speaking, the analysis of the susceptibility to the liquefaction of a given site requires:

1. the evaluation of the main characteristics of the expected seismic event (i.e., the triggering factor);
2. the geotechnical characterization of the subsoil (i.e., the predisposing factor); and,
3. the estimate of the consequent effects of the liquefaction.

In connection to the selected analysis type, the characteristics of the seismic motion should be evaluated in terms of representative parameters (for instance magnitude, PGA, duration) or the whole time history of the accelerations.

For the geotechnical characterization of the area, appropriate in situ and laboratory tests should perform to determine at least: the depth of the water table; the stratigraphic conditions; and, the physical and mechanical property of soil constituting the deposit.

Based on the results of the evaluation of the liquefaction susceptivity, if the level of damage caused by the phenomenon is not compatible with the stability of the give site, it should eventually estimate the possibility of:

- not using the site;
- improving the mechanical characteristics of soil; and/or,
- modifying the characteristics of the construction.

The following part of this paper deals with the points (1) and (2) indicates above, as they characterize the various methods of analysis for the evaluation of the susceptibility to the liquefaction. In the spirit of the performance-based design method some notes are also given of the effects of the liquefaction on the structures.

REQUIREMENTS TO EXCLUDE THE LIQUEFACTION PROBLEM

Part 5 of Eurocode 8 (EN 1998-5, 2003)

states that “An evaluation of the liquefaction susceptibility shall be made when the foundation soils include extended layers or thick lenses of loose sand, with or without silt/clay fines, beneath the water table level, and when the water table level is close to the ground surface. This evaluation shall be performed for the free-field site conditions (ground surface elevation, water table elevation) prevailing during the lifetime of the structure”.

The same document declares also: “For buildings on shallow foundations, evaluation of the liquefaction susceptibility may be omitted when the saturated sandy soils are found at depths greater than 15 m from ground surface”.

And then: “The liquefaction hazard may be neglected when $\alpha S < 0,15$ (i.e., for maximum horizontal acceleration at the site surface lesser than 0.15 g) and at least one of the following conditions is fulfilled:

- the sands have a clay content greater than 20% with plasticity index PI > 10;
- the sands have a silt content greater than 35% and, at the same time, the SPT blowcount value normalised for overburden effects and for the energy ratio $N_{1(60)} > 20$;
- the sands are clean, with the SPT blowcount value normalised for overburden effects and for the energy ratio $N_{1(60)} > 30$”.

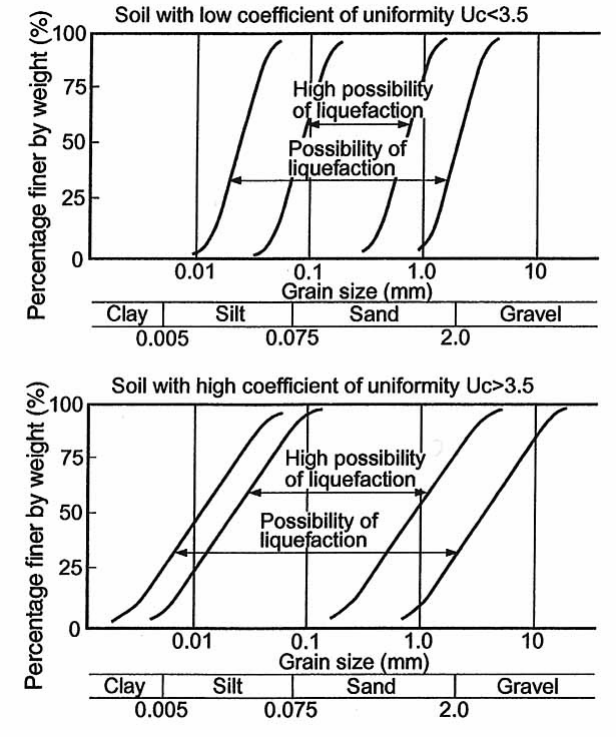

Fig 2: Grading curves for a preliminary evaluation of the liquefaction potential for soil with low and high coefficient of uniformity (after Tsuchida, 1970)

The first statement implicitly limited the necessity to perform liquefaction analysis when saturated loose sand is found. However, no detailed grading limits are indicated.

It might be suggested therefore to recall the criterion introduced by Tsuchida (1970) and recently adopted for instance by PIANC (2001) and Santucci de Magistris (2005a). The criterion is represented in Fig 2, where some bound for the grading curves in the case of uniform soils ($U_c < 3.5$) or non-uniform soils ($U_c > 3.5$) help to exclude liquefaction problems for some classes of materials.

Quoting Seed et al., (2003), coarse graded soils are poorly susceptible to liquefaction because: (1) they can be much more pervious, and so can often rapidly dissipate cyclically generated pore pressures; and, (2) due to the mass of their larger particles, the coarse gravelly soils are seldom deposited “gently” and so do not often occur in the very loose states more often encountered with finer sandy soils. Sandy soils can range from very loose to very dense, while the “very” loose state is relatively uncommon in gravelly deposits and coarser soils. However, the same Authors warned that the apparent drainage advantages of coarse, gravelly soils can be defeated if: (1) they are surrounded and encapsulated by finer, less pervious materials; (2) if drainage is internally impeded by the presence of finer soils in the void spaces between the coarser particles; or, (3) if the layer or stratum of coarse soil is of large dimension, so that the distance over which drainage must occur (rapidly) during an earthquake is large.

For fine graded soils it was recently recognised that the percent clay fines is less important than the overall contribution of the fines to plasticity, and there are numerous cases of liquefaction of soils with more than 10 or 15% clay-sized fines. Rather, it is the percent of clay minerals present in the soil and their activity that are important (Seed et al., 2003). It seems that new criteria will be soon proposed to quickly assess the liquefaction potential of

fine graded soil, based on these statements.

The second sentence quoted here from Eurocode 8 is related to a depth limit of the water table to make the liquefaction occurring.

Related to this point Day (2002) affirms that the greater the confining pressure, the less susceptible the soil is to liquefaction. Deeper water level is one of the conditions that usually generate higher effective confining pressure. Case studies have shown that the possible zone of liquefaction usually extends from the ground surface to a maximum depth of 15 meters, since below this level soils do not liquefy because of the higher confining pressure. The same Author warns, however, that in many circumstances it might be appropriate to perform liquefaction analysis for soil that is deeper than 15 m as it is the case of earthworks or alluvium soil strata being rapidly deposited.

The third statement from Eurocode allows avoid liquefaction analysis for low to medium seismic areas when some particular conditions on soil physical properties or on soil penetration resistance exist.

The latter derives from the vertical asymptote existing in the Seed and Idriss (1971) verification method, that will briefly discussed later in this paper. However, if this is the rationale of the excluding criterion, some further statements might easily introduced in the codes giving some limits values of the CPT resistance or of the shear wave velocity beyond which the liquefaction potential is negligible.

The statement on clay content and plasticity index derives from the well-known Chinese criterion (Wang, 1979) whose validity, as previously indicated, has been recently reconsidered by several researchers (see also Idriss and Boulanger, 2004; Bray et al., 2004).

The Guidelines "Geotechnical Aspect of the Design in Seismic Areas" proposes two further simplified criteria associated to a low probability of liquefaction that are:

- Moment magnitude M_w of the expected earthquake lower than 5; and,
- Maximum expected horizontal acceleration at the ground level, in free-field conditions, lower than 0.1g.

The first condition derives from the analysis of the databases of the observed liquefaction phenomena. Such data, that are usually employed to derive relationships between the magnitude of the earthquakes and the distance (from epicentre or from the fault) where the liquefaction occurred, showed that even very close to the earthquake source no liquefaction was historically observed if the earthquake has a magnitude lower than 5 (see for instance Kuribayashi and Tatsuoka, 1975; ISSMGE-TC4, 1999; Galli, 2000). It should be noticed, however, that limited liquefaction phenomena might eventually occur even for moment magnitude as low as 4.2.

The second condition was detected evaluating the peak acceleration at the ground level in correspondence to the minimum value of the cyclic resistance ratio CRR in the conventional verification charts. Assuming for CRR a value equal to 0.050, the consequent maximum acceleration, for the case of water table at the ground level, is approximately equal to 0.04g. It is worth considering that Yasuda et al. (2004) indicates evidences of liquefaction for the 2003 Tokachi-oki earthquake in Japan (M_w=8.0) in areas where the measured maximum acceleration was equal to 0.05g. The threshold was, however, moved upward considering that very low acceleration might cause liquefaction only if generated by earthquake of very long duration (i.e. recorded far from the epicentre and produced from large earthquakes) that are not expected in Italy.

It is worth underlining also, that, according to the seismic zonation currently adopted for Italy, which divides the country in four areas each characterized by different values of the peak ground acceleration on outcropping rock (OPCM 3274, 2003), the above criterion allow not performing liquefaction analysis in the lower seismic zone only.

SIMPLIFIED ANALYSIS METHODS

To estimate the occurrence of liquefaction at a given site, various methodologies were proposed, varying from simple qualitative methods to simplified analyses, dynamic analyses, up to the physical models. In this paper only simplified analysis and simplified dynamic analysis are treated.

Eurocode 8 part 5 states that "If the liquefaction hazard may not be neglected, it

shall as a minimum be evaluated by well-established methods of geotechnical engineering, based on field correlations between in situ measurements and the critical cyclic shear stresses known to have caused liquefaction during past earthquakes". It then appears that all the simplified methods which derive from the original Seed and Idriss (1971) procedure are accepted.

In this case, the safety factor against liquefaction, at a generic depth, is estimated from the ratio between the resistance available to the liquefaction and the stress states induced from the seismic action.

Both stress parameters are running normalised regarding the vertical effective stress at the examined depth, to define a cyclic resistance ratio, CRR, and a cyclic stress ratio, CSR. The term CSR is usually estimated from the value of the attended maximum horizontal acceleration at the ground level, for seismic events of an assigned "probability of exceedance" in a given reference time. The term CRR is generally estimated by means of abacuses, starting from SPT, CPT or the shear waves velocity V_s measurements. In the abacuses, the seismic loading is typically indicated in the ordinate, in the abscissa the soil resistance. A limit curve separate the representative points of case-histories where liquefaction phenomena where observed (above the curve) from points where liquefaction did not occurred (below the curve). Such curve represents the locus of the minimum cyclic stress ratio, CSR, which are needed for the liquefaction to be triggered and then represents the locus of the corresponding values of cyclic resistance, CRR.

Eurocode 8 part 5 gives some synthetic indication for the use of historical-empirical charts for the simplified analysis. In particular, Annex B is devoted to this topic.

Detailed information on the methods can be found in the paper of Youd et al. (2001), while the Italian Guidelines mainly refers to the recent paper of Idriss and Boulanger (2004). The latter has the advantage to include updated and re-evaluated information and to give all the methodologies in an analytical form, which can be easily incorporated into a worksheet.

It is worth noting that Eurocode 8 suggests evaluating seismic shear stress τ_e using the following expression:

$$\tau_e = 0.65 \frac{a_g}{g} S \sigma_{v0} \quad (1)$$

where a_g is the design ground acceleration for stiff type A ground; g is the acceleration of gravity; S is the soil factor defined in Eurocode 8 part 1; and σ_{v0} is the total overburden pressure. It is thus implicitly neglected, but on the safer side, any stress reduction coefficient that accounts for the flexibility of the soil column[1], that is always reported in the literature and also in the Italian Guidelines.

Please notice that Eurocode apparently does not give any *S* value for *S2* ground type which is constituted by deposits of liquefiable soils. Maybe, it should first assume that the soil deposit is not subjected to liquefaction and a proper S should be estimate according to the value of $v_{s,30}$; the number of blows of SPT or the value of the undrained cohesion c_u[2]. Then, if soil liquefies, specific studies are required for the definition of the seismic action on structures.

It should be considered also that the empirical methods were established for earthquakes having moment magnitude equal to 7.5. Whether this is not the case, some correction factors might be introduced, as also suggested by Eurocode 8. It is then clear that if such correction factors would be applied, designers should be able to estimate the magnitude of the design earthquake. At the moment, in Italy, no official map of the magnitude of the expected earthquake for different areas is available.

A final consideration should be done regarding the criteria to be adopted to choice between SPT, CPT, and V_s measurements for liquefaction evaluations. Some indications are again given in Youd et al. (2001). Idriss and Boulanger (2004) remarks that different in-situ tests are differently sensitive to the soil relative density D_R, that is one of the main factors influencing liquefaction potential, being the SPT the most sensitive and the Vs measurement the least.

It should be considered, however, that soils with crushable particles, as for instance some pyroclastic soils which are present in Italy,

[1] It is unknown to the Author if, instead, this is an editorial mistake.

[2] Some considerations and suggestions to improve the Eurocode on the topic of site classification can be found for instance in Lanzo, 2005.

might have a reduced penetration resistance due to the particle crushing itself, and then might have a misleading high liquefaction potential. Such elevated liquefaction potential might, on the other hands, not resulting if the computation is made using shear wave velocity measurements.

This point will be discussed in the last part of this paper, but some specific researches should be performed on this point.

SIMPLIFIED DYNAMIC ANALYSIS METHODS

While Eurocode 8 correctly concentrated on simplified methods, which are employed for the ordinary design cases, it open the doors at the use of more sophisticated procedures, that are already available in literature.

Particularly, the Italian guidelines recall some simplified dynamic analysis methods where liquefaction potential is computed, in free-field condition, evaluating seismic loading throughout a local response analysis. Therefore, the seismic action should be defined using an acceleration time history at bedrock and the geotechnical characterisation should be more detailed. In principle, the methods can be classified in: (a) methods operating in total stress; and, (b) methods operating in effective stress.

For case (a), the seismic loading is computed neglecting the pore pressure development, which is typical in a liquefaction process. At a given depth, the site response analysis, eventually performed under 1-D condition, can typically provide us the time-history of shear stress $\tau(t)$. Its maximum value τ_{max} can be introduced in the following equation that can be used to estimate the cyclic stress ratio CSR:

$$CSR = \frac{\tau_{average}}{\sigma'_{vo}} = \frac{0.65\tau_{max}}{\sigma'_{vo}} \quad (2)$$

where σ'_{vo} is the vertical effective stress at the assigned depth before the seismic event (i.e., computed without taking into account the pore pressure development).

For case (b), the seismic loading is computed after a site response analysis executed in effective stress, integrating the equations of the motion in the time domain. Such methods allow detecting at a given depth, among others, the time history of the excess pore water pressure Δu induced by the earthquake. Liquefaction potential might, then, be computed from the knowledge of the ratio $r_u = \Delta u/\sigma'_{vo}$. Safety factor FSL can be computed from the empirical relationship (Tokimatsu and Seed, 1987):

$$FSL = r_u^{-n} \quad (3)$$

where n can be taken equal to 7.

Whatever method (a) or (b) are employed to define the seismic loading, the soil resistance to liquefaction might be evaluated using in-situ or laboratory tests. A procedure of simplified dynamic analysis currently adopted in Japan, and reported in PIANC (2001) is also proposed in the Italian guidelines.

This method is divided in two stages: in the first part the likelihood of liquefaction is detected, based on normalized SPT blowcount and equivalent design acceleration.

If this part gives not clear indication whether or not the liquefaction phenomenon occurs, in the second part of the method, liquefaction potential is evaluated based on results of laboratory cyclic triaxial tests.

EVALUATION OF THE EFFECTS OF LIQUEFACTION

Eurocode 8 states that if simplified analysis methods are employed "soil shall be considered susceptible to liquefaction under level ground conditions whenever the earthquake-induced shear stress exceeds a certain fraction λ of the critical stress known to have caused liquefaction in previous earthquakes. The value ascribed to λ for use in a Country may be found in its National Annex. The recommended value is λ = 0.8, which implies a safety factor of 1.25".

Therefore, it seems that at a given site, if the "demands" exceed 0.8 times the "capacity", at any depth (or the value indicated by each single country), some "actions" should be carried out, since liquefaction is expected to be triggered.

But a question can arise. If the verification is not satisfy in a point of the given vertical, which is the real hazard of the site? Eurocode 8 partially helps in answering this question, stating that "If soils are found to be susceptible to liquefaction and the ensuing effects are deemed capable of affecting the load bearing capacity or the stability of the foundations, measures, such as ground improvement and piling (to transfer loads to layers not susceptible

to liquefaction), shall be taken to ensure foundation stability".

This means that Engineers should be able to evaluate the effects of liquefaction. But Seed et al. (2003) states that "engineering assessment of the deformations and displacements likely to occur as a result of liquefaction or pore-pressure-induced ground softening is a difficult and very challenging step in most projects, and this is an area where further advances are needed". Also, several papers warns that great care should be employed in design piles in potentially liquefiable soils, especially because failures might occurs at the border between liquefied and non-liquefied materials (see for instance Finn and Fujita, 2004).

Please notice that if liquefaction happens it does not necessarily imply the loss of serviceability or the collapse of the structures made of or interacting with the soil. Important settlements and reductions of bearing capacity depends, among others, from the thickness and the wideness of the liquefied strata, the thickness of not liquefied soils covering liquefied materials, the ground slope and the closeness of a free-surface.

Associated with the onset of liquefaction, noticeable variation of seismic motion can be observed, typically due to the attenuation of high frequency components and a general reduction of the acceleration. This does not necessarily imply a reduction of the damage capability of the earthquake.

Quantitative evaluation of the engineering effects of the liquefaction related phenomena could be obtained by advanced dynamic analysis. In this case the soil, the foundation and the superstructure should constitute the analysing system.

Some simplified methods allows however to estimate the effects of liquefaction, even though with some incertitude (see for instance Kramer (1996) or TC4-ISSMGE (1999)).

In the Italian guideline the Iwasaki et al. (1982) method is recalled, since is sometime used in practice and allow obtaining an "integral" evaluation of the liquefaction effects. Such method introduced a liquefaction potential index I_L defined by:

$$I_L = \int_0^{20} F(z)w(z)dz \tag{4}$$

where z is the depth below the ground surface, measured in meters; F(z) is a function of the liquefaction safety factor FSL, being *F(z)=1-FSL* for FSL ≤ 1.0 and *F(z)=0* if FSL> 1.0, and *w(z)=10-0.5 z*. Analysing a series of case-histories Iwasaki et al. (1982) suggested that for:

- $I_L \leq 5$ the liquefaction potential is low;
- $5 < I_L \leq 15$ the liquefaction potential is high; and
- $I_L > 15$ the liquefaction potential is very high.

AN EXAMPLE OF CALCULATION FOR THE CITY OF NAPLES

As previously mentioned, after 2002 Molise earthquake, a new seismic classification of Italy was adopted. Such classification is associated with relatively high level of peak ground acceleration on outcropping rocks (OPCM 3274, 2003).

It might be then interesting to verifying, under these new conditions, if liquefaction hazard might be of some concern in some part of Italy. Under this framework, a research project is now in progress to evaluated seismic hazard for the city of Naples, adopting the prescription of the new Italian seismic code that, as recalled before, reflects the Eurocode 8 (Evangelista, 2006). Some preliminary results are reported here.

The city of Naples was selected due to:

- its large exposure, being the third large populated city in Italy, with one of the highest population density in Europe;
- its movement from the third to the second category within the new seismic classification; and,
- the large knowledge on its subsoil, which was analyzed from several decades at the Department of Geotechnical Engineering, University of Naples, since the sixty.

Seismological outlines

Several relevant earthquakes affected the city of Naples in its history. The intensity database of damaging earthquakes in the Italian area (Monachesi and Stucchi, 1997) includes 79 events having interested the area, being the most damaging the 1456 Molise earthquake, that had in Naples an estimated (7.3)

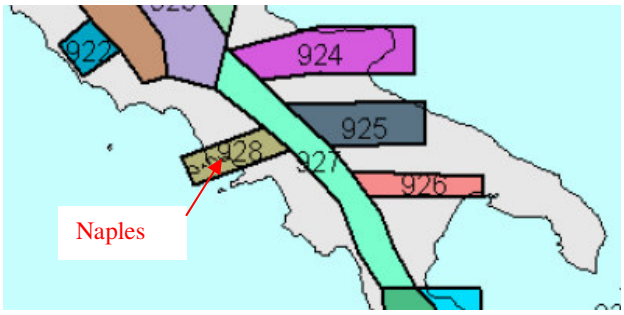

Fig 3: Seismogenic zonation ZS9 for South Italy (modified after WG, 2004).

seismic intensity equal to I_s = 8.0 MCS.

According to the new map of seismic hazard of Italy (WG, 2004), for the city of Naples the peak ground acceleration on outcropping rocks a_g, for earthquakes having a return period T_r= 475 years, ranges from 0.150 to 0.175 g. However, by the current seismic law, Naples belong to zone two, thus such acceleration should be raised up to 0.25 g in design. This acceleration was adopted in the subsequent example.

The background of the map of seismic hazard is a new model of seismogenic source called ZS9. According to this model, two zones interest the Campania prefecture, as sketched in Fig 3.

Zone SZ927 (Sannio-Irpinia-Basilicata) runs parallel to the Apennine chain and included all the sources that had given tectonic earthquakes in the past. Zone 927 was characterized by the following parameters:

- Prevailing fault mechanism: normal;
- Average depth of earthquakes: from 8 to 12 kilometres;
- Maximum observed magnitude: M_{max} =7.06;

By applying the Gutenberg-Richter recurrence law (Gutenberg and Richter, 1956) to the data belonging to ZS927 it results that the magnitude associate with a returning period T_r= 475 years is equal to 6.85.

Zone SZ928 (Ischia-Vesuvius) runs perpendicular to the previous zone and includes the earthquakes generated by the Neapolitan volcanic areas. Zone 928 was characterized by the following parameters:

- Prevailing fault mechanism: normal;
- Average depth of earthquakes: from 1 to 5 kilometres;
- Maximum observed magnitude: M_{max} =5.91;

In the following computations an expected magnitude 6.85 was adopted that is the one evaluated for SZ927. This zone is, however, not the seismogenic area closer to the city of Naples.

Overall, from the above consideration it appears that the criteria based on the expected peak ground acceleration or on the expected magnitude cannot exclude that liquefaction related phenomena might interest the city of Naples.

Geotechnical background

Subsoil is Naples is mainly generated by the volcanic activities of the nearby district of Phlegrean Fields and mount Vesuvius. The subsoil is essentially made of pyroclastic soils (pozzolana, volcanic ashes, pumices) lying on a volcanic soft rock called Neapolitan yellow tuff. The pyroclastic sequence is the result of the primary volcanic deposition on the hills of the city, while it appears as alluvial sediments on the costal zones, from continental or marine origin. The volcanic tuff is present everywhere and can be assumed as bedrock. The pyroclastic sequence overlying the tuff is mainly constituted by pozzolanic soils underlying a younger formation of thin layers of pumices and lapilli belonging to the third period of the Phlegrean eruptive cycle, covered by volcanic fly ashes and remoulded soils, together with man-made grounds, including masonry blocks often used as filling materials.

Some macro-areas can usually be distinguished in the city starting from the groundwork of Croce and Pellegrino (1967) recently updated (Grosso, 2002) (see Fig 4).

Zone 1 includes the hill area that is characterized by uneven morphology and with subsoil constituted by a layer of made-man ground and pozzolana and pumices soils with a total thickness spanning from around 10 to 30 meters. The basement is constituted by the Neapolitan yellow tuff. In the area the water table is very deep and soils are typically in a partially saturated condition.

Zone 2 is located in the western part of the city, where the subsoil is reasonably homogeneous and characterized by a thick cover (more than one hundred meters) of

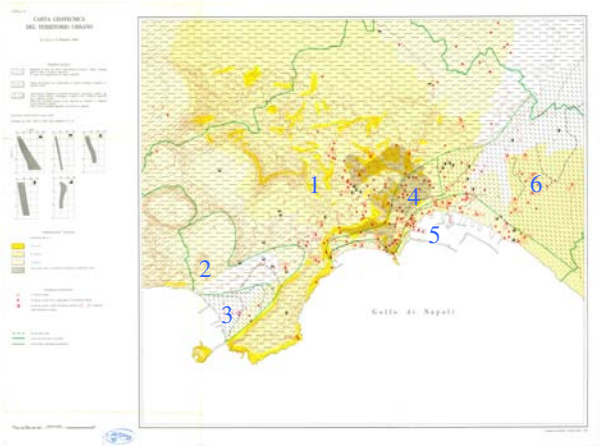

Fig 4: Geotechnical zonation for the city of Naples (modified after Croce and Pellegrino, 1967).

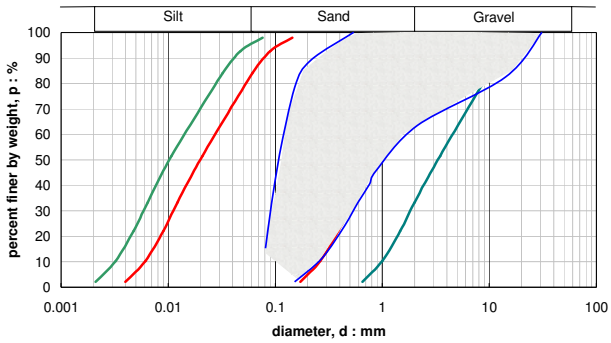

Fig 5: Grading curves for the pozzolana soil in Naples compared with the limit curves for liquefaction susceptivity.

recent pyroclastic products on marine sand or occasionally, Neapolitan yellow tuff formation.

Zone 3 is again in the west part of Naples and included a former industrial site. In this area the thick pyroclastic soils (pozzolana, pumices and lapilli) are sometime mixed with organic materials. The pyroclastic soils are sometime washed by old rivers and sometime deposited in a marine environment. Water table is often very shallow.

Zone 4 is the downtown area that is constituted by some meters of man-made ground, followed by pozzolana and pumices soils. The tuff is present at a depth varying from few up to around 30 meters from the ground level. Several cavities are present in the tuff formation. The water table spans from few to several meters from the ground level.

Zone 5 is the costal area that is often a reclaimed land, filled with different man-made materials having several meters in thickness. Such materials overlays medium-fine grading alluvial soils (with some thin pozzolanic layers), which covers, at a depth varying from 20 to 30 meters, the Neapolitan yellow tuff. Water table is close to the ground level.

Zone 6 is the eastern part of the city that is constituted from the top by recent man-made ground placed to overwhelm ancient swamps. Then, layers of sands and peat characterize a fluvio-palustrine formation, with a whole thickness from around 15 to 20 meters. Such material overlays, from a depth larger than 20 or 30 meters from the ground level, the yellow tuff formation constituted by uncemented or cemented pozzolanic material and the yellow tuff itself. Water table is at few meters from the ground level.

Some physical and mechanical properties of Neapolitan volcanic soils are reported in Pellegrino (1967). Referring in particular to the pozzolana soil, the Author claims that even though the material is heterogeneous itself, no macroscopic differences in properties are found in different part of the city. Fig 5 shows the variability of the grading curve of such material, compared with the grading curves limits to exclude liquefaction related phenomena. It clearly appears that, from the grading distribution viewpoint only, the pozzolana might have elevated liquefaction potential. Also the material does not have relevant clay fraction. Please notice that again Pellegrino (1967) claims that some pozzolana soil might be remoulded and washed by some geological phenomena. In this case the gravelly fraction disappears, but again the material is within the bounding curves for possible liquefaction.
Overall the pozzolana soil has a plasticity index spanning from zero up to around 10%. The plasticity for this material derives from some organic fraction that might be present in the soil.

Grading curves of pumices are plotted in Fig 6, together with the bonding curves for liquefaction. In this case, the material should not be subjected to liquefaction, due its coarse nature.

Finally grading curves of alluvial materials are plotted in Fig 7, together with the control

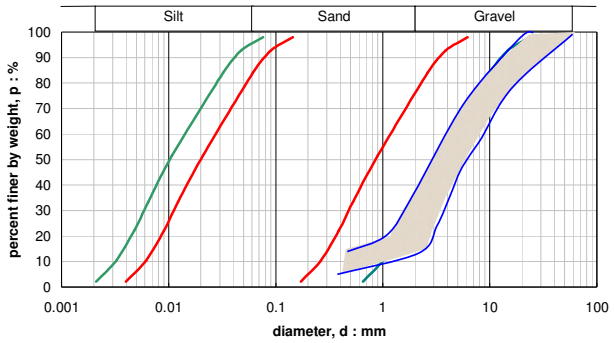

Fig 6: Grading curves for the pumices in Naples compared with the limit curves for liquefaction susceptivity.

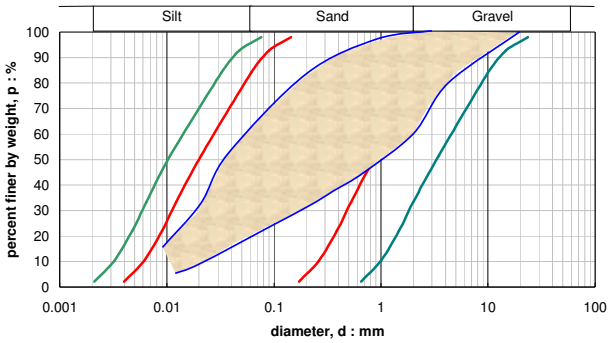

Fig 7: Grading curves for the alluvial soils in Naples compared with the limit curves for liquefaction susceptivity.

bonding curves. In this case the data are those reported by Croce and Pellegrino (1967). From the figure it appears that such materials are potentially liquefiable, even tough their grading curves are very variable.

On the whole, it appears that for all materials that constitute the Neapolitan subsoil the clay fraction is always negligible.

Liquefaction analysis by simplified methods

As underlined before, seismological and geotechnical parameters cannot a priori eliminate the problem of the liquefaction in the city of Naples. Therefore, liquefaction analysis by simplified method will be systematically performed (Evangelista, 2006). The attention is concentrate in the costal area of the city, where soils are fully saturated, being the water table very shallow. Here some calculation examples are reported for the previous defined zone 5, evaluating the cyclic resistance ratio CRR by CPT.

Fig 8a shows the variation with depth of the cone penetration resistance for a site that is constituted by marine sand above pyroclastic and tuff formation. In this particular location, the water table is 2.9 meters below the ground level.

The original test data have been smoothed averaging the cone resistance over a depth of one meter (Grosso, 2002).

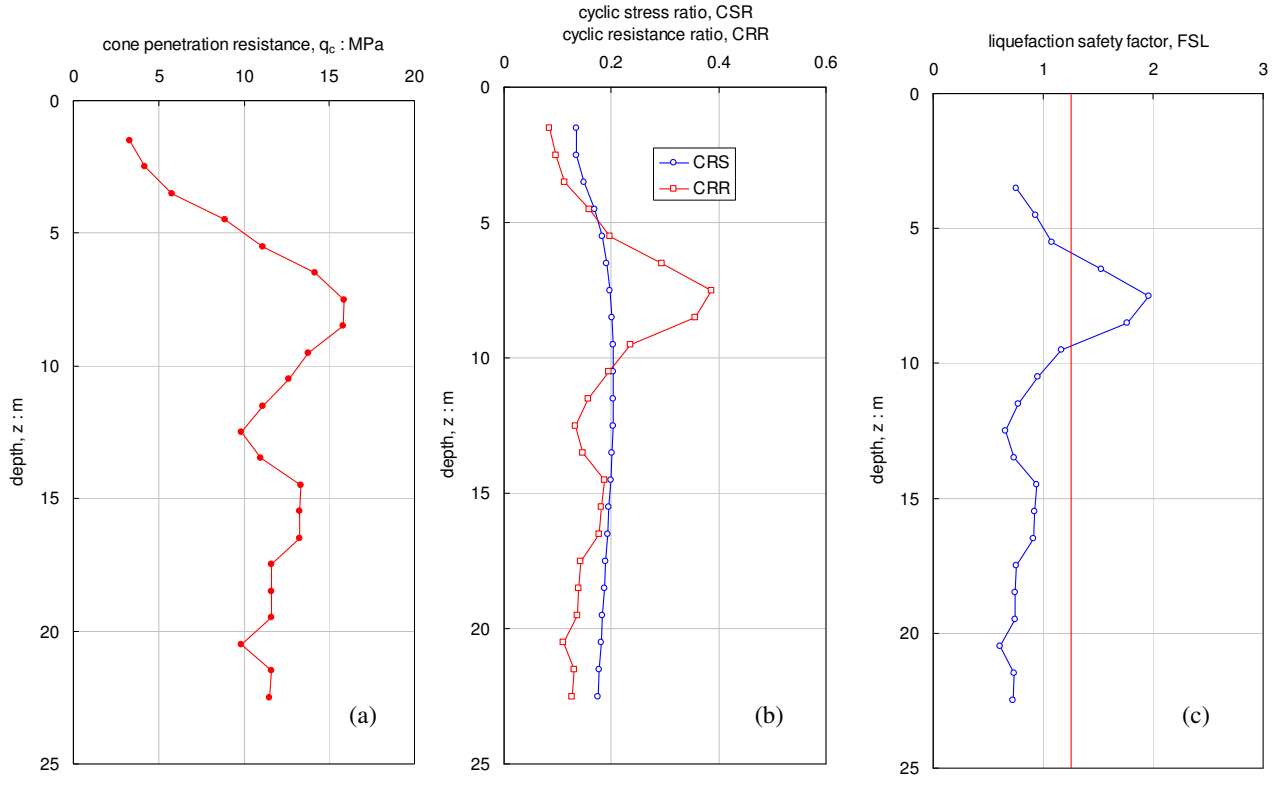

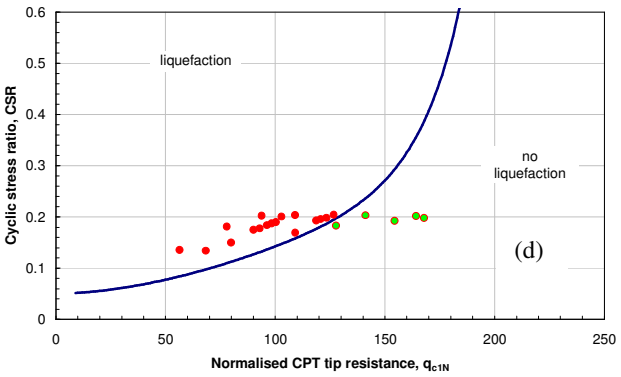

Fig 8: Liquefaction analysis by simplified method for a site in Naples: (a) CPT profile; (b) cyclic stress ratio and cyclic resistance ratio profile; (c) liquefaction safety factor profile; (d) normalized cone resistance versus cyclic stress ratio in a liquefaction chart.

Fig 8b shows the profile of the cyclical stress ratio CSR and the cyclical resistance ratio CRR. Calculations were executed following the indications in the Italian guidelines (Santucci de Magistris, 2005b), which are based on the work of Idriss and Boulanger (2004) and Boulanger and Idriss (2004). To evaluate CSR, it was assumed a soil factor S=1 that is not on the safer side. It should be considered that neither Eurocode nor the Italian guidelines allow classifying a site, and then defining the soil factor, based on the result of a cone penetration test only. It might eventually be suggested to the designer to assume a larger soil factor, even though this might sensitively influence the final result of the analysis.

It appears that, in some part of the deposit, the stress ratio exceeds the resistance and therefore the liquefaction safety factor, FSL is below the unit. This can be clearly seen in Fig 8c. In this figure, a line corresponding to a safety factor 1.25 separates point, which are or are not safe, according to the indications of Eurocode 8.

Another representation of the same data is in Fig 8d that shows the relationship between the cyclic stress ratio, CSR and the normalized cone resistance, q_{1cN} for an overburden vertical effective stress σ'_v = 100 kPa. The limit curve for clean sand is also plotted in the figure. The verification is not satisfied for several points in the analysed vertical (i.e., for the point lying on the left hand side of the limit curve).

This observation is confirmed by the previously defined liquefaction potential index, I_L that is equal to 6.94, thus indicating a high liquefaction potential for the deposit.

The CPT profile previously drawn in Fig 8a is labelled “5b” and again shown Fig 9a, together with some others representative penetration tests for zone 5 (Grasso, 2002). Some variability can be seen in the profiles that

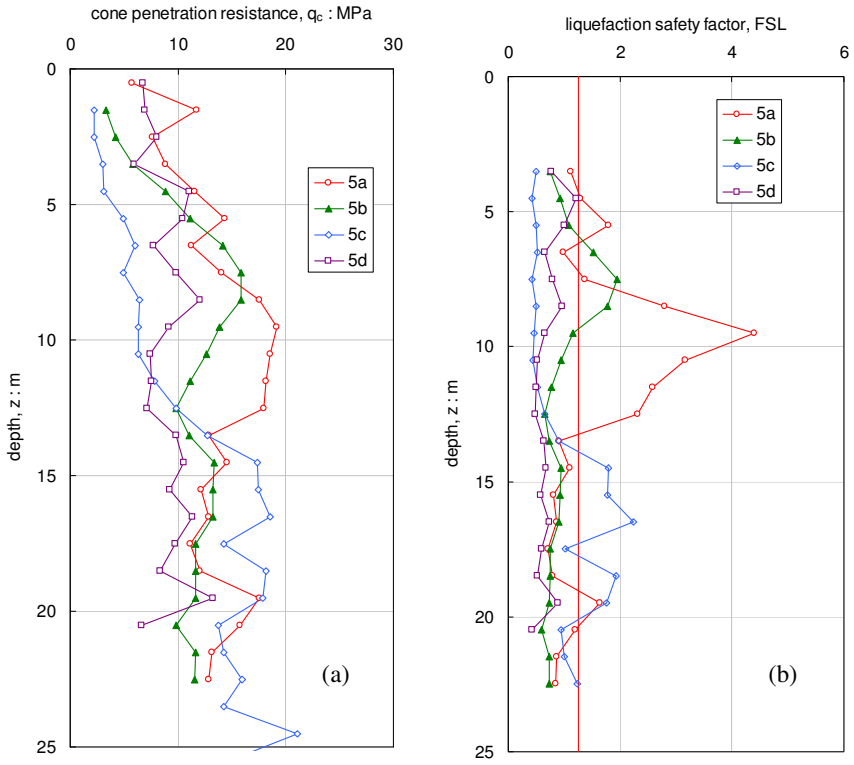

Fig 9: Liquefaction analysis by simplified method for site in the costal area in Naples: (a) CPT profile; (b) liquefaction safety factor profile.

Table 1: Liquefaction potential index for some location in the costal areas on Naples.

Profile label	Liquefaction potential index, I_L	Liquefaction potential
5a	1.53	low
5b	6.94	high
5c	31.11	very high
5d	18.32	very high

are largely reflected in the variation with depth of the liquefaction safety factor, plotted in Fig 9b.

Particularly it can be seen that while safety level for profile "5a" is relatively high, this is not the case of the profile "5c" and "5d" that show often a safety factors below the unit. Such considerations can be better summarized by the liquefaction potential index I_L that represents an integral evaluation of the safety level of the deposit. Table I reports the values of I_L for the four-studied vertical. It can be seen that for vertical 5b and for vertical 5c and 5d the liquefaction potential is respectively high or even very high. On the other hand, the liquefaction potential for the vertical labelled 5a is low, even though at some particular depth the liquefaction safety factor is below the limit value reported in Eurocode 8.

It should be underlined again that the above analyses were performed using a soil factor equal to 1. As for example, for vertical "5a" if this parameter increases from 1 up to 1.4, which is its maximum value according to Eurocode 8 part 1, the liquefaction potential index linearly increases from 1.53 up to 8.66, then moving the potential from low to high.

For the costal areas of Naples no direct shear wave velocity V_s profile are available to the Author close to the location where penetration tests were executed. However, in an attempt to evaluate the local seismic response for Naples, Nunziata (2004) adopts for the area a representative velocity profile recalled in Fig 10, based on surface and in-hole measurements. When the shear wave velocity profile is normalised for an overburden vertical effective stress σ'_v = 100 kPa (see Andrus and Stokoe, 2000 and Santucci de Magistris 2005b) almost all values overtakes the limit threshold of

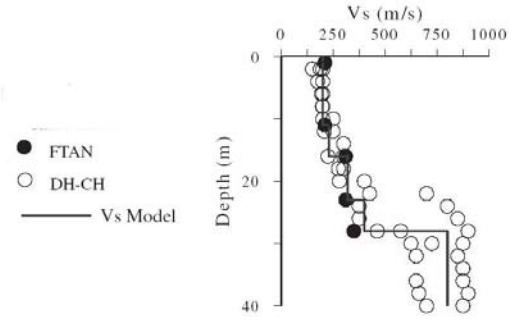

Fig 10: Selected shear wave velocity profile for the zone 5 that is the coastal area of Naples (modified after Nunziata, 2004).

V^*_{s1} = 215 m/s over which no liquefaction occurs, adopting the simplified method.

It is not clear to the Author whether such differences in the analyses are due: (a) to the soil heterogeneity that makes CPT and shear wave measurements obtained in different location no comparables; (b) limits in the simplified calculation procedures, that were created adopting no Italian case-histories or (c) to the fact that cone tip resistance underestimates the liquefaction resistance for volcanic soils, because of their grain crushability.

CONCLUSIONS

The paper summarizes a chapter of the new Italian guidelines "Geotechnical Aspects of the Design in Seismic Areas" to highlight some key points and give some comments in Eurocode 8 related to the liquefaction.

Except for some minor inaccuracies, no particular critical points appear on this topic in Eurocode 8. In fact the Eurocode looks inspired by the classical verification methods presented in the literature, while it allows also an eventual use of more enanched methodologies.

The Italian guidelines similar in the general structure of Eurocode 8 and are inspired to the newer state-of-art paper.

In the guidelines some reasons to exclude liquefaction analyses are also presented and commented here. Such points might eventually be introduced in a seismic code.

A preliminary calucaltion example is also reported for the city of Naples, where some area looks susceptibles to the liquefaction after introducing the larger design accelerations following the new Italian seismic code.

It appears that for some specific location, at some specific depth the liquefaction safety factor is below the limit value reported by Eurocode. According to the Italian guidelines, however, this does not necessary imply that some mitigation procedures should be adopted, while a more significant parameter for liquefaction susceptivity could be the liquefaction potential index rather than the liquefaction safety factor. This is particularly true when a "normal" performance grade is required for the structure; that is the structure should remain in service for ordinary earthquakes and should be in a near collapse condition for large earthquakes.

It should be finally remarked that in the calculation examples reported in this paper, no partial safety factor were applied to increase the seismic action or to decrease the soil resistance. Therefore, the resulting liquefaction safety factor has to be seen as a global factor.

REFERENCES

Andrus, D.R. and Stokoe, K.H., II "Liquefaction Resistance of Soils from Shear-Wave Velocity," *ASCE, Journal of Geotechnical and Geoenvironmental Engineering*, Vol. 126, No. 11, pp 1015-1025.

Associazione Geotecnica Italiana (2005) *Geotechnical Aspect of the Design in Seismic Areas,* Patron Editore, Bologna, pp. 416 (in Italian).

Boulanger, R.W. and Idriss, I.M. (2004) "State normalization of penetration resistance and the effect of overburden stress on liquefaction resistance", *Proceedings of the 11th ICSDEE & 3rd ICEGE*, (Doolin et al. Eds.), Berkeley, CA, USA, Vol. 2, pp. 484-491.

Bray, J.D., Sancio, R.B., Durgunoglu, T., Onalp, A., Youd, T.L., Stewart J.P., Seed R.B., Cetin, O.K., Bol, E., Baturay, M.B., Christensen, C. and Karadayilar, T. (2004) "Subsurface Characterization at Ground Failure Sites in Adapazari, Turkey", *ASCE Journal of Geotechnical and Geoenvironmental Engineering,* Vol. 130, No. 7, pp. 673-685.

Building Seismic Safety Council, B.S.S.C. (2003) *The 2003 NEHRP recommended provisions for new buildings and other structures,* National Institute of Building Sciences. (http://www.bssconline.org).

California Geological Survey (1997) *Guidelines for evaluating and mitigating seismic hazards in California*, State Mining and Geology Board Special Publication 117 (http://gmw.consrv.ca.gov/shmp/webdocs/sp117.pdf).

California Geological Survey (2004) *Recommended criteria for delineating seismic hazard zones,* State Mining and Geology Board Special Publication 118 (http://gmw.consrv.ca.gov/shmp/webdocs/sp118_revised.pdf).

Croce, A. and Pellegrino, A. (1967) "The subsoil of the city of Naples. Geotechnical characterization of the urban area", *Proc. of the 8th Geotechnical National Conference*, Cagliari, pp. 233-253 (in Italian).

Day, R.W. (2002) *Geotechnical Earthquake Engineering Handbook,* McGraw-Hill, New York.

(pr)EN 1998-1 (2003) *Eurocode 8: Design of structures for earthquake resistance – Part 1: General rules, seismic actions and rules for buildings,* CEN European Committee for Standardization, Bruxelles, Belgium.

(pr)EN 1998-5 (2003) *Eurocode 8: Design of structures for earthquake resistance – Part 5: Foundations, retaining structures and geotechnical aspects,* CEN European Committee for Standardization, Bruxelles, Belgium.

Evangelista, L. (2006) *An overview of the seismic hazard for the city of Naples*, Master Thesis, University of Naples Federico II (in Italian, in prep.).

Finn, W.D. and Fujita, N. (2004) "Behavior of Piles in Liquefiable Soils during Earthquakes: Analysis and Design Issues", *Proc. of the Fifth Case Histories in Geotechnical Engineering Conference*, New York, NY, SOAP. pp. 16.

Galli, P., and Meloni, F. (1993) "Historical liquefaction. A National Catalogue", *Il Quaternario - Italian Journal of Quaternary Sciences*, Vol. 6, pp. 271–292 (in Italian).

Galli, P., Meloni, F., and Rossi, A. (1999) "Historical liquefaction in Italy: relationship between epicentral distance and seismic parameters", *European Geophysical Society XXIIII General Assembly Natural Hazards NH3*, The Hague, Netherlands.

Galli, P. (2000) "New empirical relationships between magnitude and distance for liquefaction" *Tectonophysics*, Vol. 324, pp. 169–187 (http://www.iesn.org/dida/lique.pdf).

Grosso, V. (2002) *Geotechnical characterization of the subsoil of the city of Naples using static*

penetration tests, Master Thesis, University of Naples Federico II (in Italian).

Gutenberg, B. and Richter, C.F. (1956) "Earthquake magnitude, intensity, energy and acceleration", *Bulletin of the Seismological Society of America*, Vol. 46, pp. 105-145.

Idriss, I.M., and Boulanger, R. W. (2004) "Semi-Empirical Procedures for Evaluating Liquefaction Potential During Earthquakes", *Proceedings of the 11th ICSDEE & 3rd ICEGE*, (Doolin et al. Eds.), Berkeley, CA, USA, Vol. 1, pp. 32-56.

ISSMGE-TC4 (1999) *Manual for zonation on seismic geotechnical hazards*, The Japanese Society of Soil Mechanics and Foundation Engineering.

Iwasaki, T., Tokida, K., Tatsuoka, F., Yasuda, S., Sato, H. (1982) "Microzonation for soil liquefaction potential using simplified methods" *Proceedings of the 3rd Int. Conf. on Microzonation*, Seattle, Vol. 3, pp. 1319-1330.

Kramer, S.L. (1996) *Geotechnical Earthquake Engineering*, Prentice Hall, Inc., Upper Saddle River, New Jersey, pp. 653.

Kuribayashi, E. and Tatsuoka, F. (1975), "Brief Review of Soil Liquefaction during Earthquakes in Japan", *Soils and Foundations*, Vol. 15, No. 4, pp.81-92.

Lanzo (2005) "Approximate analytical solutions for the evaluation of the surface motion", *Geotechnical Aspect of the Design in Seismic Areas,* Patron Editore, Bologna, pp. 335-350 (in Italian).

Monachesi, G. and Stucchi M. (1997) *DOM4.1, an intensity database of damaging earthquakes in the Italian area.* (http://emidius.mi.ingv.it/DOM/home.html).

Multidisciplinary Center for Earthquake Engineering Research, M.C.E.E.R. (1995) *The New York City seismic code,* Local Law 17/95 (http://mceer.buffalo.edu/publications/sp_pubs/99-SP06/default.asp).

Nevada Earthquake Safety Council (2000) *Guidelines for evaluating liquefaction hazards in Nevada* (http://www.nbmg.unr.edu/nesc/liquefaction.htm).

Nuclear Regulatory Commission (2003) *Procedures and criteria for assessing seismic soil liquefaction at nuclear power plant sites* Regulatory Guide 1.198 (http:// www.nrc.gov).

Nunziata, C. (2004) "Seismic Ground Motion in Napoli for the 1980 Irpinia Earthquake", *Pure and applied geophysics,* Vol. 161, pp. 1239-1264.

OPCM n. 3274, (2003) " First elements on the general criteria for the national seismic classification and the technical codes for the constructions in seismic areas" *Gazzetta Ufficiale della Repubblica Italiana*, Vol. 105, May 8th 2003 (in Italian).

Pellegrino, A. (1967) "Physical and mechanical properties of volcanic soils in Naples", *Proc. of the 8th Geotechnical National Conference*, Cagliari, pp. 113-145 (in Italian).

PIANC (2001) *Seismic Design Guidelines for Port Structures* Working Group no. 34 of the Maritime Navigation Commission, International Navigation Association, 474 pp., Balkema, Lisse 2001.

Santucci de Magistris, F. (2005a) "Liquefaction", *Geotechnical Aspect of the Design in Seismic Areas,* Patron Editore, Bologna, pp. 99-108 (in Italian).

Santucci de Magistris, F. (2005b) "Evaluation of liquefaction susceptibility using simplified methods", *Geotechnical Aspect of the Design in Seismic Areas,* Patron Editore, Bologna, pp. 351-364 (in Italian).

Seed, H.B., and Idriss, I.M. (1971) "Simplified procedure for evaluating soil liquefaction potential", *ASCE Journal of Soil Mechanics and Foundations Division*, Vol. 97, n° 9, pp. 1249-1273.

Seed, R.B., Cetin, K.O., Moss, R.E.S., Kammerer, A. M., Wu, J., Pestana, J.M., Riemer, M.F., Sancio, R.B., Bray, J.D., Kayen, R.E., and Faris A. (2003) "Recent Advances in Soil Liquefaction Engineering: a Unified and Consistent Framework", *26th Annual ASCE Los Angeles Geotechnical Spring Seminar*, Keynote Presentation, H.M.S. Queen Mary, Long Beach, California, April 30, 2003.

Southern California Earthquake Center (1999) *Recommended procedures for implementation of DMG special publication 117 guidelines for analyzing and mitigating liquefaction hazards in California* (http://www.scec.org/resources/catalog/LiquefactionproceduresJun99.pdf).

Tokimatsu, K. and Seed, H.B. (1987) "Evaluation of settlement in sands due to earthquake shaking", *ASCE, Journal of Geotechnical Engineering,* Vol. 113, No. 8, pp. 861-878.

Tsuchida, H. (1970) *Prediction and countermeasure against the liquefaction in sand deposit,* Abstract of the seminar, Port and Harbour Research Institute, Yokusuka, Japan (in Japanese).

Wang, W. (1979) *Some Findings in Soil Liquefaction*, Water Conservancy and Hydroelectric Power

Scientific Research Institute, Beijing, China, August.

Working group (2004) *Redaction of the map of the seismic hazard, following the Ordinanza PCM 3274 of March 20, 2003,* Final Report for Department of Civil Protection, INGV, Milano-Roma, apr. 2004, pp. 65 + 5 annexes. (in Italian).

Yasuda, S., Morimoto, I., Kiku, H. and Tanaka, T. (2004) " Reconnaissance report on the damage caused by three Japanese earthquakes in 2003", *Proceedings of the 11th ICSDEE & 3rd ICEGE*, (Doolin et al. Eds.), Berkeley, CA, USA, Vol. 1, pp. 14-21.

Youd, T.L. et al., (2001). "Liquefaction resistance of soils: Summary report from the 1996 NCEER and 1998 NCEER/NSF workshops on evaluation of liquefaction resistance of soils", *ASCE Journal of Geotechnical and Geoenvironmental Engineering*, Vol. 127, n° 10, pp. 817-833.

Application of EC8 for the Assessment of Liquefaction Potential and for the Seismic Response Analysis of a River Embankment

C. Vrettos

Technical University of Kaiserslautern, Germany

Abstract

Within the frame of the ETC-12 work two application examples have been prepared that are derived from engineering projects. The first example deals with the assessment of liquefaction potential of cohesionless soils, while the second one addresses the seismic response analysis of river embankments on deep sedimentary strata. Some issues are identified to be considered in future modifications and improvements of EC8.

INTRODUCTION

In the frame of the ETC-12 two application examples have been worked out. The first deals with the assessment of liquefaction potential in cohesionless soils in a high seismicity region. The second one refers to the stability of embankments on very deep sediments as typically encountered in Germany along the Rhine river graben that is an area of medium seismicity. Both examples are derived from realized infrastructure projects. Suggestions for additions/modifications in the actual EC8 version are given within the text when the necessity arises during the example application.

ASSESSMENT OF LIQUEFACTION POTENTIAL

One of the more significant factors leading to ground failure during earthquakes is the liquefaction of loose to medium-dense sand and silty sands below the water table. The problem of liquefaction is addressed in EC8, Part 5, § 4.1.3 "Potentially liquefiable soils" as well in the Annex B "Empirical Charts for simplified liquefaction analysis". The fundamentals of the current state-of-practice are described e.g. by Youd et al. (2001). The method has been updated in many reports and professional papers over the last 20 years.

The data for the example presented herein are taken with some minor modifications from a recently completed immersed tunnel project, as described by Vrettos and Savidis (2004). Consider a non-homogenous soil deposit consisting of layers of sand, silty sand and clay over bedrock as given in Table 1. Excavation depth for the tunnel at this location was equal to -11 m. The investigation program carried out is in accordance with the requirements of (2) P and (3) P. Soil classification is performed on the basis of samples obtained from a borehole. During the boring a Standard Penetration Test (SPT) was conducted at various depths by measuring the penetration index N_{SPT} expressed in blows per 30 cm penetration. These values are normalized to a 60% ratio of impact energy over theoretical free-fall energy. Results are given in Table 1.

Due to the variability of dynamic soil properties a seismic site response analysis is performed to determine the shear stress each particular layer is subjected to by the earthquake. Alternatively the simplified equation (4.1) in § 4.1.3 may be used for depths smaller than 20 m.

For the analysis, the dynamic soil properties are needed which are determined either by in-situ seismic tests and/or dynamic laboratory tests (resonant column tests). The density is determined either from the SPT test results using well known empirical correlations or directly from undisturbed samples in the laboratory. Shear modulus and damping are determined by resonant column tests in

Table 1: Layered soil deposit with SPT blow-count numbers. Depth is measured from excavation level at -11 m.

Layer No.	Soil type	Depth [m]
1	Silty Sand	0.0 - 3.0
2	Sand	3.0 - 10.0
3	Silty Sand	10.0 - 14.0
4	Clay	14.0 - 17.0
5	Clay	17.0 - 20.0
6	Silty Sand	20.0 - 25.0
7	Silty Sand	25.0 - 35.0
8	Clay	35.0 - 38.0
9	Silty Sand	38.0 - 40.0
10	Clay	40.0 - 44.0
11	Clay	44.0 - 47.0
12	Clay	47.0 - 59.0
	Bedrock	

Depth [m]	N_{SPT}	Depth [m]	N_{SPT}
2.0	12	20.0	26
4.2	5	22.5	29
6.2	10	26.5	15
8.5	14	28.5	11
10.2	10	30.5	18
12.0	9	32.5	34
15.3	11	35.0	17
17.7	11	43.0	34

dependence of the effective confining pressure. The resulting small-strain shear wave velocity depth-profile is given in Fig. 1. For thin layers dynamic soil properties are put constant while for thick layers the variation of shear modulus with confining pressure and accordingly with depth within the layer is considered.

The nonlinear variation of shear modulus and damping with shearing strain amplitude is determined from resonant column tests for the particular soil type. If such relationships are not available, design curves as given e.g. by Seed et al. (1986), Vucetic and Dobry (1991) are used.

The liquefaction assessment procedure is based on the comparison between the cyclic stress ratio induced by the earthquake τ_e / σ'_{v0} and the cyclic shear strength of the soil. τ_e is the seismic shear stress and σ'_{v0} is the effective overburden pressure at the particular depth.

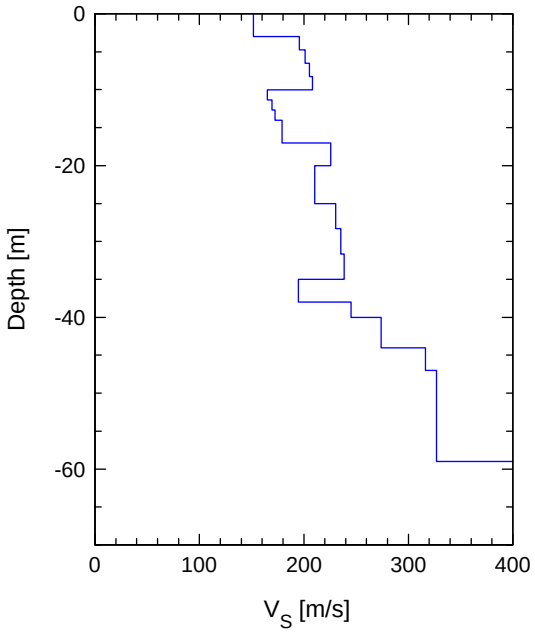

Fig 1: Depth-profile of shear wave velocity

The seismic action is specified in terms of an artificial accelerogram for an earthquake with maximum ground acceleration at rock outcrop $a_{max} = 0.3g$, where g is the acceleration due to gravity. The magnitude of the design earthquake is $M_S = 6.5$. The accerelogram and its response spectrum are given in Fig. 2.

The seismic site response analysis is conducted by using the code SHAKE which is based on an equivalent linear analysis in total stresses, Schnabel et al. (1972), Idriss and Sun (1992). The average shear stress is taken as 0.65 times the maximum shear stress. The results for the variation of the cyclic stress ratio with depth are given in Fig. 3.

The evaluation of liquefaction potential is exemplarily demonstrated for the silty sandy layer number 3 at a depth of 12 m. At this depth the measured SPT penetration index $N_{SPT} = 9$. The soil classification test shows a silty sand with 8% fines content, where fines content is defined as the percentage of material passing the 75-μm sieve. Correction for the impact energy level is not required since the test was conducted according to the standard testing procedure. The correction for overburden effects is made according to (5) in § 4.1.3 by multiplying the measured N_{SPT} value by the factor $(100 / \sigma'_{v0})^{1/2}$ where σ'_{v0} in kPa is the effective overburden pressure acting at the

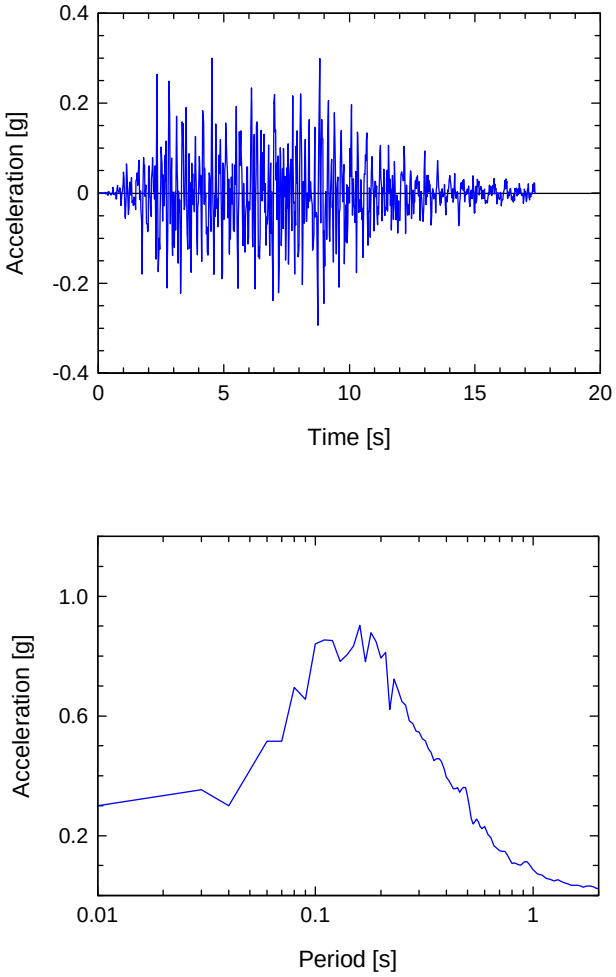

Fig 2: Design Earthquake. Time-history, and 5% damping response spectrum

depth where the SPT measurement has been made. Assuming groundwater level at ground surface and an average effective unit weight γ'= 9 kN/m^3 we obtain at a depth of 12 m σ'_{v0} = (12 + 11)·9 = 207 kPa which yields a correction factor for overburden effects equal to 0.7. Hence, the normalized standard penetration index $N_1(60)$ = 0.7·9 = 6.3. From Figure B1 of Annex B, EC8, Part 5 representing the relationship between stress ratio causing liquefaction and $N_1(60)$ for clean and silty sands we obtain a cyclic stress ratio of 0.07. The magnitude dependent correction factor for M_S = 6.5 is 1.69 yielding τ_e / σ'_{v0} = 0.07 · 1.69 = 0.12. From the seismic site response analysis we obtain for the cyclic stress ratio induced by the design earthquake at a depth of 12 m a value of 0.29, cf. Fig. 3, which is larger than 0.12. This means, that at the event of the design earthquake the soil would liquefy at this depth.

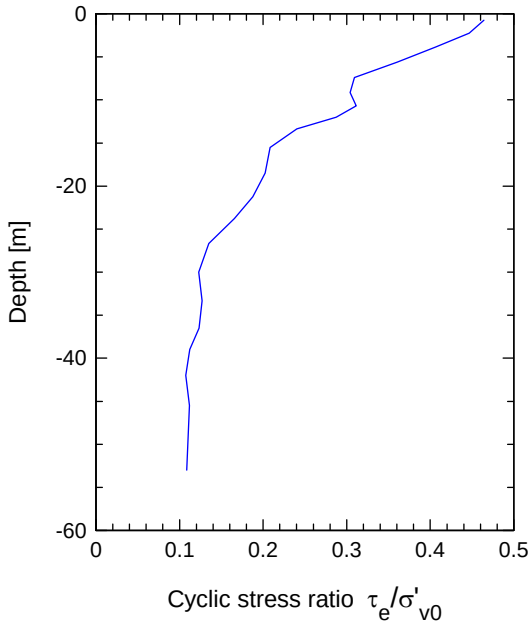

Fig 3: Variation of cyclic stress ratio with depth

Similarly we proceed for the silty sandy layer number 6 which shows 15% fines. In the middle of this layer at a depth of 22.5 m a value N_{SPT} = 29 was measured. For an average γ' = 9 kN/m^3 we obtain σ'_{v0} = (11 + 22.5) · 9 = 301.5 kPa which yields a correction factor of 0.58. Hence, $N_1(60)$ = 0.58 · 29 = 16.8. From Fig. B1 of Annex B we obtain for M_S = 6.5 the cyclic stress ratio τ_e / σ'_{v0} = 0.25 · 1.69 = 0.42. The cyclic stress ratio induced by the earthquake at this depth, cf. Fig. 3, is 0.18 < 0.42. Thus, liquefaction would not occur in that layer.

The screening procedure described above is repeated at various depths in order to establish the zone of liquefaction.

In a further step we compare the seismic shear stress τ_e estimated by equation (4.1) in EC8, Part 5 with the value computed from the seismic site response analysis:

$$\tau_e = 0.65 \cdot a_{gR} \cdot \gamma_I \cdot S \cdot \sigma_{v0}$$

where σ_{v0} is the total overburden pressure. The reference peak ground acceleration value a_{gR} is defined for class A ground. However, class A is not defined in EC8, Part 5 but in Table 3.1 “Ground types” of EC8, Part 1. γ_I is defined in § 1.5 as the importance factor, and S is named there the soil profile parameter while in EC8, Part 1 is named soil factor. The soil factor S is defined for an elastic response spectrum in

Table 3.2, EC8, Part 1. The stratigraphic profile can be classified as ground type D or S_2, Table 3.1, EC8, Part 1. Values for the associated soil factor S are given in Table 3.2, EC8, Part 1 only for ground type A to E. The prevailing soil conditions are best classified as ground type D with $S = 1.35$.

The importance factor γ_I is defined in § 3.2.1(3) of EC8, Part 1 and an additional Note is given in 2.1(4) of EC8, Part 1 and equals 1 when the reference peak ground acceleration chosen by the National Authorities for each seismic zone corresponds to the reference return period T_{NCR} of the seismic action for the no-collapse requirement. In our example we assume that the value $a_{max} = 0.3g$ assigned at rock outcrop corresponds to that return period of say 475 years. Thus, $a_{gR} = 0.3$ and $\gamma_I = 1.0$. Applying equation (4.1) to the soil conditions at depth of 12 m and assuming constant unit weight for saturated soil $\gamma = \gamma' + 10 = 19$ kN/m^3 yields for the total overburden pressure $\sigma_{v0} = 12 \cdot 19 = 228$ kPa and for the seismic shear stress $\tau_e = 0.65 \cdot 0.3 \cdot 1.35 \cdot 228 = 60$ kPa that corresponds to a cyclic stress ratio of $60 / (12 \cdot 9) = 0.56$. If ground type C with $S = 1.15$ were assumed, the cyclic stress ratio would be 0.47. Both values are considerably larger than the value 0.29 obtained from the seismic site response analysis. One reason for this discrepancy is the fact that the stress reduction factor commonly applied to τ_e is not included in equation (4.1). The average value of this reduction factor at this depth is approx. 0.85, Youd et al. (2001).

In summary, it can be said that the calculation of the liquefaction potential is straightforward but the accuracy of the simplified method based on equation (4.1) strongly depends on the selected value of the soil factor S. Consideration of the depth dependent stress reduction factor is recommended.

SEISMIC RESPONSE OF RIVER EMBANKMENT

This example application describes a situation that is typically encountered in seismic areas of Germany and refers to the seismic response and slope stability of dams or embankments of medium height. The embankment considered has a height of $H = 11.5$ m and crest width 6.5 m, Fig. 4. The site is assumed to be located along the Rhine river that belongs to the highest seismic zone in Germany, which, however, in absolute terms corresponds to an area of medium seismicity. Subsoil conditions are of particular interest due to the fact that the depth to bedrock is in the order of kilometers (graben structure). Since the stability of the particular dam is not considered critical, a detailed seismological study is not carried out and the designer is asked to perform his calculations solely on the basis of the relevant codes and state-of-the-art methodologies. The relevant German Code DIN 4149 closely follows the specifications of EC8 with design spectra considering the subsoil conditions at the various geographical units. In this example, we will use information from both codes in a complementary fashion.

In a first step the subsoil conditions are assessed. The geological data indicate that the sedimentary subsoil consisting of sand and gravel extends down to large depths and that a distinct bedrock level does not exist down to a depth of at least 150 m. According to EC8, Part 1, Table 3.1 this subsoil is classified as ground type C. DIN 4149 includes a refinement of the classification of the foundation soil by introducing sub-categories. Here, e.g. sub-category 3 referring to fine grained soil with shear wave velocity $V_S = 270$ m/s applies.

Next, we select the seismic input motion. According to the national code, here DIN 4149, the site is located in a zone of EMS intensity $7.5 \leq I \leq 8.0$ with peak ground acceleration for sound rock (a_{gR} for class A ground of EC8) equal to

$$a_{gR} = 0.8 \text{ m/s}^2.$$

The reference return period in this national building code (DIN) is equal to 475 years. However, for the particular water-retaining earth structure additional national specifications apply that dictate a higher return period for the design earthquake. The extrapolation to higher return periods requires knowledge of the magnitude recurrence law for the particular region and the magnitude-intensity relationship. To accomplish this task the assistance of a seismologist is needed. An alternative offers EC8, Part 1 under 2.1(4) by adjusting the importance factor γ_I according to

$$\gamma_I \sim (T_{LR}/T_L)^{-1/k}$$

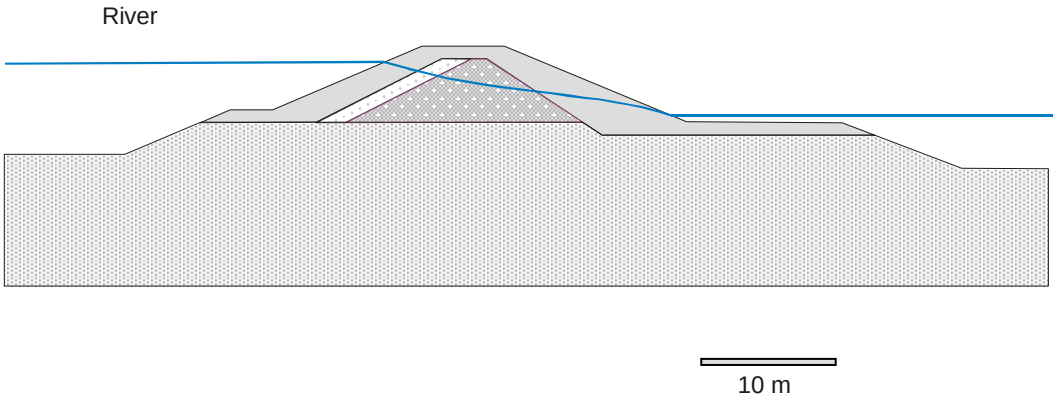

Fig 4: River embankment

where T_L is the return period for which the extrapolation is applied, T_{LR} is the reference return period, and k = 3.

Here, we select a reliability level described by a return period of T_L = 950 years, yielding an importance factor

$$\gamma_I = (475/950)^{-1/3} = 1.26.$$

This value compares well to the estimate based on more sophisticated seismological methods that was applied to the specific project.

Hence, for the specified reliability level the peak ground acceleration is:

$$a_g = 0.8 \cdot 1.26 = 1.0 \text{ m/s}^2.$$

It was decided to perform a dynamic analysis of the dam. For this purpose an accelerogram is required as input to the computation. In the absence of a project-specific seismological study the designer determines a representative time history using the code SIMQKE, Gasparini and Vanmarcke (1976). The target spectrum is that of the national code (here DIN 4149) for the particular subsoil class, as given in Fig. 5. Like in EC8, Part 1 the response spectrum of the local code considers site effects by means of a soil parameter S. Here S = 0.75. The resulting time history is given in Fig. 6 with a peak ground acceleration value

$$a_{max,\ freefield} = a_g \cdot S = 1.0 \cdot 0.75 = 0.75 \text{ m/s}^2.$$

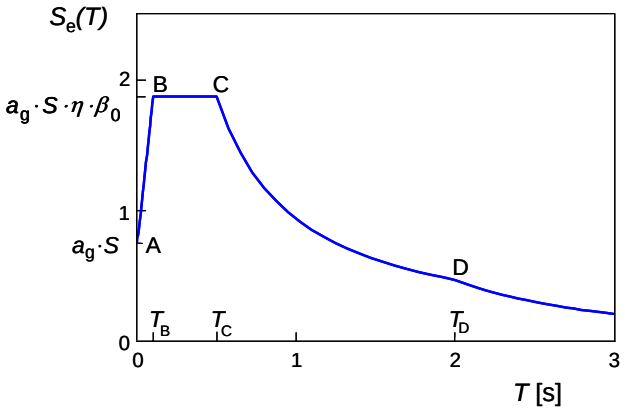

Fig 5: Horizontal elastic response spectrum according to national code (DIN 4149, subsoil class C3): S = 0.75, T_B = 0.1 s, T_C = 0.5 s, T_D = 2.0 s, η = 1, β_0 = 2.5 for 5% damping.

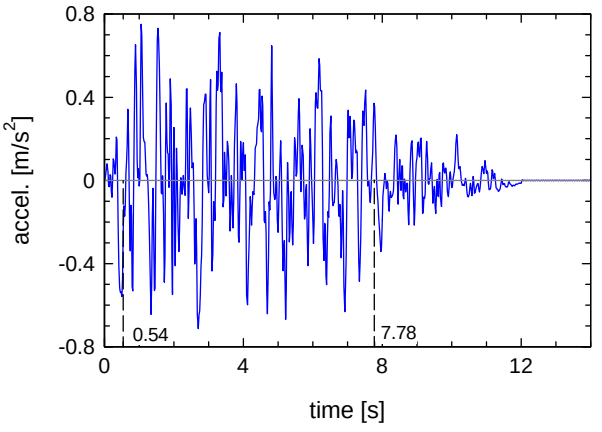

Fig 6: Synthesized design acceleration time-history for reliability level corresponding to a return period of 950 years with indication of strong ground motion duration

Both the in-situ and the laboratory soil investigation program were very poor including only some borings, DPH soundings to assess the relative density, and tests for grain size distribution. It is found that the foundation soil consists of sand-gravel mixtures while the core material is composed of alternating cohesive and non-cohesive layers of sandy silt and gravely sand, respectively. Values of relative density D_r as inferred from the soundings were 0.48 for the foundation ground and 0.63 for the dam material, respectively.

The dynamic soil properties both for the foundation soil and for the inhomogeneous dam material are estimated from own experience and empirical correlations given in the literature, cf. Kokusho and Yoshida (1997), Seed et al. (1986). While according to EC8, Part 5, § 4.2.2(5) and 4.2.2(6) this is allowed for the foundation soil being classified as type C, no information is found in EC8, Part 5 on the requirements for the dam material. First-estimate numerical values for shear modulus (or equivalently for shear wave velocity) and damping ratio at small strains are not given in EC8, Part 5. Useful would be also a note pointing to the fact that dynamic soil stiffness determined from in-situ tests is usually larger than that measured in laboratory test and how the designer has to cope with it.

For the foundation soil a small-strain shear wave velocity of 275 m/s is selected. The respective values for the three soil types of the dam material are 220, 263, and 240 m/s. Reduction factors to account for nonlinear effects are given in Table 4.1, EC8, Part 5. For the foundation soil the acceleration level is set equal to the level of seismic input motion while for the dam structure the expected average ground acceleration ratio is estimated equal to 0.15. This leads to a reduction factor for the shear wave velocity equal to 0.9 for the foundation soil and 0.8 for the dam structure. Damping ratio is also determined from Table 4.1, EC8, Part 5 to 3% and 4.5% for foundation soil and dam, respectively.

A recommendation for the variation range to be applied to these “best-estimate” numerical values of soil properties in the subsequent dynamic analysis is missing in the code. The standard deviation values given in Table 4.1 are interpreted as indication of the scatter in the data of natural soils.

Also missing are typical values for the Poisson’s ratio that is required for 2D calculations. Some comments, such as avoiding values equal to 0.5 that lead to infinite valued compressional wave velocities, would be helpful to the designer.

The FEM-Code PLAXIS, Brinkgreve and Vermeer (2002), is used for the 2D-analysis that is conducted directly in the time-domain. Since such algorithms use Rayleigh damping formulations, appropriate numerical values have to be determined from the damping ratio values. This is not an easy task, and requires engineering judgement and modelling experience.

Another source of errors is the point of application of earthquake motion, and here in particular because of the unknown depth of the bedrock. Using an iterative process we compute transfer functions for a two-dimensional soil foundation system (without dam structure) of specified thickness of 15m to determine the appropriate seismic input at the base of the problem. The de-convolution to determine the base motion is performed for a 1D-model by SHAKE. The resulting base motion is then entered as input into the 2D-model and adjusted so as to yield the synthesized spectrum-compatible surface motion. For simplicity the time history is kept unchanged and scaled down to a peak value of

$$a_{\text{max, base FEM}} = 0.54 \text{ m/s}^2$$

The subsequent 2D dynamic analysis for the dam structure resting on a 15 m thick soil layer on bedrock yields at the dam crest a peak acceleration value of 1.69 m/s^2, while for the dam slope an average representative value of the peak acceleration is determined:

$$a_{\text{max,dam}} = 1.4 \text{ m/s}^2.$$

The corresponding accelerogram given in Fig. 7 as calculated by 2D PLAXIS shows a different time-history pattern compared to that obtained from a 1D SHAKE free-field analysis, demonstrating the influence of the Rayleigh damping assumption and of the wave absorbing boundary conditions employed along the sides of the mesh.

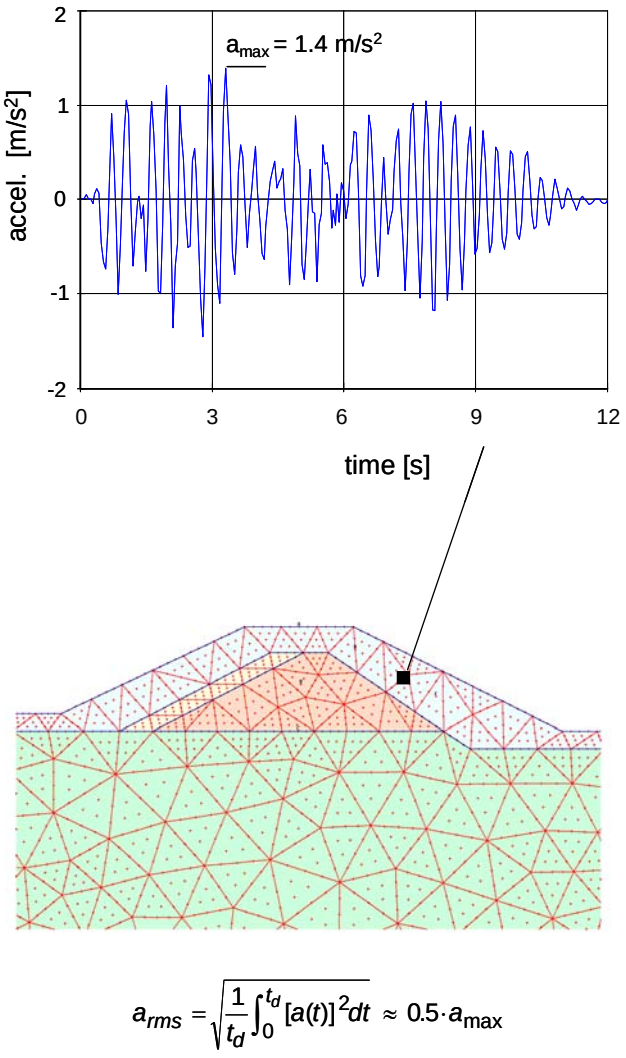

Fig 7: Embankment response and effective acceleration for slope stability analysis

Slope stability is checked following the specifications of § 4.1.2 of EC8, Part 5. It is not clear if provision § 4.1.2(1) P referring to the analysis method of response calculation would allow here a simplified pseudo-static method since the limitation § 4.1.2(3) regarding irregularity of surface topography does not apply. Limitation § 4.1.2.3(8) P does not apply since both the dam and the foundation are not susceptible to high pore water pressure increase. An additional provision restricting the application of the pseudo-static method of analysis to a maximum embankment height is necessary.

The effects of pore water pressure increase shall be considered according to § 4.1.2.4(2) by a decrease of the resisting frictional force. The estimation of the expected maximum pore pressure increment in the slope of the dam is difficult and empirical correlations, as proposed in § 4.1.2.3(9), are not verified in practice. In our example, we reduce the effective angle of friction by 1° considering the fact the in-situ relative density is medium to high and § 4.1.2.4(3).

The stability verification is carried out by means of simplified pseudo-static method following § 4.1.2.3(3). The design seismic inertia forces acting on the mass are determined from the results of dynamic analysis and compared to the provisions in § 4.1.2.3(5) P.

From the distribution of acceleration within the dam we computed an average peak acceleration value of 1.4 m/s^2, see above. An effective acceleration value is taken as the RMS value of the acceleration time history over the duration of strong motion. The latter is obtained from a Husid plot as the time required to build-up energy from 5 to 95%, Trifunac and Brady (1975), cf. Fig. 6. Here, the duration of strong motion t_d was 7.2 s and the calculated reduction factor was approx. equal to 0.5 yielding an average effective acceleration for the embankment slope equal to 0.5 · 1.40 = 0.7 m/s^2, cf. Fig. 7. This corresponds to a horizontal seismic coefficient to be used in the subsequent quasi-static slope stability analysis

$$k_h = 0.5 \cdot 1.40 = 0.7.$$

The reduction factor 0.5 is identical to the reduction factor recommended in EC8, Part 5, § 4.1.2.3(5) P to be applied to the peak ground acceleration when use is made of simplified pseudo-static analyses for slope stability calculations. Note that § 4.1.2.3(5) P refers solely to slopes, i.e. does not consider the amplification effects observed in embankment dams.

Amplification effects in the embankment can be determined using an approximate method assuming homogeneous dam material with shear wave velocity $V_{S,dam}$ = 200 m/s. First, we estimate the eigenperiod of the embankment, Gazetas (1987):

$$T_{dam} = 2.5 \cdot H / V_{S,dam} = 2.5 \cdot 11.5 / 200 = 0.14 \text{ s}$$

The response spectrum of the national code for the site-specific ground conditions yields for this period an amplification factor of A = 2.5 that

is assigned here to the dam crest. A rough approximation consists in setting the effective amplification over the embankment height equal to the average between the free-field value (A = 1) and that of the crest (A = 2.5), i.e. equal to 1.75. With this amplification value we obtain for use in the slope stability analysis:

$$a_{max,\ slope} = a_{max,\ freefield} \cdot 1.75 = 0.75 \cdot 1.75 = 1.3 m/s^2$$

This value is a good approximation to the value of 1.4 m/s^2 obtained from the dynamic FEM-analysis as given above.

A similar procedure for estimating amplification effects could be added to the present version of the EC8, Part 5, even if its application would be restricted to embankments of low to medium height.

CONCLUSIONS

The following major issues have been identified: The simplified method of liquefaction prediction is conservative, strongly depending on the value of the soil factor selected. A depth reduction factor shall be considered. Recommendations on the selection of design values for the soil parameters with their range of variation as well as some comments on numerical modelling aspects (damping, boundaries) shall be included. Provisions regarding the application of pseudo-static analyses to embankment stability could also be added. Finally, some comments on methods to estimate permanent seismic displacements would also be of interest to the designer.

REFERENCES

Brinkgreve, R.B.J. and Vermeer, P.A. (2002) *PLAXIS. Finite Element Code for Soil and Rock Analyses. User's Manual*. *Version 8*. A. A. Balkema, Rotterdam.

DIN 4149 *Bauten in deutschen Erdbebengebieten. Lastannahmen, Bemessung und Ausführung üblicher Hochbauten*, April 2005.

Eurocode 8: *Design of structures for earthquake resistance Part 1: General rules, seismic actions and rules for buildings*, May 2002.

Eurocode 8: *Design of structures for earthquake resistance. Part 5: Foundations, retaining structures and geotechnical aspects*, May 2002.

Gasparini, D. and Vanmarcke, E. (1976) *SIMQKE – A Program for Artificial Motion Generation, User's Manual and Documentation*, Department of Civil Engineering, Massachusetts Institute of Technology.

Gazetas, G. (1987) "Seismic response of earth dams: some recent developments". *Soil Dynamics & Earthq. Eng.*, 6(1), 2-47.

Idriss, I.M. and Sun, J.I. (1992) *User's Manual for SHAKE91*, Department of Civil & Environmental Engineering, University of California, Davis.

Kokusho, T. and Yoshida, Y. (1997) "SPT N-value and S-wave velocity for gravelly soils with different grain size distribution", *Soils and Foundations*, 37(4), 105-113.

Schnabel, P.B., Lysmer, J. and Seed, H.B. (1972): *SHAKE: A Computer Program for Earthquake Response Analysis of Horizontally Layered Sites*, Report No. UCB/EERC-72/12, Earthquake Engineering Research Center, University of California, Berkeley.

Seed, H.B. and Idriss, I.M. (1982) *Ground Motions and Soil Liquefaction During Earthquakes*, EERI Monograph, Earthquake Engineering Research Institute

Seed, H.B., Wong, R.T., Idriss, I.M and Tokimatsu, K.. (1986) "Moduli and damping factors for dynamic analyses of cohesionless soils", *J. Geotech. Engng. ASCE*, 112, 1016-1032.

Trifunac, M.D. and Brady, A.G. (1975) "A study on the duration of strong earthquake ground motion", *Bull. Seism. Soc. Am.,* 65, 581-626.

Vrettos, C. and Savidis, S. (2004) "Seismic design of the foundation of an immersed tube tunnel in liquefiable soil", *Rivista Italiana di Geotecnica*, 38 (4), 41-50.

Vucetic, M. and Dobry, R. (1991) "Effects of soil plasticity on cyclic response", *J. Geotech. Engng. ASCE*, 117, 89-107.

Youd, T.L., I.M. Idriss, R.D. Andrus, I. Arango, G. Castro, J.T. Christian, R. Dobry, W.D.L. Finn, L.F. Harder Jr., M.E. Hynes, K. Ishihara, J.P. Koester, S.S.C. Liao, W.F. Marcuson III, G.R. Martin, J.K. Mitchell, Y. Moriwaki, M.S. Power, P.K. Robertson, R.B. Seed, and K.H. Stokoe II. (2001) "Liquefaction resistance of soils: Summary report from the 1996 NCEER and 1998 NCEER/NSF Workshops on Evaluation of Liquefaction Resistance of Soils", *J. Geotech. Geoenviron. Eng., ASCE*, 124(10), 817-833.

A modified Newmark type-analysis according to EC-8 requirements for seismic stability analysis of natural slopes

G. Biondi & M. Maugeri

University of Catania, Italy

Abstract

In the paper the EC-8 requirements for seismic stability analysis of natural slopes are discussed with reference to the influence of soil dynamic behavior. The need of a modified Newmark-type analysis dissimilar from those available in the literature is highlighted and a procedure is proposed showing its accordance with the EC-8 provisions. Practical tools, such as stability charts and closed form solutions, are provided to evaluate the stability conditions without neglecting the effect pore pressure building-up in cohesionless soils and of cyclic degradation in cohesive soils. Examples of application of the proposed approach are also provided and proposition for improvement of EC-8 are outlined.

INTRODUCTION

EC-8 requirements and criteria for the analysis of seismic stability conditions of natural slopes are described in *paragraph 4.1.3* of Part 5 in the framework of the analysis related to the construction site requirements. No annex to *EC-8 Part 5* is provided for slope stability analysis as in the case of topographic amplification factors, evaluation of liquefaction potential, pile-head static stiffness, dynamic soil-structure interaction problems, earth retaining structures and seismic bearing capacity of foundations.

In the general requirements the verification of the slope response to a design earthquake is prescribed in order to ensure the safety and the serviceability of the structures erected on or near the slope. Consequently the limit state is defined as the state "*beyond which unacceptably large permanent displacements of the ground mass take place within a depth that is significant both for the structural and functional effects on the structures*".

Concerning the methods of analysis, different approaches are considered and the importance of the dynamic behaviour of soils is frequently highlight. In particular *paragraph 4.1.3.3* state that the response of ground slope to the design earthquake shall be evaluated performing a dynamic analysis, with the finite element method, or using simplified procedure such as the sliding block approach and the pseudo-static approach, taking into account the effect of soil dynamic behaviour. Concerning this last aspect, the effects of pore pressure build-up and of soil cyclic degradation are mentioned in *4.1.3.3.(2)* and limitation to the use of pseudo static approach is described in *4.1.3.3.(8)* due to the inadequacy of this approach into modelling the behaviour of "*soils capable of developing high pore water pressures or significant degradation of stiffness under cyclic loading*". Finally, the evaluation of earthquake induced permanent displacements using the rigid block procedure (Newmark, 1965) is prescribed in *4.1.3.3.(7)* to check the serviceability limit state.

Among the suggested approaches the sliding block procedure is the widely adopted for problems involving natural slopes for the following reasons:

- the previous described inadequacy of the pseudo-static approach into modelling the earthquake effects;
- the lack of information, which generally characterize the analyses of natural slopes, which makes the prevision of numerical seismic response analyses not enough accurate;

- among the available approaches, the sliding block procedure seems to be the better compromise between the accuracy of the model and the amount and complexity of the required data.

Since the cyclic behaviour of soils strongly affects both the seismic stability conditions and the magnitude of earthquake-induced permanent deformations, the use of a sliding block procedure incorporating the effects of earthquake-induced pore pressure and of soils cyclic degradation can be perceived through *paragraph 4.1.3.3*; in particular this modified Newmark-type analysis seems to be the better approach for the analysis of both limit state and serviceability limit state conditions. However, no practical suggestions or requirements are provided in *EC-8 Part 5* in order to perform a modified Newmark-type analysis including strength degradation effects.

OUTLINE OF METHODOLOGY

Based on these considerations, a procedure for the analysis of the influence of soil dynamic behaviour on the seismic stability condition and post-seismic serviceability of natural slopes is presented in the paper. The procedure consists in a modification of the original sliding block approach (Newmark, 1965) and is presented herein with the following aims:

- point out the accordance of the proposed procedure with the provisions of *EC-8 Part 5* with reference to the stability analysis and to the evaluation of the limit states;
- underline the importance of the requirements of *EC-8 Part 5* concerning the assessment of the limit states taking into account the effect of soil shear strength reduction;
- highlight some aspects of the dynamic soil behaviour which are not considered in *EC-8 Part 5* suggesting some improvements concerning the procedure to be adopted to incorporate the influence of pore pressure build-up and soil cyclic degradation into a modified Newmark-type analysis;
- provide practical tools, such as stability charts and closed form solutions (to be included as an annex to *EC-8 Part 5*) useful to apply the proposed procedure.

Concerning the paper, the need of a new modified Newmark-type analysis is firstly pointed out through:

- field evidences of the influence of soil dynamic behavior on the seismic response of natural slopes and earth-structures;
- a review of the modified Newmark-type analyses available in the literature for both saturated cohesionless slopes and cohesive slopes.

Then, a procedure is proposed starting form the results of Biondi (2002), Biondi et al. (2000,2002a) and Biondi & Maugeri (2005a) providing also a matching with the requirements of *EC-8 Part 5* and some numerical practical examples.

Finally, suggestions for an improvement of the *General requirements* (*paragraph 4.1.3.1*) and of the *Methods of analysis* (*paragraph 4.1.3.3*) of *EC-8 Part 5* are proposed.

REASONS FOR A MODIFIED NEWMARK-TYPE ANALYSIS IN EC-8

Field evidences of the effects of soils strength reduction on seismic stability conditions

It is well known that cyclic behaviour of soils strongly affects the seismic stability conditions of natural slopes and earth-structures and significantly influences the post-seismic serviceability in terms of amplitude of earthquake-induced permanent deformations. This matter was highlighted in the first studies and post-event reports.

During the 1964 Alaska earthquake loose saturated sands and sensitive clays suffered a loss of shear strength causing devastating landslides (Shannon & Wilson, 1964; Seed & Wilson, 1967). Despite the magnitude of the 1906 San Francisco earthquake, most of the earth dams shaken by event did not suffered heavy damages due to the rock or stiff clays foundation soils; otherwise most of the damages induced by the 1939 Ojika (Japan) earthquake to earth dams were caused by the liquefaction of saturated sandy soils. Makdisi & Seed (1978) distinguished different seismic response of embankments depending on the dynamic soil behaviour: large deformations and failures can occur in loose or medium dense sandy embankments due to the increase in pore pressure; embankments of cohesive soils, dry cohesionless soils or saturated dense sandy soils can experience

trivial permanent deformations without reaching a failure condition.

More recently several post-earthquake reports gave evidence of the influence of soil dynamic behaviour. Liquefaction of deltaic and beach deposits causes ground lateral spreading in the 1970 Chimbote (Perù) earthquake (Plafker et al., 1971). The cyclic behaviour of clay soils significantly affects the seismic and post-seismic response of several natural slopes during the 1980 Irpinia (Italy) earthquake (Maugeri & Motta, 1985; D'Elia et al., 1986; Cotecchia et al., 1986 b; Crespellani et al., 1996). Lateral deformations of gently inclined slopes was triggered by the pore pressure build-up during the 1995 Hyogoken-Nambu earthquake (Kameda & Hamada, 1998) and failures were observed in earth dams and embankments due to liquefaction (Oka et al., 1995 a,b). During the 1995 Aegion (Greece) earthquake, the pore pressure build-up in sand and silty-sand layers causes extensive submarine landslides and lateral spreading of the coastline with displacements in the order of 5-15m (Boukovalas et al., 1999). Damages to earth structures were induced by the 1995 Kozani-Grevena (Greece) earthquake due to the combined effect of earthquake-induced shear stress and reduction of shear strength of loose silty-sand soils. Finally, land loss into the sea along south coastal line of the Izmit Bay occurred during the 1999 Kocaeli (Turkey) earthquake due to the inertial effect and the loss of soils shear strength caused by the excess pore pressure (Cetin et al., 2004).

Match of traditional approaches with EC-8 requirements and provisions

Based on the previous described experiences and on other case-histories documented in the literature, a number of studies were performed in order to introduce the effect of soil dynamic behaviour in the procedures for seismic response analysis of natural slopes and earth structures.

Concerning natural slopes, simplified methods based on approximate models are often preferred to more rigorous solutions that are less practical and more time-consuming and require more detailed data. The widely adopted procedures were the pseudo-static approach and sliding block analysis performed using the Newmark (1965) method.

The pseudo static approach is nowadays considered a primitive tool due to its inadequacy in describing the time-dependent effect of earthquake shaking (*inertial effect*) and the consequent soil dynamic response which cannot, apriori, exclude a *weakening effect*; this inadequacy represent the reason of the above described limitation imposed in *paragraph 4.1.3.3.(8)* of *EC-8 Part 5* .

The Newmark sliding block model, although approximate, gives much more information than the pseudo-static analysis and requires less data and a smaller modelling effort than numerical approach for seismic response analysis. A number of studies were performed to evaluate the accuracy of this approach (Lin & Whitman, 1983; Chopra & Zhang, 1991; Gazetas & Uddin, 1994; Kramer & Smith, 1997; Bray & Rathje, 1998; Elms, 2000; Beikae, 2001; Sarma & Koukoulis, 2004).

Concerning the dynamic behaviour of soils, it is well known that the Newmark method allow a reliable and safe prediction of the slope response only if the effect of soils strength reduction is accounted for in the displacement analysis and in the evaluation of the slope critical acceleration.

Otherwise a number of studies has shown that stability analyses or displacements analyses performed neglecting the effect of soils shear strength reduction, can lead to an unsafe evaluation of the slope response. As an example Table 1 shows several case-histories of natural slopes and earth-structures for which a pseudo-static stability analysis or a displacement analysis performed without taking into account the effect of soil shear strength reduction were not able to predict the occurred failures and the magnitude of the observed earthquake-induced displacements.

In particular, in the most of the cases the values of seismic safety factor F_d greater that unity and the comparison between the maximum earthquake acceleration k_{max} and the slope critical acceleration, point out that the soil shear strength reduction represent the only explanation of the occurred instabilities and, in the same time, the triggering factor. In some other case the weakening effect together with the inertial effect, due to the

shaking, must be considered the concurrently causes of the occurred phenomena.

Review of modified Newmark-type analysis available for cohesionless soils

Different methodologies are available to perform a Newmark-type analysis including the effect of soil dynamic behaviour. In the procedure for cohesionless slopes (Sarma, 1975; Conte & Dente, 1986; Baziar et al., 1992; Loukidis et al., 2001; Tradafair & Sassa, 2005), the effect of shear strength reduction is quantified in terms of earthquake-induced pore pressure. A review of the available procedures was performed by Biondi (2002); the following aspects are of interest to match the characteristics of the procedures with the requirements of *EC-8 Part 5*:

a) all the proposed procedures emphasize that the effective stress analysis (including an evaluation of the pore pressure build-up) represent the proper approach for the stability analysis and for the assessment of permanent displacements; usually the earthquake-induced pore pressure ratio is introduced in the procedures;
b) the available procedures do not describe the combination of earthquake parameters, slope geometry and soil parameters involved in the dynamic behaviour for which a failure of the slope can occur due to the strength reduction or due to a combined weakening and inertial effect; as an example none of the available procedures highlight the fundamental influence of the soil relative density on the slope response;
c) the available procedures do not describe the combination of the previous mentioned factors for which permanent displacements can occur in slopes which were initially stable under seismic condition (before the strength reduction take place), or in slopes which become unstable during the ground motions when the weakening effect occurs;
d) in order to perform a reliable displacement analysis the time-history of the slope critical acceleration k_c must be known; then an evaluation of the time-histories of excess pore pressure is required together with the evaluation of the minimum value $k_{c,min}$ to which the slope critical acceleration drops when the excess pore pressure reaches its maximum value;
e) in them most of approaches the displacement analysis is performed using the minimum value $k_{c,min}$; only the approach by Conte & Dente (1986), Loukidis et al.(2001) and Tradafair & Sassa (2005) takes into account a time-dependent value of k_c which reduces from its initial value k_{co} (before the strength reduction take place) to $k_{c,min}$; however, Conte & Dente (1986) uses an arbitrary empirical expression to describe the reduction of k_c; Loukidis et al.(2001) suppose an arbitrary linear reduction of k_c from k_{co} to $k_{c,min}$ and Tradafair & Sassa (2005) use the results of cyclic tests to describe the change in k_c valid only for the tested soils.

For those described in b) and c), the available procedure does not provide practical tools of general validity to detect the occurrence of the weakening effect and its consequence on the slope response; moreover no suggestions are provided to detect the proper approach for a reliable displacement analysis. Concerning these aspects *point 4.1.3.4(1)* of *EC8 Part 5* suggest that "*For saturated soils in areas where αS>0.15, consideration shall be given to possible strength degradation and increases in pore pressure due to cyclic loading…*". More detailed indications on this field shall be appreciable for practical purposes and are presented in the paper in the framework of the description of the proposed approach.

Concerning the evaluation of earthquake induced pore pressure, *point 4.1.3.3(9)* of *EC8 Part 5* suggest to adopt "…*appropriate tests. In the absence of such tests, and for the purpose of preliminary design, it may be estimated through empirical correlations*.". However, due to the general lack of data, in the case of natural slopes the use of empirical relationships developed through the results of cyclic untrained tests seems to represent the better compromise. The available procedure adopts empirical relationships to evaluate the excess pore pressure with the exception of the procedures by Loukidis et al.(2001), which uses the results of numerical analyses including a pore-pressure generation model, and the procedure by Tradafair & Sassa (2005) which uses the results of laboratory

tests to detect the time-history of the available shear strength.

The use of earthquake-induced pore pressure ratio to describe the excess pore pressure effect is in accordance with *point 4.1.3.4(2)* of *EC-8 Part 5* which state that the cyclic pore-pressure increase "*may be accounted for by decreasing the resisting frictional force through an appropriate pore pressure coefficient proportional to the maximum increment of pore pressure.*". Then, threshold values of the earthquake induced pore pressure ratio may represent a practical way to quantify the influence of soil shear strength reduction on slope seismic response. As later described, this way was followed in the procedure proposed herein for slopes in cohesionless soils.

Finally, the use of literary available empirical relationships to quantify the excess pore pressure requires the evaluation of the *number of equivalent loading cycles* N_{eq} (Seed et al., (1975). Biondi et al. (2004) performed a review and a comparison of the literary available procedures showing significant differences in the predicted values of N_{eq}. No suggestions in this field are provided in *paragraph 4.1.3* and in both *paragraph 4.1.4* and *Annex B* of *EC8 Part 5* related to liquefaction problems. The convenience in the use of N_{eq} in a stability analysis which includes the effect of excess pore pressure will be described in the present paper and suggestions will provided for improvements of *paragraph 4.1.3*. of *EC8 Part 5*.

Review of modified Newmark-type analysis available for cohesive soils

Some procedures were developed to perform a Newmark-type analysis including the effect of cyclic behaviour of cohesive soils (Lemos & Cohelo, 1991; Tika-Vassilikos et al.,1993; Lemos et al., 1994; Crespellani et al., 1990, 1992, 1996; Biondi, 1998; Cascone et al., 1998). Due to the differences in the approaches a comparison between the procedures cannot be performed as in the case of cohesionless slopes. Then separate considerations are performed herein.

Lemos and co-workers (Lemos & Cohelo, 1991; Lemos et al., 1994) and Tika-Vassilikos et al.(1983) suggested a procedure for incorporating rate-dependent field strengths into numerical sliding block analysis. The procedure concern with failures in pre-existing shear surfaces and predict different slope behaviour depending on the soil response to high-speed shearing conditions: positive, neutral and negative rate effect in fast shearing can occur depending on the clay fraction. In the displacement analysis the reduction of k_c was evaluated assuming the soil ultimate shear strength as a function of the displacement rate and degree of particle orientation; however only the results of high-speed controlled ring shear tests (performed on samples pre-sheared to residual conditions), were suggested to this purpose. In soils showing positive rate effect (fast residual strength is higher that slow residual) the earthquake-induced permanent displacements were about 10 times smaller than the ones calculated using a constant strength soil model (traditional Newmark-type analysis); otherwise, catastrophic slope failures can occur during earthquakes in soil that exhibit a loss of shear strength related to the negative rate effect in fast shearing.

In the procedure suggested by Crespellani et al. (1990, 1992, 1996) both the effective and the total stress approaches are considered. The stability analysis is performed referring to the seismic and post-seismic conditions and the displacement analysis is performed taking into account the change in soil shear strength due to the earthquake-induced pore pressure and soil cyclic degradation.

In the effective stress analysis the change in soil shear strength is accounted for introducing the earthquake-induced pore pressure ratio in the evaluation of the slope safety factor and critical acceleration; in the post-seismic stability analysis the maximum value of the excess pore pressure is adopted to compute a post-seismic static safety factor. The procedure requires the estimation of the maximum earthquake-induced shear strain amplitude γ_{max} and the knowledge of the soil volumetric cyclic threshold shear strain γ_v (which is related to the plasticity index *IP* and the over consolidation ratio *OCR* through an empirical expression). The displacement analysis is performed using the minimum value $k_{c,min}$ of the slope critical acceleration (i.e the value corresponding to the maximum value of earthquake-induced pore pressure)

for the entire duration of the selected ground motion time history.

In the total stress approach the change of k_c during the earthquake is considered in the displacement analysis. To this purpose the effect of loading speed is accounted for through the *loading rate coefficient* (Poulos, 1988) and the cyclic degradation is evaluated using the *cyclic degradation index* (Thiers & Seed, 1968). The amplitude of each loading cycles imposed to the soil is compared with the cyclic threshold shear strain γ_v of the soil in order to detect those cycles that take part to the cyclic degradation phenomena. The resulting time-histories of k_c depend on which of the two effects prevails.

The procedures proposed by Biondi (1998) and Cascone et al. (1998) adopt the total stress approach and the soil strength degradation is accounted for introducing the degradation index and the degradation parameter. In this way, according to Matasovic & Vucetic (1995), both the pore water pressure generation and the simultaneously cyclic soil degradation are accounted for. The time-history of the slope critical acceleration is evaluated through a procedure that consists of the following stage: detection of the loading cycles to be considered in the degradation path, evaluation of the degradation parameter related to each cycle, calculation of the current value of soil undrained shear resistance and, finally, computation of a current value of slope critical acceleration. The application of the procedure to different earthquake records and soil geotechnical parameters shows a significant dependence of the slope displacement response on the duration, frequency and energy content of the earthquake records, on the static stability condition of the slope and, finally, on the parameters involved in the modelling of soil cyclic behaviour.

Considerations in the match of the revised procedures with the requirements of *paragraph 3.1.3* of *EC-8 Part 5* and general consideration for a possible improvement are described:

a) the total stress approach is generally adopted for two reasons: the lack of accurate empirical relationships for the evaluation of excess pore pressure and the opportunity of modelling the effective stress reduction (due pore pressure build-up) and the cyclic degradation through an accurate selection of the degradation index which allow to take into account the pore pressure build-up and the simultaneously cyclic degradation;
b) the introduction of the parameters mostly involved in the cyclic response of cohesive soils (such as *IP*, *OCR* and γ_v) represent an appreciable improvement in a modified Newmark-type analysis;
c) the displacement response of cohesive slopes and the occurrence of failures depend on the characteristic of the ground motion (duration, frequency and energy content) and on the associated cyclic behaviour of soils; then, the selection of the time histories to be adopted for the displacement analysis represent a crucial point in a modified Newmark-type analysis more than in a traditional one;
d) in a modified Newmark-type analysis, k_{co} cannot be used to reliably predict the occurrence of a failure and the magnitude of permanent displacements; then, differently, from the traditional displacement analysis, the ratio k_{co}/k_{max} cannot be considered as the only parameter governing the stability conditions;
e) since permanent displacements are significantly affected by the time history of k_c, the use of a constant value equal to $k_{c,min}$, although conservative, can lead to an overestimation of the response; otherwise, the adoption of a time-dependent value of k_c allows to take into account the influence of the amplitude and frequency of the earthquake-imposed loading cycle;
f) no parameter describing the occurrence of failures are provided both in the effective and total stress available approaches; as an example, no threshold valued of the pore pressure ratio and of degradation parameter are provided in order to detect the influence of the inertial and weakening effects; moreover no suggestions are provided to detect the proper approach for a reliable displacement analysis; again, detailed indications on this field shall be appreciable for practical purposes; indication for an improvement of *paragraph*

3.1.3 of *EC-8 Part 5* are presented in the paper in terms of threshold values of the degradation parameter.

A PROCEDURE FOR SEISMIC STABILITY ANALYSIS OF NATURAL SLOPES ACCORDING TO EC-8 REQUIREMENTS AND PROVISIONS

The procedure described herein summarizes the works by Biondi (2002), Biondi et al. (2000,2002) and Biondi & Maugeri (2005a). In the following paragraphs the procedure is summarised underline its accordance to the requirements and provisions of *EC-8 Part 5* and highlighting some possible improvements.

Reference scheme and definitions

The infinite slope (Figure 1) is the reference scheme for the procedure and solutions for both effective and total stress approach are provided. All the equations giving the relevant parameters of the procedure are reported in the appendix A of this paper. The flow chart of the proposed procedure is described in Figure 2. The definitions required to describe the procedure are those derived by Biondi (2002), Biondi et al.(2002a) and Biondi & Maugeri (2005a), which are synthesized in Table 2.

The proposed procedure allows to detect the occurrence of all the slope behaviors described in Table 2 using two threshold values of the pore pressure ratio (in the effective stress analysis) and two threshold values of the degradation parameter (in the total stress approach). The evaluation of the seismic and post-seismic stability conditions, the occurrence of permanent displacements and the selection of the proper approach for the displacements analysis represent the targets of the procedure.

Effective stress approach

The effective stress approach is adopted in the procedure for the analysis of the seismic response of saturated sandy slopes; the reduction of soil shear strength is accounted for using the earthquake-induced pore pressure ratio Δu^*_{max} and the number of equivalent loading cycles N_{eq} computed for the selected ground motion.

The relationships by Biondi (2002), is suggested to estimate Δu^*_{max}:

$$\Delta u^*_{max} = \frac{2}{\pi} \cdot \sin^{-1}\left\{ N_{eq}^{1/2a} \cdot \sin\left[\frac{\pi}{2} \cdot \Delta u_1^* \right] \right\} \quad (1)$$

$$\Delta u_1^* = r \cdot (D_r)^s \cdot \frac{0.65 \cdot k_{max}}{1 - r_u} + t \cdot (D_r)^z \quad (2)$$

In eqs. (1) and (2) r,s,t,z are numeral fitting constants which values is reported in Table 3 (in relation to the assumption for the experimental constant a), D_r represent the soil relative density and r_u is the static pore pressure ratio (see Appendix 1).

The evaluation of N_{eq} can be performed using the expressions of Table 4 derived by Biondi et al. (2004) for soils sites with $V_{s,30}$ between 180 and 360 m/s.

Two threshold values of the pore pressure ratio are introduced in the procedure:

$$\Delta u_f^* = 1 - \frac{1}{F_s} \qquad \Delta u_d^* = 1 - \frac{1}{F_{do}} \quad (3)$$

where F_s is the static factor of safety and F_{do} represent the seismic safety factor evaluated for the maximum earthquake induced acceleration k_{max}, neglecting the strength reduction (see Appendix 1).

The significances of Δu^*_f are synthesized in Figure 3 were the numerical values of this parameter are also plotted for different slope schemes. The significances of Δu^*_d are synthesized in Figure 4 together with some numerical values computed for different slope schemes and for ω=-β, ϕ'=35° and r_u=0.2.

Due to their significances, a comparison between Δu^*_{max}, Δu^*_f and Δu^*_d allows to detect the possible slope response to the selected ground motion and the superposition of the plots Δu^*_f and Δu^*_d represent useful stability charts for the evaluation of the effects of excess pore pressure on seismic stability conditions and post-seismic serviceability.

Figure 5 shows a description of the different slope behaviour that can be detected with the proposed stability charts together with a description of the proper approach to be adopted for the displacement analysis. Using eqs.(3) a number of stability charts can be plotted for different slope schemes, different slope hydraulic conditions and different values of k_{max}; examples are provided in the same Figure 5.

In alternative to earthquake induced pore pressure ratios, the procedure may be applied

referring to the values N_f and N_d of the number of equivalent loading cycles corresponding to Δu^*_f and Δu^*_d, respectively:

$$N_f = \left[\frac{\sin\frac{\pi}{2}\cdot\Delta u^*_f}{\sin\frac{\pi}{2}\cdot\Delta u^*_1}\right]^{2a} \qquad N_d = \left[\frac{\sin\frac{\pi}{2}\cdot\Delta u^*_d}{\sin\frac{\pi}{2}\cdot\Delta u^*_1}\right]^{2a} \tag{4}$$

In this way the uncertainties in selection of the empirical relationships to be adopted for the evaluation of the excess pore pressure may be overcome; however the influence of soil relative density, slope hydraulic condition and earthquake-induced shear stress are not missed out since are respectively accounted for through D_r, r_u and k_{max} involved in the estimation of Δu^*_1.

Stability charts in terms of N_{eq} , N_f and N_d with the same significances of those schematized in Figure 5 can be plotted using eqs. (3) and .(4) allowing to detect the slope response through a comparison of N_{eq} , N_f and N_d. Examples of these charts are provided by Biondi et al.(2002a).

According to Biondi et al.(2002b) the reduction of k_c take place in the time interval which gives a contribute in the conversion procedure required for the evaluation of N_{eq}. This means that the pore pressure build-up is considered to take place in the bracketed duration corresponding to a threshold acceleration level equal to 30% of k_{max}.

Finally, the effect of the earthquake shaking on the slope response can be also evaluated using the post-seismic static factor of safety F_s^{PS} which represent an index of the slope stability immediately after the end of the shaking:

$$F_s^{PS} = F_s \cdot \left(1 - \Delta u^*_{max}\right) \tag{6}$$

Stability charts with the same significances of those schematized in Figure 5 can be obtained comparing the ratios $1/F_s$ and F_s^{PS}/F_s (Biondi, 2002).

Total stress approach

The total stress approach is adopted for cohesive slopes and the effect of cyclic behaviour on slope response is accounted for using the degradation index t and the degradation parameter C_u^*:

$$C_u^* = \frac{C_{uc}}{C_{uo}} = N^{-t} \tag{6}$$

In eq. (5) C_{uo} is the static value of the soil undrained shear strength while C_{uc} represent its current value (available during the ground motion) that depends on the number of loading cycles N to which the soil is subject. The degradation index t is related to γ_{max}, IP, OCR and γ_v (Matasovic & Vucetic , 1995).

Two threshold values of the degradation parameter are introduced in the procedure:

$$C_{uf}^* = \frac{1}{F_s} \qquad C_{ud}^* = \frac{1}{F_{do}} \tag{7}$$

The significances of $C_u{}^*_f$ are synthesized in Figure 6 were the numerical values of this parameter are also plotted for different slope schemes. The significances of $C_u{}^*_d$ are synthesized in Figure 7 together with some numerical values computed for different slope schemes for the case ω=0, $C_u/\gamma D$=1.

Due to their significances, a comparison between C_u^*, $C_u{}^*_f$ and $C_u{}^*_d$ allows to detect the possible slope response to the selected ground motion and the superposition of the plots of $C_u{}^*_f$ and $C_u{}^*_d$ allows to obtain useful stability charts for the evaluation of the effects of cyclic strength degradation on seismic stability condition and post-seismic serviceability of the slope. Figure 8 shows a description of the different slope behaviour that can be detected with the proposed stability charts together with a description of the proper approach for the displacement analysis.

Using eqs.(7) a number of stability charts can be plotted for different slope geometry and static stability conditions and different values of k_{max}; examples are provided in the same Figure 8.

According to Crespellani et al. (1992) and Cascone et al. (1998) the reduction of k_c take place each times the amplitude of the earthquake-imposed loading cycles overcome the cyclic threshold volumetric shear strain.

Finally, the effect of the earthquake shaking on the slope response can be again evaluated using the post-seismic static factor:

$$F_s^{PS} = F_s \cdot C_u^* \tag{8}$$

and stability charts as those described in Figure 8 can be obtained plotting $1/F_s$ and F_s^{PS}/F_s.

Accordance with EC-8 provisions and improvements for the stability analysis

The main aspects of the proposed procedure are discussed herein to check its accordance with the provisions of *EC*-8 Part 5 and to propose some improvements:

- the theoretical assumption adopted in the proposed procedure for the effective stress analysis (i.e. the sliding block approach and the evaluation of pore pressure build-up) are in accordance with *paragraphs 4.1.3.3.(2) and 4.1.3.3.(7)*; then the proposed stability charts (Figure 5) represent useful and reliable tools which can be proposed to be added as a new Annex to *EC-8 Part 5* or as closed form solutions (eqs.3 and other of interest from Appendix A of this paper);
- the influence of the degradation index and of the degradation parameter accounted for in the total stress analysis, agree with field, laboratory and theoretical available results; then suggestions to adopt these parameters in a total stress analysis should be added to paragraph *4.1.3.* of *EC-8 Part 5* as in the case of excess pore pressure (see *4.1.3.3.(2), 4.1.3.3.(9), 4.1.3.4.(1)* and *4.1.3.4.(3)).*
- for the reasons above described the stability charts proposed for the total stress approach (Figure 8) represent useful and reliable tools for a stability analysis including cyclic degradation effects and can be proposed both in the form of stability charts (to be added in a new Annex of *EC-8 Part 5*) or as closed form solutions (eqs.7 and other of interest from Appendix A of this paper);
- the adoption of N_{eq} for the assessment of the excess pore pressure represent a crucial point in the procedure presented herein and in all other procedures which can be adopted following *4.1.2.3.(2)* and *4.1.2.3.(9)*; for these reasons, suggestions in order to compute N_{eq} should be added to *EC-8 Part 5* together with practical evaluation tools (such as diagrams and closed form solutions);
- the solution proposed herein for the assessment of N_{eq} was derived by Biondi et al. (2004) using a large number of earthquake records (the greater among other similar studies available in the literature) and accurate multi-regression analyses; moreover, its validity was checked and results significantly higher with respect to other available solutions; then, neglecting the uncertainties in the evaluation of excess pore pressure, the effective stress approach proposed herein can be also applied through N_{eq}, N_f and N_d in spite of the pore pressure ratios;
- due to the importance of N_{eq} (also for liquefaction potential assessment: see *paragraph 4.1.4* of *EC-8 Part 5*) and the dependence of the selected earthquake record motion from sites characteristics , all the numerical solutions derived by Biondi et al. (2004), for *ground types* ranging from *A* to *E*, are suggested for an improvement of *EC-8 Part 5*. The solutions were adopted by the Italian Geotechncial Society in the guidelines for geotechnical design in seismic areas (AGI, 2005).

DISPLACEMENT ANALYSIS ACCORDING TO EC-8 REQUIREMENTS

Based on the procedure proposed herein, the permanent displacements response of a slope can be evaluated using a modified Newmark-type analysis, which take into account the effect of pore pressure build-up in saturated cohesionless slopes or the effect of soils cyclic degradation in cohesive slopes.

Examples of application of the proposed procedure (from the stability analysis to the permanent displacements evaluation) were proposed by Biondi (2002) and Biondi et al. (2002b) for saturated sandy slopes and by Biondi (1998) and Biondi & Maugeri (2005b) for cohesive slopes. Some of the examples are described herein order to:

- highlight the procedure capabilities and its accordance to the requirements of *EC-8 Part 5*;
- shows the importance of a displacement analysis which takes into account the dynamic soil behaviour;
- highlight the inability of the traditional Newmark type-analysis in the prediction of weakening and inertial-weakening instabilities;
- propose some suggestions to be added to the provisions of *EC-8 Part 5* to detect the proper approach for the displacement

analysis and to restrict the field of validity of the traditional Newmark-type analysis.

Stability and displacement analysis for cohesionless slopes

The examples proposed for cohesionless saturated slopes are related to the slope schemes and earthquake records described in Tables 5 and 6; the obtained results (Table 6) are showed in Figures from 9 to 11.

Figures 9 and 10 shows the influence of the soil relative density and of slope initial stability conditions predicted by the proposed procedure. For each of the considered case, the analysis through the stability charts (figures 9a,10a), the reduction of slope critical acceleration (figures 9b,10b), the pore pressure build-up (figures 9c,10c) and the displacement response (figures 9d,10d) are plotted.

Slope 1 is initially unstable referring to the earthquake record #*A* (Tables 5,6) then, inertial, weakening and inertial-weakening instabilities may occur. The following consideration can be outlined using the obtained results (Figure 9):

- for D_r=65% and D_r=75% the reduction in shear strength brings k_c to zero; the slope experiences large permanent displacements and a flow failure (*zone 6* of the stability charts) is predicted; the displacement time-history is affected by the occurrence of the slope failure since, regardless the inertial effect, displacements increase following a trend predominantly imposed by gravity;
- for D_r=85% the procedure predicts the potential occurrence of a deformation failure (*zone 4*); the displacement analysis confirm this hypothesis but shows the occurrence of a moderate permanent displacement to be ascribed to the combined inertial and weakening effects;
- the traditional Newmark approach (*T.N.A.*) estimates a smaller value of permanent displacement overestimating the post-seismic serviceability of the slope; then even if the increase in pore pressure is negligible the consequence on the displacement response may be estimated carefully; for these reason the suggestion provided in point *4.1.3.4.(4)* of *EC-8 Part 5* should be accurately investigated.

Slope 2 is initially stable referring to the earthquake record #*G* (Tables 5,6), then only instabilities due to the pore-pressure build-up may occur; otherwise the slope remain stable during the ground motion. The following consideration can be outlined using the obtained results (Figure 10):

- for D_r=65% a flow failure (*zone 6*) is predicted with large slope displacements driven by gravity;
- for D_r =75% and D_r =85% the procedure predicts the possible occurrence of a weakening instability (*zone 3*); no significant permanent displacements develop, standing that, the slope response depends not only on the reduced value of slope critical acceleration but also on the shape of the selected record and on the degradation pattern followed by k_c; since the reduction of k_c is related to assumption on the pore pressure build-up, more detailed indications may be added to point *4.1.3.3.(2)* of *EC-8 Part 5* for those concern with a displacement analysis which take into account "*the possible effect of pore pressure increase under earthquake loading*".

Figure 11 shows the displacement response of *slopes A*, *B* and *C* to the earthquake records #*A* and #*F* (Table 5). The slopes were selected in order to be characterized by the same value of k_{co} then a traditional Newmark-type analysis would invariably predict the same permanent displacement (in this case no permanent displacement since $k_{co} > k_{max}$). However, due to the different state of stress and hydraulic condition, different seismic response of soils to the cyclic loading may be envisaged.

For the earthquake record #*A* the following response were evaluated (Figure 11):

- for *slope A*, despite the increase in pore pressure, no permanent displacements occur; then, the need of supplementary suggestions on the degradation path to be adopted for k_c is again pointed out and specification of point *4.1.3.3.(2)* of *EC-8 Part 5* are evident*;*
- for *slope 2*, the considerable increase in pore pressure produces a reduction in k_c and a remarkable permanent displacement, even if the slope was initially stable; a *weakening instability* occurs (zone 3);

- for *slope 3*, soil liquefaction affect the stability conditions and the displacement response shows the typical trend of flow failure (zone 6).

For the earthquake record #*F* (Tables 5,6) the same consideration outlined for the earthquake record #*A* may be pointed out; however, significant differences in the magnitude of displacements triggered by the strength reduction can be observed even if the same k_{max} characterize the records and even if similar values of the pore pressure build-up and $k_{c,min}$ were computed. These differences range from about 130% for *slope C* to about 200% for *slope B* and must be ascribed to the differences in the energy and frequency content and strong motion duration of the records which lead to different values of N_{eq} (Table 5) and different length of the time interval in which the pore pressure build-up take place. Again, a detailed indication of the approach to be adopted for evaluating the influence of N_{eq} should be added to *EC8 Part 5* in the provisions for including the excess pore pressure effects.

Stability and displacement analysis for cohesive slopes

The examples proposed for cohesive slopes are related to the slope schemes and earthquake records described in Tables 7 and 8. The obtained results (Table 8) are showed in Figures 12 and 13 in terms of displacement response computed for different values of the degradation index *t* ranging from 0 to 0.20. To simplify the understanding of the results, the displacement response were computed using a constant value of the degradation index during the whole ground motion duration.

The slope S1 is initially unstable for both the selected ground motions (k_{max}/k_{co}=5); then, regardless the occurrence of the strength reduction, permanent displacements occurs due to the inertial effect. As a consequence of the different soil cyclic behavior (described through the different values of the degradation index) different displacement response were computed. As an example an increase in the degradation parameter from *t*=0.1 to *t*=0.2 produce and increment of the permanent displacements equal to about 260% for the earthquake record #CT (Figure 12) and to about 150% for the earthquake record #TZ (Figure 13). Those differences must be ascribed to the different frequency and energy content of the records and to the different degradation path of k_c;, again, the need of exhaustive recommendations on the theoretical assumption to perform a modified Newmark-type analysis are highlighted and explanations to the requirements of *paragraph 4.1.3.3.(2)* of concerning a displacement analysis which take into account "*the softening of the response with increasing strain level*" are evident.

Similar conclusions can be derived with reference to the slope S2. In this case, the same reduction of the soil degradation index produces a less evident increase in the permanent displacements equals to about 140% for both records (Figures 12 and 13). This behavior can be explained considering that in this case (k_{max}/k_{co}=7) the contribution of the inertial effect is greater than those computed for slope S1 (k_{max}/k_{co}=5); then, despite the same records were adopted and the same degradation index were considered, the displacement response suffer a less evident weakening effects with respect to the inertial one.

Finally, for both slopes the comparison with the results of a traditional Newmark-type analysis (*T.N.A.*) highlight a general underestimation of the response if the cyclic strength reduction is neglected; the differences in the displacement response depends on the adopted values of the degradation index and than is related to the cyclic soil behavior associated to the soil degradation properties and to the selected ground motion.

CONCLUDING REMARKS

General conclusions

The need of a new modified Newmark-type analysis is pointed out in the paper through the analysis of several field evidences of the seismic response of natural slopes and through a review of the modified Newmark-type analyses available in the literature.

A modified Newmark-type analysis for the evaluation of the seismic stability condition of saturated cohesionless slopes (taking into account the effect of pore pressure build-up)

and of cohesive slopes (taking into account the effect of cyclic degradation) is presented in the paper showing its match to the requirements of *EC-8 Part 5* and highlighting an evident necessity of a more detailed indication concerning a displacement analysis which take into account "*the softening of the response with increasing strain level, and the possible pore pressure increase under cyclic loading…"*.

Several numerical examples are provided in order to shows the main characteristics of the proposed procedure and the influence of the parameters directly involved in the seismic response of natural slopes in term of stability condition and permanent displacements. In particular the influence of the static slope stability conditions, of the earthquake induced shear stress, of the relative density of cohesionless soils and of the degradation index for cohesive soils is pointed out.

Propose of improvements to Part 5 EC-8

The following suggestions for improvements to the provisions and requirements of Part 5 of Eurocode 8 are outlined in the paper:

- since the theoretical assumption of the proposed procedure for the effective stress analysis are in fully accordance with the *General Requirements* of *paragraphs 4.1.3*, the proposed stability charts (see Figure 5) and the introduced threshold values of the earthquake-induced pore pressure ratio (see eq.3) and number of equivalent loading cycles (see eq.4) may be added to *Part 5 of Eurocode 8* (as a new Annex) in the forms of diagrams or closed form solutions together with other relevant equations described in the Appendix A of this paper;
- the assumptions of the proposed approach for the total stress analysis agree with field, laboratory and theoretical available results and with the few indications of the *General Requirements* of *paragraphs 4.1.3*; then the proposed stability charts (see Figure 8) together with the threshold values of the degradation parameters introduced in the proposed procedure (see eqs.7) may be added to *Part 5 of Eurocode 8* (as a new Annex) in the forms of diagrams or closed form solutions together with other relevant equations described in the Appendix A of this paper;
- since N_{eq} represent a crucial parameter in the estimation of the excess pore pressure required by *4.1.2.3.(2)* and *4.1.2.3.(9)* and due to the accuracy of the solutions presented in the paper, the formulas reported in Table 4 may be added to *EC-8 Part 5* providing, also, a useful tool for problems involving the liquefaction potential assessment (*paragraph 4.1.4*). Moreover, due to the site-dependence of the design ground motion selected for the stability analysis, all the solutions derived by Biondi et al. (2004), for *ground types* ranging from *A* to *E*, can be considered in the proposed improvement; these relationships were added to the recent guidelines of the Italian Geotechnical Society for the geotechnical design in seismic areas (AGI, 2005).
- the parameters and the assumptions involved in a Newmark-type analysis modified in order to include the strength degradation effect are numerous; the paper clearly shows that the displacement response is significantly affected by the chose of the pore pressure generation model, the selection of the time interval in which it takes place, the computation of cycles involved in the degradation effect and, finally, the computed degradation path of the slope critical acceleration; then, more detailed indications should be added in the *Method of analysis* (*paragraph 4.1.3.2*) in order to clarify the requirements of point *1,2,7,8* and *9.*

Table 1. Case-histories of natural slopes and earth-structures that suffered damages due to the weakening and inertial effects during earthquakes.

Earthquake	Slope/earth structure		Effect	References
Santa Barbara (1925)-M=6.3	Sheffield dam	k_H=0.10 F_d=1.2	Complete failure	Seed (1979)
San Fernando (1971) - M_w=6.6	Lower San Fernando dam	k_H=0.15 F_d=1.3	Upstream slope failure	Seed (1979)
San Fernando (1971) - M_w=6.6	Upper San Fernando dam	k_H=0.15 F_d=2÷2.5	Downstream shell including crest slipped of about 6 ft: d≈180cm	Seed (1979)
Near Izu Oshima (1969)	Tailing Dam on the Oshima island (Japan)	k_H=0.20 F_d≈1.3	Failure of the dam with release of tailing due to the soil shear strength reduction	Seed (1979)
Irpinia (Italy) 1980 M_s=6.5 k_{max}=0.177g	Natural slopes near Andretta (Avellino)	β_{av}=8° F_s≈1 k_{co}=0.02 Δu^*_f =0.2	Displacements of the crown: d_H=1-2m Displacements of the toe: d_H=20-30 m Slope movement after the end of the shaking.	D'Elia et al. (1986)
Irpinia (Italy) 1980 M_s=6.5 k_{max}=0.176g	Natural slopes near Calitri	β_{av}=10° F_s>1 k_{co}=0.017-0.045	Displacement (d=1-2m) due to the earthquake-induced pore pressure, soil cyclic degradation and post-seismic recompression.	Crespellani et al. (1996)
Kozani-Grevena (1995) M_s=6	Rimino bridge embankment	k_{co}=0.325	Failure due to the inertial effect and to the soil shear strength reduction: d_H=0.8-2m	Tika & Pitilakis (1999)
Hokkaido-Nansei-Ohi (1994)	Road embankment	"*sufficient resistance against seismic inertia forces*"	Failure due to the inertial effect and to the soil shear strength reduction	Towhata & Mizutani (1999)
Kushiro-Oki (1993)- M_{JMA}=7.8	Left bank of Kushiro River	H = 7m β_{av}=17°	The crest of the dike settled about 2 m. Movement of the slope take place towards the river: d≈ 2-3m	Finn (1999) Sasaki et al. (1995)
Kushiro-Oki (1993) - M_{JMA}=7.8 k_{max}=0.5	Embankment near the Kushiro Airport	H = 65m β_{av}=22° Δu^*_{max} =0.2	Toe displacement of about 2-3 m due to the soil shear strength reduction and inertial effect: d_V=2÷4 cm d_H =10 cm	Iai *et al.* (1999)
Aegion (1995) M_S=6.2 k_{max}≥0.29	Natural slope near Eratini (Corinthian Gulf) coast line	β_{av}=6.8° - 10.2° F_s=1.5 - 3.3 k_{co}=0.09 - 0.38	Failure triggered by the excess pore pressure Post earthquake landslides	Bouckovalas *et al.* (1999)

F_d:	Seismic safety factor evaluated with the pseudo-static approach using a seismic coefficient equal to k_H
k_{max}:	Maximum value of the earthquake induced acceleration (g) recorded near the slope/earth-structure
k_{co}:	Slope critical acceleration evaluated without taking into account the effect of soil shear strength reduction
d, d_H, d_V:	Value of permanent displacement (d) and of its horizontal (d_H) and vertical (d_V) components
H , β_{av}:	Slope/earth-structure height and average slope angle
F_S:	Static factor of safety
Δu^*_{max}:	Earthquake-induced pore pressure ratio
Δu^*_f:	Earthquake-induced pore pressure ratio required for slope failure

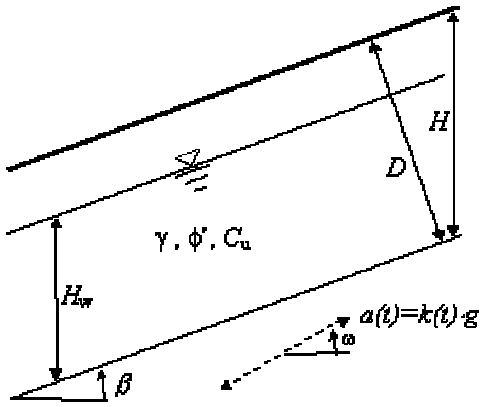

Fig 1. Reference slope scheme for the proposed procedure.

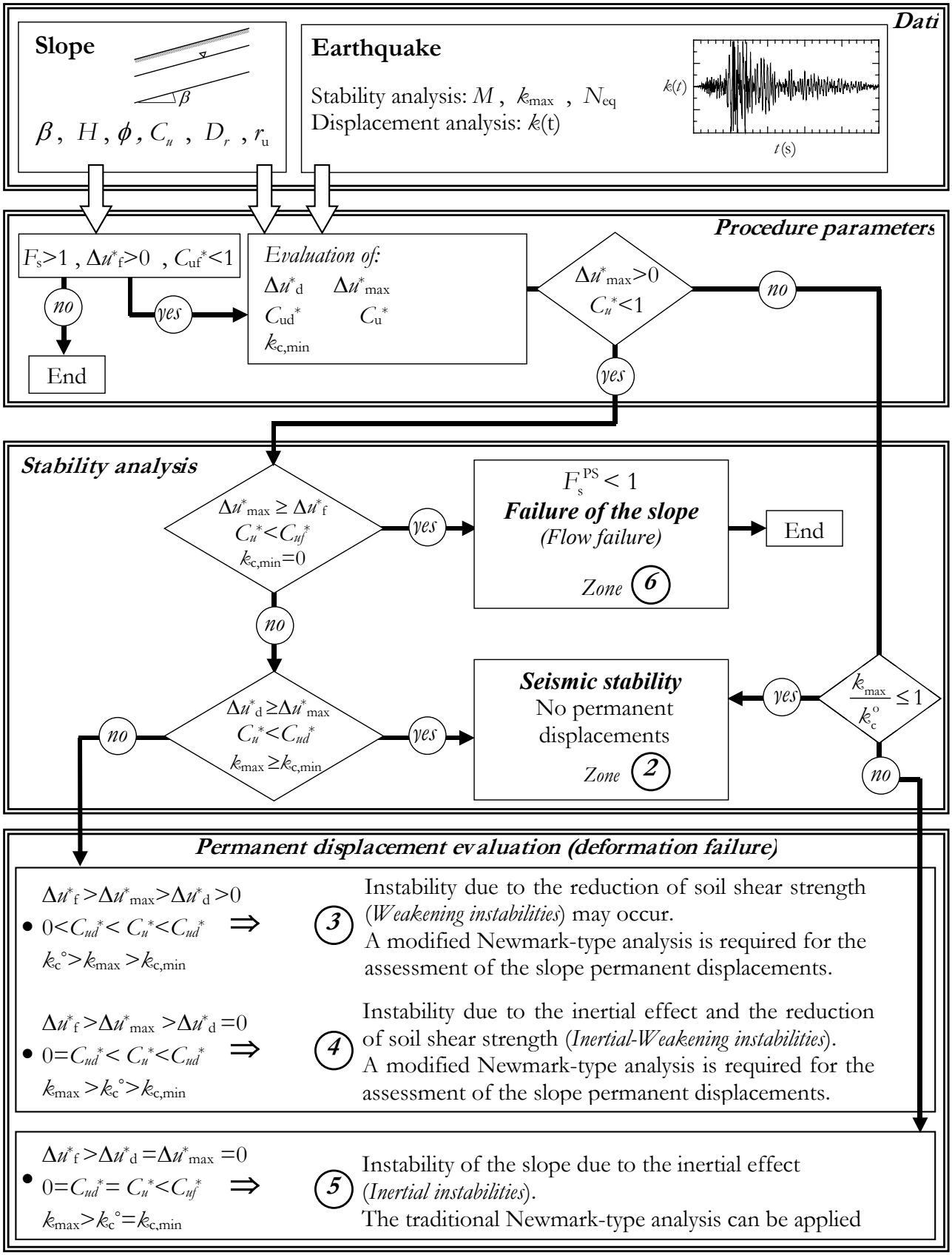

Fig 2. Flow chart of the proposed procedure (Biondi 2002).

Table 2. Definition adopted in the procedure by Biondi et al. (2002, 2004).

Earthquake effects	
inertial effect:	change in soil stress-state induced by the ground motion;
weakening effect	stiffness and strength degradation of soils due to pore pressure change and cyclic degradation effect

Types on instabilities	
inertial instability	- instability mainly ascribed to the inertial effect and triggered by the temporarily unbalanced driving forces; - no significant strength reduction take place;
weakening instability	- instability mainly ascribed to the reduction in soil shear strength; - the inertial effect is negligible
inertial-weakening instability	- instabilities due to both inertial and weakening effects - the slope response depends on which effect prevails

Types of weakening instabilities	
failure	- failure of a slope which occurs with very large deformations triggered by the strength reduction; - strength capacity drops below the values required for the static equilibrium and deformation are mainly ascribed to gravitational forces; - in slopes of loose or medium dense saturated sands the term *flow failure* is usually adopted to describe the quick failure due to the pore pressure build-up; - in cohesive slope the triggering factors are the pore pressure build-up and the cyclic degradation and failures can occur during or after the ground motion ends
deformation failure	- the strength capacity temporarily drops below the strength demand but remain higher than the values required for slope static equilibrium; - the slope does not experience a failure condition and its response must be analysed in term of admissibility of permanent displacements

Slope behavior in relation to the initial stability condition and to the occurrence of strength reduction	
initially stable slopes ($k_{co}/k_{max}\geq 1$)	*Possible slope behaviour*: - no strength reduction take place ($k_c=k_{co}$) in the soil and the slope remain stable without experience permanent displacements; - despite the strength reduction ($k_c<k_{co}$) k_c remains greater that k_{max} and no permanent displacements happens; - due to the strength reduction the slope becomes unstable (i.e. k_c drops to values lower than k_{max}) and a weakening instabilities may occur; in this case permanent displacements (*deformation failure*) or *failure* of the slope may happen.
initially unstable slopes ($k_{co}/k_{max}<1$)	*Possible slope behaviour*: - if no strength reduction happens ($k_c=k_{co}$) an inertial instability occurs; - if a strength reduction take place an inertial-weakening instability occurs and the slope can experience permanent displacements (*deformation failure*) or reach a *failure* condition

Table 3. Numerical fitting constant for equation (2) (modified by Biondi, 2003).

Experimental constant *a*	***r***	***s***	***t***	***z***
Seed & Booker (1977): $a= 0,7$	0,85134	-2,25052	0,13365	-1,50651
Fardis & Veneziano (1981): $a= 0.96 \cdot D_r^{0.83}$	1,00369	-1,90532	0,15198	-1,30758

Table 4. Formulas for the estimation of the number of equivalent loading cycles (modified by Biondi et al., 2003).

$\ln N_{eq} = -3.8370 + 2.670 \cdot \ln M - 0.3436 \cdot \ln a_{Max}$	
$\ln N_{eq} = -0.1533 - 1.8841 \cdot \ln a_{Max} + 0.9097 \cdot \ln I_{a,TB}$	
$\ln N_{eq} = 0.3854 - 2.2617 \cdot \ln a_{Max} - 0.3856 \cdot \ln D_{TB} + 1.0525 \cdot \ln I_{a,TB}$	
$\ln N_{eq} = -2.3679 - 2.3460 \cdot \ln a_{Max} + 0.9194 \cdot \ln v_o + 1.1911 \cdot \ln I_{a,TB}$	
$\ln N_{eq} = -1.9231 - 2.5467 \cdot \ln a_{Max} + 0.8657 \cdot \ln v_o - 0.2278 \cdot \ln D_{TB} + 1.2613 \cdot \ln I_{a,TB}$	
M:	earthquake magnitude
a_{Max}:	maximum ground acceleration of the selected time-histories [m/sec^2]
D_{TB}:	Trifunac & Brady (1975) s*trong-motion* duration [sec]
$I_{a,TB}$:	Arias Intensity evaluated in the s*trong-motion* duration [m/s]
v_o:	frequency of zero crossing estimated in the s*trong-motion* duration [Hz]

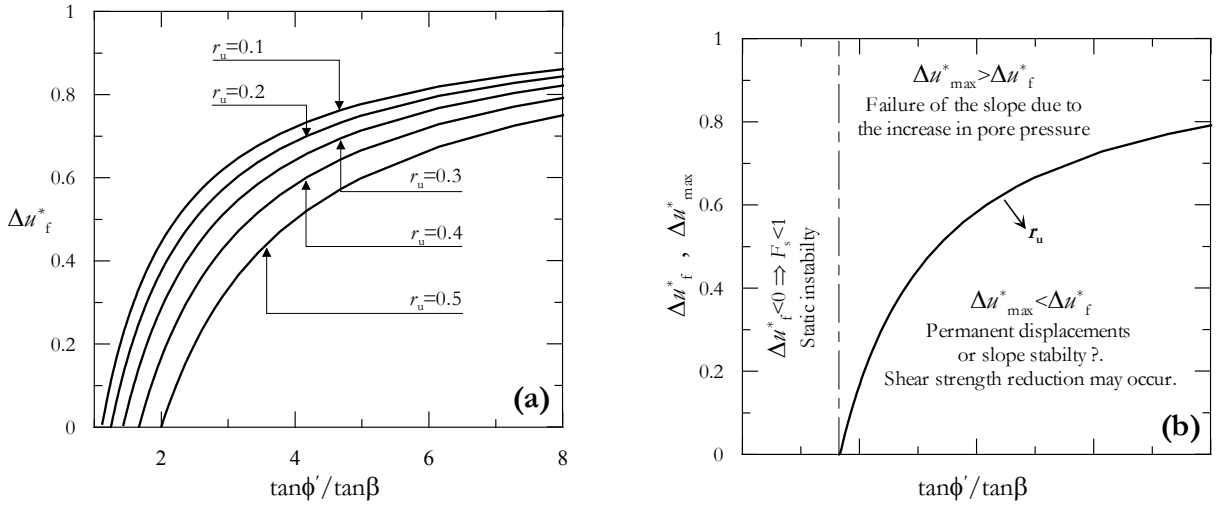

Fig 3. a) Values of Δu^*_f; b) possible slope behaviours (modified from Biondi et al. 2002a).

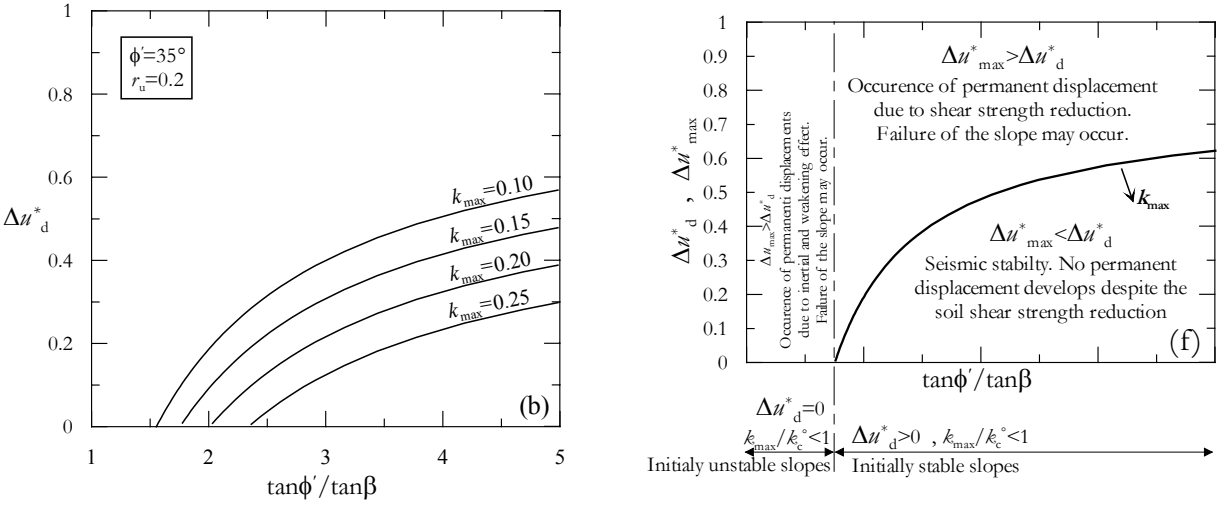

Fig 4. a) Some values of Δu^*_d; b) possible slope behaviours (modified from Biondi et al. 2002a).

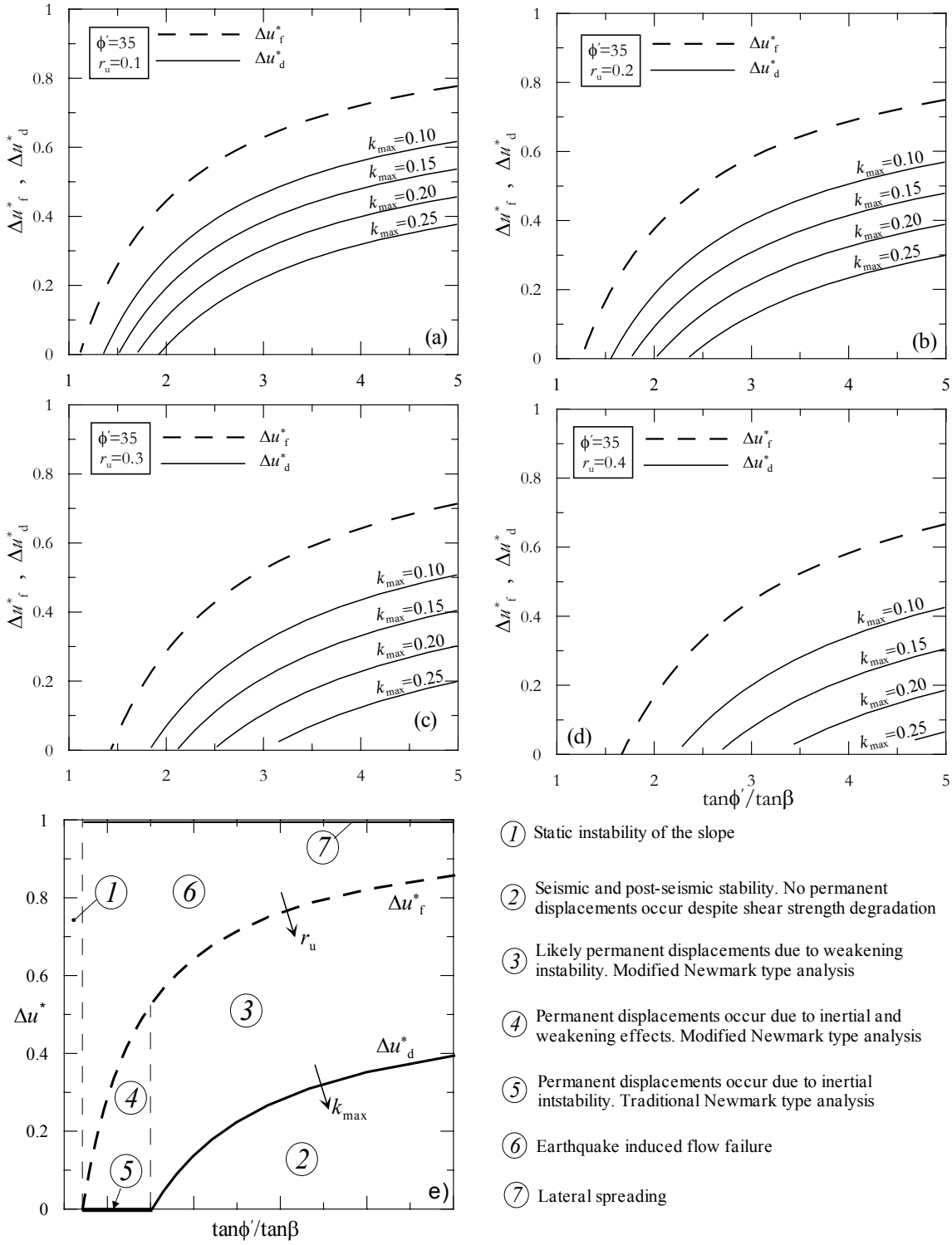

Fig 5. a,b,c,d) Example of the stability charts proposed for the effective stress analysis (modified from Biondi et al. 2002a); e) Scheme of the stability charts proposed for the effective stress analysis (modified from Biondi et al. 2002a).

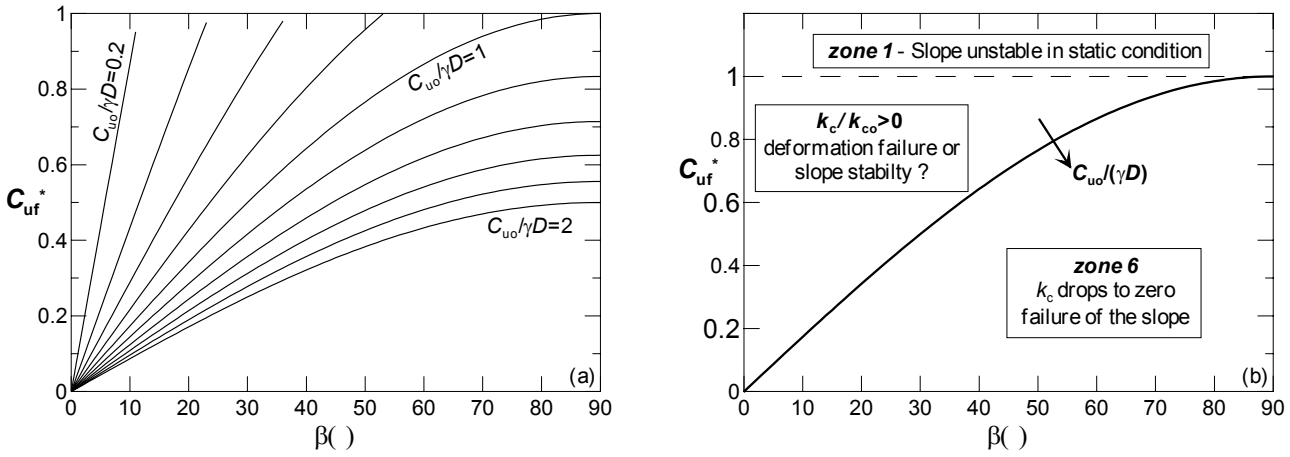

Fig 6. a) Values of $C_u^*{}_f$; b) possible slope behaviours depending on the values of C_u^* and $C_u^*{}_f$ (Biondi & Maugeri, 2005 a)

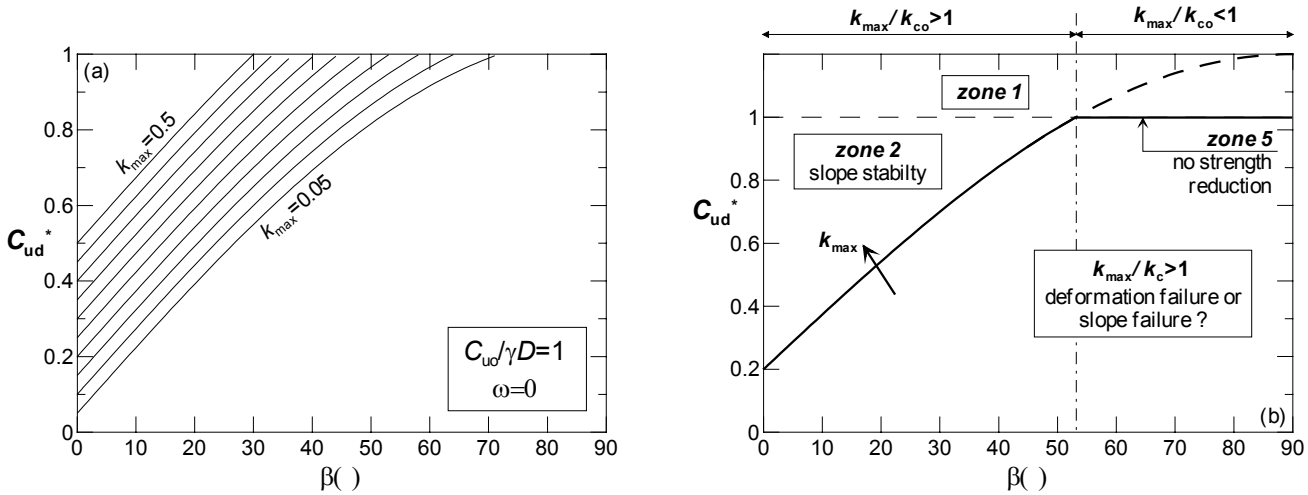

Fig 7. a) Some values of $C_u^*{}_d$; b) possible slope behaviours depending on the values of C_u^* and $C_u^*{}_d$ (Biondi & Maugeri, 2005 a).

.

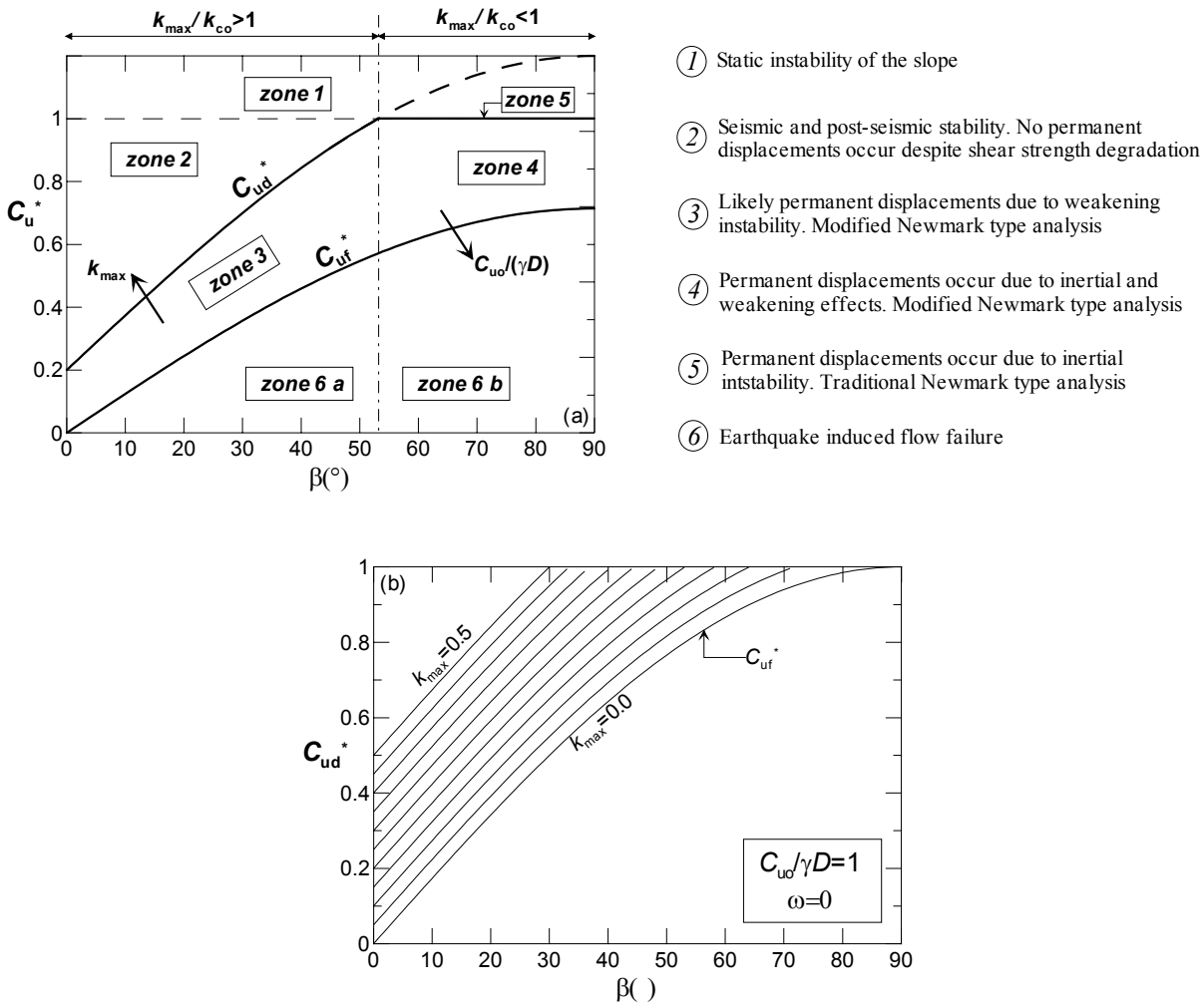

Fig 8. a) Scheme of the stability charts proposed for the total stress analysis. b) example of the stability charts proposed for the total stress analysis.

Table 5. Characteristics of the earthquake record adopted in the examples provided for saturated cohesionless slopes.

Earthquake	M_w	M_s	M_L	Station	V_s(m/s)	k_{max}	N_{eq}
#A Morgan Hill (USA 1984)	6.2	6.1	6.2	Gilroy #4	180-360	0.224	4.46
#F Northridge (USA 1994)	6.7	6.7	6.6	Hollywood Storage	180-360	0.231	7.55
#G Loma Prieta (USA 1989)	6.9	-	7.1	Gilroy #7	180-360	0.226	11.07

Table 6. Scheme of the slope considered in the examples provided for cohesionless saturated slopes and parameters of the proposed procedure.

Slope	ϕ'	$\tan\phi'/\tan\beta$	r_u	F_s	k_{co}	Δu^*_f
1	35°	2	0.1	1.8	0.264	0.444
2	35°	2	0.3	1.4	0.132	0.286

Slope	*Earthquake record*	Δu^*_d	Δu^*_{max} D_r=65%	Δu^*_{max} D_r=75%	Δu^*_{max} D_r=85%
1	#*G*	0.06	0.82	0.36	0.21
2	#A	0.00	0.79	0.36	0.21

Slope	ϕ'	$\tan\phi'/\tan\beta$	r_u	F_s	k_{co}	Δu^*_f
A	35°	2	0.07	1.9	0.284	0.46
B	35°	3	0.25	2.3	0.284	0.56
C	35°	5	0.39	3.1	0.284	0.67

Slope	*Earthquake record*	Δu^*_d	Δu^*_{max}	k_{max}/k_{co}	F_{do}	$k_{c,min}$
A	#*A*	0.10	0.29	0.79	1.11	0.106
	#*F*	0.09	0.26	0.81	1.09	0.124
B	#*A*	0.12	0.51	0.79	1.13	0.023
	#*F*	0.10	0.47	0.81	1.12	0.044
C	#*A*	0.14	1.00	0.79	1.17	0.00
	#*F*	0.13	1.00	0.81	1.14	0.00

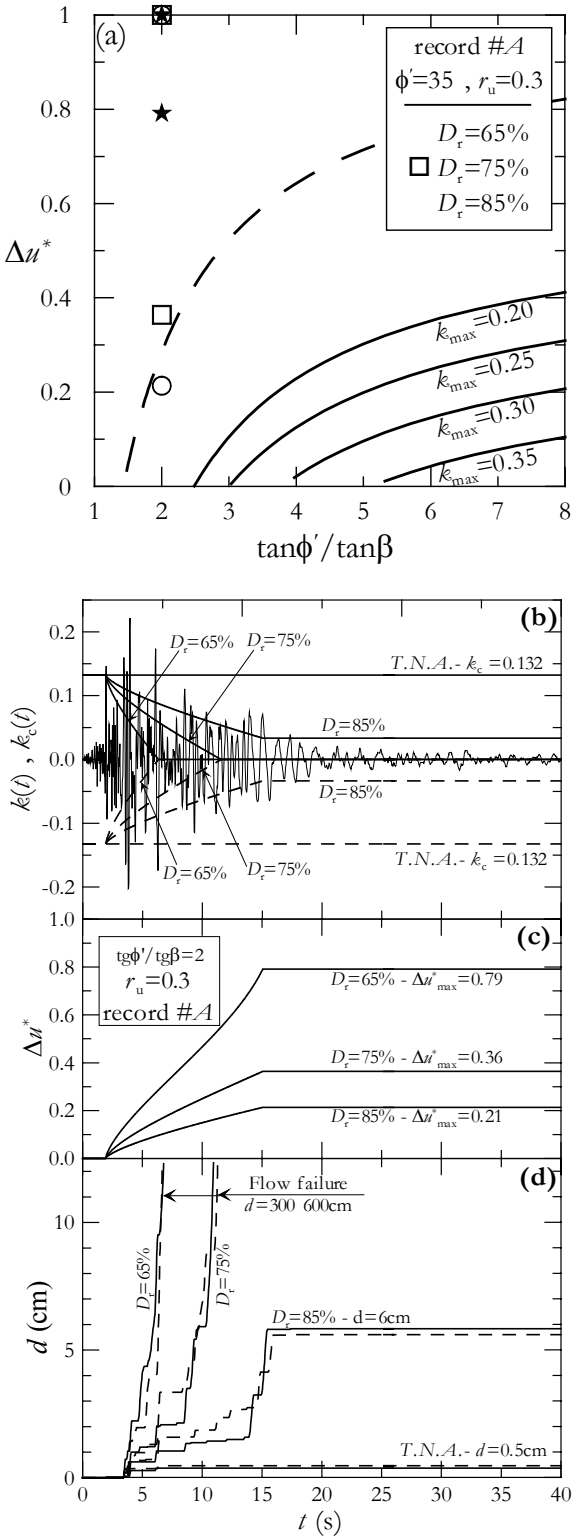

Fig 9. Influence of soil relative density on the stability conditions and on the displacement response of slopes initially unstable under seismic conditions.

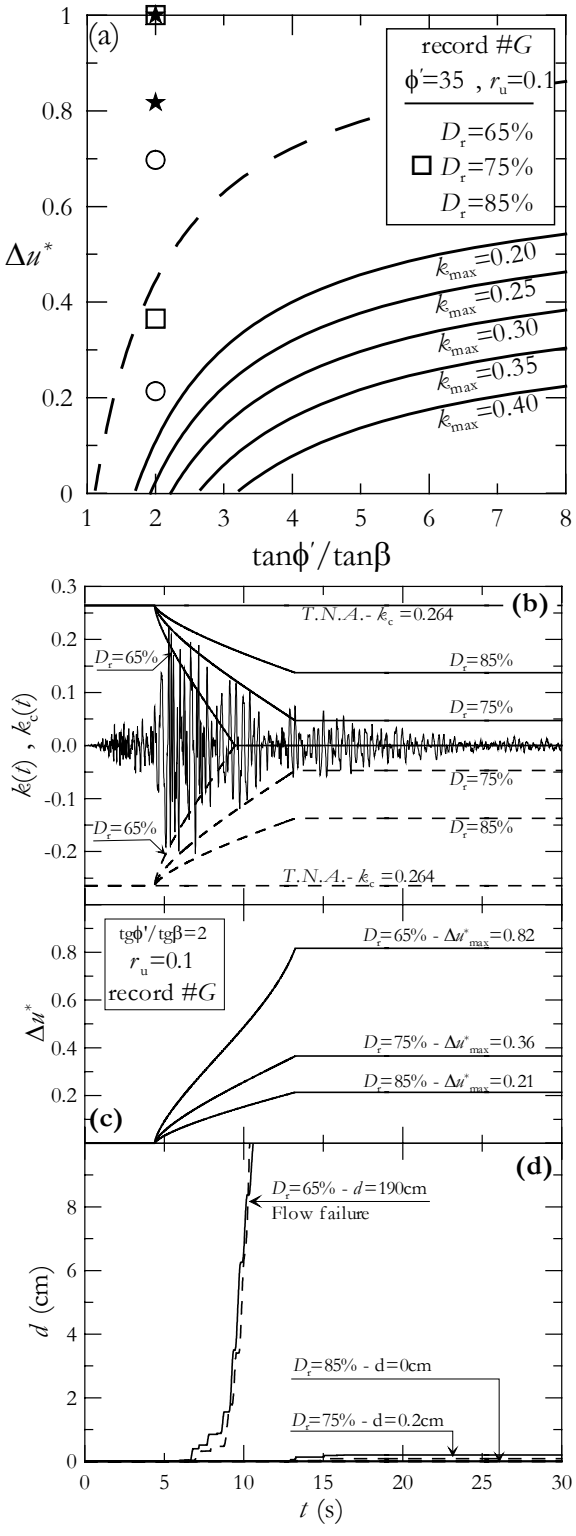

Fig 10. Influence of soil relative density on the stability conditions and on the displacement response of slopes initially stable under seismic conditions.

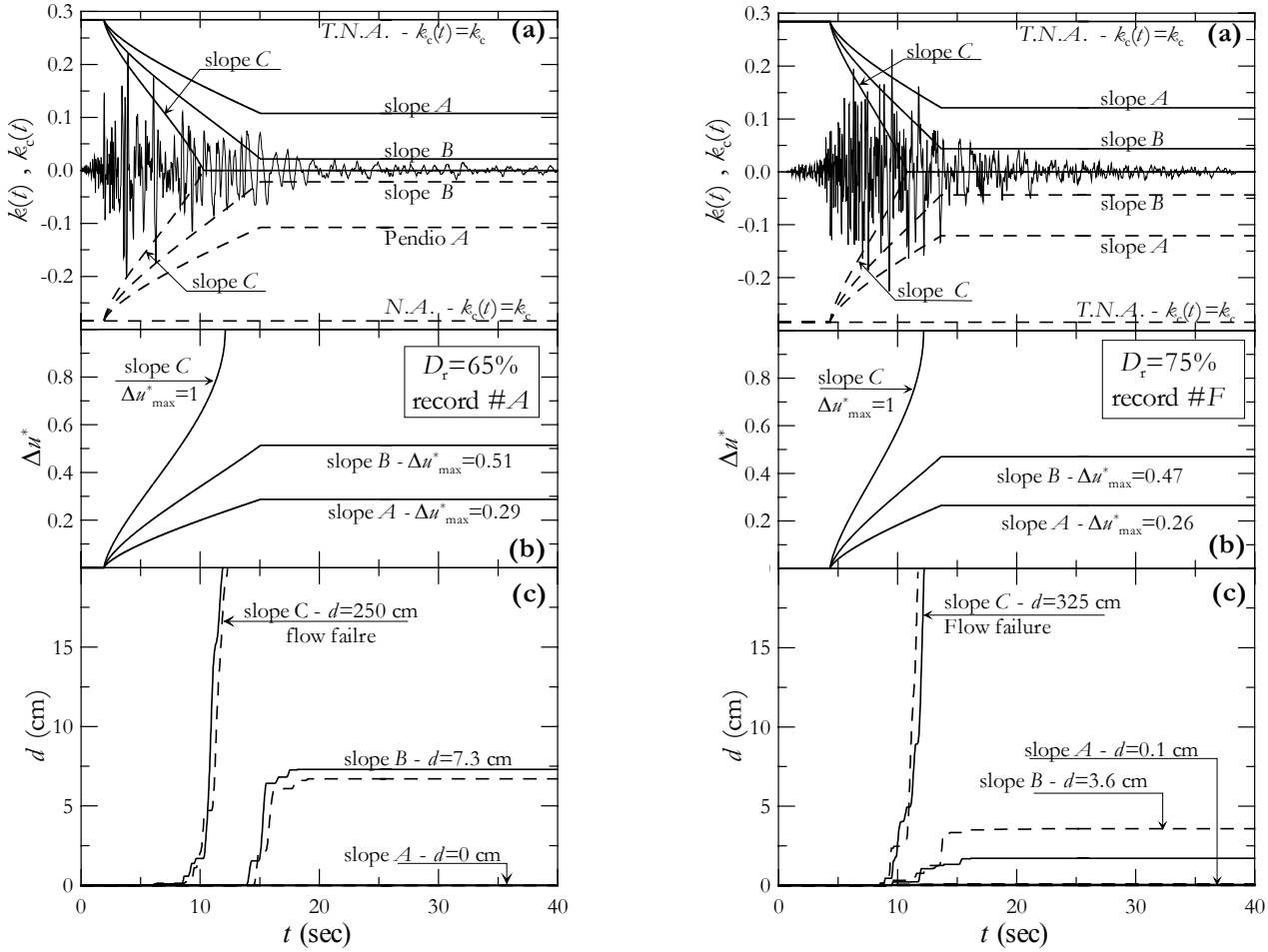

Fig 11. Effectiveness of the procedure for a modified Newmark-type analysis.

Table 7. Characteristics of the earthquake records adopted in the examples for cohesive slopes.

Earthquake		*M*	Station	k_{max}	scaled k_{max}
#CT	Sicilia (Italy, 13-12- 1990)	5.4	Catania, E-W component	0.24	0.50
#TZ	Friuli (Italy, 6-5-1976)	6.4	Tolmezzo, N-S component	0.35	0.50

Table 8. Scheme of the slopes considered in the examples provided cohesive slopes and parameters of the proposed procedure.

Slope	$C_u/\gamma D$	k_{co}	F_s
S1	*0.500*	0.10	1.22
S2	*0.464*	0.07	1.154

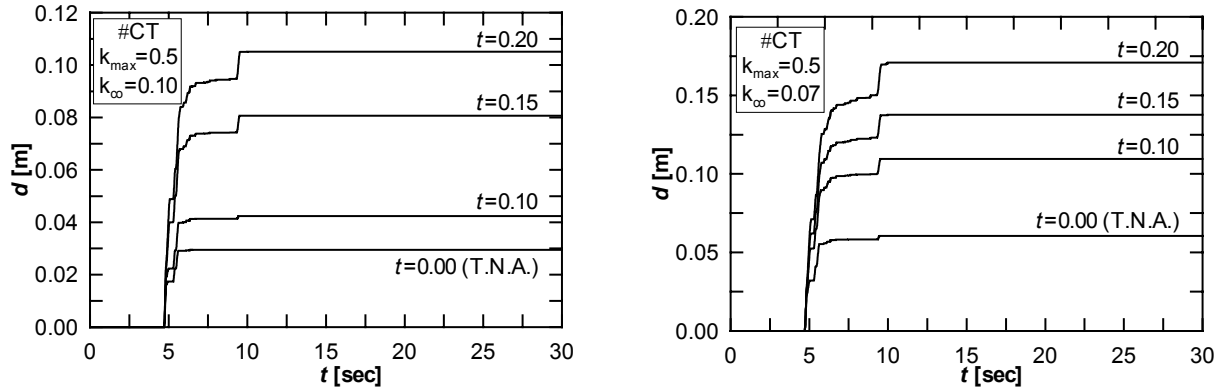

Fig 12. Results of displacement analyses performed taking into account the cyclic degradation effect of cohesive soils.

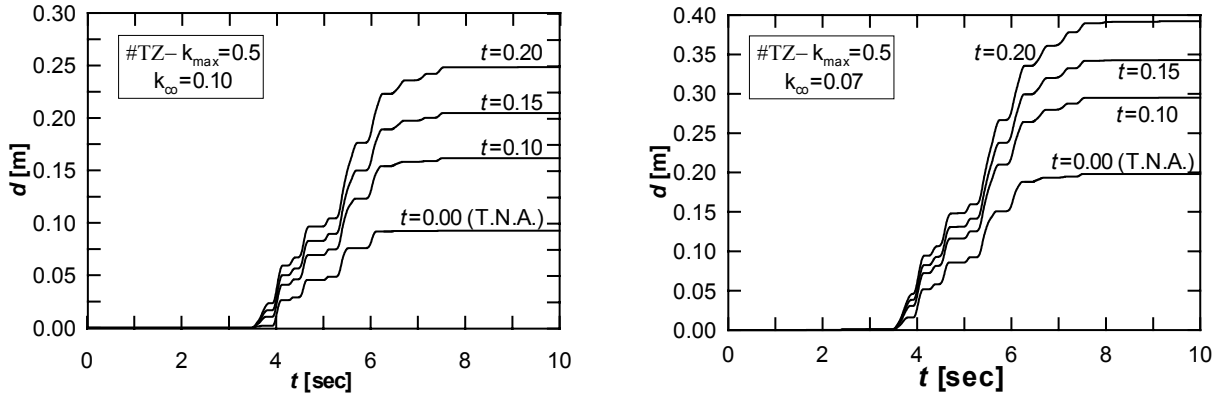

Fig 13. Results of displacement analyses performed taking into account the cyclic degradation effect of cohesive soils.

REFERENCES

AGI. Italian Geotechnical Society (2005). Aspetti geotecnica della progettazione in zona sismica. Linee guida. March, 2005 Version (In Italian).

Baziar M.H., Dobry R., Elgamal A-W.M. (1992). Engineering evaluation of permanent ground deformations due to seismically-induced liquefaction. Tech. Rep. NCEER-92-0007, National Center for Earthquake Engineering Research, Buffalo, NY, March 24.

Beikae M. (2001). Is Newmark method conservative? . Proc. 4th Int. Conf. on Recent Advances in Geotechnical Earthquake Engineering and Soil Dynamics, San Diego, CA, March 26-31. Paper 5.16.

Biondi G. & Maugeri M. (2005a): "Effect of cyclic behaviour of soils on seismic response of clay slopes" Proc. Satellite Conference of the 16th Int. Conf. on Soil Mechanics and Geotechnical Engineering, September 12-16, Osaka, Japan

Biondi G. & Maugeri M. (2005b). "Un'estensione del metodo di Newmark per lo studio dei fenomeni di instabilità sismica dei pendii in presenza di riduzioni della resistenza al taglio dei terreni. Proc. "Convegno in memoria del Prof. A. Pellegrino", Naples, Italy (In italian).

Biondi G. (1998). "Pore pressure effect on seismic response of slopes". Diploma Thesis, University of Catania (In Italian).

Biondi G. (2002). "Seismic instability of sandy slopes due to earthquake-induced pore pressure". Ph.D. Thesis, University of Catania (In Italian).

Biondi G., Cascone E., Maugeri M. (2004): "Number of uniform stress cycles equivalent to seismic loading". Proc. 11 Int. Conf. on Soil Dynamics & Earthquake Engineering and 3rd Int. Conf. on Earthquake Geotechnical Engineering, 7th – 9th January, 2004, University of California, Berkeley, California, Vol.2, pp.705-712.

Biondi G., Cascone E., Maugeri M., Motta E. (2002b): "Earthquake effects on the displacements of liquefiable slopes". Proc. 12th European Conference on Earthquake Engineering, Elsevier Science Ltd., London 2002 (Paper n. 509).

Biondi, G., Cascone, E. and Maugeri, M. (2002a) "Flow and Deformation Failure of Sandy Slopes", *Soil Dynamics and Earthquake Engineering*, Elsevier, Vol.22, pp. 1103-1114.

Biondi, G., Cascone, E., Maugeri, M. and Motta, E. (2000) "Seismic Response of Saturated Cohesionless Slopes", *Soil Dynamics and Earthquake Engineering,* Elsevier, Vol. 20, N° 1-4, pp. 209-215.

Bouckovalas G., Gazetas G., Papadimitriou A.G. (1999). Geotechnical aspects of the 1995 Aegion, Greece, earthquake. Proc. 2nd Int. Conf. on Earthquake Geotechnical Engineering, Lisboa, Portugal, 21-25 June, 1999, pp. 739-748

Bray J.D. & Rathjie E.R. (1998). Earthquake-induced displacement of solid waste landfills. Journal of Geotechnical and Geoenvironmental Engineering, Vol. 124, No. 3, pp. 242-253.

Cascone E., Maugeri M., Motta E. (1998). Seismic response of clay slopes. Proc. 11th European Conference on Earthquake Engineering, Paris.

Cetin O.K. Youd T.L., Seed R.B., Bray J.D., Stewart J.P., Durgunoglu H.T., Lettis W. & Yilaz M.T. (2004). "Liquefaction-induced lateral spreading at Izmit Bay during the Kocaeli (Izmit)-Turkey earthquake". Journal of Geotechnical and Geoenvironmental Engineering, ASCE, Vol. 139, No. 12, p. 1300-1313.

Chopra A.K. & Zhang L. (1991). Base sliding response of concrete gravity dams to earthquakes. Earthquake Engineering Research Center, Report No. UCB/EERC-91/05, University of California, Berkeley, California, USA, May 1991, 165 pp.

Conte E. & Dente G. (1986). Deformazioni permanenti indotte da carichi sismici nei pendii sabbiosi in falda. A.G.I., XVI Convegno Nazionale di Geotecnica, Bologna 14-16 Maggio 1986.

Costanzo A., Silvestri F., Lampitiello S., Olivares, L. Lanzo G. & Tommasi P. (2004). "Vulnerabilità sismica di centri storici su rilievi: i casi di Bisaccia, Orvieto, Gerace". Atti del XI Congresso Nazionale "L'ingegneria Sismica in Italia", Genova 25-29 Gennaio 2004.

Cotecchia V., Lenti V., Salvemini A. & Spilotro G. (1986). "Reactivation of the large Buoniventre slide by the Irpinia earthquake on 23 Novembre 1980". Proc. International Symposium on Engineering Geology Problems in Seismic Areas, Bari.

Crespellani T., Ghinelli A., Madiai C., Vannucchi G. (1990). Analisi di stabilità dei pendii naturali in condizioni sismiche. Rivista Italiana di Geotecnica XXIV, No.2.

Crespellani T., Madiai C., Maugeri M. (1996). Analisi di stabilità di un pendio in condizioni sismiche e post-sismiche. Rivista Italiana di Geotecnica XXX, No.1.

Crespellani T., Madiai C., Vannucchi G. (1992). Seismic stability analisys of slopes including amplification effects. Proc. of French-Italian Conference on Slope Stability in Seismic Areas, Bordighera, Italy, 14-15 May 1992.

D'Elia B.,Federico G., Pescatore T.S., Rippa F. (1986). "Occurrence and development of a large landslide (Andretta, Italy) reactivated by the nov. 23, 1980 earthquake ". Proc. International Symposium on Engineering Geology Problems in Seismic Areas, Bari.

Elms D. (2000). Refinements to the Newmark sliding block model. Proc. 12 World Conference on Earthquake Engineering, Auckland, New Zealand, paper 2132

Gazetas G. & Uddin N.(1994). Permanent deformazion on pre-exiting slidign surface in dams. Journal of Geotechnical Engineering Division, ASCE, Vol. 120 (11), pp. 2041-2061.

Idriss I.M., Dobry R., Singh A.M. "Nonlinear behaviour of soft clays during cyclic loading", Journal of Geotechnical Engineering, ASCE, 1978, 104(12), pp. 1427-1447.

Kameda H. & Hamada M. (1998). "Engineering management of civil infrastructures in Japan following the 1995 Hyogoken-Nambu (Kobe) earthquake". Proc. 11th European Conference on Earthquake Engineering. Paris, 1998, Balkema, Rotterdam.

Kramer S.L. & Smith M.W. (1997). Modified Newmark Model for seismic displacement of compliant slope. Journal of Geotechnical and Geoenvironmental

Engineering Division, ASCE, Vol. 123, No. 7, pp.635-644.
Lemos L.J.L. & Coelho P.A.L.F. (1991). Displacements of slopes under earthquake loading. Proceedings of the 2nd International Conference on Recent Advances in Geotechnical Earthquake Engineering and Soil Dynamic, St. Louis, Missouri, Vol.2, pp. 1051-1056.
Lemos L.J.L., Gama A.M.P., Coelho P.A.L.F. (1994). Displacement of cohesive slopes induced by earthquakes loading. Proc. 13th Int. Conf. On Soil Mechanics and Foundation Engineering, New Delhi, 5-10 January, 1994.
Lin J.S. & Whitman R.V. (1983). Decoupling approximation to the evaluation of ef earthquake-induced plastic slip in earth dams. Earthquake Engineering and Structural Dynamics, Vol. 11, No. 5, pp. 667-678.
Loukidis D., Lee S.H., Yi Q., Bourdeau P.L. (2001). “Analytical study of the Nikawa Landslide”. Proc. 4th International Conference on Recent Advances in Geotechnical Earthquake Engineering and Soil Dynamics, San Diego, CA, March 26-31.
Makdisi F.I. & Seed H.B. (1978). Simplified procedure for estimating dam and embankment earthquake - induced deformations. Journal of the Geotechnical Engineering Division, ASCE, Vol.104, No. GT7, pp. 849-867.
Matasovic N. & Vucetic M. (1995). “Generalized cyclic-degradation-pore pressure generation model for clays”, Journal of Geotechnical Engineering, ASCE, 121, No.1, pp. 33-42.
Maugeri M. & Motta E. (1985). "A note on the residual strength in a landslide induced by the 1980 Italian earthquake". Proc. of Discussion Session 7B of the Eleventh International Conference on Soil Mechanics and Foundation Engineering, San Francisco, 11-16 August 1985. Ed. Shamsher Prakash, pp.37-40.
Newmark N.M. (1965). Effect of earthquakes on dam and embankment, The Rankine lecture, Geotèchnique , Vol. 15, No.2.
Oka K., M Sugito and A. Yashima, 1995 a. "The Great Hanshin Earthquake Disaster; The January 17, 1995, South Hyogo Prefecture Earthquake, Preliminary Investigation Report, Part 1, 25 January 1995". Report of Civil Engineering Department, in Japanese, Gifu University, Gifu, Japan, 56 p.
Oka K., M Sugito and A. Yashima, 1995 b. "The Great Hanshin Earthquake Disaster; The January 17, 1995, South Hyogo Prefecture Earthquake, Preliminary Investigation Report, Part 2, 2 February 1995". Report of Civil Engineering Department, in Japanese, Gifu University, Gifu, Japan, 24 p.
Plafker G., Ericksen G.E., Fernandez C.J. (1971). “Geological aspect of the May 31, 1970, Perù earthquake“. Bulletin of the Seismological Society of America, Vol. 61, p.543-578.
Poulos H. G. (1988), Marine geotechnics, Unwin Hyman Ltd, london.
Sarma S. K., Kourkoulis R. (2004). “Investigation into the prediction of sliding block displacements in seismic analysis of earth dams”. Proc. 13th World Conference on Earthquake Engineering, Vancouver, B.C., Canada, August 1-6., paper n. 1957.
Sarma S.K. & KoukoulisR. (2004). Investigation into the prediction of sliding block displacement in seismic analysis of earth dams. Proc. 13th World conference on Earthquake Engineering, Vancouver, B.C., Canada, paper n.1957.
Sarma S.K. (1975). “Seismic stability of earth dam and embankments”. Geotèchnique, Vol. 25, No.4. London
Sarma S.K. (1975). Seismic stability of earth dam and embankments. Geotèchnique Vol. 25, No.4.
Seed H.B. & Wilson D. (1967). The Turnagain Heights Landslides, Anchorage, Alaska. Journal of Soil Mechanics and Foundation Division, ASCE, Vol. 93, No. SM4, July, pp. 325-353.
Seed H.B., Idriss I.M., Makdisi F., Banerjee N. (1975). Representation of irregular stress time histories by equivalent uniform stress series in liquefaction analysis, Report No. EERC 75-29, Earthquake Engineering Research Center, University of California, Berckeley.
Shannon & Wilson Inc. (1964). Report on Anchorage area soil studies, Alsaka. To U.S. Army Engineer District, Anchorage, Alaska. Seattle, W.A.
Thiers G.R., Seed H.B. (1968). “ Cyclic stress-strain characteristics of clay” Journal of Soil Mech. and Found. Div., Proc. ASCE, vol..94.
Tika-Vassilikos T.E., Sarma S.K., Ambraseys N. (1993). Seismic displacement of shear surfaces in cohesive soils. Earthquake Engineering and Structural Dynamics, Vol. 22, pp. 709-721.
Tradafair A.C. & Sassa K. (2005). Seismic triggering of catastrophic failures on shear surfaces in saturated cohesionless soils. Canadian Geotechnical Journal 42, p. 229-251.

APPENDIX A: equation giving all the parameters involved in the procedure

This appendix describes all the equations giving the relevant parameters of the proposed procedure and the correlated notation. The expressions for both effective and total stress analysis are provided.

Notation

β: slope angle
D: depth of the failure surface
ϕ': angle of soil shear strength
r_u: static pore pressure ratio
C_{uo}: static value of the undrained soil shear strength
γ: soil unit weight
$\beta^* = \beta + \omega$
ω: inclination of the earthquake-induced acceleration k. $\omega = tg^{-1}(k_v/k_h)$
k_h,k_v: horizontal and vertical component of earthquake-induced acceleration k
k_{max}: maximum value of the earthquake-induced acceleration
k_{co}: initial value of the slope critical acceleration (before the strength reduction take place)
k_c: current value of the slope critical acceleration
C_{uc}: current value of the undrained shear strength available under cyclic loading

Relevant equations

Static factor of safety:

$$F_s = \frac{\tan\phi'}{\tan\beta}\cdot(1-r_u)$$

$$F_s = \frac{C_{uo}}{\gamma\cdot D\cdot\sin\beta}$$

Earthquake-induced pore pressure ratio:

$$\Delta u^*(t) = \frac{\Delta u(t)}{\sigma'_o} = \frac{\text{excess pore pressure}}{\text{effective static normal stress}}$$

Earthquake-imposed degradation parameter:

$$C_u^* = \frac{C_{uc}}{C_{uo}} = N^{-t}$$

Current value of the slope critical acceleration:

$$k_c(t) = \frac{\cos\beta\cdot\tan\phi'\cdot(1-r_u)\cdot\left[1-\Delta u^*(t)\right]-\text{sen}\beta}{\cos\beta^* + \tan\phi'\cdot\text{sen}\beta^*}$$

$$k_c(t) = \frac{C_u^*(t)\cdot C_{uo}/(\gamma\cdot D)-\sin\beta}{\cos\beta^*}$$

Initial value of the slope critical acceleration:

$$k_{co} = \frac{\cos\beta\cdot\tan\phi'\cdot(1-r_u)-\text{sen}\beta}{\cos\beta^* + \tan\phi'\cdot\text{sen}\beta^*}$$

$$k_{co} = \frac{C_{uo}/(\gamma\cdot D)-\sin\beta}{\cos\beta^*}$$

Factor of safety evaluated for $k=k_{max}$ neglecting the pore pressure build-up ($\Delta u^*=0$):

$$F_{do} = \frac{\cos\beta\cdot(1-r_u)-k_{max}\cdot\text{sen}\beta^*}{\text{sen}\beta + k_{max}\cdot\cos\beta^*}\cdot\tan\phi'$$

$$F_{do} = \frac{C_{uo}}{\gamma\cdot D}\cdot\frac{1}{\sin\beta + k_{max}\cdot\cos\beta^*}$$

Earthquake-induced pore pressure ratio and degradation parameter required for slope failure:

$$\Delta u_f^* = 1-\frac{1}{F_s} \qquad C_{uf}^* = \frac{1}{F_s}$$

Earthquake-induced pore pressure ratio and degradation parameter required to trigger permanent displacements:

$$\Delta u_d^* = 1-\frac{1}{F_{do}} \qquad C_{ud}^* = \frac{1}{F_{do}}$$

Number of equivalent loading cycle required for slope failure (see eq.(2) for Δu^*_1):

$$N_f = \left[\frac{\sin\frac{\pi}{2}\cdot\Delta u_f^*}{\sin\frac{\pi}{2}\cdot\Delta u_1^*}\right]^{2a}$$

Number of equivalent loading cycle required to trigger permanent displacements (see eq.(2) for Δu^*_1):

$$N_d = \left[\frac{\sin\frac{\pi}{2}\cdot\Delta u_d^*}{\sin\frac{\pi}{2}\cdot\Delta u_1^*}\right]^{2a}$$

Post-seismic static safety factor:

$$F_s^{PS} = F_s\cdot(1-\Delta u_{max}^*)$$

$$F_s^{PS} = F_s\cdot C_u^*$$

Slope stability analysis according to EC-8 and Italian seismic regulations

A.L. Simonelli, S. Sica, F. Moccia

Università del Sannio, Engineering Faculty, Benevento (Italy)

Abstract

The aim of the paper is to compare the results of slope stability analyses performed according to Eurocode 8 (EC-8) with those obtained by the pseudo-static approach of the pre-existing Italian seismic code (D.M. 16.1.1996). In applying the European code to the simple case of a dry, infinite and incoherent slope the acceleration values defined in the recent Italian seismic zonation (OPCM 3274/2003) have been utilised for determining both the pseudostatic and pseudo-dynamic actions. Although it may not be possible to make an immediate comparison of the different design methods in that they make use of non "homogeneous" seismic actions, it may be observed that the Eurocode 8 pseudo-static method, combined to the Italian OPCM 3274 ground accelerations, leads to a much more conservative design than that obtained by the pre-existing Italian seismic regulation. On the other hand, more reliable Newmark displacement analyses, performed according to EC-8, do not confirm the results of the EC-8 pseudostatic method. This evidence suggests that more work has to be done in defining the parameters and coefficients to be entered in the EC-8 pseudo-static procedure.

INTRODUCTION

Traditionally the seismic stability of both natural and artificial slopes has been evaluated by the classical pseudostatic approach where the seismic actions are traduced in equivalent static forces by means of the so-called seismic coefficients. They are related to the seismic intensity observed at the site and specified in national codes.

In recent years, more advanced approaches have been tested and validated such as the pseudo-dynamic approaches (Newmark method or its derivatives) or dynamic approaches solved numerically by different techniques (FEM, FDM, etc.). Both pseudodynamic and dynamic approaches model the earthquake in a more realistic way generally by utilising a time-acceleration function.

More advanced approaches have been contemplated in recent European codes (see Part 1 (EN 1998-1) and Part 5 (EN 1998-5) of Eurocode 8, henceforth indicated as EC-8) and national codes such as the Italian regulation OPCM 3274 of March 2003. In these documents, however, the classical pseudo-static approach is still contemplated but the seismic coefficients have been correlated to the maximum ground acceleration expected at the site.

In this paper the Italian seismic regulation OPCM 3274 will often be recalled, which acknowledges Eurocode 8 criteria. Further, it proposes initial values of parameters such as the reference peak ground acceleration agR, the soil factor S, etc., which are required to perform pseudostatic, pseudodynamic or dynamic analyses in the spirit of the Eurocodes. In this sense it could be intended as a National Annex.

The objective of the paper is to compare the results of slope stability analyses performed in the traditional way as suggested in the old Italian seismic regulation (D.M. 1996) and those obtained by applying the more recent EC-8 and OPCM 3274 normative.

In the paper the above objective is attained in two stages:

1) comparing the results of the pseudostatic analyses performed by following the old Italian seismic code (D.M. 1996) and the new criteria

of EC-8 (combined to OPCM 3274 ground accelerations);

2) comparing the results discussed at the previous item with those obtained applying the Newmark method (according to EC-8 criteria and OPCM 3274 acceleration values).

METHODS OF ANALYSIS

The pseudostatic approach is the most consolidated method adopted to analyse slope stability under seismic actions. This popularity, especially in the professional field, may be due to the fact that the pseudostatic approach is very simple and further it was the only one contemplated in old seismic codes.

Referring to literature for the basic concepts of the method, only some features will be recalled. The method assumes that the earthquake actions are represented by equivalent static actions F_h and F_v acting both horizontally and vertically, whose magnitudes are proportional to the weight W of the unstable mass by means of the so-called seismic coefficients K_h and K_v:

$$F_h = K_h \cdot W \tag{1}$$

$$F_v = K_v \cdot W \tag{2}$$

The method consists in comparing the resisting forces acting along the failure surface to the driving ones. The failure surface is not known *a priori* and should be found tentatively. The ratio between the resisting and the driving forces represents the pseudostatic safety factor, PSF, which allows to assess the slope stability. In the particular case of a dry, infinite and incoherent slope the PSF has the following expression:

$$PSF = \frac{\left[(1-K_v)W\cos\beta - K_h W\sin\beta\right]tg\varphi'}{\left[(1-K_v)W\sin\beta + K_h W\cos\beta\right]} \tag{3}$$

where φ' is the friction angle and β is the slope inclination with respect to the horizontal direction.

In spite of its simplicity, the crucial aspect of the pseudostatic approach is the equivalence criterion between the pseudostatic forces, constant in time and space, and the earthquake actions, variable in time and space. As a matter of fact the analysis results are strongly dependent on values assigned to the seismic coefficients K_h and K_v.

The seismic stability of a slope can be assessed also on the basis of its performance during the earthquake; the performance can be evaluated by means of the pseudo-dynamic or dynamic approaches. Among these, the simple Newmark model (1965) allows the evaluation of the final displacement suffered by the slope at the end of the earthquake. The earthquake action is represented in a more realistic way, by means of a time-acceleration function. To assess the safety condition of a slope under seismic actions, the computed displacement should be compared to an admissible limit value which depends on the slope boundary conditions (performance based design) and has therefore to be defined for the particular case in hand. The magnitude of the seismic-induced displacement is strongly dependent on the accelerogram features: peak value, length and frequency content. These features vary with the earthquake source mechanism, the seismic wave pattern and with the nature of soils at the specific site which may induce amplification phenomena. Hence, for a correct prediction of the final displacement the Newmark method requires a suitable choice of the input motion set. This aspect is crucial especially when applying the method in the professional field.

As well known, the Newmark model analyses the sliding of a rigid block on a plane surface, assuming a rigid-plastic behaviour at the interface between them (Fig 1). From simple limit equilibrium considerations, the threshold acceleration value a_c can be evaluated, above which the surface moves faster than the block, which instead still saves the threshold acceleration.

The relative displacement between the block and the surface can be computed by integrating relative accelerations twice, until the velocity between them returns to zero again.

The threshold acceleration a_c is given by:

$$a_c = k_c\, g \tag{4}$$

where k_c is the critical acceleration coefficient which can be determined by a pseudostatic analysis imposing a unit safety factor (PSF=1).

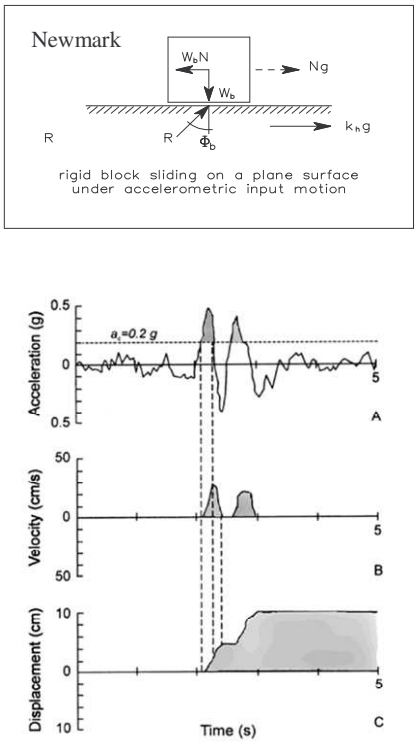

Fig 1: Newmark (1965) model for displacement analysis

The threshold acceleration a_c is therefore function of the geometrical and mechanical properties of the slope. For the simple case of a dry, infinite and incoherent slope the expression of the critical acceleration coefficient is very simple (Simonelli, 1993):

$$k_c = tg(\varphi' - \beta) \tag{5}$$

where φ' and β have been already defined. From the above two equations it emerges that the threshold acceleration is only function of the difference between φ' and β and does not depend on their single values.

The differential equation regulating the relative displacement $U(t)$ between the block and the surface is given by:

$$\frac{d^2U(t)}{dt^2} = \frac{\cos(\varphi'-\beta)}{\cos\varphi'}\left[a(t) - k_c g\right] \tag{6}$$

Equation (6) indicates that for the simple case here considered, the relative displacement between the block and the surface markedly depends on the difference between φ' and β whilst the influence of the term 1/cosφ' is less relevant (Simonelli & Fortunato, 1996).

If the vertical component of the accelerogram is also taken into account, the threshold acceleration varies with the direction of the input motion (Sarma 1975 and 1999). In the simple case of a dry, infinite and incoherent slope the formulation of the critical acceleration coefficient and of the displacement equation can be found in Simonelli & Di Stefano (2001). The latter work actually shows that with reference to three seismic events occurred in Italy, namely the Friuli 1976, the Irpinia 1980 and the Umbria-Marche 1997 earthquakes, the influence of the vertical component of the motion on the computed final displacement is practically negligible.

ITALIAN SEISMIC CODES FOR SLOPE STABILITY ANALYSES

In Italy the reference codes regulating the seismic slope stability are the D.M. 1996, still in force, and the OPCM 3274/2003, still under revision, that for the most part acknowledges the Eurocode criteria. This paper will often recall these rules, hence a brief description of what they suggest on slope stability analysis will be provided.

In the past, the Italian codes classified the seismic areas into three categories (I, II and III) characterized by different degrees of seismicity (S=12, 9 and 6). A large part of the territory has not been recognized as seismic area. This classification was essentially based on maps of macro-seismic Intensity, derived from the observation of the effects induced by past earthquakes on the physical environment, on buildings and on people. The D.M. 1996 with reference to the above classification of the national territory, defines the seismic coefficients C which are equal to 0.1, 0.07 and 0.04, respectively for the seismic category I, II and III. In the D.M. 1996 the role played by the "local" soil conditions has been taken into account through the so-called foundation coefficient ε, that increases seismic actions by 30% only in the case of alluvial deposits of thickness varying between 5 and 20 m, overlying stiff soils or rocks. This coefficient thus represents a sort of magic number based exclusively on the nature of the deposit and not on quantitative evaluations of the real mechanical characteristics of the soils.

For the stability analysis of slopes the D.M. 1996 exclusively suggests the use of the pseudostatic approach, considering only the horizontal force F_h, thus disregarding the effect of the earthquake in the vertical direction. The equivalent pseudostatic force F_h is linked to the seismic coefficient C by the following relation:

$$F_h = C\,W \tag{7}$$

that is in all similar to equation (1) if it is assumed C=K_h.

In assessing the seismicity of a given area, the OPCM 3274 adopts the reference peak ground acceleration a_{gR}, which is the maximum acceleration on a stiff outcropping formation (later defined as ground type A). On the basis of the expected a_{gR}, 4 seismic zones have been defined as shown in Table 1.

Table 1: Peak ground accelerations on ground type A for the 4 seismic Italian zones (OPCM 3274)

Zone	a_{gR}
1	0.35 *g*
2	0.25 *g*
3	0.15 *g*
4	0.05 *g*

Moreover the OPCM 3274 takes into account the amplification of the seismic motion due to local soil conditions by identifying 7 different types of subsoil (ground types from A to E plus the special category S1 and S2) such as those defined in the EC-8-part 1.

For the first 5 types of subsoil (from A to E) an amplification factor of the acceleration a_{gR} is given, named soil factor S.

According to OPCM 3274, the soil factor assumes the following values: 1.0 for subsoil type A; 1.25 for subsoils B, C and E; 1.35 for ground type D. The special subsoil classes S1 and S2 require *ad hoc* studies for characterizing the site amplification. The OPCM 3274 further takes into account topography effects by means of the factor S_T which amplifies the ground acceleration for slopes with inclination greater than 15° and a difference in height greater than 30 meters. Recommended values of S_T are 1.2 and 1.4.

With respect to slope stability analysis the OPCM 3274, as EC-8, suggests the use of the pseudostatic approach taking into account both the horizontal and vertical forces given by:

$$F_h = \pm 0.5\,S\,S_T\,(a_g/g)W \tag{8}$$

$$Fv = \pm 0.5\,F_h \tag{9}$$

For particular slope conditions the use of dynamic approaches is contemplated, in which the seismic action is represented by means of accelerograms and the soil is described by suitable constitutive law simulating soil response under cyclic loading conditions.

In conclusion, the OPCM 3274 acknowledges the EC-8 criteria and proposes initial values of the parameters that must be defined nationally, such as a_{gR}, S and S_T, in order to determine the ground acceleration. In this study the OPCM 3274 therefore plays the role of a National Annex.

PSEUDOSTATIC ANALYSIS

As stated above, in order to compare the results of pseudostatic analyses performed in the traditional Italian way (D.M. 1996) with those derived from the application of EC-8 (combined to OPCM 3274), the simple case of a dry, infinite and incoherent slope has been considered. In such a context the simplicity of the selected case has been a prerequisite to better appreciate the differences among the results of the two approaches, since a huge difference in the definition of seismic actions exists: on the basis of the seismic coefficient in the D.M. 1996; on the basis of the peak ground acceleration for the EC-8.

In the case of a dry, infinite and incoherent slope the static safety factor SF is given by:

$$SF = \frac{tg\,\varphi'}{tg\,\beta} \tag{10}$$

If seismic actions are considered the pseudostatic safety factor PSF computed according to the old D.M. 1996 is given by:

$$PSF = \frac{tg\varphi'}{tg(\beta + arctgC)} \qquad (11)$$

derived from equation (3) by considering $Kh=C$ and $Kv=0$.

The pseudostatic safety factor, considering the EC-8 or the OPCM 3274 normative, is given by the following equation:

$$PSF = SF\frac{(1-K_v)-Kh\ tg\beta}{(1-K_v)+\frac{Kh}{tg\beta}} \qquad (12)$$

where:

$$Kh = S \cdot S_T \cdot (a_g / g) \qquad (13)$$

$$K_v = 0.5K_h \qquad (14)$$

The analyses have been performed parametrically considering three different friction angles φ' (i.e., 15°, 30° and 45°) and changing the slope inclination β from 1° to φ'. For each combination of φ' and β the following parameters were computed:

1) the static safety factor SF;
2) the pseudostatic safety factor according to the D.M. 1996 for the old three seismic categories in which the Italian territory was subdivided before March 2003.
3) the pseudostatic safety factor according to the EC-8, considering the 9 different values of ground acceleration (obtained combining S, S_T and a_g) characterizing the 4 seismic zones in which the OPCM 3274 nowadays classifies the Italian territory.

Comparing the pseudostatic safety factors computed according to the D.M. 1996 and the EC-8 for homogeneous seismic zones (for example, the 1st seismic category of the pre-existing D.M. 1996 and Zone 1 of the new classification) a huge discrepancy in the results obtained can be observed in Fig 2. This could be attributed to the quite different values in the magnitude of the horizontal pseudostatic force: the D.M. 1996 considers a horizontal force equal to 0.1W in a 1st category seismic zone while the OPCM 3274 provides horizontal pseudostatic forces of magnitude between 0.175W and 0.33W for seismic Zone 1. Further, the addition of the vertical pseudostatic force in the latter case contributes to exasperate the difference. In other words any artificial slope designed in the past in Italy, nowadays is no longer verified by applying EC-8 with the ground accelerations provided by OPCM 3274.

In Fig 2 the static and pseudostatic safety factors are plotted as functions of the difference (φ'-β) for a soil with friction angle φ'=30° and for the most severe seismic zone (the I[st] category according to D.M. 1996 and Zone 1 according to the OPCM 3274).

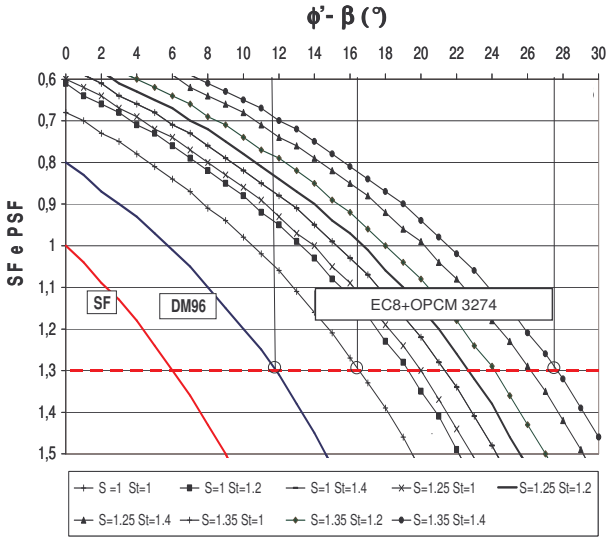

Fig 2: Pseudostatic analysis (φ'=30°): static and pseudostatic safety factors according to the D.M. 1996 and the EC-8 combined to the OPCM 3274 for seismic Zone 1.

It could be observed that if a safety factor equal to 1.3 is required for slope stability, when applying the EC-8 in conjunction to the OPCM 3274, higher (φ'-β) values are required, that is to say, lower slope inclinations β (between 13° and 3°), well below the value required by the D.M. 1996 (β=18°).

PSEUDODYNAMIC ANALYSIS

For the pseudo-dynamic analyses, the main accelerograms recorded during the 1980 Irpinia-Lucania earthquake have been adopted as input motions (Bagnoli Irpino, Brienza,

Calitri, Mercato San Severino, Torre del Greco and Sturno).

The horizontal component of each accelerogram has been scaled in magnitude in order to obtain the 36 PGA values established for the 4 seismic zones up to a maximum peak ground acceleration equal to 0.66g. The accelerograms have been selected in such a way that their original PGA value was as close as possible to the maximum value required by the regulation. Since the vertical component of each accelerogram has also been considered, this was scaled consistently with the horizontal one.

As for the pseudostatic analyses, three different values of the soil friction angle φ' (i.e., 15°, 30° and 45°) were considered and the slope inclination □ varied from 1° to φ'. As already found in previous studies (Simonelli, 1993; Simonelli and Fortunato, 1996) the final displacements computed applying the sliding block model depend significantly on the difference (φ'-□) while the influence of the single values of φ' and □ is less relevant. Actually, the final displacement slightly increases with the values of φ'. Further, it changes in each seismic zone and within a unique zone it depends on the particular combination of both the soil and topography factors, respectively S and ST.

For the sake of simplicity in this study all displacements computed in each seismic zone have been adopted to obtain the so-called upper bound curve (Ambraseys and Menu, 1988) that represents the safest correlation between the maximum seismic-induced displacement and the ratio between the slope threshold acceleration and the maximum ground acceleration, i.e. the ratio Kc/Km. The displacement upper bound curve reflects both the maximum ground accelerations at the specific site and the features of the accelerogram time histories adopted in the displacement analysis. As a matter of fact, the upper bound curves should have regional validity. The upper bound curve shown in Fig 3, for example, refers to seismic Zone 1 of the Irpinia region since the accelerograms recorded during the 1980 Iprinia-Lucania earthquake have been adopted.

Similar curves have also been obtained for Zones 2, 3 and 4.

The upper bound curves may be adopted either to verify the displacement suffered by a slope during an earthquake, or to design artificial slopes and embankments.

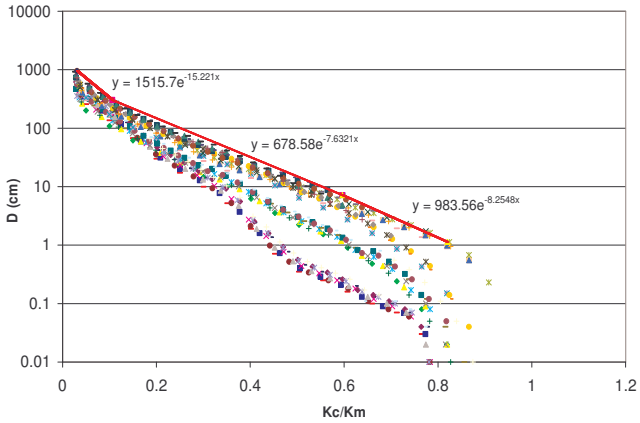

Fig 3: Upper bound curve for Zone 1 in the Irpinia region for a dry, infinite and incoherent slope (accelerograms scaled up to 0.66g)

To verify the stability of a dry, infinite and incoherent slope, it could be firstly determined the critical acceleration coefficient Kc according to eq. (5) and the site maximum expected acceleration (Km g) so that the threshold acceleration ratio Kc/Km could be determined; later from Fig 3 the maximum expected displacement in Zone 1 could be estimated. This value has to be compared to a maximum displacement, judged admissible for the particular case in hand.

To design an artificial slope, suitable design charts may be obtained from the upper bound curves. Fixing the displacement D, representing the maximum one allowed for the slope, the upper bound curve of Fig 3 could allow the deduction of the corresponding ratio Kc/Km. Hence, the threshold acceleration coefficient Kc and the slope inclination β can be easily determined.

In Fig 4, for example, the design chart relative to Zone 1 of the OPCM 3274 is shown. The upper plot shows the iso-displacement curves (D=1, 3, 5, 10, 30, 50 and 100 cm) as function of the difference (φ'-β) and of the maximum ground acceleration Amax (Amax=Km g). If the maximum ground acceleration at the site and the maximum admissible displacement D are known, the slope can be designed.

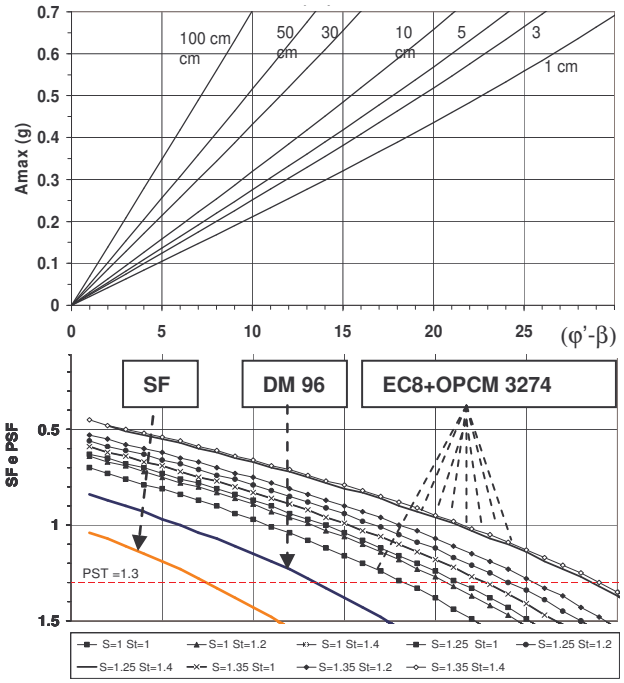

Fig 4: Design chart for artificial slopes in Zone 1 (OPCM 3274) of the Irpinia region (φ'=45°)

In the lower plot of Fig 4 the results of the pseudostatic application are shown as well, to allow an immediate comparison between the two approaches.

From the two plots of Fig 4 it could be observed that fixing a reasonable value of the admissible displacement (for example 10 cm) the design according to the pseudostatic approach of the EC-8 combined to the OPCM 3274 results strongly underdimensioned. Conversely, the design according to the D.M. 1996 seems more reasonable and better corresponding to the slope performance predicted by the pseudodynamic approach, especially when the ground accelerations at the site are less significant due to the favorable combination of site and topography conditions (lower values of S and S_T).

CONCLUSIONS

Slope stability analyses have been carried out according to EC-8 and the Italian pre-existing normative (D.M.96). The reference acceleration for defining the EC-8 seismic actions have been obtained from the recent Italian OPCM 3274 seismic zonation.

The comparisons among the analysis results have given rise to interesting conclusions:

- the D.M.96 and EC-8 pseudo-static methods provide very different designs, being the EC-8 design much more severe;
- a pseudo-dynamic analysis, based on the Newmark sliding-block model, with a proper set of accelerometric input motions fitting the requirements of EC-8 and OPCM 3274 normative, has confirmed that the EC-8 pseudo-static design is actually over-conservative;
- the difference between the pseudo-static design results of the D.M.96 and EC-8 essentially depends on the different evaluation of EC-8 seismic actions on the slope (correlated to the ground acceleration expected for a severe earthquake).

In conclusion, the present EC-8 pseudo-static method for slopes, together with the ground acceleration values of the OPCM 3274 Italian seismic zonation, appears to be inapplicable. An effective design can be achieved by more advanced dynamic analyses, with a suitable accelerometric representation of the seismic motion, as suggested by EC-8.

On the other hand, since the application of pseudo-static methods is well consolidated in the engineering practice, it would be very useful to save the EC-8 pseudo-static approach. At this aim, it would be necessary to better calibrate the correlation between the ground accelerations and the pseudo-static actions on the slope, by the introduction of proper model coefficient values, which have to effectively convert the real and complex dynamic action into a pseudo-static force, or, in alternative, to define different partial safety factor values for verifying the slope under the severe design earthquakes.

REFERENCES

Ambraseys, N. and Menu, J.M. (1988), Earthquake induced round displacements, Earthquake Engineering and Structural Dynamics, 16, 985-1006

DM LL.PP. 16/1/96, Norme tecniche per le costruzioni in zone sismiche, Gazzetta Ufficiale della Repubblica Italiana, n. 29 del 5/2/1996.

EN 1998-1, (December 2003). Eurocode 8: Design of structures for earthquake resistance - Part 1: General rules, seismic actions and rules for

buildings. CEN European Committee for Standardization, Bruxelles, Belgium.

EN 1998-5, (December 2003). Eurocode 8: Design of structures for earthquake resistance - Part 5: Foundations, retaining structures and geotechnical aspects. CEN European Committee for Standardization, Bruxelles, Belgium.

Newmark, N.M. (1965), Effects of earthquake on dams and embankments, Geotecnique, n.15, pp. 139-160.

OPCM n. 3274 (20/3/03), Primi elementi in materia di criteri generali per la classificazione sismica del territorio nazionale e di normative tecniche per le costruzioni in zona sismica, Gazzetta Ufficiale della Repubblica Italiana, n. 105 dell' 8/5/03.

Sarma,S.K.,(1975), Seismic stability of earth dams and embankments, Geotechnique, No 25, pp. 743-761.

Sarma, S.K. (1999), Seismic slope stability: the critical acceleration, Proc. II Int. Conf. On Earthquake Geotechnical Eng., Lisbon, Balkema, Rotterdam, pp. 1077-1082.

Simonelli, A.L. (1993), Displacement analysis in earth slope design under seismic conditions, Proc. VI Conference on Soil Dynamics and Earthquake Engineering, Bath, CMP, Southampton & Elsevier, London.

Simonelli, A.L. and Di Stefano P. (2001), Effects of vertical seismic accelerations on slope displacements, Proc. IV International Conference on Recent Advances in Geotechnical Earthquake Engineering and Soil Dynamics, San Diego, CA, USA.

Simonelli, A.L. and Fortunato E. (1996), Effects of earth slope characteristics on displacement based seismic design, Proc. 11 World Conference on Earthquake Engineering, Acapulco, Pergamon, Oxford.

SESSION 3: Topography Effects - Retaining Walls

NUMERICAL INVESTIGATION OF 3D SEISMIC AMPLIFICATION BY REAL STEEP TOPOGRAPHIC PROFILES AND CHECK OF THE EC8 TOPOGRAPHIC AMPLIFICATION COEFFICIENTS

R. Paolucci[1]

[1] *Department of Structural Engineering, Politecnico di Milano, Italy*

Abstract

In this paper the results of several 3D numerical analyses of seismic wave propagation in steep topographic irregularities are presented. Namely, 4 real configurations have been selected from the Italian geological context, where the steepness of site topography make significant site amplification effects during earthquakes highly probable. After evaluation of numerical transfer functions and convolution with a significant number of real accelerograms, the response spectrum of each synthetic accelerogram at the mountain surface was calculated, together with the ratio r(T) with respect to the response spectrum of the input motion. The variation with period T of such ratio is small, so that a single, period-independent, topographic amplification factor F was calculated as the average value of r(T). The value of F was found to be in reasonable agreement with that recommended by Eurocode8, for topographic profiles elongated in one direction ("2D configurations") , while in the case of steep isolated hills the F factor is significantly higher.

INTRODUCTION

Amplification of seismic waves in the presence of topographic irregularities has generally received limited attention. One reason for the scarcity of research on this subject is that topographic site effects are generally smaller than those due to stratigraphic irregularities and that, at the same time, there is a lack of good quality instrumental data. Furthermore, topographic effects are typically 3D, and still few research groups have the capabilities of simulating them with appropriate numerical codes. Therefore, most published results and parametric solutions, including the topographic amplification factors of the Annex A of the Eurocode8 Part5 (CEN 2004), are derived from 2D wave propagation analyses.

It is still to be verified if such solutions apply also for typical 3D topographic profiles, such as the numerous examples occurring in Italy and other Mediterranean countries, where the historical centers of many small towns are located at the top of isolated steep cliffs. It should also be considered that very often such unfavourable conditions come together with high vulnerability levels due to the quality of the built environment and to the possible occurrence of sliding movements of the soil. Therefore, even a moderate increase of the seismic site amplification factor may be of practical relevance for the earhquake risk evaluation.

METHOD AND RESULTS

The seismic response of some of the numerous cases of steep or very steep topographic irregularities in the Italian geological environment is studied through 3D numerical models, for which a spectral element grid has been constructed based on a digital elevation model (DEM) of the site. To focus on topographic effects alone and avoid the complex coupling of stratigraphy and topography amplification, soil properties are homogeneous throughout the numerical model, and are selected according to the predominant surface rock materials.

The selected cases are the following:

Civita di Bagnoregio, Lazio, Central Italy (isolated hill, 110 m high)
Altino, Abruzzo, Central Italy (isolated hill, 65 m high)
Mt. Titano, San Marino Republic (massive ridge, about 250 m high)
Castellaro, Liguria, Northern Italy (steep ridge, 240 m high)

The procedure followed for the evaluation of topographic amplification factors for each of the selected cases is the following:

- calculation of the 3D numerical transfer functions;
- convolution with the previous transfer functions to obtain the surface response to a significant set of real accelerograms, from earthquakes with magnitude ranging from 5.4 to 7.4, and representative of rock or stiff soil conditions;
- obtention of the 5% damping acceleration response spectrum of each accelerogram;
- calculation of the average ratio r(T), over all the accelerograms considered, of the previous response spectrum with respect to that of the input motion;
- r(T) turns out to be roughly constant with the structural period T and its average value over T can be assumed as the topographich amplification factor for the site.

An example of the topographic amplification numerical results is reported for the case of Civita di Bagnoregio. Civita lies on a steep isolated hill, about 110 m high, reaching 442 m above sea level (Figure 1). On June 11, 1695, it was badly hit by a strong earthquake with local MCS intensity ranging from IX to X. The enormous damage in Civita, together with the occurrence of several landslides, may suggest a significant site amplification, possibly due to the steep topography. This is also supported by the fact that other surrounding villages, with site topography less prominent than Civita, suffered less damage.
Site geology at Civita is fairly complex, with surface layers consisting of tuff overlaying softer clays. However, for the reasons mentioned previously, the numerical model is homogenous, with shear wave velocity β = 600 m/s, representative of tuff materials, and Poisson coefficient ν=0.25.

Fig 1: Picture of Civita di Bagnoregio, taken from W.

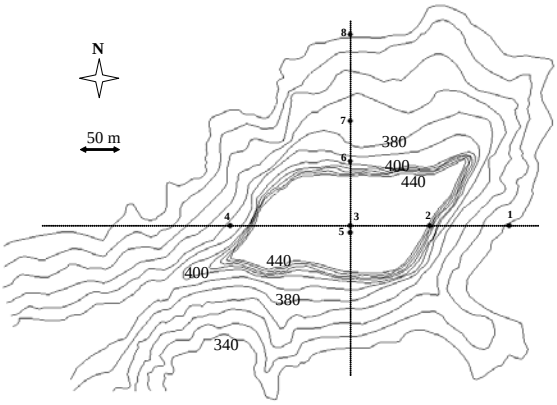

Fig 2: Contour level map of Civita, with location of receivers

Numerical transfer functions for the receivers on an EW cross-section indicated in Figure 2 are reproduced in Figure 3. Note that the spectral ordinates should be divided by 2, i.e. by the free surface amplification factor, to obtain the actual topographic amplification.
A prominent peak at about 1 Hz appears in all transfer functions at the hill top, indicating the fundamental frequency of vibration. For a thorough discussion on the relation of such peaks with closed-form expression of the fundamental vibration frequency of topographic profiles refer to Paolucci (2002).

EVALUATION OF A TOPOGRAPHIC AMPLIFICATION FACTOR

A single, period-independent, topographic amplification factor was calculated for each case under study with the procedure outlined in the following.

First the surface response at the receiver highest in elevation was convolved with a significant set of real accelerograms, from earthquakes with magnitude ranging from 5.4 to 7.4, and representative of rock or stiff soil conditions. The range of magnitude ensures that both low and high frequencies, up to about 4-5 Hz, are excited.

Subsequently, the acceleration response spectrum of each accelerogram was divided by that of the input motion and the average (±1s.d.) over all accelerograms was calculated. Due to the frequency limitations of the numerical analyses, such operations were performed in the period range 0.2÷3 s. In this way, an average ratio r(T), T being the natural period of the single degree-of-freedom oscillator, was obtained for each of the four real cases illustrated (Figure 4).

The dispersion of the curves is not indicated since it is very low (ranging from 2% to 5% of the average): this indicates that the dependence of r(T) on the input motion is negligible. Besides, the variations with period of r(T) are small in the indicated range of periods, with peaks that do not exceed 2, even for the Civita case where the highest topographic amplification levels were obtained. Taking the average of r(T) for each case, a constant topographic amplification factor (F) can be introduced for a quantitative evaluation of topographic effects on the design spectrum.

The F values obtained for the different topographic configurations analyzed are reported in the fourth column of Table 1.

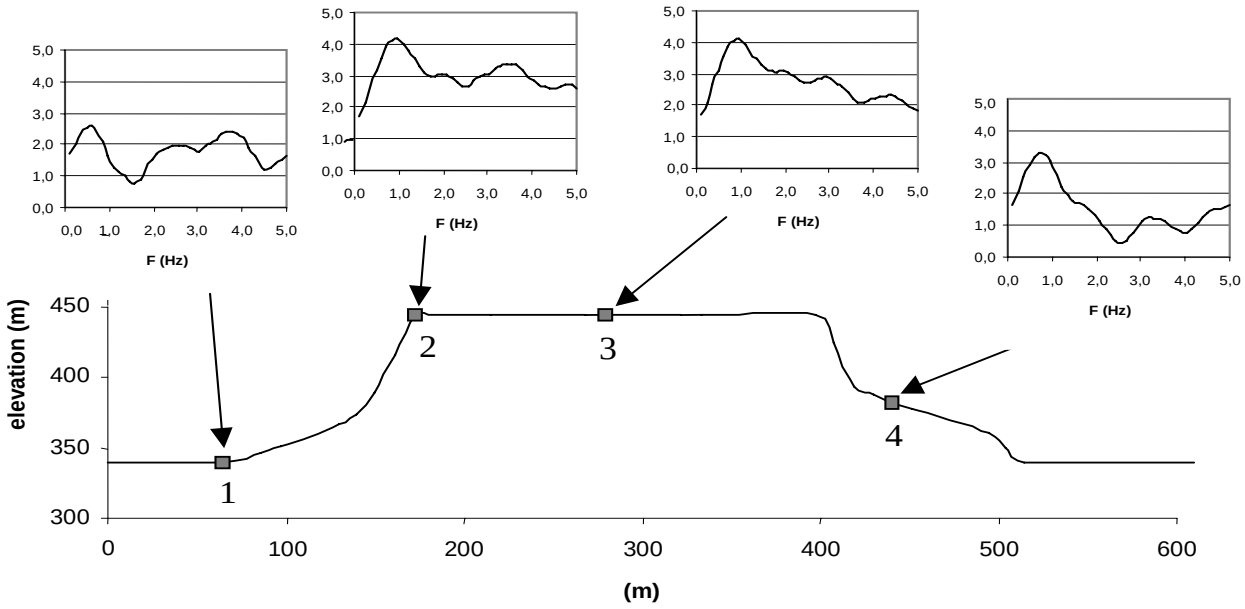

Fig 3: Numerical transfer functions at Civita at selected receivers, located in Figure 2. Input motion: vertically incident plane S-wave polarized in the EW direction.

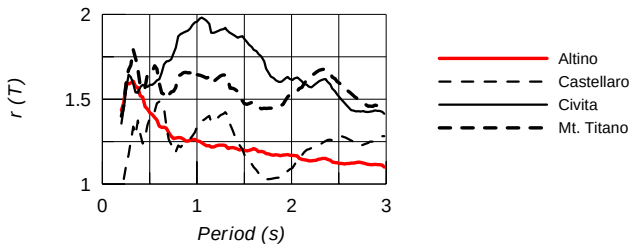

Fig 4: Average ratio of output vs. input acceleration response spectra from 3D numerical analyses.

CONCLUSIONS AND INDICATIONS FOR EC8

The topographic amplification factors obtained in this study, both for 2D and for 3D numerical analyses are compared in Table 1 with the corresponding factors of Annex A of Eurocode 8 Part 5. It turns out that the EC8 recommendations in terms of topographic amplification factors are generally satisfactory. However, there are some cases, like that of Civita di Bagnoregio, for which the EC8 factor is not conservative and underestimates the numerical value by about 40%.

Tentatively, these cases may be characterized by the combined presence of the following features:

- isolated cliff with height H > [60] m ;
- similar dimensions of the width (W) and length (L) of the crest (e.g., [1/3] < L/W < [3]);
- average slope angle > [30]° and maximum slope angle > [60°].

For these cases, a topographic amplification factor $S_T \geq [1.7]$ to be used at the top of the slope may be suggested.

Values between square parentheses are indicative and should be carefully checked with further 3D numerical simulations.

REFERENCES

CEN (Comité Européen de Normalisation). *Eurocode 8: Design of structures for earthquake resistance. Part 5: Foundations, retaining structures and geotechnical aspects*. EN 1998-5, Brussels, Belgium, 2004.

Paolucci, R. (2002) “Amplification of earthquake ground motion by steep topographic irregularities”, *Earthquake Engineering and Structural Dynamics*, Vol. 31, pp. 1831-1853.

Table 1: Topographic amplification factors from 3D and 2D numerical analyses, against EC8 factors and EC8 classification of the site. After Paolucci, 2002.

SITE	Site classification according to EC8	*EC8*	*3D*	*2D SH*	*2D SV*
CIVITA 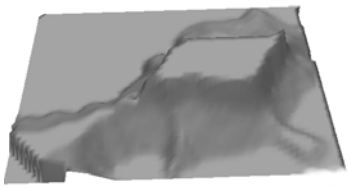	*Isolated cliff*	*1.2*	*1.75 +46%*	*1.40 +17%*	*1.30 +8%*
ALTINO 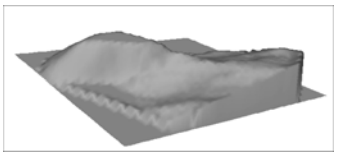	*Isolated cliff*	*1.2*	*1.30 +8%*	*1.22 +2%*	*1.22 +2%*
MT. TITANO 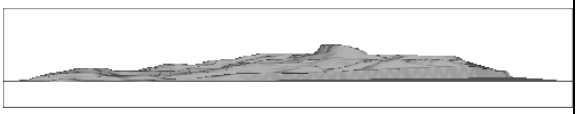	*Ridge with crest width significantly less then the base width and average slope angle > 30°*	*1.4*	*1.58 +13%*	*1.18 -16%*	*1.32 -6%*
CASTELLARO 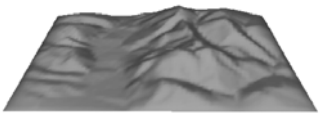	*Ridge with crest width significantly less then the base width and average slope angle < 30°*	*1.2*	*1.25 +4%*	*1.09 -9%*	*1.28 +7%*

Aggravation of Seismic Ground Motion due to Slope Topography

Achilleas G. Papadimitriou[1], George D. Bouckovalas[2]

[1] *Research Associate, National Technical University of Athens, Greece*
[2] *Professor, National Technical University of Athens, Greece*

Abstract

This paper presents results of numerical analyses for the seismic response of step-like ground slopes in uniform visco-elastic soil, under vertically propagating SV seismic waves. The aim of the analyses is to explore the effects of slope geometry, predominant excitation frequency and duration, as well as dynamic soil properties on seismic ground motion in a parametric manner, and provide qualitative as well as quantitative insight to the phenomenon. Among the main conclusions of this study is that this kind of topography may lead to intense amplification or de-amplification variability at neighboring (within a few tens of meters) points behind the crest of the slope, especially for high frequency excitations. Nevertheless, a general trend of amplification near the crest and de-amplification near the toe of the slope seems to hold for the horizontal motion. As a result of these two findings, it becomes evident that reliable field evidence of slope topography aggravation is extremely difficult to establish. Furthermore, this study highlights the generation of a parasitic vertical component of motion in the vicinity of the slope, due to wave reflections at the slope surface, that under certain preconditions may become as large as the horizontal. Criteria are established for deciding on the importance of topography effects, while approximate relations are provided for the preliminary evaluation of the topographic aggravation of seismic ground motion and the width of the affected zone behind the crest.

INTRODUCTION

The effect of step-like slope topography on seismic ground motion has not been thoroughly examined in the literature, despite that there is indisputable evidence of its significance even from the late 1960's [1]. In fact, this form of surface topography has drawn the least attention among scientists, as compared to hills and canyons, despite its significance in engineering practice. One possible reason is the non-symmetric geometry of step-like slopes, which complicates analytical solutions and favors mostly site-specific numerical simulations whose conclusions are difficult to generalize. Another reason could be the fact that conclusive results from field measurements are difficult to obtain, due to the wave scattering that a step-like slope produces, as discussed later in this paper. As a result, approximate relations and design guidelines are rare in the literature, while relevant provisions have not yet been implemented in most modern seismic codes.

Among the published studies, the majority concerns either specific geometries and seismic excitations (e.g. [1], [2], [3], [4], [5], [6]), or examines specific aspects of the phenomenon such as the wave scattering generated at the vicinity of the slope [7] and the effects of a soft soil cap in the area of the slope [8]. The only systematic parametric study found in the literature is that by [9] and [10], which provides valuable insight to the effects of slope inclination i and height H, wave type (P, SH and SV) and wavelength λ, as well as the angle of wave incidence β. Nevertheless, the results of the analyses are presented solely at the crest and at distances equal to H, $2H$ and $4H$ behind it. Furthermore, these studies do not address the effect of two factors that are commonly accounted for in most seismic ground response analyses: the hysteretic damping ratio of the soil ξ and the duration of the shaking or the number of equivalent uniform excitation cycles N. Thus, the presented results cannot be readily used for a quantitative assessment of the effect of slope topography on seismic ground motion, in the form of either simple approximate relations or seismic code provisions.

Aiming at this goal, results are presented

from an extensive parametric study of step-like slope topography effects, performed with the Finite Difference method [12]. The relevant research was triggered from recent evidence that such effects played an important role in the extent of damage caused by two recent destructive earthquakes in Greece ([3], [4], [11] and [6]): the 1995 Aigion and the 1999 Athens events. Compared to the study by [9] and [10], our study is narrower in the sense that it focuses merely on the case of vertically propagating SV waves. On the other hand, it explores in detail the effects of a larger number of problem parameters and provides a continuous assessment of slope topography effects along the ground surface, for a sufficient length behind the crest and in front of the toe of the step-like slope. It should be underlined, that the quantitative assessments hereby provided apply conservatively to SH waves as well, since SH topographic amplification has been shown smaller than that of SV waves ([9], [10]). Note that details on the hereby presented numerical results can be found in [16]. This presentation adds to the work of [16] in terms of the topographic seismic ground motion aggravation envelope, as a tentative code provision.

OUTLINE OF METHODOLOGY

The numerical analyses were performed with the Finite Difference method [12], for linear visco-elastic soil with V_S = 500m/s, Poisson's ratio v = 1/3 and mass density ρ = 2Mg/m^3. A schematic illustration of the 2-D analyzed mesh and the boundary conditions is provided in Fig. 1. More specifically,

- 28000 to 120000 quadrilateral zones were used to simulate the uniform soil mass, with a maximum height equal to 1/10 – 1/20 of the predominant wavelength of the seismic excitation in order to avoid the numerical distortion of its frequency content.
- The width and the height of the mesh were usually set at *20H* and *5H* respectively, in order to reduce the effects of artificial wave reflections from the boundaries at the area of interest (near the slope).
- For the same purpose, transmitting boundaries were applied at the base of the mesh, while boundaries simulating the free field were applied at its right and left sides.

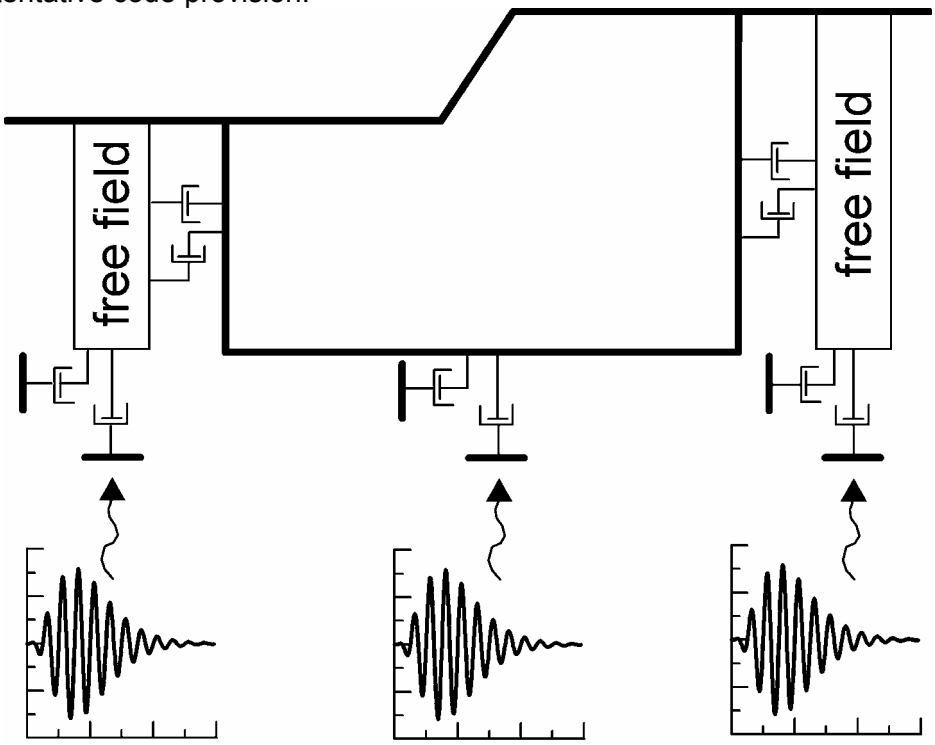

Fig 1: Schematic illustration of Finite Difference model for the numerical analyses of step-like slope topography effects

Unlike common practice that introduces the seismic excitation at the base of the mesh as a time history of acceleration (or velocity, or displacement), in our analyses a time history of stress was used, in order to avoid artificial wave reflections at the base of the mesh, which are unavoidable in analyses of common practice. Most of the parametric analyses were performed either with a harmonic excitation of 20 – 40 uniform cycles, or with a Chang's Signal excitation aimed to simulate the limited duration as well as the gradual rise and decrease of shaking amplitude (Fig. 1). In addition, a limited number of parametric analyses were performed for actual seismic excitations to explore the effect of a much wider frequency content.

The overall accuracy of the numerical methodology was verified through comparison with analytical solutions for the seismic response of the ground surface across semi-circular shaped canyons, for uniform soil and vertically propagating harmonic SV waves [13]. The choice of this analytical study was dictated by the fact that there are no analytical solutions for step-like slope topography in the reviewed literature and that it is well established and commonly used for calibration of new methods or studies in the literature. A typical comparison between numerical and analytical predictions for the horizontal (U_h) and the (parasitic) vertical (U_v) components of the peak ground surface displacement is shown in Fig. 2, for the particular case of canyon radius R=25m and wavelength ratio λ/R = 2.

It is important to notice that the numerical methodology previously outlined does not take consistently into account the effect of soil non-linearity. Namely, shear moduli remain constant (elasticity) and material damping is of the Rayleigh type, i.e. it is frequency dependent and the reference damping of each analysis is the damping value for the frequency of the excitation. For this reason, as well as for the benefit of generalization, the results of the numerical analyses are not evaluated directly, but following normalization against the free-field response of the ground, which is free from any topography effects. For this purpose, each basic 2-D analysis was supplemented by two 1-D analyses: one for the free field in front of the toe of the slope and the other for the free field behind its crest. This approach is cumbersome, but more accurate than evaluating the free-field response from the results of the 2-D analyses alone, at nodes at large distance away from the slope. The reason is that topography effects decrease asymptotically with distance from the slope and may not completely disappear within the analyzed mesh, thus underestimating the overall amplification effects, especially for low intensity motions with small soil damping.

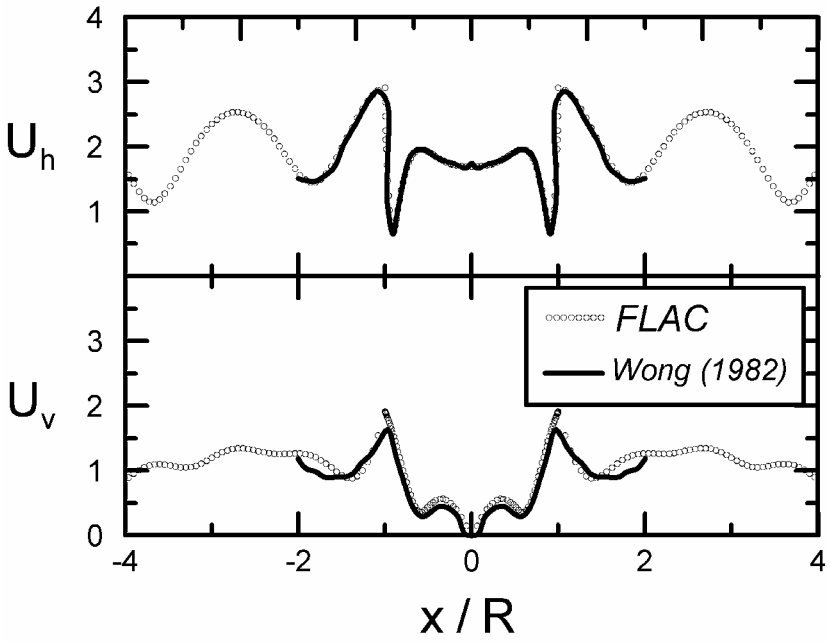

Fig 2: Analytical verification of numerical scheme for canyon topography (vertical SV wave, R=25m, λ/R=2)

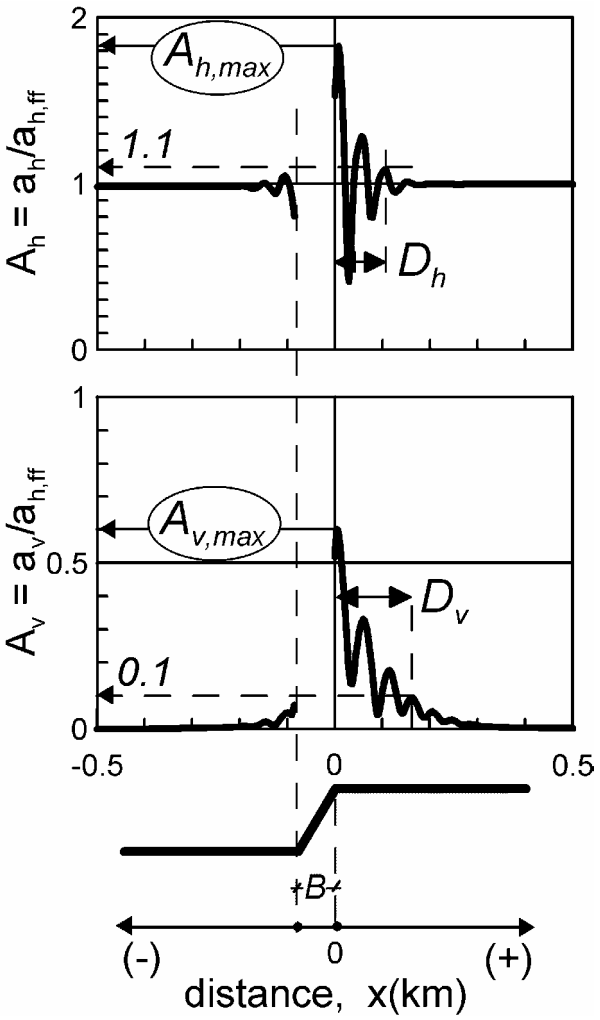

Fig 3: Typical results for the topographic amplification of the peak horizontal A_h and the parasitic vertical A_v acceleration, as a function of horizontal distance x from the crest (results for H/λ=2, i=30°, N=6, ξ=5%)

It is important to notice that the numerical methodology previously outlined does not take consistently into account the effect of soil non-linearity. Namely, shear moduli remain constant (elasticity) and material damping is of the Rayleigh type, i.e. it is frequency dependent and the reference damping of each analysis is the damping value for the frequency of the excitation. For this reason, as well as for the benefit of generalization, the results of the numerical analyses are not evaluated directly, but following normalization against the free-field response of the ground, which is free from any topography effects. For this purpose, each basic 2-D analysis was supplemented by two 1-D analyses: one for the free field in front of the toe of the slope and the other for the free field behind its crest. This approach is cumbersome, but more accurate than evaluating the free-field response from the results of the 2-D analyses alone, at nodes at large distance away from the slope. The reason is that topography effects decrease asymptotically with distance from the slope and may not completely disappear within the analyzed mesh, thus underestimating the overall amplification effects, especially for low intensity motions with small soil damping.

TYPICAL RESULTS

Typical results from the numerical analyses are presented in Fig. 3, for the specific case of uniform soil, slope inclination i = 30°, normalized height H/λ = 2.0, critical damping ratio ξ = 5% and six significant cycles of base excitation (N = 6). This figure shows the variation of the topography aggravation factors $A_h=a_h/a_{h,ff}$ and $A_v=a_v/a_{h,ff}$ with distance from the crest x, where a_h and a_v denote the peak horizontal and peak vertical accelerations at each point of the ground surface.

Parameter $a_{h,ff}$ denotes the free-field value for the peak horizontal acceleration and is used for normalization of both a_h and a_v, since $a_{v,ff}$ = 0 for a vertically propagating SV wave in a uniform horizontal soil. Review and interpretation of this figure alone may provide insight to the mechanisms, which control topography effects and lead to some first conclusions of practical interest. Namely:

(a) Even a purely horizontal excitation, as a vertically propagating SV wave, results in considerable (parasitic) vertical motion at the ground surface near the slope. This component of ground motion is independent from any vertical excitation induced to the base of the slope by the earthquake itself and, consequently, it has to be superimposed to it. The results of the parametric analyses show that the vertical (parasitic) component of seismic motion may become comparable to the horizontal free-field motion.

(b) The topography aggravation of the horizontal ground motion, expressed through the acceleration ratio $A_h=a_h/a_{h,ff}$, fluctuates intensely with distance away from the crest of the slope, alternating between amplification ($A_h > 1.0$) and de-amplification ($A_h < 1.0$) within very short horizontal lengths. For the typical results of Fig. 3, this

length is approximately 25m, i.e. equal to $H/2$ (or equal to λ for this case of $H/\lambda = 2$). Similarly, the topographic apparition of parasitic vertical motion expressed via A_v is also intensely variable with distance. The local maxima and minima of A_v occur again at distances equal to $H/2$, but their locations do not necessarily coincide with the respective points for the A_h. These findings regarding the fluctuation of topographic aggravation imply that its experimental verification through inverse analysis of structural damage is very crude, and that actual ground motion recordings near slopes must be obtained via very dense seismic arrays.

(c) It is also worth noticing that the horizontal ground motion is de-amplified at the toe of the slope and amplified near the crest. As a result, topography aggravation may be seriously overestimated, when calculated as the peak seismic ground motion at the crest over that at the toe of the slope. For example, for the results of Fig. 3, this procedure would give $A_h \cong 1.70/0.80 = 2.13$, which is higher than the peak topography aggravation behind the crest $A_{h,max} = 1.83$. This overestimation may reach 100% for steeper slopes (see Fig. 5) and may explain, at least in part, why field measurements (without appropriate free field selection) of topography aggravation are usually significantly higher than analytical predictions [14].

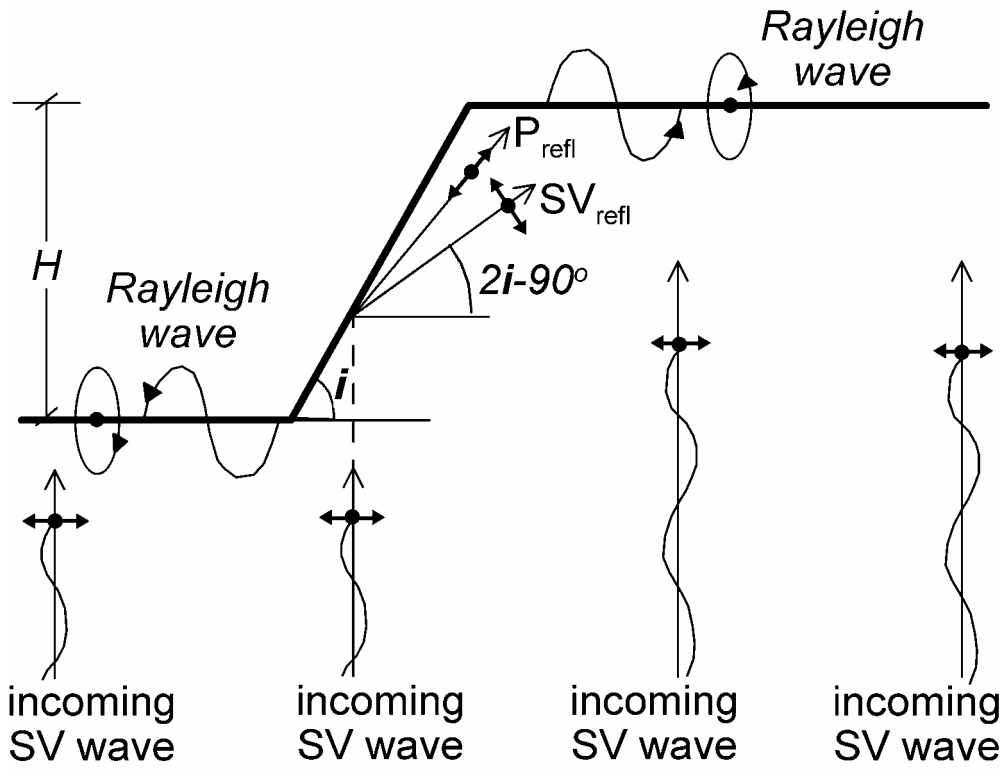

Fig 4: Schematic illustration of incoming SV waves and induced P_{refl}, SV_{refl} and Rayleigh in the case of step-like slopes ($i \geq 45^o$)

Findings (a) and (b) above can be readily attributed to the reflection of the incoming SV waves on the inclined free surface of the slope (Fig. 4), which leads to reflected P and SV waves impinging obliquely at the free ground surface behind the crest, as well as Rayleigh waves. All these induced waves have a strong vertical component. In addition, they arrive with a time lag and a phase difference at the different points of the ground surface so that their superposition to the incoming SV waves may lead either to amplification or to de-amplification of the horizontal seismic motion.

APPROXIMATE RELATIONS

In all, ninety (90) parametric analyses were performed in order to assess the effect of the following *potentially* important parameters (see Tables 1 and 2):

- the slope inclination *i(deg)* or *I=i/90*,
- the normalized height of the slope H/λ, where λ denotes the predominant wave length of the incoming SV waves,
- the number of significant excitation cycles *N*, defined for a stress level equal to the 1/2 of the peak,
- the critical hysteretic damping ratio ξ of the soil.

Note that the 90 parametric analyses were performed for base excitations with a predominant period T_e ranging from 0.05 – 2.0sec, a range practically covering the large majority of possible earthquake events. This range of T_e is what produces the range of H/λ = 0.05 – 2.0 shown in Tables 1 and 2, since all analyses were performed for a slope of height H = 50m and uniform V_S = 500m/s. Nevertheless, topographic aggravation results coincide for step-like slopes with different values of H and λ but the same value of H/λ, a fact that allows for the generalization of the presented results for a very large range of soil and excitation conditions.

Table 1: Pairs of normalized height H/λ and slope angle i for the parametric analyses of step-like slopes with small soil damping ($\xi \leq 5\%$), under harmonic base excitation.

$i(^o)$ \ H/λ	0.05	0.10	0.15	0.20	0.30	0.45	0.70	1.00	1.30	2.00
10		X		X		X		X		
20		X		X		X		X		
30	X	X	X	X	X	X	X	X	X	X
45	X	X	X	X	X	X	X	X	X	X
60	X	X	X	X	X	X	X	X	X	X
75		X		X		X		X		
90		X		X		X		X		

Table 2: Pairs of significant excitation cycles *N* and soil damping ξ for the parametric analyses of step-like slopes with H/λ = 2.0 & i = 30^o (X) or H/λ = 0.20 & i = 75^o (O), under Chang's signal base excitation

$\xi(\%)$ \ N	1	2	3	4	6	8	12
0	X	X , O	X	X	X , O	X	X , O
2	X	X	X	X	X	X	X
5	X	X	X	X	X	X	X
10	X	X , O	X	X	X , O	X	X , O
20	X	X , O	X	X	X , O	X	X , O

Figures 5 through 8 present selected results from the parametric analyses demonstrating the effects of slope angle i, normalized height H/λ, number of significant excitation cycles N and soil damping ξ. In broad terms, it is observed that the slope angle i and the normalized height of the slope H/λ have a significant and non-univocal effect on the aggravation of the horizontal and vertical ground motions (factors A_h and A_v), as well as on the distance to the free field in front and behind the slope (see Figures 5 and 6). On the contrary, Figures 7 and 8 show that the hysteretic damping ratio of the soil ξ has a significant effect only on the distance to the free field, while the number of significant excitation cycles N has a relatively minor overall effect. Practically speaking, our results in terms of A_h and A_v from analyses for small soil damping ($\leq$ 5%) agree in both qualitative and quantitative terms with the work of [9] and [10].

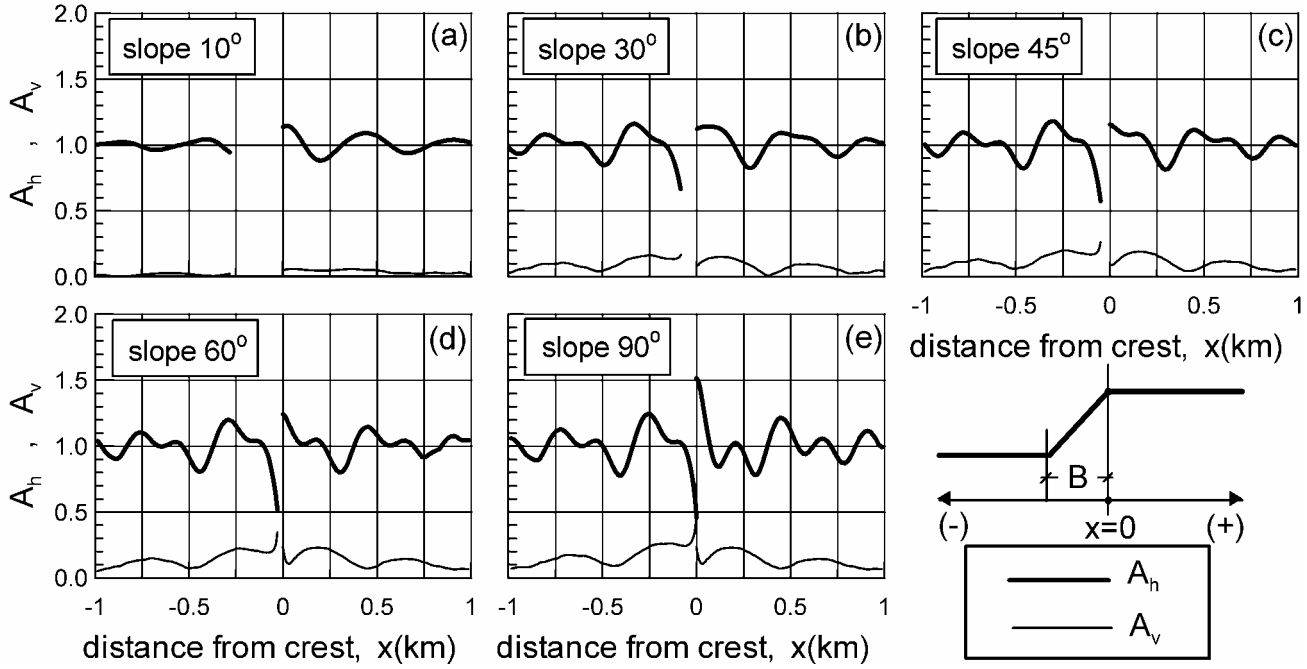

Fig 5: Effect of slope inclination *i* on the amplification of peak horizontal A_h and apparition of parasitic vertical A_v acceleration, as a function of horizontal distance x from the crest of a step-like slope (H/λ = 0.2, harmonic motion, ξ < 5%)

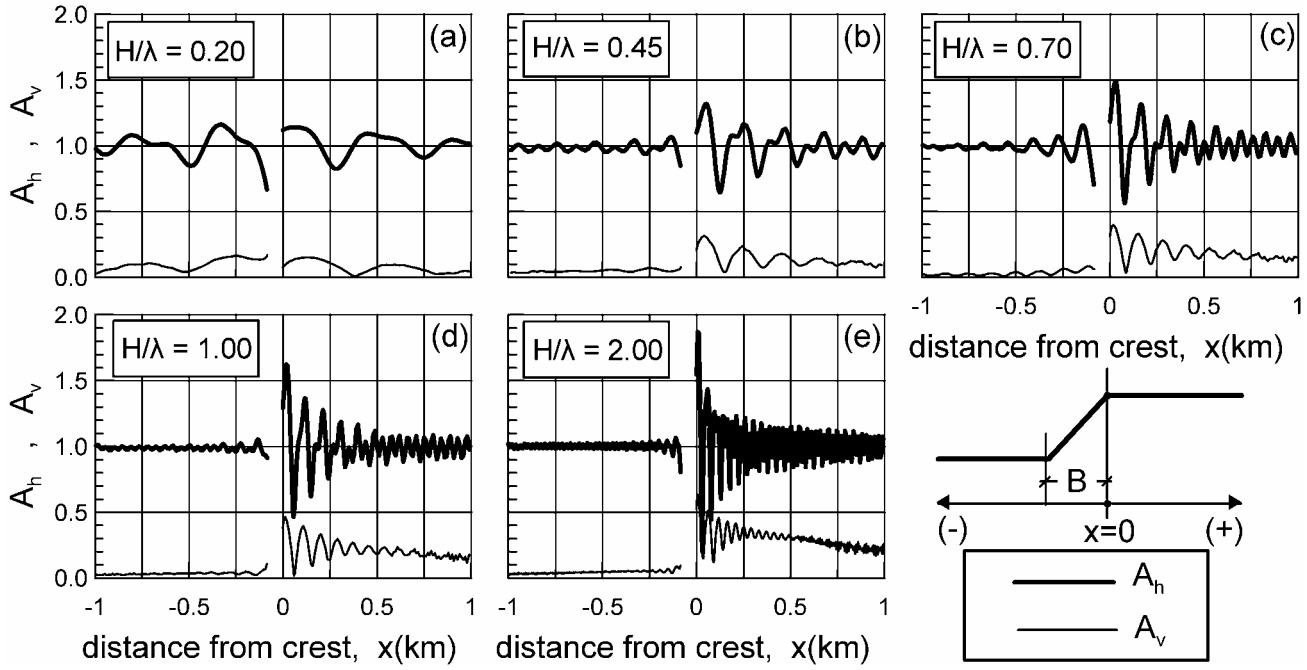

Fig 6: Effect of normalized height H/λ on the amplification of peak horizontal A_h and apparition of parasitic vertical A_v acceleration, as a function of horizontal distance x from the crest of a step-like slope (i=30°, harmonic motion, ξ < 5%)

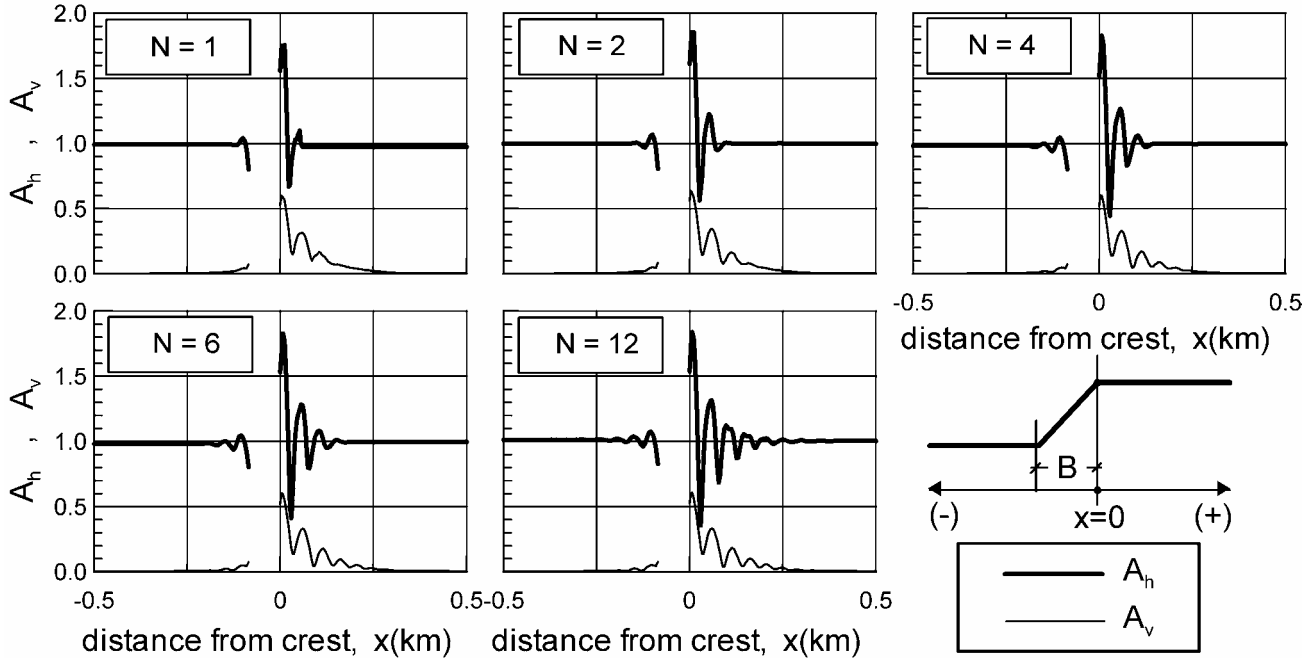

Fig 7: Effect of number of significant cycles N on the amplification of peak horizontal A_h and apparition of parasitic vertical A_v acceleration, as a function of horizontal distance x from the crest of a step-like slope (H/λ = 2, i=30°, ξ = 5%)

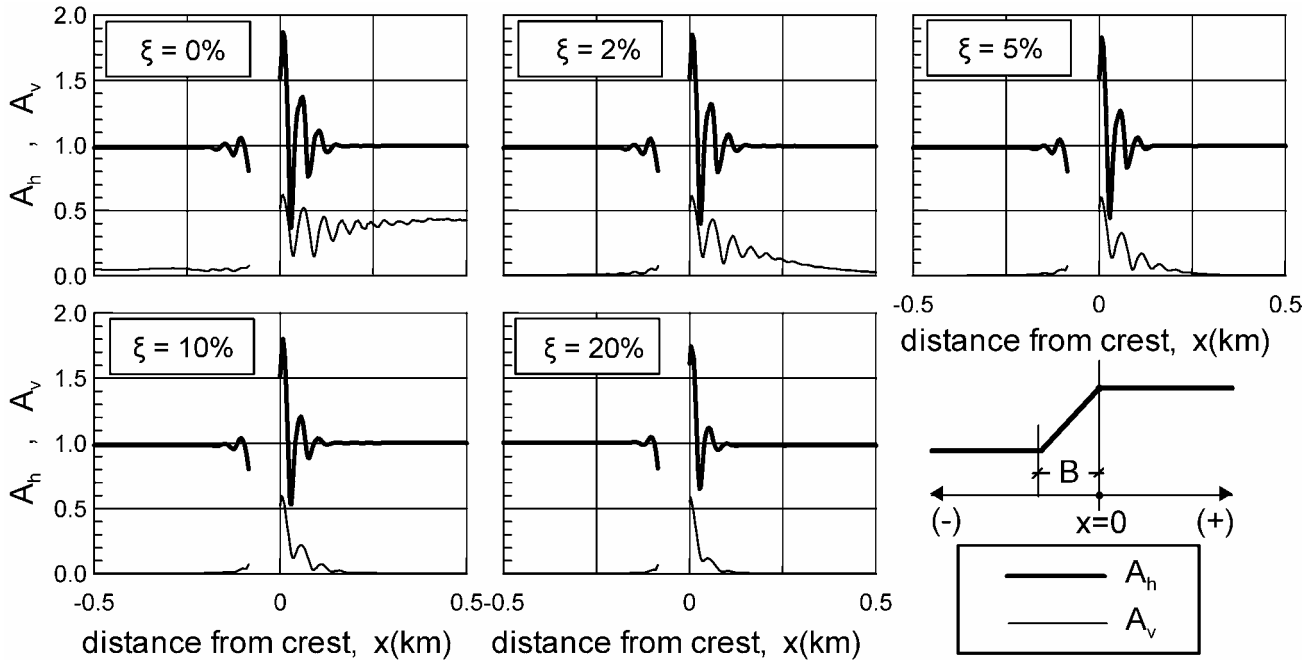

Fig 8: Effect of number of soil damping ξ on the amplification of peak horizontal A_h and apparition of parasitic vertical A_v acceleration, as a function of distance x from the crest of a step-like slope (H/λ = 2, i =30°, N = 4)

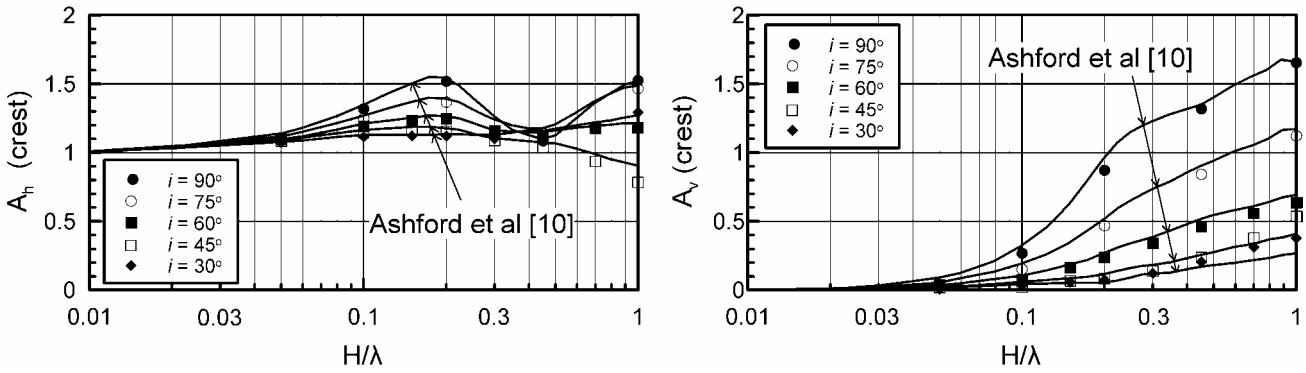

Fig 9: Comparison of results from parametric analyses with published predictions for the crest of step-like uniform slopes ($\xi < 5\%$, harmonic base excitation)

As an example, Figure 9 compares our results in terms of A_h and A_v at the crest of step-like slopes (symbols) with the respective results (lines) from [10] and shows that the two distinctly different methodologies of analyses (Finite Difference method here versus generalized consistent transmitting boundary method in [9] and [10]) produce practically identical results.

Furthermore, in order to increase the applicability of the results of the parametric analyses, a database was created tabulating the most important input variables and output parameters of all analyses. Namely, the input of each analysis was introduced in terms of variables *I(=i/90), H/λ, N* and *ξ*. The selection of the output parameters was less straightforward. Addressing this issue from an engineering point of view, of interest for design purposes are the peak values of the topography aggravation factors $A_{h,max}$ and $A_{v,max}$ behind the crest, in the horizontal and vertical direction, respectively (see Fig. 3). Moreover, of practical importance is also the distance behind the crest for which topography aggravation is significant, defined separately for the horizontal and for the vertical directions and denoted by D_h and D_v respectively. Note that, from an engineering point of view, it was assumed that *free field* conditions apply at distances D_h and D_v behind the crest where $A_h \leq 1.10$ and $A_v \leq 0.10$ respectively (see Fig. 3).

Hence, four (4) output parameters were tabulated in the database, which were sequentially related to the four (4) input variables via the following general expressions:

$$A_{h,\max} = 1 + \mathrm{F_{Ah}}\left(\frac{\mathrm{H}}{\lambda}\right)\mathrm{G_{Ah}}(\mathrm{I})\mathrm{H_{Ah}}(\xi)\mathrm{J_{Ah}}(\mathrm{N}) \quad (1)$$

$$A_{v,max} = \mathrm{F_{Av}}\left(\frac{\mathrm{H}}{\lambda}\right)\mathrm{G_{Av}}(\mathrm{I})\mathrm{H_{Av}}(\xi)\mathrm{J_{Av}}(\mathrm{N}) \quad (2)$$

$$D_h/H = \mathrm{F_{Dh}}\left(\frac{\mathrm{H}}{\lambda}\right)\mathrm{G_{Dh}}(\mathrm{I})\mathrm{H_{Dh}}(\xi)\mathrm{J_{Dh}}(\mathrm{N}) \quad (3)$$

$$D_v/H = \mathrm{F_{Dv}}\left(\frac{\mathrm{H}}{\lambda}\right)\mathrm{G_{Dv}}(\mathrm{I})\mathrm{H_{Dv}}(\xi)\mathrm{J_{Dv}}(\mathrm{N}) \quad (4)$$

The final form of functions F, G, H and J in Equations 1 to 4 are analytically defined in Table 3 and shown graphically in Fig. 10. Note that for better accuracy, the statistical analysis that produced the form of functions F, G, H and J was performed in two steps. First, the effect of each (practically independent) variable was explored separately, by selecting cases for which the values of the remaining variables varied within a narrow range, so that the general form of functions F, G, H and J could be identified. The quantitative expression of the proposed relations was consequently established from a multivariable regression analysis of the entire database, according to the Newton-Raphson iterative procedure.

The comparison between approximate and numerical predictions of $A_{h,max}$, $A_{v,max}$, D_h/H and D_v/H is shown in the four plots of Figure 11.

Table 3: Analytical form of functions F, G, H and J in the proposed approximate relations for topography aggravation (Eqs 1 to 4)

Parameter	F(H/λ)	G(I)	H(ξ)	J(N)
$A_{h,max}$	$(H/\lambda)^{0.4}$	$\frac{I^2+2I^6}{I^3+0.02}$	$\frac{1}{1+0.9\xi}$	0.225
$A_{v,max}$	$(H/\lambda)^{0.8}$	$I^{0.5}+1.5I^5$	$\frac{1}{1+0.15\xi^{0.5}}$	0.75
D_h/H	$\frac{(H/\lambda)}{(H/\lambda)^2+0.2}$	$\frac{I^{1.5}+3.3I^8}{I^4+0.07}$	$\frac{1}{0.71+3.33\xi}$	$N^{0.43}$
D_v/H	$\frac{(H/\lambda)}{(H/\lambda)^2+0.2}$	$\frac{I^{1.5}+3.3I^8}{I^4+0.07}$	$\frac{0.233}{\xi^{0.78}}$	1.00

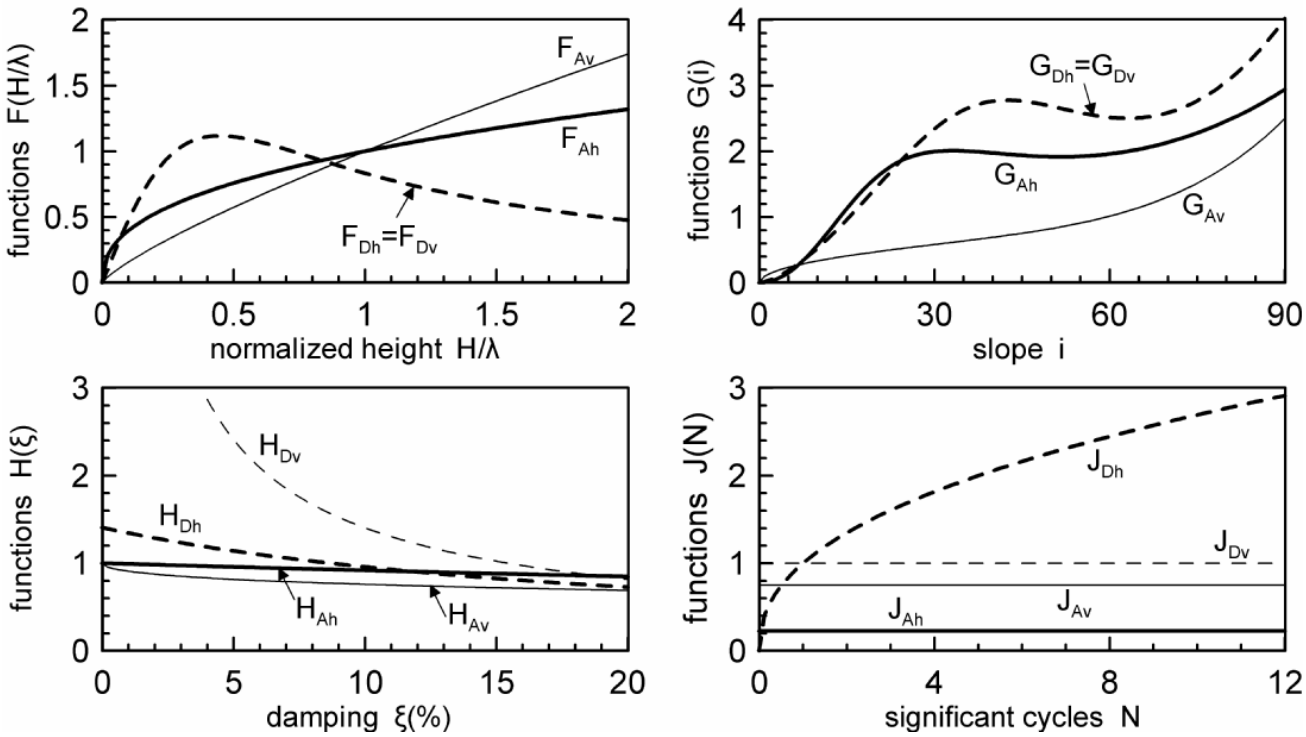

Fig 10: Form of functions F(H/λ), G(i), H(ξ) and J(N) entering the approximate relations for the estimation of parameters $A_{h,max}$, $A_{v,max}$, D_h/H and D_v/H

In the plots of Fig.11, each symbol corresponds to a different analysis and is obtained, on one hand, using as coordinates the value of the parameter from the numerical analysis, and, on the other hand, the respective value from the approximate relation. The diagonal lines in each plot correspond to perfect match between the compared values, while the shaded area provides an estimate of the anticipated relative difference. Observe that, the symbols are equally scattered on both sides of the diagonal lines and that the standard deviation of the relative error of the approximate relations ranges from 29 to 40%, depending on the parameter at hand.

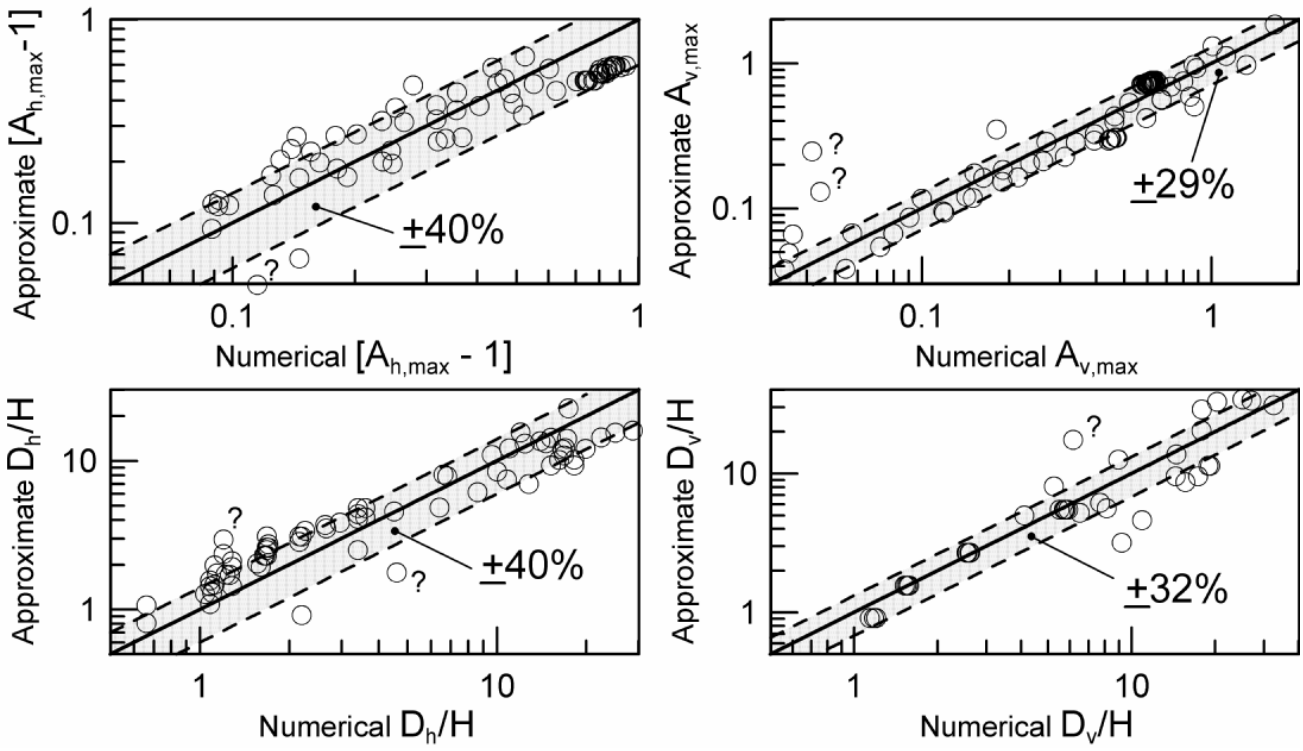

Fig 11: Comparison of $A_{h,max}$, $A_{v,max}$, D_h/H and D_v/H estimates from approximate relations and numerical analyses for all the cases in the database

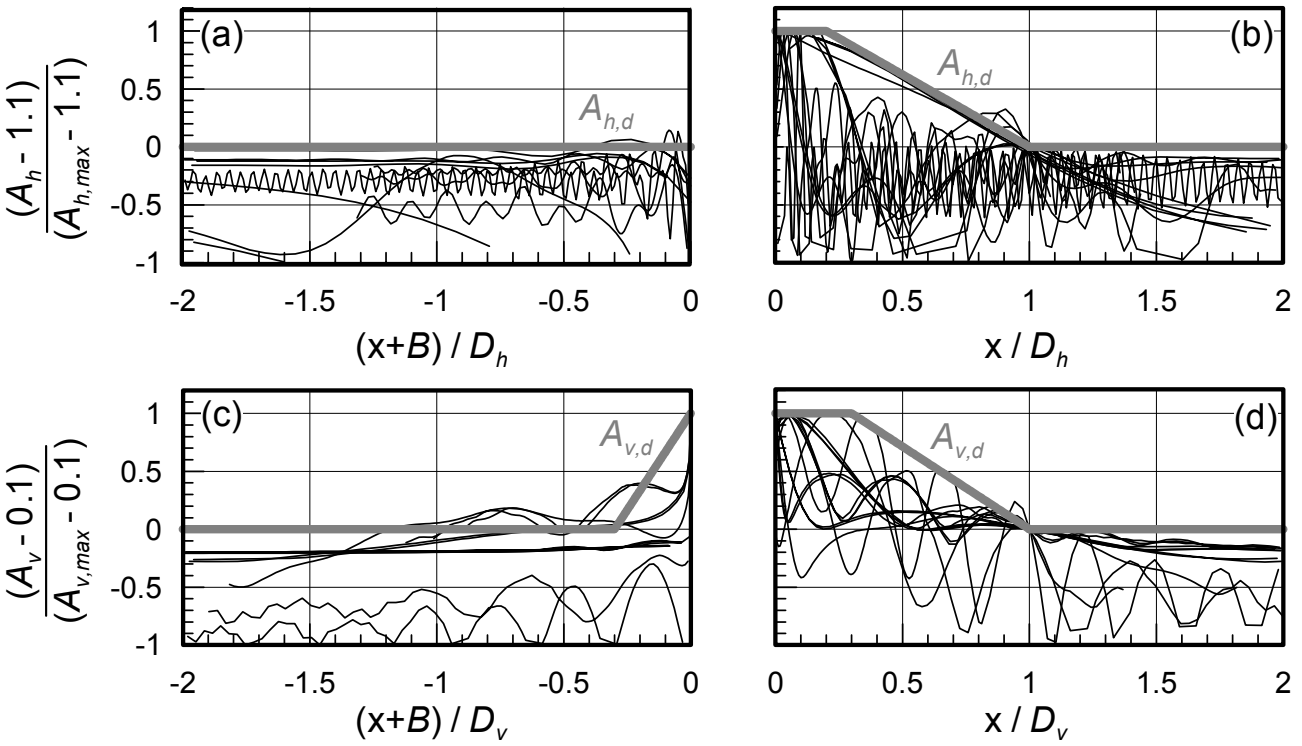

Fig 12: Design envelopes $A_{h,d}$ and $A_{v,d}$ of the topography aggravation factors A_h and A_v with distance x from the crest of the slope ($B = H/\tan i$).

The topographic aggravation of the seismic motion in the horizontal and vertical directions as a function of $A_{h,max}$ and $A_{v,max}$ for the whole distance D_h and D_v behind the crest is considered extremely conservative and non compliant to the results of the analyses. Hence, the results of the variation of A_h and A_v with distance x from the crest of the slope for each one of the ninety (90) analyses were normalized to the respective values of $A_{h,max}$, $A_{v,max}$, D_h and D_v and plotted together in Figure 12. Based on this figure, design envelopes were defined, denoted as $A_{h,d}$ and $A_{v,d}$, for the geographic variation of A_h and A_v with distance x from the crest of the slope. These design envelopes are given by eqs. (5) and (6) below:

$$A_{h,d} = \begin{cases} 1.0 \div 1.1 & , \quad x \le -B \\ 1.1 + \dfrac{A_{h,max} - 1.1}{B}(x + B) & , \quad -B \le x \le 0 \\ A_{h,max} & , \quad 0 \le x \le 0.2D_h \\ A_{h,max} - \dfrac{A_{h,max} - 1.1}{0.8D_h}(x - 0.2D_h) & , \quad 0.2D_h \le x \le D_h \\ 1.0 \div 1.1 & , \quad D_h \le x \end{cases}$$

$$A_{v,d} = \begin{cases} 0.0 \div 0.1 & , \quad x \le -(B + 0.3D_v) \\ 0.1 + \dfrac{A_{v,max} - 0.1}{0.3D_v}(x + B + 0.3D_v) & , \quad -(B + 0.3D_v) \le x \le -B \\ A_{v,max} & , \quad -B \le x \le 0.3D_v \\ A_{v,max} - \dfrac{A_{v,max} - 0.1}{0.7D_h}(x - 0.3D_v) & , \quad 0.3D_v \le x \le D_v \\ 0.0 \div 0.1 & , \quad D_v \le x \end{cases}$$

COMPARISON WITH CODE PROVISIONS

The comparison of the foregoing results with code provisions leads to useful conclusions regarding the compatibility between the codes and the theory-based simulations.

Extensive search in the literature showed that only EC-8 (2000 and draft of 2002) and the French Seismic Code PS-92 have provisions related to the topographic aggravation of seismic motion. In particular, for the topography of a slope the two codes prescribe an increase of the peak horizontal acceleration by 20% and 40%, respectively, while they both disregard the apparition of parasitic vertical motion. In EC-8, the increase of the horizontal acceleration is prescribed for areas "*near the top edge*", i.e. the distance to the free field is not clearly defined. On the contrary, the PS-92 code provides specific relations for the estimation of this distance, according to which this distance rarely exceeds the height H of the slope.

In addition, the two codes prescribe lower bounds for the geometric dimensions of the slope, below which topographic aggravation of seismic ground motion should be ignored. Namely, the EC-8 prescribes topographic aggravation only if the slope height $H > 30$m and the slope inclination $i > 15^o$, while the PS-92 adopts the following bounds: $H > 10$m and $i > 22^o$.

To perform a comparison of the foregoing code provisions with the results of our analyses, the latter should be processed in order to establish:

(a) Average values of $A_{h,max}$, $A_{v,max}$ and the distance D_{ff} to the free field behind the crest (i.e. of the maximum of the D_h and D_v) for common cases of practical interest.
(b) Criteria for the relative significance of the topographic aggravation

In most cases, the input parameters of the relations take the following values: $H/\lambda = 0.2 \div 1.0$, $i = 25 \div 75^o$ and $\xi = 5 \div 15\%$. These values lead to a usual range of $A_{h,max} = 1.20 \div 1.50$ and $A_{v,max} = 0.10 \div 1.10$, while the distance D_{ff} ranges from $2H$ to $8H$. Hence, the code provisions are compatible with the theoretical predictions in terms of the amplification of the peak horizontal acceleration, but clearly underestimate the distance to the free field. In addition, the fact that the parasitic vertical motion is found relatively significant in common cases of practice, shows a problem of the existing code provisions.

In order to establish criteria for the relative importance of topographic aggravation, Figure 13 presents the pairs of values for the most important parameters H/λ and $I=i/90^o$ for which the values of $A_{h,max} \ge 1.10$ & 1.20 and $A_{v,max} \ge 0.10$ & 0.20. The value of damping ξ in Figure 13 has a small effect on the results, and was assumed equal to 10%, a value characteristic of strong earthquake motion. From Figure 13 it is concluded that the criteria for significant topographic aggravation of the horizontal acceleration (i.e. $A_{h,max} \ge 1.10$ & 1.20) are more strict than those for the apparition of significant parasitic vertical motion (i.e. $A_{v,max} \ge 0.10$ & 0.20). Hence, adopting the former:

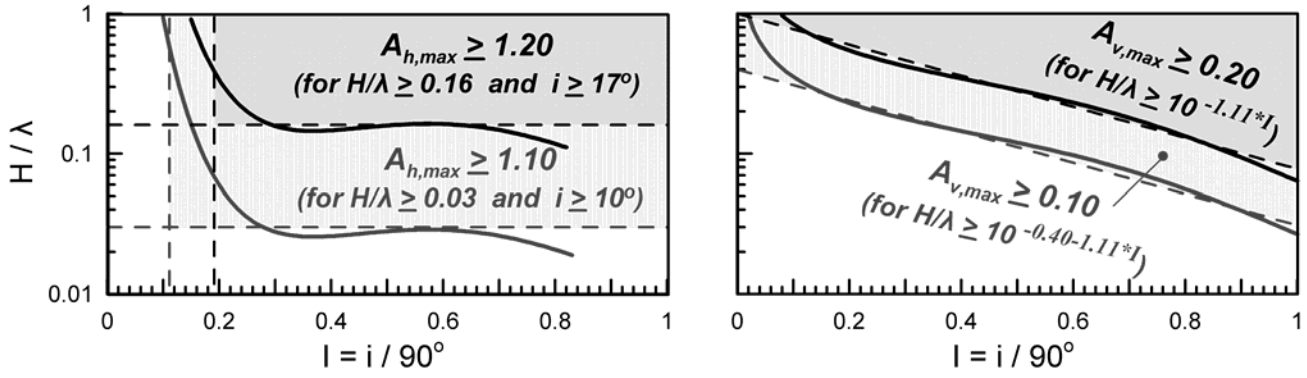

Fig 13: Lower limits of normalized slope height H/λ and slope angle i, for which topography effects become significant.

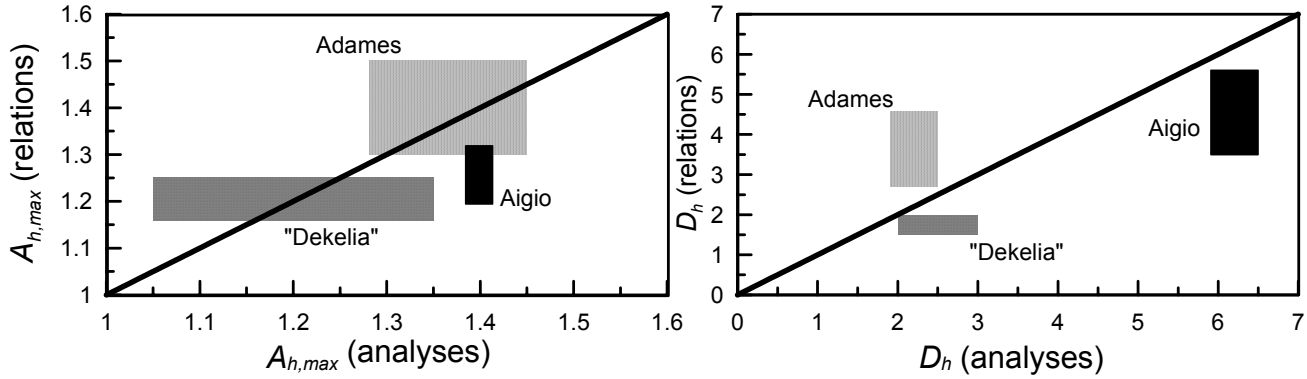

Fig 14: Comparison of topographic aggravation predictions in terms of $A_{h,max}$ and D_h for case histories, as resulting from detailed numerical analyses and the proposed relations .

– $H/\lambda > 0.03$ and $i > 10^o$ for at least 10% topographic aggravation of the horizontal motion, and
– $H/\lambda > 0.16$ and $i > 17^o$ for at least 20% topographic aggravation of the horizontal motion.

The foregoing criteria are considered more rational than the purely geometrical criteria of the code provisions, since they include the predominant wavelength λ, which takes into account (in an approximate manner) the local soil conditions and the characteristics of the seismic excitation. Yet, for usual cases of slopes that have $V_S > 400$m/s (stiff soils or soft rocks) and for common seismic excitations with a predominant period larger than 0.20s, the code provisions for lower bounds are in broad agreement with the hereby proposed criteria for 20% topographic aggravation that lead to $H >$ 13m and $i > 17^o$.

COMPARISON WITH CASE STUDIES

The excitations used to perform the parametric analyses were harmonic or nearly harmonic (Chang signal), with a very narrow frequency spectrum as compared to seismic recordings. To explore the importance of this limitation, the on the accuracy of the proposed relations, they have been applied to predict the results of 3 numerical case studies for seismic events in Greece, namely:

a) the slope in Aigion with an inclination $i \cong 45^o$, height $H \cong 80$m in the Aigion earthquake (15-6-95), from Bouckovalas et al (1999).
b) the slope of the Kifissos river in Adames with an inclination $i \cong 30^o$, height $H \cong 40$m in the Athens earthquake (7-9-99), from Gazetas et al (2002).
c) the slope of the Kifissos river at the site of hotel "Dekelia" with an inclination $i \cong 16^o$, height $H \cong 35$m in the Athens earthquake (7-9-99), from Athanasopoulos et al (2001).

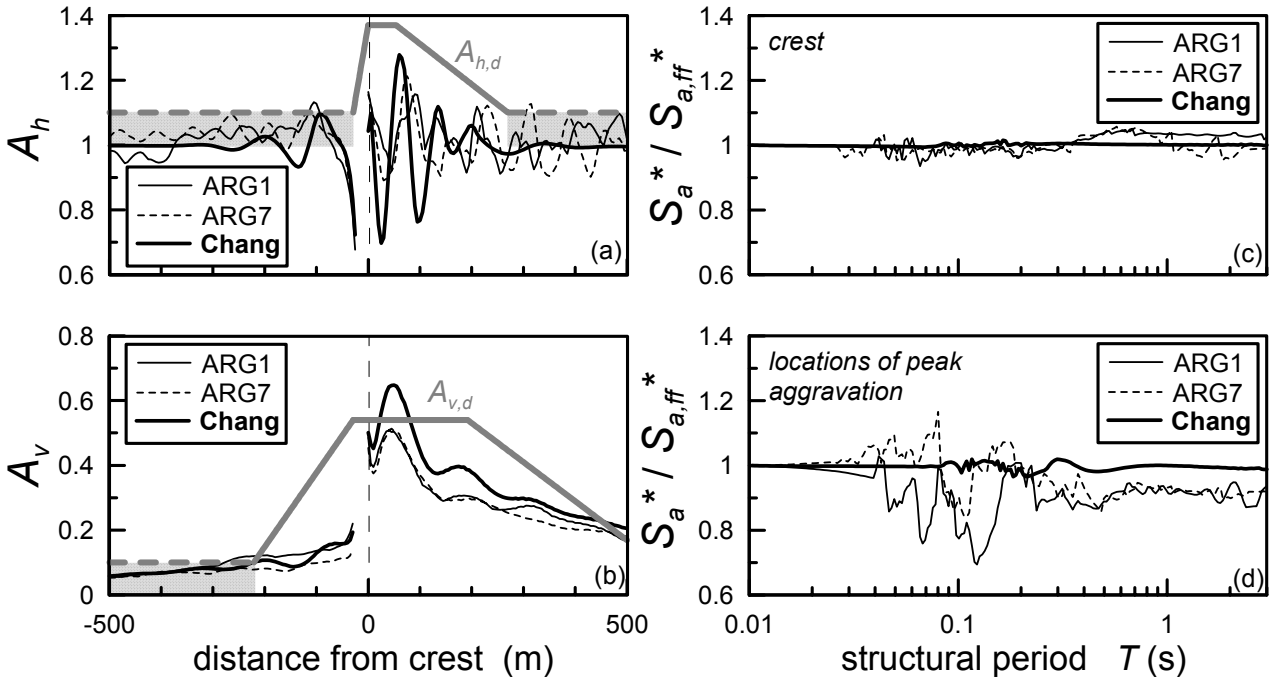

Fig 15: Comparison of topographic aggravation from the proposed approximate relations and numerical analyses with seismic recordings (ARG1 and ARG7) and an equivalent Chang signal.

The comparison of results from the case specific analyses and the approximate relations in terms of the peak amplification of the horizontal motion $A_{h,max}$ and the distance to the free field D_h for the aforementioned case studies is presented in Figure 14, from which a satisfactory agreement is observed. Details on these comparisons are presented by [16].

In addition, a numerical "experiment" was performed, i.e. a slope with H = 50m, i = 60^o consisting of a linear visco-elastic soil with V_S = 500m/s, Poisson's ratio v = 1/3 and mass density ρ = 2Mg/m^3 was subjected to three (3) excitations, two recordings (ARG1 and ARG7) with similar values of T_e = 0.14 – 0.16s and N = 2 – 4.5 and a Chang signal with similar characteristics. Figures 15a and 15b compare the variations of A_h and A_v with distance from the crest resulting from the three (3) numerical analyses to the respective aggravation envelopes $A_{h,d}$ and $A_{v,d}$ from Equations (1) to (6). The results from the three (3) analyses compare well with one another, with the Chang signal analysis being rather conservative. In addition, the results from all three (3) analyses generally fall below the proposed design envelope, with the exception of a small under-prediction of the $A_{v,max}$ but only in the Chang signal analysis.

Furthermore, Figures 15c & 15d present the topographic aggravation of the normalized elastic response spectrum (5% damping) $S_a^* = S_a/a_h$ at two points: a) the crest and b) the location of peak aggravation (where $A_h = A_{h,max}$), disregarding the fact that the locations of peak aggravation do not coincide in the three analyses. These results show that topography seems to affect mostly the peak ground acceleration and less so its frequency content.

CONCLUSIONS & PROPOSED EC-8 CHANGES

The basic conclusions from this study are the following:

(a) Slope topography alters (increases and decreases) mainly the peak acceleration and less so the frequency content of the horizontal seismic motion. In addition, it creates a parasitic vertical motion. These effects are pronounced in the vicinity of the slope and decrease with distance.

(b) Amplification of the horizontal motion is generally expected behind the crest of the slope, while the opposite effect (i.e. de-amplification) is generally expected in front of the toe of the slope. Despite the foregoing trends, intense geographic variability of the (horizontal and vertical) seismic motion is expected, even within tens of meters. Hence, the detection of topography

aggravation effects on the basis of field recordings can only be achieved with very dense arrays.

(c) This paper presents approximate relations for the estimation of the coefficients of topographic aggravation of the peak horizontal and vertical acceleration $A_{h,max}$ and $A_{v,max}$, as well as their relative distances to the free field, D_h and D_v. In addition, a geographic design envelope of topographic aggravation is proposed for the horizontal and vertical motion, $A_{h,d}$ and $A_{v,d}$. Overall, the proposed approximate relations are in satisfactory agreement with analyses of case histories.

(d) Topography aggravation is considered significant only when $H/\lambda > 0.16$ and the slope inclination $i > 17^o$. In such cases, the values of the coefficients of topographic aggravation for the horizontal and vertical seismic motion range from $A_{h,max}$ = 1.20 – 1.50 and $A_{v,max}$ = 0.10 – 1.10, while the distance to the free field ranges from D_{ff} = 2H – 8H.

(e) The only Seismic Codes that deal with topographic aggravation (EC-8 and PS-92) give rational values for the amplification of the horizontal acceleration. Nevertheless, they disregard the generation of parasitic vertical motion and seriously underestimate the distance to the free field. In closure, the criteria of significance of topography effects that the codes prescribe yield rational lower bounds for slope height and inclination, but do not take into account the effects of soil and excitation conditions.

Based on the commentary and comparisons presented above, modifications are proposed to the (Informative) Annex A of EC-8 pertaining to topographic amplification factors. In particular, the following changes (in bold face) are proposed:

A.1 This annex gives some simplified amplification factors for the seismic action used in the verification of the stability of ground slopes **and the design of important structures ($\gamma_I > 1.0$) in the vicinity of ground slopes**. Such factors, **denoted S_{hT} and S_{vT} for the horizontal and vertical directions respectively**, multiply as a scaling factor the ordinates of the **horizontal** elastic design response spectrum given in EN 1998-1:2004. **The resultant design spectra for the horizontal and vertical directions lead to amplified horizontal seismic actions and additional vertical seismic actions (on top of those resulting from the vertical elastic response spectrum given in EN 1998-1:2004.**

A.2 These topographic amplification factors should in preference be applied when the slopes belong to two-dimensional topographic irregularities. **In cases of slopes, these amplification factors may be neglected if the average slope inclination $i < 17^o$ and the height of the slope $H < 0.16\lambda$, where λ is the predominant wavelength of the shear waves in the slope**

a) In slopes that are both higher and steeper than the above lower bounds, the topographic amplification factors vary with location. If x is the horizontal distance from the crest of the slope (where x > 0 behind the crest), the amplification factors are given by:

$$S_{hT} = \left\{ \begin{array}{ll} 1.1 + \dfrac{A_{h,max} - 1.1}{B}(x + B) & , \quad x \le 0 \\ A_{h,max} & , \quad 0 \le x \le 0.2D_h \\ A_{h,max} - \dfrac{A_{h,max} - 1.1}{0.8D_h}(x - 0.2D_h) & , \quad 0.2D_h \le x \end{array} \right\} \ge 1.0$$

$$S_{vT} = \left\{ \begin{array}{ll} 0.1 + \dfrac{A_{v,max} - 0.1}{0.3D_v}(x + B + 0.3D_v) & , \quad x \le -B \\ A_{v,max} & , \quad -B \le x \le 0.3D_v \\ A_{v,max} - \dfrac{A_{v,max} - 0.1}{0.7D_h}(x - 0.3D_v) & , \quad 0.3D_v \le x \end{array} \right\} \ge 0.0$$

where B = $H/\tan i$, $A_{h,max}$ and $A_{v,max}$ the coefficients of topographic aggravation for the horizontal and parasitic vertical motions and D_h and D_v are the distances to the free field behind the crest for the horizontal and parasitic vertical motions, that are given in simplified form by:

$$A_{h,max} = 0.2(H/\lambda)^{0.4}\left(\frac{I^2 + 2I^6}{I^3 + 0.02}\right)$$

$$A_{v,max} = 0.7(H/\lambda)^{0.8}\left(I^{0.5} + 1.5I^{5}\right)$$

$$D_h/H = 2\left[\frac{(H/\lambda)}{(H/\lambda)^2 + 0.2}\right]\left(\frac{I^{1.5} + 3.3I^{8}}{I^{4} + 0.07}\right)$$

$$D_v = 0.7D_h$$

where I = i/90°.

Notice that the remaining provisions of Annex A of EC-8 for *ridges with crest width significantly less than the base width* (A.2.b), for the *presence of a loose surface layer* (A.2.c), the *spatial variation of amplification factor* (A.2.d) and A.3 have not been addressed in this effort.

REFERENCES

[1] Idriss I, Seed HB. Response of earthbanks during earthquakes. *Journal of Soil Mechanics and Foundations Division*, ASCE, 93(SM3), pp. 61–82, 1967

[2] Idriss I. Finite Element analysis for the seismic response of earth banks. *Journal of Soil Mechanics and Foundations Division*, ASCE, 94(SM3), pp. 617-636, 1968

[3] Athanasopoulos GA, Pelekis PC, Xenaki VC. Topography effects in the Athens 1999 earthquake: the case of hotel Dekelia. In: Proc. *4th International Conference on Recent Advances in Geotechnical Earthquake Engineering and Soil Dynamics*, San Diego, March, (in CD-ROM), 2001

[4] Bouckovalas GD, Gazetas G, Papadimitriou AG. Geotechnical aspects of the Aegion (Greece) earthquake. In: Proc. *2nd International Conference on Geotechnical Earthquake Engineering*, Lisbon, June, vol. 2, pp. 739 – 748, 1999

[5] Castellani A, Peano L, Sardella. Seismic response of topographic irregularities. In: Proc. *3rd International Earthquake Microzonation Conference*, Seattle, vol. II, p. 533-540, 1982.

[6] Gazetas G, Kallou PV, Psarropoulos PN. Topography and soil effects in the Ms=5.9 Parnitha Athens earthquake: the case of Adames. *Natural Hazards*, vol. 27, pp. 133-169, 2002

[7] Boore DM, Harmsen SC, Harding ST. Wave scattering from a step change in surface topography. *Bulletin of the Seismological Society of America*, 71(1): 117 – 125, 1981.

[8] Ohtsuki A, Harumi K. Effect of topography and subsurface inhomogeneities on seismic SV waves. *Earthquake Engineering and Structural Dynamics* vol. 11, pp. 441-462, 1983

[9] Ashford S, Sitar N. Analysis of topographic amplification of inclined shear waves in a steep coastal bluff. *Bulletin of the Seismological Society of America*, vol. 87, no. 3, pp. 692-700, 1997

[10] Ashford S, Sitar N, Lysmer J, Deng N. Topographic effects on the seismic response of steep slopes. *Bulletin of the Seismological Society of America*, vol. 87, no. 3, pp. 701 – 709, 1997

[11] Bouckovalas GD, Kouretzis GK. A review of soil and topography effects in Athens 09/07/199 (Greece) earthquake. In: Proc. *4th International Conference on Recent Advances in Geotechnical Earthquake Engineering and Soil Dynamics*, San Diego, March, (in CD-ROM), 2001

[12] Itasca Consulting Group Inc. FLAC: Fast Lagrangian Analysis of Continua. *User's Manual*, 1993

[13] Wong HL, "Effect of surface topography on the diffraction of P, SV and Rayleigh waves", *Bulletin of the Seismological Society of America*, vol. 72, no. 4, pp. 1167 – 1183, 1982.

[14] Geli L, Bard PY, Jullien B. The effect of topography on earthquake ground motion: a review and new results. *Bulletin of the Seismological Society of America*, vol. 78, no. 1, pp. 42 – 63, 1988

[15] PS-92. Règles de construction parasismique: Règles PS applicables aux bâtiments. *Normes NF P 06-013*, Troisième Tirage, 1999

[16] Bouckovalas G. D. and Papadimitriou A. G. (2005), "Numerical evaluation of slope topography effects on seismic ground motion". *Soil Dynamics and Earthquake Engineering*, 25 (7-10): pp. 547 – 558

Numerical study of the topography effects at the Nicastro (Southern Italy) cliff and comparison with EC8 recommendations

A. Pagliaroli, G. Lanzo, B. D'Elia

Dipartimento di Ingegneria Strutturale e Geotecnica, Università di Roma "La Sapienza", Rome, Italy

Abstract

Seismic amplification of ground motion due to topographic effects at the Nicastro cliff (Calabria, Southern Italy) is investigated. Linear 2D numerical analyses are carried out on representative cross-sections using FLAC finite difference computer code. Additionally linear 1D analyses accounting only for stratigraphic effect are also carried out. A topographic amplification factor at the crest is then obtained taking the ratio of 2D over 1D horizontal peak acceleration and Fourier spectrum. The calculated amplification factors are compared with those recommended by EC8.

INTRODUCTION

It is well recognised that ground motion amplification occurring during earthquakes in a soil deposit with plane ground level resting on horizontal bedrock is mainly affected by the stratigraphic profile and by the physical-mechanical soil properties. This so called "stratigraphic" amplification is associated with phenomena such as trapping of body waves and interference between trapped and incoming waves (resonance). The stratigraphic amplification is nowadays routinely modelled through numerical one-dimensional (1D) analyses and can provide accurate results if both the geotechnical model of the soil deposit and a representative reference input motion at the outcropping bedrock are available.

Seismic amplification of ground motion can be also associated with the surface topography. The physical phenomena responsible for amplification are the focusing of seismic waves as well as the diffraction of body and surface waves propagating downwards and outwards the topographic feature. The effects related to these 2D phenomena are indicated as "topographic" amplification.

Limited case-histories of topographic amplification referring to past (Friuli, Italy, 1976; Irpinia, Italy, 1980) and more recent (e.g. Northridge, USA, 1994, Aegion, Greece, 1995, Athens, Greece, 1999) earthquakes are available in the literature. The related topographic effects are mainly reported as macroseismic observations (e.g. has been documented that buildings located at hill tops suffered more damages than those located at the base) while only few instrumental data are available.

Quantification of topographic amplification is a very difficult issue as it depends from many factors among which one of the most important is the coupling between stratigraphy and topography. Usually, the main difficulty arises from the insufficient knowledge of the geological and geotechnical site characteristics which renders problematic to separate stratigraphic from topographic effects. Besides, especially for the experimental studies, the difficulty of finding a reference station free of site effects (i.e. located on an unweathered and horizontal outcropping bedrock) can further complicate the quantitative evaluation of topographic amplification. These above mentioned difficulties probably explain the quantitative differences between theoretical predictions and observed topographic amplifications.

Conventionally, in the numerical studies, topographic amplification can be estimated through the ratio of 2D (accounting for both stratigraphic and topographic effects) over 1D (depending only on stratigraphic effects) seismic motion parameters. Usually this ratio is calculated in terms of peak acceleration (Ashford and Sitar, 1997; Rathje and Bray, 2001), Fourier (Kallou et al., 2001; Assimaki and Gazetas, 2004) or acceleration response spectra (Bouckovalas and Kouretzis, 2001). In frequency domain this ratio has been defined

as the “topographic aggravation factor” (TAF).

The inherent difficulties in quantifying the amplitude of topographic amplification explains why the incorporation of these effects in seismic codes is usually overlooked. Only AFPS (1995) and EC8 (2003) provide some recommendations. In particular EC8 incorporates surface topography via the soil parameter S_T variable between 1.2 and 1.4 depending on the slope angle and the topographic feature. Typically, for mean slope angles <15° the topography effects can be neglected. For isolated cliffs and slopes, near the top edge $S_T \geq 1.2$ is recommended. For ridges with crest width signficantly less than the base and slope height H>30 m, the recommended values are $S_T \geq 1.2$ and $S_T \geq 1.4$ for mean slope angle exceeding 15° and 30°, respectively. The highest values apply near the top of the slopes while the amplification factor can be assumed to linearly decrease towards the base, where it becomes unity. The suggested amplification factors are increased by at least 20% in case of an existing surficial zone more than 5 m thick. Comparisons between topographic amplification factors by EC8 and those calculated from numerical and analytical studies can be found, among others, in Paolucci (2002) for ridges and cliffs, Pitilakis et al. (2005) and Klimis and Anastasiadis (2002) for slope- and canyon-like topography, respectively.

The present study aims to quantitatively investigate the topographic amplification by means of 2D numerical analyses of the seismic response of the Nicastro cliff (Southern Italy). The topographic amplification factors estimated by the numerical analyses are compared to those suggested by EC8.

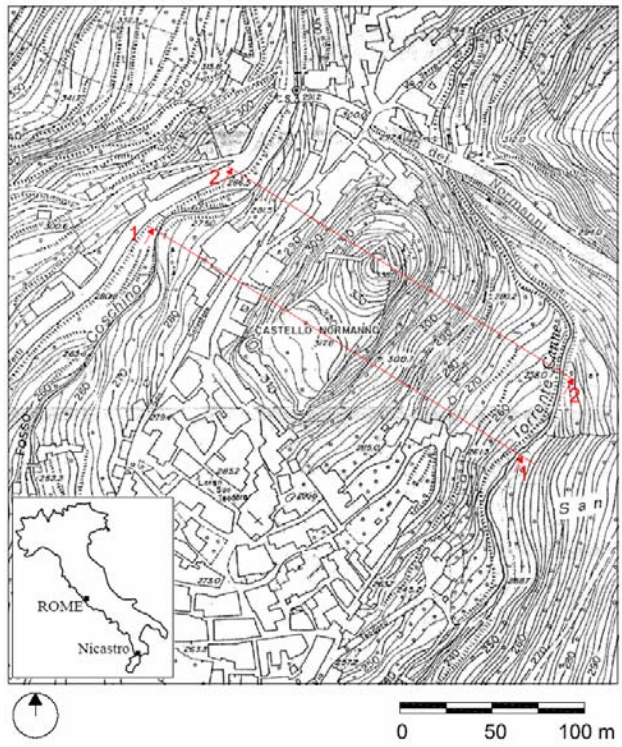

Fig 1: Plain view of Nicastro and picture of the upper part of the cliff taken from North.

SITE DESCRIPTION AND SUBSOIL CHARACTERISATION

Nicastro cliff is located in Calabria (Southern Italy), one of the most active seismic region of the Mediterranean area. The cliff is elongated in the NE-SW direction, about 60 m high; the width at the crest varies between 30 and 60 m moving from NE to SW while it is about 200 m at the base (Fig. 1). The ridge flanks are quite irregular with slope angles varying generally between 20° and 50° and almost subvertical in the northern part of the cliff. On the crest lie the remains of the ancient Norman castle, which is 100 m long and 20 to 55 m wide. The castle was built in the period 1100-1500 and was severely damaged during the two strong earthquakes of 1638 and 1783. In the last 200 years the castel was completely abandoned and only recently has been subjected to consolidation works.

From 1998 to 2003 several geotechnical in situ surveys have been conducted. Altogether 31 boreholes have been carried out reaching a maximum depth of about 40 m below ground level. Further, five refraction seismic profiles

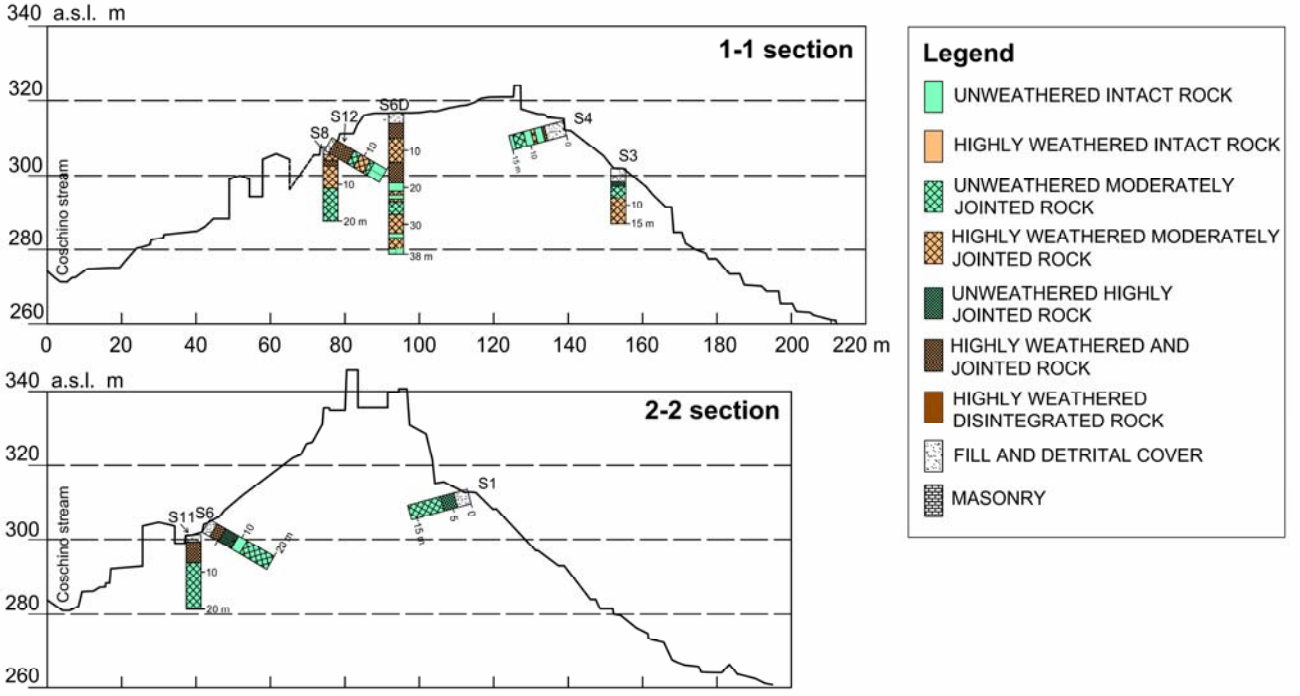

Fig 2: Cross-sections 1-1 and 2-2 of the Nicastro cliff.

and two down-hole tests have been performed.

The cliff is constituted by metamorphic rocks, characterised by extremely variable degree of weathering and jointing which strongly affect the mechanical behaviour of the cliff.

In Fig. 2 the cross sections 1-1 and 2-2 (see Fig. 1) are reported together with the stratigraphic profiles obtained from the boreholes located along the sections. By examining all the available profiles, seven types of rocky material have been identified, characterized by different degree of weathering and jointing, as displayed in the legend of Fig. 2. It can been seen that the material ranges from unweathered intact rock to highly weathered disintegrated rock. Locally the cliff is covered by fill or debris material mainly made of gravel in a silty matrix, characterised by a maximum thickness of 5 m. Although the identified rock types appear extremely variable even at small distances, it is possible to recognise some sufficiently homogeneous “macro-zones” constituting the cliff. Finally, the shear wave velocity profiles obtained from the down-hole tests are reported in Fig. 3. These test were carried out in the boreholes S3D, located about 50 m north of 2-2 cross-section, and S6D, located in correspondance of the 1-1 cross-section.

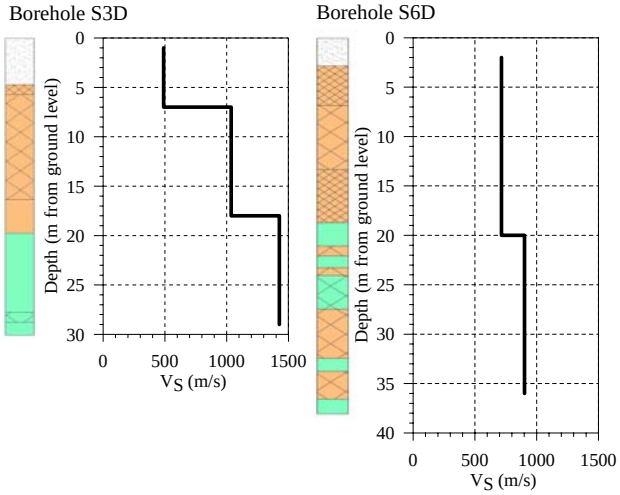

Fig 3: Estimated shear wave velocity profiles from down-hole tests.

SEISMOTECTONIC OUTLINES AND SELECTED INPUT MOTION

Calabria in the past has been struck by the most catastrophic earthquakes ever occurred in Italy. In fact, as documented by historical sources, at least 19 earthquakes with magnitude (M) greater than 6 occurred since 91 b.C. The strongest events are the 1783 seismic sequence (M=5.1-7.1), the 1905 Monteleone (M=7.5) and the 1908 Messina (M=7.3) earthquakes. In the Nicastro area, the most distructive event is the earthquake of

March 27, 1638 (M=7.1) which produced a local macroseismic intensity I = XI MCS.

For evaluating a reference rock outcropping motion for seismic response analyses, the study of the historical seismicity of Nicastro and of the seismotectonic outlines of the region was carried out. The historic seismicity of the area was characterised by the construction of a seismic catalogue which reports the intensities felt at the site or estimated through attenuation relationships. The epicentral intensities of these historical events are depicted in Fig. 4. Then the seismotectonic study led to the identification of the main regional seismogenic sources, characterised in terms of maximum potential magnitude and distance from Nicastro. In Fig. 4 the main sesimogenic areas and the active fault systems are illustrated.

Two controlling *near-field* and *far-field* seismogenic zones were identified, characterised by the following minimum source-to-site distance, D, and maximum historically observed magnitude M_{max} : D = 10 km and M_{max} = 7.1 km (*near-field* - seismogenic area #4); D = 100 km and M_{max} = 7.3 (*far-field* - seismogenic area #6). Following a deterministic approach, using the attenuation relationships by Ambraseys and Douglas (2003) and Ambraseys et al. (1996) for the *near-field* and *far-field* conditons respectively, the expected ground motion parameters at outcropping rock were estimated. It resulted PGA= 0.35g and PGA= 0.04g for the *near-field* and *far-field* conditons respectively. The corresponding acceleration response spectra (mean and mean ± standard deviation) are illustrated in Fig. 5. In the same figure the response spectra of several *free-field* rock outcropping accelerograms, selected from european and world-wide databases matching the required M_{max} and D values, if necessary scaled to the expected PGA, are illustrated.

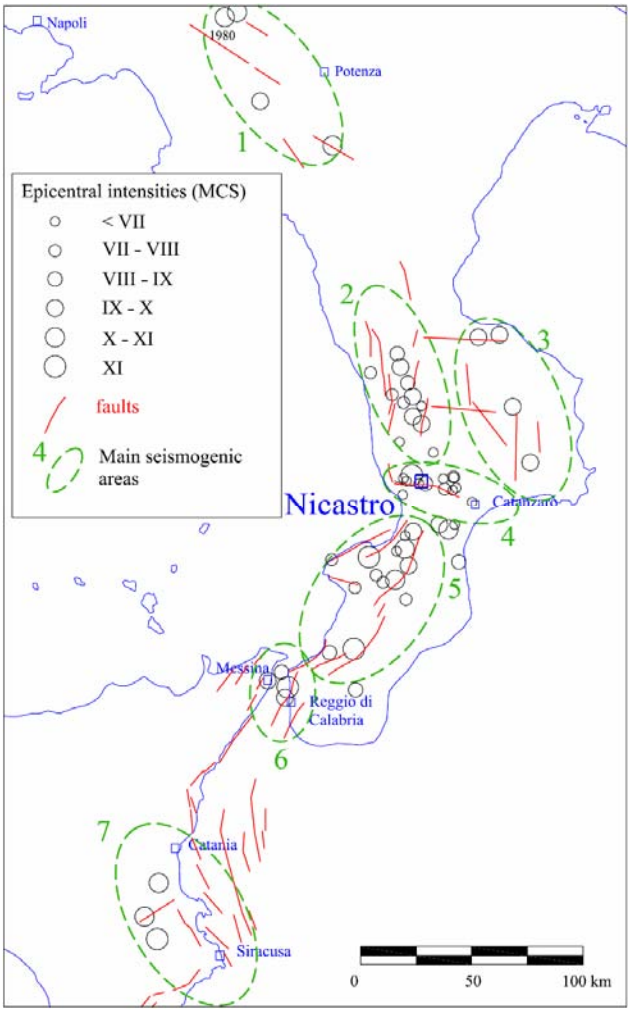

Fig 4: Principal historical seismic events and main seismogenic sources in the studied region.

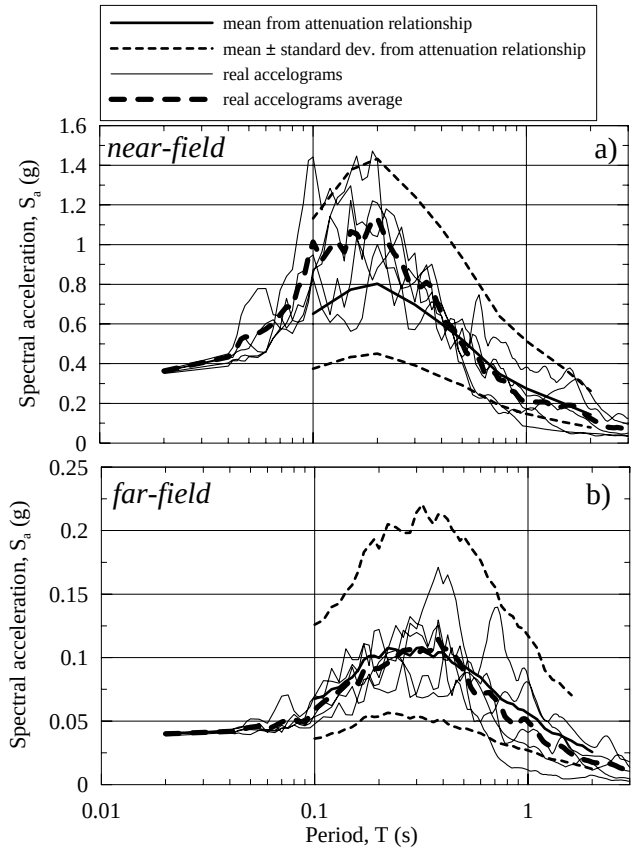

Fig 5: Real accelerograms selected for (a) *near-* and (b) *far-field* conditions.

NUMERICAL ANALYSES

Numerical analyses were carried out by the dynamic option of FLAC finite difference computer code (Itasca, 2002). The input motion was applied at the base of the model as vertically incident SV waves. Wave reflection at model boundaries were minimised by specifying free-field conditions at the sides of the mesh and viscous boundaries at the bottom. Only linear analyses were performed; this latter hypothesis can be considered a satisfactory approximation of material behaviour take into account its high stiffness.

The dynamic response of the cliff was investigated for both sections, characterised by different morphological and stratigraphic conditions. The shape ratio H/L (where H is the average cliff height and L is the half-width at the base) is equal to 0.55 and 0.8 for cross-sections 1-1 and 2-2, respectively. Further, cross-section 2-2 is characterised by stiffer material with respect to 1-1 section, as it is apparent from Fig. 3.

In order to obtain preliminary physical insights on the bi-dimensional phenomena affecting the dynamic response of the cliff, a simple homogeneous model was examined first. A more realistic heterogeneous model was then analysed. Results of the numerical analyses for both the homogeneous and heterogeneous models are presented hereafter.

Homogeneous model

Numerical results are shown only for the stiffest and steepest cross-section 2-2, characterised by an average height H=70 m and an average width at the base 2L= 180 m. As representative values of the main physical and mechanical properties of the rocky material constituting the cliff, it was assumed γ =26 kN/m^3, V_S=1200 m/s, ν=0.25 and D_0=0.4% (being D_0 the small-strain damping ratio). For the half-space beneath the cliff, the same properties were assigned.

The horizontal peak acceleration (a_{max}) surface profile, for one of the selected *near-field* accelerogram, is displayed in Fig. 6a. Anyway, similar results were also obtained for the others selected input motions. The a_{max} values are normalised with respect to the peak acceleration at outcropping half-space (a_{out}). The ratio $A_T = a_{max}/a_{out}$ can be considered as a measure of topographic amplification in time

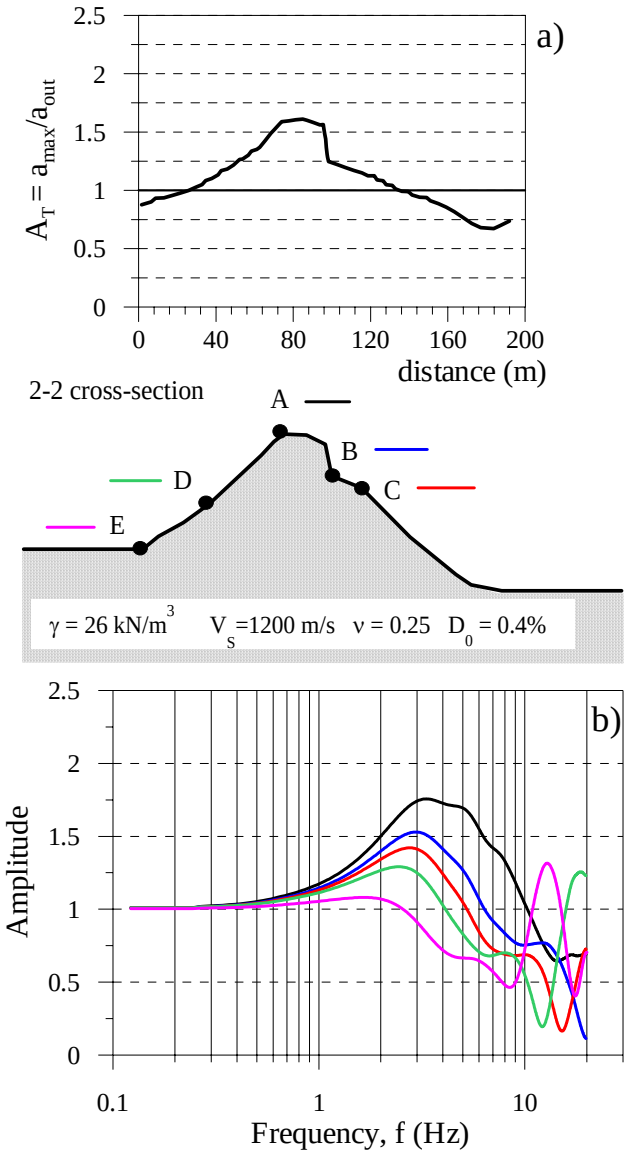

Fig 6: Homogeneous model for 2-2 cross-section: (a) horizontal peak acceleration surface profile and (b) transfer functions at several nodes along the surface.

domain. It is clearly seen in the figure that the horizontal peak acceleration increases from the base to the crest of the cliff: at the toe the motion is deamplified with respect to the outcropping bedrock ($A_T \approx 0.7$ on the right side) while at the crest the maximum amplification ($A_T \approx 1.6$) is attained.

In Fig. 6b the transfer functions at different nodes along the section are shown. These functions, that represent an estimate of topographic amplification in the frequency domain, were obtained by taking the ratio of smoothed Fourier spectra of output and input motions. The amplification occurs essentially in

the frequency range 2-7 Hz. These frequency values correspond to incident wavelength λ comparable with the cliff width 2L. In fact, for V_S=1200 m/s and 2L=180 m, it results 2L/λ =0.3-1.0. As far as the amplitude of spectral amplification is concerned, it increases moving from the base to crest, reaching a maximum value of 1.75 at the crest. A clear peak at about 3-4 Hz appears in the transfer functions at the cliff crest (nodes A, B and C in Fig. 6). This peak corresponds to the fundamental frequency of vibration (f_{2D}) of the cliff estimated by the Rayleigh method applied to homogeneous triangle-shaped asymmetric ridges (Paolucci, 2002):

$$f_{2D}= f_{SV} V_S/(2L) \quad (1)$$

where f_{SV} is a factor usually variable between 0.6 and 1.0 according to geometric features of the cliff and the Poisson ratio. In fact, for 2L=180 m and V_S=1200 m/s, equation (1) yields f_{2D}=4-6 Hz. Therefore, topographic amplification can be interpreted as a bi-dimensional resonance phenomenon.

Heterogeneous model

The geotechnical model for the heterogeneous case was constructed subdividing the cliff in homogeneous macro-zones. Three different macro-zones were considered, i.e., from bottom to surface: moderately weathered and jointed rock, moderately weathered and highly jointed rock, highly weathered and jointed rock. In addition, only for cross-section 1-1, a detrital cover was also considered in the geotechnical model. The physical and mechanical material properties are reported in Table 1.

The representative finite difference meshs for both cross-sections are shown in Fig. 7. In the same figure the horizontal peak acceleration surface profiles for all the selected input motions are illustrated. As the homogeneous case, a_{max} was normalized with respect to the peak value at the outcropping bedrock. For both cross-sections the amplification of horizontal peak acceleration increases from the base to the crest of the cliff, with maximum values at the crest generally between 2 and 2.5. As expected, these values are greater than those calculated for the homogeneous model because of the stratigraphy effect. In order to evaluate the magnitude of the stratigraphic amplification, 1D analyses for the vertical columns corresponding to two representative nodes at the crest of the cliff (node 1A and 2A for cross-sections 1-1 and 2-2 respectively in Fig. 7) were carried out.

In time domain topography effect was then evaluated through the 2D over 1D ratio of horizontal peak acceleration. The resulting topographic amplification factor A_T is about 1.5 and 1.9 for cross-sections 1-1 and 2-2, respectively. These values are an average of the amplification factors calculated for all the selected *near-field* and *far-field* accelerograms. Further, it can be noted that the topographic amplification for the heterogeneous case is almost 15% higher than that calculated for the homogeneous one.

In the frequency domain the topographic amplification was estimated by TAF, calculated in terms of smoothed 2D over 1D Fourier spectra ratio at the above mentioned nodes 1A and 2A for all the selected input motions (Fig. 8). It can be noted that the input motion does not affect the variation of TAF with frequency. The maximum spectral amplification occurs between 3-5 Hz for both sections, therefore essentially at the same frequency as it was found for the homogeneous model. The amplitude of spectral amplification is about 1.8 and 2.5 for sections 1-1 and 2-2 respectively; therefore, the maximum spectral amplification is about 30% higher than that corresponding to the homogeneous case.

This quantitative discrepancy can be explained by the difficulty in fully uncoupling stratigraphic from topographic effects and by the more complex wave field in a heterogeneous subsoil with respect to a homogeneous one.

Table 1: Heterogeneous model: physical and mechanical material properties.

Material	γ (kN/m^3)	ν	V_S (m/s)	D_0 (%)
cover	21	0.35	350	1
highly weathered and jointed rock	23	0.25	700	1
moderately weathered, highly jointed rock	24	0.25	900 - 1000	0.4
moderately weathered and jointed rock	26	0.25	1200	0.4
bedrock	27	0.25	1500	0.1

Finally, it seems that TAF is capable of capture the main features of topographic amplification, from qualitative and quantitative point of view. In other words, TAF allows the estimation of the order of magnitude of topographic amplification and frequency at which maximum occurs.

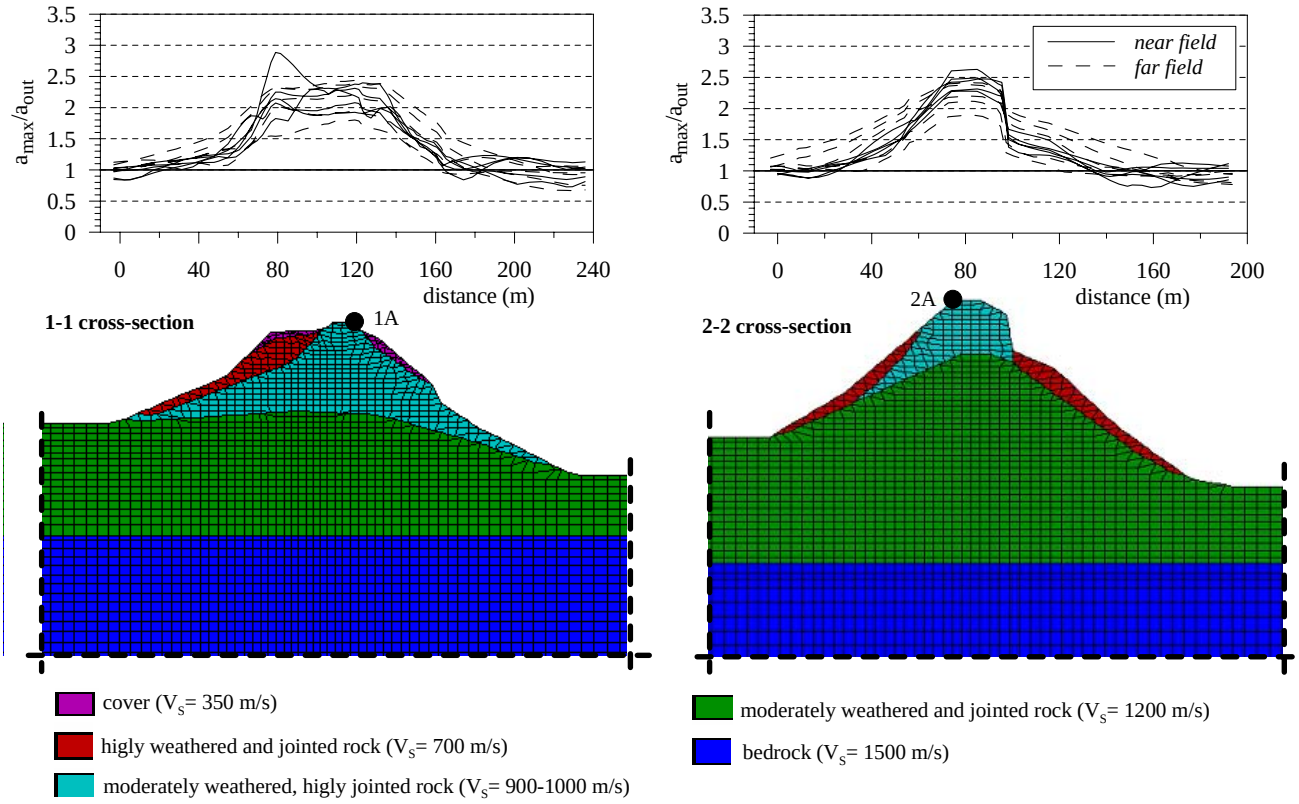

Fig 7: Normalised horizontal peak accelerations computed at the surface of cross-sections (a) 1-1 and (b) 2-2 for the *near-field* and *far-field* input motions.

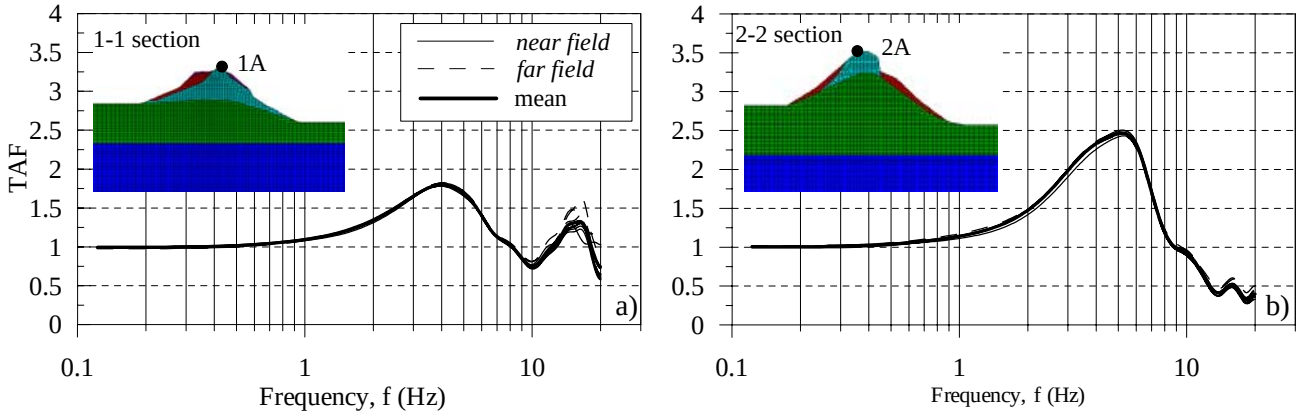

Fig 8: Topographic aggravation factor (TAF) computed at the crest of cross-sections (a) 1-1 and (b) 2-2 for the *near-field* and *far-field* input motions.

COMPARISON OF TOPOGRAPHIC AMPLIFICATION FACTORS CALCULATED IN THIS STUDY WITH THOSE OBTAINED FROM LITERATURE AND SUGGESTED BY EC8

Topographic amplification factors derived from numerical and analytical studies available in literature were compiled and analysed (Pagliaroli, 2006). Both ideal and real isolated cliffs and ridges subjected to SH and SV waves with variable incident angle were considered. The gathered data refer to surface points in which maximum topographic amplification occurs (usually at the crest of the topographic feature). Most of the studies concern homogeneous models while only few cases assuming heterogeneous subsoils are available. In this latter case topographic amplification was computed as the ratio between 2D and 1D analyses results, as done in the present study. Further, amplification factors estimated using a reference station affected by topographic effects (e.g., base of the ridge) were also excluded from the collected data.

These topographic amplification factors are reported in Figg. 9a and 9b in terms of horizontal peak acceleration and peak spectral values, respectively, as a function of the shape ratio H/L. The data were plotted with different symbols depending on the type of incidence wave (SH or SV) and on the geometry of the problem (2D or 3D). Most data points refer to incident SH waves while only few data are available for SV waves and 3D analyses. It is also apparent from the figure that data referring to spectral ratios are more limited and scattered (Fig. 9b). A linear regression analysis of the data was carried out and the resulting lines are plotted in Fig. 9 (dashed line). In Fig. 9a the analytical solution by Sanchez-Sesma (1990) for a triangular shaped ridge subjected to incident SH waves is also plotted as continuos line and satisfactory approximates the whole set of data.

The topographic amplification factors S_T suggested by EC8 for ridges with crest width significantly less than the base width are also displayed in Fig. 9. It can be observed that S_T changes sharply from 1.2 to 1.4 for a shape ratio H/L corresponding to 30° slope angle (H/L=0.58). It can be noted that the amplification factors suggested by EC8 fall at the lower bound of the literature data.

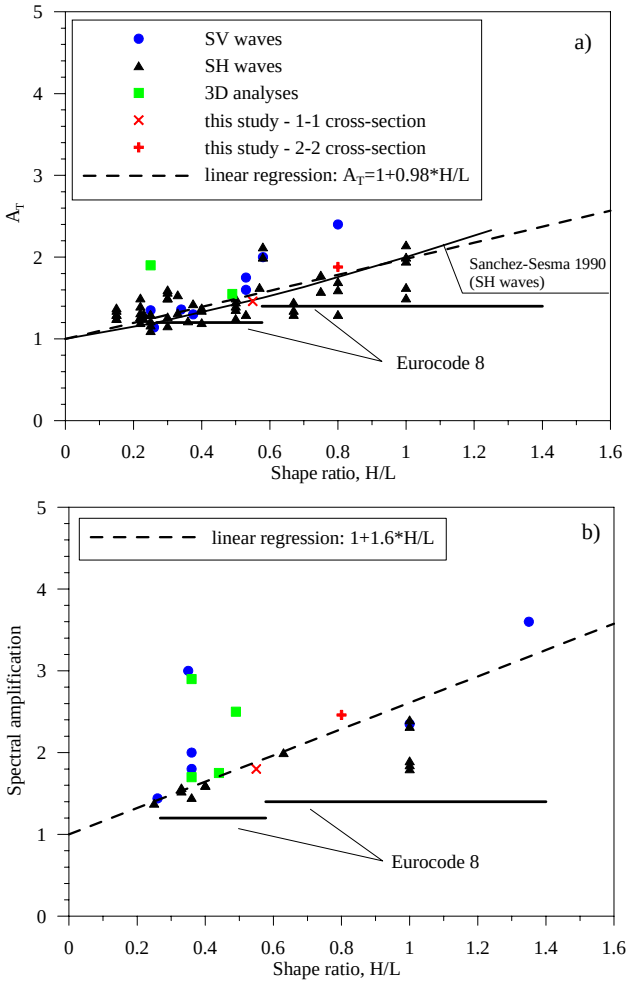

Fig 9: Topographic amplification as a function of shape ratio H/L in terms of (a) horizontal peak acceleration and (b) spectral values.

For comparison, in Fig. 9 the topographic amplification factors obtained in this study at the crest nodes 1A and 2A are also plotted. As it is clearly seen, data are located in correspondence of the average values of the literature data range and therefore above those by EC8. In particular, the topographic amplification factors A_T obtained for the Nicastro hill are about 25% and 35% higher than the EC8 recommended values for section 1-1 and 2-2, respectively (Fig. 9a). Greater differences are observed if the comparison is made with reference to spectral values (Fig. 9b).

CONCLUSIONS

Seismic amplification of ground motion due to topographic effects was investigated through the comparison between 2D and 1D numerical analyses. These analyses were carried out on

two representative cross-sections of the Nicastro cliff (Southern Italy).

It was found that amplification occurs for wavelengths comparable with the cliff base width; it was also found that resonance dominates the frequency response, i.e. the peak spectral amplification occurs at the 2D fundamental frequency of vibration of the whole cliff, calculated as suggested by Paolucci (2002).

Surface topography at the crest may amplify the horizontal motion. It has been found that topographic amplification factors in terms of peak acceleration can be 25% to 35% higher than the values suggested by EC8. These underestimation is even greater if the comparison is made in terms of spectral values. This is expected considering that the EC8 values are frequency independent and therefore they do not take into account that topographic amplification is band-limited and usually occurs at the fundamental frequency of vibration of the ridge.

REFERENCES

AFPS'95 (1995) "Recommandations pour la redaction de regles relatives aux ouvrages dans les regions sujettes aux seismes" .

Ambraseys, N. N., Simpson, K. A., and Bommer, J. J. (1996) "Prediction of horizontal response spectra in Europe" *Earthquake Engineering Structural Dynamics*, Vol. 25, pp. 371-400.

Ambraseys, N. N., and Douglas, J. (2003) "Near-field horizontal and vertical earthquake ground motions" *Soil Dynamics and Earthquake Engineering*, Vol. 23, pp. 1-18.

Ashford, S. A. and Sitar, N. (1997) "Analysis of Topographic Amplification of Inclined Shear Waves in a Steep Coastal Bluff" *Bulletin of the Seismological Society of America*, Vol. 87, pp. 692-700.

Assimaki, D., and, Gazetas, G. (2004) "Soil and topographic amplification on canyon banks and the 1999 Athens earthquake" *Journal of Earthquake Engineering*, Vol. 8, pp. 1-43.

Bouckovalas, G. D., and Kouretzis, G. (2001) "Review of soil and topography effects in the September 7, 1999 Athens (Greece) earthquake" *Proc. of 4th Int. Conf. on Recent Advances in Geotechnical Earthquake Engineering and Soil Dynamics*, San Diego, California.

Eurocode 8 (2003) "Design Provisions for arthquake Resistance of Structures — Part 5: Foundations, retaining Structures and Geotechnical Aspects" ENV 1998-5, CEN European Committee for Standardisation, Brussels.

Itasca (2002) "FLAC – Fast Lagrangian Analysis of Continua – Version 4.0" *User's Guide*, Itasca Consulting Group, Minneapolis, USA.

Kallou, P.V., Gazetas, G., and Psarropoulos, P.N. (2001) "A case history on soil and topographic effects in the 7th September 1999 Athens earthquake" *Proc. of 4th Int. Conf. on Recent Advances in Geotechnical Earthquake Engineering and Soil Dynamics*, San Diego, California.

Klimis, N. S. and Anastasiadis, A. J. (2002) "Comparative Evaluation of Topography Effects via Code Recommendations and 2-D Numerical Analysis" *12th European Conference on Earthquake Engineering*, Barbican Centre, London, UK.

Paolucci, R., (2002) "Amplification of earthquake ground motion by steep topographic irregularities" *Earthquake Engineering and Structural Dynamics*, Vol. 31, pp. 1831-1853.

Pagliaroli, A. (2006) "Studio numerico e sperimentale dei fenomeni di amplificazione sismica locale di rilievi isolati" *Ph.D. Thesis*, Università di Roma "La Sapienza", Roma, in italian (in press).

Pitilakis, K., Ktenidou O.-J., Apostolidis, P., Raptakis, D., Manakou, M., Makropoulos, K. and Diagourtas, D. (2005) "Experimental and theoretical studies of topographic effects" *Proc. 16th ICSMGE*, Osaka, Japan, pp. 175-182.

Rathje, E.M., and Bray, J.D. (2001). "One- and two-dimensional seismic analysis of solid-waste landfills" *Canadian Geotechnical Journal*, Vol. 38, pp. 850-862.

Sanchez-Sesma, F. J. (1990) "Elementary solutions for response of a wedge-shaped medium to incident SH and SV waves", *Bulletin of the Seismological Society of America*, Vol. 80, pp. 737-742.

Pseudo-static and pseudo-dynamic gravity wall design according to Eurocode 8

A.L. Simonelli

University of Sannio, Benevento, Italy

Abstract

The aim of the paper is to compare the results of the EC8 pseudo-static and pseudo-dynamic gravity wall design, with those obtained by the pseudo-static approach of the pre-existing Italian seismic code (D.M. 16.1.1996). First the criteria are outlined for assessing seismic actions on the ground according to the European code (EC8), and for determining the actions on retaining walls. Hence four retaining walls designed according to the D.M. 96 have been verified by means of two EC8 approaches, the pseudo-static analysis and a more accurate pseudo-dynamic one, with the acceleration values provided by the recent Italian OPCM 3274 normative. The comparisons give rise to interesting results: the D.M. 96 and the EC8 pseudo-static analyses provide very different designs, while the EC8 pseudo-dynamic approach gives results congruent with those by D.M. 96. This evidence suggests that more work has to be done in defining the parameters and coefficients to be entered in the EC8 pseudo-static procedure.

INTRODUCTION

The objective of the paper is the evaluation of the effectiveness of the gravity retaining wall design methods suggested by Eurocode 8 (alias EC8). At this aim, the comparison between the pseudo-static and pseudo-dynamic EC8 approaches and the traditional Italian pseudo-static design (D.M. LL.PP. 16.1.96, alias D.M.96) has been performed. In a previous paper (Simonelli, 2003) the comparison between the D.M.96 and EC8 pseudo-static approaches was carried out. Recently other pseudo-static analyses have carried out and the comparison with the first results obtained by means of a pseudo-dynamic approach have been illustrated (Simonelli and Lafratta, 2005). This paper is just an extended version of the latter, since the results of the pseudo-dynamic analyses for all the seismic areas of the Italian country are shown, and the relevant design charts are drawn.

A major difference between the two codes consists in the evaluation of seismic actions, because according to the Italian D.M.96 they are related to the observed macroseismic Intensity, while according to EC8 they are related to the values of the maximum accelerations expected at the ground surface.

The two following paragraphs are devoted to the illustration of EC8 ground seismic actions (*EN1998-1, FINAL DRAFT*, December 2003), and to the retaining structures (*EN1998-5, FINAL DRAFT*, December 2003). The last paragraph deals with the application of EC8 criteria to retaining wall design, and the comparison with the traditional national design.

EUROCODE 8 – PART 1: EVALUATION OF SEISMIC ACTIONS

In the past, the Italian codes have classified the seismic areas into three categories (I, II and III) characterised by different degrees of seismicity (12, 9 and 6) to which there correspond the so-called seismic C coefficients, equal to 0.1, 0.07 and 0.04 respectively; a large part of the territory has not been recognised as seismic area. The classifications have always been based on maps of macro-seismic Intensity, derived from the observation of the effects induced by past earthquakes on the

physical environment, on buildings and on people. The role played by the "local" soil conditions has been taken into account through the so-called foundation coefficient ε, that increases seismic actions by 30% only in the case of alluvial deposits of thicknesses varying between 5 and 20 m, overlying stiff soils or rocks.

The Eurocode approach in assessing the seismicity of a given area is completely different, since the earthquake phenomenon is observed "from below" and "*a priori*", instead of "from above" and "*a posteriori*" (Simonelli, 2004). In fact the seismic actions are related to the value of the *reference peak ground acceleration* a_{gR}, which is the maximum acceleration of the seismic motion expected on a stiff outcropping formation (later defined as ground type A), at the end of the travel path of the seismic waves from the source (hypocentre) to the site (Fig. 1), but before the seismic input produces any damage to whatever lies on the surface.

The peak acceleration is determined with reference to two levels of earthquakes, characterised by very different return periods (Eurocode 8-Part 1, alias EC8-1): a severe phenomenon, with a low probability of excess during the time-life of the structure, for which no collapse requirements have to be verified; a much less severe earthquake, with a higher probability of excess, for which damage limitation requirements have to be verified. The Eurocode suggests as severe earthquake the one characterised by a 10% probability of excess in a 50-year period (conventional structure time-life), with a return period T_{NCR} of 475 years.

Moreover the amplification of the seismic motion due to the local soil conditions is taken into account by identifying 7 different types of subsoil (see Table 1), on the basis of the nature of the soils and some specific parameters of mechanical behaviour. For the first 5 types (A to E *ground types*) an amplification factor of the acceleration a_{gR} is given, named *soil factor S*, whose values vary from 1.0 to 1.4 going from the stiffer subsoil (type A) to the less stiff one (type E); for any kind of subsoil, the ground surface acceleration is the product of a_{gR} times *S* (see Fig 1). For the same 5 subsoil types (A to E), characteristic values of reference periods of the site response spectra are also given. On the other hand, for the remaining two *ground types* (S_1 and S_2), characterised by very low mechanical properties, no indications are given but specific amplification studies are required. Eurocode 8 does not provide the values of the expected ground accelerations, which vary among the EU countries, and have to be defined locally.

In Italy a seismic zonation of the peak acceleration expected on a stiff subsoil, with reference to the severe earthquake (T_{NCR} = 475 years), has been acknowledged by the Italian Presidency of the Council of Ministers with Decree n. 3274 dated 20th March 2003 (henceforth referred to succinctly as OPCM 3274) and published in G.U. n. 105 dated 8.5.2003.

The same OPCM 3274 has also edited a new seismic normative, still in progress, which is substantially derived from Eurocode8, Part 1 and Part5.

In this context of continuous evolution of seismic design normative proposals, the Italian Geotechnical Association (AGI) has formed a scientific committee, that in about one year has produced a wide guideline document on geotechnical aspects in earthquake design (AGI, 2005).

EUROCODE 8 - PART 5, CH.7 : EARTH RETAINING STRUCTURES

Retaining structures are dealt with in Ch. 7 of Eurocode8-Part 5 (alias EC8-5); a detailed comment on the whole chapter is given in Simonelli (2004). Here it is worthwhile reminding what is stated in the beginning (ch. 7.1 "General requirements", clause (2)): "Permanent displacements, in the form of combined sliding and tilting, the latter due to irreversible deformation of the foundation soil, may be acceptable if it is shown that they are compatible with functional and/or aesthetic requirements". This concept is very important, and will be taken into account later in the evaluation of the seismic action on the structure.

The methods of analysis are dealt with in Ch. 7.3, and it is stated that: "Any established method based on the procedures of structural

Table 1: Ground types of Eurocode 8

Ground Type	Description of stratigraphic profile	Parameters		
		$v_{s,30}$ (m /s)	N_{SPT} (blows / 30cm)	c_u (kPa)
A	Rock or other rock-like geological formation, including at most 5 m of weaker material at the surface	> 800	-	-
B	Deposits of very dense sand, gravel, or very stiff clay, at least several tens of m in thickness, characterised by a gradual increase of mechanical properties with depth	360 – 800	> 50	> 250
C	Deep deposits of dense or medium-dense sand, gravel or stiff clay with thickness from several tens to many hundreds of m	180 – 360	15 - 50	70 - 250
D	Deposits of loose-to-medium cohesionless soil (with or without some soft cohesive layers), or of predominantly soft-to-firm cohesive soil	< 180	< 15	< 70
E	A soil profile consisting of a surface alluvium layer with v_s values of type C or D and thickness varying between about 5 m and 20 m, underlain by stiffer material with v_s > 800 m/s			
S_1	Deposits consisting – or containing a layer at least 10 m thick – of soft clays/silts with high plasticity index (PI> 40) and high water content	< 100 (indicative)	-	10 – 20
S_2	Deposits of liquefiable soils, of sensitive clays, or any other soil profile not included in types A – E or S_1			

and soil dynamics, and supported by experience and observations, is in principle acceptable for assessing the safety of an earth retaining structure" (Ch. 7.3.1, clause (1)P). Nevertheless, after this foreword, particular attention is devoted to the pseudo-static analysis, regarded as the main simplified method (Ch. 7.3.2).

Simplified methods: pseudo-static analysis

The procedure based on the pseudo-static analysis is quite articulate (as illustrated in Simonelli, 2004); here only the main features are recalled. The pseudo-static method is based on the well-known theory of Mononobe (1929) and Okabe (1926). Pseudo-static seismic actions both in the horizontal and vertical directions are taken into account. As for the vertical action, this may act both upwards and downwards.

The total design thrust E_d, which is the thrust affected by the partial safety factors (see *EN 1997-1 – Geotechnical Design*, 2003, alias EC7), is given in *Annex E*, points *E3* and *E4* (see Fig 2):

$$E_d = 0.5 \cdot \gamma^* \cdot (1 \pm k_v) \cdot K \cdot H^2 + E_{ws} + E_{wd} \quad (1)$$

where γ^*=soil unity weight; k_v=vertical seismic coefficient; H=wall height; E_{ws}=static water force; E_{wd}=hydrodynamic water force; K=earth pressure coefficient (static + dynamic).

The vertical seismic coefficient k_v is a function of the horizontal one k_h :

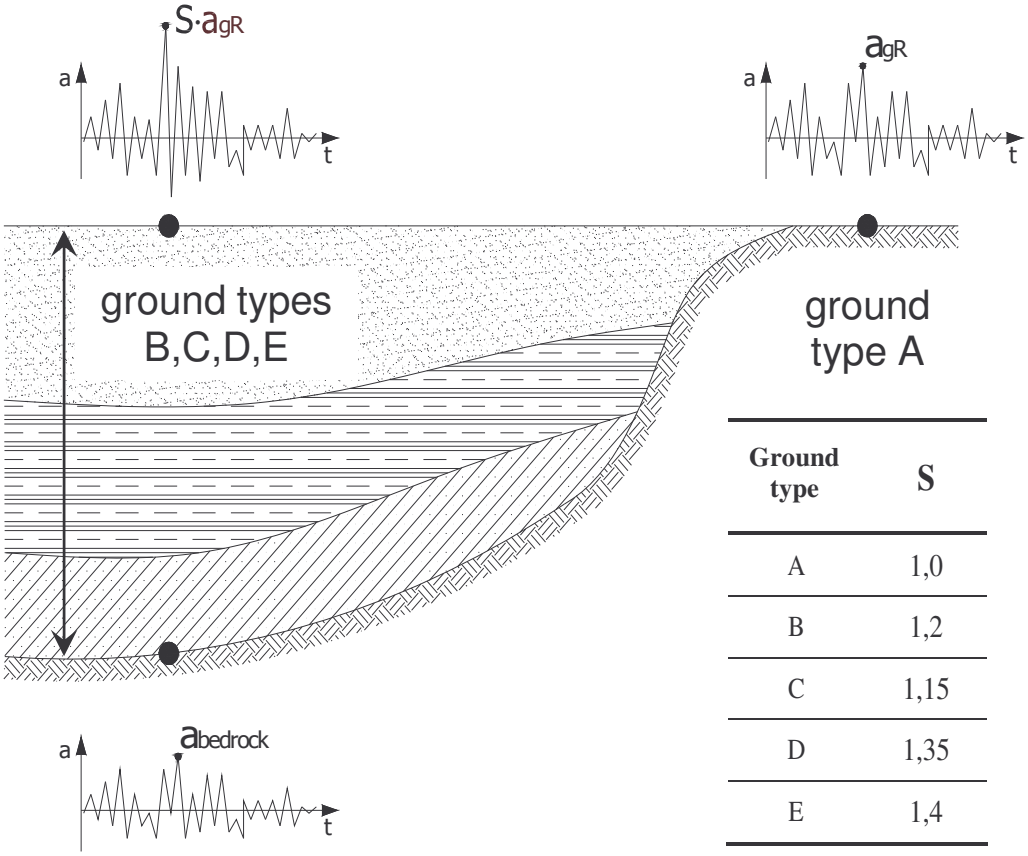

Ground type	S
A	1,0
B	1,2
C	1,15
D	1,35
E	1,4

Fig 1: Schematic representation of the accelerations (at bedrock and on the surface) and of the soil factor *S* of the subsoil classes of Eurocode 8

Thrust: $E_d = \frac{1}{2}\,\gamma^{*}\,(1 \pm k_v)\,K \cdot H^2 + E_{ws} + E_{wd}$

Active thrust coefficient (static + dynamic):

$$K = \frac{\sin^2(\psi + \phi'_d - \theta)}{\cos\theta \sin^2\psi \sin(\psi - \theta - \delta_d)\left[1 + \sqrt{\frac{\sin(\phi'_d + \delta_d)\sin(\phi'_d - \beta - \theta)}{\sin(\psi - \theta - \delta_d)\sin(\psi + \beta)}}\right]}$$

Per $\beta \le \varphi'_d - \theta$

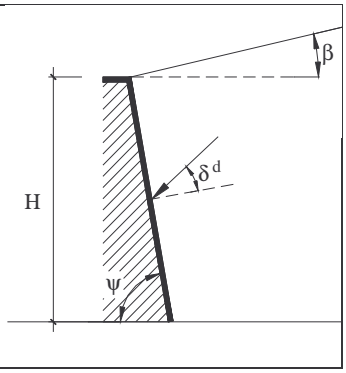

Fig 2: Active thrust of the soil in seismic conditions

Table 2: EC8-5: factor *r* values for the evaluation of the horizontal seismic coefficient

Type of retaining structure	*r*
Free gravity walls that can accept a displacement up to $d_r = 300\ \alpha S$ (mm)	2
Free gravity walls that can accept a displacement up to $d_r = 200\ \alpha S$ (mm)	1.5
Flexural reinforced concrete walls, anchored or braced walls, reinforced concrete walls founded on vertical piles, restrained basement walls and bridge abutments	1

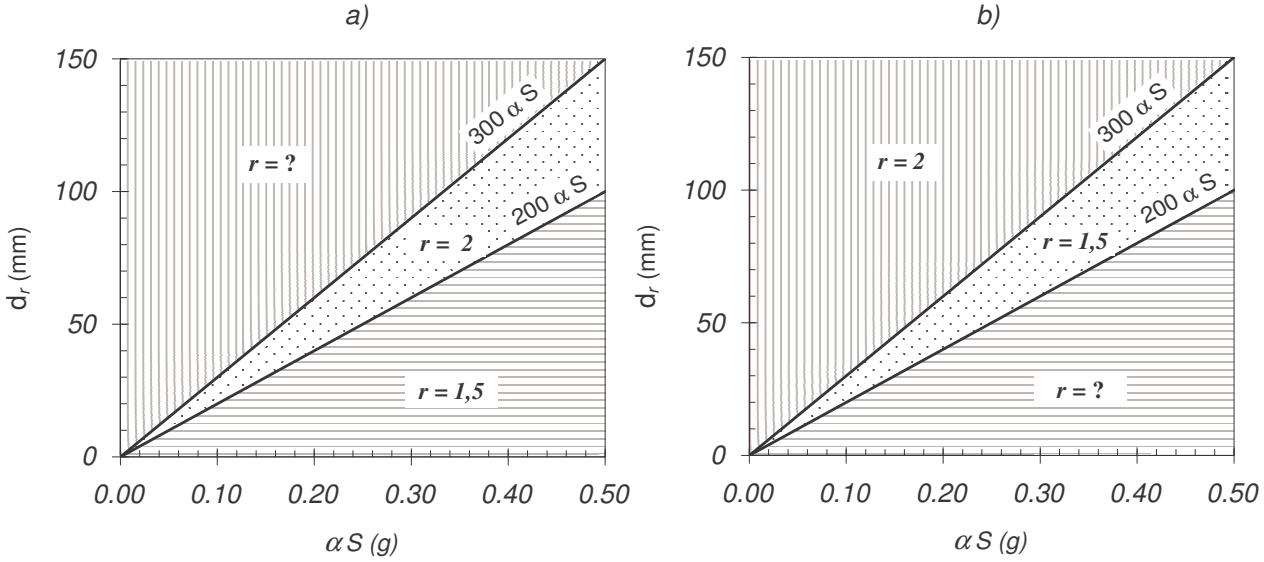

Fig 3: Graphic interpretations of the correlation among the *r* factor, the acceptable displacement d_r (*free gravity wall*) and the peak ground acceleration (see Table 2)

$$k_v = \pm 0.33 \cdot k_h \quad \text{or} \quad k_v = \pm 0.5 \cdot k_h \qquad (2)$$

depending on the ratio between the vertical and horizontal design accelerations (see E8-Part 5, ch. 7.3.2.2, clause (4)P).

The horizontal seismic coefficient k_h is:

$$k_h = a_{gR} \cdot \gamma_I \cdot S / (g \cdot r) \qquad (3)$$

where γ_I = importance factor of the structure; *r*=factor that depends on the allowable wall displacements (in the Final Draft of EC8-5 the formula is $k_h = \alpha \cdot S / r$, where $\alpha = (a_{gR}/g) \cdot \gamma_I$). The seismic coefficient shall be taken as being constant along the height, for walls not higher than 10 m.

The values to be adopted for the factor *r* are listed in Table 2 (which is the copy of the EC8-5 Table 7.1). In brief the factor should be taken equal to 1 for structures that substantially cannot accept any displacement, while it assumes 1.5 and 2 values as the acceptable displacement increases. The threshold values of the displacement d_r are proportional to the peak ground acceleration ($\alpha \cdot S$) expected at the site.

Nevertheless, in the Author's opinion, it is not very clear if the threshold values d_r are the upper or the lower limit values for the acceptable displacement. In particular, if d_r identifies the upper limit values, then Table 2 should be read as shown in Fig 3a, but the doubt still remains on the *r* value to be adopted for walls that can accept a displacement greater than 300 $\alpha \cdot S$ (mm); probably even for these walls a factor *r* value equal to 2 should be adopted (and in Fig 3a the line $d_r = 300\ \alpha \cdot S$

should be eliminated). On the other hand, if d_r identifies the lower limit values for the acceptable displacement, then Table 2 should be read as shown in Fig 3b, but the doubt still remains on the r value to be adopted for walls that can accept a displacement lower than 200 $\alpha \cdot S$ (mm); moreover, in this case, the threshold condition d_r = 300 $\alpha \cdot S$ (mm) for applying r=2 would be quite severe, implying very large acceptable displacement values for the walls.

The intensity of the seismic forces therefore depends on the value of the ground surface acceleration $a_g \cdot S$, and on the amount of allowable displacement of the wall (by means of the factor r).

The equation of the active earth pressure coefficient K is given in Fig 2, where the symbols are φ'_d = design value of the soil friction angle; δ_d = design value of the wall-soil friction angle; θ = inclination of the mass forces acting on the soil wedge.

At this point it is worthwhile making a consideration on the utilization of the design approaches defined in EC7-1 (2003). As a matter of fact the adoption of φ'_d and δ_d in the equation of the earth pressure coefficient K would imply that the strength properties should always be reduced by the partial safety factors; hence only the design approaches DA1 Combination 2 (DA1C2) and DA3 could be effectively utilised, while the DA1C1 and DA2 ones would be ineffective.

Going back to the angle θ, for dry soil it is given by the equation:

$$tan\ \vartheta = \frac{k_h}{1 \mp k_v} \tag{4}$$

For saturated soils the expression of θ changes for the two cases of low and high permeability soil under dynamic actions, and proper values of E_{ws} and E_{wd} must be taken into account; it is worthwhile to underline that in any case the soil strength is always computed in drained conditions.

Once the design action E_d has been determined, the wall must be verified against the sliding and bearing capacity failures: in both cases, E_d must be lower or equal to the design resistance R_d, which is the resistance affected by the partial safety factors:

$$R_d \geq E_d \tag{5}$$

Dynamic analysis

As recalled before, any established method based on the procedures of structural and soil dynamics, and supported by experience and observations, is in principle acceptable for assessing the safety of an earth retaining structure. Obviously such procedures imply the definition of time-history seismic input motion.

In particular, according to clause (1)P of Ch. 2.2 of EC8-5, both artificial accelerograms and real strong motion recordings may be used; their peak values and frequency contents have to be in agreement with the rules specified in EC8-1, Ch. 3.2.3.1. It is worthwhile to recall that, if recorded accelerograms are utilised, the samples used must be adequately qualified with regard to the seismogenetic features of the sources and to the soil conditions appropriate to the site, and their values must be scaled to the value of the ground surface acceleration ($a_g \cdot S$) for the zone under consideration (Ch. 3.2.3.1.3, clause (1) P.

Returning to EC8-5, clause (2) of Ch. 2.2, it is stated that "in verifications of dynamic stability involving calculations of permanent ground deformations, the excitation should preferably consist of accelerograms recorded on soil sites in real earthquakes, as they possess realistic low frequency content and proper time correlation between horizontal and vertical components of motion." Moreover it is stated that the strong motion durations have to be selected consistently with EC8-1, Ch. 3.2.3.1; mainly the duration has to be consistent "with the magnitude and the other relevant features of the seismic event underlying the establishment of a_g" (Ch. 3.2.3.1.2, clause (2)P).

APPLICATION OF EC8 CRITERIA TO RETAINING WALL DESIGN

Formulation of the application

In order to compare EC8 and the pre-existing Italian seismic code, at first, four retaining walls have been designed according to D.M.96, then the designed walls have been verified by means of EC8 pseudo-static and pseudo-dynamic analyses.

The seismic coefficients and the time-history

input motion utilised for the EC8 analyses have been determined adopting the peak ground accelerations provided by the recent Italian seismic zonation, included in the OPCM 3274 normative.

Wall design according to D.M.96

A simple soil configuration has been chosen, whose main characteristics are: cohesionless soil with internal soil friction angle $\varphi' = 35°$; absence of groundwater table; friction angle between the wall and the backfill soil $\delta=0°$; friction angle between the wall and the foundation soil $\varphi_b' = 35°$; backfill slope $\beta=0°$ (see Fig 4).

According to D.M.96, the Mononobe (1929) and Okabe (1926) theory has been utilised, adopting the seismic coefficients C and global safety factors given by the code; the walls have been verified against sliding, overturning, and bearing capacity failures. The results of the design are illustrated in Fig 4: the walls for the I, II and III seismic categories have been called Wall 1, Wall 2 and Wall 3 respectively (see Simonelli, 2004); Wall 4 is the wall designed for the non-seismic area.

APPLICATION OF (EC8 + OPCM3274): PSEUDO-STATIC APPROACH

OPCM 3274 normative: seismic actions

The new seismic zonation attached to OPCM 3274 converts the I, II and III categories into Zone 1, 2 and 3 respectively, while the non-seismic area has been classified as seismic Zone 4. For these zones the values of the *reference peak ground acceleration* a_{gR} have been defined, varying from 0.35*g* to 0.05*g*, as reported in Table 3.

Table 3 OPCM 3274: values of maximum horizontal acceleration on the ground surface, type A soil, for the seismic zones in Italy

Zone	Acceleration (g)
1	0.35
2	0.25
3	0.15
4	0.05

According to EC8, OPCM 3274 defines several ground types to take into account the amplification of the seismic motion due to the local soil conditions, but with slightly different soil factor *S* values (see Table 4).

Table 4 OPCM 3274: values of *soil factor S* for the different subsoil categories

Ground type	*Soil factor*
A	1
B, C, E	1.25
D	1.35

Taking into account the 4 a_{gR} and the 3 soil factor values, 12 ground surface accelerations characterise the entire Italian territory, as listed in Table 5.

Table 5 OPCM 3274: values of the peak ground accelerations for the different seismic zones and subsoil categories

Zone	Peak ground acceleration (g)		
	Ground type		
	A	B, C, E	D
1	0.35	0.44	0.47
2	0.25	0.31	0.34
3	0.15	0.19	0.20
4	0.05	0.06	0.07

These values will be utilised both in the following analysis to determine the pseudo-static seismic coefficients, and later to scale the accelerometric input motion for the pseudo-dynamic analyses.

Pseudo-static analysis results

The design approaches DA1 (C1 and C2 combinations), DA2 and DA3 have been utilised, with the partial safety factors given by *EN1997-1* (April 2003) as schematically represented in Fig 5 and Table 6. For a full treatment of the different *design approaches* and of the articulated classification of the safety factors of the Eurocodes, see Scarpelli (2004), Aversa & Squeglia (2004) and Frank (2005). Here it is worthwhile making some ulterior considerations on the choice of the design approaches and the partial safety factors, after having previously observed that the equation of

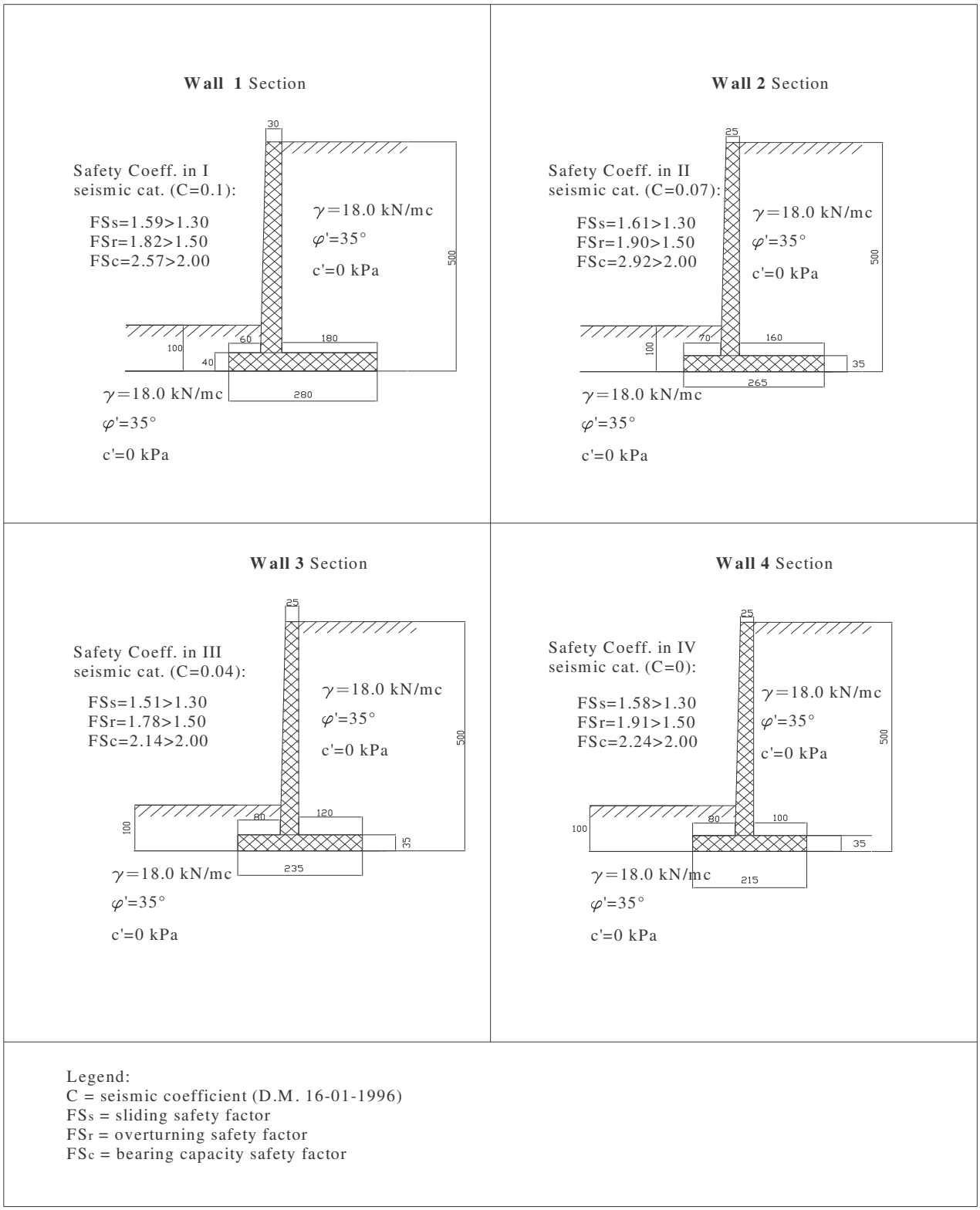

Fig 4: Walls 1 to 4 (designed according to D.M. 16.1.1996): soil characteristics and wall sections

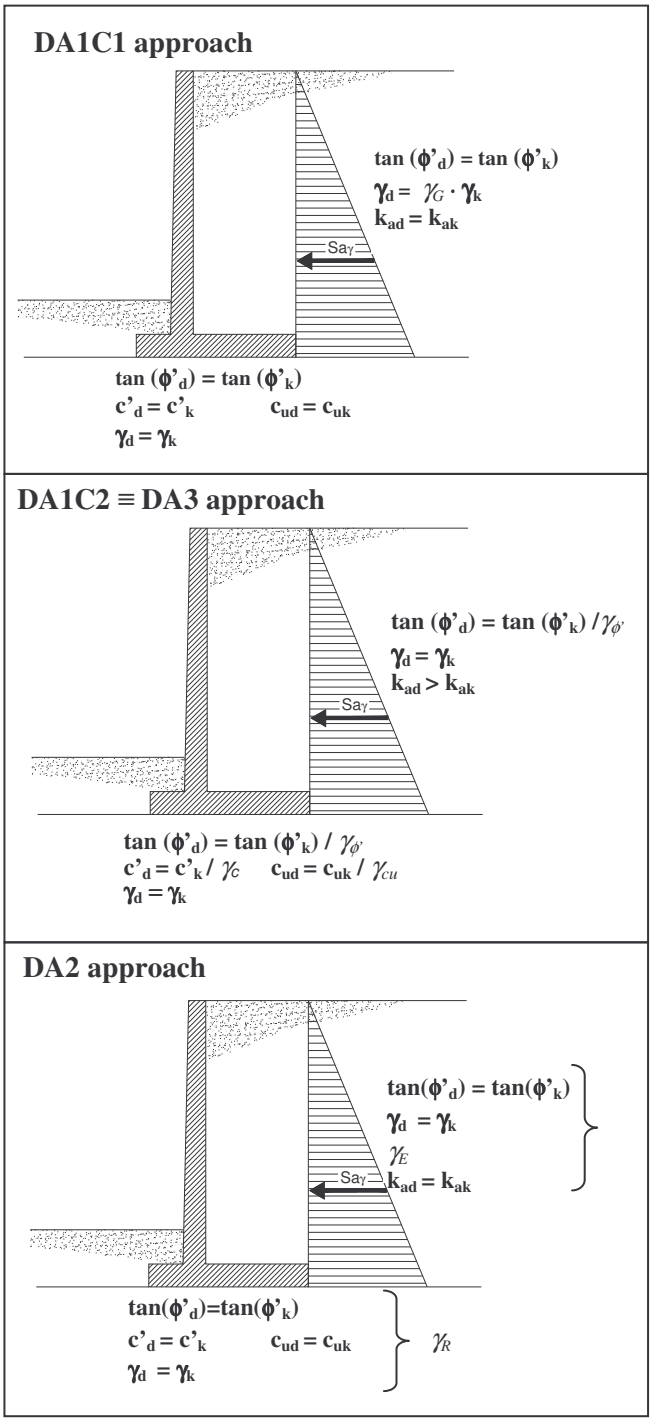

Fig 5: Scheme of the design approaches and the partial safety factors for the case of a gravity wall

Table 6: Partial safety factor values utilised

Design approach	Partial safety factor
DA1C1	γ_F = 1.35
DA1C2=DA3	$\gamma_{\phi'}$ = 1.25
DA2	γ_E = 1.35
	γ_R = 1.1

K in Fig 2 would imply that the reduced values of the strength properties should always be used.

Actually, with regard to the partial safety factors on seismic actions, the Eurocode EN1990 (2004) states that they should be chosen equal to 1. Hence once again the design approaches DA1C1 and DA2 would be ineffective, and only the DA1C1 and DA3 would be significant. In truth, this is not congruent with the indications of EC7-1, which considers that in principle all the design approaches can be effective for the design.

In conclusion, since some doubts remain on the interpretation of EC7 and EC8, in the following application all the design approaches have been tested, utilising the partial safety factor values defined within EC7. It must be said that the application will show that, for the examined cases, the design approach DA1C1 results to be less conservative than the DA1C2, while the DA2 is, at most, as conservative as the DA1C2 and DA3 approaches. Therefore the conclusions drawn by the analyses' results will not be affected by the choice of applying other design approaches other than the DA1C2 and DA3.

The sliding and overturning failure mechanisms have been verified. It must be underlined that for the tilting mechanism, that is not accounted for in EC7, the same 1.1 value for the γ_R coefficient (DA2 approach) has been adopted, as for the case of the sliding mechanism.

The vertical pseudo-static forces do not significantly affect the analysis results (e.g. see the diagrams in Fig 6).

For all the walls the sliding mechanism is the critical one, as shown in Fig 7. The results have shown that the design approaches DA with the partial safety factors would provide results congruent with those obtained by means of the traditional methods with the global safety factors, since in both cases the designed wall would tolerate about the same pseudo-static seismic action.

On the other hand the comparison has pointed out that the walls designed according to the D.M.96 would be dramatically under-dimensioned according to EC8+OPCM 3274 approach, as illustrated here in Fig 8. In the figure, for each wall (Wall 1 to Wall 4) and with

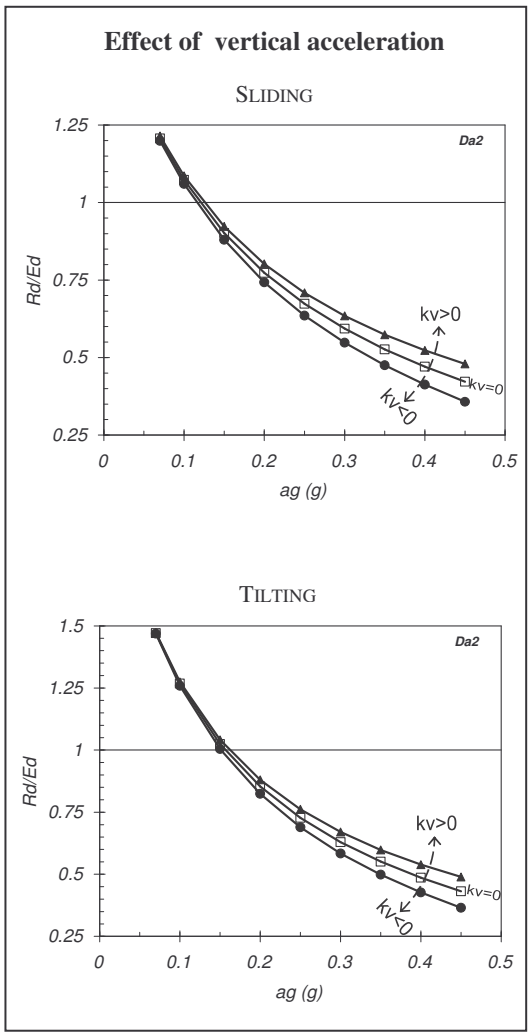

Fig 6: EC8 – Pseudostatic analyses: effect of the vertical acceleration ($k_v \cdot g$) for the sliding and tiling mechanisms (Simonelli, 2003).

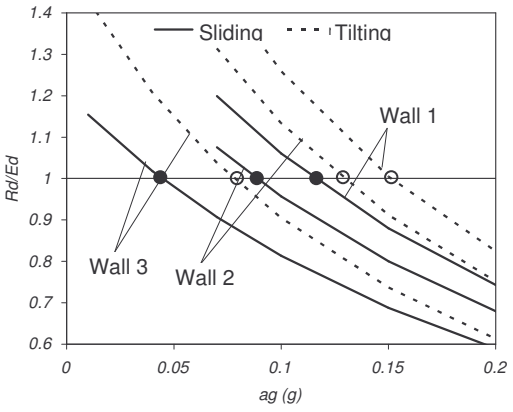

Fig 7: EC8 – Comparison between the sliding and tilting pseudostatic analysis results for the identification of the critical mechanism (Simonelli, 2003).

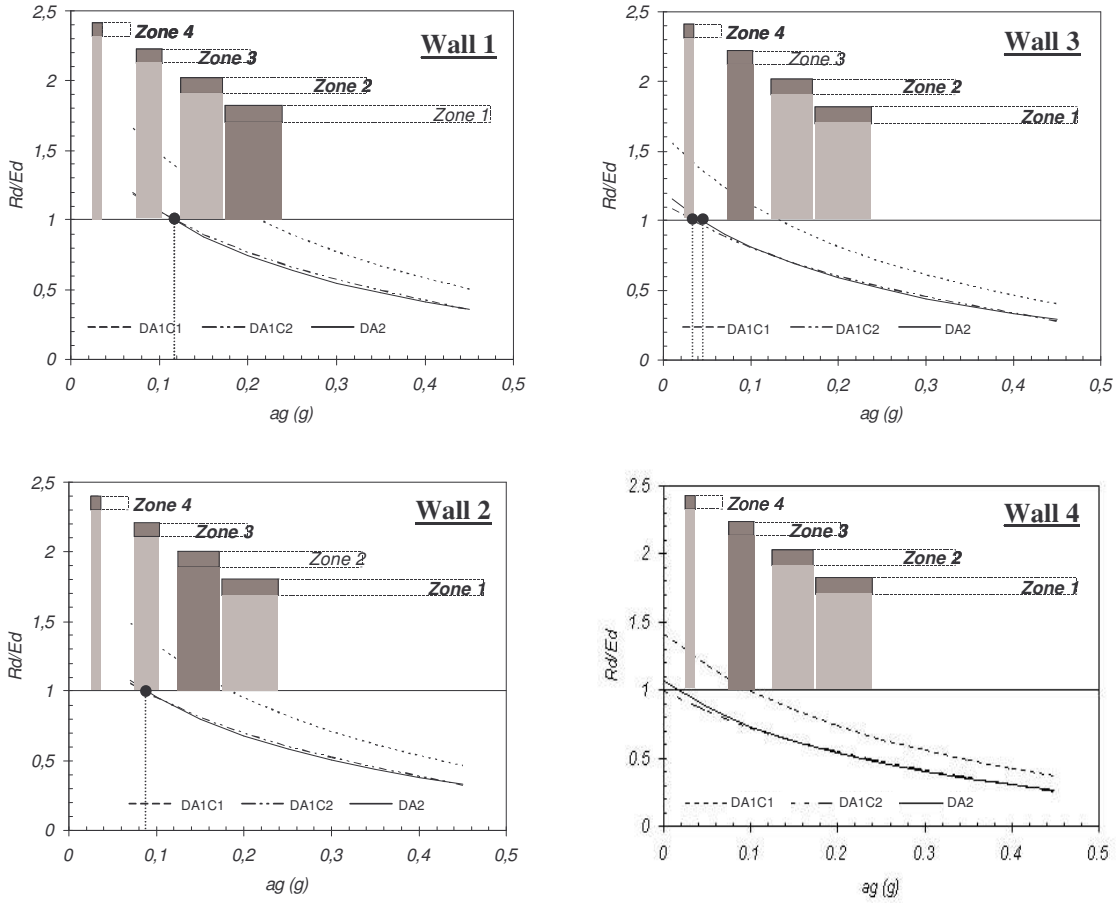

Fig 8: Walls 1 to 4 (designed according to D.M. 16.1.1996): results of the EC8 pseudo-static analyses (R_d/E_d ratio vs. the "global" pseudo-static acceleration *ag*) and comparison with the range of *ag* values for the 4 seismic zones defined by OPCM 3274

reference to each of the design approaches utilised, the ratio between the design resistance R_d and the design action E_d (for the sliding mechanism) is plotted against the horizontal acceleration *ag*, that represents the "global" acceleration to be used for computing the pseudo-static actions ($ag=k_h \cdot g$, where k_h is given by eq. (3), and hence takes account of the maximum horizontal acceleration value on outcropping rock (Table 2) and of the *soil factor S* (Table 3) of the OPCM 3274, and also takes account of the eventual reduction of the action through the coefficient *r*). In the upper part of the figure the range of the global accelerations expected at each seismic zone of the Italian territory is also reported (the restricted field highlighted in grey corresponds to the value of *r*=2). The maximum global acceleration allowable for the wall must be read on the more conservative design approach curve, and corresponds to the unit value of the ratio R_d/E_d: as a matter of fact, for each zone the expected global acceleration values (which have to be taken into account for the "new" design of retaining walls) are much higher than the allowable one (e.g. Wall 1, designed for the old I seismic category, would be under-dimensioned not only for the correspondent Zone 1, but even for the Zone 2 of the new seismic classification).

APPLICATION OF (EC8 + OPCM3274): PSEUDO-DYNAMIC ANALYSIS

According to EC8, a pseudo-dynamic method has been utilised, for assessing the response of the wall in terms of permanent horizontal displacements induced by the dynamic excitations. At this aim a sliding block model (Zarrabi, 1979) derived by the original

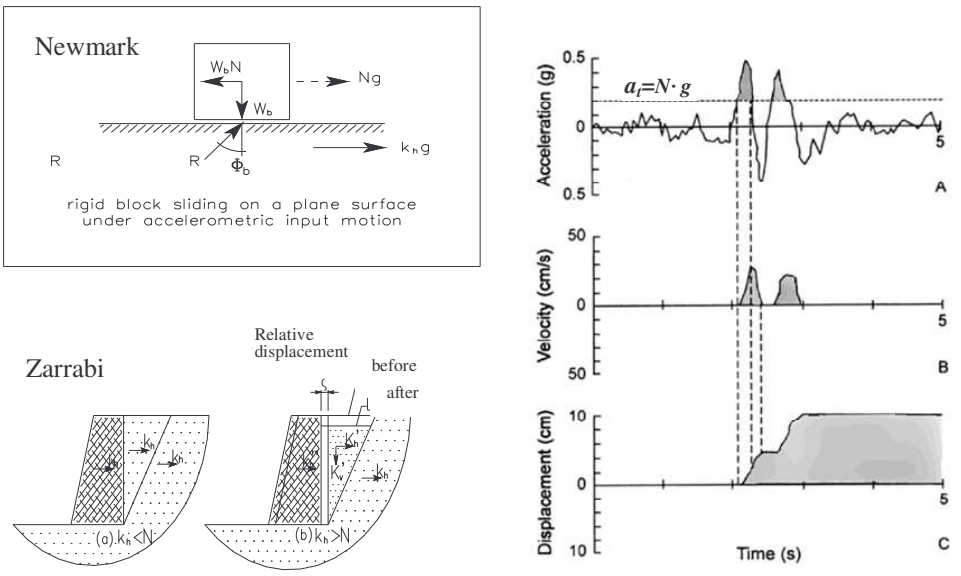

Fig 9: Newmark (1965) and Zarrabi (1979) models for displacement analysis

one proposed by Newmark (1965) has been adopted. Moreover a proper accelerometric input motion has been elaborated in order to fit EC8 and OPCM 3274 requirements.

As well known, the Newmark model analyses the sliding of a rigid block on a plane surface, assuming a rigid-plastic behaviour at the interface between them. From simple limit equilibrium considerations, the threshold acceleration value can be evaluated, over which the surface moves faster than the block, which instead still saves the threshold acceleration. The displacement between the block and the surface can be computed by integrating the relative accelerations twice, until the velocity between them returns to zero again (see Fig 9).

Zarrabi model improves the retaining wall analysis, since it takes into account the congruency among the displacements of the backfill, the soil wedge and the wall (Fig 9): as a consequence, the threshold acceleration value is not constant, but varies with the amplitude of the input acceleration. The effectiveness of this model has been validated by proper laboratory tests on the shaking table apparatus (Crewe et al., 1998 and Simonelli et al., 2000).

Further, according to EC8 requirements, both the horizontal and the vertical components of the accelerograms have been considered as input motion for the displacement analysis.

Accelerometric seismic input according to OPCM 3274

The data recorded at several sites during two of the major Italian earthquakes have been adopted for the pseudo-dynamic analyses: Friuli 1976 earthquake (Tolmezzo and Forgaria Cornino accelerograms), and Irpinia 1980 earthquake (Sturno, Brienza, Calitri, Bagnoli Irpino and Torre del Greco accelerograms); six of them are illustrated in Fig 10. The accelerograms have been grouped in function of their maximum values, in order to be properly scaled at the closest values of the 12 ground surface acceleration of the Italian territory (listed in Table 5). The coherence of the scaled accelerograms with the spectra of EC8 has also been checked.

Pseudo-dynamic analysis results

For the Walls 1 to 4, the horizontal displacements induced by the accelerograms elaborated for the different subsoil conditions of each seismic zone have been computed.

The main displacement results are summarised in Table 7, together with the results of the pseudo-static approaches (for the sliding mechanism). For each Zone the results of the correspondent Wall (with the threshold acceleration a_t value in parenthesis) are reported: on the left the D.M.96 pseudo-static safety factor PSF and the R_d/E_d ratios for the

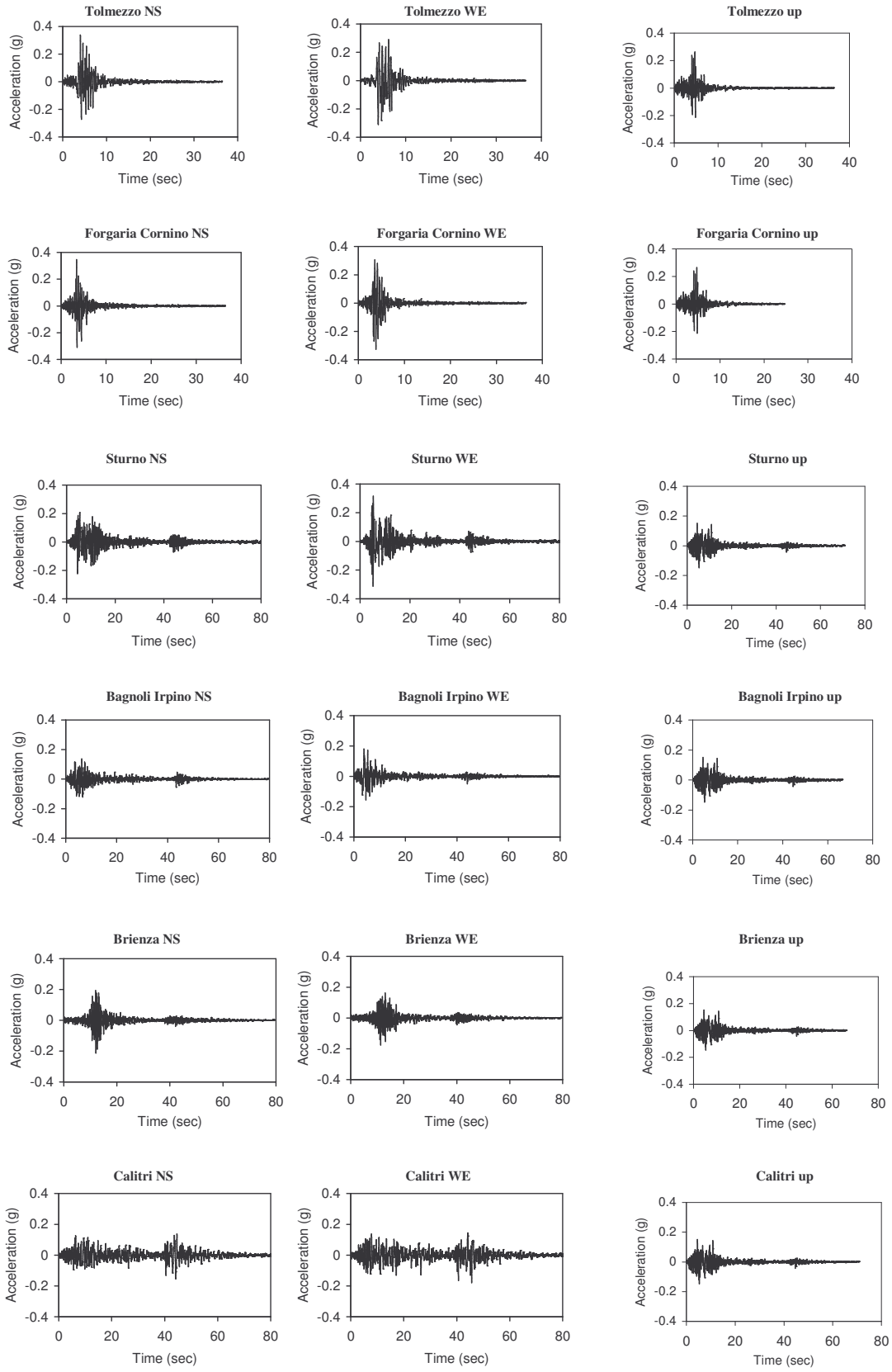

Fig 10: Friuli 1976 (Tolmezzo and Forgaria Cornino) and Irpinia 1980 (Sturno, Bagnoli Irpino, Brienza and Calitri) recorded accelerograms

Table 7 Analysis results for Zones and Walls 1 to 4. Pseudo-static analyses: global safety factor PSF (DM 1996) and R_d/E_d ratio values (EC8). Pseudo-dynamic analysis: permanent displacements D induced by Italian scaled accelerograms

Zone 1 - Wall 1 (threshold acceleration a_t = 0.250 *g*)						
Pseudo-static approach				**Displacement Analysis : D (cm)**		
D.M. 1996	Site	Peak ground acc.	EC8		Earthquake	
PSF		a_g (g)	R_d/E_d	Tolmezzo	Forgaria C.	Sturno
	A	0.35	0.77	0.56	0.19	1.47
1.59	B-C-E	0.44	0.69	2.15	1.13	4.24
	D	0.47	0.65	3.52	1.69	5.87

Zone 2 - Wall 2 (threshold acceleration a_t = 0.219 *g*)						
Pseudo-static approach				**Displacement Analysis : D (cm)**		
D.M. 1996	Site	Peak ground acc.	EC8		Earthquake	
PSF		a_g (g)	R_d/E_d	Tolmezzo	Forgaria C.	Sturno
	A	0.25	0.85	0.06	0.02	0.21
1.61	B-C-E	0.31	0.77	0.53	0.20	1.41
	D	0.34	0.74	0.72	0.40	1.50
D.M. 1996	Site	Peak ground acc.	EC8		Earthquake	
PSF		a_g (g)	R_d/E_d	Bagnoli I.	Brienza	Calitri
	A	0.25	0.85	0.03	0.02	0.11
1.61	B-C-E	0.31	0.77	0.63	0.16	1.69
	D	0.34	0.74	1.28	0.26	2.98

Zone 3 - Wall 3 (threshold acceleration a_t = 0.165 *g*)						
Pseudo-static approach				**Displacement Analysis : D (cm)**		
D.M. 1996	Site	Peak ground acc.	EC8		Earthquake	
PSF		a_g (g)	R_d/E_d	Bagnoli I.	Brienza	Calitri
	A	0.15	0.85	0.00	0.00	0.00
1.51	B-C-E	0.19	0.80	0.02	0.01	0.07
	D	0.20	0.78	0.06	0.03	0.25

Zone 4 - Wall 4 (threshold acceleration a_t = 0.131 *g*)					
Pseudo-static approach				**Displacement Analysis : D (cm)**	
D.M. 1996	Site	Peak ground acc.	EC8	Any	Earthquake
PSF		a_g (g)	R_d/E_d		
	A	0.05	0.91	0	
1.58	B-C-E	0.06	0.89	0	
	D	0.07	0.88	0	

different ground types are recalled; on the right side the displacements induced at any site by the scaled accelerograms are listed.

The table for Zone 1 and Wall 1 indicates that, while the pseudo-static approach always gives unsatisfactory results (R_d/E_d ratio values much lower than 1 for any site), the induced displacement, increasing from site A to site D, are generally acceptable. In particular Wall 1 behaves well on ground type A (displacement D < 1.5 cm), and quite well on B-C-E subsoils, where only Sturno input motion induces a displacement of about 4 cm. For D site the displacements are higher, and reach the maximum value of about 6 cm under Sturno excitation.

For Zone 2 and Zone 3, the correspondent Walls 2 and 3 behave even better, suffering displacements of a few centimetres or less (notwithstanding R_d/E_d values range from about 0.7 to 0.85).

Finally Wall 4 (designed for the no-seismic area of D.M.96, and having R_d/E_d values equal to about 0.9) would suffer no displacements at all in Zone 4, being its threshold acceleration (a_t=0.131*g*) higher than the expected maximum accelerations (ranging from 0.05*g* at site A to about 0.07*g* at site D).

For each Zone (1 to 4) and Site (A to E), the results of the displacement and pseudo-static analyses have been effectively represented in a graph, in order to visualize significant comparisons (Figs 11-14).

In the upper part of each figure the displacement curves relative to different input motion are drawn vs. the wall weight factor *w.w.f.*, which substantially represents the size of the wall, and is univocally linked with the wall threshold acceleration (Simonelli & Viggiani, 1992 and Simonelli, 1994):

$$w.w.f. = \frac{W_w}{0.5 \cdot \gamma \cdot H^2} \qquad (6)$$

where W_w=weight of wall, γ=soil unit weight and H=wall height.

In the lower part the R_d/E_d ratio for the different design approaches and the D.M.96 pseudo-static safety factor PSF (over the minimum allowable factor PSF_{min}, equal to 1.3) are plotted vs. the *w.w.f.*; the horizontal line passing through unity divides the unsatisfactory values of the curves above from the satisfactory ones below.

On the abscissa, the Walls 1 to 4 have been represented with different symbols, in order to visualize their response in terms of displacements and pseudo-static analysis results.

The graph for Zone 1 - Site A (Fig 11), confirms that Wall 1 behaves very well, suffering very small displacements (even Wall 2 would undergo acceptable displacements). On the other hand, Wall 1 would have unsatisfactory R_d/E_d values (except that for the design approach DA1, combination C1). As a matter of fact, whatever design approach is taken into account, the achievement of the value R_d/E_d =1 would require a much heavier *w.w.f.*.

Going directly to the graph for Zone 1 - Site D, the displacements induced on Wall 1 vary between a few millimetres up to about 6 cm (for at least 2 accelerometric input motions); the acceptability of such displacement amounts should be verified case by case, depending on the particular boundary conditions. On the other hand the “pseudo-static response” of Wall 1 appears to be absolutely unsatisfactory (R_d/E_d ~ 0.6); at the same time the analyses would suggest extremely huge walls according to the design approaches DA1 and DA3 (R_d/E_d =1 for *w.w.f.*~2).

At this point it is worthwhile noting that in these calculations the *r* factor value equal to 2 has been adopted; hence it is assumed that the walls can accept displacements of the order of ten centimetres (in particular d_r = 9.4 cm in the hypothesis illustrated in Fig 3a, and d_r = 14.2 cm in the hypothesis of Fig 3b). As a matter of fact, the displacements induced on Wall 1 would be much lower than the maximum one the wall is able to tolerate.

Considerations analogous to those illustrated for Zone 1 can be made for Zones 2, 3 and 4, as can be deduced by Figs 12-14. In particular it must be observed that, passing from Zone 1 to Zone 4, the response of the correspondent Wall (1 to 4) is always better.

On the basis of the previous considerations, further elaborations of the displacement and

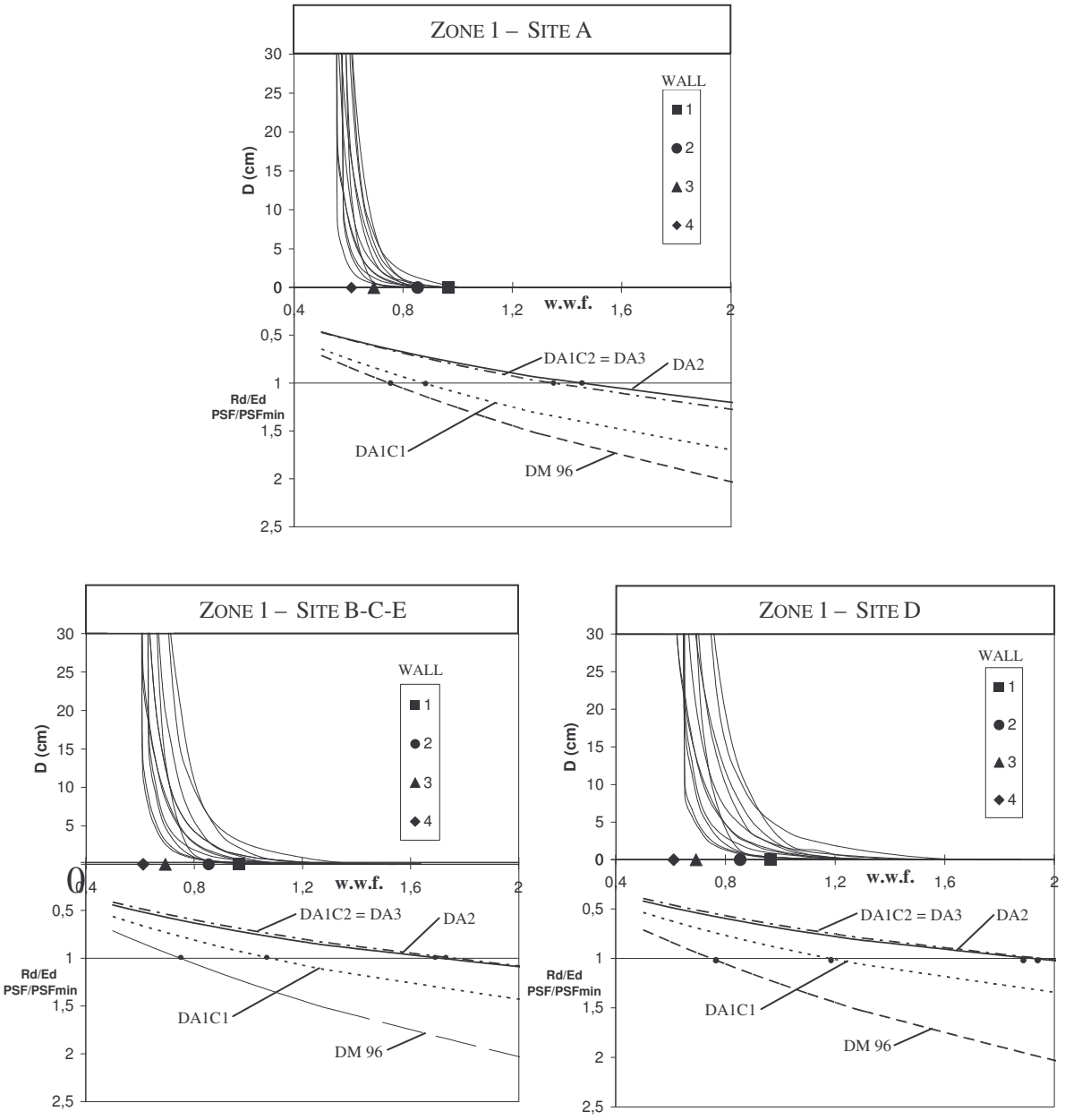

Fig 11: Zone 1 analysis results. Above: displacement induced by different scaled accelerograms vs. wall weight factor *w.w.f.*. Below: R_d/E_d ratio for different design approaches (according to EC8) and PSF/PSF_{min} (according to D.M. 16.1.1996) vs. *w.w.f.*

pseudo-static results have been represented in specific charts, which could represent design tools for each seismic Zone. These new graphs are illustrated in Fig 15.

For each Zone, in the upper part the maximum displacements induced at the three ground types (site A, sites B-C-E and site D) are plotted versus the wall weight factor.

In the lower part of the figure the lowest R_d/E_d values (given by the more conservative DA) are plotted for each of the three ground types, together with the above explained PSF/PSF_{min} ratio. On the abscissa, the Walls 1 to 4 have been represented with different symbols, in order to compare the D.M.96 design results (i.e. Wall 1 to 4) with those

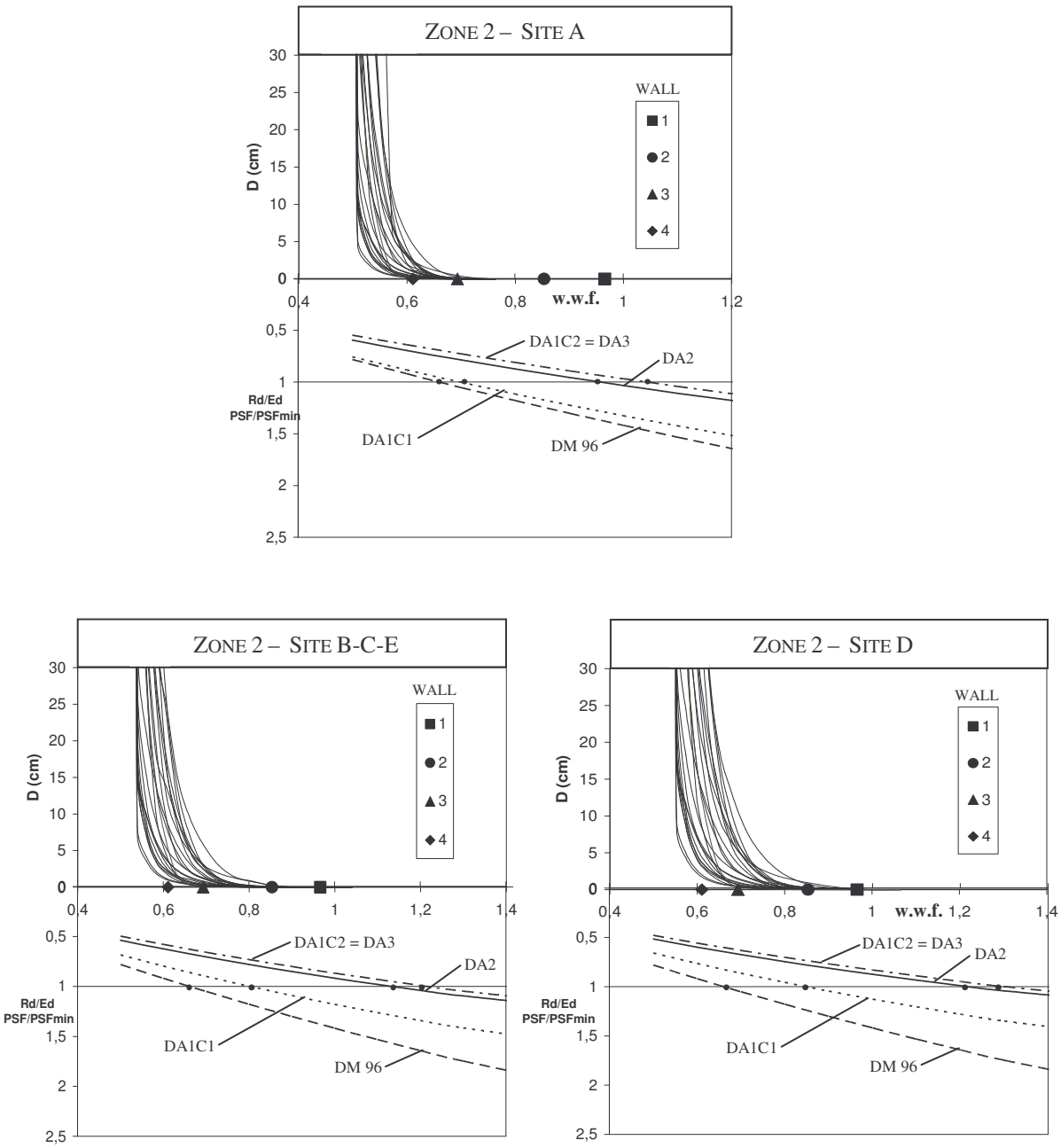

Fig 12: Zone 2 analysis results. Above: displacement induced by different scaled accelerograms vs. wall weight factor *w.w.f.*. Below: R_d/E_d ratio for different design approaches (according to EC8) and PSF/PSF_{min} (according to D.M. 16.1.1996) vs. *w.w.f.*

obtained by the EC8 pseudo-static and displacement analyses.

Zone 1 chart indicates that Wall 1 would be dramatically underdimensioned according to EC8 pseudo-static approach (R_d/E_d values much lower than 1 for any site). On the other hand, according to the displacement analysis, Wall 1 would behave very well in Site A (displacement D~0); for sites B-C-E and D the computed displacements are of the order of centimetres, and the behaviour of the wall would depend on the amount of the displacement allowable for the specific case under examination. In any case the wall

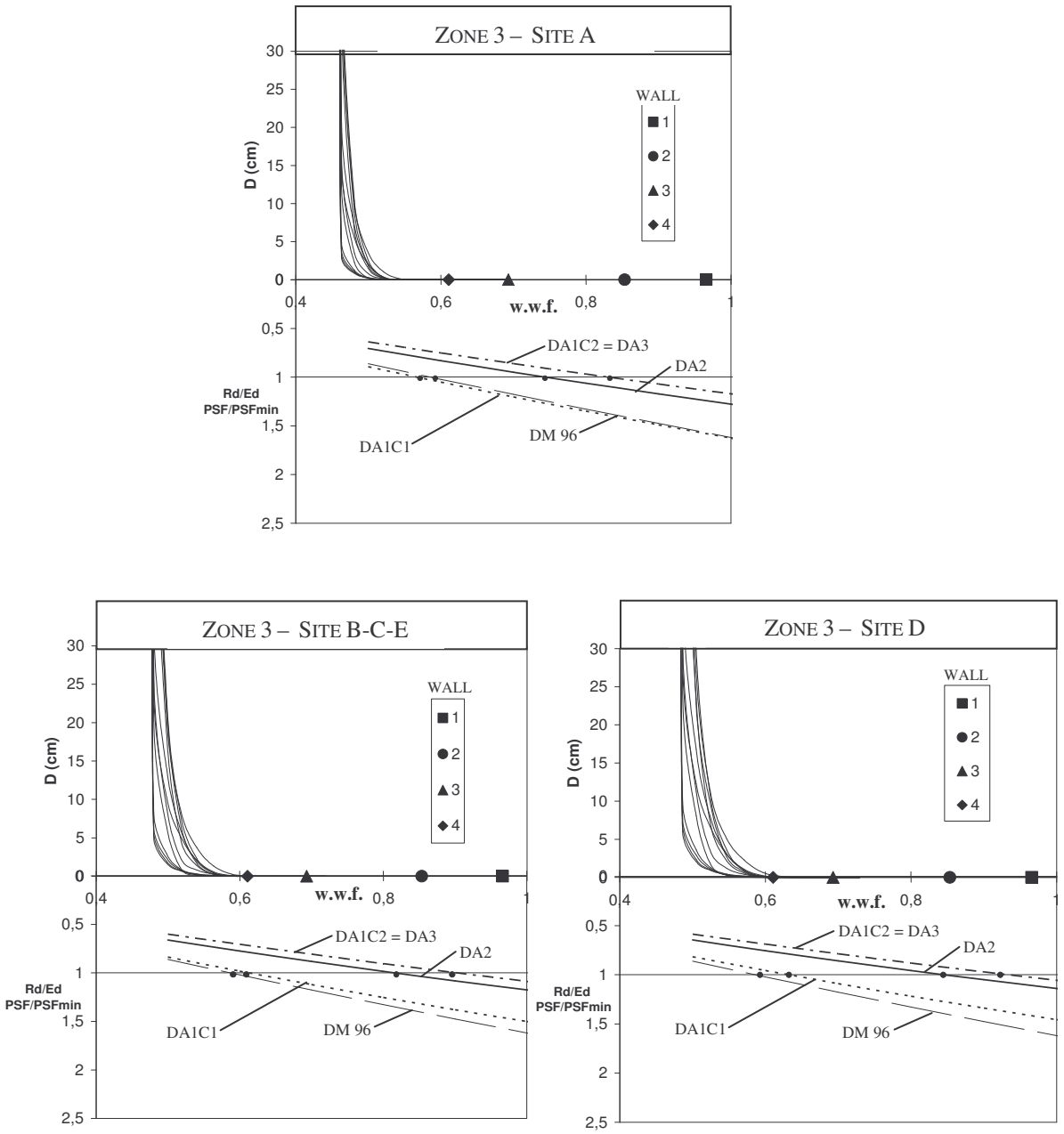

Fig 13: Zone 3 analysis results. Above: displacement induced by different scaled accelerograms vs. wall weight factor w.w.f.. Below: R_d/E_d ratio for different design approaches (according to EC8) and PSF/PSF_{min} (according to D.M. 16.1.1996) vs. *w.w.f.*

design suggested by the present EC8 pseudo-static method appears to be overconservative: in fact, even a performance based design imposing no displacement at all would provide *w.w.f.* values lower than those provided by EC8 pseudo-static approach.

The charts for Zone 2 and 3 again confirm that, according to EC8 pseudo-static method, Wall 2 and Wall 3 would be noticeably underdimensioned. On the other hand, according to the displacement analysis, they would behave very well at any site (from A to E) suffering displacement of a few centimetres (Wall 2 in Site D) or displacements about zero

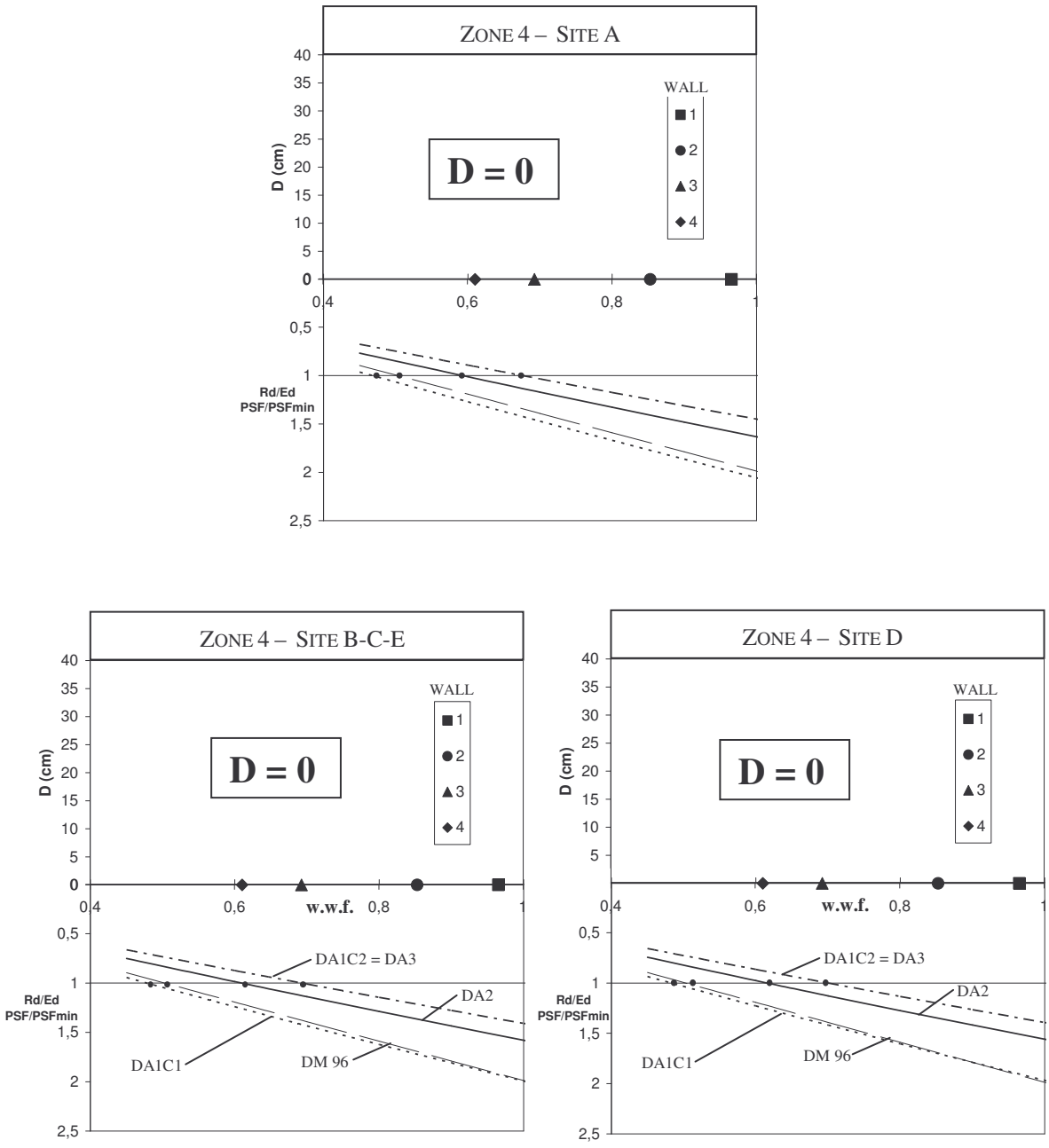

Fig 14: Zone 4 analysis results. Above: displacement induced by different scaled accelerograms vs. wall weight factor w.w.f.. Below: R_d/E_d ratio for different design approaches (according to EC8) and PSF/PSF_{min} (according to D.M. 16.1.1996) vs. *w.w.f.*

for all the other cases. Hence the wall design suggested by the present EC8 pseudo-static method must absolutely be considered overconservative.

Analogous conclusions can be drawn for Zone 4 and Wall 4 too. In this case, the wall designed according to the D.M.96 would not suffer any displacements under the seismic input motion set out for Zone 4, even if the R_d/E_d values still remain under the unity for all the sites.

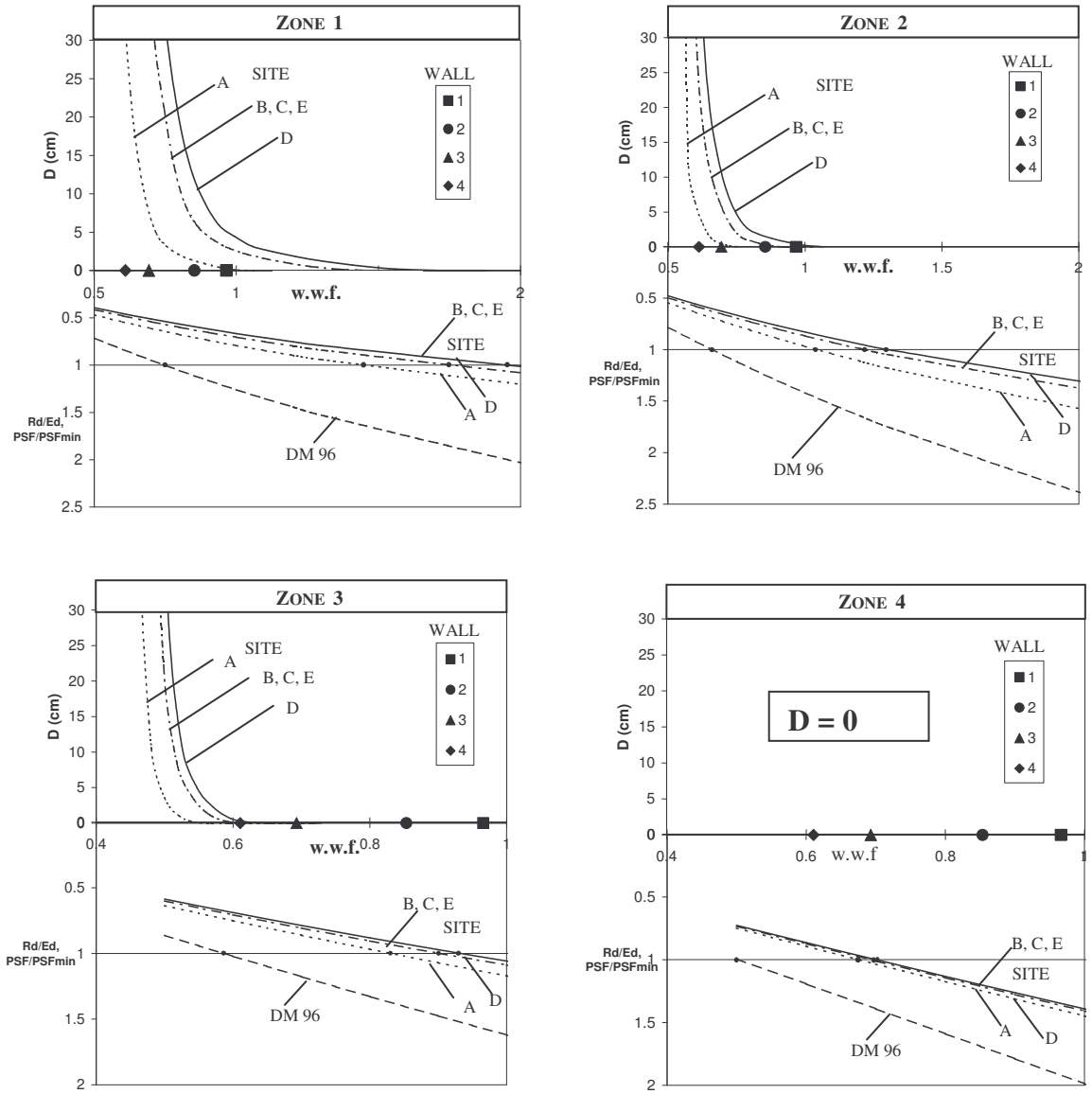

Fig 15: Zone 1 to 4: results and design charts. *Above*: maximum displacement induced at sites A to D vs. wall weight factor w.w.f. (for performance based design). *Below*: R_d/E_d ratio for A to D sites (for pseudo-static design according to EC8) and PSF/PSF_{min} (according to D.M. 16.1.1996) vs. *w.w.f.*

CONCLUSIONS

Four retaining walls (namely Wall 1 to Wall 4) designed according to the Italian pre-existing normative (D.M.96) have been verified by means of two EC8 design approaches: the pseudo-static method and a pseudo-dynamic displacement analysis.

The reference acceleration values for the input motion have been taken from the recent Italian OPCM 3274 normative.

The comparisons among the analysis results have given rise to interesting conclusions:

- the D.M.96 and EC8 pseudo-static methods provide very different designs, being the EC8 wall design much more severe;
- a pseudo-dynamic analysis, based on a Newmark-derived sliding-block model, and utilising a proper set of accelerometric input motion fitting the requirements of EC8 and OPCM 3274 normative, has shown that Walls 1 to 4 generally behave quite well in terms of

suffered displacements, hence confirming that EC8 pseudo-static design is actually overconservative;

- the difference between D.M.96 and EC8 pseudo-static design results does not depend on the use of the new EC7 design approaches with the partial safety factors (which would give results similar to those obtained by the traditional pseudo-static method with the global safety factors), but depends on the different evaluation of EC8 seismic actions on the wall (correlated to the ground acceleration expected for a severe earthquake).

In conclusion, the present EC8 pseudo-static method for retaining wall design, together with the ground acceleration values of the OPCM 3274 Italian seismic zonation, appears to be inapplicable. An effective design can be achieved by more advanced dynamic analyses, utilising proper accelerometric representation of the seismic motion, as suggested by EC8.

Nevertheless, since the application of pseudo-static methods is well consolidated in the engineering practice, it would be very useful to save the EC8 pseudo-static approach. At this aim, it would be necessary to better calibrate the correlation between the ground accelerations and the pseudo-static actions on the wall, by the introduction of proper model coefficient values, which have to effectively convert the real and complex dynamic action into a pseudo-static force, or, in alternative, to define different partial safety factor values for verifying the wall under the severe design earthquakes.

REFERENCES

AGI - Associazione Geotecnica Italiana (2005). Linee Guida su “Gli aspetti geotecnici della progettazione antisismica”. Provisional edition, March 2005, Patron Editor, Bologna.

Aversa, S., and Squeglia, N. (2003). Il dimensionamento delle opera di sostegno. *Italian Geotechnical Journal*

Crewe, A.J., Scotto di Santolo, A. and Simonelli, A.L. (1998). Shaking table tests of scale models of gravity retaining walls. *The Sixth SECED Conference on Seismic Design Practice into the Next Century*, Oxford, UK

DM LL.PP. 16/1/96**.** *Norme tecniche per le costruzioni in zone sismiche*. Gazzetta Ufficiale della Repubblica Italiana, n. 29 del 5/2/1996.

EN 1990 (June 2004). *Eurocode: Basis of Structural Design*. CEN European Committee for Standardization, Bruxelles, Belgium.

EN 1997-1 (2002). *Eurocode 7 Geotechnical Design – Part 1: General Rules*. CEN European Committee for Standardization, Bruxelles, Belgium.

EN 1998-1 (December 2003). *Eurocode 8: Design of structures for earthquake resistance – Part 1: General rules, seismic actions and rules for buildings.* CEN European Committee for Standardization, Bruxelles, Belgium.

EN 1998-5 (December 2003). *Eurocode 8: Design of structures for earthquake resistance – Part 5: Foundations, retaining structures and geotechnical aspects*. CEN European Committee for Standardization, Bruxelles, Belgium.

Frank, R. (2005). Eurocodice 7: Progettazione geotecnica. Regole generali: Approccio concettuale e principi di base. *Atti delle Conferenze di Geotecnica di Torino, XX Ciclo*, Torino.

Mononobe, N. (1929). Earthquake proof construction of masonry dams. *Proc. of World Conference*, vol 9

Newmark, N. M. (1965). Effects of earthquake on dams and embankments. *Geotechnique*, n.15, pp. 139-160

Okabe, S. (1926). General theory of earth pressure. *Japanese Society of Civil Engineers*, vol. 12, no. 1.

OPCM n. 3274 (20/3/03). *Primi elementi in materia di criteri generali per la classificazione sismica del territorio nazionale e di normative tecniche per le costruzioni in zona sismica*. Gazzetta Ufficiale della Repubblica Italiana, n. 105 dell’ 8/5/03.

Scarpelli, G. (2003). I possibili approcci alla progettazione secondo l’Eurocodice 7. *Italian Geotechnical Journal*.

Simonelli, A.L. (1994). Earth retaining wall displacement analysis under seismic conditions. *X European Conference on Earthquake Engineering*, Vienna

Simonelli, A.L. (2003). Eurocodice 8: valutazione delle azioni sismiche al suolo ed effetti sulla spinta dei terreni. *Italian Geotechnical Journal*

Simonelli, A.L., Carafa, P., Feola, A., Crewe, A.J. and Taylor, C.A. (2000). Retaining walls under seismic actions: shaking table testing and numerical approaches. *XII World Conference on Earthquake Engineering*, Aukland, New Zealand

Simonelli, A.L. and Lafratta, A. (2005). Eurocode 8: retaining wall design based on pseudo-static approach and displacement analysis. *EC7 Workshop on the "Evaluation" of Eurocode 7*, ERTC 10, Dublin.

Simonelli, A.L. and Viggiani, C. (1992). Some remarks on retaining wall design under seismic conditions. *X World Conference on Earthquake Engineering*, Madrid

Zarrabi-Kashani, K. (1979*). Sliding of gravity retaining walls during earthquakes considering vertical acceleration and changing inclination of failure surface.* M.S. Thesis, Dept. of Civil Eng., Massachusetts Institute of Technology, Cambridge

Pseudo-static seismic design of embedded retaining structures

L. Callisto
University of Rome "La Sapienza", Italy

Abstract

The application of a simplified pseudo-static approach based on Mononobe-Okabe theory to the seismic design of embedded retaining walls is affected by a number of uncertainties, deriving by soil layering, evaluation of passive pressure, effect of pore water pressure, and soil deformability. This paper discusses the application of the pseudo-static approach to the analysis of embedded retaining walls, and outlines possible methods to take into account the factors above. The important issue of the choice of an appropriate seismic coefficient for pseudo-static analysis is also addressed.

INTRODUCTION

In EC8 Part 5, a simplified method is described for the seismic analysis of retaining walls, based on the pseudo-static approach of Mononobe-Okabe (MO). While MO method is very useful for the pseudo-static analysis of gravity walls, its use for the seismic analysis of embedded retaining walls is not straightforward. This is due to a number of reasons:

- Equilibrium of embedded retaining walls is often ensured primarily by the passive resistance of soil below dredge level. The validity of MO approach to the evaluation of passive resistance must be confirmed.

- MO method is an extension of Coulomb's sliding-wedge analysis, which is suited for a homogeneous soil. Embedded retaining walls, extending well below dredge level, almost inevitably interact with heterogeneous, layered deposits.

- Gravity retaining walls retain a soil volume which is either partially (for excavations) or entirely (for backfilled walls) man-made, in which it is possible to construct a drainage system. Therefore, the effect of pore pressures on the forces acting on the wall is often negligible. On the contrary, drainage in the vicinity of an embedded retaining wall is not usually performed and the effect of pore pressures must be accounted for.

- For the same reason, in gravity retaining walls it is possible, to a certain extent, to chose the grain size distribution of the backfill hence actions due to a clayey backfill in undrained conditions is seldom an issue. Conversely, the soil interacting with the wall and providing active and passive pressure may well be fine-grained. A seismic analysis in undrained condition is often necessary.

- Deformability of both the retaining wall and the soil can significantly modify the resultant actions on the wall.

In the following, a brief discussion of each of the above points will be presented, aimed at highlighting the main uncertainties related to the use of the pseudo-static approach for the seismic analysis of embedded retaining structures and suggesting possible approaches to deal with them. The effect of the soil-wall deformability on the choice of pseudo-static seismic coefficients is also discussed.

PASSIVE RESISTANCE

Results from experiments on small-scale models have shown that MO theory provides a reasonable approximation to measured passive resistance (Richards & Elms 1992). This result have been obtained using smooth walls with small soil wall friction. For higher soil-wall friction angles δ, as in the case of cast-in-situ reinforced concrete walls, it may be anticipated that MO *formulae* will overestimate passive resistance, just as Coulomb's theory does in static condition. This happens because, for high

δ values, the curvature of sliding surfaces becomes significant. Therefore, it is recommended that for high soil-wall friction alternative solutions are used to compute the pseudo-static passive resistance, which take into account the curvature of the sliding surface, such those published by Chang (1981) and Chen & Liu (1990), based on an upper bound limit analysis approach.

LAYERED DEPOSITS

Just like Coulomb's theory, MO method was developed for a homogeneous sliding wedge, and is not readily applicable to layered soils.

Under static conditions, it is common to study the limit equilibrium of embedded retaining walls in layered soils using a hybrid approach, in which active and passive horizontal effective stresses, σ'_a and σ'_p, are computed multiplying vertical effective stresses by active and passive earth pressure coefficients, which in turn are obtained using Coulomb's theory. In principle, such a method could be adopted also in seismic conditions; for instance, active and passive effective horizontal stresses could be evaluated as:

$$\sigma'_{aE} = -2c'\sqrt{K_{aE}} + K_{aE}\sigma'_v \quad (1)$$

$$\sigma'_{pE} = 2c'\sqrt{K_{pE}} + K_{pE}\sigma'_v \quad (2)$$

where the suffix E refers to seismic conditions, and c' is the effective cohesion. Pseudo-static active and passive earth pressure coefficients. K_{aE} and K_{pE}, can be computed according to MO theory or similar. This procedure takes into account a distribution of effective stress consistent with soil layering and pore water pressure.

Application of MO theory to layered soil deposits also brings about the issue of the point of application of the seismic earth pressure.

For active pressures, shaking table results (Ishibashi & Fang 1987) and simplified calculations (Richards *et al.* 1999) show that the location of the total active force is a function of the type of movement associated with a limit state. A tentative summary of these findings in shown is Figure 1. Under static conditions, the wall movement has an influence on the distribution of active pressure which is not dissimilar from that shown in Figure 1. For instance, if, under working conditions, horizontal displacements at the top of the wall are restrained, say, by a prop, then active pressure will not be completely mobilised near the top of the wall, and the centre of the earth pressure distribution will move up. While this may have an effect on bending moments in the wall, in an ultimate limit state calculation full mobilization of active limit state should be assumed in order to check stability.

Evidence for passive limit states under seismic conditions are somewhat limited: Richards & Elms (1992) report a position of the resultant passive force slightly lower than that associated to static conditions.

Calculations carried out by Chang & Chen (1990) based on the Dubrova (1963) approach show that the type of soil movement have an influence on the position of the resultant earth forces more limited than that shown in Fig. 1: the distance of the resultant force from the base of the wall ranges from 0.3 to 0.37 H for the active case and from 0.28 to 0.4 H for the passive case.

Examining the above information, it does not seem unreasonable to extend to the seismic analysis of embedded retaining walls in layered soils the approach used under static conditions, i.e. to evaluate the distribution of effective horizontal stresses using equations (1) and (2), and perform stability checks with the usual limit equilibrium method, without any further assumption on the position of the resultant forces.

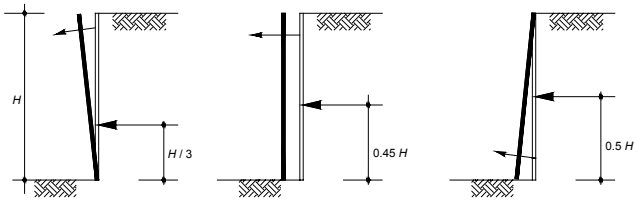

Fig. 1: Approximate location of resultant of active forces, from results of Ishibashi & Fang (1987) and Richards & *et al.* (1999).

EFFECT OF PORE PRESSURE

In EC8 Part 5, Annex E, a method is proposed to account for the effect of pore water pressure in pseudo-static calculation: it consists

in a multiplication of the seismic horizontal and vertical coefficients k_h and k_v by appropriate values of saturated, dry, or submerged unit weight of the soil (Matsuzawa *et al.* 1984). While this method may yield reasonable results (Steedman 1998), its physical basis does not seem obvious. Also, it is not applicable to the frequent cases of layered soils and to non-hydrostatic conditions, and it does not seem to account for excess pore pressures induced by the earthquake.

In principle, for a homogeneous soil it is not difficult to update MO analysis to the case in which there is a known distribution of pore pressure along the sliding surface (Figure 2). In this case, a closed form solution may not exist, and the resultant active (passive) force should be maximised (minimised) with respect to the slope α of the active (passive) wedge.

Pore pressure increments produced by the earthquake Δu_E should be calculated separately using, for instance, the procedures proposed by Seed & Booker (1977) and Matsui (1980), and should be included into the resultant force *U* in Fig. 2.

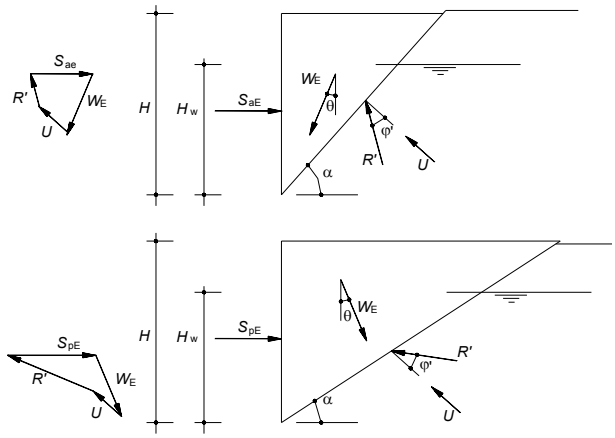

Fig 2: Mononobe-Okabe analysis modified to account for the presence of pore water pressure.

For layered soil deposits, in drained conditions, the complete pore pressure distribution should be evaluated in the soil interacting with the excavation. In general, the pore pressure *u* at a point will be:

$$u = u_S + \Delta u_E \qquad (3)$$

where u_S is the static steady-state pore water pressure, that in general may not be hydrostatic, and Δu_E is the change in pore water pressure produced by the earthquake. Then, equations (1) and (2) can be used to compute the effective stresses in the active and passive limit state, which should be added to *u* in order to write equilibrium equations.

UNDRAINED CONDITIONS

For excavations in clay, two limit conditions can be envisaged:

A. the earthquake occurs soon after the excavation, while the soil is still in undrained conditions. In this case, the pore pressure at a point would be:

$$u = u_S + \Delta u_0 + \Delta u_E \qquad (4)$$

where Δu_0 are the changes in pore water pressure produced by the excavation. Often, the uncertainties in the evaluation of Δu_0, along with their strong spatial variability, make an effective stress analysis unfeasible. Then, calculations of active and passive resistances should be carried out in terms of total stresses, and the effect of Δu_E be accounted for by reducing the undrained shear strength using, for instance, the concept of degradation index (Idriss *et al*. 1978).

B. the earthquake occurs after the excavation has reached drained conditions, and values of Δu_0 have become negligible. In this case, the analysis can be carried out in terms of effective stress, accounting for steady state pore pressure and changes produced by the earthquake as discussed in the previous section.

DEFORMABILITY AND CHOICE OF SEISMIC COEFFICIENTS

In EC8 part 5, at 7.3.2.2 clause (4), it is stated that the horizontal seismic coefficient k_h, necessary to calculate equivalent pseudo-static forces on a retaining structure, should be evaluated as:

$$k_h = \frac{a_g}{g}\frac{S}{r} \qquad (5)$$

where a_g is the peak acceleration on type A ground (rock-like), S is the amplification coefficient, depending on soil type (over a depth of 30 m), and r is a function of the displacement d_r that the retaining structure can accept. For non-gravity wall, the prescribed value for r is 1 (EC8 Pert 5, Table 7.1) that is, the pseudo-static analysis of an embedded retaining wall should be carried out assuming that the soil interacting with the wall is subjected to a value of the horizontal acceleration which is: a) constant in space and time (this is implicit in a pseudo-static analysis); b) equal to the peak acceleration expected at the soil surface.

Deformability of the soil can produce amplification of acceleration, that is incorporated in coefficient S, but that can be better evaluated through a site response analysis.

For many structures, including embedded retaining walls, there may be reasons to question the assumption that the structure should be designed assuming a constant peak acceleration. The validity of the two assumptions (spatial and temporal invariance) will be examined separately for clarity.

Figure 3.a shows a MO active wedge which interacts with a vertically propagating harmonic shear wave of frequency f and velocity V_s, characterised by a wavelength $\lambda = V_s/f$ larger that the height of the wedge H. In this case, the variation of the acceleration along the height of the wedge is small, inertial forces (per unit mass) are about constant and the motion of each horizontal element is approximately in phase.

In Figure 3.b a case is depicted in which, either because V_s is smaller (the soil is more deformable) or f is larger, λ is small compared to H. In this case, at a given time t, different horizontal wedge elements are subjected to different inertial forces, and their motion is out of phase. Therefore, at each t the assumption of spatial invariance of the acceleration is no longer valid, and, at each t, the resultant inertial force on the wedge must lead to a smaller resultant force S_{aE} than that predicted with the MO analysis. Steedman & Zeng (1990) have proposed a method for evaluating the effect of spatial variability of the inertial forces on the values of S_{aE}, maintaining the hypothesis that the wedge is subjected to a harmonic wave. Figure 4 shows some results obtained using this method. Expressing the resultant force as usual:

$$S_{aE} = \frac{1}{2}\gamma H^2 K_{aE} \qquad (6)$$

the calculation results can be expressed in terms of equivalent values of the coefficient of active pressure K_{aE}, plotted as a function of the ratio H/λ, for different values of the amplitude of the shear wave a_g. The equivalent values of K_{aE} can be quite smaller than the corresponding MO ones (obtained for $H/\lambda = 0$): in the example given in Figure 4, K_{aE} decreases by about 40 % for the stronger wave, as H/λ tends to 1. Values of K_{aE} decrease for increasing wall height, decreasing soil stiffness (quantified by V_s), and increasing frequency of the incident wave.

This approach may be used in practical applications by performing a site response analysis, selecting a value of V_s derived by the average secant shear modulus mobilised along the wall height, and choosing f as the dominant frequency of the seismic motion at a characteristic elevation along the retaining wall.

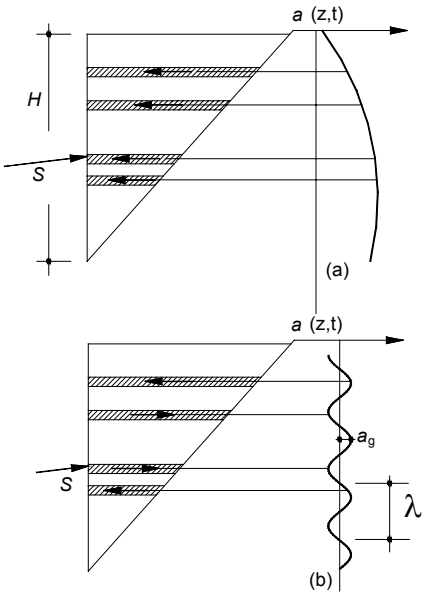

Fig 3: Mononobe-Okabe wedge interacting with harmonic wave characterised by (a) small wavelength; (b) large wavelength.

The assumption of a peak acceleration constant in time for the pseudo-static analysis of an embedded retaining structure can be questioned on different grounds.

It should be clear that coefficient r in equation (5) depends on the displacements that the structure can accept with no loss of strength. That is, it may be acceptable that over a small temporal period during an earthquake the acceleration is higher than a critical value producing limit conditions, provided that this will lead to acceptable displacements and that these displacements do not produce any strength degradation. This is equivalent to state that the behaviour of the structure should be ductile, i.e. that strength should not drop as the displacements increase.

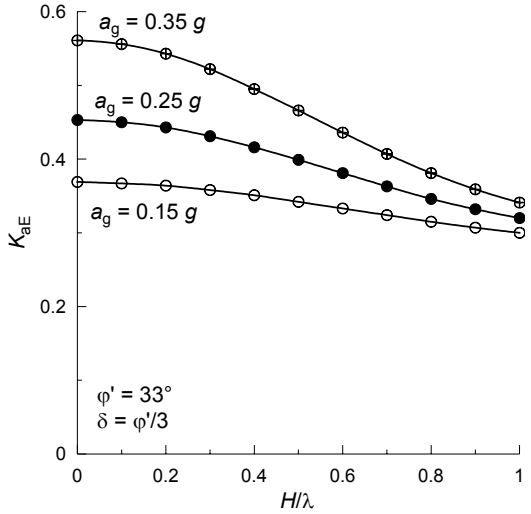

Fig 4: Results of the Steedman & Zeng (1990) method: seismic coefficient of active pressure as a function of H/λ for three different peak acceleration of the harmonic wave.

Therefore, the prescribed value of $r = 1$ in EC8 for non-gravity walls reveals the underlying hypothesis that the behaviour of such structures is fragile. In this perspective, any possibility of a Newmark-type displacement analysis is also ruled out. However, as for many other structures, it may be advantageous to rely on ductility, allowing a significant part of the energy transferred by the earthquake to be dissipated by the plastic, hysteretic behaviour of the materials, rather than designing very strong, non-dissipative structures.

It is then natural to investigate whether embedded retaining structures have a ductile behaviour, and which are the possible causes leading to a fragile behaviour. The following is a tentative list of possible sources of fragility and relative measures for increasing ductility:

- rupture of the steel tendon of a prestressed anchor: this is an obvious fragile phenomenon, which should be avoided by increasing the tendon strength;
- overstressing of the wall structure: walls should be designed to be intrinsically ductile in bending and shear, for instance by a proper design of reinforcement in a concrete wall;
- buckling of a horizontal prop: props should be designed to fail in compression for loads smaller than those producing instability;
- fragile mechanical behaviour of contact between anchor active length and soil: the anchor skin friction should be designed using strength parameters for the surrounding soil evaluated for large displacements, i.e. constant volume angle of friction for coarse grained soils, post-peak to residual angle of friction for fine grained soils;
- fragile mechanical behaviour of soils providing active pressure and passive resistance: design should be carried out with strength parameters relative to large strains, effective cohesion should be neglected.

For an embedded retaining structure characterised by a ductile behaviour, it can be anticipated that the equivalent value of the acceleration to use in a pseudo-static calculation, as if it were constant in time, should be significant smaller than the expected peak acceleration (Anastassopoulos *et al.* 2004). Such a reduction should be evaluated by a review of available case histories, and through parametric advanced numerical analysis of embedded retaining structures in which the dissipative properties of both soil and structural elements are properly modelled.

REFERENCES

Anastassopoulos I., Gazetas G., and Psarropoulos P.N. (2004). "On the seismic response of flexible retaining structures." *Proc. 11th Int. Conf. On Soil Dynamics and Earthquake Engineering – Proc. 3rd Int. Conf. On Earthquake Geotechnical Engineerning,* Vol. 1, 96-103.

Chang M.F. (1981). *Static and seismic lateral earth pressures on rigid retaining structures*. Ph.D. Thesis, School of Civil Engineering, Purdue University.

Chang M.F. & Chen W.F. (1990). "Some practical considerations in design of rigid retaining

structures." In: Chen W.F. & Liu X.L. (1990). *Limit analysis in soil mechanics*. Elsevier Science Publishers, 231-308.

Chen W.F. & Liu X.L. (1990). *Limit analysis in soil mechanics*. Elsevier Science Publishers.

Dubrova G.A. (1963). *Interaction of Soils and Structures*. Renhoy Transport, Moscow.

Idriss I.M., Dobry R., and Singh R.D. (1978). "Non linear behaviour of soft clays during cyclic loading". *Journal of Geotechnical Engineering*, Vol. 104, No. 12, 1427-1447.

Ishibashi I. and Fang Y.S. (1987). "Dynamic earth pressures with different wall movement modes, soils and foundations." *Japanese Soc. Of Soil Mech. And Found. Engrg.*, Vol. 27, 4, 11-22.

Matsui T., Ohara H., and Ito T. (1980). "Cyclic stress-strain history and shear characteristics of clay". *Journal of Geotechnical Engineering*, Vol. 106, No. 10, 1101-1120.

Matsuzawa H., Ishibashi I. & Kawamura M. (1984). "Dynamic soil and water pressures of submerged soils." *Journal of Geotechnical Engineering*, Vol. 111, No.10, 1161-1176.

Richards R. & Elms D.G. (1992). "Seismic passive resistance of tied-back walls." *Journal of Geotechnical Engineering*, Vol. 118, No. 7, 996-1011.

Richards R., Huang C., and Fishman K.L. (1999). "Seismic earth pressure on retaining structures." *Journal of Geotechnical and Geoenvironmental Engineering*, Vol. 125, No.9, 771-778.

Seed H.B. and Booker, J.R. (1977). "Stabilization of potentially liquefiable san deposits using gravel drains." *Journal of Geotechnical Engineering*, Vol. 103, No. 7, 757-768.

Steedman R.S. & Zeng X. (1990). "The influence of phase on the calculation of pseudo-static earth pressure on a retaining wall." *Géotechnique* Vol. 40, No. 1, 103-112.

Steedman R.S. (1998). "Seismic design of retaining walls." *Geotechnical Engineering*, Vol. 131, Jan., 12-22.

SESSION 4: Soil Structure Interaction - Faults

Soil plasticity and uplifting effects on soil-structure interaction

G. Abate, M. R. Massimino, M. Maugeri

Department of Civil And Environmental Engineering, University of Catania, Italy

Abstract

The present paper deals with the seismic response of the Catania fire-station (Italy), which is, up to now, a no-seismically designed structure, despite its important function. Numerical DSSI analyses are performed by means of a FEM commercial code, including soil plasticity and soil-foundation plastic hinges. Particularly, sliding at the soil-foundation interface, uplifting of the foundation from the soil and mobilisation of the bearing capacity failure are taken into account. Artificial accelerograms, generated so as to match the elastic response spectrum given by the new Italian Seismic Regulation (O.P.C.M. 3274/2003) for soil of class A, are considered as input motions at the bedrock. The aim of the paper is, above all, to investigate the effects of soil elasto-plastic constitutive equations and foundation uplifting on the acceleration transmission and so on the structure bending moments and shear forces. A special attention is also devoted to the transient and permanent deformed configuration of the structure. The study performed leads to conclude that the effects of DSSI are numerous and difficult to predict without specific analyses. First of all, if it is true that, as suggested by EC8, DSSI causes an increasing of the structure fundamental period of vibration, it is at the mean time true that the predominant period of several recent earthquakes has been longer than those predicted by EC8 and so very probably close to the fundamental period of vibration of many structures. In this case DSSI is certainly detrimental. Furthermore, for guaranteeing not only the safety but also the functionality of all the structures, which is strictly related to the structure deformed configuration, "displacement-based" design and so DSSI analysis should always be performed. Finally, DSSI analyses should be encouraged in order to achieve the most economical design. In fact, to consider fixed-base structure can lead sometime to an exaggeratedly anti-economic design. The large acceleration levels recorded in several recent earthquakes would imposed an enormous ductility demands to structures if soil-foundation plastic hinging had not taken place to limit the transmitted accelerations.

INTRODUCTION

Several papers of Earthquake Geotechnical Engineering published in the last decades have demonstrated the important effects of dynamic soil-structure interaction (DSSI) in the seismic response of buildings (Mylonakis and Gazetas, 2000; Prakash, 2004). Eurocode 8 (EC8 – Part 5, 2003), devotes a chapter (Chapter 6) and a related annex (Annex D) to DSSI; but, the attention devoted to this field appears not to be exhaustive. Particularly, EC8 recognises that "*As a results of dynamic SSI, the seismic response of a flexibly-supported structure will differ in several ways from that of the same structure founded on rigid ground (fixed base)*", but it concludes that "*for the majority of common building structures the effects of SSI tend to be beneficial*" and so invites the reader to perform DSSI analyses only for a few number of structures, i.e.: i) structures where *P-*δ effect plays a significant role; ii) structures with massive or deep-seated foundations; iii) slender tall structures; iv) structures supported on very soft soils (Vs < 100 m/s). Furthermore, EC8 does not give any practical suggestion for performing DSSI.

However, the effects of DSSI are numerous and difficult to predict without specific analyses. Certainly, the effects of DSSI are strictly related to the predominant period of the input motion. According to EC8 we must recognise that "*the*

fundamental period of vibration of the flexibly-supported structure will be longer than that of the fixed-base structure"; this leads generally to a smaller design acceleration, considering the design spectra suggested by EC8. But, different recent earthquakes (Bucharest, 1977; Mexico City, 1985; Kobe, 1995) have been characterised by response spectra significant different from those suggested by EC8 in terms of predominant period, which has been longer than those predicted by EC8 and so approximately coincident with the fundamental period of vibration of most flexibly-supported structures (Fig. 1). This finding should invite to a deeper revision of the response spectra suggested by EC8.

Furthermore, even if DSSI analysis could lead to a design acceleration and so to bending moments and shear forces lower that those obtained analysing the fixed-base structure, it can lead to a permanent configuration not allowable for the functionality of the structure, as demonstrated by the behaviour of some structures hit by the 1999 Turkey earthquake. Fig. 2 shows a building, which rotated of about 30° due to the earthquake and in the following days of other 30° due to a consequent *P-*δ effect. The building lost its functionality, even if no significant structural damage occurred. Thus, DSSI analysis should always be performed to guarantee not only the safety but also the functionality of all the structures.

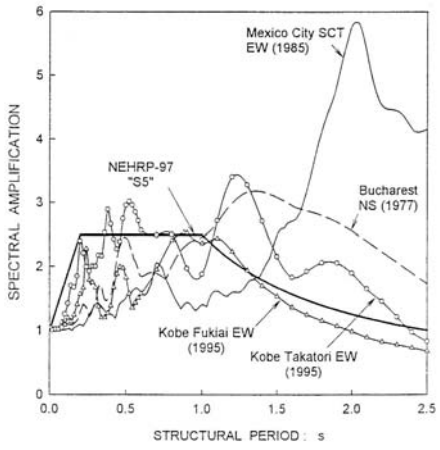

Fig 1: Comparison of a typical seismic code design spectrum to actual spectra from catastrophic earthquakes with strong long-period components; ξ = 5% (after Mylonakis and Gazetas, 2000).

Fig 2: Effects of the 1999 Turkey earthquake.

Finally, DSSI analyses should be encouraged in order to achieve not only the safest design, but also the most economical design. In fact, to consider fixed-base structure can lead sometime to an exaggeratedly anti-economic design in the evaluation of the bending moments and shear forces. As recently underlined by Maugeri et al. (2004) and by Gazetas (2005), the large acceleration levels recorded in several recent earthquakes (1986 San Salvator a_{max} = 0.75g; 1994 Northridge a_{max} = 0.98g; 1995 Kobe a_{max} = 0.85g; 1999 Chi-Chi a_{max} = 1.01g; 2001 Tattoni-Ken Seibu a_{max} = 0.95g) would imposed an enormous ductility demands to structures if soil-foundation plastic hinging had not taken place to limit the transmitted accelerations. If we consider these recorded accelerations in seismic design of new buildings or in seismic retrofitting of existing buildings, without extending the inelastic analysis of structures also to the supporting foundations and soil, we will often arrive to design not technically or economically feasible. Thus, it appears necessary to consider soil-foundation plastic hinges, which consist of: i) sliding at the soil-foundation interface; ii) separation and uplifting of the foundation from the soil; iii) mobilisation of the bearing capacity failure.

The present paper deals with the seismic response of the Catania fire-station, which, despite its important function, is a no-seismically designed structure in a seismic area. A numerical DSSI analysis is performed including the above mentioned plastic hinges. Interesting results are achieved in terms of structure displacements as well as bending moments and shear forces.

FEM ANALYSIS OF THE SEISMIC RESPONSE OF A THREE-STOREY BUILDING

The structure and its subsoil

The Catania fire-station was built at the end of 1950'. It consists of eight buildings. All the buildings have a classical reinforced-concrete structure designed to resist only to gravitational loads and so characterized by open frames and isolated square footings of different sizes. The present paper refers to the seismic behaviour of one significant 2-D frame located at the fire-station gate (Fig. 3). In particular, the frame is characterized by long cantilever beams, which cause a great axial force on the contiguous columns. For all the three square footings a plane section of 1.60m x 1.60m and an embedment of 1.00 m is assumed. The computation of gravitational loads to be applied on the frame is performed as suggested by O.P.C.M. 3274/2003.

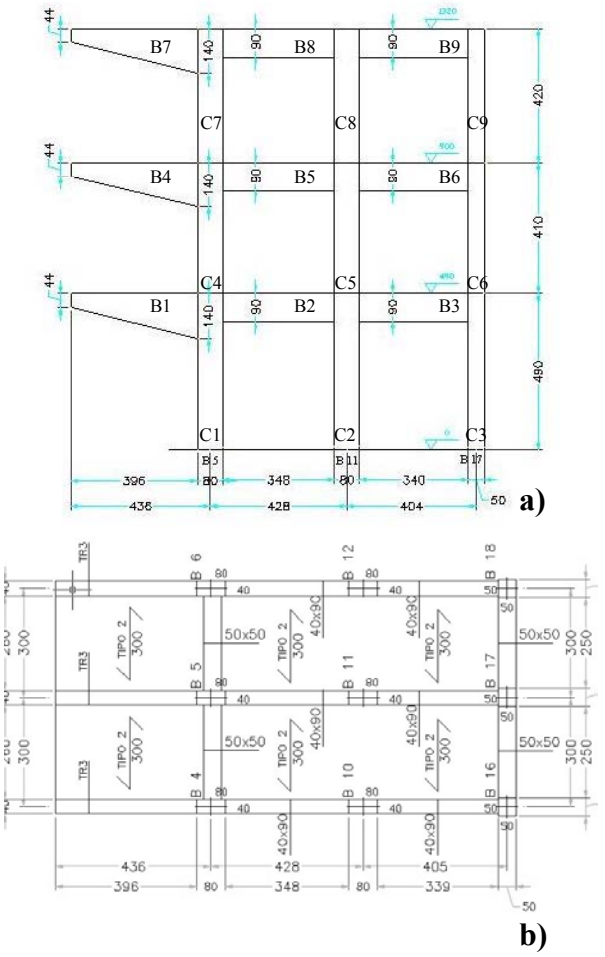

Fig 3: Analysed 2-D frame: a) section; b) typical structural plan (after Abate et al., 2006).

The subsoil consists on: i) sand-gravel from the soil surface up to the depth of 8.00 m; ii) basalts from 8.00 m up to 25.00 m. No water-table was found (DICA, 2000). The main properties of the sand-gravel deposit are: γ = 17.30 kN/m^3; D_r = 70-85 %; V_s = 300 m/s; φ' = 34°; c' = 0 kPa; E_0 = 80 MPa; ν = 0.33 (Cavallaro and Maugeri, 2004). This soil can be assimilated to a ground type E according to EC8-Part 1 (2003) and O.P.C.M. 3274/2003.

For more details on the structure and the subsoil see Abate et al., 2006.

FEM models

Two different numerical models are adopted for studying the seismic response of the 2-D frame shown in Fig. 3, by means of the ADINA finite element code (Bathe, 1996).

The first model (named *Fixed-base model*) consists of only the structure fixed at the base; the second model (named *S-S model*) involves both the structure and the interacting subsoil. In this last case the horizontal bottom boundary is 8.00 m from the structure, according to the soil profile discussed in the previous paragraph. Similarly, the two lateral boundaries are 8.00 m from the structure (Fig. 4). For the horizontal bottom boundary the vertical displacements are fixed equal to zero, while a horizontal displacement time-history is given, as will be explained better in the following paragraph. For the lateral boundaries the vertical displacements are free, while the horizontal displacements are constrained in the following way: each point of the left lateral boundary is constrained to have the same horizontal displacement of the point of the right lateral boundary located at the same depth. This constraint law is given in order to have a stable model minimizing, at the mean time, the horizontal boundary effects (see *Results* paragraph).

Three contacts are fixed at the soil-foundation contact areas; these allow us to simulate frictional sliding at the soil-foundation interface and uplifting of the foundations from the soil. Fig. 4 shows the contact nodes 11, 12 and 13, which represent the middle points of each foundation; the corresponding contact nodes, which belong to the soil, are 9106, 9392 and 9678.

The Rayleigh damping factors *a* and *b* are fixed equal to 4.20 and 0.015 respectively

(Abate et al., 2006). Finally, in order to investigate the soil non-linearity effects both the linear elastic constitutive model and the Mohr-Coulomb elasto-plastic constitutive model are utilized for the soil. More sophisticated soil constitutive models, such as elasto-plastic constitutive models involving isotropic and kinematic hardening and/or softening (Gajo and Muir Wood, 1999), incrementally non linear (Darve, 1990) or hypoplastic (Chambon et al., 1994) models should be utilized for a better simulation of dynamic soil behaviour. Unfortunately, at the moment these constitutive models are not implemented in commercial codes, such as ADINA code. The Catania Geotechnical group has recently implemented an elasto-plastic constitutive model involving isotropic/kinematic hardening/softening in the ADINA code. The new version of this code is at the moment in a validation phase (Abate et al., 2005).

Input motions

Ten artificial accelerograms generated so as to match the elastic response spectrum given by O.P.C.M. 3274/2003 for soil of class A are considered. The elastic spectra obtained from these accelerograms for a structure damping ratio ξ = 5% should be such that their medium elastic spectrum has ordinates, whose distances from those of the spectrum suggested by O.P.C.M. 3274/2003 are not more than 10% in the period range 0.15-2.0 s.

The chosen accelerograms are then opportunely integrated twice to obtain ten horizontal displacement time-histories.

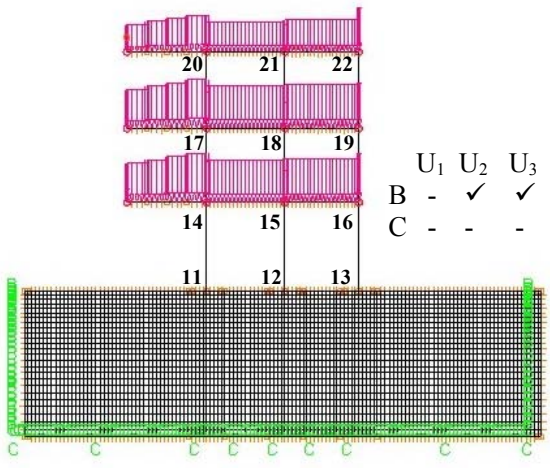

Fig 4: Numerical *S-S model* showing the foundation nodes 11, 12 and 13.

These latter are applied to the bottom horizontal boundary of the *S-S model* (Fig. 4). Due to lack of space, the results obtained for only one of these accelerograms(Fig. 5), are presented in the following.

This input motion does not lead clearly to foundation uplifting, even if an important rocking component of the structure behaviour is found. Thus, in order to deeper investigate on foundation uplifting effects, the amplitude of the previous displacement time-history is increased of 20 mm, so a new amplified input motion is also considered (Fig. 6).

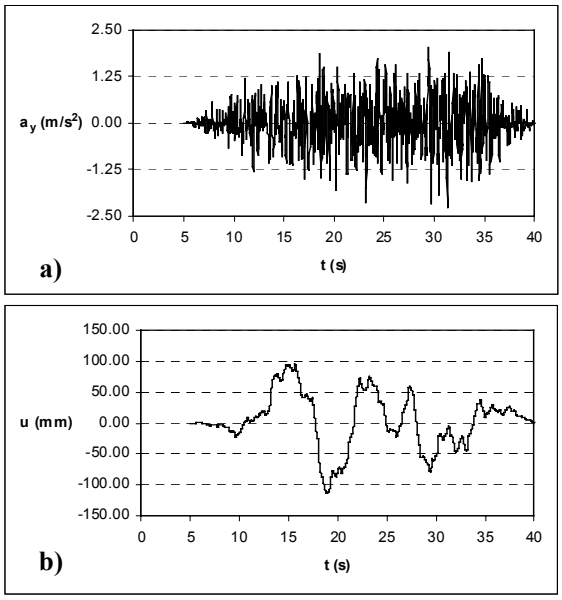

Fig. 5: Seismic input: a) artificial accelerogram; b) corresponding horizontal displacement time-history.

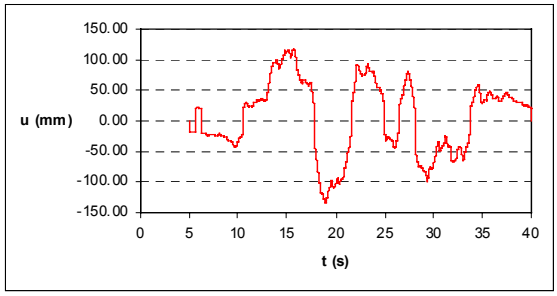

Fig. 6: Amplified horizontal displacement time-history applied to the bottom boundary of the *S-S model*.

RESULTS

First of all, it is interesting to observe, as predicted by EC8 (EC8-Part 5, 2003), the significant increasing of the fundamental period of vibration of the investigated system, moving from the fixed-base structure to the flexibly-supported structure (Fig. 7). This leads to a considerable decreasing of the acceleration transferred to the structure. The main important consequence of this phenomenon is the significant decreasing of the total shear force *V* at each storey (Fig. 8), as well as to a general considerable reduction of the bending moments on the beams (Table 1) and on the columns (Table 2), moving from the fixed-base structure to the flexibly-supported structure.

Analysing also the acceleration time-histories of the soil-foundation contacts, it is possible to see a perfect acceleration transmission from the subsoil to the structure for the node pair 11-9106; while a considerable acceleration reduction occurs moving from node 9678 to node 13 (Figs. 9 and 10). The great values obtained for nodes 13 and 9678 considering the linear elastic soil behaviour and for all the soil-foundation contact nodes considering the Mohr-Coulomb soil behaviour are due to numerical instability typical of contact zones. Going away from contact zones this instability disappears immediately, but the important aspect of the different acceleration transmission for node pairs 11-9106 and 13-9678 remains.

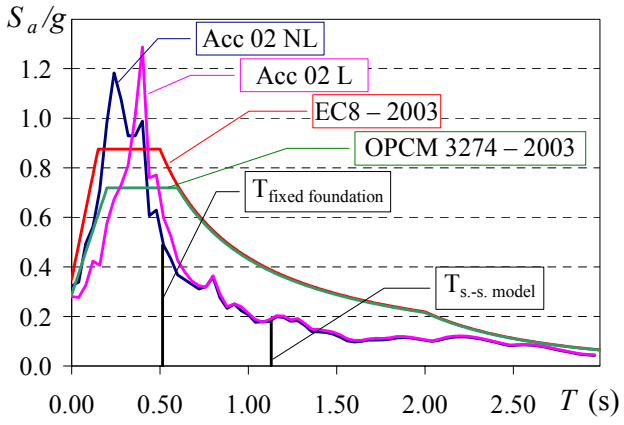

Fig 7: Decreasing of the fundamental period of vibration of the system moving from the fixed-base structure to the flexibly-supported structure.

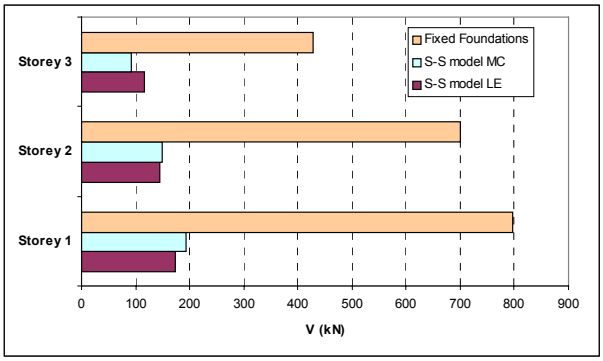

Fig 8: Peak values of the total shear forces *V* per each storey.

Table 1: Peak values of the bending moments on the beams [kNm]

Beam	Node	Fixed Foundations		L.E. Soil Model		M.C. Soil Model	
		Min	*max*	*min*	*max*	*min*	*max*
B1	sx						
	dx	-371.39		-371.39		-371.39	
B2	sx	-669.15	1119.04	-7.52	445.65	-80.61	408.73
	dx	-586.79	530.43	-229.34	52.38	-300.17	21.71
B3	sx	-579.73	609.33	-64.88	184.71	0	343.06
	dx	-1064.87	976.84	-274.60	203.38	-295.32	187.04
B4	sx						
	dx	-371.41		-371.41		-371.41	
B5	sx	-413.195	798.16	0	352.76	0	258.17
	dx	-462.90	364.88	-185.39	27.83	-301.24	0
B6	sx	-370.52	436.83	0	210.75	0	309.70
	dx	-705.09	621.81	-86.63	196.66	-55.34	236.47
B7	sx						
	dx	-287.39		-287.39		-287.39	
B8	sx	-48.51	449.85	0	274.06	0	227.41
	dx	-205.76	138.80	-126.94	0	-220.80	0
B9	sx	-107.32	169.68	0	121.85	0	225.95
	dx	-284.34	256.37	-39.64	96.53	-22.83	115.46

Table 2: Peak values of the bending moments on the columns [kNm]

Beam	Node	Fixed Foundations		L.E. Soil Model		M.C. Soil Model	
		min	*max*	*min*	*max*	*min*	*max*
C1	down	-557.46	633.54	-127.66	33.55	-39.13	185.72
	up	-470.50	587.56	-93.52	221.8	-102.29	267.57
C2	down	-632.94	660.57	-67.38	66.55	-148.33	39.73
	up	-621.51	641.97	-111.21	211.51	-269.61	130.29
C3	down	-632.94	660.57	-67.38	66.55	-148.33	39.73
	up	-621.51	641.97	-111.21	211.51	-269.61	130.29
C4	down	-276.52	456.88	0	164.18	0	187.71
	up	-301.62	479.46	0	165.73	0	198.36
C5	down	-517.72	527.62	-139.67	82.71	-97.61	102.86
	up	-514.35	527.25	-134.77	85.28	-101.97	98.35
C6	down	-517.72	527.62	-139.67	82.71	-102.41	102.86
	up	-514.35	527.25	-134.77	85.28	-101.97	98.35
C7	down	-138.19	305.25	0	149.32	0	153.68
	up	-162.14	336.22	0	156.98	0	162.70
C8	down	-301.84	306.17	-103.81	54.53	-86.95	34.93
	up	-308.48	313.09	-105.78	55.53	-87.75	35.61
C9	down	-301.84	306.17	-103.81	54.53	-86.95	34.93
	up	-308.48	313.09	-105.78	55.53	-87.75	35.61

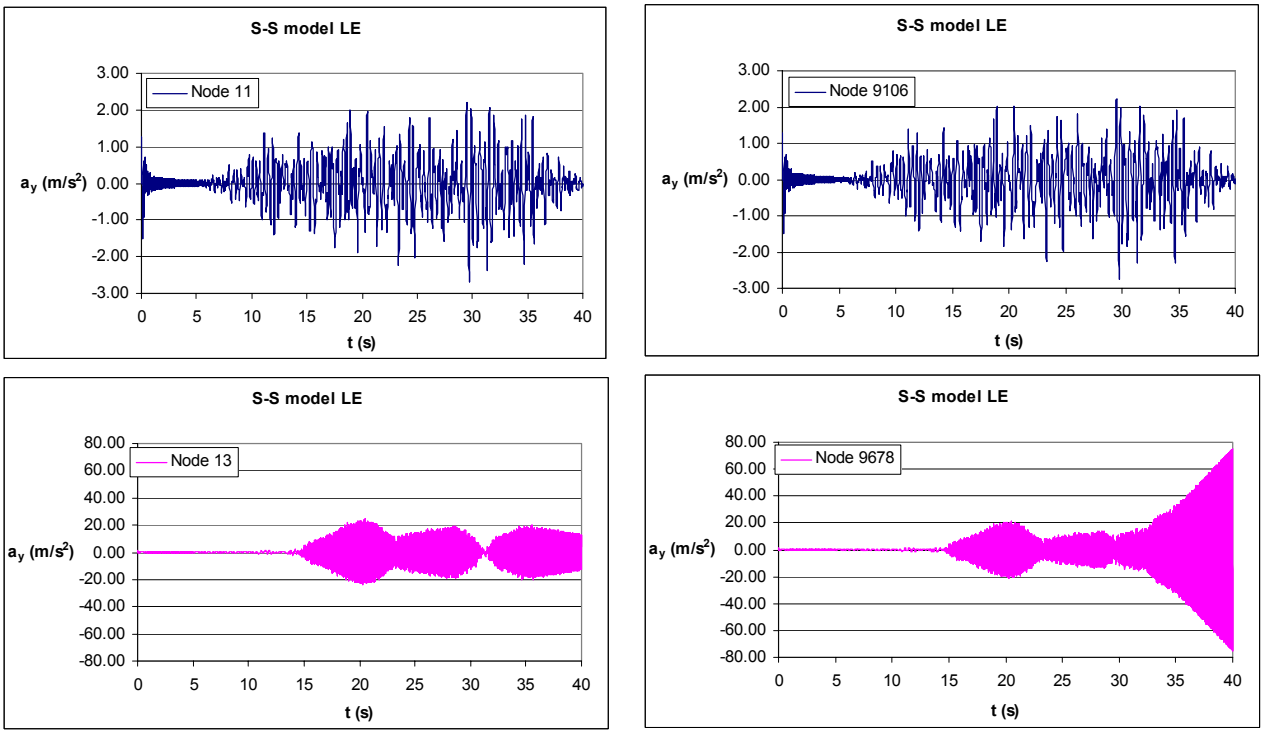

Fig 9: Horizontal acceleration time-histories for soil-foundation contact node pairs 11-9106 and 13-9678, considering the linear elastic soil constitutive model.

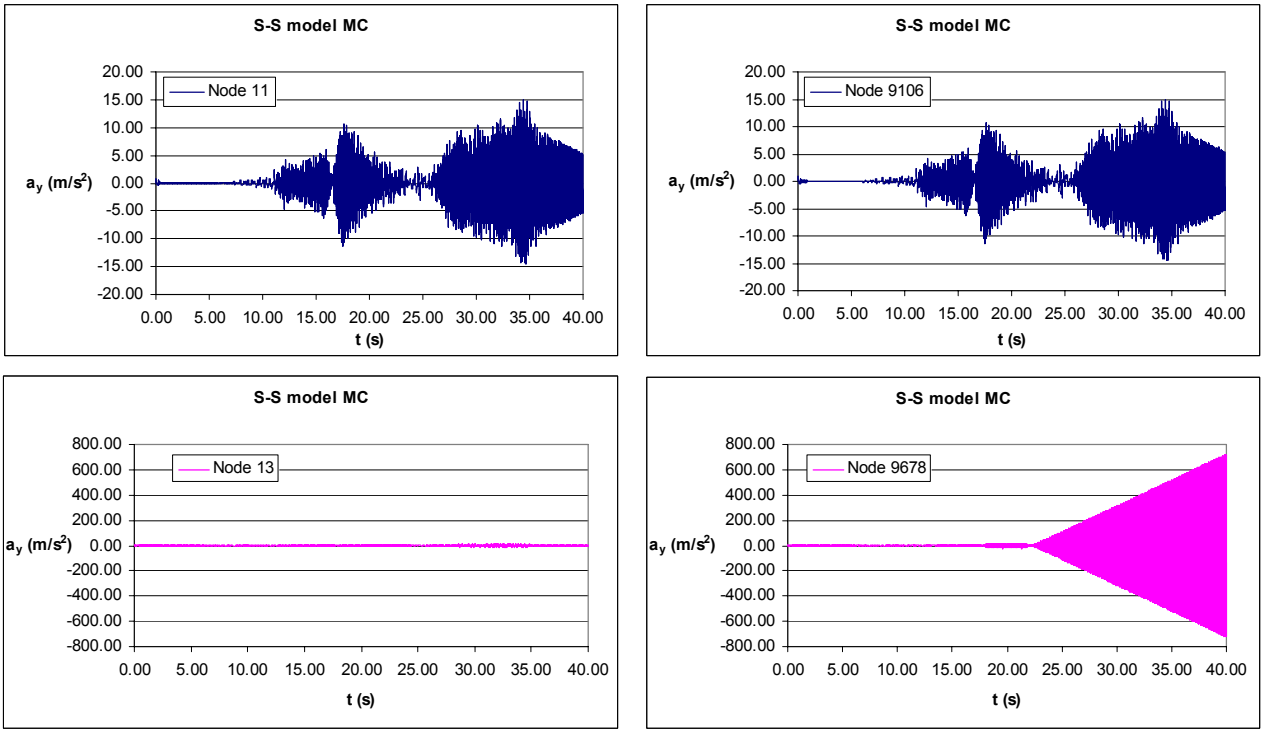

Fig 10: Horizontal acceleration time-histories for soil-foundation contact node pairs 11-9106 and 13-9678, considering the Mohr-Coulomb soil constitutive model.

The analysis of seismic response of structures should be also founded on "*displacement-base*" design concept, to avoid deformed configurations not allowable for building functionality. With this aim the performed numerical analyses are also devoted to investigate on structure displacements. In particular, Fig. 11 shows the vertical displacement time-histories of the foundation nodes 11 and 13, considering the linear elastic soil constitutive model (Fig. 11.a) and the Mohr-Coulomb soil constitutive model (Fig. 11.b). In this last case, because of the possibility to account for plastic strains, a significant permanent positive vertical displacement is reached for node 11, while node 13 shows a light foundation uplifting, due to the quite rigid rotation of the structure. Furthermore, significant differential vertical displacements can be observed both in terms of peak and permanent values (Tables 3 and 4).

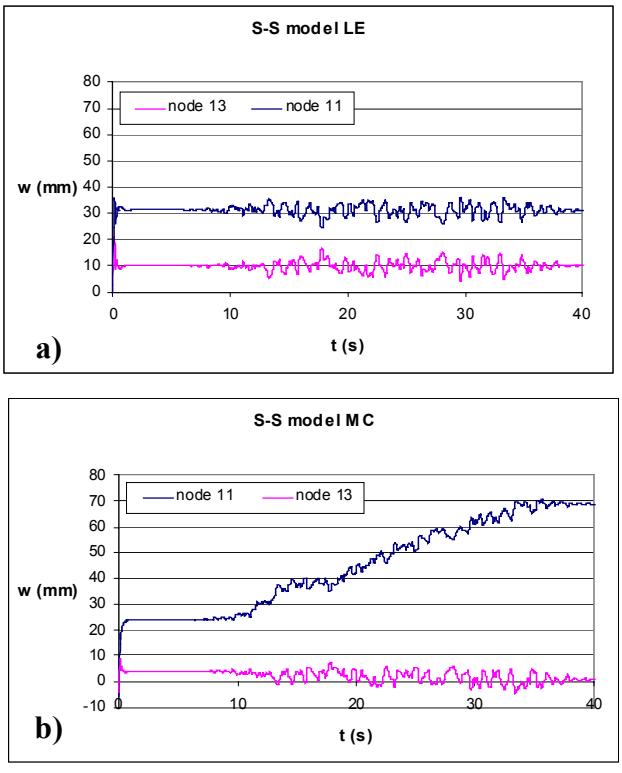

Fig 11: Vertical displacement time-histories for the foundation nodes 11 and 13, considering: a) the linear elastic soil constitutive model; b) the Mohr-Coulomb soil constitutive model

A great agreement exists for the horizontal displacements of all the isolated foundations, considering the linear elastic soil constitutive model, while a low divergence appears considering the Mohr-Coulomb soil constitutive model (Fig. 12).

Furthermore, the time-histories of the foundation horizontal displacements are very similar to the time-history of the input motion (Fig. 5), but sliding at the soil-foundation interface occur for the right foundation, as it is possible to observe comparing the horizontal displacements of nodes 13 and 9678 (Tables 3 and 4).

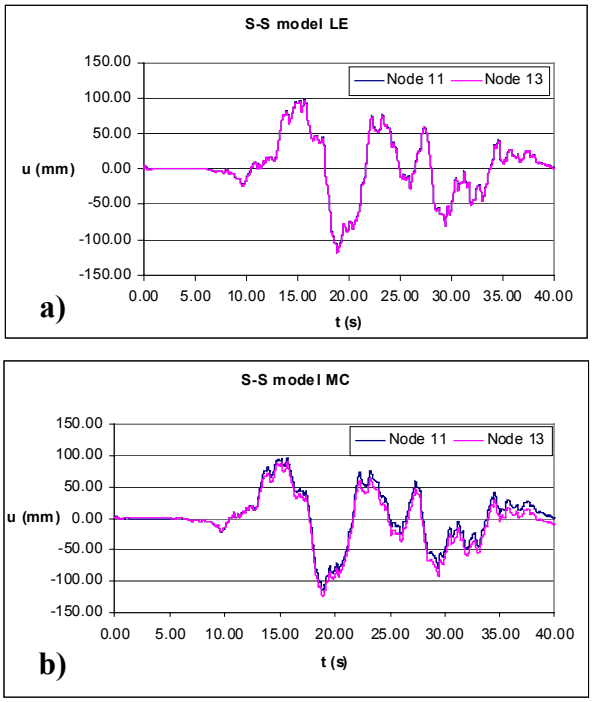

Fig 12: Horizontal displacement time-histories for the foundation nodes 11 and 13, considering: a) the linear elastic soil constitutive model; b) the Mohr-Coulomb soil constitutive model

Table 3: Peak values of the vertical and horizontal foundation displacements

Absolute displacement					
	11	**12**	**13**	**9106**	**9678**
			w_{max} [mm]		
L. E. Soil Model	36	28	21	36	21
M. C. Soil Model	70	33	9	70	9
			u_{max} [mm]		
L. E. Soil Model	117	118	118	117	118
M. C. Soil Model	116	115	126	116	115
Differential displacement					
	11 –12	**12 – 13**	**11 –12**	**12 – 13**	
	Δw_{max} [mm]		Δu_{max} [mm]		
L. E. Soil Model	17	15	2	0.7	
M. C. Soil Model	40	35	4	15	

Table 4: Permanent vertical and horizontal foundation displacements

Absolute displacement					
	11	**12**	**13**	**9106**	**9678**
			***w* [mm]**		
L. E. Soil Model	31	20	10	31	18
M. C. Soil Model	69	32	1	69	2
			***u* [mm]**		
L. E. Soil Model	0.7	-0.2	-0.01	0.7	0.3
M. C. Soil Model	-0.2	2	-12	-0.2	4
Differential displacement					
	11 –12	**12 – 13**	**11 –12**	**12 – 13**	
	Δ*w* [mm]		**Δ*u* [mm]**		
L. E. Soil Model	11	10	0.9	0.2	
M. C. Soil Model	37	31	2	14	

Table 5: Horizontal displacements of nodes 11, 13, 20 and 22

Peak value						
		u_{max} [mm]			Δu_{max} [mm]	
	11	**20**	**13**	**22**	**11-20**	**13-22**
L. E. Soil Model	117	150	117	150	33	33
M. C. Soil Model	117	179	125	179	62	54
Permanent value						
		u_{max} [mm]			Δu_{max} [mm]	
	11	**20**	**13**	**22**	**11-20**	**13-22**
L. E. Soil Model	0.69	-32	-0.01	-32	33	32
M. C. Soil Model	-0.18	-111	-12	-111	111	99

Due to the large eccentricity of structural gravitational loads, the soil-foundation seismic displacements, as well as the displacements due to static loads, causes also significant total and differential displacements on the over-structure(Table 5 and Fig. 13).

A limitation for the differential horizontal displacements between nodes (i. e. between nodes 11 and 20 and nodes 13 and 22 of Fig. 4) should be prescribed to avoid *P-δ* effect, dangerous for the structure serviceability.

Finally, considering the amplified input motion of Fig. 6 the results achieved are qualitatively very similar to those above discussed. Of course, significantly bigger accelerations and displacements are experimented by the structure and in particular, the foundation uplifting appears clearly. Thus, the Authors consider not useful to show the results related to the amplified input motion in terms of bending moments and shear forces; while it is very interesting to show the deformed configurations of the system for some time steps. In particular, Fig. 14 shows the deformed configurations for the following time steps: a) *t* = 21.80 sec; b) *t* = 25.00 sec; c) *t* = 25.12 sec; d) *t* = 26.52 sec.

In the first two configurations (a and b), which are related to a negative peak value of the amplified input motion (see Fig. 6), the soil mass is moving toward right and the structure is following the soil movement but with an evident delay; the opposite behaviour can be observed for the last two configurations (c and d), which are related to the following positive peak value of the amplified input motion.

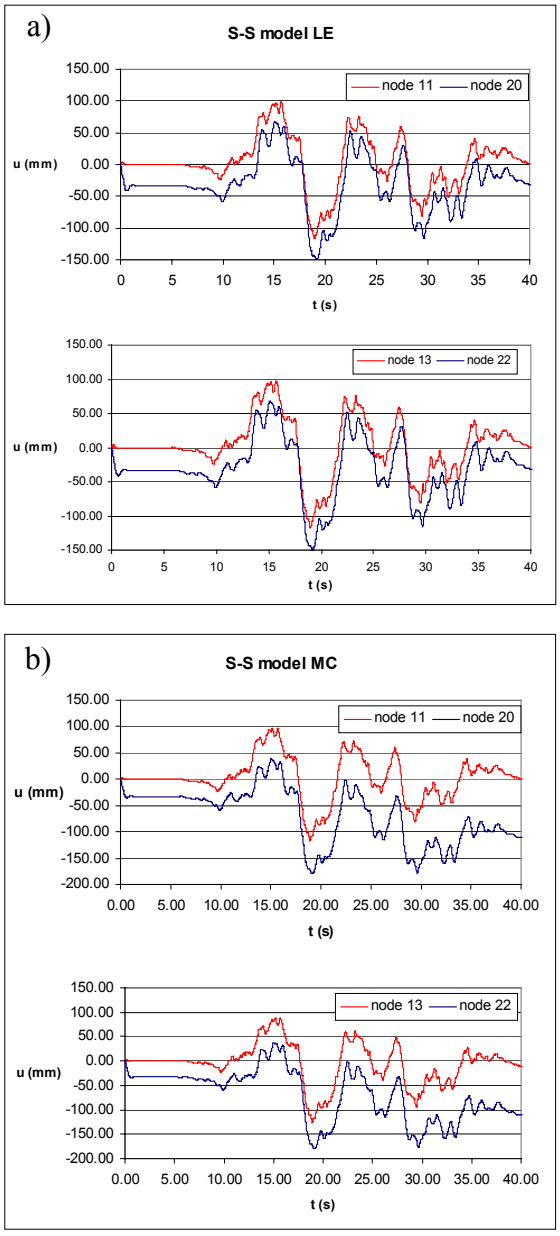

Fig 13: Horizontal displacement time-histories for the node pairs 11-20 and 13-22, considering: a) the linear elastic soil constitutive model; b) the Mohr-Coulomb soil constitutive model.

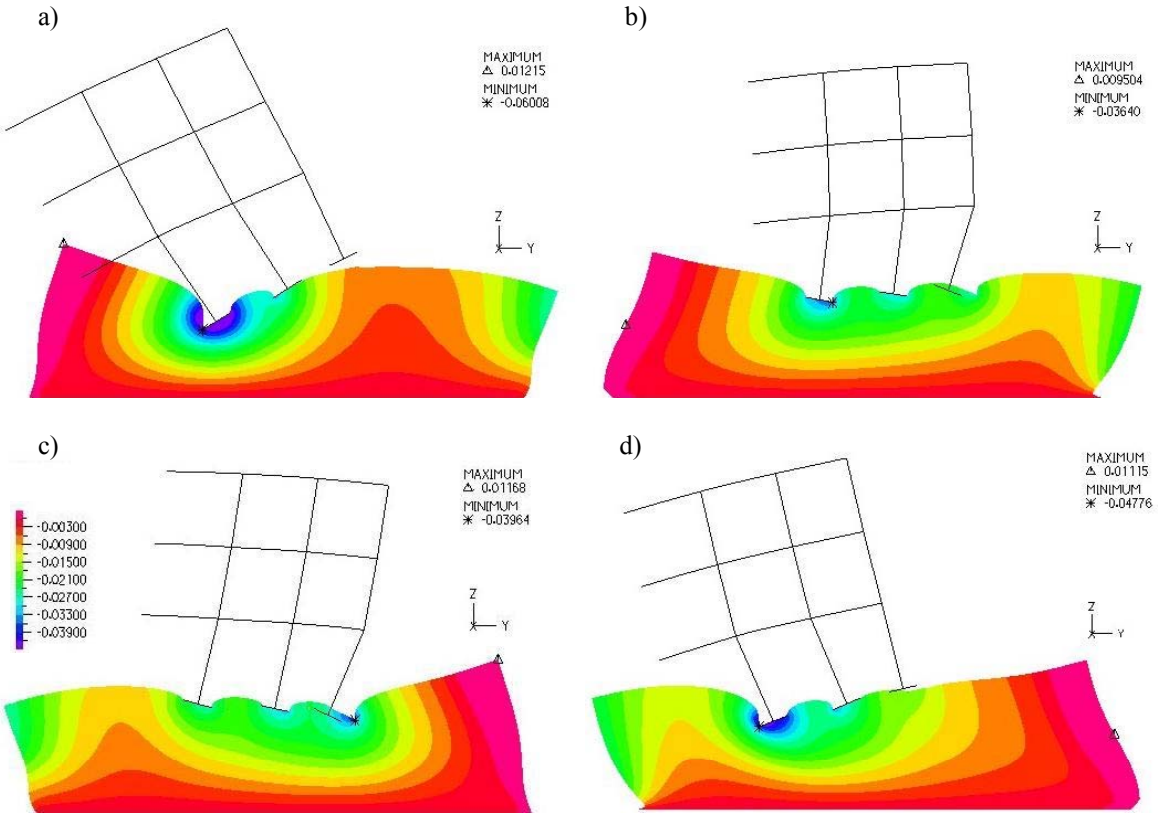

Fig. 14: Deformed configuration of the system under amplified seismic input, including soil vertical displacement band plot for the time steps: a) *t* = 21.80 sec; b) *t* = 25.00 sec; c) *t* = 25.12 sec; d) *t* = 26.52 sec (linear-elastic soil constitutive model - displacement amplification factor = 70).

From Fig. 14 it is also possible to see the movement of the lateral soil boundaries, which follow quite well the soil motion, reducing considerably the boundary effects on the transmission of the input motion through the soil, due to the imposed boundary conditions (see *FEM models* paragraph).

CONCLUSIONS

The present paper investigates DSSI by means of the analysis of one case-history. In particular, the seismic response of the Catania (Italy) fire-station is taken into account. Nevertheless, the majority of the results achieved can be qualitatively considered of general interest and sufficient to propose some integrations to EC8. So, based on the results presented in the paper the following conclusions can be made:

a) It is certainly to encouraged the performing of DSSI for all the structure typologies, instead of limiting it only to some kinds of structures, as suggested by EC8. The effects of DSSI are numerous and difficult to predict without specific numerical analyses.
b) The fundamental period of vibration of the flexibly-supported structure is longer than that of the fixed-base structure. Thus, generally, DSSI is beneficial. Nevertheless, considering the great predominant period of several recoded earthquakes, sometimes DSSI can be detrimental. So, specific studies to estimate site-dependent design spectra, which could have predominant period longer than those suggested in EC8-Part 1, should be encouraged in order to avoid dangerous resonant phenomena.
c) Considering the large acceleration levels of several recorded earthquakes, transient and permanent foundation displacements, as well as sliding at the soil-foundation interface, separation and uplifting of the foundation from the soil and mobilisation of the bearing capacity failure should be taken into consideration, in order to avoid not technically and economical feasible design. In this context numerical codes involving elasto-plastic, hypoplastic or incrementally non linear soil constitutive models are welcomed.

d) The results of DSSI should be taken into account in the foundation design, which should be founded not only on the "capacity" design principle, but also in the "displacement-based" design principle, in order to guarantee both the safety and the functionality of structures.

REFERENCES

Abate G., Massimino M.R., Maugeri M. (2005). "A kinematic-isotropic hardening constitutive model for granular soils: implementation in a FEM code and application to finite problems", *Computers & Mathematics with Applications*, Elsevier, Special Edition for the Symposium on "Granular Matter: Mathematical Modelling and Physical Instance", Reggio Calabria, June 26-29, 2005 (submitted).

Abate G., Bosco M., Massimino M.R., Maugeri M. (2006). "Limit state analysis for the Catania fire-station (Italy)". *Proc. 8NCEE*, San Francisco, 18-22 April, 2006 (accepted).

Bathe K.J. (1996). "Finite Element Procedures". *Prentice Hall*, Englewood Cliffs, NJ, 1996.

Cavallaro A., Maugeri M. (2004). "Dynamic Geotechnical Characterization for the Microzonation of the Seismical Area of Catania". *Proc. 5th Int. Conf. on Case Hist. in Geot. Eng.*, New York, 13-17 April 2004.

Chambon R., Desrues J., Hammad W., Charlier R. (1994). "CloE : a new rate type constitutive model for geomaterials. Theoretical basis and implementation". *Int. J. Num. Anal. Meth. Geomech.* Vol. 18, pp. 53-78.

Darve F. (1990). "Incrementally non-linear constitutive relationships". *Geomaterials Constitutive Equations and Modelling*. F. Darve ed., Elsevier Applied Science, pp. 213-238.

DICA (2000). "Progetto di consolidamento ed adeguamento sismico della Caserma dei Vigili del Fuoco di via C. Beccaria,Catania – Relazione Geologica". *Convenzione tra il Dipartimento di Ingegneria Civile ed Ambientale, Università di Catania e VIII Area Tecnica Provincia Regionale di Catania*.

EC8-Part 1 (2003). "Design of structures for earthquake resistance– Part 1: General rules, seismic actions and rules for buildings". *European Prestandard, ENV 1998*, Europ. Com. for Standard., Brussels.

EC8-Part 5 (2003). "Design of structures for earthquake resistance– Part 5: Foundations, retaining structures and geotechnical aspects". *European Prestandard, ENV 1998*, Europ. Com. for Standard., Brussels.

Gajo A., Muir Wood D. (1999). "A kinematic hardening constitutive model for sands: the multiaxial formulation". *Int. Journ. for Numerical and Analytical Methods in Geomechanics*, Vol. 23, pp. 925-965.

Gazetas G. (2005). "Seismic analysis of shallow foundations: beyond EC8". *Proc. Conferenze di Geotecnica di Torino XX Ciclo*, 22-23 November, 2005, Tourin.

Maugeri M., Castelli F., Massimino M. R. (2004). "Analisi, modellazione e miglioramento sismico delle fondazioni di edifici esistenti". *Invited lecture for XXII Convegno Nazionale di Geotecnica*, Palermo (Italy), 22-24 September, 2004, Italian Geotechnical Journal (to appear).

OPCM 3274/2003 (2003). "Norme tecniche per il progetto, la valutazione e l'adeguamento sismico degli edifici". Gazzetta Ufficiale Repubblica Italiana, 25.03.2003.

Mylonakis, G., Gazetas, G. (2000). "Seismic soil-structure interaction: beneficial or detrimental?", *Journ. of Earthquake Engineering*, Vol. 4, No. 3, pp. 277-301.

Prakash S. (2004). "Evaluation of soil-structure interaction effects of embedded structure by simple method". *Proc. 13th WCEE*, Vancouver, B.C., Canada, August 1-6, 2004, paper No. 3405.Ishibashi, I., and Zhang, X. (1993) "Unified Dynamic Shear Moduli and Damping Ratios of Sand and Clay", *Soils and Foundations*, Vol. 33, No. 1, pp. 182-191

SUPPLEMENTARY CRITERIA FOR SHALLOW FOUNDATION DESIGN CLOSE TO SEISMICALLY ACTIVE FAULTS

R. Paolucci[1] and M.T. Yilmaz[2]

[1] *Department of Structural Engineering, Politecnico di Milano, Italy*
[2] *Department of Engineering Sciences, Middle East Technical University, Turkey*

Abstract

The construction of buildings is restricted in the proximity to seismically active faults by clause 4.1.2 of Eurocode 8 Part 5. However, there is no clear definition of the safe distance to fault, and the uncertainty related to the location of main and secondary traces of rupture for a future event can prevent the reduction of fault-breakage related risks to acceptable levels. The diversion of the surface trace of rupture by massive structures seated on thick soil deposits can be beneficial for the risk reduction. The scope of this contribution is to introduce simple supplementary criteria for shallow foundation design close to seismically active faults, based on the application of methods based on limit analysis and yield design theory, to assess the possibility of foundation-induced fault diversion.

INTRODUCTION

According to clause 4.1.2 of Eurocode 8 Part 5 (Proximity to seismically active faults) “Buildings of importance classes I, II, III (...) shall not be erected in the immediate vicinity of tectonic faults recognised as being seismically active in official documents issued by competent national authorities”. Large research efforts have been recently made for mapping known seismically active faults in the European, and namely Mediterranean, environment, as documented by the production of Databases of potential sources of earthquakes larger than M5.5 in Europe and Italy.

However, the main difficulty in the mapping activity is that active faults in Europe are generally characterized by relatively small dimensions (up to few tenths of km) and by small rates of slip (of the order of few mm/year or fractions of mm/year), corresponding to relatively large average return periods of the major (characteristic) earthquakes produced by a given fault, of the order of one or more thousands of years. Even the identification of the causative fault of major seismic events in the Mediterranean region may lead seismologists to conflicting viewpoints, such as for the Southern Calabria earthquake sequence of February-March 1783 (Galli and Bosi, 2002). As noted by Valensise and Pantosti (2001), in a recent review paper on the investigation of potential earthquake sources in Italy, there are systematic evidences of (a) the lack of correlation between seismological and geological structures and (b) the tendency for many large earthquakes not to coincide with mapped faults.

In addition to the uncertainty related to mapping activity, there is also no indication in the Eurocode 8 for the quantitative definition of the proximity to the fault. As a reference, the “Alquist-Priolo earthquake fault zoning Act”, that regulates since 1972 in California the mitigation of hazard of surface faulting to structures for human occupancy, states that “before a project can be permitted, cities and counties must require a geologic investigation to demonstrate that proposed buildings will not be constructed across active faults. An evaluation and written report of a specific site must be prepared by a licensed geologist. If an active fault is found, a structure for human occupancy cannot be placed over the trace of the fault and must be set back from the fault (generally 50 feet)”.

Therefore, the typical situation that may arise in the vicinity of a mapped seismically active fault, is that the designer does not know

at which distance the Eurocode 8 requirement applies. The problem is enhanced by two important considerations:

- structures that are adequately engineered against dynamic loads during a severe earthquake can still have a significant risk of seismic failure due to excessive permanent ground displacements induced by the surface fault breakage (Berrill, 1983);
- secondary ruptures can also contribute significantly to the overall damage due to excessive ground displacements, and these ruptures can be located at relatively large distances from the location of the main trace of the fault rupture (see e.g. Dong et al., 2003, for the Chi Chi Taiwan earthquake of Sept. 1999).

As for the latter problem, it is worth to point out that during the Landers 1992 earthquake most ground breakages occurred in an area some tens of meters wide, but extensional cracks were also observed several hundreds of meters from the main trace (Lazarte et al., 1994). Furthermore, around 45% of all Landers earthquake surface ruptures fell outside the established Alquist-Priolo Special Studies Zones (Hart et al., quoted by Lazarte et al., 1994).

Therefore, in cases where there is a significant degree of uncertainty in the mapping of the fault, or the risk induced by secondary ruptures cannot be avoided, engineering approaches are needed to limit the damage potential. Such approaches may involve use of ductile compacted fill or reinforced fill, utilization of foundation systems to resist the induced stresses due to the excessive ground displacements, and utilization of structural or foundation members with increased ductility to prevent collapse (Lazarte et al., 1994).

A further effect that may be helpful to reduce the damage potential of fault ruptures to buildings is the possible diversion of the surface breakage in the presence of heavy structures with strong shallow foundations, as was first noted for the Banco Central de Nicaragua building during the 1972 Managua earthquake, where the rupture was diverted by the presence of the building, leaving the structure itself essentially intact (Niccum et al., 1977). Several cases of satisfactory performances of buildings located next or on the surface fault breakage during the 1999 Kocaeli earthquake are reported by Lettis et al. (2000), such as the massive concrete bunkers at Golcuk Naval Base that diverted the surface fault rupture with no observable structural damage (Fig 1).

Considering the similar features of the reported cases of good performance of foundation systems against fault rupture, it seems that high bearing loads coupled with sufficiently deep soil deposits are the key elements for the possibility of diversion of rupture.

The scope of this contribution is to introduce some simple engineering criteria to assess whether the interaction of the shallow foundation with the fault rupture can result in the diversion of the rupture itself, with beneficial effects on the safety of the structure. These criteria, that essentially provide minimum values for the weight of structure depending on the thickness of the surface soil deposit, may be helpful in risk reduction for those areas located in the vicinity of mapped active fault zones, where the maps and relevant studies for the location of the main and secondary fault ruptures involve significant uncertainty and limitations

The studies involved in this report have been developed within the European Commission funded QUAKER project ("Fault-Rupture and Strong Shaking Effects on the Safety of Composite Foundations and Pipeline Systems"), where the first author (RP) is involved as a scientific consultant of Studio Geotecnico Italiano, Milano (SGI), partner of the project. In the QUAKER project a substantial experimental activity in the centrifuge apparatus of the University of Dundee is being carried out to support the theoretical results presented in this report.

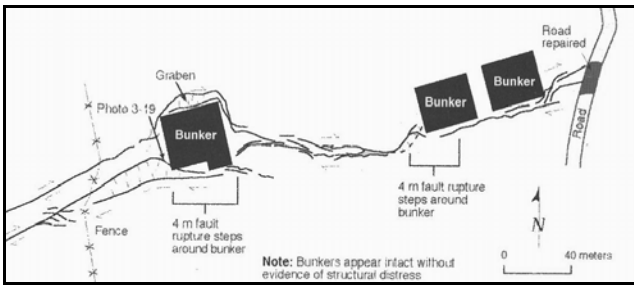

Fig 1: The surface rupture diverted by the concrete bunkers at Golcuk Naval Base (Lettis et al., 2000)

CRITERIA FOR FAULT-RUPTURE DIVERSION

Berrill's approach for strike-slip faults

For the case of strike-slip faults, the equations proposed by Berrill (1983) can be utilized to estimate the minimum dead load on foundation that is required for the diversion of the rupture, as a function of the soil layer thickness beneath the foundation, and the friction angle for the foundation-soil interface.

Berrill (1983) proposed a simple method to estimate the minimum bearing load that is needed to divert the fault rupture around the foundations. The method considers a strip foundation having width B, and resting on a soil layer of thickness H. In the two-dimensional problem statement, the soil is assumed to behave as a rigid-plastic material, obeying Mohr-Coulomb yield criterion with the strength parameters Φ (angle of internal friction) and c (cohesion). The strike of purely strike-slip fault coincides with the central axis of the strip foundation.

Based on the formulations provided in the study of Berrill, it is possible to develop the relationships in Fig 2, which shows the minimum values of normalized bearing load required to divert the rupture. For the case of drained cohesionless soil layer (c=0), the bearing load (V) is normalized by the unit weight of soil (γ) and the square of the foundation width (B^2). For the case of purely cohesive soil (Φ=0), the bearing load (V) is normalized by undrained shear strength (c_u) and width (B). The normalized value of V is also dependent on the friction between soil-foundation interface. Thus, for the case of cohesionless soil, the value of V is dependent on R, the friction ratio, which is formulated as

$$R = \frac{\tan\delta}{\tan\Phi} \qquad (1)$$

where, δ is the friction angle between soil-foundation interface. For the purely cohesive soil case, the limiting values of V are directly related to the value of tan δ, and the multiplication V·tanδ/B cannot exceed the value of c_u.

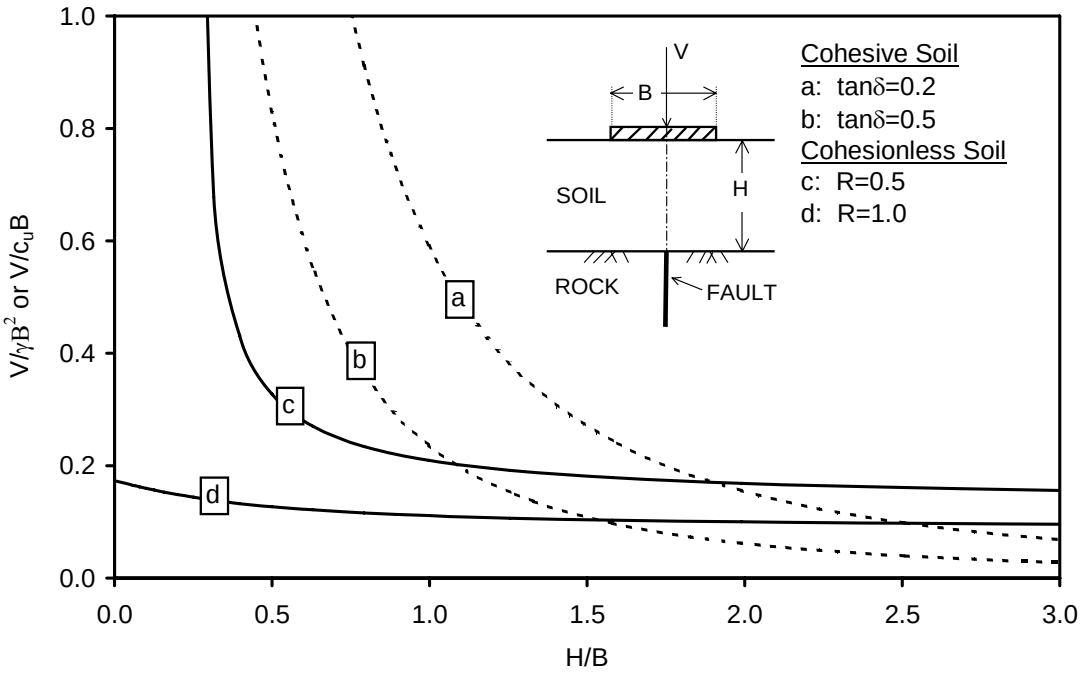

Fig 2: Typical chart to estimate the minimum normalized bearing load or minimum soil layer thickness to divert rupture due to a strike-slip fault, based on the method of Berrill (1983).

By using plots similar to the one in Fig 2, it is possible to decide whether site conditions and bearing load on shallow foundations are appropriate to divert the surface trace of rupture. However, the simple approach proposed by Berrill is valid for the cases with strike-slip faults, and similar simple relationships are needed for the normal and reverse faults.

Reverse and normal faults

In Fig 3, the problem is stated for the case of reverse faulting. The approach is similar to the two dimensional problem considered by Berrill (1983), except the fault type and the variability of the location of the faulting in the rock. The normal fault case can also be defined simply by reversing the direction of fault displacements in Fig 3. The parameters considered in the problem statement are as follows: B is the width of the shallow foundation, V is the vertical (bearing) concentrated load acting on the centre of the foundation, H is the thickness of the soil layer resting on rigid rock, x* is the horizontal distance between left edge of foundation and the location of the rupture at the soil-rock interface, c and Φ are the Mohr-Coulomb (or Tresca, when Φ =0) yield criterion parameters that reflect the cohesion and angle of internal friction of the soil layer, and β is the dip-angle of the fault rupture.

The solution procedure is based on the kinematic approach of limit analysis and yield design theory. Skipping the mathematical details, for which the reader is referred to specialized textbooks (e.g., Chen 1975, Salençon, 2002), the main steps involved by the application of this approach are the following:

- assume a rigid-plastic soil behaviour;
- define several kinematically admissible failure mechanisms;
- for each kinematic mechanism, calculate the maximum resisting power (P_{res}), depending on the adopted failure criterion for the soil, and the power of the external forces applied to the system in the admissible velocity field adopted;
- by an optimization procedure, find the limit external load that satisfies the stability condition

$$P^{ext}(U) \leq P^{res}(U) \qquad (2)$$

Further details of the implementation of the approach for the cohesive soil case can be found in Yilmaz and Paolucci (2006).

It is worth to be noted that in this case the external load to be optimized is the force that drives the fault movement, instead of the foundation load, as in the classical applications of the method for bearing capacity problems (see e.g. Paolucci and Pecker, 1997). Of course there is no engineering interest in calculating such force, but the main output of the procedure is the kinematic mechanism itself, which will indicate whether the fault rupture will intersect or not the foundation.

An example of one of the five kinematically admissible mechanisms proposed in this work is shown in Fig 4. In this case, the optimization procedure aims at finding the geometrical parameters α and y_0, that uniquely define the kinematic mechanism.

This approach also allows the identification of the non-dimensional parameters that govern the problem. Namely, for the Tresca soil, which represents the behaviour of purely cohesive soil layer, the parameters can be normalized by c_u (undrained shear strength) and foundation width B, while for the Mohr-Coulomb case, representing the drained behaviour for cohesionless soils, the parameters are normalized by γ (unit weight of soil) and B. The soil layer is assumed to be homogeneous. The non-dimensional parameters used in the analyses are summarized in Table 1.

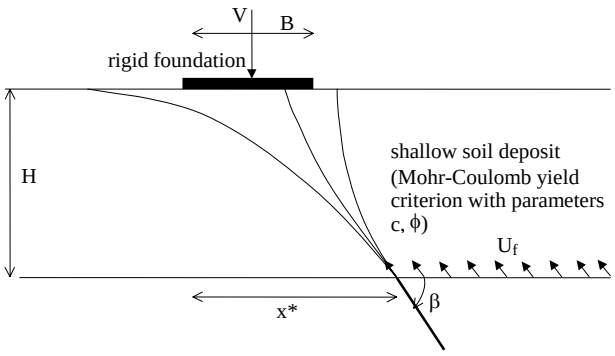

Fig 3: The parameters considered in the problem statement for the diversion of rupture, considering the reverse faulting.

Fig 5 summarizes the results for a typical case of reverse fault intersecting a drained soil layer, with β=60º, Φ=30º, and H/B=1.0. The region in black denotes the undesired case that the surface trace of fault rupture intersects the foundation footstep. The kinematic mechanisms predicted by our approach that result in diversion of fault rupture are also presented in Fig 5.

The minimum vertical foundation load to divert the fault rupture is dependent on the value of x*. However, the exact value of x* can not be known accurately in practice. Therefore, we have decided to select a representative value of the minimum bearing load to be considered in engineering applications as the highest load value for which diversion occurs for any x*. Considering again Fig. 5, the critical value of x*/B for the given set of parameters is 1.74, and the minimum value for the normalised bearing load acting on foundation ($[V/\gamma B^2]_{min}$) required to divert the rupture is 0.20. The minimum values of normalised bearing load were determined accordingly for all ranges of parameters considered in this study.

Table 1: Non-dimensional parameters used in the analyses.

Non-dimensional Input Parameters	Tresca Material (Undrained)	Mohr-Coulomb Material (Drained)
Soil layer thickness	$\overline{H} = \frac{H}{B}$	$\overline{H} = \frac{H}{B}$
Coordinate of fault rupture intersection at soil-rock interface	$\overline{x^*} = \frac{x^*}{B}$	$\overline{x^*} = \frac{x^*}{B}$
Fault dip angle	β	β
Bearing load on foundation	$\overline{V} = \frac{V}{c_u B}$	$\overline{V} = \frac{V}{\gamma B^2}$
Angle of internal friction	-	Φ
Unit weight	-	1

For the same set of parameters, the results of parametrical analyses are presented for the case of normal fault in Fig 6. The critical x*/B value is determined as 0.99, and the corresponding minimum value of normalised bearing load required to divert the rupture is 0.67. The comparison of Fig 5 and 6 reveals that the most critical value of x* for the reverse fault corresponds to the intersection of the surface trace of fault rupture beneath the left (far) side of the foundation, whereas for the normal fault case it corresponds to the intersection with the right (close) side of the foundation.

In Fig 7, the purely cohesive soil case is considered utilizing the set of parameters β=60º and H/B=1.0, and for the case of reverse fault. A minimum normalized bearing load of 1.0 is required for diversion of rupture. This value corresponds to a bearing capacity safety factor of 5.14 in practice, due to Prandtl solution for the ultimate bearing capacity. The diversion of surface trace of rupture by lower values of bearing load is possible in cases that the soil layer is thicker.

In order to provide a relationship between the minimum bearing load required to divert fault rupture for any x*, soil layer thickness and fault type (i.e., reverse or normal) for purely cohesive (undrained) and cohesionless (drained) soils, a set of parametric analyses have been carried out, that considers a range of dip angles (β) and soil strength parameters relevant to practical applications. Thus, the selected dip angle values were restricted between 60° and 90° for both fault types, and the angle of internal friction (ϕ) is set to 20° and 30° for consecutive sets of analyses.

The summary of results for cohesionless soil is presented in Fig 8. The minimum value of bearing load ($[V/\gamma B^2]_{min}$) required to divert the rupture is observed to be dependent on the fault type, soil layer thickness, β and ϕ. For the case of reverse fault, the highest values of bearing load are obtained by setting β=90° and ϕ=30°, whereas for the normal fault case, the set of parameters β=60° and ϕ=30° provides the most critical case. Thus, the relationship between β and $[V/\gamma B^2]_{min}$ is different for the two fault types: for reverse faults, increasing the dip angle β results in increasing values of $[V/\gamma B^2]_{min}$ for a given set of parameters, but the trend is opposite for the normal fault case.

The effect of the variation in ϕ is similar for both types of faults, and the increasing tendency for $[V/\gamma B^2]_{min}$ with increasing ϕ is clearly observable in Fig 8.

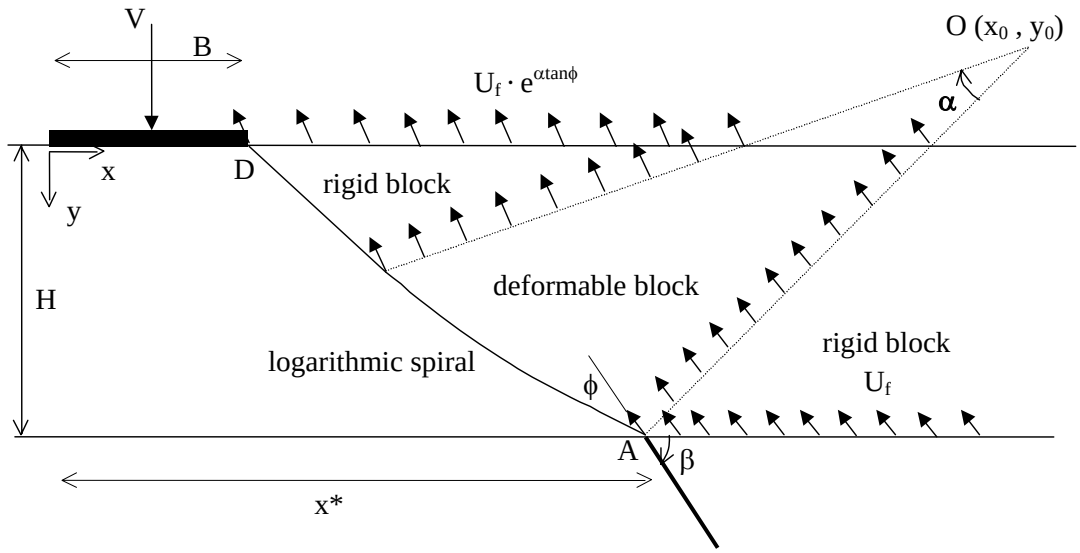

Fig 4: Kinematically admissible mechanism for the fault rupture – shallow foundation interaction problem.

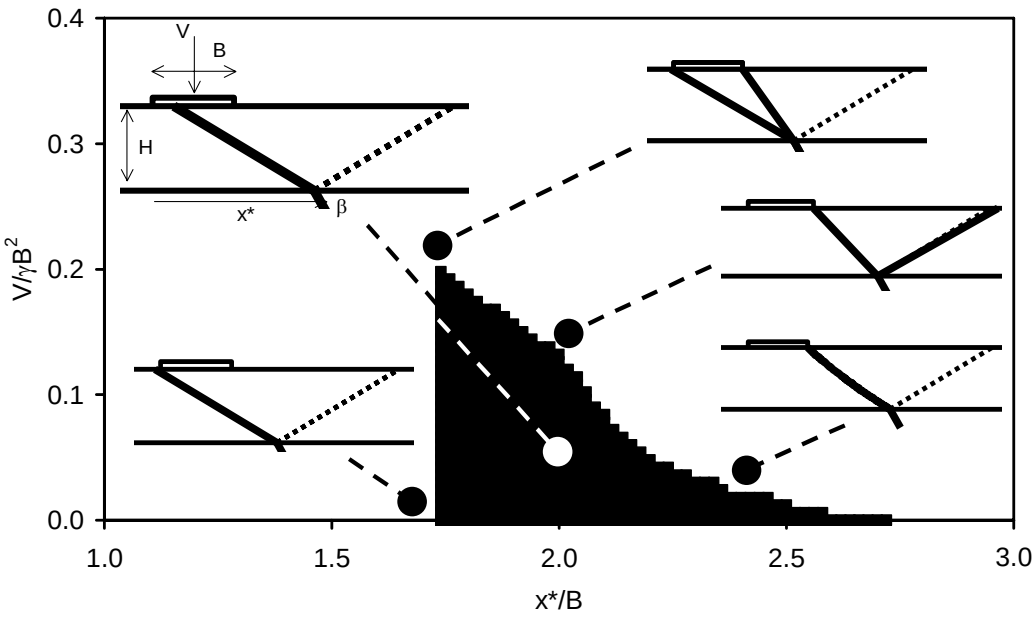

Fig 5: Summary of results for the reverse fault and cohesionless soil behaviour case with parameters β=60º, Φ=30º, and H=B. x* denotes the location of the fault rupture at the bedrock – layer interface with respect to the left edge of the foundation. Black region denotes no diversion of rupture.

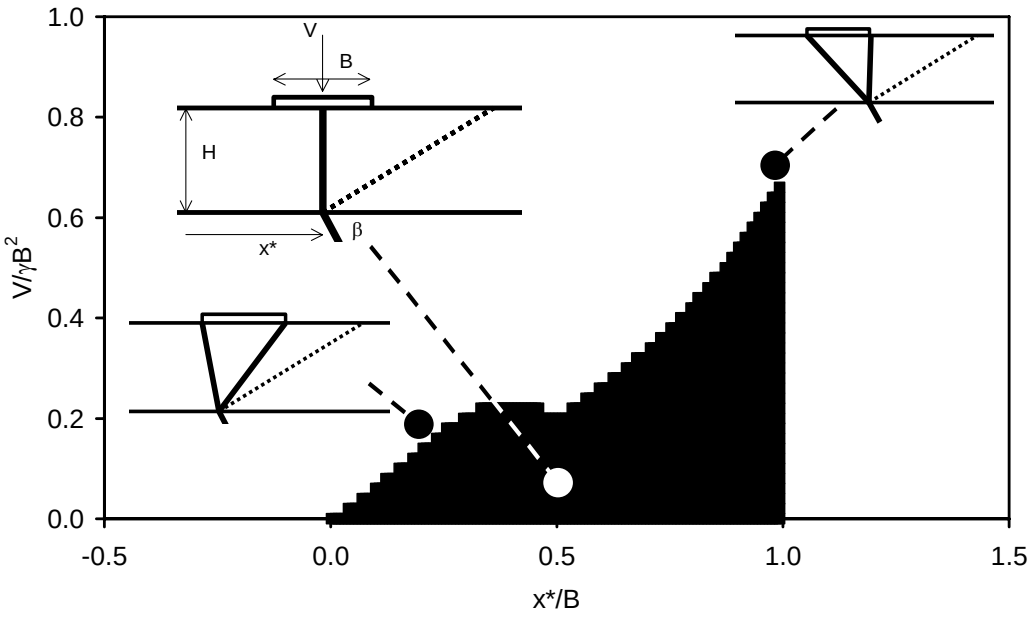

Fig 6: Summary of results for the normal fault and cohesionless soil behaviour case with parameters β=60º, Φ=30º, and H=B. Black region denotes no diversion of rupture.

In this respect, note that the proposed approach yields a theoretical upper bound solution for the limit load only if the flow rule is associative, i.e., the friction angle coincides with the dilation angle for the Mohr-Coulomb material. Since what we are interested in is the kinematic mechanism rather than the limit load itself, our mechanisms may be quite different from the actual ones. The preliminary comparisons with the experimental centrifuge results that are being obtained at the University of Dundee within the QUAKER project, and with FEM numerical simulations as well, suggest that the best agreement is obtained when the dilation angle is considered, instead of the friction angle. As well known, and also demonstrated by Cole and Lade (1984) for the problem at hand, the soil dilation angle typically reduces to considerably low values for large shear strains.

Owing to these considerations, the results plotted in Fig. 8 for cohesionless soil should be better interpreted by viewing ϕ as the dilation, rather than the friction angle. Thus, the estimated $[V/\gamma B^2]_{min}$ can be quite conservative when the representative value of the angle of internal friction is selected as 30°.

The previous problem is fortunately less relevant for purely cohesive soil, for which the associative flow rule applies and the upper bound solution of the kinematic approach tends to the actual limit load, and the theoretical mechanisms are close to the actual ones. As discussed by Yilmaz and Paolucci (2006), for cohesive soils the theoretical mechanisms and those provided by nonlinear FEM analyses are generally in quite good agreement. Referring to Yilmaz and Paolucci (2006) for further details, the summary of results for purely cohesive soil is presented in Fig 9. The minimum normalised bearing load to divert the rupture $[V/c_uB]_{min}$ is observed to be independent of the dip angle and the fault type. Thus, a single relationship between $[V/c_uB]_{min}$ and H/B is provided.

Finally, it is worth noting that the range of values represented in Figs. 8 and 9 is similar to the corresponding range obtained by Berrill for strike-slip faults (Fig 2).

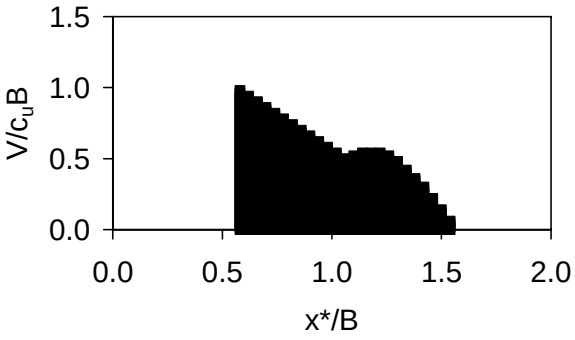

Fig 7: Summary of results for the reverse fault and purely cohesive soil behaviour case with parameters β=60º, and H=B. Black region denotes no diversion of rupture.

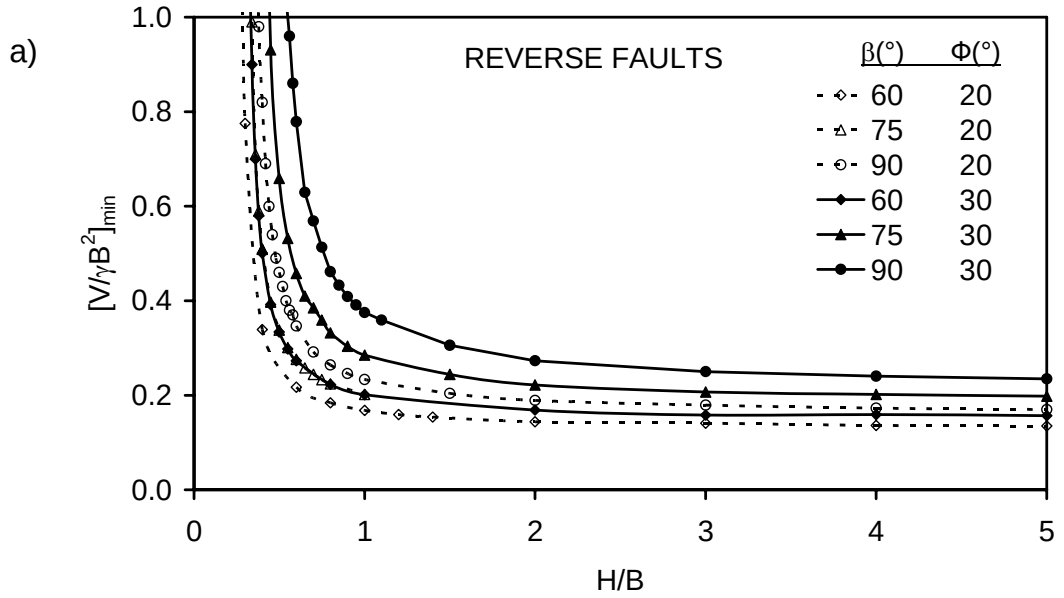

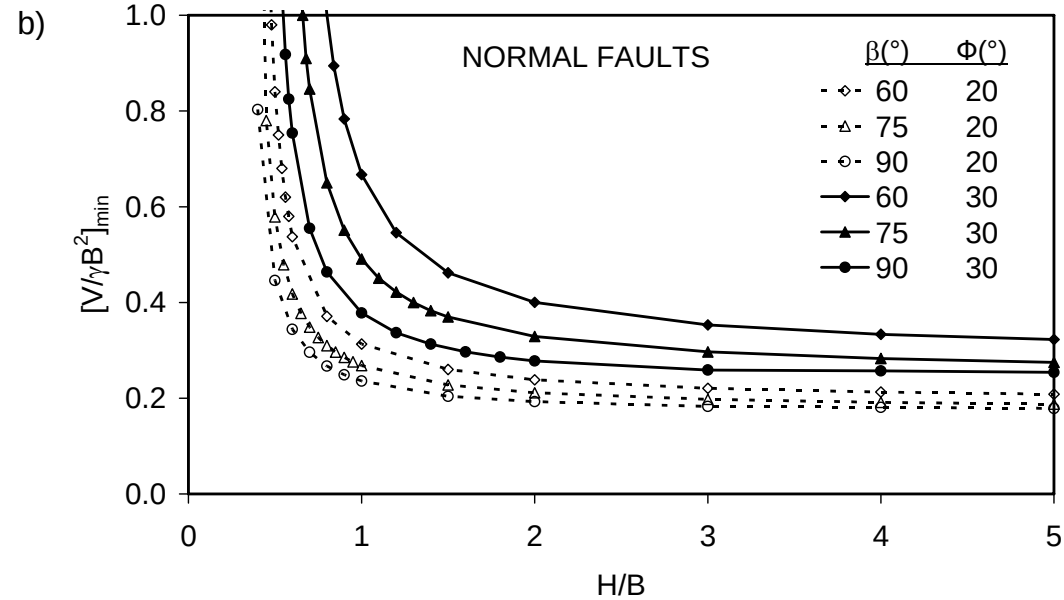

Fig 8: The relationship between the minimum bearing load, $[V/\gamma B^2]_{min}$, and the cohesionless soil layer thickness, H/B, for the cases of (a) reverse fault, and (b) normal fault.

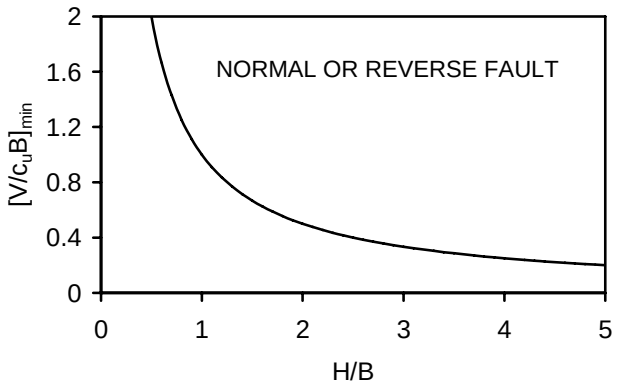

Fig 9: The proposed relationship between the minimum bearing load, $[V/c_uB]_{min}$, and the purely cohesive soil layer thickness, H/B.

CONCLUSIONS

Problems arising in accurately mapping seismically active faults and the possible occurrences of secondary ruptures far from the main fault may limit the applicability of clause 4.1.2 of Eurocode 8 Part 5, that prevents construction of buildings in the immediate vicinity of seismic faults.

The concept of diversion of fault rupture by relatively heavy buildings can be viewed as a simple but engineering sound approach, in cases where this type of risk cannot be reduced to an acceptable level by preventing building construction in a reasonably narrow zone (not specified by Eurocode 8) around the fault trace. For this purpose, Berrill (1983) devised a simple approach for the strike-slip fault case, and the conditions for rupture diversion are stated in Fig 2.

The kinematic approach of the yield design theory is used in this study, to propose similar criteria applicable for the reverse and normal fault cases. Thus, the conditions for rupture diversion for soils overlying reverse or normal faults are presented in Figs. 8 and 9, considering cohesionless and purely cohesive soils, respectively. While for the purely cohesive soil case, the conditions for rupture diversion were found to be independent of the dip angle and fault type, the same does not apply for the cohesionless soil case.

The main limitation of the proposed approach is for the cohesionless soil case, for which the preliminary comparison with experimental results obtained in centrifuge at the University of Dundee within the QUAKER project, suggest that the dilation angle should be used to provide accurate theoretical rupture mechanisms, instead of the friction angle. Waiting for a clarification on this subject, that will be possible when the set of experimental analyses at Dundee and the corresponding nonlinear FEM simulations will be accomplished, the plots of Fig. 8 can be viewed as a conservative estimation of the minimum bearing load required to divert the surface fault rupture.

We can summarize the results of this study by stating that the proposed supplementary criteria can improve the safety of structures located on sites where the potential risk due to the interaction with the surface trace of fault rupture cannot be decreased to acceptable levels by the conventional fault mapping approach. For the validity of the proposed criteria, strong shallow mat (or, raft) foundations should be used, so that the foundation can keep its intact form when exposed to large soil deformations. The required minimum bearing load can be deduced from the plots in Fig. 2 for strike-slip faults, from Fig. 9 for cohesive soils and both normal and reverse faults, while for cohesionless soils the plots in Fig. 8, namely those for ϕ = 30°, should be viewed as a conservative estimation, waiting for a thorough analysis of the experimental results that are becoming available within the QUAKER project.

As a final remark it should be considered that these simplified criteria do not take into account the dynamic nature of earthquake loading, but are based on the idea of a (pseudo) static application of the fault displacement. It is obvious that if the fault rupture process is fast enough to produce large velocity and acceleration pulses in the vicinity of the fault itself, the interaction with the foundation system and the supporting structure may be much more complicated than assumed in this study.

ACKNOWLEDGEMENTS

This research was partially funded by the European Commission within the QUAKER project (“Fault-Rupture and Strong Shaking Effects on the Safety of Composite Foundations and Pipeline Systems”), n. EVG1-2001-00069.

REFERENCES

Berrill, J.B. (1983). “Two-dimensional analysis of the effect of fault rupture on buildings with shallow foundations,” *Soil Dynamics and Earthquake Engineering*, Vol. 2, pp. 156-160.

CEN (Comité Européen de Normalisation). *Eurocode 8: Design of structures for earthquake resistance. Part 5: Foundations, retaining structures and geotechnical aspects*. EN 1998-5, Brussels, Belgium, 2004.

Chen , W.F. (1975). *Limit Analysis and Soil Plasticity. Developments in Geotechnical Engineering*, 7, Elsevier , Amsterdam, 638 pp.

Cole, D.A., Lade, P.V. (1984). “Influence zones in alluvium in dip-slip zones,” *Journal of Geotechnical Engineering*, Vol. 110, No. 5, pp. 559-615.

Dong, J.J., Wang, C.D., Lee, C.T., Liao, J.J., and Pan, Y.W. (2003). “The influence of surface ruptures on building damage in the 1999 Chi-Chi earthquake: a case study in Fengyuan City,” *Engineering Geology*, Vol. 71, pp. 157-179.

Galli, P. and Bosi, V. (2002). “Paleoseismology along the Cittanova fault: implications for seismotectonics and earthquake recurrence in Calabria (Southern Italy)”, *Journal of Geophysical Research*, Vol. 107, No. B3.

Lazarte, C.A., Bray, J.D., Johnson, A.M. and Lemmer, R.E. (1994). “Surface breakage of the 1992 Landers Earthquake and its effects on structures,” *Bulletin of the Seismological Society of America*, Vol. 84, No. 3, pp. 547-561.

Lettis, W., Bachhuber, W. and Witter, R. as coordinators (2000). “Chapter 2: surface fault rupture,” *Earthquake Spectra*, Vol. 16, Supplement A: 1999 Kocaeli, Turkey, Earthquake Reconnaissance Report, pp. 11-53.

Niccum, M.R., Cluff, L.S., Chamorro, F., and Wyllie, A.L. (1977). “Banco Central de Nicaragua: a case history of a high-rise building that survived surface fault rupture,” *Proceeding of the 6th World Conference on Earthquake Engineering*, New Delhi, pp. 2423-2428.

Paolucci, R., and Pecker, A. (1997). “Seismic bearing capacity of shallow strip foundations on dry soils”. *Soils and Foundations*, Vol. 37, pp. 95-105.

Salençon, J. (2002). *De l’Elastoplasticité au Calcul à la Rupture*, Presses de l’Ecole Nationale des Ponts et Chaussèes, Paris, pp. 262.

Valensise, G. and Pantosti, D. (2001). “The investigation of potential earthquake sources in peninsular Italy: a review”. *Journal of Seismology*, Vol. 5, pp. 287-306.

Yilmaz, M.T. and R. Paolucci (2006). “Earthquake fault rupture – shallow foundation interaction in undrained soils”, submitted for publication to *Earthquake Engineering and Structural Dynamics*.

On the Design of Structures to Resist Fault Displacement, with Applications in Greece

I. Anastasopoulos[1] and G. Gazetas[2]

[1] *Post Doctoral Researcher, National Technical University, Athens, Greece*
[2] *Professor, National Technical University, Athens, Greece*

Abstract

Older seismic codes demanded that "*buildings and important structures not be erected in the immediate vicinity of active faults*". This restriction has proved not only very difficult to obey for long structures such as bridges, tunnels, and embankments, but also unnecessarily conservative as the exact location of the surface outbreak of a fault is rarely known reliably; Moreover, recent earthquakes have shown that structures with suitable foundation can withstand with minimal damage a direct "hit" by a fault. Thus, modern Seismic Codes (e.g. Greek Anti-Seismic Code – EAK, 2000) allow building in the vicinity of active faults, but only after a special study. This paper outlines a two-step methodology to design structures against major fault ruptures. The first step applies non-linear finite elements to analyse fault rupture propagation in the free-field, ignoring the presence of a structure. Then, knowing the location of rupture outcropping in the free field, the structure is placed on top, and the analysis of the soil-structure system is performed. The first step analysis, i.e. fault rupture propagation in the free-field, is validated through successful comparison with real case-histories, earlier laboratory experiments, and Class "A" predictions of centrifuge Experiments. Case-histories from the 1999 Kocaeli earthquake are studied to validate (qualitatively) the second step of the developed methodology. Then, three applications in Greece are presented : (a) the design of a three-span road bridge in Rhodes, (b) the fault-resistant design of the buildings of a housing complex in Atalanti, and (c) the design of highway cut-and-cover tunnels against fault rupture in Kamena Vourla.

INTRODUCTION

The threat of a major seismic fault rupturing underneath a structure is an important part of the earthquake hazard. Lack of understanding of the mechanics of the rupturing process and the limited experience on how structures behave on top of a fault had led to an absolute prohibition of building "in the vicinity" of a fault in all seismic codes. The term "vicinity" was interpreted differently in various codes, ranging from a few hundred meters to a few kilometers.

However, recent earthquakes have shown that a more optimistic attitude is justified. In the Kocaeli 1999 earthquake, for instance, several simple structures have survived with minimal damage a fault dislocation of more than 2 meters. Clearly, the type of foundation and the nature of the supporting soils played a decisive role in the behaviour of the structure.

Indeed, recent analytical studies (Anastasopoulos, 2005) have shown that a structure on top of the ground interacts with the deforming soil and the outcropping fault rupture. The presence of a structure may lead to a diversion of the rupture path, as the latter propagates to the ground surface, as well as to a modification of the surface displacement profile caused by the emerging fault rupture. Depending on the rigidity and weight of the foundation-structure system, even a complete diversion of the fault path may take place. Additionally, depending on soil compliance, a distinct (and steep) fault scarp may be "diffused" by the structure to a widespread differential settlement. This dual interaction mechanism, named hereafter "Fault Rupture–Soil–Foundation–Structure Interaction (FR–SFSI), is of great significance for the performance of a structure.

The Greek Seismic Code (EAK 2000), in agreement with the aforementioned reasoning, allows building in the vicinity of active faults, but only after a "special seismic–geologic–geotechnical–structural study" is conducted. Until now there was no specific methodology to conduct such a study. This paper presents the developed methodology to conduct such a special study, providing the ability to safely design structures against fault rupture.

METHODOLOGY

The analysis is conducted in two steps. First, fault rupture propagation through soil is analysed in the free field, ignoring the presence of a structure (Fig.1a). Then, knowing the exact location of rupture outcropping in the free field, the structure is placed on top, and the analysis of the soil-structure system is performed (Fig1b). By comparing the results of the two analyses, the effect of FR-SFSI is visualized and quantified.

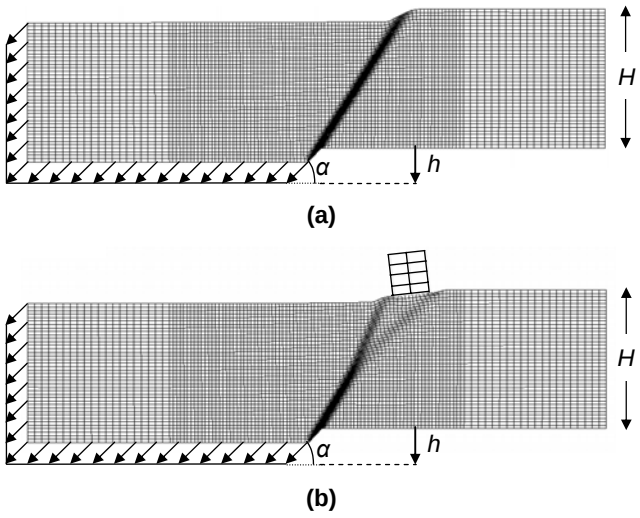

Fig. 1 Analysis Methodology : (a) fault rupture propagation in the free-field, (b) FR-SFSI

To explore the interplay between a rupturing fault and a structure two-dimensional plane-strain analyses are performed. However, the fault rupture is always significantly longer than a structure, and the rupture rarely crosses a structure exactly perpendicularly to its axis; therefore, the plane-strain assumption can be seen as a practical approximation. Although the scope of our research is not the exhaustive analysis of fault rupture propagation in the free-field, its realistic simulation is a prerequisite for the second step of our methodology.

Hence, a parametric study of fault rupture propagation through soil in the free field has been conducted (Anastasopoulos, 2005). The results of these analyses have been compared with case-histories, earlier experimental results, earlier numerical studies (Bray et al, 1994), and centrifuge experiments (Davies & Bransby, 2005).

FAULT RUPTURE PROPAGATION THROUGH SOIL : METHODOLOGY AND VALIDATION

Methodology

Only a few attempts utilising the finite element (FE) method have been reported in the literature to model fault rupture propagation through soil. One such study, by Bray et al (1994) concluded that FE modeling can be successful if certain conditions are satisfied, such as the use of a very refined mesh in the neighborhood of the potential rupture and of a nonlinear constitutive law for the soil.

The problem studied herein along with the FE discretisation is displayed in Fig. 1a. It refers to an H = 40 m thick soil layer at the base of which a dip slip fault, dipping at an angle α, ruptures and produces a downward movement of vertical amplitude h. Our model has a total width $B = 4H$, following the recommendation of Bray (1990) that a $B : H = 4 : 1$ ratio is sufficient to minimize parasitic boundary effects. At the central 80 m of the model the discretisation is finer, with the quadrilateral elements being 1 m x 1 m (width x height). At the two edges, where the deformation is expected to be negligible, the mesh is coarser : 2 m x 1 m. The differential displacement is applied to the left part of the model in small consecutive steps.

Following a thorough review of the literature (Anastasopoulos, 2005), we adopted an elastoplastic constitutive model : Mohr-Coulomb failure criterion, with an isotropic strain softening rule. Strain softening is applied to cohesion c ; friction angle φ, and dilation angle ψ. Denoting γ_f the plastic shear strain at which soil reaches its residual strength, we consider c, φ and ψ as linearly decreasing with the total plastic strain down to their residual values c_{res}, φ_{res} and ψ_{res}. Typical values of γ_f range from 5% to 15%. Equally important is the "yield" strain γ_y, which depends on the strength parameters as

well as on the shear stiffness. Both γ_y and γ_f , are calibrated through numerical simulation of the direct shear test.

The capability of the constitutive model to reproduce actual soil behaviour has been verified through the analysis of idealised soil samples tested in direct shear (Anastasopoulos 2005). Despite its simplicity and lack of generality, our constitutive model can capture adequately the predominant mode of deformation of the studied problem, providing a reasonable simplification of the complex soil behaviour.

Validation : Centrifuge Experiments

A parametric study of fault rupture propagation through soil in the free field can be found in Anastasopoulos (2005). The results have been compared with case-histories, experimental results, and earlier numerical studies. Additionally, Class A ("blind") predictions were conducted before performing centrifuge tests. The latter were performed on Fontainebleau sand at the University of Dundee, as part of the "QUAKER" research project (Davies & Branby, 2005).

The specimen were prepared by pluviating Fontainebleau sand (Gaudin, 2002) from a height of 1.57 m, resulting in a density of about 80%. The prototype model dimensions were H = 25 m combined with a width of 65.9 m. The dip angle was set to 60^o for both normal and thrust faulting. The experiment was performed at 100 g centrifugal acceleration.

Fig. 2 compares our analytical predictions with the experimental results. The predictions are quite successful for both faulting types. The analysis predicts successfully not only the correct location of the fault break-out at the surface, but the localization of deformation at a narrow band. In the case of normal faulting (Fig. 2a), the prediction can be seen as equally successful for both h = 0.6 m as well for 1.0 m. Similarly, in the case of thrust faulting (Fig. 2b),the prediction is also satisfactory for both h = 0.8 m and 1.0 m.

The validation of the developed free-field fault rupture propagation analysis methodology against case histories from the literature, and our successful Class "A" predictions gives us the necessary confidence in using our numerical modeling methodology.

FAULT RUPTURE–SOIL–FOUNDATION–STRUCTURE INTERACTION (FR–SFSI) : METHODOLOGY AND VALIDATION

Analysis Methodology

Having analysed fault rupture propagation in the free-field, we proceed to the next step of our methodology. The model of the structure (simplified 2-D buildings), consisting of beam elements, is placed on top of the soil model and connected through special contact (gap) elements. These elements are infinitely stiff in compression, but offer no resistance in tension. In shear, their behavior follows Coulomb's friction law. Thus, the structure is not bonded to the ground, and both uplifting and slippage can realistically occur.

The main factors influencing FR-SFSI are :

(a) The type of the foundation system (for example, isolated footings, mat foundation, box-type foundation, piles).
(b) The flexural and axial rigidity of the foundation system (thickness of mat foundation cross-section and length of tie beams, etc.)
(c) The dead load of the superstructure.
(d) The stiffness of the superstructure (cross section of structural members, grid spacing, presence or not of shear walls).
(e) The soil stiffness (G), strength (φ, c) and kinematic characteristics (ψ).

Since the exact relative position x of the outcropping fault to the structure cannot be determined with validity, it is also varied parametrically. Three values are usually adequate to capture the dominant interaction modes : x/B = 0.2, 0.5, and 0.8 (where B is the width of the structure).

Given the multitude of the structure–foundation–fault position combinations to be analysed, a dip angle α = 60^o has been selected for normal faulting, and α = 45^o for reverse. Two idealized soil types were analysed: *dense* and *loose* sand. The idealized *dense* sand is stiffer, reaching failure at low strains, exhibiting "brittle" behaviour, and allowing for the rupture to outcrop at relatively small normalized bedrock displacement h/H. On the other hand, the idealized *loose* sand is more compliant and reaches failure at higher strain levels, exhibiting more "ductile" behaviour, and allowing for the rupture to delay its emergence.

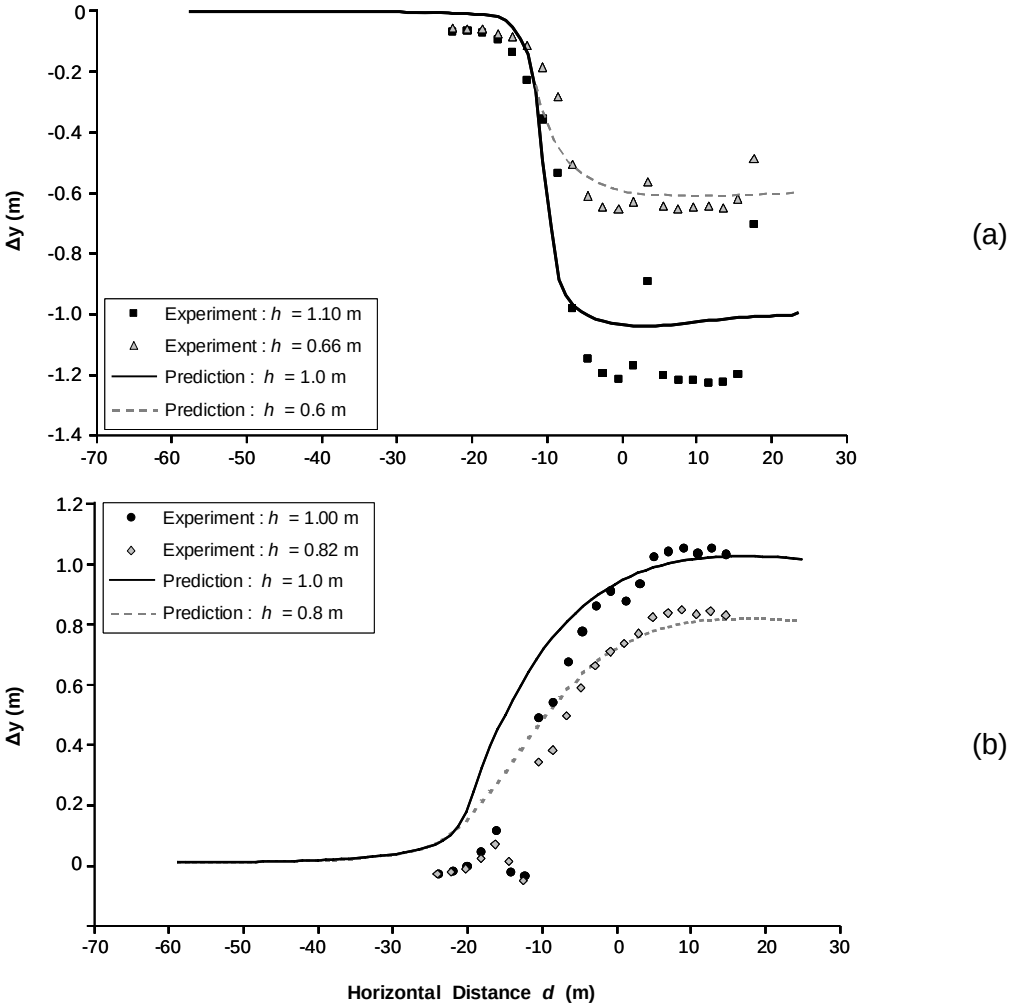

Fig. 2 Comparison of analytical Class "A" prediction with experimental results – vertical displacement at the surface : (a) normal, and (b) thrust faulting

A detailed parametric study, examining all the aforementioned factors, can be found in Anastasopoulos (2005). Without under-estimating the general importance of the details of a superstructure, all of the analysed structures were treated as "equivalent" in this respect, changing only the number of stories, to allow for an insight on the influence of the type and stiffness of their foundation. Due to space limitation it is impossible to present the results of the parametric investigation. We will therefore solely focus on the analysis of the case-histories of Gölcük, which is also the qualitative validation of our FR–SFSI methodology.

Validation : The Case-histories of Gölcük

The disastrous 1999 M_w7.4 Izmit earthquake was triggered by reactivation of a 125 km segment of the North Anatolian Fault (NAF). With its epicenter 5 km southwest of Izmit, it struck the industrialized corridor around the Marmara Sea, causing more than 30,000 fatalities. The earthquake caused tectonic surface rupture over an area exceeding 110 km in length, with maximum offset of 5 m. General overviews of the behaviour of numerous structures in various locations can be found in Earthquake Spectra (2000). The differential displacement of the Gölcük relative to the Sapanca segment produced a 4 km NW-SE (110^o) normal fault east of of Gölcük, crossing the small community of Denizevler, with maximum vertical displacement of 2.4 m. The geometry of ruptures and the geomorphology, in combination with palaeo-seismicity studies confirm the tectonic origin of the event (Tutkun et al, 2001; Pavlides et al, 2003).

The dislocation crossed several residential structures. As expected, many of them collapsed or were severely damaged. Surprisingly, several structures survived,

essentially unharmed, with the rupture path seeming to have deviated, as if to “avoid” them. In other cases the damage was substantial even though the dislocation was “masked” by the near-surface soil, not creating a distinct scarp. The rigidity of the foundation appears to have been one of the crucial factors affecting the performance. The involved structures were supported on a variety of foundation types, ranging from isolated footings, to rigid box-type foundations, and piles.

Within an area of 1 km, five residential buildings, a mosque, a basketball stadium, an automobile factory, and a high-voltage electricity pylon were crossed by the outcropping dislocation. Although the vertical differential displacement exceeded 2 m, only few of these structures collapsed. Four buildings survived with minor or no damage, with the surface rupture being diverted. Soil conditions do not differ significantly from point to point, and therefore differences in the behavior can be attributed to the foundation, in addition to the location of the rupture relative to the building.

A detailed investigation of the area can be found in Anastasopoulos (2005). From east to west, a first impressive success was that of the high-voltage electricity pylon, that did not collapse, sustaining only minor damage despite the “loss” of two of its four supports. Further west, a 4-story building (Bldg.1) on the hanging wall, sustained no damage at all, with the rupture deviating around it. To its west, a Mosque was very heavily damaged.

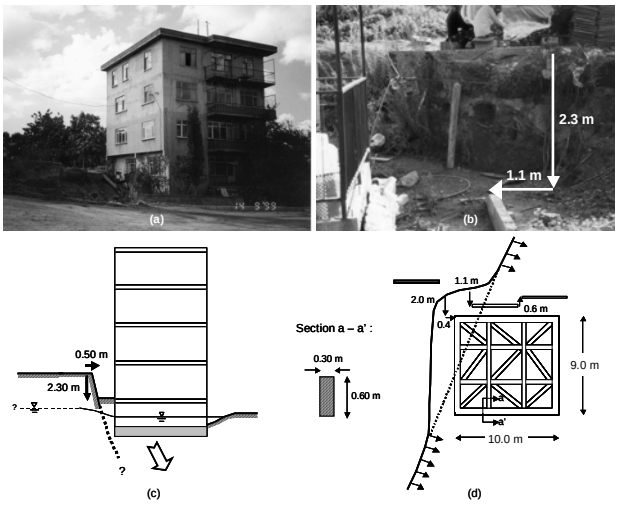

Fig. 3 The case-histories of Gölcük : Building 1, four stories plus basement ; Minor Damage

Next to it, a 1-story building (Bldg. 2) was literally cut by the fault. Building 3 (2 stories + attic) remained on the “footwall”, without any dam-age, avoiding a direct hit thanks to diversion of the fault rupture. Finally, a newly built Basketball Court, founded on piles, sustained severe damage. Due to space limitations we will focus only on Bldgs. 1 and 2.

Building 1

As depicted in Fig. 3 the surface rupture diverted and just avoided the 4-story reinforced-concrete structure, leaving it totally unharmed. The downward settlement reached 2.3 m, accompanied by a strike component of 1.1 m. The only apparent damage was the flooding of the basement, due to the local modification of the water table. The owners were inside the house during the earthquake and felt no vertical falling. Evidently, the vertical displacement was of a quasi-static nature. The foundation of the 9 x 10 m building consists of strip footings ~0.6 m x ~0.3 m (height x width) transversely connected through tie beams of similar dimensions.

The results of our FR-SFSI analyses are discussed in terms of the deformed mesh and the distribution of plastic strains. The differential settlement Δy of the foundation and the maximum bending moment M_{max} in the superstructure (beams or columns) are also reported to provide an estimate of the relative distress of each structure.

As clearly seen in Fig. 4 the rupture path is diverted away from the building (towards the footwall), as it approaches the ground surface (topmost 10 m of the propagation path). As it deviates to the right of the building, the plastic strain does not remain as concentrated as

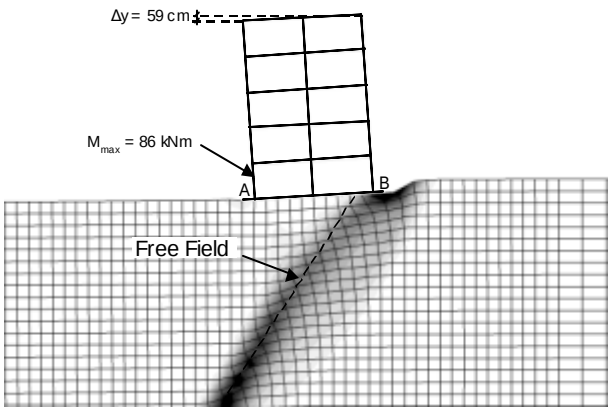

Fig. 4 The case-histories of Gölcük : FE analysis of Building 1 – deformed mesh and plastic strain

along the free-field rupture path, but is diffused over a wider area. The building tilts towards the hanging wall and the differential settlement reaches 59 cm. Despite this significant differential settlement the maximum bending moment M_{max} in the superstructure does not exceed 86 kNm. The rigid foundation not only managed to divert the rupture, but also allowed the building to rotate essentially as a rigid body, without stressing its superstructure.

Although the differential settlement is significant (6 % is much higher than the usually accepted maximum of 1/300), the analysis does not indicate significant distress of the building's superstructure. This agrees fairly well with the observed performance: the building sustained no structural damage. However, the tilting of the building was not as large as the predicted. We identify two possible explanations: (i) post-seismic consolidation near-the-edge of the building due to the increased contact stresses under that part, (ii) the rupture did not cross the structure perpendicularly as assumed in our analysis: it intersected only at the corner of the building, which is more favorable than our plane strain assumption.

Building 2

Building 2 was a simple 1-story structure. Its wooden tile-roof was supported on cinder-block walls. The walls were practically founded directly on the soil, without any decent foundation. This poor building could not have been expected to perform well subjected to a differential displacement of 1.5 m, and indeed it was torn apart by the rupture (Fig. 5). However, it did not collapse completely, not causing fatalities. The rupture crossed its north-east corner tearing it apart from the rest.

The model is only an approximation of the actual cinder-wall superstructure. The rupture is only locally diverted towards the hanging wall to avoid the far-left "footing" of the building (Fig. 6). The dislocation follows the same propagation path as in the free field, with the exception of the top 4 m. The building tilts towards the hanging wall, with the differential settlement reaching 33 cm. Part of the edge footing looses its support from the ground. Despite the smaller differential settlement, M_{max} reaches 469 kNm. Evidently, such a distress could not be accommodated by this structure. FR-SFSI does not appear to affect either the path of dislocation, or the deformations along the surface. The analysis agrees quite well with the observed performance, despite the crude modeling of the superstructure.

Conclusion

Applying our analysis to each of the Denizevler case histories, we demonstrate adequate qualitative accuracy with our field observations following the 1999 earthquake. The presence of a structure on top of an outcropping fault may have a significant influence on the rupture path : with heavy structures founded on rigid box-type foundations, the path diverts substantially and may avoid rupturing underneath the structure. The latter undergoes rigid body rotation, with its foundation sometimes loosing contact with the ground, but in most cases retaining its integrity. By contrast, buildings on isolated footings and, perhaps surprisingly, piles exert a smaller diversion of the rupture which is thus likely to outcrop between the footings or pile caps ; the latter may then undergo devastating differential displacements.

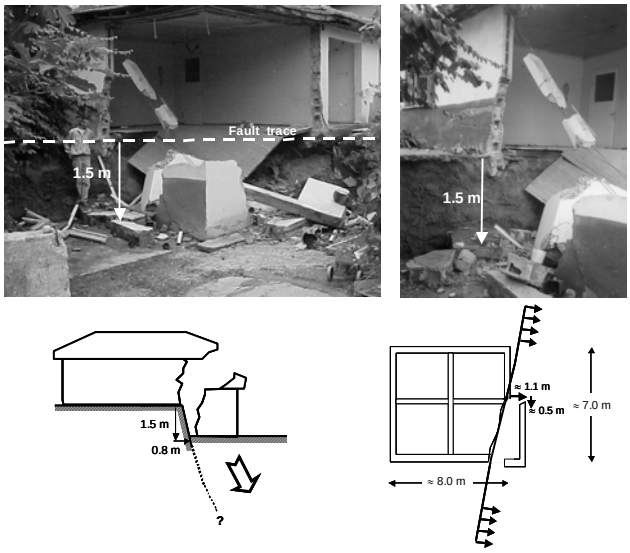

Fig. 5 The case-histories of Gölcük : Building 2, one story cinder-block structure ; Collapse

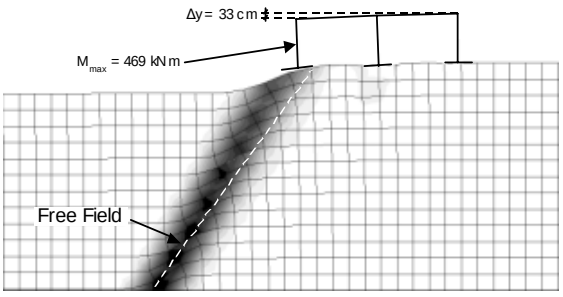

Fig. 6 The case-histories of Gölcük : FE analysis of Building 2 – deformed mesh and plastic strain

RHODES : A THREE–SPAN ROAD BRIDGE

Introduction

The under study three–span road bridge is situated in the island of Rhodes, being part of the new ring-road of the homonymous city. As depicted in Fig. 7a, the bridge is 72 m in length, with a central span of 24.8 m and two slightly shorter spans of 23.6 m. The pre-stressed concrete deck consists of a box girder 1.7 m in height and 11.3 m in (total) width, with a web thickness of 0.25 m. According to the initial design (Fig. 7a), the continuous deck would be supported through lead-rubber bearings on the two abutments (A1, and A2) and the two piers (M1, M2). The wall-type piers are 1.4 m in thickness, 7 m in width, with their height ranging from 7.3 m to 7.9 m. The foundation of piers and abutments consists of 2 x 4 groups of 1.2 m diameter piles, connected to the pier through 1.6 m thick pilecaps.

The scope of our study was the design of the bridge against a possible fault rupture. The alternative solution of a continuous deck monolithically connected to the piers was put out-of-the-question right from the beginning of the study : such a structural system is extremely sensitive to tectonically-induced differential settlement and tensile deformation. The first logical solution was a continuous deck supported on piers and abutments through lead-rubber bearings (Fig. 7a). Although such a structural system is definitely much more resilient than a monolithic one, this solution was also abandoned. As it will be demonstrated in the sequel, our FR-SFSI analysis showed that the stressing of the deck could easily become unacceptable. Finally, to minimize the fault-induced stressing of the bridge, a structural system comprising three separate simply supported decks, supported on lead-rubber bearings was adopted (Fig. 7b).

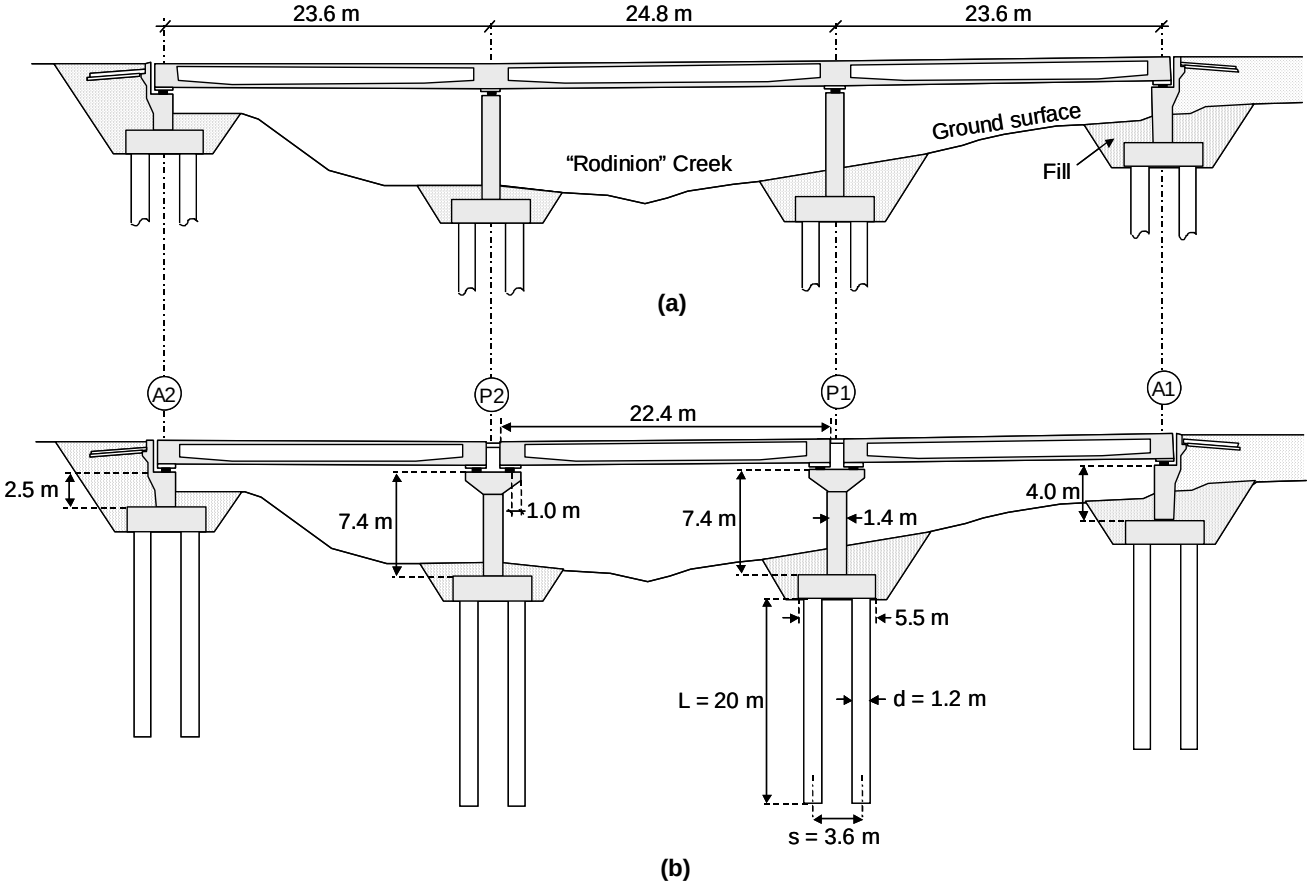

Fig. 7 Design of a three-span road bridge in Rhodes against possible fault rupture : (a) cross section of the initial design with a continuous deck supported on lead-rubber bearings, (b) modified design, offering seismo-tectonic isolation (three separate simply supported decks, supported on lead-rubber bearings).

This solution provides "seismo-tectonic" isolation of the bridge, allowing for large differential displacements without structural damage. To avoid intermediate joints (excessive noise and wear), the three decks are connected through a continuous concrete slab. In case of a significant tectonic displacement, the slab is designed to fail.

Seismic Hazard of the Area

The broader area of the island of Rhodes is of high seismicity. During the last 100 years the greatest earthquake in Greece, of magnitude M_s8, took place very close to the island. Within a 100 km radius, the greatest recorded earthquake was of magnitude M_s7.2. According to a seismic hazard study of the area (Lekkas, 1994), the maximum earthquake magnitude (with 63% probability) is M_s 6.8 and 7.2 for the next 50 and 100 years, respectively.

The city of Rhodes is traversed by five active faults. The Rodinion fault, more than 15 km in length and practically coinciding with the homonymous creek, intersects with the bridge almost perpendicularly. The fault is active and its reactivation is possible in the future.

Geotechnical Data and Soil Profile

Eight boreholes were conducted during the geotechnical exploration. The water table was found to be at ~6.5 m depth. Before proceeding to the analysis, we visited the area. Walking along the Creek, downstream of the bridge, several rock outcrops were spotted at both buttresses, forming discontinuities. Close to borehole B4 a 3 m deep trench had been excavated. The soil within the trench consisted of medium to dense clayey sand with gravel. The data from the geotechnical exploration, in combination with our field observations, were utilized to set up the idealized soil profile (Fig.8). The possible rupture zones at both buttresses have not been verified in detail. They are based on our field observations, the geomorphology of the area, and the hypothesis that the Rodinion fault coincides with the homonymous creek.

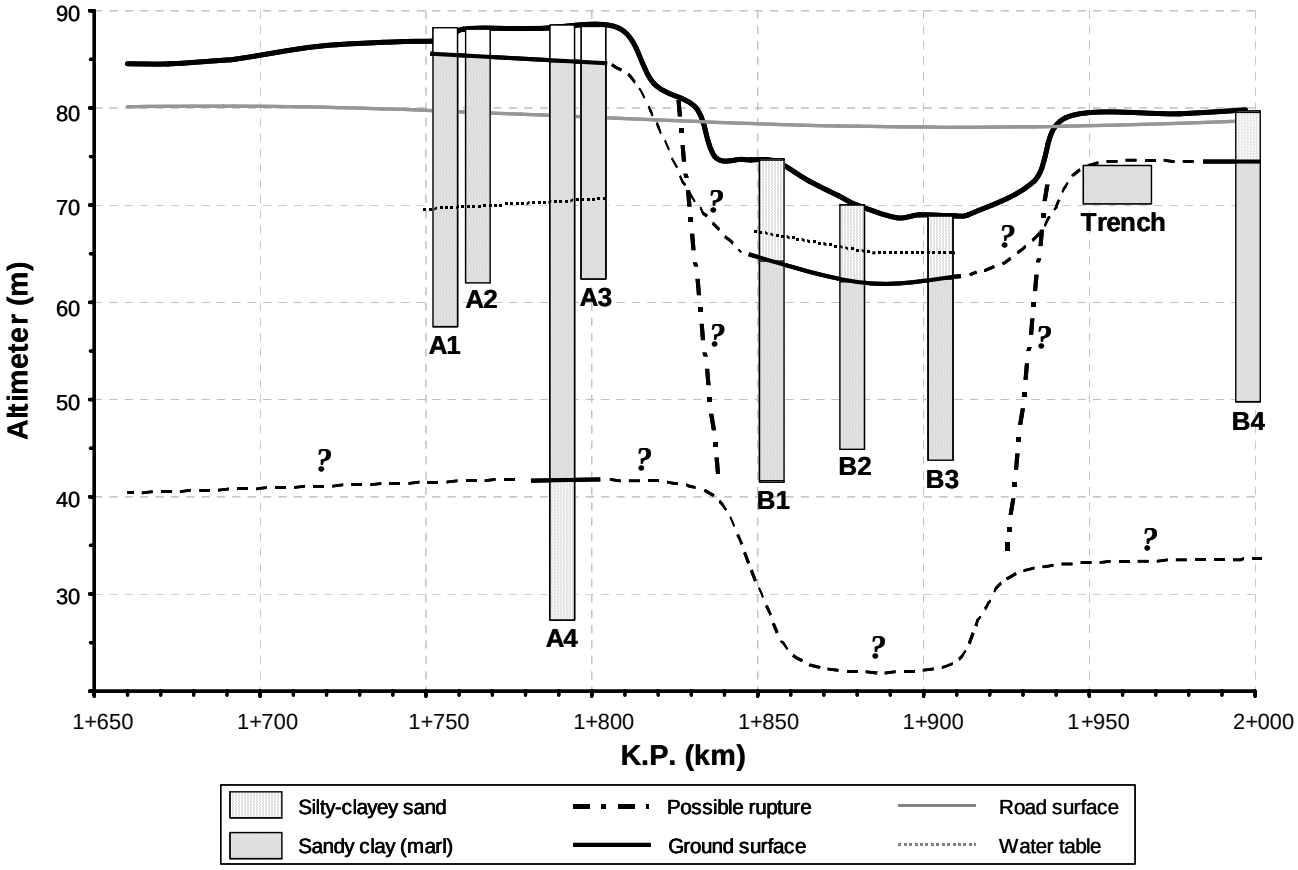

Fig. 8 Design of a three-span road bridge in Rhodes against possible fault rupture : Idealised geotechnical cross-section based on the conducted geo-exploration in conjunction with our field observations.

Based on the findings of our field visit (not described in detail herein), we came up to the hypothesis that the morphologic trench, through which the Rodinion Creek flows, is probably the outcome of tectonic displacement of the fault and the formation of a gravity graben. Although this hypothesis cannot be proven, it can easily explain the morphology of the area and the discontinuities at both buttresses.

Analysis Methodology

Given the available data, the possible (expected) tectonic displacement of the Rodinion fault is unknown : a special seismo-tectonic study would be required. To this end, we utilize the widely accepted empirical correlations of Wells & Coppersmith (1994). Since the length of the fault (= surface rupture length) may be greater than 15 km (Lekkas,1994), we assume a possible fault length L_f = 8 km to 20 km, yielding a possible moment magnitude M_s6 to 6.5. For this magnitude range, and for a normal fault, the average displacement is AD = 7 – 40 cm, and the maximum MD = 20 – 70 cm. Given the small jump of the Rodinion fault (in the order of 20 m), we hold the maximum value of MD not realistic and of low probability. In fact, values even lower than the average should be expected : D = 20 – 40 cm. It is noted that the tectonic displacement can either take place during a single event, or be of a cumulative nature (during multiple seismic episodes). Additionally, the occurrence of co-seismic displacements along the fault cannot be excluded. Therefore, we investigate the effect of the imposed tectonic displacement h parametrically : h = 0.1 m to 0.7 m.

As already discussed, the idealized soil profile of Fig. 8 is based on the hypothesis that the Rodinion fault coincides with the homonymous creek, and that the trench, through which the Rodinion Creek flows, corresponds to the formation of a gravity graben. From all eight boreholes, only A4 reached 60 m, without however “hitting” the bedrock. Therefore, the depth of the soil layer H remains unknown, along with the fault dip α. Therefore, we estimated both parameters (H and α) through back-analysis of the formation of the observed trench (= graben). The back analysis, not discussed herein due to space limitations, yielded $\alpha \approx 45^o$ and $H \approx 100$ m.

Having estimated h, H, and α, along with conservative soil parameters, we conduct our analysis in two steps. First, fault rupture propagation through soil is analysed in the free field, ignoring the presence of the bridge, and then, knowing the location of fault rupture outcropping in the free field, the bridge is placed on top, and the analysis of the soil-structure system is performed. Given that the exact location of the fault is unknown, we investigate 6 possible scenarios concerning its relative location to the bridge (Fig. 9). Based on the aforementioned back-analysis, “1” is the most probable location of the fault. However, since our back-analysis is quite approximate, and given that there is no real guarantee that the fault will “break” at the same location in a future event, locations “2” to “6” cannot be excluded.

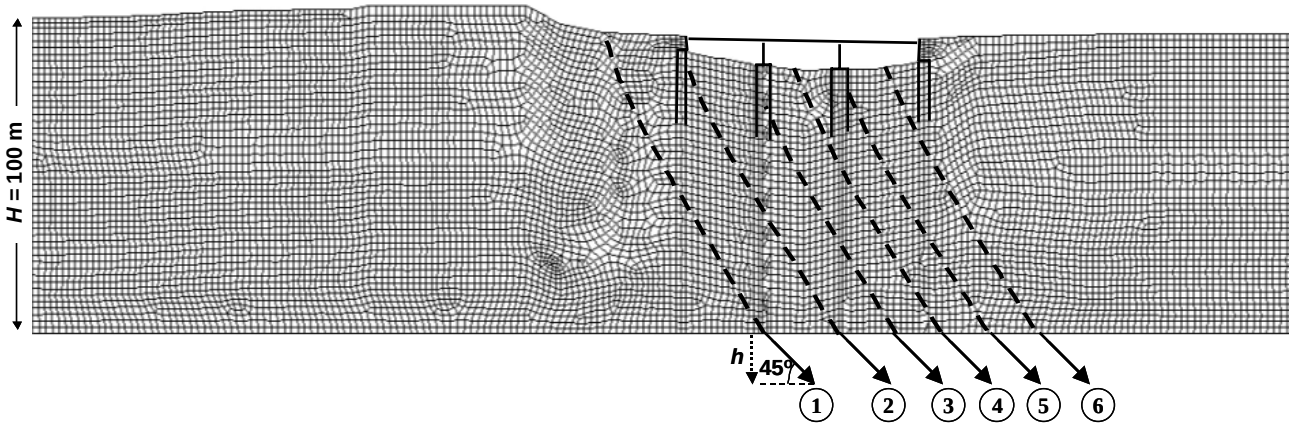

Fig. 9 Design of a three-span road bridge in Rhodes against possible fault rupture : finite element discretisation, along with the six likely scenarios of fault rupture that were analysed.

Results : Continuous vs. Isolated Deck

As already discussed, the aim of the study was the design of the bridge against fault rupture. The solution of a continuous deck monolithically connected to the piers was out-of-the-question, since it would not allow any differential settlement or tensile deformation. In this section we compare our analysis results for : (a) the initially envisioned solution of a continuous deck supported on the piers through lead-rubber bearings (Fig. 7a), and (b) the final solution of three separate simply supported decks on lead-rubber bearings, offering "seismo-tecnonic" isolation (Fig. 7b).

Fig 10 compares the results for the two design alternatives, in terms of deformed mesh and bending moment along the deck(s). The performance of the "seismo-tectonically" isolated alternative is definitely favorable. Observe the deformed mesh (Fig 10b) (magnification factor of 6) to note that the imposed tectonic displacement does not cause any bending of the deck in the case of the second alternative: the simply supported decks are only subject to rigid-block type rotation and displacement. On the contrary, the continuous deck alternative is subjected to serious bending (Fig 10a). The bending moment diagrams clearly attest this difference in the performance: while with isolation *M* is practically insensitive to *h,* in the case of a continuous deck *M* almost linearly increases with *h*. Even for *h* = 20 cm, M reaches 15 MNm, almost three times higher than the moment due to dead load ; for *h* = 40 cm, *M* reaches 54 MNm, a value which would certainly cause damage to the deck.

We have therefore proposed the "seismo-tectonically" isolated alternative, as the safest solution, in terms of fault rupture resistance. Several parametric analyses were then carried out to validate the performance, and determine the design sectional forces of piers and piles.

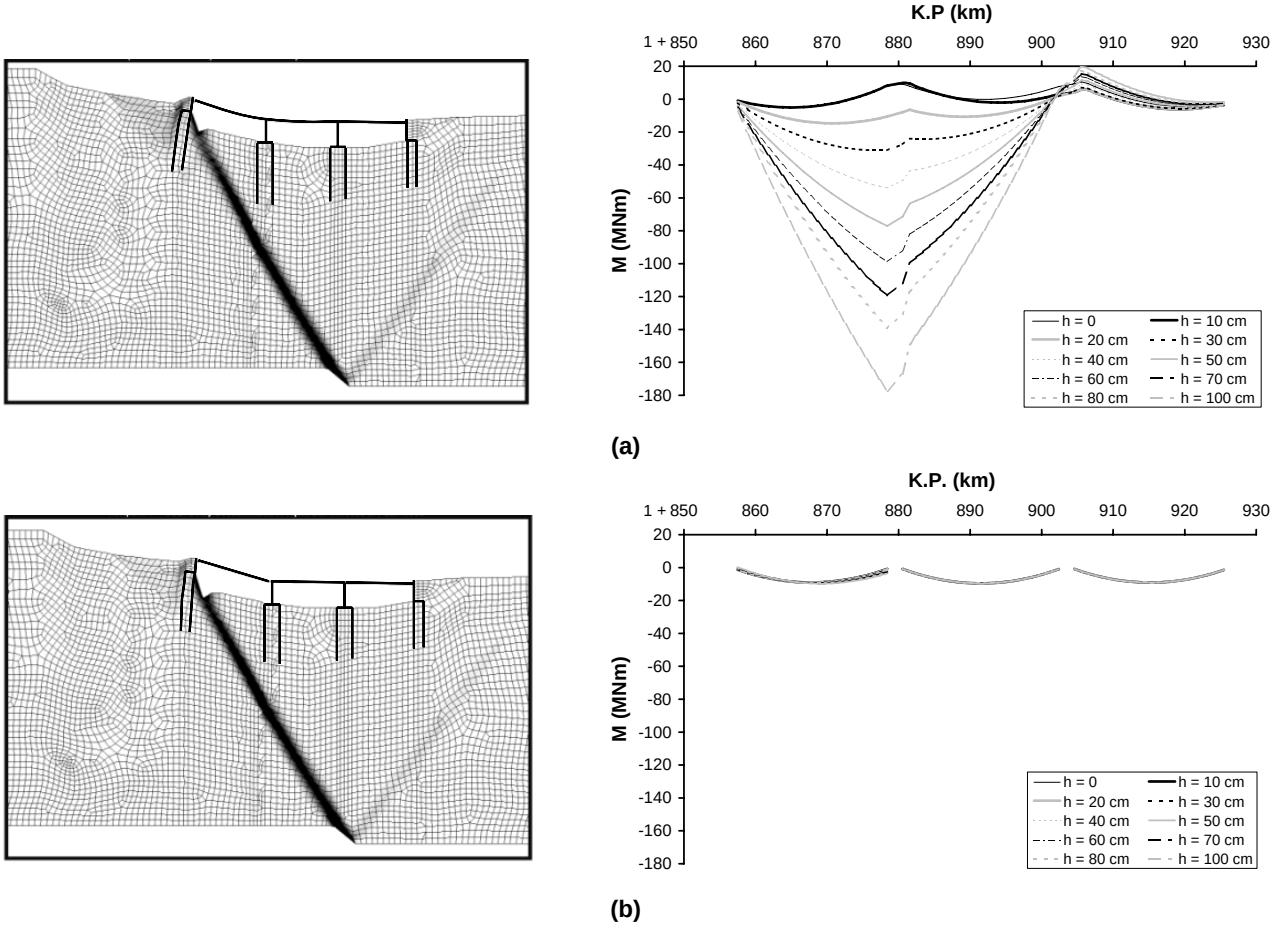

Fig. 10 Design of a three-span road bridge in Rhodes against possible fault rupture : deformed mesh with plastic strain, and bending moments along the deck, for scenario 2 fault rupture (a) initial design – continuous deck, and (b) modified design, offering "seismo-tectonic" isolation.

ATALANTI : OEK HOUSING COMPLEX

Introduction – History of the Project

OEK is the Workers Housing Organization of Greece. The buildings of our study (Fig. 11) belong to a housing project, in the region of Atalanti. The problem with the site was its proximity to the well-known Atalanti fault. Building was first attempted in 1986. For more than 15 years OEK was unable to proceed with construction, due to the ongoing debate concerning the seismic hazard and the possibility of a direct hit from the Atalanti fault. In 2003 we decided to make a "revolutionary" proposal that would give an end to this long-going debate : Instead of debating on the existence and exact location of the faults, let us assume their existence and apply our FR-SFSI methodology to design the buildings against a possible fault rupture.

Tectonics of the area and the Atalanti fault

The area of study is situated in Central Greece, to the east of the city of Atalanti. The site is situated within the Atalanti plain, relatively close (< 1 km) to the fault trace of the 1894 earthquake. Fig.12a depicts the geodynamic setting of the Aegean region (Pantosti et al, 2001), while the active faults of Central Greece, as modified from Roberts & Jackson (1991) and Armijo et al (1996) are illustrated in Fig. 12b. Northern Evoikos is a tectonic graben that was formed during the Tertiary period. Its seismic activity is quite intense, characterized from normal faults of NW-SE direction. The main rupture zones include the predominant Atalanti fault, as well as the faults of Thermopyles, Kamena Vourla, Agios Konstantinos, Arkitsa, and Kallidromon. While the broader area comprises Mesozoic and Tertiary layers, the site is clearly within quaternary sediments (Fig. 12c), i.e. alluvial and lacustrine deposits, and cones of debris. The fault trace of the 1894 earthquake is clearly not within the site. However, the distance to the Atalanti fault not exceeding 500 m – 800 m, clearly characterizes the site as in the vicinity of the fault.

In 1894 two seismic events struck the broader area of Atalanti. The two episodes took place only a week apart, on April 20 and 27, with the first one of smaller magnitude. The magnitudes of the two earthquakes have been estimated to be 6.4 and 6.9, according to Ambraseys & Jackson (1990). According to contemporary authors , the earthquakes

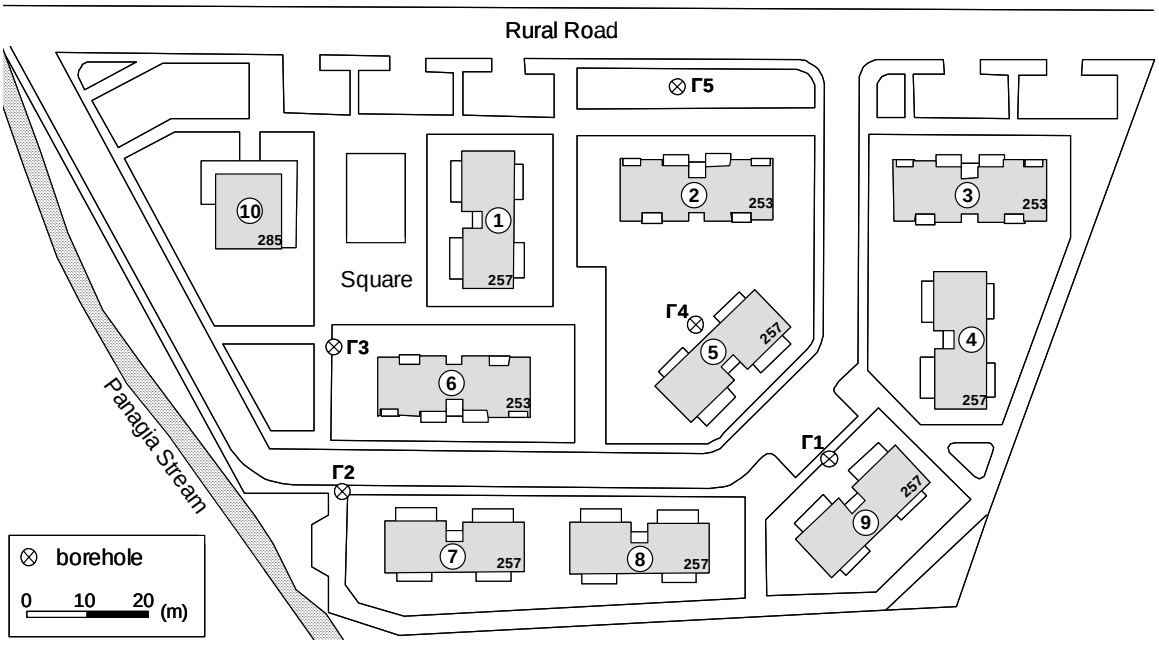

Fig. 11 OEK's housing complex in Atalanti : ten buildings in total, six of type 257 (4 apartments each x 6 = 24 in total), three of type 253 (4 apartments each x 3 = 12 in total), and one of type 285 (union building).

produced ground ruptures and major disturbances of the landscape. However, there was a debate on the location and extent of the ground ruptures. More specifically, there was an issue concerning the main fault rupture. According to Skouphos (1894), Papavassiliou (1894), and Philippson (1894) the “chasm” was tectonic, continuing in depth. On the other hand, Mitsopoulos (1895) believed that the rupture was a superficial gravitational feature.

The first shock seems to have produced smaller ruptures in addition to landslides and liquefaction (Skouphos, 1894). Contrarily, the second earthquake created surface fault ruptures systematically arranged along the Atalanti fault. Skouphos (1894) describes a 60 km long dislocation with vertical displacement in the order of 30 cm in limestone. The dislocations were much larger, reaching 2 m, wherever the fault was outcropping through alluvium.

Rondoyianni (1984) provides the first analytical geological and neotectonic study and mapping of the region, including the central and southern segment of the Atalanti fault. Pantosti et al (2001), re-mapping the remnants of the 1894 ruptures, concluded that the Atalanti fault ruptured only during the second event (April 27), while the first one (April 20) was caused either by the Malessina fault, or an offshore fault parallel to the Atalanti fault. They concluded that the April 27 rupture (i.e. the Atalanti fault) was 32 km to 40 km long, 12 km wide with a 1.5 m slip at depth, yielding a magnitude of 6.8.

According to Buck & Stewart (2000) the maximum subsidence was not higher than 0.5 m within the bedrock. However, wherever the fault was outcropping through sediments the maximum movement reached 2 m to 4m. The coastline “sank” significantly with the 1894 earthquake (Pavlides, 2003), implying a co-seismic subsidence of 1.5 m (Buck & Stewart, 2000). Based on all of the above data, our seismo-tectonic study (Pavlides, 2003) concluded that the Atalanti fault must be in the order of 30 km in length, with slip rates not exceeding 0.5 mm/yr, classifying it as a typical active fault of medium to high seismicity. If the whole fault is activated, the maximum possible magnitude will be M_s = 7.0, with a 50 year non-exceedance probability of 95%.

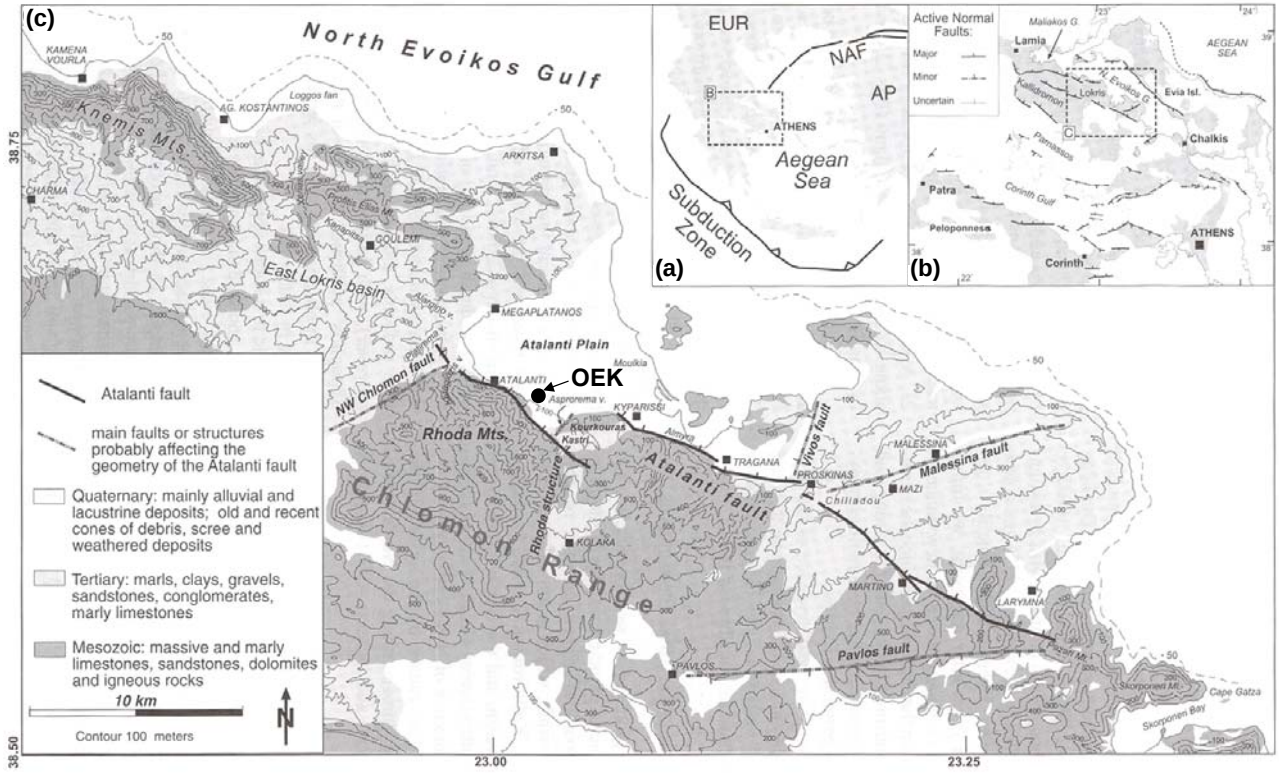

Fig. 12 OEK’s housing complex in Atalanti : (a) Simplified geodynamic setting of the Aegean region, (b) Active Faults in central Greece, modified from Roberts & Jackson [1991] and Armijo et al. [1996], (c) Geology and Topography of the broader area between Ag. Konstantinos and Cape Gatza, mapping the Atalanti fault along with other secondary faults [Pantosti et al, 2001].

The site is 500 to 800 m from the 1894 fault trace, and 200 to 300 m from secondary branches. The two geological trenches, that we conducted within the site, did not reveal any fault. No land-sliding phenomena or significant co-seismic gravitational movements should be expected within the site. However, given the seismo-tectonic history of the area, and the proximity to secondary fault branches, the study (Pavlides, 2003) proposed a 10 – 20 cm tectonic-induced differential settlement to be taken into account for the design of the buildings.

Geotechnical Data

Five boreholes were conducted within the site during the geotechnical exploration. Five generalized soil layers were identified : (a) low plasticity sandy clay, (b) very dense clayey sand and gravel, (c) very dense medium to high plasticity sandy clay with gravel, (d) medium to loose low plasticity sandy clay, and (e) very dense medium plasticity clayey sand. Based on the results of the geotechnical exploration (in situ and laboratory), two idealized soil profiles were synthesized (Fig.13). The estimation of both the strength and the deformational characteristics of the idealized soil profiles was not done "conservatively", at least in the usual meaning of the term. When FR-SFSI is the issue, it is non-conservative to assume lower values for either the strength characteristics (c, φ), or for E. In fact, the softer the soil the more favourable the response of the structure (Anastasopoulos, 2005). In that sense, for FR-SFSI both the strength and the deformational parameters of soil must be estimated as realistically as possible, and not "conservatively". In fact, conservatism in FR-SFSI is exactly in the opposite sense : *assume higher strength and deformational parameters.*

Analysis Methodology

As in the previous cases, the analysis is conducted in two steps. First, fault rupture propagation through soil is analysed in the free field, ignoring the presence of the structure. The depth of the soil deposit was conservatively assumed to be equal to H = 40 m. Given that all of the boreholes had reached 40 m depth, this was the only safe way to go.

For the modeling of soil behavior we applied our modified Mohr-Coulomb constitutive model with isotropic strain softening. The differential displacement h was applied to the left part of the model at an angle α = 55°, in small consecutive steps. According to the geotectonic study of Pavlides (2003) a maximum differential displacement in the surface of 10 – 20 cm should be adequate. Therefore, to be conservative we applied h_{max} = 0.4 m.

Then, knowing the location of fault outcropping in the free field, the three different types of structures were placed on top, and the analyses of the soil-structure systems were performed. To model FR-SFSI as accurately as possible, the two-dimensional beam and shell elements of the superstructure were given equivalent plane-strain properties. This way the stiffness of the superstructure relative to the soil was modeled correctly, even though the structure is in reality three-dimensional. The same principal was applied to all the loads of the superstructure.

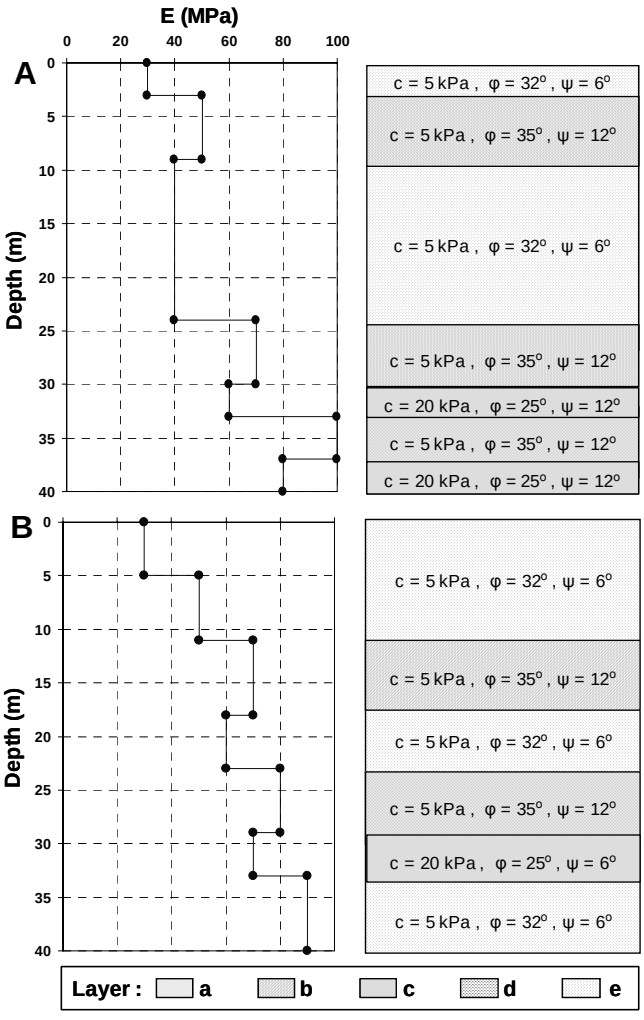

Fig. 13 OEK's housing complex in Atalanti : The idealized soil profiles used for the analysis.

For all three buildings, the outcropping fault rupture was assumed to be perpendicular to their larger dimension. This assumption is conservative and the results can safely be applied to the other direction, as well. For each building type three different fault rupture outcrop relative locations were parametrically investigated. In this paper we will focus on building Type 253 (Fig. 14).

As depicted in Fig. 15, the building was placed at three different locations, relative to the fault outcrop (in the free field) :

(i) fault rupture outcropping at distance x = 6 m from the left edge of the building (i.e. the rupture outcrops at the left 1/4 of the width),
(ii) fault rupture outcropping at x = 13 m from the left edge of the building (i.e. the rupture outcrops at the middle of the building), and
(iii) fault rupture outcropping at x = 6 m from the right edge of the building (i.e. the rupture outcrops at the right 1/4 of the building).

In the first case (i), the building is mainly in contact with the footwall, while in the last case (iii) the building finds support mainly on the hanging wall. The second case (ii) is an intermediate positioning, possibly generating the highest stressing.

The foundation of the building constitutes the main concern of the study. FR-SFSI does not only depend on the stiffens of the superstructure, but also on the stiffness and characteristics of the foundation system (Anastasopoulos, 2005). Isolated footings were put out of the question right from the beginning, and only slab and box-type foundation systems were anticipated. Four different foundation types were parametrically investigated :

1) Slab foundation, of thickness t = 0.2 m,
2) Slab foundation, of thickness t = 0.5 m,
3) Box-type foundation, of t = 1.0 m, and
4) Box-type foundation, of t = 1.5 m.

The box-type foundation consists of a grid of 0.5 m thick strips, sandwiched between a bottom and a top slab, 0.2 m in thickness. The voids between the strips and the slabs are filled with compacted soil material. This type of foundation combines increased stiffness and dead load with significant savings in concrete. Both the stiffness of the foundation as well as the increased dead load have proven to be advantageous in FR-SFSI, both in terms of fault diversion and of “smoothing” of the settlement profile. Given that building type 253 has a basement with stiff reinforced concrete walls, we analyzed only the first three foundation types.

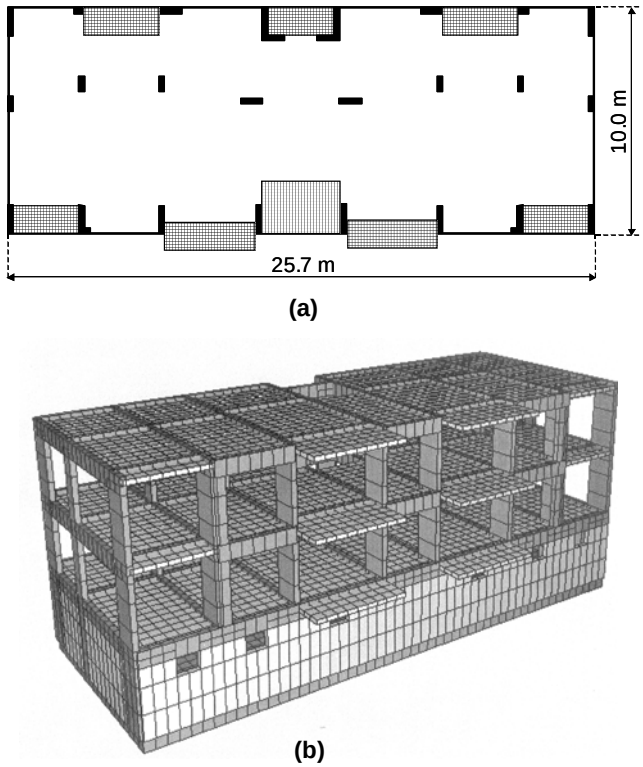

Fig. 14 OEK’s housing complex in Atalanti : Building type 253 (a) plan view, and (b) 3-D structural model (after Sigalas, 2004)

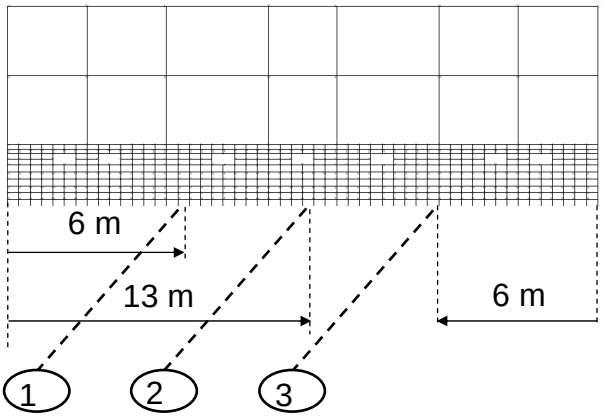

Fig. 15 OEK’s housing complex in Atalanti : the three scenarios of fault rupture location relative to the building (type 253) that were analysed.

Summary of Results and Conclusion

The results of our study were presented in detail in the relevant Technical Reports. Since the basement walls were believed to play an important role, to visualize their effect we also conducted FR-SFSI analyses of building 253 without basement walls. The analytical review of all the results is clearly not within the scope of the paper. We will therefore present only some characteristic results, giving emphasis on our conclusions and design considerations.

Fig.16 illustrates the deformed mesh and plastic strains for building Type 253, founded on the t = 0.5 m slab foundation, with and without basement walls. When the fault rupture is at a distance of 6 m from the left edge of the structure (Fig.16a), the rupture is diverted to the left but not enough to avoid outcropping underneath the building. The building uplifts mainly at its left edge and only slightly at the right. In the scenario of the fault rupture outcropping at a distance of 13 m from the left edge of the structure (Fig.16b), the rupture is diverted by about 5 m to the left, but obviously not enough to avoid the building. Now, the building finds support at its left edge, and at the middle. Uplifting occurs between the two supporting sections, as well as at the right edge. Finally, when the rupture is at a distance of 6 m from the right edge (Fig.16c), it is not only diverted to the right, but is also separated (diffused) in two separate branches. From the two branches, one outcrops near the middle of

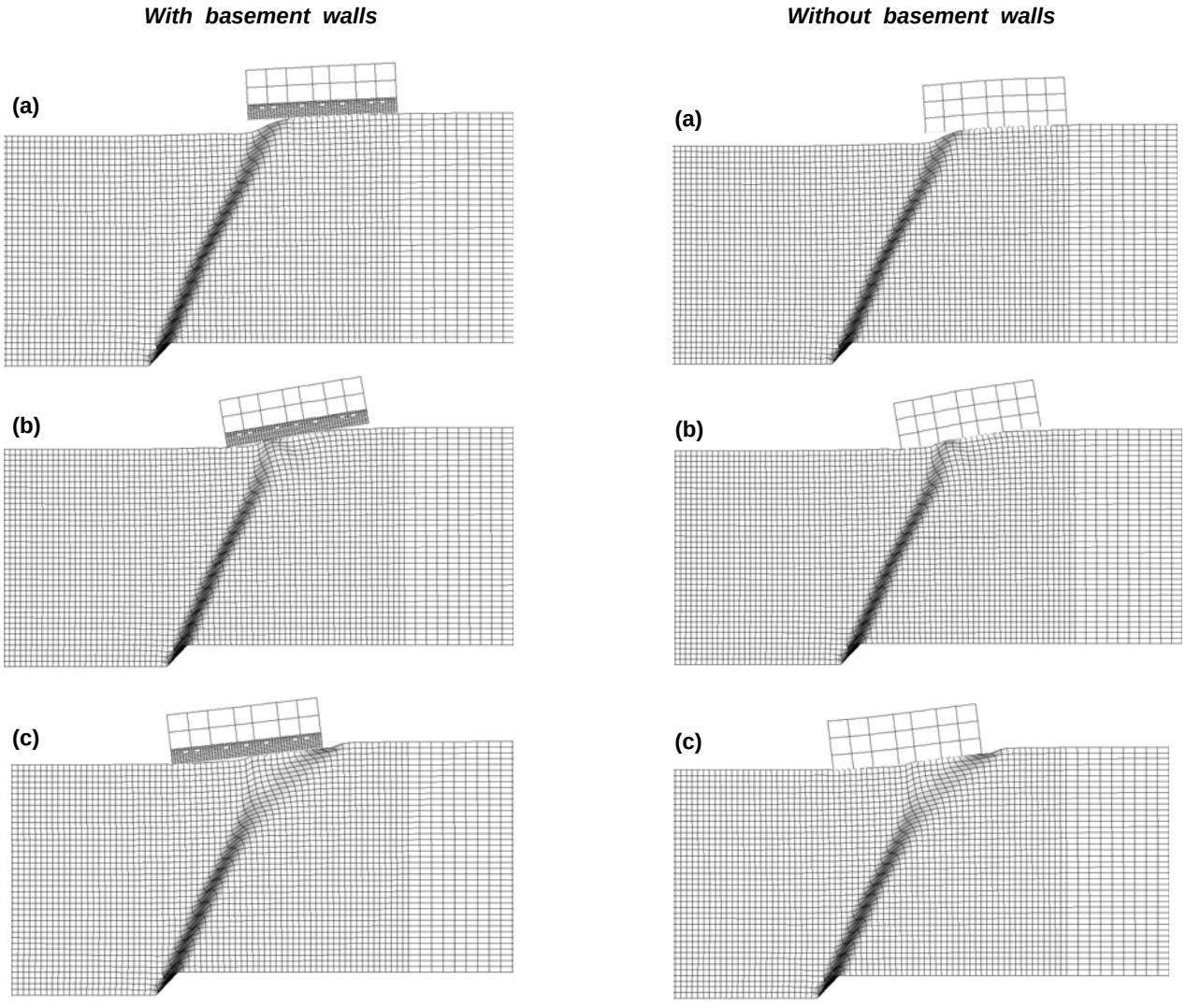

Fig. 16 OEK's housing complex in Atalanti : Deformed mesh (magnified by a factor of 10) and plastic strains for building Type 253, founded on t = 0.5 m slab foundation. Fault rupturing : (a) 6 m from the left edge of the structure, (b) 13 m from the left edge (at the middle), and (c) 6 m from its right edge. Building with basement walls on the left, and without on the right.

the structure, and the second one emerges at the right edge. Now, the building is supported at the left edge and at a greater portion near its right edge, with uplifting taking place from the middle to the left support.

Fig. 17 depicts the sectional forces and basement wall stresses for the same building–foundation system with the rupture at 6 m distance from its left edge, with respect to the applied bedrock displacement *h*. Interestingly, after *h* has reached 0.2 m, all of the bending moments and basement wall stresses remain practically constant. Although phenomenally paradox, this response is quite logical and easy to explain. The fault rupture outcrops for *h* = 0.2 m. After the fault has outcropped, there is no reason for the structure to be subjected to higher stressing. Since the building is supported on the footwall, with its left edge acting as a cantilever, it does not really matter if the hanging wall subsides by 0.2 m or 0.4 m, or even more. As already explained, since the soil–foundation interface cannot transmit tensile forces to the structure, the distress is mainly due to uplifting. The increase of the downward displacement does not really change the extent of the uplifted region near the left edge.

The situation is a little different when the relative fault–structure location is moved to the middle of the building. As illustrated in Fig. 18, not all of the sectional forces are stabilized for $h \geqslant 0.2$ m. Of course, the response is highly non-linear and the rate of increase decreases significantly with the increase of *h*. The difference can be attributed to the different geometry of the problem. Now, the building finds support at the middle, uplifting at both of its edges. It seems that the "equilibrium" is not reached that fast, with the increase of *h* increasing the uplifted parts of the structure. Of course, if we increase *h* further, the aforementioned "equilibrium" will finally be attained.

Even more interesting is the scenario of fault outcropping near the right edge of the structure (Fig. 19). This time, the sectional forces are not only stabilized, for $h \geqslant 0.3$ m, but some of them are even observed to slightly decrease.

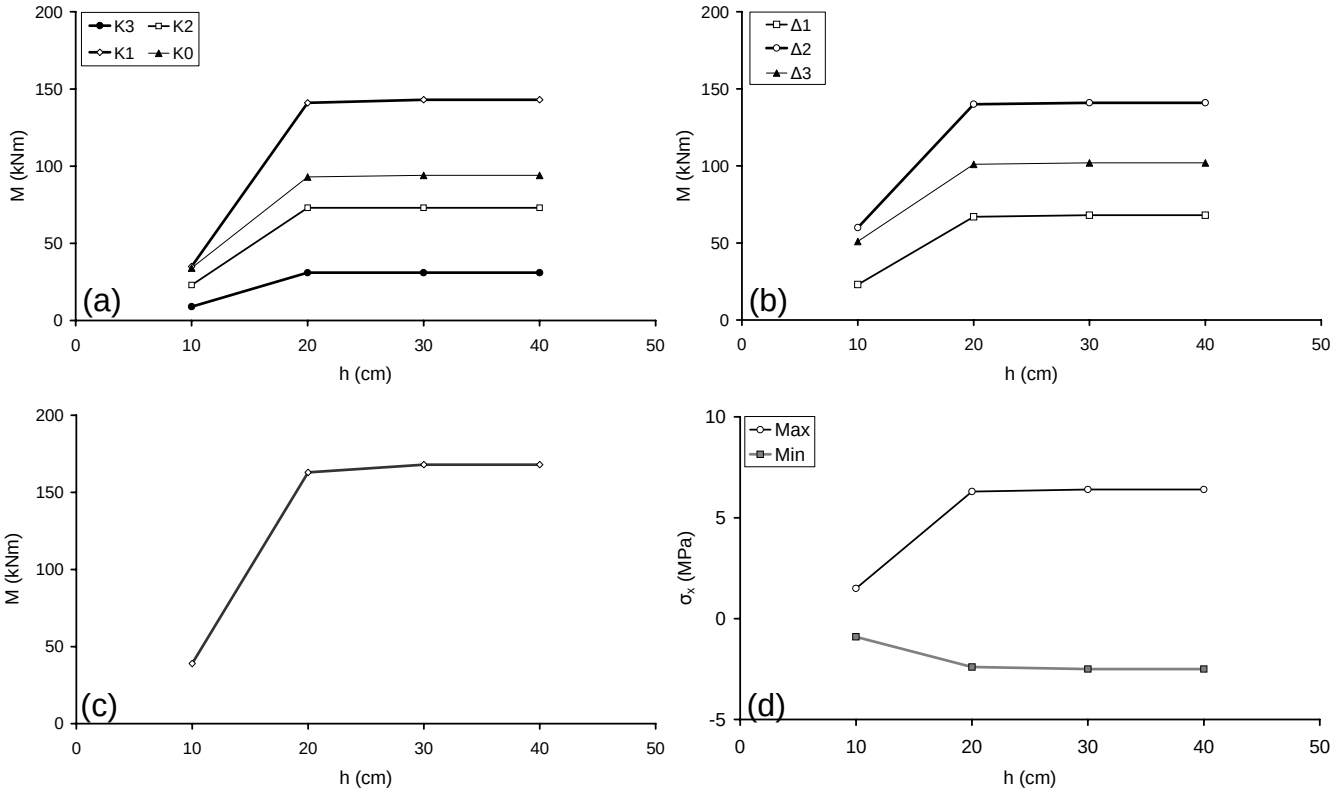

Fig. 17 OEK's housing complex in Atalanti : Effect of bedrock displacement *h* on the sectional forces and basement wall stresses for building Type 253, founded on *t* = 0.5 m slab foundation, with the rupture 6 m from its left edge : (a) bending moments *M* in columns, (b) bending moments *M* in beams, (c) bending moments *M* in the foundation slab, and (d) horizontal stresses σ_x in the basement walls.

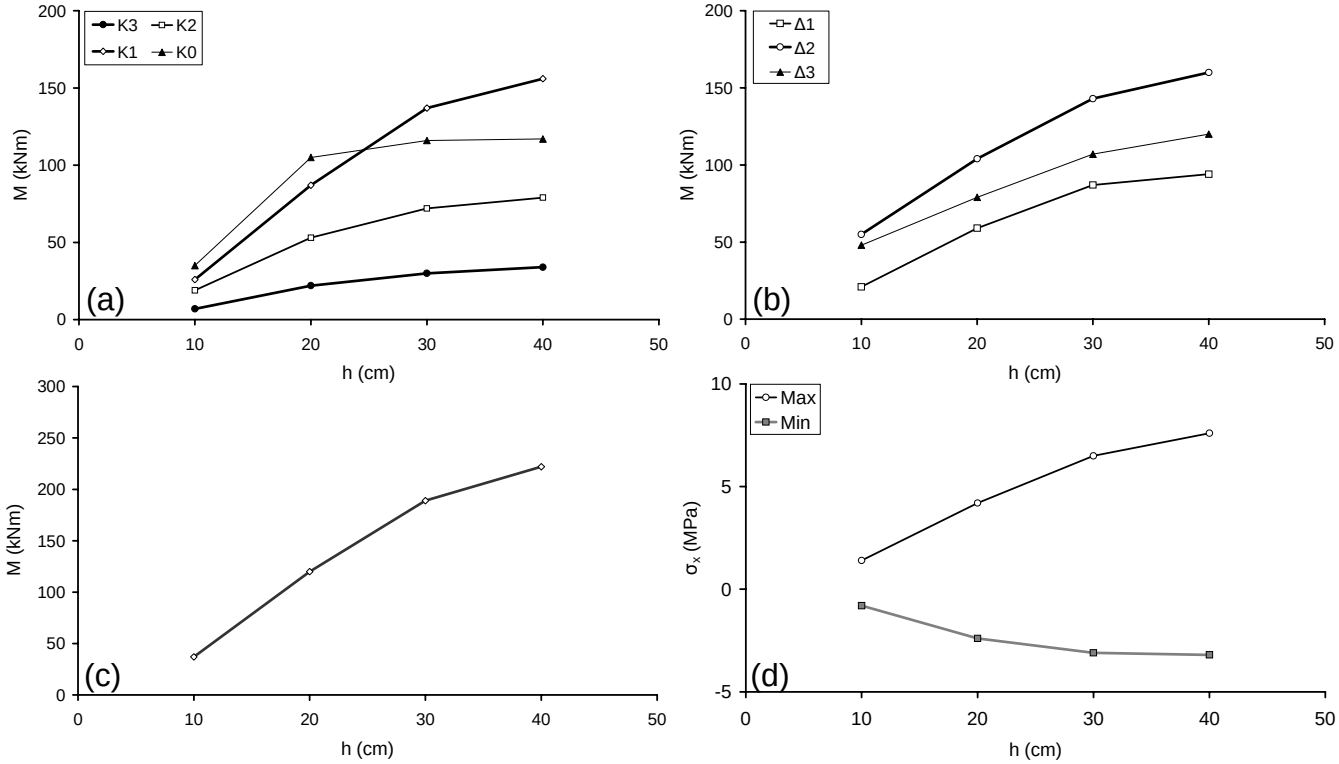

Fig. 18 OEK's housing complex in Atalanti : Effect of bedrock displacement *h* on the sectional forces and basement wall stresses for building 253, founded on *t* = 0.5 m slab foundation, with the fault rupture 13 m from its left edge : (a) bending moments *M* in columns, (b) bending moments *M* in beams, (c) bending moments *M* in the foundation slab, and (d) horizontal stresses σ_x in the basement walls.

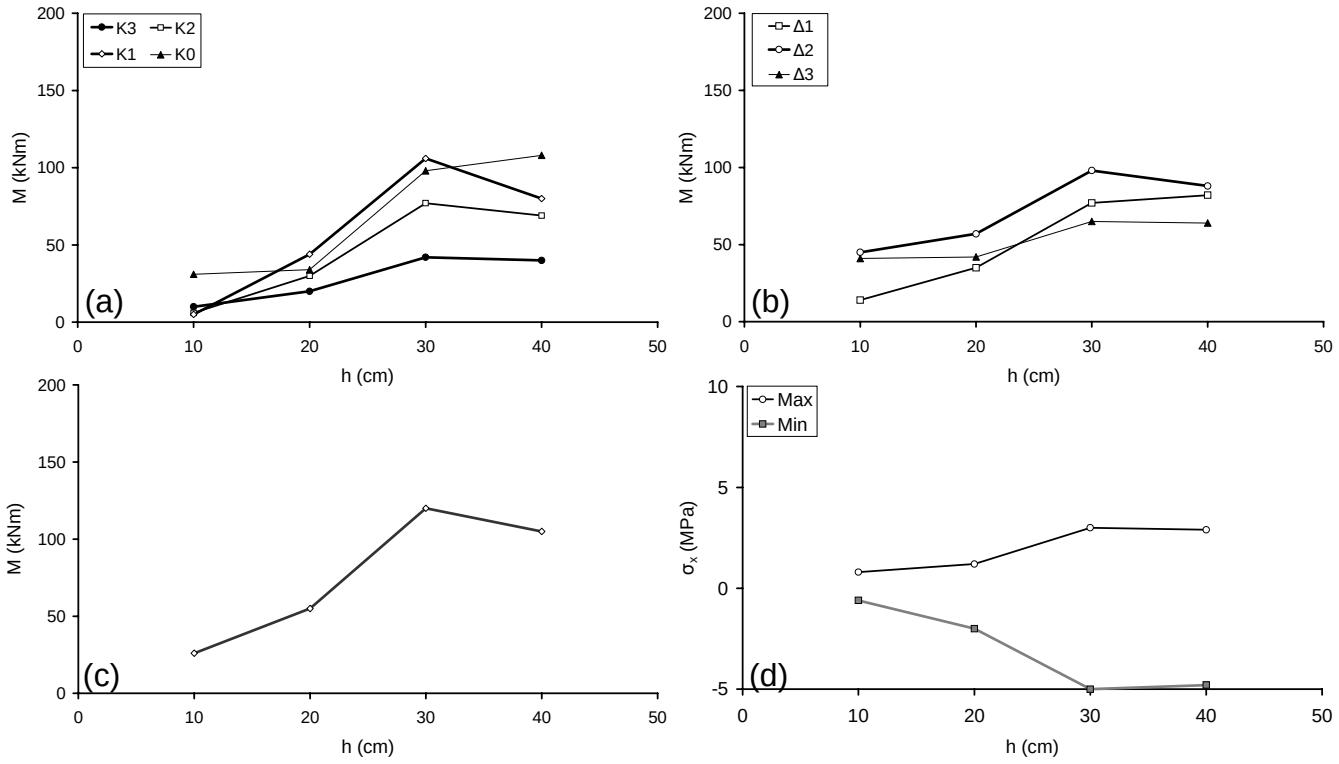

Fig. 19 OEK's housing complex in Atalanti : Effect of bedrock displacement *h* on the sectional forces and basement wall stresses for building 253, founded on *t* = 0.5 m slab foundation, with the fault rupture 6 m from its right edge : (a) bending moments *M* in columns, (b) bending moments *M* in beams, (c) bending moments *M* in the foundation slab, and (d) horizontal stresses σ_x in the basement walls.

The answer for this behaviour resembling "softening" can be found in Fig.16c. Observe that for h = 0.4 m the deformation is diffused over a wide area underneath the structure. This diffusion, due to soil non-linearity, is responsible for the observed "softening" behaviour. Due to the geometry of outcropping relative to the structure, the effective width of the foundation becomes too narrow to bear the load of the structure. Consequently, the soil fails creating this diffused deformation zone, and the effective width of the foundation is increased. This means that the uplifted areas decrease in width, decreasing the distress of the structure, consequently.

Quite interesting is the response of the same building without basement walls. As illustaretd in Fig. 16, the response is very similar in all cases, with the only exception being the distress of the structure. Observe the difference in the deformation of the structure. While in the case of the building with basement walls the structure rotates almost as a rigid body, without any deformation being easily observed, without the basement walls the deformation is evident. Table 1 summarizes the main results of our study for building type 253.

The sectional forces clearly confirm the severe stressing of the structure without basement walls.

The main conclusions of our study are :

[1] In all cases FR-SFSI modifies the soil settlement profile and the outcrop location,

[2] The rupture tends to be diverted either to the left or to the right of the building, depending on the fault–structure relative location. However, due to the "small weight" of the structure (2-stories + basement, only), in combination with its significant length (25.7 m), the rupture cannot avoid outcropping underneath the building.

[3] The increase of the foundation stiffness (and weight) does not seem to cause a significant amelioration of the response. The basement walls, in combination with the foundation and ground-floor slabs create a very stiff box section capable of "absorbing" most of the stressing.

[4] The foundation system would have to become stiffer than the basement walls to observe some amelioration of the response. This is not necessary since the response of the building is quite satisfactory.

Table 1 OEK's housing complex in Atalanti : Summary of Results

Distance from fault (m)	Superstructure	Foundation	Differential Settlement (cm)	M_{max} – superstructure distress			Bsmt. Walls	
				Columns (kNm)	Beams (kNm)	Foundation (kNm)	σ_{max} (MPa)	σ_{min} (MPa)
6 L*	With Basement Walls	Slab foundation t = 0.2 m	12	140	141	149	5.5	-3.1
		Slab foundation t = 0.5 m	13	143	141	168	6.4	-2.5
		Box-type t = 1.0 m	15	166	153	776	6.9	-2.5
	Without Bsmt. Walls	Slab foundation t = 0.5 m	15	520	569	368	–	–
13L**	With Basement Walls	Slab foundation t = 0.2 m	31	135	142	17	5.8	-3.3
		Slab foundation t = 0.5 m	29	137	143	189	6.5	-3.1
		Box-type t = 1.0 m	26	147	146	768	6.3	-2.9
	Without Bsmt. Walls	Slab foundation t = 0.5 m	30	525	611	362	–	–
6R***	With Basement Walls	Slab foundation t = 0.2 m	20	108	102	16	3.2	-4.4
		Slab foundation t = 0.5 m	19	106	98	120	2.9	-5.0
		Box-type t = 1.0 m	18	110	97	480	2.5	-4.6

* : 6 m from the left edge of the structure ** : 13 m from the left edge of the structure *** : 6 m from the right edge of the structure

[5] The above statement is true, provided that all of the structural members are reinforced adequately. Especially the basement walls must be reinforced to undertake bending to the horizontal, which is certainly different to their usual reinforcing (to sustain shaking–induced shear loading).

[6] Given that the exact location of the fault outcrop relative to the building cannot be predicted, the building can be subjected to either direction of bending. Therefore, beams, slabs, and basement walls must be reinforced for both directions of bending.

Structural Design of the buildings

The soil settlement profiles computed through our FR-SFSI analyses were utilized for the structural design of the buildings (Sigalas, 2003). Three-dimensional models (Fig. 14b) of the three building types were developed and subjected to the fault-induced displacements. The displacements were transmitted to the 3-D structural models through special non-linear elements, infinitely stiff in compression with tension cut-off. The sectional forces and basement wall stresses were found to compare well with the equivalent 2-D FR-SFSI analyses, validating the equivalency of the two analyses.

KAMENA VOURLA : CUT-AND-COVER TUNNELS

Introduction

The under study cut-and-cover tunnels are situated in Kamena Vourla, being part of the new highway connecting Southern Greece with Northern Greece (PATHE). They are within the bypass section of the homonymous city. The scope of our study was the design of the cut-and-cover tunnels against a major fault rupture. Their proximity to the well known, and mapped, Kamena Vourla fault gave rise to the question of their seismo-tectonic performance.

Four tunnels were studied. Due to space limitations we will only focus on the first tunnel. As depicted in Fig 20, the tunnel is of double section, with 1 to 5 m cover. Its cross-section is 24.4 m wide and 9.5 m in height, with a bottom slab of 1.3 m thickness and a top slab of 1.2 m. The side walls are 1.0 m in thickness, and the middle one 1.4 m. Based on seismic risk assessment studies (OTM, 1997), AD = 1 m and MD = 2 m.

Geotechnical Data

The geotechnical conditions of the site have been explored in the relevant geotechnical exploration. Two generalized soil layers were identified. The first one, from the surface to about 10 m depth, consists of alternating layers of dense silty to clayey sand and gravel with cones of debris. Within this layer, the blows of the standard penetration test N_{SPT} ranged from 31 to 50. Deeper, the second generalized soil layer consisted of very dense silty to clayey gravel, with interlayers of sound rock. The N_{SPT} blows were consistently $\geqslant$ 50.

Analysis Methodology and Results

Based on the geology of the area, the depth of the soil layer was estimated to be H = 50 m. As always, the soil was modeled with quadrilateral plane-strain elements, and the tunnel with beam elements. The tunnel is connected to the soil through special interface elements, allowing for uplifting and sliding.

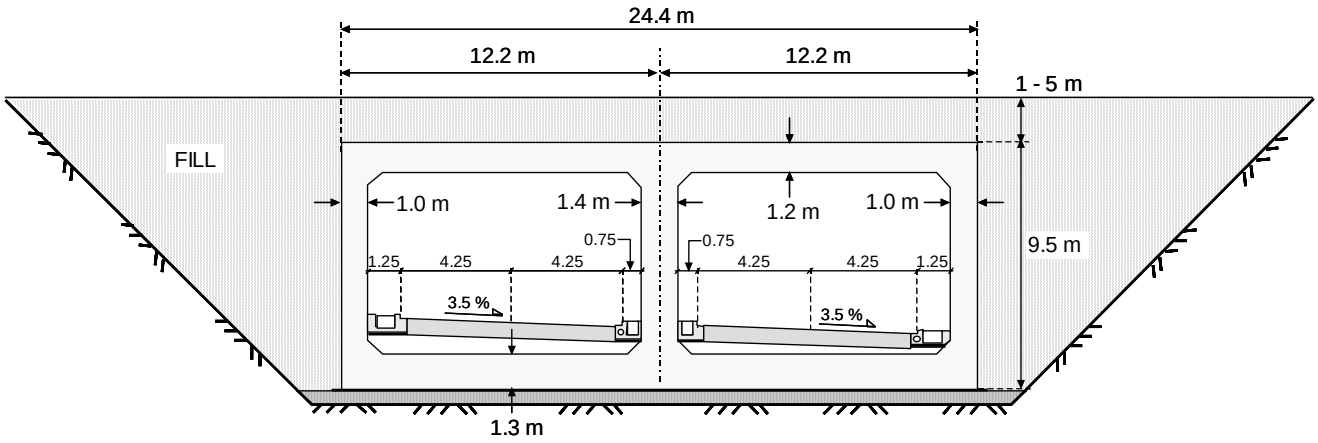

Fig. 20 Design of Cut-and-Cover Tunnels in Kamena Vourla against a major fault rupture : typical tunnel cross-section

Soil behavior is modeled through our modified Mohr-Coulomb constitutive law with isotropic strain softening. As in the previous cases, the analysis is performed two steps. First, fault rupture propagation through soil is analysed in the free field, ignoring the presence of the tunnel. The differential displacement h was applied to the left part of the model at an angle $\alpha = 60^o$, in small consecutive steps. According to the aforementioned geotectonic studies, a differential displacement from 1 m to 2 m should be taken into account. Therefore, to be conservative, we conducted our analyses applying maximum displacement $h_{max} = 2$ m.

Having conducted the analysis of fault rupture propagation, and knowing the location of fault break-out in the free field, the soil-tunnel model was subject to three different rupturing scenarios, with respect to the relative fault-tunnel location :

(1) fault rupture outcropping at distance $x = 6$ m from the left edge of the tunnel (i.e. left 1/4),

(2) fault rupture outcropping at $x = 12$ m from the left edge of the tunnel (i.e. at the middle),

(3) fault rupture outcropping at $x = 6$ m from the right edge of the tunnel (i.e. at the right 1/4).

The three scenarios, along with the finite element discretisation are illustrated in Fig. 21.

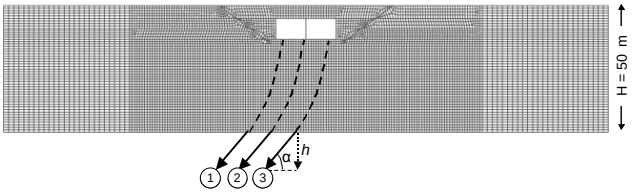

Fig. 21 Design of Cut-and-Cover Tunnels in Kamena Vourla against a major fault rupture : FE discretisation, along with the three scenarios of fault rupture location relative to the tunnel.

Typical results, in terms of deformed mesh and plastic strain accumulation, are presented in Fig. 22, corresponding to rupturing scenario "1" of the cut-and-cover tunnel with 5 m cover. At the beginning, $h = 0.5$ m, a single rupture outcrops close to the left edge of the tunnel. The rupture seems to have been significantly diverted, without however avoiding the structure. Increasing the imposed bedrock displacement leads to a pronounced bifurcation of the rupture plane. A second rupture outcrops almost at the middle of the tunnel, while at the same time some diffusion can be observed close to its base. The tunnel seems to rotate almost as a rigid body, without being distressed extensively.

Fig. 23 depicts the bending moments along the structural members of the tunnel, with respect to the imposed displacement. As it

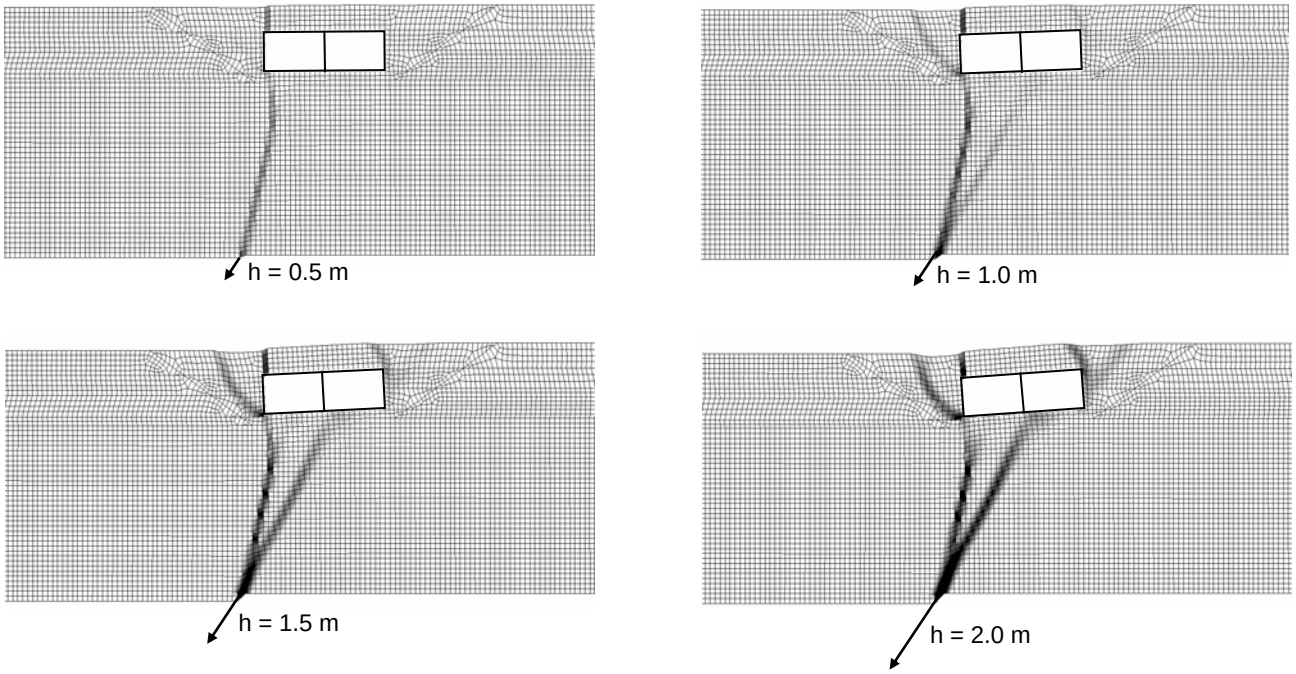

Fig. 22 Design of cut-and-cover tunnels in Kamena Vourla against a major fault rupture : Deformed mesh (magnified by a factor of 2) and plastic strains for rupture scenario 1, for imposed bedrock displacement h ranging from 0.4 m to 2 m. Notice the bifurcation of the outcropping rupture plane with the increase of h.

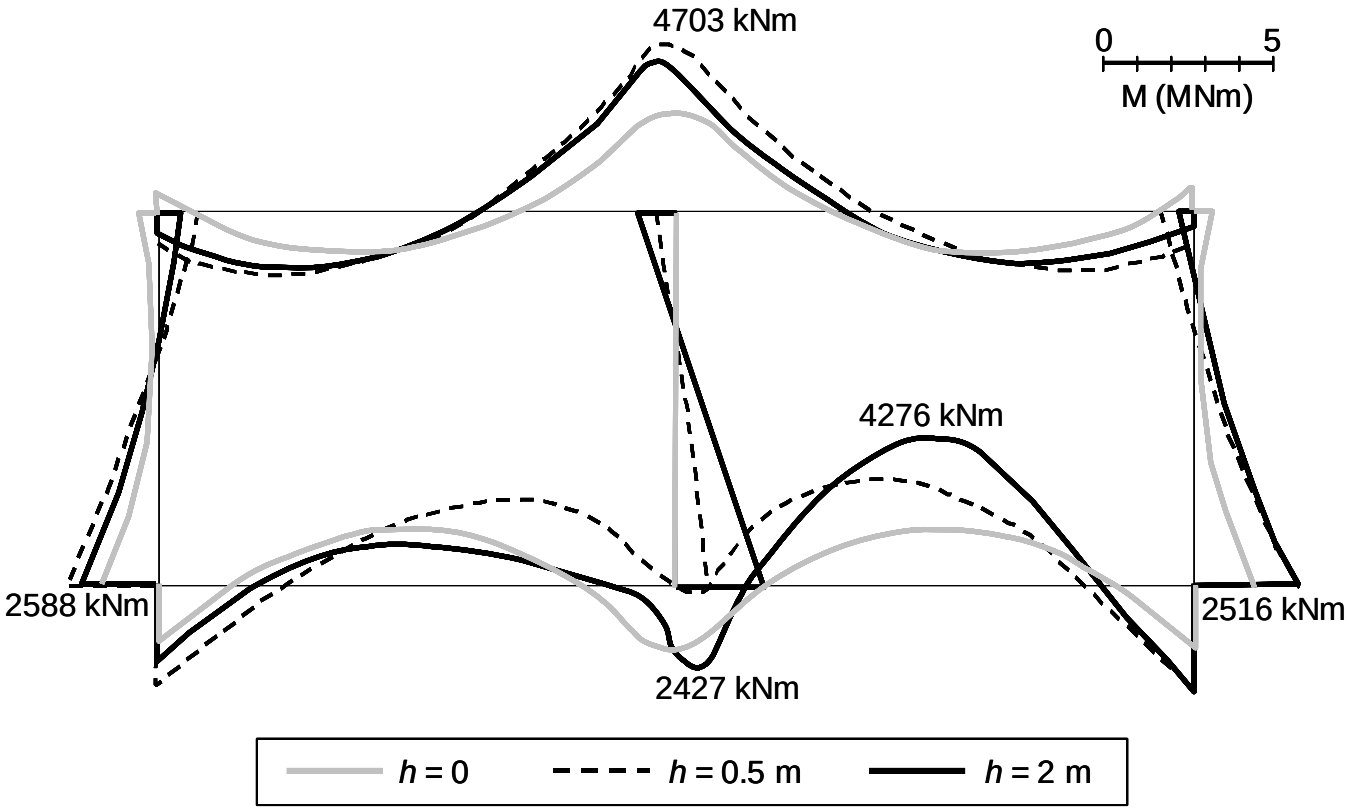

Fig. 23 Design of cut-and-cover tunnels in Kamena Vourla against a major fault rupture : Bending moments with respect to the imposed bedrock displacement *h,* for rupture scenario 1, with 5 m cover.

would be expected, the maximum stressing of the base slab of the tunnel (4276 kNm) takes place for the maximum imposed displacement, h = 2 m. Interestingly, the response of the top slab is different. The maximum bending moment of 4703 kNm is attained for h = 0.5 m. Then, the increase of h only leads to a slight decrease of the bending moment. The same observation also holds for the left wall and the left half of the bottom slab. This performance is indicative of the strong non-linearity that characterizes the interplay between the rupturing fault, the bearing soil, and the tunnel.

Conclusion

The analysis has clearly shown that the rupture path is strongly affected by the presence of the tunnel. The rupture is not only diverted, but is also subject to bifurcation and diffusion. More importantly, due to the developing interaction between the tunnel and the rupture, the fault does not outcrop underneath the tunnel with the form of a distinct scarp. Instead, the imposed displacement is converted to a diffuse differential displacement on the tunnel base. This is attributed to the significant stiffness of the tunnel, along with its increased weight (structure + 5 m of soil cover).

This combination of stiffness and dead load proves to be favorable for the response of the tunnel. The soil underneath the tunnel is subjected to significant loading (exerted from the rotating tunnel). Such a loading cannot be undertaken by the bearing soil, which in turn fails, leading to the observed diffusive behavior. This way, the tunnel practically remains in almost complete contact with the soil, and is therefore subjected to acceptable levels of stressing.

The sectional forces of our study, where used as the design values for the tunnel.

REFERENCES

Akyüz, H.S., Barka, A., Altunel, E., Hartleb, R., Sunal, G. (2000), “Field Observation and Slip Distribution of the November 12, 1999 Düzce Earthquake (M=7.1), Bolu – Turkey, The 1999 Izmit and Düzce Earthquakes: Preliminary Results”, *Istanbul Technical University*, pp.63-70.

Ambraseys, N.N, & Jackson, J.A. (1990), “Seismicity and associated strain of central Greece between 1890 and 1988”, *International Journal of Geophysics*, Vol. 126, pp. No.3, pp. 663-708.

Anastasopoulos, I. (2005), “Fault Rupture – Soil – Foundation – Structure Interaction”, *Doctoral Dissertation*, National Technical University, Athens, pp. 570.

Armijo, R., Mayer, B., King, G.C.P., Rigo, A., and Papanastassiou, D. (1996), Quaternary evolution of the Corinth Rift and its implications for the late Cenozoic evolution of the Aegean, International Journal of Geophysics, Vol.126, pp. 11-53.

Bray, J.D. (1990), “The effects of tectonic movements on stresses and deformations in earth embankments”, *Ph.D Dissertation*, University of California, Berkeley.

Bray, J.D., Seed, R.B., Cluff, L.S., and Seed, H.B. (1994), “Earthquake Fault Rupture Propagation through Soil”, *Journal of Geotechnical Engineering*, ASCE, Vol. 120, No.3, pp. 543-561.

Buck, V., & Stewart, I. (2000). “A critical reappraisal of the classical texts and archaeological evidence for earthquakes in the Atalanti region, central mainland Greece”, in: McGuire, Griffiths, Hancock, and Stewart (editors), *The Archaeology of Geological Catastrophes, Geological Society of London, Special Publications*, Vol. 171, pp. 33-44.

Davies, M.C. & Branby F. (2005), “Centrifuge experiments for fault rupture propagation”, *University of Dundee*, to be published.

E.A.K. 2000 (2001), “Hellenic Seismic Regulation”, *published by O.A.S.P.*, Athens, April 2001 (in Greek).

Earthquake Spectra (2000), “Kocaeli, Turkey, Earthquake of August 17, 1999 Reconnaissance Report”, *Suppl. A to Vol. 16*.

Gaudin, C. (2002), “Experimental and theoretical study of the behaviour of supporting walls: Validation of design methods”, *Ph.d Dissertation*, Laboratoire Central des Ponts et Chaussées, Nantes, France.

Lekkas, S. (1994) “Study of Seismic Hazard and Catastrophic Geodynamic Phenomena for the city of Rhodes”, *Technical Report.*

Mitsopoulos, K (1895), “The Mega-earthquake of Lokris in April 1894”, *Ethnikon Typografeion,* Athens, 40 pp. (in Greek).

Pantosti, D., De Martini, P.M., Papanastassiou, D., Palyvos, N., Lemeille, F., and Stavrakakis, G. (2001), “A Reappraisal of the 1894 Atalanti Earthquake Surface Ruptures, Central Greece”, *Bulletin of the Seismological Society of America*, Vol. 91, No. 4, pp. 760-780

Papavassiliou, M.S. (1894), “Sur le tremblement de terre de Locride (Grèce) du mois d’ Avril 1894”, *C. R. Acad. Scienc.,* Paris, Vol. 19, pp. 112-114 (in French).

Pavlides, S.B. (2003), “Study of the Geology and the Seismic Hazard of Northern Atalanti”, *Technical Report* (in Greek).

Pavlides, S., Tutkun, Z., Chatzipetros, A., Özaksoy, V., and Doğan, B. (2003), “Trenching along the Gölcük 1999 normal fault: evidence for repeated recent seismic activity”, *International Workshop on the North Anatolian, East Anatolian and Dead Sea Fault Systems: Recent Progress in Tectonics and Paleoseismology, and Field Training Course in Paleoseismology*.

Philippson, A. (1894), “Das dies jahrige Erdbeben in Lokris”, *Zeitschrift Ges. Erdkunde zu Berlin*, Vol. 21, pp. 332-334 (in German).

Roberts, S., and Jackson, J. (1991), “Active normal faulting in central Greece: and overview, in The Geometry of Normal Faults”, A.M. Roberts, G. Yielding, and B. Freeman (Editors), *Geological Society Special Publ. 56*, pp. 125-142.

Rondoyanni, Th. (1984), “Etude néotectonique des ravages occidentaux du canal d’Atalanti, Grèce, Centrale”, *Thèse 3eme cycle*, Université de Paris-XI, 190 pp. (in French).

Sigalas, I. (2003), “Investigation of the Hazard of a Possible Seismic Rupture of the Atalanti Fault and Design Proposal for the Buildings of O.E.K. to undertake it : Static Design of Bldgs 253, 257, and 285”, *Research Project Report*, Vol 1–3.

Skouphos, T. (1894), “Die zwei grossen Erdbeben in Lokris am 8/20 und 15/27 April 1894”, *Zeitschrift Ges. Erdkunde zu Berlin,* Vol. 24, pp. 409-474 (in German)..

Tutkun, Z., Pavlides, S., and Doğan, B. (2001), “Small scale structural pattern along the surface rupture traces of the Izmit – Kocaeli (Turkey) 1999 earthquake”, *4th International Symposium on Eastern Mediterranean Geology*.

Wells, D.L. and Coppersmith, K.J. (1994), “New Empirical Relationships among Magnitude, Rupture Length, Rupture Width, Rupture Area, and Surface Displacement”, *Bulletin of the Seismological Society of America*, Vol. 84, No. 4, pp. 974-1002.

OTM – Omilos Technikon Meleton (1997) “New Athens-Thessaloniki Highway, Ag. Konstantinos Kammena Vourla : Technical Seismologic Study”, *Technical Report.*